



HAL
open science

Use of nanocellulose for security paper

Johanna Desmaisons

► **To cite this version:**

Johanna Desmaisons. Use of nanocellulose for security paper. Mechanics of materials [physics.class-ph]. Université Grenoble Alpes, 2018. English. NNT : 2018GREAI055 . tel-04213532

HAL Id: tel-04213532

<https://theses.hal.science/tel-04213532v1>

Submitted on 21 Sep 2023

HAL is a multi-disciplinary open access archive for the deposit and dissemination of scientific research documents, whether they are published or not. The documents may come from teaching and research institutions in France or abroad, or from public or private research centers.

L'archive ouverte pluridisciplinaire **HAL**, est destinée au dépôt et à la diffusion de documents scientifiques de niveau recherche, publiés ou non, émanant des établissements d'enseignement et de recherche français ou étrangers, des laboratoires publics ou privés.

THÈSE

Pour obtenir le grade de

DOCTEUR DE LA COMMUNAUTE UNIVERSITE GRENOBLE ALPES

Spécialité : **Matériaux, Mécanique, Génie civil, Electrochimie**

Arrêté ministériel : 25 mai 2016

Présentée par

Johanna DESMAISONS

Thèse dirigée par **Dr. Julien BRAS, Grenoble-INP Pagora**, et
codirigée par **Pr. Alain DUFRESNE, Grenoble-INP Pagora**

préparée au sein du **Laboratoire Génie des Procédés Papetiers**
dans **l'École Doctorale I-MEP 2 – Ingénierie – Matériaux,
Mécanique, Environnement, Énergétique, Procédés,
Production**

Use of nanocellulose for security paper

Thèse soutenue publiquement le **14 septembre 2018**,
devant le jury composé de :

Pr. Aji P. MATHEW

Professeur, Stockholm University, rapporteur

Pr. Thaddeus MALONEY

Professeur, Aalto University, rapporteur

Dr. José Maria LAGARON

Directeur de recherche, Spanish National Research Council, président

Dr. Julien BRAS

Maître de conférences à Grenoble-INP, directeur de thèse

Pr. Alain DUFRESNE

Professeur à Grenoble-INP, co-directeur de thèse

M. Giuseppe MOSELE

Senior R&D expert, European Central Bank



Acknowledgments

I am very grateful to all the people who have contributed to make this PhD an unforgettable adventure.

First, I would like to thank Giuseppe Mosele, Gilles Roberty and Marion Lutsche without whom this project would not exist. Thank you for your support, your help and all our interesting discussions during these 3 years. I will really miss this project.

Thank you Alain Dufresne and Julien Bras for supervising this PhD, I learned a lot from your scientific knowledge and expertise. You helped me always with kindness to give the best of myself.

Thank you Aji Mathew, Thaddeus Maloney, and Jose Maria Lagaron for accepting to be involved in this project as jury members. Thank you for the great discussion.

I also really enjoyed all the enriching collaborations. Thank you to all the people from Université de Bretagne Sud, 3SR, Mc Master University. Special thanks to Emily Cranston and her team for their nice welcome in their lab. Thank you to Emil Gustafsson for sharing RESIST project.

Thank you to all the LGP2 members. I spent great time in this lab thanks to the sympathy and great source of knowledge from all the people I met. A few words in French now. Merci à tous les doctorants pour les moments de convivialité. Merci en particulier à toute la Matbio'team pour la bonne ambiance, les moments passés au labo, autour d'un verre ou d'un resto. Merci à ceux avec qui j'ai partagé des conférences ou training school en France, en Suède, au Japon, au Canada, à la Nouvelle Orléans (et merci à mes directeurs de thèse de m'avoir donné autant d'opportunités). Merci à Cécile pour son aide précieuse mais aussi pour sa gentillesse.

Merci à mon premier bureau trop cool, Fanny, Claire, Jordan et Marcos. C'était vraiment top de commencer ma thèse avec vous. Merci à mon bureau 2ème génération avec Manon, Gabriel (Mister papèt!), et Estelle. C'était tout aussi top de finir ma thèse avec vous.

Merci à toutes les copines du midi pour ces bons moments qui vont me manquer.

Enfin pendant cette thèse, mais aussi pendant l'expérience PAGORA qui a précédé, j'ai rencontré des personnes qui sont devenues de vraies amies maintenant et sans qui ça n'aurait vraiment pas été pareil. Merci Fleur et Hélène pour ces 6 années de partage, de galères communes et de papotages. Merci Manon, toujours de bonne humeur et attentive pour m'écouter râler. Merci Fanny (H) pour ton peps et ta sagesse, merci Fanny (T) pour ta gentillesse et les bons moments passés autour d'un jeu ou dans un escape game (on a failli gagné). Merci les filles pour tous les chouettes souvenirs que j'ai de ces trois ans et pour les prochains à venir.

Pour finir, merci à ma famille de toujours me porter vers le haut et me soutenir. J'ai beaucoup de chance de vous avoir. Merci à Anaïs, pour son amitié depuis 15 ans. Merci à Killian, d'avoir été présent et de l'être toujours 800 km plus loin.

Table of content

General Introduction.....	11
I. Literature review.....	19
Introduction.....	23
1. Banknote papers: production and challenges.....	25
2. Crumpling and dog-ears defects: solutions and expectations.....	36
3. From cellulose to nanocellulose.....	44
4. Nanocellulose for use with polymer and in paper industry.....	63
Conclusion.....	81
References.....	83
II. Introduction of cellulose nanocrystals in polyvinyl alcohol matrix for dog-ears limitation.....	95
Introduction.....	99
1. Extension of buckling-based metrology to thick cellulose nanocrystal-reinforced polyvinyl alcohol coatings.....	101
2. Impregnation of paper with cellulose nanocrystal-reinforced PVOH: synergistic effect of infrared drying and CNC content on polymer crystallinity.....	121
3. Use of cellulose nanocrystals in a polyvinyl alcohol matrix to decrease banknotes dog-ears defect.....	145
References.....	173
Supplementary data.....	179
III. Design of a multilayer material containing cellulose nanofibrils for crumpling limitation.....	183
Introduction.....	187
1. A new quality index for benchmarking of different cellulose nanofibrils.....	189
2. Hybrid nanopaper of cellulose nanofibrils and PET microfibers with high tear and crumpling resistance.....	211
3. Influence of pretreatment and degree of defibrillation on cellulose nanofibril cryogel properties and strategies to introduce a porous CNF layer inside a papermaking process.....	229
4. Introduction of cellulose nanofibril as a paper middle layer: three strategies for crumpling limitation and tear-resistant material.....	247
References.....	271
Supplementary data.....	281
IV. Scale-up and combination of the two strategies.....	293
Introduction.....	297
1. Project scale-up: pilot tests and industrial tests.....	299
2. Combining of the two strategies: influence of CNC reinforced PVOH impregnation, CNF middle layer and banknote calendaring on the whole paper properties.....	319
References.....	333
General conclusion and perspectives.....	335
Résumé Français - Extended French abstract.....	343

Scientific contributions (2015 – 2018)

Due to confidentiality reasons, no communication was performed relative with dog-ears and crumpling banknote damages.

Publications in scientific journal

1. J. Desmaisons, E. Boutonnet, M. Rueff, A. Dufresne, J. Bras, « A new quality index for benchmarking of different cellulose nanofibrils », **Carbohydrate Polymers** **2017**, 174 318 – 329. DOI : 10.1016/j.carbpol.2017.06.032
2. J. Desmaisons, M. Rueff, J. Bras, A. Dufresne, « Impregnation of paper with cellulose nanocrystal-reinforced PVOH : Synergistic effect of infrared drying and CNC content on crystallinity », **Submitted in Journal of Material Science**
3. J. Desmaisons, E. Gustafsson, A. Dufresne, J. Bras, « Hybrid nanopaper of cellulose nanofibrils and PET microfibers with high tear and crumpling resistance », **Submitted in Cellulose**
4. J. Desmaisons, E. Niinivaara, E. D. Cranston, A. Dufresne, J. Bras, « Extension of buckling-based metrology to thick cellulose nanocrystal-reinforced polyvinyl alcohol coatings », **Submitted in Langmuir**

Author's contribution

Publication 1: Johanna Desmaisons, Julien Bras and Alain Dufresne were responsible for the experimental design and planning of the work. Johanna Desmaisons supervised the 3-month internship of Elisa Boutonnet, performed experiments, analyzed the results and wrote the manuscript as principal author under the supervision of Dr. Julien Bras and Pr. Alain Dufresne. Martine Rueff helped us with the statistical analysis (correlation matrix and principal component analysis).

Publication 2: Johanna Desmaisons, Julien Bras and Alain Dufresne were responsible for the experimental design and planning of the work. Johanna Desmaisons performed all the experiments, analyzed the results and wrote the manuscript as principal author under the supervision of Dr. Julien Bras and Pr. Alain Dufresne. Martine Rueff supervised the experiments relative with infra-red drying modeling.

Publication 3: Johanna Desmaisons and Emil Gustafsson have both performed the experiments and they shared the writing of the manuscript under the supervision of Dr. Julien Bras and Pr. Alain Dufresne.

Publication 4: Johanna Desmaisons, Dr. Julien Bras and Dr. Emily Cranston were responsible for the experimental design and planning of the work. Dr. Elina Niinivaara and Dr. Emily Cranston helped Johanna Desmaisons during her stay at Mc Master University (Canada) and shared their expertise on buckling metrology. Johanna Desmaisons performed all experiments and wrote the manuscript as first author under the supervision of Dr. Julien Bras, Dr. Emily Cranston, Pr. Alain Dufresne and Dr. Elina Niinivaara.

Patents

1. J. Bras, A. Dufresne, J. Desmaisons, G. Roberty, M. Lutsche, « Use of nano cellulose on a paper product », EP3228744 A1, **2017**
2. J. Bras, A. Dufresne, J. Desmaisons, G. Roberty, M. Lutsche, G. Mosele, « Use of nano cellulose to decrease crumpling of paper », patent application in submission

Oral presentations in international conference

1. J. Desmaisons, U. Gill, E. Niinivaara, A. Dufresne, E. Cranston, J. Moran-Mirabal, J. Bras, « Buckling-metrology adaptation for determining mechanical properties of PVOH-CNC thick coated layers », in **ACS** - American Chemical Society, USA, **2018**.
2. J. Desmaisons, A. Dufresne, B. Seantier, C. Jiménez Saelices, S. Molina-Boisseau, J. Bras, « Influence of cellulose nanofibrils chemical and mechanical treatments on nanocellulosic foam properties » in **ICC** – The 4th International Cellulose Conference, Japan, **2017**.
3. J. Desmaisons, A. Dufresne, J. Bras, « What is the difference between different Cellulose nanofibrils? The Quality Index », in **TAPPI** – International conference of nanotechnology for renewable materials, Canada, **2017**
4. J. Desmaisons, A. Dufresne, J. Bras, « A New Quality index for benchmarking of different cellulose nanofibrils », in **Action Cost FP1205** – Innovative applications of regenerated wood cellulose fibres, Germany, **2017**

Poster presentations in international conference

1. J. Desmaisons, A. Dufresne, B. Seantier, C. Jiménez Saelices, S. Molina-Boisseau, J. Bras, « Influence of cellulose nanofibrils chemical and mechanical treatments on nanocellulosic foam properties » in **ICC** – The 4th International Cellulose Conference, Japan, **2017**.
2. J. Desmaisons, A. Dufresne, B. Seantier, C. Jiménez Saelices, S. Molina-Boisseau, J. Bras, « Influence of nanofibrillation degree on nanocellulosic foam properties », in **ACS** - American Chemical Society, USA, **2017**
3. J. Desmaisons, A. Dufresne, J. Bras, « Mechanical properties of cellulose nanocrystal based coating layer – Buckling method », in **TAPPI** - International conference of nanotechnology for renewable materials, France, **2016**

Other communications

1. E. Gustafsson, J. Desmaisons, A. Dufresne, J. Bras, « Hybrid nanopaper of cellulose nanofibrils and PET microfibers with high tear resistance », in TAPPI - International conference of nanotechnology for renewable materials, USA, **2018**
2. J. Bras, J. Desmaisons, « Know your starting Materials: What About CNF? », in TAPPI nano Worskhop, USA, **2018**

Abbreviations

Chemical and materials

CNCs	Cellulose nanocrystals
CNFs	Cellulose nanofibrils
CNFs-	Anionic cellulose nanofibrils
CNFs+	Cationic cellulose nanofibrils
CMC	Carboxymethyl cellulose
EPTMAC	Epoxypropyltrimethylammonium chloride
GF	Glass fibers
PAE	Polyamideamine epichlorohydrin
PDMS	Polydimethylsiloxane
PET	Polyethylene terephthalate
PS	Polystyrene
PTFE	Polytetrafluoroethylene
PVOH	Polyvinyl alcohol
TEMPO	(2,2,6,6-Tetramethylpiperidin-1-yl)oxyl
TiO₂	Titanium dioxide
TTAB	Tetradecyltrimethylammonium bromide

Methods

AFM	Atomic Force Microscopy
ANOVA	Analysis of variance
BET	Brunauer Emmett Teller
DLS	Dynamic Light Scattering
DMA	Dynamic Mechanical Analysis
DSC	Differential Scanning Calorimetry
EAR	Elastic angle recovery
FEG-SEM	Funnel Electron Gun Scanning Electron Microscopy
FFT	Fast Fourier Transform
IR	Infra-red
NBS	National Bureau of Standard
SEM	Scanning Electron Microscopy
SIEBIMM	Strain-Induced Elastic Buckling Instability for Mechanical Measurements

General Introduction

General introduction

Principal actors of this PhD. This PhD, called **RESIST** project, is a collaboration between the R&D department of European Central Bank (**ECB**, Frankfurt, Germany) and the Laboratory of Pulp and Paper Science (**LGP2**, Grenoble, France) (Figure 1). The banknote research section at ECB focuses on three axes: (i) the improvement of security features to remain technologically ahead of counterfeiters, (ii) the improvement of banknote production technology, and (iii) the development of banknote processing or handling technology. This work fits into the second axis, and the main purpose is the development of **new banknote substrates** to increase their lifetime and ensure a material with state of the art technology. Two classical banknote defects are especially targeted in this project: **dog-ears** (folded corners) and **crumpling**, which are accountable for quick banknotes deterioration, imposing a significant replacement cost to the community. In parallel, LGP2 develops research in the field of production processes and final properties of biobased materials with a multidisciplinary and integrated approach, from the building block to the final material. This laboratory also developed for many years a strong expertise on **nanocellulose** and collaborates with many paper and packaging industries for the development of innovative fibrous materials.

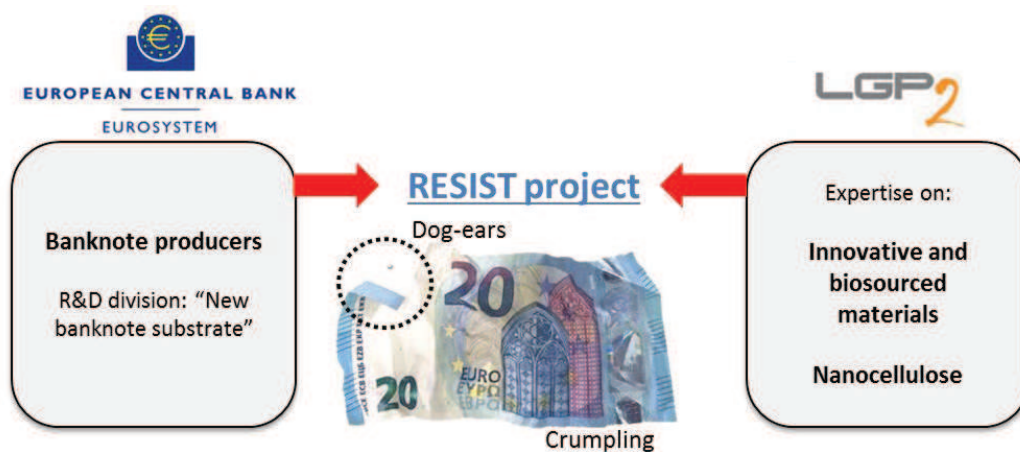


Figure 1: PhD subject: Improvement of banknote dog-ears and crumpling resistance thanks to the introduction of nanocellulose in the paper substrate

Industrial context. The banknote industry combines large volumes and high added value. There are today 20.2 billion of euro banknotes in circulation and an average of 7 billion of euro banknotes are fabricated yearly. Five accredited paper-mills and eleven printing companies exist in Europe, working in parallel on banknote fabrication with the best possible quality control to ensure the same final properties. France is the first euro banknote paper producer in volume with approximately 2000 tons/year of banknote paper produced. These papers, symbol of an economic value, are daily exchanged and submitted to strong solicitations because of manual handling (folding, crumpling), storage conditions (pockets, wallets,...), or ambient climate (humidity, extreme temperatures, rain). Despite these harsh conditions, the role of ECB and central banks is to guarantee secure banknotes with high visual and mechanical properties. Consequently, banknotes which do not

meet these quality requirements are destructed in sorting centers. Consequently, the banknote average lifetime is between a few months and three years, depending on their denomination and country habits. Some defects particularly impact this duration and increase the number of banknotes shredded in sorting centers. The first reason of banknote destruction is soil, the second one is the flapped corners also called “dog-ears”, responsible for 10% of destroyed banknotes. With a cost of 15 cents per banknote production, the economic loss due to dog-ears is huge. Among the other classical banknote defects, crumpling is also responsible for a loss of banknote quality. However, there is still no sensor able to detect crumpling in sorting centers and this defect remains out of statistics in spite of being the cause of several banknotes destruction (e.g. issue with dimensions or with image analysis in sorting machines).

Challenges associated to banknote dog-ears and crumpling. Dog-ears and crumpling are responsible for banknote destructions and sorting center issues for different reasons. The first consequence of dog-ears is the increase in thickness in the area of the folded corner, which complicates the automatic transportation of banknotes in sorting machines and can cause paper jams. Otherwise, the dog-ears corners can be separated by tear from the paper product. Dog-ears can also weaken the barrier layer of banknotes and allow penetration of soil. Finally, it can also cause storage problems as the banknotes are stored in boxes with specific heights and an increase in banknote thickness limits the number of packaged banknotes. The presence of multiple dog-ears can also impair proper operation of automatic processing: a banknote can be caught in another one, or the folded tip can cover security features. The situation concerning crumpled banknotes is more complex. First, the crumpled banknotes can be put back in circulation even if they do not meet the visual quality requirements, because of no detection of the defect. Otherwise, crumpling can also increase banknotes local thickness and promote conditioning issues. The so-called spring-effect can appear during supply chain resulting from a loss of paper rigidity, increasing the needed tension to maintain banknotes in their packaging box. Finally, crumpled banknotes in circulation are weakened and wrinkled areas can be easily teared. In the worst cases, a loss of mechanical properties leads to the circulation of limp banknotes. Today, no satisfying solutions exist for the limitation of these two defects.

Some countries such as Australia, Canada or New Zealand, have opted for polymer-based banknotes to increase banknote lifetime, mechanical properties and resistance to soil. However, these plastic banknotes present also some disadvantages such as their higher upfront production cost and cause issues in manual handling and in adaptation to automatic payment or vending machines. Up to now, the Eurosystem has decided to remain in a paper-based strategy and looked into the wide possibilities offered by nature to gain in performance.

Nanocellulose for innovative and performant materials in paper industry. Over the past two decades, the potential of nanocellulose has emerged in papermaking industry. This material combines the well-known properties of cellulose such as mechanical resistance, abundance and renewability with the innovative and outstanding properties offered by the nanoscale. The term

General Introduction

“nano” refers to materials having at least one dimension below 100 nm. Two kinds of nanocellulose can be extracted from the raw cellulosic fiber: cellulose nanofibrils (“CNFs”) and cellulose nanocrystals (“CNCs”). The first one is obtained after a mechanical disintegration of the fiber and results in long and flexible fibrils often imaged as “spaghett-like” form, with the diameter of a hair that would have been cut by 1000 in the width direction. The second one is obtained after an acid hydrolysis treatment that dissolves the amorphous regions of the fiber, and releases small and rigid crystals which can be imaged as a “grain of rice” with a diameter divided by 106 (Figure 2-A). These materials have raised an industrial interest during the last decade which is exponentially increasing as we can see with the evolution of patents (Figure 2-B).

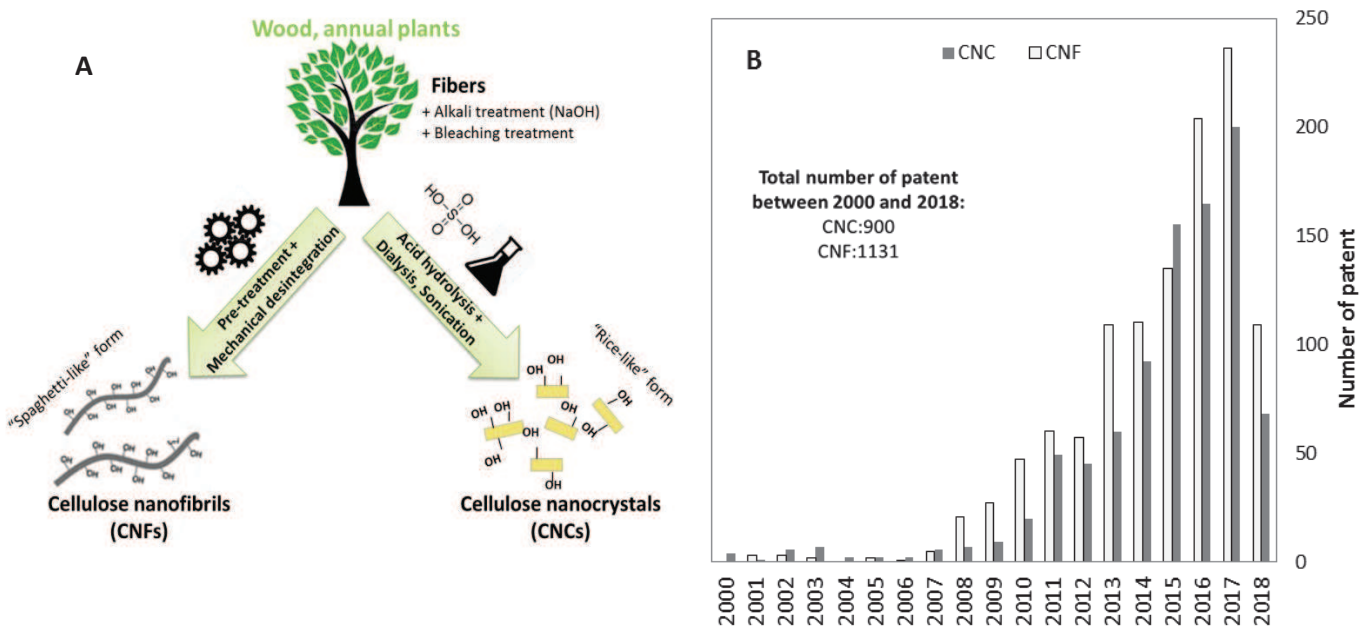


Figure 2: A) Schematic description of CNF and CNC and B) number of patent published with nanocellulose. Based on SciFinder research. Descriptors for CNF: Cellulose + CNF, Cellulose + MFC, Cellulose + NFC, Cellulose nanofibers, nanofibrillated cellulose, cellulose nanofibrils. Descriptors for CNCs: Cellulose + CNC, Cellulose + NCC, Cellulose nanocrystals, Nanocrystalline cellulose, Cellulose nanowhiskers.

The use of nanocellulose as additive in paper-making is a wide source of interest since the beginning of the 2010’s as both CNFs and CNCs present similar composition than paper, but their exceptional properties at the nanoscale confers paper quality enhancement (Campano et al. 2018). One of the main reasons for the expansion of nanocellulose in paper industry is the up-scaling in production of both cellulose nanofibrils and nanocrystals since 2012 and breakthrough to decrease the costs, accessibility and homogeneity of these materials. There are two approaches for the use of nanocellulose in paper: (i) insert nanocellulose in the bulk material, or (ii) coat them at the surface. Cellulose nanofibrils are mostly used in bulk for improving wet and dry mechanical properties (Madani et al. 2011; Hassan et al. 2011), increasing the filler content (Torvinen et al. 2011), decreasing the fiber refining (González et al. 2012) or decreasing the paper basis weight (Hamann 2011). Both cellulose nanofibrils and cellulose nanocrystals are used in surface, alone or as a polymer additive, in order to enhance oil resistance (Aulin et al. 2010), air resistance (Syverud and Stenius

2009), grease resistance (Kumar et al. 2017), improve surface smoothness (Afra et al. 2016), or printing properties (Luu et al. 2011). These applications are already used in traditional papers, in papers which target additional functional properties, in food packaging or in cardboard industries, but also in specialty papers and even in banknote. Indeed, a recent patent has been filed two years ago by Oberthur security and propose the use of CNCs in banknote varnish for increasing soil and oil resistance (Le Berre et al. 2015). However, no patent or publication ever reported the use of CNC and CNF for dog-ears and crumpling applications.

RESIST project and chapters description. The RESIST project aims to use both CNC and CNF potential in two different strategies for limiting the damages caused by banknote dog-ears and crumpling. This project is divided into 4 phases (Figure 3) and proposes fundamental studies, applied science and pilot or industrial tests conducted at Banque De France.

- **Phase 1: Selection of the raw materials.** *This preliminary study was performed by the same authors in a master thesis which is not part of this manuscript.* As the actual fiber used in banknote substrate is cotton, this first phase studied the possibility to overcome the commercial supply of nanocellulose with a self-ruling and home made in site nanocellulose production from the same cotton pulp, or from an eucalyptus pulp. As such, different kinds of nanocelluloses were prepared and characterized: CNF were prepared with different pretreatments (anionic, cationic, and enzymatic) followed by a super-grinding treatment, and CNCs were produced by acid hydrolysis followed eventually by anionic or cationic post-treatments. These suspensions have been successfully produced at lab-scale, with dimensions and properties comparable with commercial sources. Up-scaling of the CNF production was proposed by adapting the Masuko ultrafine super-grinder equipment of the laboratory with a recirculation system. Furthermore, the energy consumption of this mechanical treatment has also been successfully decreased thanks to small addition of abrasive fillers, such as titanium dioxide or glass fibers. However, the up-scaling of CNC production was not achieved because of time-consuming washing steps (centrifugation and dialysis). Phase 1 concluded that, for the next steps of the project, CNF could be produced from ECB cotton directly in the paper mill with adapted equipment while CNCs will always be supplied by commercial productions.
- **Phase 2: Impregnation of CNC-reinforced PVOH for dog-ears limitation.** *This phase is described in **Chapter II** of this manuscript.* A banknote substrate is composed of two cotton fiber layers. At the end of the paper-machine, the paper is impregnated in a bath of polyvinyl alcohol (PVOH). The strategy of this chapter consists in introducing small amount of CNCs to reinforce the PVOH matrix. This nanocomposite is expected to change the mechanical properties of the banknote substrate and act on the dog-ears resistance.
- **Phase 3: Design of a multilayer containing CNF for crumpling limitation.** *This phase is described in **Chapter III** of this manuscript.* In this part, a CNF layer of 5 g.m⁻² will be introduced between the two fiber layers composing a classical banknote, one with a basis

weight of 25 g.m⁻² and the other with a basis weight of 60 g.m⁻². This CNF layer is expected to increase the paper resistance under crumpling deformation. As CNF materials are extremely sensitive to tear, a special attention on the multilayer paper tear resistance will also be paid, and different strategies including mixing with polyethylene terephthalate synthetic fibers or porous CNF beads will be investigated.

- Phase 4: Combination of the two strategies and up-scaling.** This phase is described in **Chapter IV** of this manuscript. The results of the two previous chapters were conducted independently, and at lab scale. This last chapter proposes a transition from applied research to industrialization and describes the trials which were performed on pilot machine and on industrial paper machine at Banque De France facilities. This chapter also gathers the two strategies and study symmetrically the influence of CNCs on crumpling resistance and the influence of CNF and dog-ears resistance.

The context of this work, its challenge and the important scientific concepts are reported in the literature review (**Chapter I**) for a better understanding of the project and for introducing the following chapters.

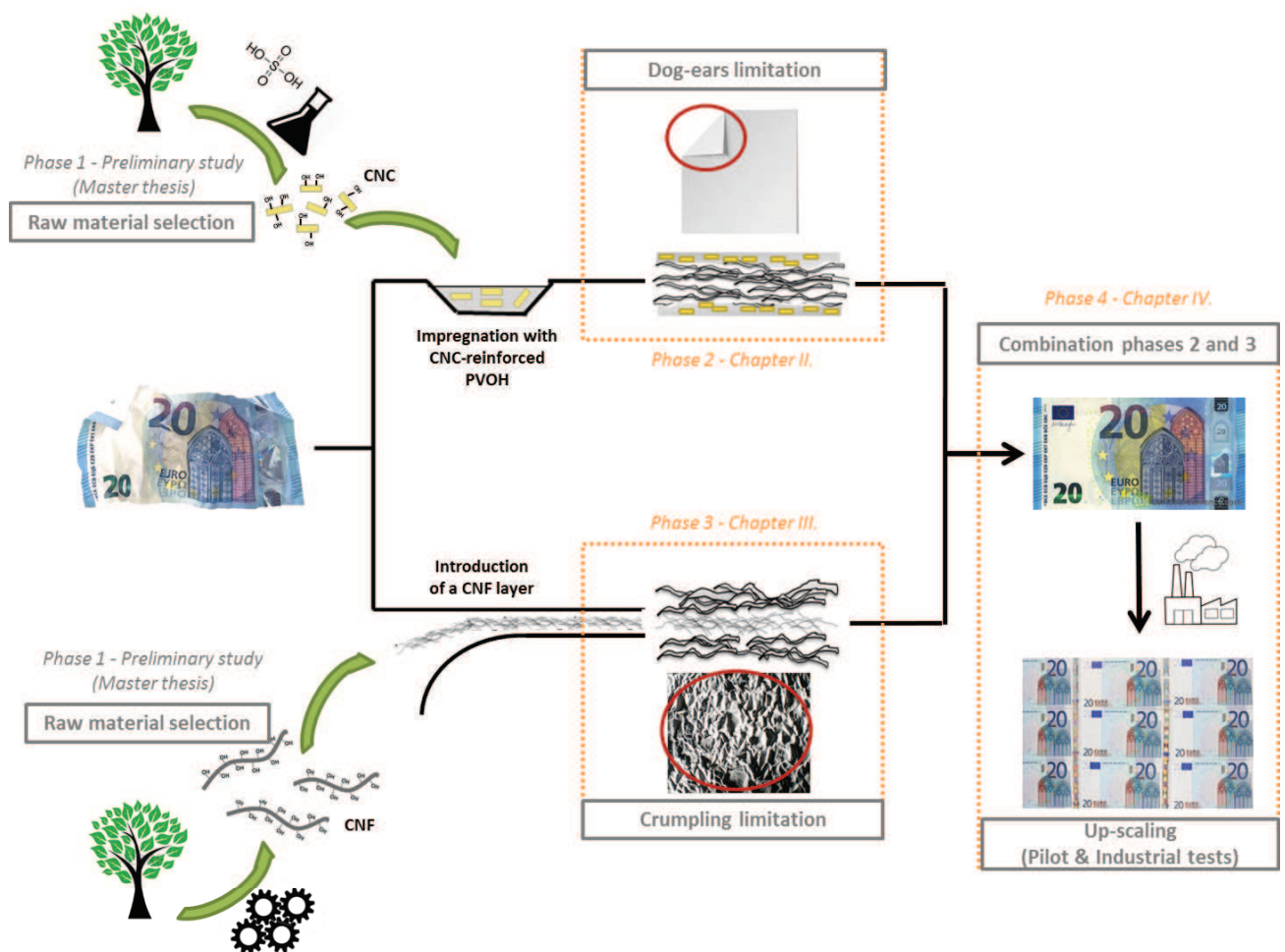


Figure 3: PhD overview and organization of the different chapters

References

- Afra E, Mohammadnejad S, Saraeyan A (2016) Cellulose nanofibils as coating material and its effects on paper properties. *Prog Org Coat* 101:455–460. doi: 10.1016/j.porgcoat.2016.09.018
- Aulin C, Gällstedt M, Lindström T (2010) Oxygen and oil barrier properties of microfibrillated cellulose films and coatings. *Cellulose* 17:559–574. doi: 10.1007/s10570-009-9393-y
- Campano C, Merayo N, Balea A, et al (2018) Mechanical and chemical dispersion of nanocelluloses to improve their reinforcing effect on recycled paper. *Cellulose* 25:269–280. doi: 10.1007/s10570-017-1552-y
- González I, Boufi S, Pèlach MA, et al (2012) Nanofibrillated cellulose as paper additive in eucalyptus pulps. *BioResources* 7:5167–5180. doi: 10.15376/biores.7.4.5167-5180
- Hamann L (2011) Wet-end applications of NFC. SUNPAP Workshop, Espoo, Finland
- Hassan EA, Hassan ML, Oksman K (2011) Improving Bagasse Pulp Paper Sheet Properties with Microfibrillated Cellulose Isolated from Xylanase-Treated Bagasse. *Wood Fiber Sci* 43:76–82. doi: 10.1177/0021998312453189
- Kumar V, Ottesen V, Syverud K, et al (2017) Coatability of Cellulose Nanofibril Suspensions: Role of Rheology and Water Retention. *BioResources* 12:7656–7679. doi: 10.15376/biores.12.4.7656-7679
- Le Berre M, Gillot J, Borde X (2015) Process for the surface treatment of a security document and associated security document. Oberthur Fiduciaire, WO2015091873 A1
- Luu WT, Bousfield DW, Kettle J (2011) Application of nano-fibrillated cellulose as a paper surface treatment for inkjet printing. PaperCon Conference
- Madani A, Kiiskinen H, Olson J, Martinez DM (2011) Fractionation of microfibrillated cellulose and its effects on tensile index and elongation of paper. *Nord Pulp Pap Res J* 26:306–311. doi: 10.3183/NPPRJ-2011-26-03-p306-311
- Syverud K, Stenius P (2009) Strength and barrier properties of MFC films. *Cellulose* 16:75–85. doi: 10.1007/s10570-008-9244-2
- Torvinen K, Helin T, Kiiskinen H, et al (2011) Nanofibrillated cellulose as a strength additive in filler-rich SC paper. TAPPI International Conference on Nanotechnology for Renewable Materials, Arlington USA

Chapter I

Literature review

Table of content chapter I

Introduction	23
1. Banknote papers: production and challenges	25
1.1. Generalities about banknote	25
1.1.1. Eurosystem in brief	25
1.1.2. Description of a banknote from Europa serie	26
1.2. Paper industry overview and focus on banknote application	28
1.2.1. Banknote paper within paper industry market.....	28
1.2.2. Paper machine review and banknote production	29
1.3.1. Banknote lifecycle	32
1.3.2. Crumpling and dog-ears defects	33
2. Crumpling and dog-ears defects: solutions and expectations.....	36
2.1. What is happening during paper folding and crumpling	37
2.2. Dog-ears and crumpling modeling: characterization and key parameters	38
2.2.1. Paper folding.....	39
2.2.2. Paper crumpling.....	41
2.3. Solutions in paper industry to limit dog ears and crumpling.....	43
3. From cellulose to nanocellulose.....	44
3.1. Properties of cellulose	44
3.2. Cellulose nanofibrils	47
3.3. Cellulose nanocrystals	54
3.4. Nanocellulose up-scaling and market prospects	57
4. Nanocellulose for use with polymer and in paper industry	62
4.1. CNCs nanocomposites and generalities on crystallization mechanisms	62
4.1.1. Use of CNC in nanocomposites	62
4.1.2. CNC reinforced polyvinyl alcohol nanocomposites	64
4.1.3. Crystallization mechanisms of CNC reinforced polymer composites	66
4.2. Use of nanocellulose in paper industry: context	71
4.3. Bulk improvement of papers	71
4.4. Surface coatings.....	75
4.4.1. Pure CNF/CNC coating in one or multilayer application	75
4.4.2. CNF/CNC as coating additive	77
4.5. Synthesis of nanocellulose strengths and weakness in paper industry and application for dog-ears and crumpling limitation	79
Conclusion.....	81
References	83

Introduction

The present chapter aims to give both non expert and expert readers the keys to understand the general background of this project, through the state of the art of technologies, actual challenges and society expectations. In this literature review, 236 references have been used to build the pillars of the following chapters.

The **first part** gives an overview of the **banknote industry** and starts with a brief description of the Eurosystem in term of history, functioning and volumes at stake. Then, a focus on banknote in the paper industry helps us to figure out the different steps involved in banknote production. Finally, the description of the banknote lifecycle introduces the challenges and expectations of this high-added value market and ends by presenting the two defects which especially concern this study: the crumpling and the dog-ears.

These **crumpling and dog-ears defects** are complex paper phenomena and have been a wide source of debate and study for paper physicists. **The second part** is hence dedicated to summarise the key parameters, explanations and characterizations of these mechanisms.

The strategy of this project consists in decreasing both dog-ears and crumpling defects of banknote thanks to the innovative use of **nanocellulose**. Two different families of nanocellulose with their own procedures of extractions, dimensions, properties and applications are detailed: the cellulose nanofibrils and the cellulose nanocrystals. **This third part** aims to give the reader the fundamental knowledge on these raw materials and highlights their outstanding potentials in our society.

Finally, the last part details the **use of nanocellulose as a nanocomposite and in paper industry**. This part proposes an understanding of the different approaches and potential improvement brought by the use of nanocellulose in coating or bulk insertion in a paper machine process.

To sum-up, this chapter identifies the main challenges of this industrial project and emphasizes the scientific questions to understand and keep in mind for the next chapters presenting the results.

1. Banknote papers: production and challenges

1.1. Generalities about banknote

1.1.1. Eurosystem in brief

Data, dates and general information, if no other source mentioned, are all provided from European central bank and Banque de France official websites (www.ecb.europa.eu, www.banque-france.fr) and discussions.

In 1992, at the occasion of the Maastricht Treaty, countries members of the European Union took the official decision to create the euro currency. Ten years later, banknote and coins began to circulate between nineteen countries members of the European Union (Figure 1-A). Since October 2006, **euro** is the first currency in the world regarding the amount of banknotes in circulation. Today, the euro is also the second largest currency in the world for transactions, behind the US dollar and ahead the Chinese yuan. According to European Central Bank estimates, at the end of December 2016, there were approximately 20.2 billion banknotes in circulation around the Eurozone, corresponding to a currency value of approximately €1.1 trillion.

Totally, 7 dominations of euro banknotes exist with values ranging from 5 to 500 euros. Each banknote paper has its proper dimensions, color, and design honoring European architecture history from the Classical movement to the Modern style of the 20th century. Furthermore, the euro banknotes contain many complex security features such as watermarks, invisible ink, holograms and microprinting to prove their authenticity.

In November 2012, the European Central Bank announced that the first series of banknotes would be replaced by a second generation of euro banknote, with reinforced security features and better protection against counterfeit. These new series are called “Europa”, as two of its new security features include a portrait of Princess Europe, the mythology princess which gave its name to our continent. On 2 May 2013, the second generation of “5 euro” banknote has been put in circulation, followed by the 10 euros in 2014, 20 euros in 2015, and 50 euros in 2017 (Figure 1-B). For the 5 euros and 10 euros, corresponding to the most manipulated banknotes, a new protecting coating has been added to reinforce their mechanical and grease resistance with a view of increasing their lifetime.

This **banknote lifetime** is a key economic aspect for ECB and the proper objective of this PhD work. There is today an average of 20.2 billion of banknotes in circulation and it is 7 billion of euro banknotes which are fabricated each year. Among the seven euro banknote denominations, low or intermediate values of banknotes are most frequently used for daily payments: 45% of banknotes in circulation are 50€, 18% are 20€, and 10% 5€ (CB Statistical Data Warehouse, May 2016). Because of the high quantity of manipulations, their average lifetime is between a few months and 3 years, depending on the denomination and country habits. Some defects particularly impact this duration

and increase the number of **unfit banknotes** in sorting centers. In 2009, 33 billion banknotes were sorted within the Eurosystem and 5.4 billion were shredded because they did not answer the quality requirements. The first reason of unfit banknotes is soil, the second ones are the flapped corners also called “dog-ears”, responsible for 10% of destroyed banknotes. With a cost of 15 cents per banknote production, the economic loss due to dog-ears can reach extreme high values.

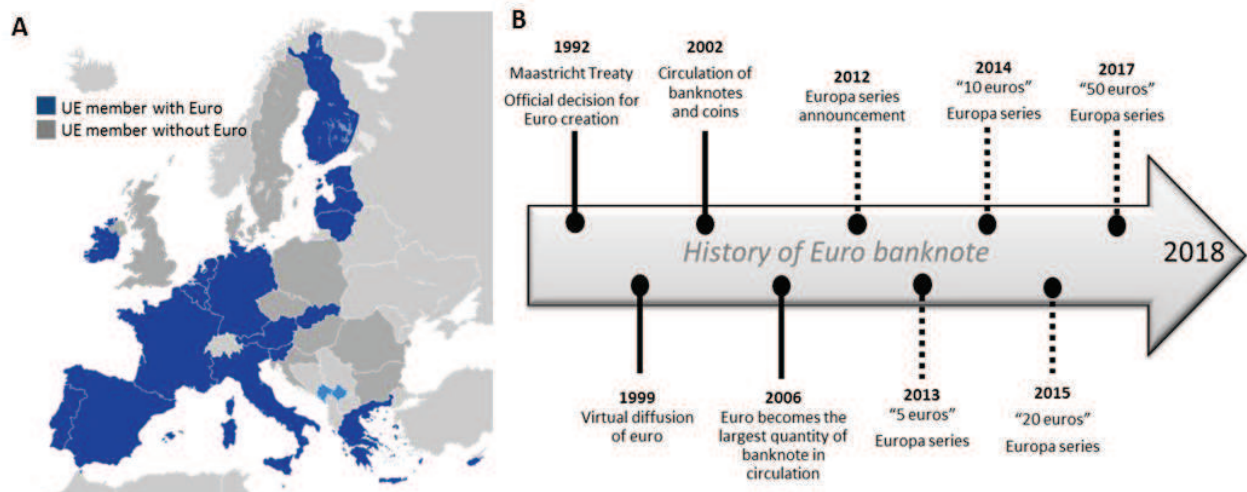


Figure 1: A) Countries currently using euro currency and B) Timeline of special events in Euro banknote

1.1.2. Description of a banknote from Europa serie

The banknote paper is a high added value quality product with strong quality requirements. This complex and secure material combines aesthetic qualities (patterns and halftones of the watermark, whiteness, opacity) and special technical characteristics (ability to receive many impressions, circulate in automatons, resistance to soiling, bending, and other mechanical defects).

Each banknote holds various security features to protect it against counterfeits (Figure 2-A). It exists different levels of security: the first level contains publicly known features, the second level of security features can be detected by specialized equipments, and the third level is only known by central banks. The first level is composed of features which can be detected thanks to the method “touch, look and tilt”:

- “Touch”: On the front, there is a series of short raised lines on the left and right edges. They make it easy to identify the banknote, especially for visually impaired people. The main image, the lettering and the large value numeral also feel thicker.
- “Look”: If the banknote is looked against the light, a faint image becomes visible and shows a portrait of Europa (Watermark), the value of the banknote and the main image. If, however, you put the banknote on a dark surface, the light areas become darker. The portrait also appears in the hologram. The security thread also appears under the form of a dark line.

- “Tilt”: The silvery stripe reveals a portrait of Europa in a transparent window and the emerald number displays an effect of the light that moves up and down.

It also exists additional features with magnetic inks, and properties which can be seen only under UV lights or infrared. Furthermore, each banknote denomination has its own dimensions, weight, color and style (Figure 2-B). Thanks to its high level of technicality, only 331,000 counterfeit euro banknotes were removed from circulation in the first half of 2014 (across the euro area). Considering 16 billion of banknotes in circulation at that time, it only corresponds to 0.002%.

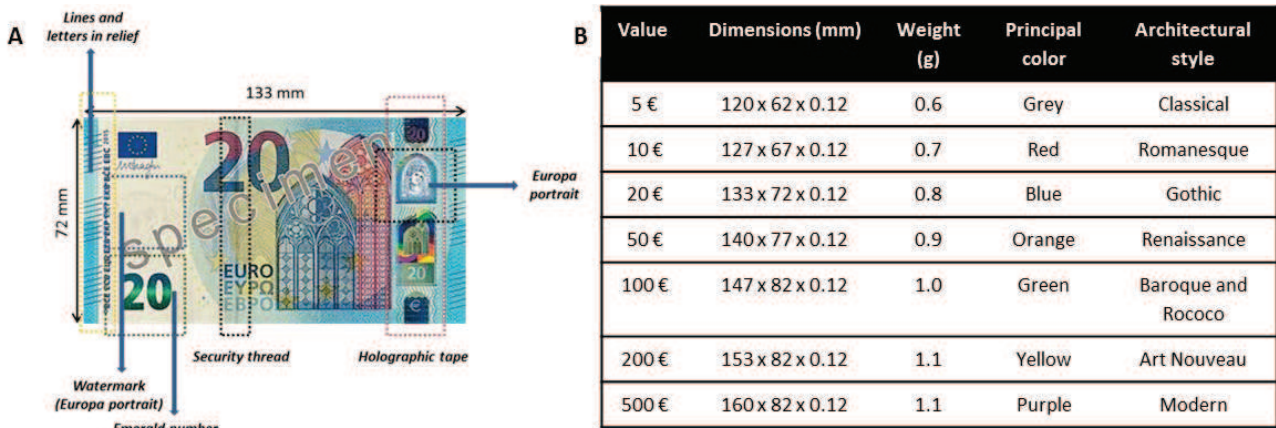


Figure 2: A) Classical features of 20 euros banknote and B) general properties of each banknote denomination

Some countries (e.g. New Zealand, Australia, Canada) are developing plastic banknotes to limit classical issues in banknote recirculation. After a debate, ECB has decided in early 2010’s to carry on with paper substrate and its industry.

1.2. Paper industry overview and focus on banknote application

1.2.1. Banknote paper within paper industry market

The worldwide production of paper and board has still increased from 400 to 420 million tons from 2013 to 2017, corresponding to an evolution of 5% in 4 years. Especially, paper and board production in Europe (CEPI members) has increased by 1.5% between 2016 and 2017 and reached 92.3 Million tons (Figure 3, purple curve). On the other hand, European consumption of paper and board is decreasing as well as the number of Paper and Board mills (Figure 3, blue curve). These half-tone statistics are characteristic of our modern society where digital empire and environmental challenges tends to slow down the old paper and cardboard industry and reveals a new one looking for new functionalities and performances.

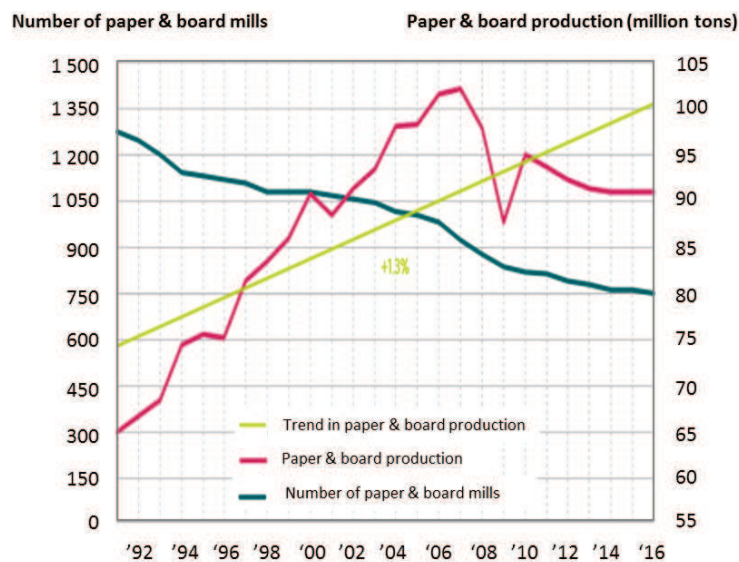
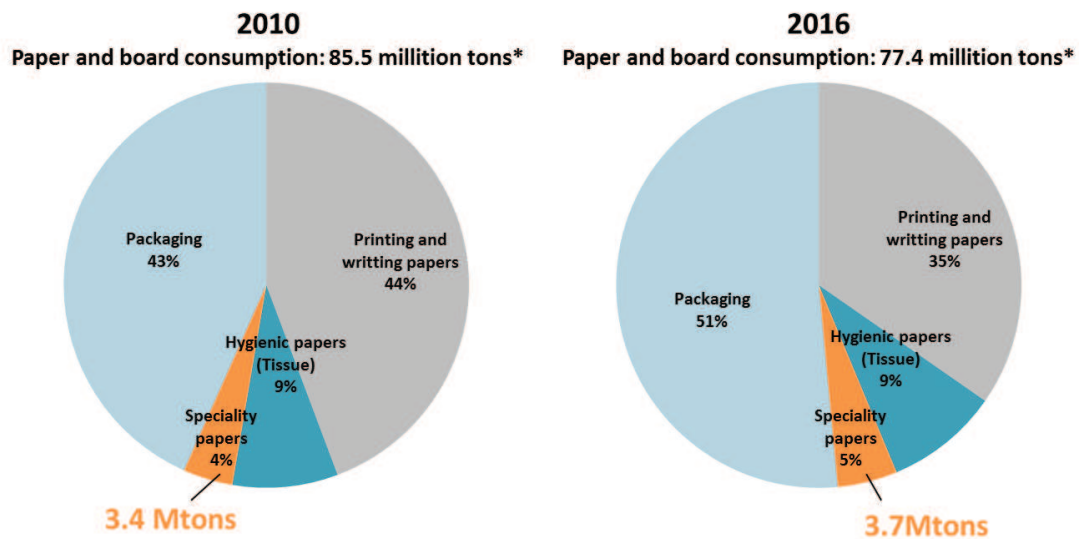


Figure 3: Number of Capi Paper & Board mills and Paper & Board production, (Capi 2017)

The paper industry is usually divided into four main categories: Printing and writing papers, hygienic papers, packaging and speciality papers. Convenience papers used for graphic communication, such as newsprint or printing paper, have declined significantly in the last decade in Western Europe and North America. This trend is expected to continue and spread to other regional markets as the digitization of communications continues. In parallel, specialty papers are becoming one of the growth forces of the paper industry, with tissue paper and packaging (Capi 2017).

Speciality papers are usually high added value papers with unique characteristics. Among them, we can find decor and wallpaper, Fiduciary or security papers, cigarette papers, filters and industrial papers, thermal and carbonless papers. They usually are a combination of state-of-the art sciences and their European consumption, instead of printing or writing papers, is growing (Figure 4). Furthermore, even if speciality papers represent only a small percentage of the overall production in terms of volume, they represent an important percentage in terms of income (Bardet 2014).

Smithers Pira's latest report (Smithers Pira 2017) has predicted a 2.2% annual growth from 2017 to 2022 for the global speciality paper market, which would result in 27 million tonnes worldwide by 2022.



*Figure 4: Paper and board consumption repartition *in CEPI area (Confederation of European Paper Industries). Values extracted from CEPI 2011 and 2017 Key statistics.*

Banknote paper belongs to speciality papers category. At the end of December 2016, 20.2 billion euro banknotes with a nominal value of 1.12 trillion € were in circulation. Compared with end-2015, banknote circulation had increased by 0.7% in volume terms and by 3.9% in value terms. Five paper-mills and eleven printing companies exist in Europe, working on banknote fabrication with the best possible quality control to ensure the reproducibility. France is the first euro paper producer in volume with 2500 tons/year. This production capacity is expected to double with the new developments of Europafi, the subsidiary papermill of Banque de France. Europafi has indeed launched a new investment plan of 75 million euros to change its paper machine in Vic-le-Comte. France is also the first printer of euro banknotes among the 14 other Europeans printer. Twenty billion of banknotes were produced at Vic le Conte and printed at Chamalières from the beginning of euro currency, corresponding to 22% of the total volume.

1.2.2. Paper machine review and banknote production

The paper is made in a wet environment, from a fibrous suspension that is deposited on a canvas. The main principle is to remove water and create a strong fiber network. The paper machine is composed of several sections where water flows, the fibrous mattress consolidates, is then pressed to give a special texture, and finally dried. The most common process is the flat table (Or Foudrinier wire) and corresponds to fast and large width machines, with a marked orientation of the fibers in the direction of manufacture ("machine direction", as opposed to "cross direction"). The other process is the round shape (Figure 5). This process is older and corresponds to machines more

specifically dedicated to the Fine Arts: it leads to papers having a more homogeneous formation, a more marked texture, and a more anisotropic distribution of the fibers (the fibers are less oriented than in the case of a flat table). This last process also produces papers more stable to moisture, which further strengthens a composition based on cotton fibers. This is also the used process for banknote fabrication in ECB paper producers and more specifically in Banque de France at Vic-Le-Conte.

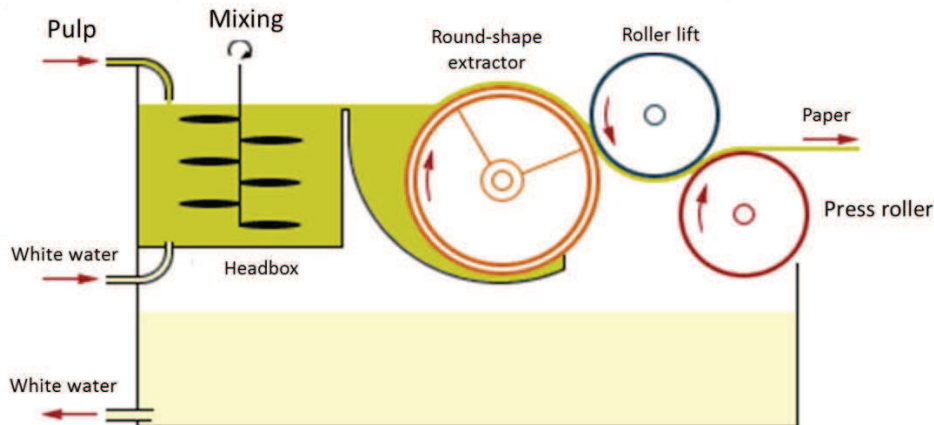


Figure 5: Round-shape section of the paper-machine, invented by Dickinson in 1809 for paper industrial production.. Adapted from (Coste 2004).

As conventional papermaking processes, the paper machine of Banque de France follows the same traditional steps: preparation of the fiber material, web forming, pressing, drying and calendaring. All banknotes papers are produced from cotton fibers, delivered from different locations such as Pakistan or India. These fibers are pre-refined between 60 and 70 SR° to ensure fibrillation, hydration and swelling of the fibers. Then, the papermill of Vic-le-compte produces the final paper thanks to a cylinder mold system, with a speed of 68m/min and a width of 746.5 mm. This speed of production is very low in comparison with classical paper machines which can reach more than 1500 m/min, but this slowness can be explained by the high level of technicity required for such papers.

The new paper machine of Banque de France, manufactured by Allimand, has a width of 2.55 m (3 times bigger than the former one) and a length of 100 m. This paper machine is effective since October 2017. However, in this project, industrial tests have been performed on the former paper machine and the following description is consequently representative of the older paper machine (still running). As conventional paper machines, a banknote paper machine is composed of a wet-end part, a wet press section, a pre-drying section, followed by a surface coating (impregnation), post-drying, a soft calendaring and finally a reeling area of the produced paper (Figure 6).

- **Wet end section.** Two round shape formers distribute the suspension across the machine width onto the wire. Two layers are produced: A thinner layer of refined cotton (20 g/m²) and a second one thicker (60 g/m²) which also contains the watermark. This watermark is produced by variation of thickness of the mattress. Water is then pressed out of the web by

mechanical means in the **press section**, and residual water is evaporated by heat in the **pre-drying section** (convective drying at 120°C).

- **Coating section.** Banknote substrate is plunged into a bath of polyvinyl alcohol heated around 60°C. This polyvinyl alcohol is a secret mixture of long-chain and short-chain PVOH. It is followed by the **Post-drying section** where the wet coating is dried. The drying section is composed of hot cylinders section and air driers section. The air dryer section is divided into 3 groups of 6 m each. A temperature between 80 and 90°C is set in the two first sections and the third one is classically not alimented but keeps a temperature of approximately 66°C. Exact dryer temperatures, but also time in drying section (machine speed) and pump speed are regulated as a function of final paper shrinkage and moisture. Indeed, humidity of the final paper has to be close to 5.8%. If it decreases below 5.5%, paper breaking during the process could happen.
- Finally, the paper goes through a **soft calendaring** section to smooth the paper surface and in **reeling section** where the paper web is reeled at the reeler at full width.

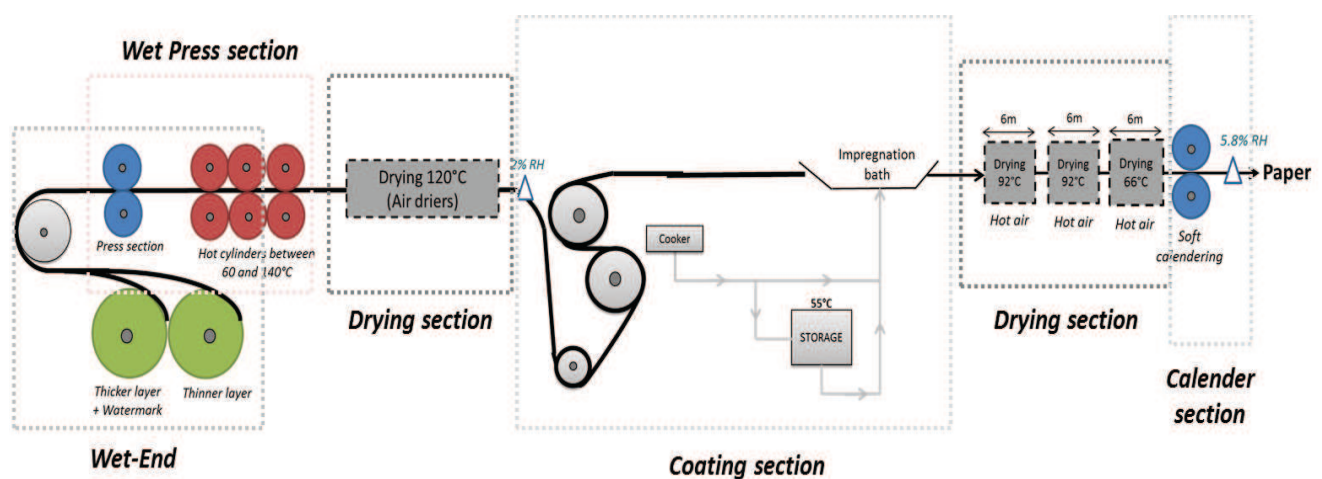


Figure 6: Overview of an example of banknote paper machine

1.3. Banknotes lifecycle: challenges and expectations

Because of their daily manipulations, banknotes deteriorate and decrease in quality during their lifespan. In 2009, 33 billion banknotes were sorted within the Eurosystem and 5.4 billion were destroyed because they did not meet the quality requirements. Consequently, the lifetime of banknotes is reduced between 3 years and a few months, depending on the value and country habits, and the economic loss is huge.

On average, every note in circulation returns every six months to the counters of the national central banks. The average lifetime of a banknote is three years, but it varies a lot depending on the value: about 1 year and a half for 10€ banknote and up to more than thirty years for the 500€. Banknotes from 100 € to 500 € are most often used for hoarding purposes, they are better preserved and their lifetime is longer. In addition to the goal of staying one step ahead of counterfeiters, the introduction of the new "Europe" series banknotes should allow extending their lifetime.

1.3.1. Banknote lifecycle

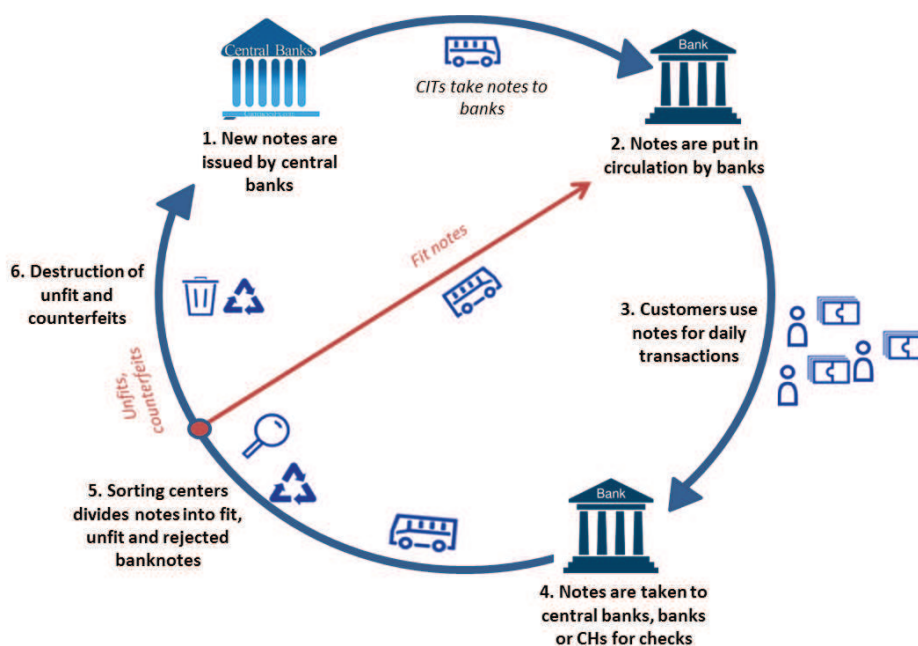


Figure 7: Banknote lifecycle in Eurosystem. Adapted from (Deinhammer and Ladi 2017)

Classical path of a banknote from production to destruction is described in Figure 7.

1. Banknotes are emerging in one of the printing mill in the euro area. They are transported to central banks where they are stored before being put in circulation.
2. Banks, through the funds carriers, collect at the counters of the Bank of France the notes they have previously ordered.

3. These notes are then made available to the public at bank counters or via ATMs. Notes, once in the hands of the public, are used daily to make various payments to merchants.
4. Merchants deposit the banknotes received at the Bank. Banks return the notes to central banks, which then send them to sorting centers.
5. In sorting centers banknotes are submitted to various sensors (magnetic sensors, inks scan, features detection level 1, 2 and 3, fluorescent detector, light source transmission, ...) measuring more than 600 parameters on each banknote. Depending on quality requirements, the tested banknote will be fit (put back in circulation) or unfit (destroyed). It exists a third possibility if the machine does not recognize the paper as a banknote (banknote is folded, two banknotes are superimposed, the banknote is not in the good place, there is a problem of orientation, the banknote is too close of the following, the machine doesn't recognize the banknote number/value,...), then it is rejected. Rejected banknotes are then manually observed and put again in the machine. Most of the time, the banknote is accepted the second time. If the banknote is still not accepted, it will be manually treated by people to identify the problem.

In France, 6 billion banknotes are treated by year, in 58 centers. Paris is the biggest center with 1 billion banknote/year. Machines can treat between 20 and 23 banknotes/s. Almost 11% of treated banknotes are detected unfit. As an example, a 5 euros banknote is usually destructed at the third passage in the sorting machine, and a 10 euros at the fifth. Unfit banknotes are replaced by new ones, which are given when orders are made by the banks. 5 euros, 10 and 20 euros are the most remaking banknotes, with an annual volume between 1.2 and 2 billion.

1.3.2. Crumpling and dog-ears defects

Soiled, limped, crumpled, folded, defaced (any form of writing or scribbling on a banknote), ink wear banknotes (due to chemical reactions, harsh friction or washing) are automatically removed from circulation. Other defects are also prohibitive, such as tears, holes (Any holes bigger than 5 mm found on a note would deem unfit for circulation), repairs (with tape or glue), burns or miss of security features.

The first reason of unaccepted banknotes is soil (due to human sebum or dirt particles), responsible for 88.6% of unfit banknotes, followed by dog-ears defect, responsible for 10.2% of unfit banknotes. Eurosystem has defined minimum thresholds to define limits for any of the defect categories but, at is it the case for crumpling, they are sometimes only based on visual criteria. Unlike soil or dog-ears defects, there are indeed no data existing to quantify the effect of crumpling, as crumpling cannot be detected by any sorting machine due to the lack of crumpling sensors or high speed measurement techniques. Next parts will focus on dog-ears and crumpling damage (Figure 8) as they are the main topics of this PhD work.

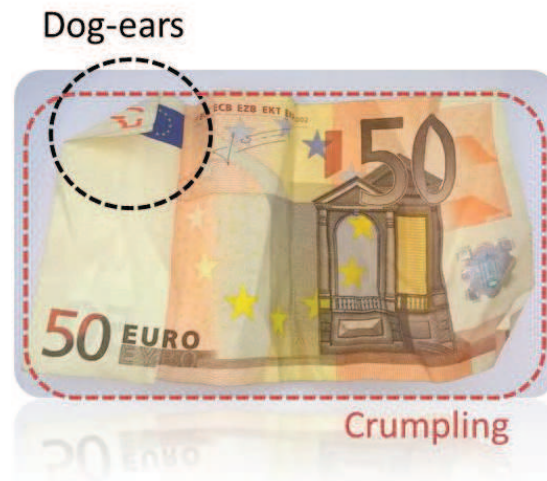


Figure 8: Crumpling and Dog-ears defects on banknotes

Crumpling defect. The situation concerning crumpled banknotes is complex. First, no sensor exists in sorting machines to detect the crumpling, and crumpled banknotes can be put back in circulation even if they do not meet the visual quality requirements. Crumpling can also increase banknote local thickness and can induce conditioning troubles. Indeed, at the exit of sorting machine, fit banknotes are packaged. If the thickness of banknotes increases drastically due to crumpling, the number of banknotes in a single packed stack is reduced. This creates further difficulties and can have an effect on both the speed of sorting and the cost of sorting banknotes. Furthermore, the package of several crumpled papers together can lead to a “spring effect” and increase the difficulty in conditioning banknotes.

Crumpled banknote can also create additional troubles during the sorting process as security features might not be detected. This issue leads to rejected banknotes. These rejected banknotes present an extra effort because they need to undergo more labor-intensive manual sorting. Finally, crumpled banknotes in circulation are weakened and wrinkled areas can be easily teared and excessive folding and crumpling results in a breakdown of the structure of banknotes and results in limpness banknotes.

The purpose of new banknote series in Europe was both the extension of the lifetime and the improvement of its security features. For the first expectation, an additional varnish has been introduced to 5 euros and 10 euros banknotes. This varnish has the particularity to limit soiling, but has in return contributed to accentuate the crumpling.

Today, there is a two-faced challenge associated to crumpled banknotes: (i) the development of quantitative methods to characterize the crumpling (at lab scale but also automated detection), and (ii) the research of technologies to reduce the occurrence of crumples in banknotes. With regards to characterization methods, there is almost no method described publicly and the few confidential internal methods are executed as part of the physical & chemical resistance testing for

banknotes and focus mainly on the stability of security features rather than on the detection of crumbles.

Dog-ears defect. The presence of folds weakens the banknote substrate and it is the second defect responsible for banknote elimination after soiling. “Dog-ears” defect corresponds to flapped corners appearing during banknote manipulation. Unlike crumpling defect, dog-ears defect can be detected by sorting machine using thickness captors and profilometry. These dog-ears can be responsible of direct damages; the banknotes will so be “unfit” and removed from the circulation, or can create treatment issues in sorting centers. The first reason is the increase of thickness in the area of folded corner, which complicates automatic transportation of banknotes in sorting machines and can in particular cause paper jams. Otherwise, the dog ears corners of a paper product can be separated from the paper product and the banknote will then be unfit. Dog-ears can also weaken the barrier layer of banknotes and allow penetration of soil. Finally, it can also cause storage issues as the banknotes are stored in boxes with specific heights in order to store a specific number of banknotes. Other problems can also prevent proper operation of automatic proceedings: a banknote can be caught in another one, or the fold can cover security features.

A banknote is considered as “unfit” due to dog-ears defect if there ar at least three dog-ears, if there are one dog-ears with dimension of the fold line $> 26\text{mm}$, if the cumulative area of the dog ears is superior to 200 mm^2 , if one dog-ear alone has a dog-ears area superior to 130 mm^2 .

2. Crumpling and dog-ears defects: solutions and expectations

Sometimes perceived as a defect, sometimes solutions of engineering problems in aerospace, architecture or textile (Gioia et al. 2012), folds and wrinkles add a tactile dimension and 3D perception for the better or for the worse. The first discipline which has raised the question of folding/unfolding concept is the origami art: born in the 6th century, this discipline has been deeply studied in the field of paper science since 1960-1970 (Gjerde 2008). Origami design is governed by mathematical laws, which if better understood, could be applied in engineering for a better understanding of folding mechanisms. Indeed, the characterization of paper crumpling and/or folding has for a long time been empirical and theoretical models have been developed mostly during the last decades (Barbier et al. 2006). Nevertheless, mechanical information and mechanisms during paper folding/unfolding (Pradier et al. 2016) and crumpling are still lacking.

Crumpling and folding of a paper are at first sight very different : the first one is random and stochastic while the second one is regular and deterministic (Deboeuf et al. 2013). Nevertheless, these two phenomena can easily be connected as they come from similar mechanisms. In particular, the stiffness that builds up in the two processes has the same nature. It is indeed well known that the force necessary to fold more than six or seven times a sheet of paper is so huge that it makes it impossible. In parallel, if trying once to crumple a paper in ball shape, the final material will be composed by 80% of air.

Paper is a particularly complex material due to its heterogeneous fibrous structure. Furthermore, in everyday life, a paper can be manually folded in large possibilities of direction and intensity. Consequently, the folding and crumpling processes are difficult to control and repeat and that's a reason why only few studies have tried to explain the mechanisms involved. Banknote are particularly submitted to damaging treatments: they can be folded/crumpled due to daily exchanges or storage (in a pocket, in a wallet,...). Therefore, increase banknote fold (in particular, the folds at the corner called dog-ears) and crumpling resistance are challenging and bring out lot of questioning: Why does a paper fold when subjected to high bending strain? From what phenomenon a permanent fold or crumpling pattern happens? What paper properties need to be modified in order to produce fold- and crumple-resistant paper? This study will explain in the first part what is happening during paper folding and crumpling, how these phenomena are characterized in the literature and what are the existing solutions to prevent these defects.

2.1. What is happening during paper folding and crumpling

It is well known that a permanent fold may form if the deformations induced by the fold exceed the elastic limit of the material (Narain et al. 2013) (Gagliardi and Gruntfest 1950). It results in plastic deformation which can be analysed at the macroscopic scale (Pradier et al. 2016) and microscopic scale (Xia et al. 2002). At the macroscopic scale, we observe a decrease of thickness and stiffness along the axis of the fold (Francis et al. 2013) and the fold can be modeled as a hinge-like behavior where the paper is assimilated to a thin plate and the fold to a mechanical joint (Pradier et al.). If we look at microscopic dimensions, when a fold is created in a thin material such as a paper, the fibers localized at the fold are placed in a position of strain. The fibers on the outside of the bend are subjected to a tensile stress and are elongated, while those inside the bend are under compression. Somewhere in the middle of the bend region, in the neutral plane of deformation, the fibers are neither stretched nor compressed. The stress is distributed between the H bonds of hydroxyl groups, van der Waals forces and primary valence bonds of the fibers. The bonds take up the stress and strain, and some bonds break. The fibers do not recover completely from their extension, and hence an irreversible fold is formed (Sharma 2011) and the paper locally loses its stiffness (Figure 9).

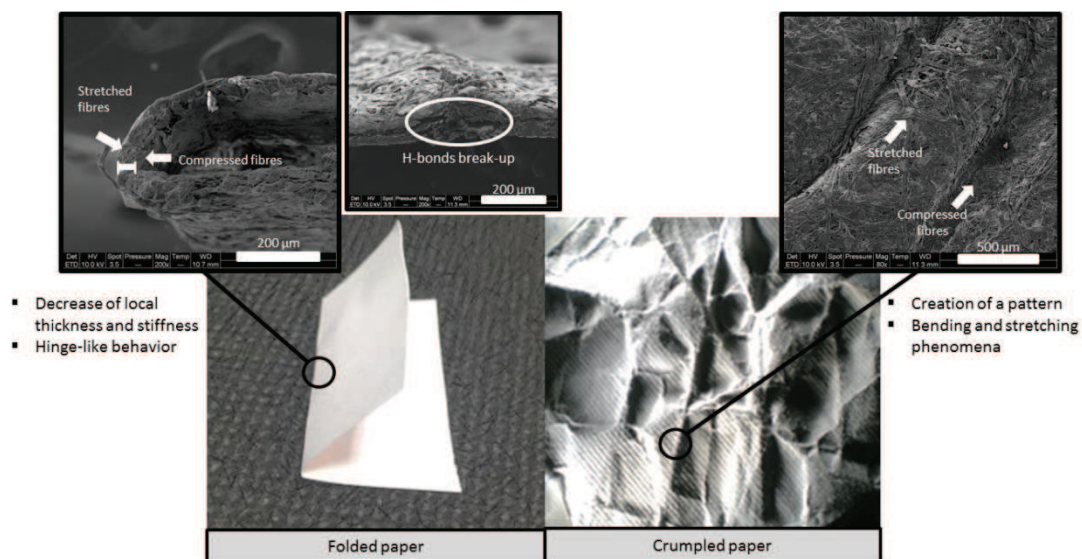


Figure 9: Folded and crumpled papers

For crumpling, similar phenomena occur but have the particularity of creating a pattern. The crumpling process induces a network of wrinkles that fold the initial paper into a smaller structure. From the elasticity theory, we know that thin elastic plates have two modes of deformation: bending, which involves curving the plates, and stretching, which changes the distances on the plate. Bending is much less expensive energetically than stretching, and is consequently the first mechanism of deformation during the paper handling. Here again, when the deformation exceeds the elastic zone,

the expensive stretching energy will appear under the form of permanent wrinkle pattern (Sultan and Boudaoud 2006). The process is irreversible as the energy is accumulated in small regions leading to localized plastic deformation, and enhanced because of the paper slenderness. Various aspects of the crumpling mechanisms are still elusive or controversial, and a general physical understanding is lacking. The difficulties arise from the fact that crumpling involves the formation of a complex network of localized folds where plastic deformations take place in addition to self-avoiding interactions. The self-avoiding interaction can be described as inter-particle repulsions which prevent the paper to collapse upon itself or to fold through itself to access unphysical configurations.

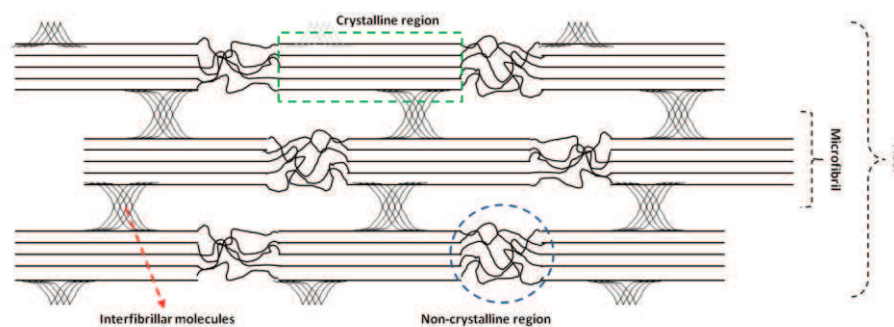


Figure 10: Structure of cellulose, extracted from (Börjesson and Westman 2015)

A fiber is composed of both crystalline areas, with chain molecules packed in regular formation, and amorphous areas, with chains in disordered formation (Figure 10). Cellulose fiber structure will be deeply explained in the next part (3.1.). In crystalline regions, the symmetry and regularity of the chain allow accentuated bonding between OH-groups while randomness organization in amorphous regions gives rise to weaker attraction between OH groups of cellulose chains. In the crystalline regions, the β -glucose chains are fully extended and are responsible for tenacity, high modulus of elasticity and resistance towards bending. On the other hand, the amorphous regions, thanks to the freedom of movement of the chains, are more responsible for the flexibility and extensibility of the material.

From these explanations, it appears that crystallinity and stiffness (Young's modulus) are key parameters to increase paper fold and crumpling resistance.

2.2. Dog-ears and crumpling modeling: characterization and key parameters

Crumpling and folding are connected phenomena and often put in parallel in literature study. Indeed, crumpling can be viewed as arising from successive folding events and predictions from simple folding models can capture many of the complicated features of the crumpling process (Deboeuf et al. 2013; Francis et al. 2013).

However, issues and challenges regarding these two phenomena are not the same. The folding process is easily reproducible and characterization focused on (i) modelling of the force

needed to create the fold (Deboeuf et al. 2013; Pradier et al. 2016) or (ii) calculation of residual strength after folding (Guyot et al. 1992). Other studies propose to calculate a “hinge index”, or a torque, to model two faces in rotation around a straight fold (Francis et al. 2013; Pradier et al. 2016). Regarding crumpling, finding a method allowing a repeatable and representative crumple of a sheet is already complicate. Some studies just create a ball of paper manually (Habibi et al. 2017). Most of the time, a compaction method is used: the paper is rolled and then compressed by the action of a piston. This last method is close to the one used by National Bureau of Standard for artificial crumpling of banknotes. Then, characterization of crumpling has raised various modelling from physicists (Narain et al. 2013). Most of the time, the characterization consists in the description of the crumpled pattern thanks to profilometry¹.

Following pages try to synthesize the key parameters for an understanding of folding and crumpling processes.

2.2.1. Paper folding

Paper dimensions. Folding a paper in half is independent of the paper dimensions (except thickness). An easy example is that the number of times one can fold a sheet of paper is only six or seven, and this is completely independent of the initial size of the sheet.

Bending rigidity and paper Young’s modulus. The force needed to create a fold is a clear indication of the paper fold resistance. It has been proved (Deboeuf et al. 2013) that the elementary force to create a unique fold F_0 (N) is proportional to $\frac{B}{h}$ (Eq 1), with B the bending rigidity (mN.m) and h the paper thickness (m). Furthermore, the bending rigidity is also directly correlated with the paper Young’s modulus and Poisson’s ratio (Eq 2). That can explain why, in a lot of studies, the question of foldable/unfoldable properties is directly linked to the need of stiffness (Gioia et al. 2012).

Paper thickness. From the previous explanations, it appears that the thinner the paper is, the easiest it is to create a fold (decrease of F_0).

Number of folds. When the sheet is folded n times repeatedly, there is a hierarchical creation of folds and the energy balance leads to (Eq3). Thus the force grows exponentially with the number of folds.

$$F_0 \sim \frac{B}{h}$$

Eq 1

F_0 : Elementary force (mN)
B: Bending rigidity (mN.m)

h: paper thickness (m)

$$B = \frac{E h^3}{12 (1 - \nu^2)}$$

Eq 2

E: Paper Young’s modulus
 ν : Paper Poisson ratio

¹ More details in crumpling methods are proposed in **chapter 3.4**.

$$F(n) \sim \frac{2^{3n} B}{2^n h} \sim F_0 \cdot 2^{2n}$$

Eq 3

n: number of time the paper is folded
 F(n): Force necessary to create n folds repeatedly (at the same place)

Degree of compaction. Repeated the folding in half is not the only possible way to fold. Different degrees of compaction (Figure 11) lead to different final material geometries. They also lead to different mechanical models. In the case of this manuscript, dog-ears of banknote can be assimilated to 1D compaction model. Consequently, higher compaction models will not be fully detailed here. To simplify, it exists a compaction ratio defined by the ratio between the initial and final size of the sheet. Therefore, this compaction ratio depends on the precise geometry and dimensionality of the compaction process.

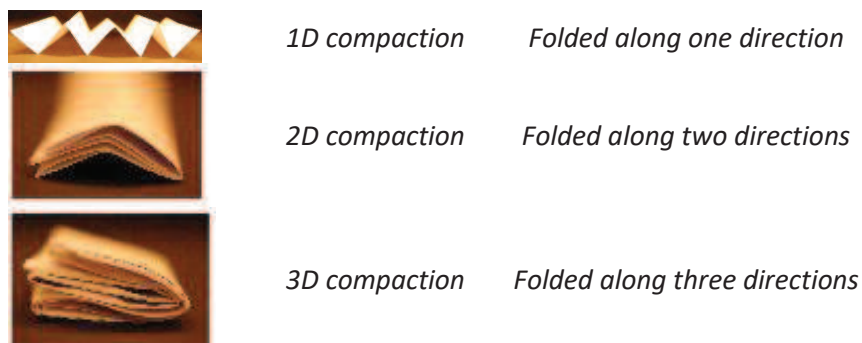
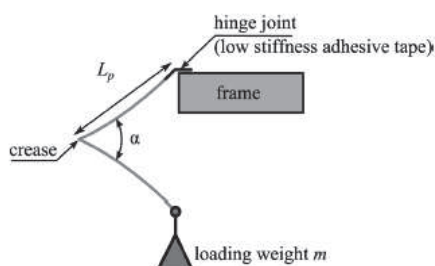


Figure 11: Different degrees of compaction for a paper, adapted from (Deboeuf et al. 2013)

Hinge Index. After the measurement of the force needed to create a fold, another metric characterization has been proposed to analyze the paper behavior when it is folded, called the “Hinge index” (Francis et al. 2013; Pradier et al. 2016). This method consists in folding a paper in half, attaching a weight at the end of one part and measuring the resulting angle α (Table 1). Kinetically, folds act like a torsional spring, storing energy as the sheet rotates relative along the axis of the fold (Gardiner, 2011). This method consists in the calculation of the torque, or the ability of the material to rotate around an axis (the fold) following the equation (Eq 4):

Table 1: Hinge index method and calculation, extracted from (Pradier et al. 2016)



$$t = m \cdot g \cdot L_p \cdot \cos(\alpha/2)$$

Eq 4

t = torque
 m = loaded weight
 g = gravitational force
 Lp = the distance between the fold and the extremity of the paper
 α = opening angle

It has been proved in this study that the torque is proportional to the fold length: the highest is the fold length, the highest is the torque.

Orientation of the fibers. In a classical paper presenting a machine direction and cross direction, the paper stiffness strongly depends on paper orientation. However, the case of the fold is different due to its complex but localized behavior: the involved physical phenomena (large strains, damage, etc.) occur at small scale (the paper thickness) and depends on the local paper constitution close to the fold. The fold behavior is driven by the cross section along the fold line, with a complex process at this scale that may allow local fiber rotation (Pradier et al). Consequently, the fraction of the crossed fibers is the first order influent parameter, leading to a similar behavior independently of the fold direction. Fold orientation appears to have only a second-order influence.

2.2.2. Paper crumpling

The process of crumpling results in the formation of a highly complex network of folds and facets, and its topology cannot be described in a straightforward manner (Hanaor et al. 2017). Many authors have tried to characterize paper crumpling properties analytically (Lobkovsky and Witten 1997; Ben Amar and Pomeau 1997), numerically (Vliegenthart and Gompper 2006), and experimentally (Lobkovsky and Witten 1997; Blair and Kudrolli 2005; Sultan and Boudaoud 2006; Boué et al. 2006). In particular, studies have tried to describe the ridge network of crumpled paper (Blair and Kudrolli 2005; Andresen et al. 2007).

Characterization of crumpling is always source of debate and uncertainties. The dependence of crumpling final pattern with the initial paper material is also in debate. Some references suggest that the material properties have only a minor effect on crumpling (Balankin et al. 2007). For others, crumpling structure depends on elasto-plastic properties of the material (Tallinen et al. 2009).

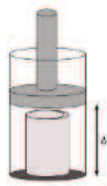
Elasto-plastic properties of the sheet. As it is well known from unfolding a crumpled paper ball, plasticity causes irreversible small-curvature wrinkles. For an ideal elastic sheet, such wrinkles will disappear when higher compactions are achieved. For elasto-plastic materials this is not the case, which causes shrinkage of the effective area of the sheet. Paper is an elasto plastic material and it is also a thin material. These two properties combined tend to localize stretching deformations in small plastic regions along creases.

Self-avoidance. The “self-avoidance” property is the primary source of resistance against the crumpling force. This property consists in the tendency of wrinkles formed to turn away from one another. In other words, it is the physical constraints which prevent the path folding back upon itself. Under moderate compression, the force–compression relationships of self-avoiding sheets are found to obey universal power-law behaviors (Vliegenthart and Gompper 2006).

Applied force to create a crumpling pattern. In the case of a paper crumpled by compaction (Table 2), the applied force to crumple a paper shows a power law dependence on the size of the crumpled object (Eq 3), with an exponent β which depends on the material properties (among them, the Young’s modulus), the compaction protocol and the self-avoidance phenomenon (Deboeuf et al.

2013; Habibi et al. 2017). Despite the various experimental, theoretical and statistical studies, these different phenomena remain difficult to disentangle.

Table 2: Modeling of crumpling extracted from (Deboeuf et al. 2013)



$$F(\Delta) = \alpha \left(\frac{\Delta}{D} \right)^{\beta} = \alpha \phi^{\beta} \quad \text{Eq 3}$$

F: force to crumple the paper

D : paper size

Δ: gap between piston and the bottom of the device

α: characteristic force scale

β: exponent of the power law

φ: compaction ratio

Repeatability. There are two main contributions to the crumpling force: the mechanical response of the crumpled network and the force needed for the creation of the wrinkle pattern (Habibi et al. 2017). Consequently, the force needed to crumple a paper for the first time is larger than for a paper that has been crumpled before. For a banknote substrate which is daily manipulated, the main contribution of crumpling is due to the mechanical response of the crumpled network since most of the crease pattern has already been created.

Fold-length distribution. Many studies have proposed models to determined fold-length distributions. It has been found that sheets obey an universal power-law behavior (Vliegthart and Gommer 2006). The fold-length distribution for crumpled sheets is determined and it is found to be well described by a log-normal distribution. This chapter will not enter into details but information can be found in the literature (Vliegthart and Gommer 2006; Andresen et al. 2007; Deboeuf et al. 2013; Narain et al. 2013; Habibi et al. 2017).

2.3. Solutions in paper industry to limit dog ears and crumpling

The first industry which has been concerned by the decrease of folds and crumpling is the textile industry. Solutions to limit fold and crumpling have consequently widely been studied in textile industry. However, it is much more limited in paper industry.

Solutions in textile industry. In textile industry, the ability to resist to crumpling and to recover from bending deformations is determined by many factors, as the stress-strain properties of the fibers, the geometric construction and arrangements of its yarns, and the presence or absence of finishing agents on or within the fibers (Gagliardi and Gruntfest 1950). Furthermore, for resisting a fold deformation, textile industries are looking for fibers with high extensibility, high elastic fiber recovery and high modulus or fiber stiffness. The stiffer fibers not only will better resist to the action of bending stresses, but also in the formation of a close fold in the fabrics such fibers can more readily adjust themselves to a position of a minimum strain than can limp fibers. One primary reason why fabrics made of rayon and cotton fibers crease or wrinkle easily is the poor elastic recovery of these fibers (Sharma 2011). In order to increase the elastic recovery of fibers, chemical modification can be performed. Chemical cross-linking with anti-creasing (Frick et al. 1960; Abidi et al. 2007; Lam et al. 2010) is the most popular method for improving the wrinkle resistance of tissue. Satisfactory dimensional stability and crease resistance can be achieved by cross-linking cellulose fibers, whose OH groups react with the cross linker. Today, the most promising formaldehyde-free cross-linking agent for cotton cellulose is 1,2,3,4-butanetetracarboxylic acid (BTCA) (Lam et al. 2010).

Solutions in paper industry. During the last decades, some studies appear in order to characterize and quantify the paper foldability or crumpling, but really few have proposed solutions to reduce these defects. One of the first sectors concerned is security papers. In banknote industry, some solutions have already been proposed to reduce dog-ears defect. The first alternative has proposed to use special paper structure like round corners (Cassidy and Doublet 1993). This proposition had the advantage to reduce paper jam in automatic transportation of banknotes, but completely changes banknote design and requires adaptations in sorting machines. A second alternative which has been patented (Pearson and Howland 2008) was corners reinforcement by watermarks. However, such a localized reinforcement of the corner regions by forming watermarks requires a complex adaptation of the paper manufacturing process. Another patented solution has been the impregnation of the substrate with an aqueous solution containing hydroxylated polymeric binder (Sarrazin 2013). This method is not selective and highly demanding in polymer with adaptation of paper machine in both impregnation and drying sections. Consequently, no satisfying method exists for now.

3. From cellulose to nanocellulose

The society is in constant demand for state-of-the art performance in all sectors, including the paper industry. Consumers and industrials are looking for (i) additional properties for tomorrow's products (for example intelligent or active papers) or (ii) optimization of today's product (increased lifetime, resistance,...). To achieve such properties which are unusual for cellulosic materials such as hydrophobicity, high electrical conductivity, antimicrobial, grease-resistance, high mechanical strength, specific raw-materials and processes are used. These new properties often result from physical or chemical modification of the paper bulk or surface. Recently, a new biobased material has become industrially available and sounds very promising for achieving high-performance materials in a large field of applications including papermaking (in particular, specialty papers): nanocellulose.

3.1. Properties of cellulose

Nature is the largest source of high-performance biocomposites, consisting in a matrix reinforced by fibrous polymers (Dufresne 2017). In 1839, Anselme Payen has discovered one of these reinforcing elements from plants: cellulose, which confers its mechanical properties to higher plant cells. For the last 180 years, the potential of cellulose has been widely developed. With its 200 Gt/year production (mainly thanks to vegetal photosynthesis), cellulose is the most abundant polymer on Earth and only less than 5% are extracted for applications (Klemm et al. 2005). A first look at this polymer reveals properties particularly in accordance with environmental challenge from our time such as abundancy, renewability and sustainability. With a closer look on its structure, a hierarchical skeleton appears and gives a glimpse on its flexibility and high strength performance. In nature, this strength plays an essential role in maintaining the structure of plant cell walls. In daily life, cellulose fibers (Demirbas 2007) have been used for a wide range of applications (paper, textile, food additives, medicines, biofuels...) (Habibi et al. 2010) but paper and cardboard industries are the largest consumers (Dufresne 2017).

Cellulose is a linear polysaccharide of glucose ($C_6H_{12}O_6$), in the form of β -1,4-linked anhydro-D-glucose. This polymer can be found in a large variety of sources such as wood (hardwood or softwood), seed fibers (such a cotton), bast fibers (flax, hemp, jute, ramie,...) but also algae, fungi, invertebrated and bacteria (Varshney and Naithani 2011). It is however mainly found in the protective cell walls of plants, embedded in a hemicellulose and lignin matrix. The cellulose content can vary depending on the source, from 40% (coir, cereal straw) to 90% (cotton). Each cellulose monomer unit, also named "anhydroglucose unit", has three hydroxyl groups available for reactions. This characteristic opens the doors of wide possibilities for functionalization with tuneable properties. Furthermore, these hydroxyl groups are also responsible for the strong intra- and inter-molecular hydrogen bonding (Figure 12). During biosynthesis of cellulose, van der Waals connections between the chains layers, H-bonding between hydroxyl groups, and covalently linked oxygen of adjacent molecules promote parallel stacking of multiple cellulose chains that can be call "microfibrils". The two networks formed by the van der Waals forces and hydrogen bonding are also

responsible for rearrangement of cellulosic chains into parallel and ordered regions called “crystals”, while the disordered regions are called “amorphous”. It exists four polymorphs of cellulose crystal, called cellulose I, II, III and IV, and cellulose I is the most abundant in nature (O’Sullivan 1997). The microfibrils are then arranged in different orientations and are embedded in a polymeric network of hemicelluloses, pectins and lignins (Somerville et al. 2004) corresponding to the biocomposite matrix. The arrangement of these microfibrils into stacked microfibrils composed the cell walls of vegetable fiber.

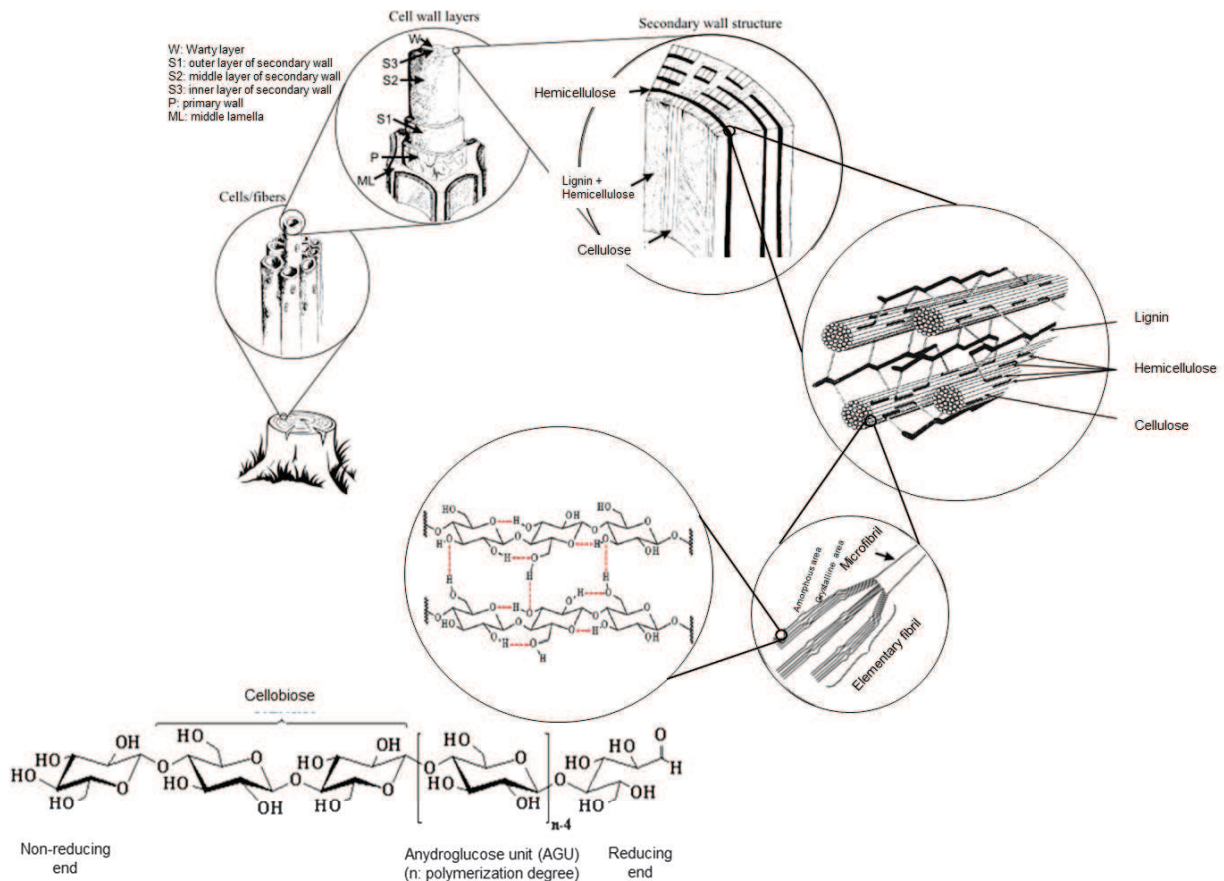


Figure 12: Hierarchical structure of wood, adapted from (Pérez et al. 2002; Nechyporchuk et al. 2014)

The degree of crystallinity of native cellulose is between 54 and 88% (Moon et al. 2011), depending on the source, and the resulting material is highly cohesive. The degree of polymerization of cellulose is on average 10 000, also depending on the source, and reaches nearly 15 000 for native cellulose in cotton (Sjostrom 1981). These degrees of polymerization are based on the anhydroglucose unit (AGU). However, the repeating unit of the polymer chain is called “cellobiose”: adjacent monomer units are arranged so that glucosidic oxygens point in opposite directions and form the cellobiose. Cellobiose units ($C_{12}H_{22}O_{11}$), whose molecular weight is 342 g/mol, are covalently linked in an extended, insoluble, straight linear chain. The two end-groups of cellulose are not chemically equivalent with a non-reducing end and a reducing end (aldehyde).

Physical properties of natural fibers, advantages and disadvantages in biocomposites

Physical properties of natural fibers are influenced by many factors, particularly the chemical composition and location in plants (Dufresne 2017). In most natural fibers the microfibrils orient themselves at an angle to the fiber axis (“microfibril angle”). In general, the fiber strength increases with increasing cellulose content and decreasing this spiral angle. This means that the most efficient fibers are those with high cellulose content and low microfibril angle. Maturity, separating process, microscopic and molecular defects, type of soil and weather conditions under which they were grown have also an impact. Physical properties of some natural fibers are reported (Table 3). The density is usually around 1.5 g/cm³ and the mechanical properties are interesting even if they often remain below synthetic fibers. Growing interest of the use of natural fibers as reinforcing elements comes from their low density, high mechanical properties, low cost, renewability, biodegradability, availability in a variety of forms throughout the world, flexibility, non-abrasive nature, non-toxicity, easiness to handle, and high ability for surface modification. However, their hydrophilic character leads to a poor adhesion and dispersion in non-polar matrix, high moisture absorption and limited thermal stability, leading to low permissible temperatures of processing and use.

Table 3: Characteristic values for the density, diameter and mechanical properties of vegetable and synthetic fibers, table adapted from (Dufresne 2017)

Fiber	Density (g/cm ³)	Young's modulus (GPa)	Tensile strength (MPa)	Elongation at break(%)
Cotton	1.5 – 1.6	5.5 – 12.8	287 - 800	7 - 8
Jute	1.3-1.5	13 – 26.5	393-800	1.2-1.5
Flax	1.5	27.6	690	2.7-3.2
Hemp	1.47	70	690	1.6
Ramie	1.55	61.4-128	400-938	1.2-3.8
Sisal	1.45	9.4-22	468-700	2-7
Carbon	1.78	240-425	3400-4800	1.4-1.8
E-glass	2.55	73	3400	2.5
Kevlar	1.44	60	3000	2.5 – 3.7

From cellulose to nanocellulose.

The hierarchical structure of natural fibers can be deconstructed using a top-down deconstruction strategy in order to obtain materials with amplified performances. This strategy consists in extracting the microfibrils sub-elements: long and flexible cellulose nanofibrils (CNFs) and smaller and rigid cellulose nanocrystals (CNCs). These two families of materials result from different processes and have their own morphologies, properties and applications (Figure 13).

The term “nano” refers to materials having at least one dimension below 100 nm. Cellulose nanofibrils are obtained after submitting cellulose fibers to high shearing forces which come to peel the fibers. This process results in fibrils which kept both their amorphous and crystalline structures, with diameters ranging from 20 to 60 nm and micrometric lengths (Turbak et al. 1983; Siró and Plackett 2010). Due to their high aspect ratio and the flexibility resulting from the amorphous part, this material is often imaged as “spaghetti-like” form, with the diameter of a hair that would have

been cut by 1000 in the width direction. On the other hand, cellulose nanocrystals are chemically obtained after dissolving the amorphous regions of the cellulosic fiber. In this case remains only the individualized crystals, with diameters ranging from 5 to 30 nm and length between 150 to 500 nm (Habibi et al. 2010). In this case, the image can be that of a grain of rice, small and rigid, with a diameter divided by 10^6 .

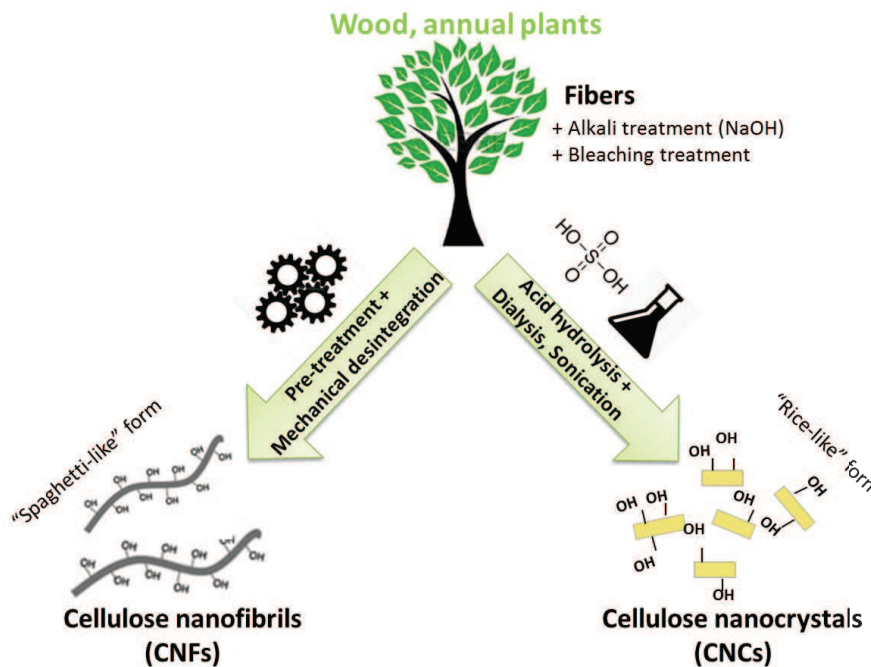


Figure 13: General procedure to obtain nanocellulose

3.2. Cellulose nanofibrils

Cellulose nanofibrils were discovered by Turbak et al. in 1983 (Turbak et al. 1983). This material is now widely available on the market as a commercial product and has more and more interest in industrial applications, as shown by patent studies (Charreau et al. 2013) and book chapters and reviews (Siró and Plackett 2010; Bardet and Bras 2014; Nechyporchuk et al. 2014; Dufresne 2017). However, their up-scale production is the result of decades of researches for the isolation and characterization of this complex material.

What is a cellulose nanofibril suspension?

Cellulose nanofibrils (Figure 14) are a material consisting of both amorphous and crystalline domains. Their Morphology, aspect ratio and degree of crystallinity are determined by two factors: the cellulose source and the extraction method, but their classical dimensions range between 20 to 60 nm for the diameter and are micrometric in length (Turbak et al. 1983; Siró and Plackett 2010). It is not a 100% cellulosic material, as it still remains bonded agents such as hemicelluloses. Their high aspect ratio, high specific surface area, and their nanodimensions lead to an entangled nanoscale network maintained by numerous hydrogen bonds. As their production is mainly performed in a

water medium, cellulose nanofibril suspensions are under the form of a viscous gel even at low solid contents, with shear-thinning and thixotropic behavior.

Cellulose nanofibrils have a maximum tensile strength of 130 MPa and a maximum strain to failure of 22% (Dufresne, 2017) and can reach a Young's modulus of more than 100 GPa (Moon et al. 2011). These impressive mechanical properties make them comparable with Kevlar. Due to these extraordinary properties, nanocelulose is used for a variety of applications in several industries: automotive and aerospace, packaging, electronics, pharmaceutical and medical devices, paper and packaging and many more as detailed in the following part.

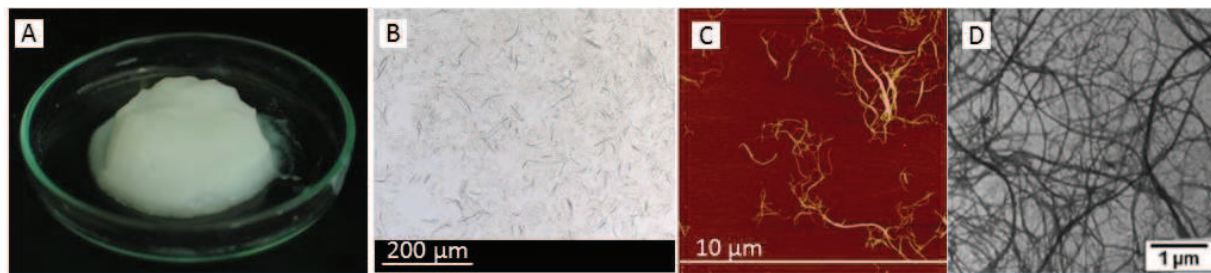


Figure 14: Cellulose nanofibril suspension A) by photography B) by optical microscopy C) by AFM and D) by TEM. The TEM image was extracted from (Dufresne et al. 1997)

How can we produce cellulose nanofibrils?

Cellulose nanofibrils are basically extracted by inducing a high shear mechanical treatment to the fiber. In previous decades, the challenge associated with the isolation of cellulose nanofibrils was the high energy demand required by the mechanical disintegration process. Since 2007, the application of pre-treatments has reduced the energy from about 30,000 kWh/t (Siró et al. 2011; Spence et al. 2011) to less than 2,000 kWh/t (Saito et al. 2007; Tejado et al. 2012) and has unlocked large-scale production.

These pre-treatments can be mechanical (refining), biological (enzymes), chemical (grafting of repulsive charges) or a combination of them. All these treatments lead to irreversible changes in the fibers, increasing their bonding potential by modifying their morphology and size. They also present the particularity to weaken the structure and ease the following mechanical disintegration of the fibers. In the case of chemical pre-treatments, anionic (Tempo oxidation, sulfonation, carboxylation, carboxymethylation) or cationic charges can be grafted as described in Figure 15. A lot of other pre-treatments have been developed or are currently in progress but will not be detailed, such as periodate oxidation, phosphorylation, or solubilizing in deep eutectic solvent (Dufresne 2017). This work will focus on two famous pre-treatments which are (i) the enzymatic hydrolysis and (ii) the tempo oxidation of the fibers.

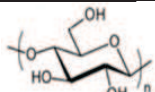
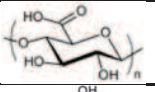
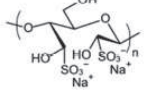
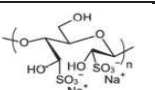
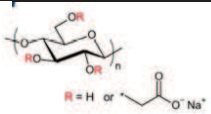
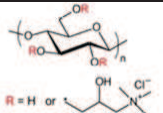
AGU	Charge	Pre-treatment name	Reference	Grafted molecule	Grafting rate	Grafted AGU
	Anionic	TEMPO-mediated carboxylation	(Saito et al. 2007)	Carboxylic groups	1.7 mmol/g	
	Anionic	Periodate-chlorate carboxylation	(Liimatainen et al. 2012)	Carboxylic groups	0.38 to 1.75 mmol/g	
	Anionic	Sulfonation	(Zhang et al. 2008)	Sulfonate groups	0,18-0,51 mmol/g	
	Anionic	Carboxymethylation	(Naderi et al. 2014)	Carboxylic groups	590 µeq/g (DS = 0.1)	
	Cationic	Cationic	(Olszewska et al. 2011)	EPTMAC*	DS = 0.015-0.5	

Figure 15: Classic chemical pre-treatments for the production of cellulose nanofibrils

In this work, two pre-treatments have been considered: the enzymatic hydrolysis and the TEMPO-oxidation.

Enzymatic hydrolysis. As patented in 1962, some enzymes can catalyse the hydrolysis of cellulose and hence enhance its fibrillation (Bolaski and Gallatin 1962). Since, the enzymatic hydrolysis has been included as a pre-treatment in the CNF process (Pääkkö et al. 2007; Henriksson et al. 2007). Usually, a mechanical refining is previously performed to increase the cellulose swelling and to make it more accessible for the enzymes. The enzyme which is able to hydrolyze the cellulose is called “cellulase”, and cellulase can be divided into endoglucanases, exoglucanases and cellobiohydrolases. Endoglucanase randomly attacks and hydrolyses the amorphous regions while exoglucanases randomly attacks and hydrolyzes the reducing or non-reducing ends of cellulose chains. These enzymatic treatments have the advantage to cause only small loss of material. Furthermore, the selectivity of endoglucanases for amorphous regions let intact the crystalline zones. Enzymes degrade or modify hemicellulose and lignin, while retaining the cellulose part of the fibers. Another effect is the reduction of fiber length. Indeed, endoglucanase enzymes randomly hydrolyse intramolecular glucosidic bonds in cellulose chains, reducing consequently the degree of polymerization. It results in oligosaccharides.

Tempo oxidation. 2,2,6,6-tetramethylpiperidine-1-oxyl (TEMPO)-mediated oxidation of cellulosic fibers is the most commonly used chemical pre-treatment (Saito et al. 2006). For native cellulose fibers, the oxidation reaction proceeds throughout the fibers but occurs only at the surface. This pre-treatment introduces charged carboxylate groups, and therefore the fibers become negatively charged. The conversion into carboxylates is regioselective and occurs on primary alcohol groups (C6 hydroxyls in the cellulose chain) (Dufresne, 2017). These negative charges will promote repulsion between the fibers, thus weakening the macrostructure and enhance their dispersion. Moreover, the presence of surface charges allow these suspensions to remain stable indefinitely. The chemical treatment would preferentially oxidize the amorphous domains, as they are more

accessible and thus more reactive, but COO⁻ groups are grafted in both amorphous regions and exterior of the crystals.

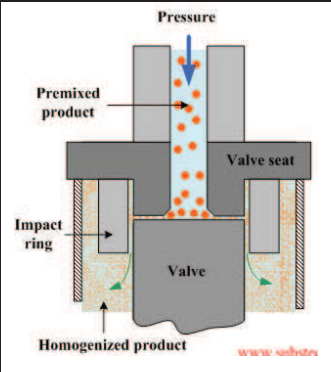
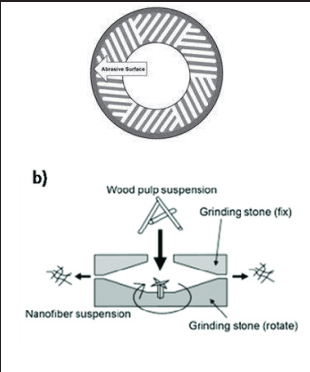
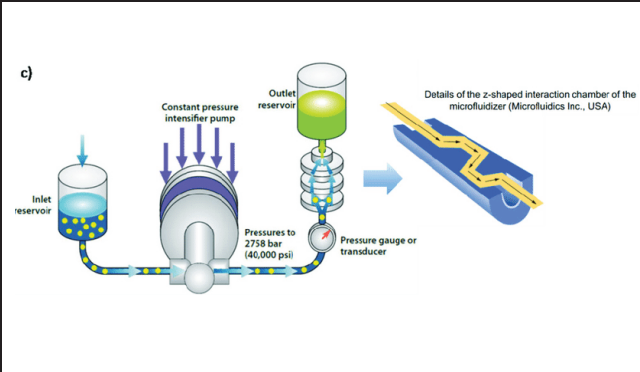



For the mechanical disintegration step, many possibilities are also possible. The first production of cellulose nanofibrils has used a softwood pulp passed several time through a high-pressure homogenizer (Turbak et al. 1983). Since this study, new processes arise for the production of CNFs. Among them, three classical methods based on intense mechanical treatments are presented in Table 4.

High-pressure homogenizer (Turbak et al. 1983): Dilute slurries of fibers (close to 0.7% w/w) are pumped at high pressure and fed through a spring high-pressure loaded valve assembly. As this valve opens and closes in rapid succession, the fibers are subjected to a large pressure drop with shearing and impact forces. This combination of forces promotes a high degree of fibrillation of the cellulose fibers and results in the progressive release of CNFs. the pressure drop is typically around 55 MPa (8,000 psi) and the fibers are cycled through the homogenizer approximately 10–20 times (Spence et al. 2011).

Super-grinding (Taniguchi and Okamura 1998): The cellulose suspension is passed through an ultrafine grinder where the upper stone is static and the lower stone rotating. The processing time depends on the raw materials used. During the grinding, the multilayered structure and bonds are broken down by the shearing forces produced by the grinding stones, and the CNFs can be isolated from the pulp.

Microfluidizer (Microfluidics Inc., USA): Cellulosic pulp is passed through an intensifier pump that increases the pressure to 276 MPa (40,000 psi), then the fiber suspension passes through thin z-shaped chambers and enter in collision with the walls. The microfluidizer operates at a constant shear rate, compared to the homogenizer, which operates at a constant processing volume. The interaction chamber can be designed with different geometries to produce different sized materials.

Table 4: Common mechanical process to produce cellulose nanofibrils

High-pressure homogenizer	Super-grinding	Microfluidizer
		
		



Recent reviews detail many possibilities for CNF production (Nechporchuk et al. 2014; Abdul Khalil et al. 2014; Bharimalla et al. 2015) and, in practice, a large number of treatment combinations is possible. With the same starting fibers, tens of distinct CNF suspensions may be produced, inducing a large number of different characteristics. Research still continues to focus on the optimization of the existing technique for the CNF production and development of alternative less energy consuming methods and with high final dry content (Rol et al. 2017). These axes of research are expected to increase the productivity, decrease the water content of the final material or give cellulose nanofibrils with new properties.

What tools for the characterizations of cellulose nanofibrils?

A lot of different cellulose nanofibrils are produced at lab-scale or available on the market, from different sources, and from different processes. Meanwhile, cellulose nanofibrils are a complex material to characterize. For a while, advanced technologies have been used to visualize and measure the dimensions of these nanoparticles. However, understanding a CNF suspension by looking in a nano-scale window is as representative as the tip of the iceberg. It is now well-known that a cellulose nanofibril suspension is not only composed of nanoscale component but is a highly heterogeneous mixture of fibers (millimeter scale), poorly fibrillated fibers (micrometer scale), nanofibrils (diameters less than 100 nm), and sometimes even soluble oligomers in water, in unknown proportions (Kangas 2014). That is also the reason why even the denomination of this complex mixture is still in debate: Cellulose nanofibrils (Ahola et al. 2007; Henriksson et al. 2008), cellulose microfibrils (Dufresne et al. 1997; Panaitescu et al. 2007), fibril aggregates (Cheng et al. 2007) are some examples of terms used for a same multiscale material. TAPPI, ISO and CSA standards approved “cellulose nanofibrils” (CNF) nomenclature and this term was also chosen for this manuscript.

As there is no single device allowing the characterization from nanometer to millimeter scale at the same time, a complete characterization of this material requires the use of several analyses. Kangas et al. (Kangas 2014) reported 25 possible techniques based on different measurement techniques (optical, mechanical, chemical). Microscopic tools at different magnifications allow studying the appearance, morphology, size and shape of CNFs. Surface chemistry (carboxyl content for natural CNFs and other grafted groups), degree of polymerization, specific surface area, crystallinity, turbidity, rheology or amount of nanomaterials in the suspension are also characteristic parameters. Similarly to fibers, which after filtration and drying can produce paper, nanofibrils can produce nanopapers. Mechanical and optical properties of these nanopapers give also key information of the CNF quality. In Table 5 some classical properties of cellulose nanofibrils are reported. Some are directly measured on the CNF suspension, and others are measured on CNF films or nanopapers. Thanks to the low dimensions and high hydrogen bonding ability, the gel-like and transparent suspension can form, similarly to paper forming, cohesive nanopapers which have the particularity to be transparent and with strong mechanical properties.

Table 5: Classic properties of cellulose nanofibrils as a hydrogel or nanopaper form

	Parameter	Increase of defibrillation degree...	CNF suspension properties
CNF Suspension 	Morphology, shape, dimensions	Lower dimensions, higher specific surface	Length: micrometric scale Diameter: 20 to 60 nm (Siró and Plackett 2010) Specific surface: 100 m ² /g
	Turbidity	Suspensions become more and more transparent	< 400 NTU Transmittance by UV light 10 – 65% (Qing et al. 2013)
	Viscosity	Viscosity increase shear-thinning and thixotropic behavior	gel-like properties ($G' \gg G''$) even at low concentrations, e.g., 0.125 wt.% (Pääkkö et al. 2007)
Nanopaper 	Contexture	Lower particle dimensions leading to higher density, lower porosity	Basis weight: 20-90 g/m ² Porosity: 8 – 40% Density: 0.8 – 1.2
	Optical properties	Lower porosity leading to higher transparency and transmittance at 550 nm	
	Mechanical properties	Denser material and higher cohesion, increase of H-bonds: decrease of tear resistance but increase of tensile properties	Tear resistance: < 60 mN Young's modulus: 10-20 GPa Tensile strength: 100 – 150 MPa
	Barrier properties	Low porosity, entangled network and strong interactions lead to increased barrier properties	Air permeability: 9-13 nm/Pa.s Oxygen permeability: mL/m ² .day Water vapor permeability: 5-10.1011 g/m.s.Pa (source: (Reverdy 2017))

Due to (i) the multiplicity of pre-treatments and mechanical treatments leading to as much different CNFs, (ii) the heterogeneity of the final material and (iii) the multiplicity of characterization techniques focusing on different aspects of the suspension, it is still difficult for producers and customers to have a global idea of the market. Researches are focused on the determination of a degree of fibrillation².

² A publication in this PhD work has been dedicated to the determination of a characterization tool called the Quality Index. According to this method, the impact of different parameters such as pulp conditioning, refining

Cellulose nanofibril foams or aerogels

The CNF suspension can also produce highly porous structures called “foams” or “aerogels” (Figure 16). The denomination “aerogel” mostly refers to “highly porous solid of ultra-low density and with nanometric pore sizes” (Sehaqui et al. 2010), obtained using supercritical drying. During drying, the original solvent (usually water) is replaced by a supercritical fluid (usually CO₂). As these two liquids are not miscible, there is an intermediate step consisting in replacing water by, for example, ethanol or acetone. At the critical point (specific temperature and pressure conditions), there is no more distinctions between liquid and gas. Then, the pressure is gradually decreased to release the gas. Aerogels have a mesoporous porosity, meaning between 2 and 50 nm in diameter, and a porosity higher than 90% (Lavoine and Bergström 2017). The denomination “foam”, on the other hand, refers to “solid porous material with micrometric pore size” (Martoia et al. 2016) and with a final material porosity higher than 50%. These foams are classically obtained thanks to freeze-drying technique, where the liquid is quickly frozen into ice, and then sublimated into gas thanks to freeze-drying technique. There are in this case two phase transitions.

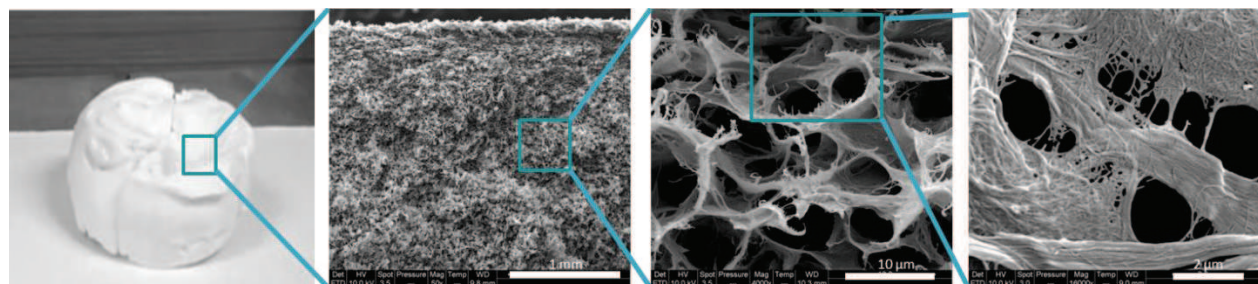


Figure 16: CNF-based foam produced by freeze-drying, observed at multi scale by scanning electron microscopy

The morphology and pore size of CNF-based foams depend on the size of ice crystals, which depends on the freezing temperature. From -196°C to -80°C, the ice nucleation is predominant over the ice crystal growth and the freezing forms a large number of small ice crystals. On the other hand, if the cooling temperature is in the range of -80°C to -13°C, ice crystal growth is predominant over the ice nucleation and we observe a small number of large ice crystals.

The combination of ultra-low density, tunable and porous architecture of this material combined with the outstanding mechanical properties of CNFs make them of interest for a wide range of applications including biomedical scaffolds, thermal or sound insulation, fire retardant materials or devices for energy storage (Lavoine and Bergström 2017). New techniques are nowadays developed to produce highly porous materials without supercritical drying or freeze-drying, which are hardly up-scalable processes. Among these techniques, there is for example solvent exchange and filtration (Sehaqui 2011) or the use of Pickering emulsions (Cervin et al. 2013)³.

and hemicelluloses content on the defibrillation process was highlighted, and a benchmarking has also been proposed (Chapter III.1.).

³ Chapter III.3. is dedicated to the production of CNF-based porous beads with or without the use of freeze-drying, and these strategies will be fully developed in this work.

3.3. Cellulose nanocrystals

From raw cellulosic fibers, the dissolution of amorphous regions allows to recover only the crystalline parts. The first reported production of stable CNCs suspension was conducted by Rånby et al. in the 1950s (Rånby and Ribi 1950). Contrary to cellulose nanofibrils which have a high aspect ratio, cellulose nanocrystals are rod-like, highly crystalline cellulose nanoparticles. Furthermore, it is a 100% cellulosic material. They are obtained after acid hydrolysis, commonly with sulfuric acid as described by Revol and co-workers (Revol et al. 1992), leading to CNCs with sulfate groups at the surface (Figure 17).

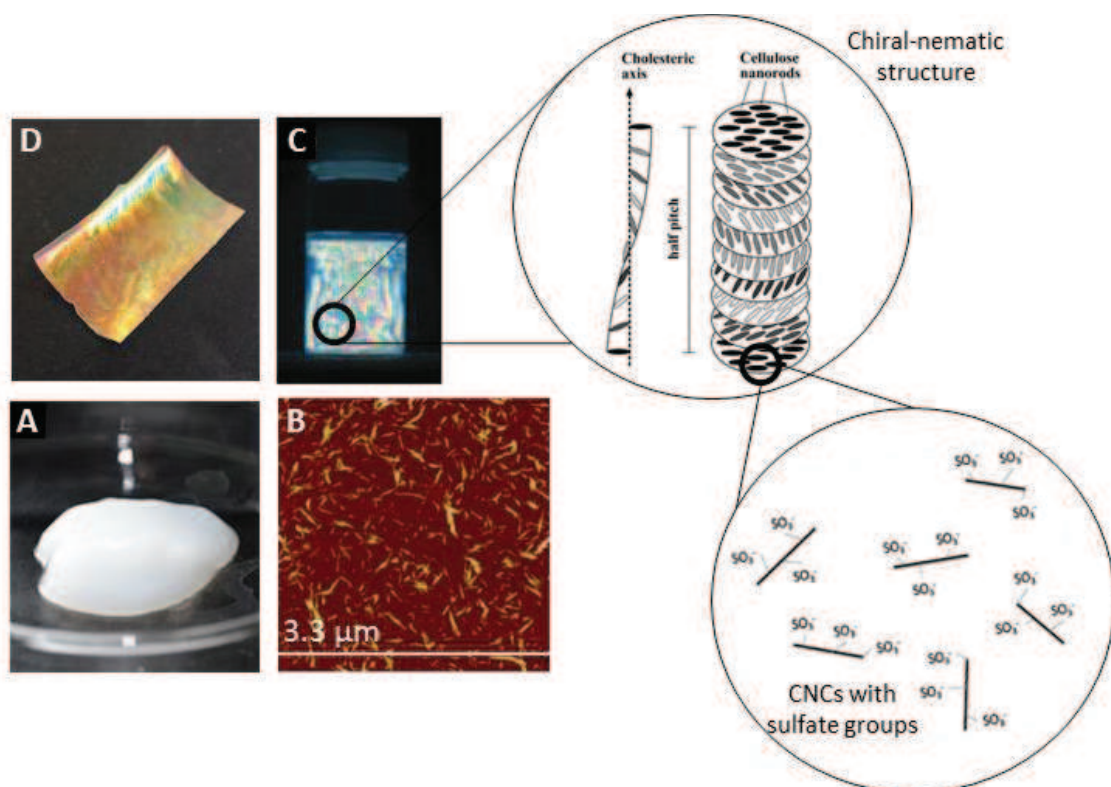


Figure 17: A) CNC gel B) AFM picture of dilute CNC suspension, C) Dilute CNC suspension observed between crossed polarizers (Araki and Kuga 2001) and D) Iridescent film of CNC

Production of cellulose nanocrystals

The starting cellulose fiber is made up of highly crystalline regions connected by amorphous regions that are much more susceptible to be hydrolysed. Therefore, after diffusion of the acid within the fibers, the linkages in amorphous regions are preferentially broken, releasing rod-like cellulose crystallites in the medium. The acid treatment can be for example with hydrochloric acid, sulfuric acid, or ammonium persulfate. The sulfuric acid has the advantage to convert part of the surface OH groups into negatively charged sulfate ester groups, providing electrostatic repulsions and leading to the spectacular self-organization properties of nanocrystals into liquid crystalline assemblies (Oksman et al. 2014). That is the reason why sulfuric acid is widely used. This acid hydrolysis is performed under controlled temperature, agitation and time (usually 64 wt%, 40-45°C and 30 min). It

is followed by washing steps by centrifugation and dialysis to remove residual reagents and salt residues, and sonication to separate the crystal domains. Conditions of hydrolysis have been shown to have an important impact on the final yield. CNCs present negative charges and are well dispersed at a pH ranging from 3 to 10.5.

Cellulose nanocrystals main properties

CNCs have a rod-like shape and typical dimensions of approximately 150-500 nm in length and a diameter of 5-30 nm (Habibi et al. 2010; Dufresne 2013). Above a certain concentration (depending on process and surface charge), suspensions of cellulose nanocrystals form a chiral nematic phase (Revol et al. 1992), whose birefringence may be viewed by polarized light microscopy. The chiral nematic phase shows a twisting of the molecules perpendicular to the director axis. The pitch “p” refers to the distance over which the molecules undergo a full 360° twist (but note that the structure of the chiral nematic phase repeats itself every half-pitch, since in this phase directors at 0° and ±180° are equivalent). These ordered structures may be preserved in solid films prepared by evaporation of the solvent and form films with controlled iridescence. By playing on the pitch length, it is possible to change the iridescence color. These properties have inspired researchers to produce pigments, security paper and inks (Chindawong and Johannsmann 2014; Bardet et al. 2015; Chen et al. 2016).

Cellulose nanocrystal properties mainly depend on the cellulose source, and at a lower level on the process (Klemm et al. 2011; Moon et al. 2011). The acid hydrolysis increases indeed the crystallinity index and hydrophilicity and decreases the thermal stability.

Table 6: Main characteristics of cellulose nanocrystals

	Parameter	Detail
Cellulose nanocrystals	Low density	1.6 g/cm ³
	High aspect ratio	Diameter from 5 to 20 nm Length from 100nm to a few micrometer (Habibi et al. 2010)
	High crystallinity	70% - 90%
	High elastic modulus	150 +/- 50 GPa (Klemm et al. 2011)
	High tensile strength	7.5 +/- 0.5 GPa
	High surface area	150 - 800 m ² /g (Habibi 2014)
CNC suspension	Colloidal stability	Colloidal stability in aqueous media due to presence of negative charges on the surface
	chiral nematic structure	(Revol et al. 1992; Beck et al. 2011)
CNC viscosity	< 3wt%	Near-Newtonian fluid with small shear thinning behavior at high shear (>1000 s ⁻¹)
	> 3 wt%	Shear thinning behavior due to organization of CNCs in the sens of the flow (Gicquel 2017)
CNC films	Iridescence	(Bardet et al. 2015)

Cellulose nanocrystals present the advantage of being biodegradable, renewable and abundant all over the world. Their most important properties are their viscosity (shear thinning behavior), size or aspect ratio, surface chemistry (sulfate groups if hydrolysed with sulfuric acid), and dispersibility in a matrix. Cellulose nanocrystals also exhibit superior mechanical properties which make them attractive as reinforcing filler in polymer composites, with a Young’s modulus close to

150 GPa (Klemm et al. 2011; Dufresne 2017). Due to the presence of three hydroxyl groups in each anhydroglucose unit, CNCs exhibit also good surface reactivity and allow the introduction of new groups by OH functionalization (Habibi 2014). Their main properties are reported in Table 6.

Unfortunately, their trend to absorb humidity and swell limits their adhesion with the matrix. Moreover, due to hydrogen bonding between their surface hydroxyl groups, unmodified CNCs aggregate easily and are often difficult to disperse in a hydrophobic matrix (Vardanyan et al. 2014). That is the reason why chemical post-treatments can be considered: as anionic and cationic pre-treatments are used for cellulose nanofibrils in order to facilitate their repulsion, anionic and cationic post-treatments can be used for cellulose nanocrystals in order to facilitate their disaggregation and improve their compatibility with a hydrophobic matrix.

Cellulose nanocrystals applications

Thanks to these impressive properties, cellulose nanocrystals are excellent candidates for the design of high performance nanomaterials in many applications. Recently, several reviews have described the potential applications of CNCs functionalized or not (Salas et al. 2014; Giese et al. 2015; Bardet et al. 2015; Abitbol et al. 2016; De France et al. 2017). They are found in a large range of applications such as composites (Abitbol et al. 2016), electronics (Hoeng et al. 2016), biomedical (Sunasee et al. 2016), cosmetic (Kalashnikova et al. 2011), paper and paints (Gicquel et al. 2017), and security (Chindawong and Johannsmann 2014).

3.4. Nanocellulose up-scaling and market prospects

In a context wherein green chemical market is expected to grow by 20% per year to exceed US \$500 billion by 2017 (Future Markets, Inc 2017) meaning about 35 millions tons/year, nanocellulose can add competitive performance while offering environmental and sustainability advantages. Nanocellulose presents indeed many advantages such as: abundance, renewability, biodegradability, biocompatibility, enhanced mechanical properties, high thermal stability, lightweight, optical transparency, high water binding capability, high surface area, chemical functionality and dimensional stability. Their outstanding potential has been proved in many scientific publications whose number is exponentially increasing since the beginning of 2000's (Figure 18-A).

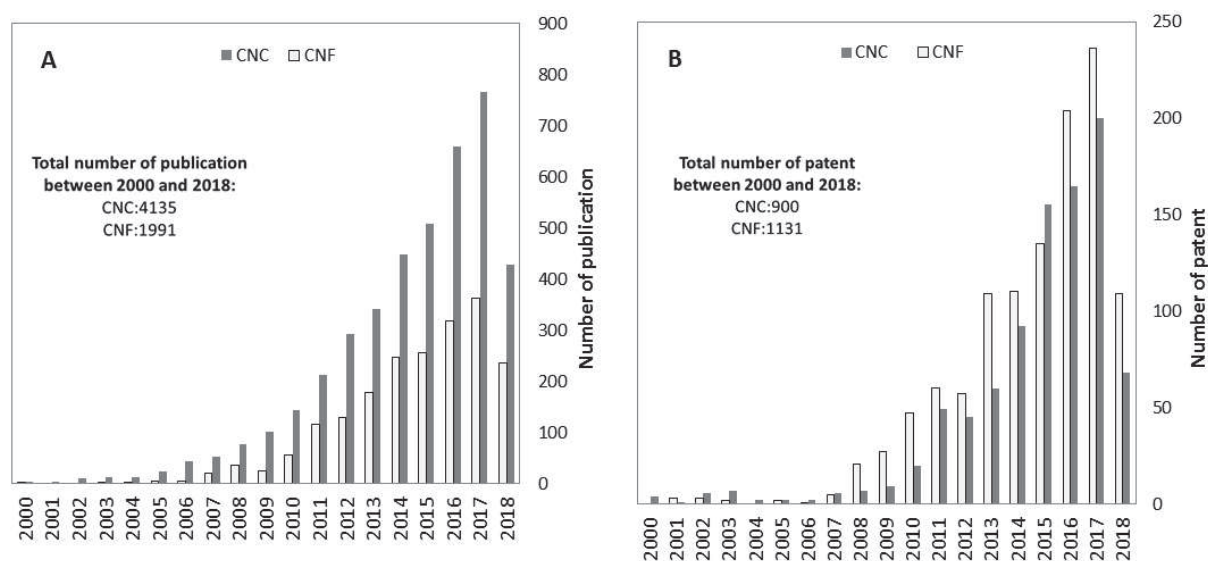


Figure 18: Overall number and distribution of A) publications and B) patents from 2000 to 1st May 2018. Based on SciFinder research. Descriptors for CNF: Cellulose + CNF, Cellulose + MFC, Cellulose + NFC, Cellulose nanofibers, nanofibrillated cellulose, cellulose nanofibrils. Descriptors for CNCs: Cellulose + CNC, Cellulose + NCC, Cellulose nanocrystals, Nanocrystalline cellulose, Cellulose nanowhiskers.

However, despite the major advantages of nanocellulose, the transition from research to commercialization took a long time to emerge. Several problems have been raised such as the high energetic consumption for the production of cellulose nanofibrils, the lack of universal characterization tools for this complex material, the time-consuming process and the production of nanocellulose with water content higher than 90% (causing transportation issues). The scientific contribution helped to overcome this brakes and the number of patents followed the same trend as the number of publications (Figure 18-B), confirming the industrial interest for nanocellulose⁴.

Furthermore, the cost of this material, which has been declared to be between 25 and 100\$/kg by Global Markets for CNCs and CNFs, respectively (Future Markets, Inc 2017), has decreased a lot this last decade due to (i) the recent commercial availability of these materials in large quantities, (ii) the decrease of water content and (iii) the development of new pre-treatments

⁴ The last chapter of this work is dedicated to the transfer from lab-scale to industrial scale, with special tests on Banque De France pilot and paper machines.

or mechanical treatments for CNF less energy consuming (Rol et al. 2017). For these reasons, a large panel of applications have reached the commercialization step (Table 7), especially in paper and packaging industries or in polymer composites⁵.

Table 7: Use of nanocellulose by field of application, position on the market and volume. Data collected from (Future Markets, Inc 2017)

Application	Use of nanocellulose	Position on the market	Volume
Cement additive			Large
Hygiene and absorbent products			Large
Paper and packaging coatings	Ink adhesion, optical properties	Commercially available (In operation or fully tested)	Large
Paper filler	Strength and weight reduction		Large
Cosmetics	Rheology modifiers, filler		Small
Filter membrane			Medium
Replacement of transparent films for food packaging	Durability, barrier properties (Grease, oil, water)	Final prototype	Large
Insulation	Sound, temperature barriers		Medium
Paint additives		Basic prototype	Medium
Automotive composites	Glass fiber replacement		Large
Bio sensors			Small
Drug delivery		Lab tested	Small
Textiles for clothing			Large
Medical implants			Small
Aerospace composite		Proof of concept	Small
Flexible and recyclable electronic			Small

If high-added value applications have been developed in priority (speciality papers, medical, cosmetics), these times are progressively changing and nanocellulose is now incorporated into existing products and processes targeting additional properties (for example, anti-bacterial diapers) or decreasing cost (decrease of paper weight and refining) for large volume applications. Precursors for massive nanocellulose industrialization are Japanese markets, with the commercialisation of shoes using CNF (The national advanced industrial Science and Technology), ballpoint pens with CNF thickener for gel inks (Mitsubishi Pencil Co Ltd and DKS Co Ltd), toilet cleaner (Daio Paper Corp.), adult diapers (Nippon Paper Industries Co., Ltd) and audio speakers (Onkyo Corp.). High-volume applications of nanocellulose by now include biocomposites, paints and other materials where the nanocellulose can be incorporated relatively easily (such as coatings). Main applications currently targeted by producers, especially in Europe and North America, are as reinforcing agent in paper, cement, biocomposites and plastic films for packaging.

However, there is still room for new patents and discovery in a lot of possible applications which have not cross yet the gap between research and industrialization, such as the use of CNF for drug delivery (Kolakovic et al. 2012), medical implants (Cherian et al. 2011) or biosensors (Schyrer et al. 2014).

⁵ These applications are the main concern of this project and will be developed in the next part.

The production capacity of nanocellulose has drastically increased this last decade, with a production of 9 tons in 2009, 1350 tons in 2014, and 3558 tons in 2017 (Bajpai 2016). At the beginning of the 2000s, the industrialization of nanocellulose was restricted to a couple of companies and research centers, mainly from Scandinavian countries, France and Japan for CNFs and North America for CNCs. Landscape has changed since that time. It exists now a large panel of producers (Table 8) with capacity of thousands kg/day. North America is the first producer of nanocellulose with 79% of the total production capacity, followed by Europe (20%) and Asia-pacific (1%).

Table 8: Cellulose nanofibrils and nanocrystals producers, adapted from (Reverdy 2017)

Company	Country	Yearly capacity	Production type
Cellulose nanofibrils plant			
FiberLean	France/switzerland	10,000 t	CNF with fillers
Performance	Canada	2,000 t	Nanofilament
Kruger/FPIInnovation	Canada	1,000 t	Nanofilament
Borregaard	Norway	1,000 t	CNF
Paperlogic	USA	730 t	CNF
Nippon Paper	Japan	300 t	CNF Tempo
American Process	USA	180 t	CNF
University of Maine	USA	110 t	CNF
Chuetsu Pulp & DKS	Japan	50 t	CNF
Sugino Machine	Japan	50 t	CNF Tempo
Oji Holdings	Japan	40 t	CNF
Suzano	Brazil	36 t	CNF
Innventia	Sweden	35 t	CNF
CTP	France	35 t	CNF
PFI	Norway	35 t	CNF
Seiko PMC	Japan	30 t	CNF
Tokushu Tokai Paper	Japan	30 t	CNF
VTT	Finland	15 t	CNF
Inofib	France	0.5 t	CNF
Icar-Circo	India	11 t	NA
EMPA	Switzerland	5 t	CNF
SAPPI	Netherlands	8 t	CNF
Daio Paper	Japan	NA	CNF
DIC corporation	Japan	NA	CNF
Daicel Corporation	Japan	NA	CNF
Stora Enso	Finland	NA	CNF
UPM	Finland	NA	CNF
Bettulium	Finland	NA	CNF Tempo
Norske Skog	Sweden	NA	CNF
Weidmann	Switzerland	NA	MFC
Cellucomp	UK	NA	CNF
BioNC	Spain	NA	CNF
Cellulose nanocrystals plant			
Celluforce	Canada	365 t	Sulfated
American Process	USA	200 t	NA
Holmen/Melodea	Sweden	35 t	Sulfated
Icar-Circo	India	10 t	NA
Alberta Innovates	Canada	7 t	Sulfated
Blue Goose	Canada	4 t	Sulfated
FPIInnovations	Canada	4 t	Sulfated
University of Maine	USA	4 t	Sulfated
Melodea	Israel	NA/ Pilot	Sulfated

The key point for the rise of nanocellulose is to identify applications and markets where nanocellulose is both superior and cost competitive. Researches in improvement of production process to increase the cost efficiency are crucial and allow this material to compete in high volume markets. Eyes are now on pulp and paper industries, which gather 51% of the industry demand for nanocellulose (Figure 19-B). Global Market Inc. put paper, board and packaging composites at the top of market opportunity assessments for nanocellulose regarding different criteria such as stage of commercialization, economic impact in 2017, potential for high volume, competitive landscape and cost. This can be explained by the need to achieve significant improvement in performance/weight ratio in paper and packaging products and also the need for new packaging material that incorporate barrier, anti-bacterial, dimensional and thermal stabilities and lightweight/high strength properties. This evolution is encouraging as end user markets (composites, packaging and construction) are potential high volume markets (Figure 19-A).

Indeed, it has been reported that nanocellulose could reach a part of 5% in the paper and board industry in next years, and the optimistic demand for nanocellulose in next year corresponds to a volume of 1000 thousand tons. This volume is just in second position behind the pharmaceutical industry, where the part of nanocellulose could reach 10% with future translation of this application from research to massive industrialisation.

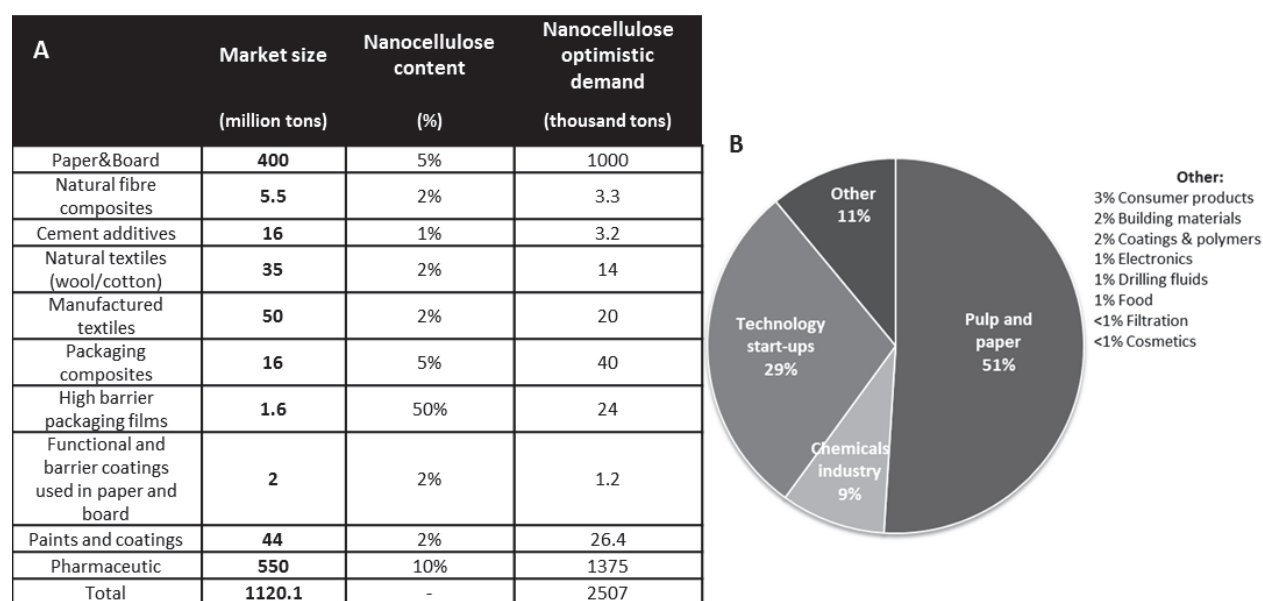


Figure 19: A) Potential volume estimates and penetration of nanocellulose into key markets and B) Volume industry demand for nanocellulose by nanocellulose producer sales in 2017. Data collected from (Future Markets, Inc 2017)

4. Nanocellulose for use with polymer and in paper industry

This project targets two of the most promising applications of nanocellulose: the use as composite and the use in paper sheets. This part will especially focus on (i) the use of cellulose nanocrystals with polymers and (ii) the use of both cellulose nanocrystals and cellulose nanofibrils in paper (bulk or surface).

4.1. CNCs nanocomposites and generalities on crystallization mechanisms

4.1.1. Use of CNC in nanocomposites

The physical properties of polymers, such as mechanical, optical or barrier characteristics, can be tailored thanks to the introduction of suitable fillers to form composites (Natterodt et al. 2018). For example, a lot of applications are reported with calcium carbonates, glass fibers, carbon black, or graphene. The nanocomposite approach has emerged in the last two decades as an efficient strategy to upgrade the structural and functional properties of polymers. Nanocomposites are materials in which nanoscale organic or inorganic particles are generally dispersed in a polymer matrix in order to drastically improve the polymer properties (Armentano et al. 2010; Dufresne et al. 2013). These materials represent a new alternative and allow increasing the Young's modulus, barrier properties, solvency, heat resistance, without detrimental effect on ductility. Previously, nanofillers used to prepare nanocomposites were mainly inorganic and their processability, biocompatibility and biodegradability were much more limited than with organic fillers.

Cellulose nanocrystals are good candidates for preparing biocomposites with polymers due to their low density, easy processability, non-abrasive nature and their impressive mechanical properties with the added benefits of low environmental impact and origin from renewable resources. Due to their hydrophilic nature, they are particularly used with hydrophilic polymers as it results in excellent interfacial compatibility and good dispersion between the filler and the polymer matrix, resulting in enhanced mechanical properties.

The first use of cellulose nanocrystals from tunicin (cellulose from tunicate) as reinforcing phase in a synthetic polymer matrix has been reported in 1995 via solvent casting from aqueous dispersion (Favier et al. 1995). Since, the use of CNC from various sources such as ramie (Habibi and Dufresne 2008), potato (Dufresne et al. 2000), cotton and wood has been extensively investigated for the preparation of high performance composites (Habibi and Dufresne 2008; Brinchi et al. 2013; Mariano et al. 2014; Oksman et al. 2016). CNCs have been shown to enhance the mechanical properties of many polar polymers such as polyvinyl alcohol (Roohani et al. 2008), poly(vinyl acetate) (Kaboarani et al. 2012), or poly(ethylene oxide) (Zhou et al. 2011). However, fabrication of nanocomposites with hydrophobic polymer matrices, such as polyethylene, natural rubber or polypropylene, remains challenging. Indeed, CNCs tend to form inter-CNC hydrogen bonds which may result in aggregation in hydrophobic environments and thus reduce their reinforcement potential in apolar matrices (Ben Azouz et al. 2012). To increase the compatibility of CNCs with

hydrophobic matrices, different surface modifications of CNCs have been reported in the literature such as physical adsorption of surfactants (Bondeson and Oksman 2007), attachment of nonpolar molecules (Ávila Ramírez et al. 2017), or covalent polymer grafting (Ljungberg et al. 2005).

Twenty-three years after the first use of CNC in nanocomposite, the method of production and applications of these nanocomposites have also evolved towards actual society concerns. The challenge in nanocomposite processing is the need to develop low cost and simple methods to produce nanocellulose composites with uniform dispersion of the filler (Salehpour et al. 2018). A classical method to produce such composites is the casting-evaporation process. However, this method is a relatively slow process and can consequently result in self-aggregation of the nanoparticles within the matrix. To obtain faster preparation, researchers have developed melt compounding techniques such as extrusion (Nagalakshmaiah 2016) or freeze-drying followed by classical extrusion process or hot pressing (Dufresne 2010). CNCs can also just be mixed with the polymer phase and coated in plastic films, packaging or paper applications (Huang et al. 2017).

In addition to the well-known reinforcing effect of cellulose nanocrystals, they are nowadays targeting new applications such as optical sensors, security marking and functional coating (Xu et al. 2018) which take advantage of their iridescent properties, but they are also used for their adhesive properties in latex films (Ouzas et al. 2018) or for their combined optical and barrier properties in food packaging films (Carvalho et al. 2018) and for their antibacterial potential in wound dressing applications (Hasan et al. 2017). It is worth noting that the resulting properties of the nanocomposites are widely dependant on several parameters such as: the CNC percolation threshold, the dispersion of CNCs, the interfacial compatibility between the filler and the matrix, the polymer molecular weight and its degree of crystallinity, the humidity level, the thickness of the nanocomposite and drying procedure⁶.

In this project, cellulose nanocrystals will be used as additive in a polyvinyl alcohol (PVOH) matrix and a further look of CNC-reinforced PVOH composites will consequently be done in the next section.

⁶ A part of this work is dedicated to the development of buckling metrology and assesses the influence of these parameters on thin PVOH-CNC coated layers.

4.1.2. CNC reinforced polyvinyl alcohol nanocomposites

Poly(vinyl alcohol) (PVOH) is the largest synthetic water-soluble polymer produced in the world (Ding et al. 2002). It is known for its thermal stability, good oxygen barrier properties, good adhesive properties, biodegradability (Garaeva et al. 2012), excellent chemical and physical properties, easy processing and low cytotoxicity (Chiellini et al. 2003). It has hence been widely used in many applications such as drug delivery, adhesives, packaging, heavy metal ions absorption, acoustic noise reduction (Tanpichai and Oksman 2018) and paper coatings (Lee et al. 2018). However, the poor mechanical properties of PVOH limit its use (Bai and Li 2006). The introduction of a reinforcing material in the PVOH matrix has been reported to improve its mechanical properties.

A broad range of nanocomposites have been prepared using PVOH as matrix and nano-reinforcement such as silica nanoparticles and carbon nanotubes (Paiva et al. 2004; Guo et al. 2007). Recently, polyvinyl alcohol has also widely been used as matrix for cellulose nanocrystals nanocomposite (Table 9) and the annual number of publications about CNC-PVOH nanocomposites tends to increase. Since 2010, 35 papers have been published reporting the use of CNC to reinforce polyvinyl alcohol or polyvinyl acetate matrix.

Table 9: Cellulose nanocrystals reinforced polyvinyl alcohol, *date of study: 02 March 2018

Year	Number of publication	References
2018*	3*	(Tanpichai and Oksman 2018; Noshirvani et al. 2018; Song et al. 2018)
2017	4	(Huang et al. 2017; Rouhi et al. 2017; Zhou et al. 2017; Popescu 2017)
2016	8	(Aloui et al. 2016; Choo et al. 2016; Kumar et al. 2016; Lee et al. 2016; Meree et al. 2016; Noshirvani et al. 2016; Song et al. 2016; Tanpichai and Oksman 2016)
2015	5	(Kamal and Khoshkava 2015; Montes et al. 2015; El Miri et al. 2015; Sirviö et al. 2015; Voronova et al. 2015)
2014	5	(Peresin et al. 2014; Zhang et al. 2014; Gonzalez et al. 2014; Rescignano et al. 2014; Mandal and Chakrabarty 2014)
2013	4	(Fortunati et al. 2013b, a; Silvério et al. 2013; Xu et al. 2013)
2012	3	(Uddin et al. 2012; Ago et al. 2012; Kaboorani et al. 2012)
2011	1	(Lu et al. 2011)
2010	2	(Peresin et al. 2010b, a)

Hydrogen bonding between CNC and PVOH (Figure 21) is particularly expected to increase the mechanical properties of the matrix (Peresin et al. 2010a; Gonzalez et al. 2014). For example, the addition of cellulose nanostructures was found to produce 100% improvement in the tensile modulus of certain PVOH nanocomposites (Qua et al. 2009). Chen et al also reported an increase of 33% in tensile modulus with 2% CNCs in PVOH matrix (Chen et al. 2012). This increase in mechanical properties is still in debate and the CNC content appears to be determinant. Indeed, Peirera (Pereira

et al. 2014) observed an increase in mechanical properties for a loading of CNCs in polyvinyl alcohol matrix up to 3%, while 5% CNCs reduced these properties. This increase in mechanical properties with 3% CNCs has also been reported by Gonzalez (Gonzalez et al. 2014) which reported an increase of nanocomposite hydrogel Young's modulus from 0.8 to 1.1 MPa. On the other hand, some researchers did not observe any mechanical reinforcement effect of CNCs in PVOH matrix (Fortunati et al. 2013b) whatever the CNC content (1, 2 and 5 wt%). These observations have led to the conclusions that the reinforcing ability of CNCs depends on many factors, such as interfacial interaction between CNCs and PVOH (Chen et al. 2012), the polyvinyl alcohol molecular weight and degree of hydrolysis (Figure 20), the percolation threshold (proportion of CNF or CNC that is just sufficient to fill the volume with an interconnecting structure (Dufresne 2008; Moon et al. 2011)) and the dispersion of CNCs within the matrix. To obtain strong interactions between the polymer matrix and cellulose, different approaches have been tested, such as chemical modification of CNCs and cross-linking between the polymer and the reinforcing phase (Chen et al. 2012; Spoljaric et al. 2014).

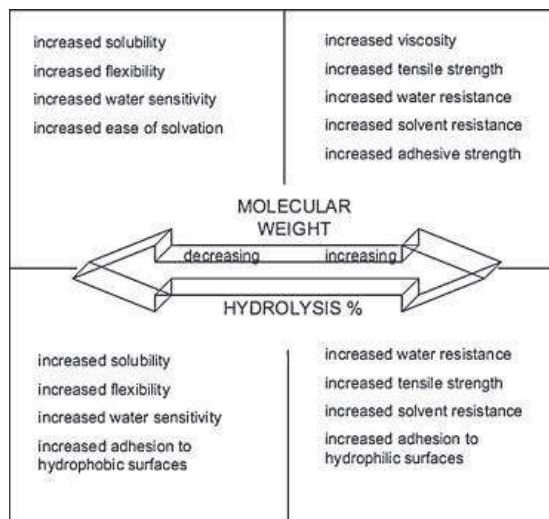


Figure 20: Property of polyvinyl alcohol as a function of degree of hydrolysis and molecular weight (Tang and Alavi 2011)

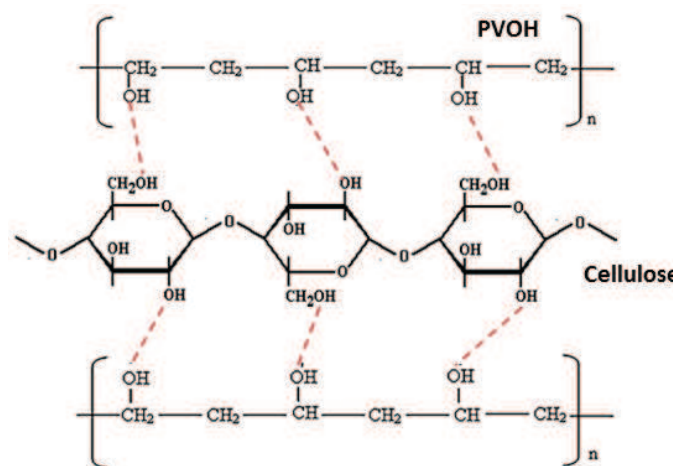


Figure 21: Possible hydrogen bond formation between cellulose nanocrystals and PVOH

The impressive mechanical properties of CNCs are not the only reason for the mechanical performance of CNC-reinforced PVOH composites. The crystallinity of the polymeric matrix is also widely influenced by the presence of the nanomaterial⁷. As the PVOH crystallinity will be a large source of discussion during this work, the next part has been dedicated to the description of polymer crystallization mechanisms.

⁷ In chapter II., a publication will especially study the influence of CNCs on PVOH drying and crystallization kinetics and the resulting impact on paper dog-ears resistance.

4.1.3. Crystallization mechanisms of CNC reinforced polymer composites

Polymers can be divided into two categories: thermoplastics and thermosetting polymers. Thermosetting polymers are composed of crosslinked macromolecules and form a tridimensional polymer, whose lateral connections are ensured by covalent links. Because of this tridimensional network, such polymers are amorphous, and hence infusible and insoluble. On the other hand, thermoplastic polymers (such as polyvinyl alcohol) are composed of linear or branched macromolecules. Their lateral connexions are ensured by secondary links and they can be amorphous or semi-crystalline. Consequently, they can be melted under high temperature, their processing is easier and thermo-reversible.

During polymerization, different configurations lead to different properties. Macromolecules can have an arbitrary arrangement: this is an “amorphous” zone, with a low compactness and a high flexibility. Macromolecules can also have a structured organization: in this case, the compactness and rigidity are higher and a crystal is formed.

Case of PVOH

Polymer properties strongly depend on the chain length and flexibility but also on the crystallization conditions (Pennings 1980). The growth and morphology of polymer crystals are generally determined by molecular processes such as mass and heat transfer, adsorption, desolvation, surface diffusion and liquid-crystal interface kinetics, and additionally by changes in the molecular conformation and topological constraints such as entanglements (Pennings 1980).

PVOH is a semi-crystalline polymer. The crystalline phase consists in plate-like single crystals (lamellae) 10-20 nm thick that are bound to each other by the amorphous phase. The degree of crystallinity of polyvinyl alcohol is an important characteristic that determines many macroscopic properties of the polymer: with a higher crystallinity, the mechanical properties are improved, the water resistance increases, and the permeability to gases and liquids increases (Tretinnikov and Zagorskaya 2012).

Crystallization of polymers

If a linear polymer in the melt state (such as poly vinyl alcohol) is rapidly frozen, then its structure will consist in amorphous zones. However, if a slow cooling is performed, the polymer chains have time for a partial reorganization and form alignment of polymeric chains (crystalline part). To start a crystallization process, the molecular chains have to be mobile. The crystallization temperature is consequently higher than the glass transition of the polymer T_g . There are two different steps during the crystallization:

- **Nucleation step** (“primary crystallization”). Nucleation starts with the movement of the polymeric chains and their organisation into parallel segments, first at nanometer scale. The nucleation can be homogeneous (from a melted polymer) or heterogeneous (from

an external element, for example the wall of the container or an additive). A small solid, the nucleus, is formed. If this nucleus reaches the critical nucleus size, the growth of the crystal can happen.

- **Growth** (“secondary crystallization”). If the nucleus reaches the critical nucleus size, the growth of the crystal can happen. The parallel chains are packed together into a platelet, a structure called “lamellae” (Figure 22). Crystallization from molten state can then assemble in superstructures: spherulites (polycrystalline spherical arrays) (Brandrup et al. 1999).

These embryos of lamellae, with dimensions smaller than 10 nm, can have an unidirectional growth along the length of the lamella at both ends (Li et al. 1999). When their lengths are longer than 0.5 – 1 μm , the lamellae begins to form banches. It then forms branching of lamella connected by amorphous regions, forming the skeleton of spherical semi-crystalline regions, called spherulite. Their formation is directly linked to the number of nucleation sites, the structure of the polymer molecules, and the crystallization process (rate, temperature). Depending on these parameters, the spherulite diameter can vary in a wide range from a few micrometers to millimeters.

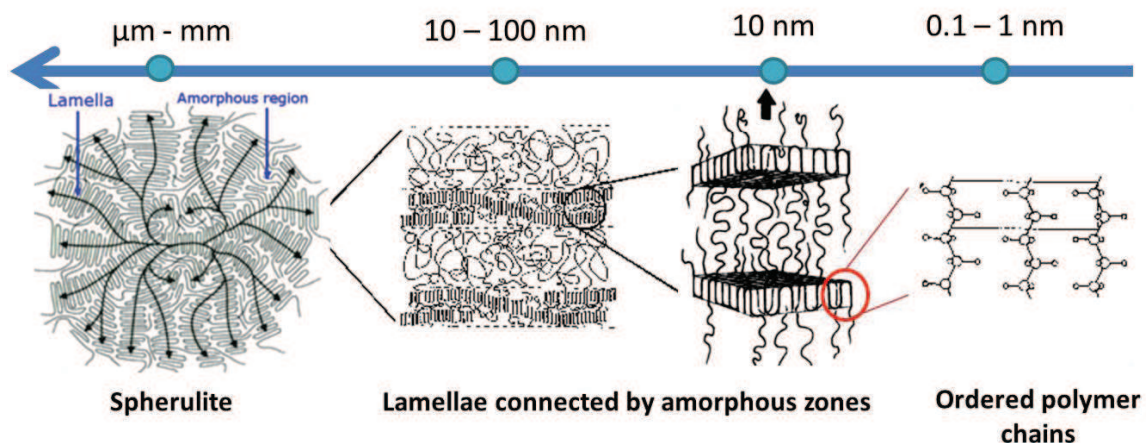


Figure 22: Organisation of a spherulite. Extracted and modified from (Myers et al. 2014)

The phase transformation depends upon the polymer type, monomer size and placement of the monomer units forming the macromolecules (Brandrup et al. 1999).

Mechanical properties. The properties of semi-crystalline polymers strongly depend on their crystalline structure (Pukánszky et al. 1997). For more than 20 years, many studies have looked for mathematic correlation between polymer structure and properties. For example, yield stress of polypropylene has been found to be a function of the spherulite size. The formation of spherulites affects many properties of the polymer material. For example, they are reported to increase the crystallinity, density, tensile strength and Young's modulus of the polymer. This increase is due to the lamellae fraction within the spherulites, where the molecules are more densely packed than in the amorphous phase. Stronger intermolecular interactions within the lamellae increases hardness. The

lamellae are connected by amorphous regions which provide elasticity and impact resistance. Changes in mechanical properties of polymers upon formation of spherulites however strongly depend on the size and density of the spherulites. Indeed, if the total volume of spherulites is too high, it can result in polymer shrinkage and spherulite interactions leading to brittleness and cracking along the boundaries of the spherulites (Ehrenstein and Theriault 2000) .

Temperature effect. When the temperature increases, the thermal motion can destroy the nuclei formed. Consequently, the critical size before growth is higher when the temperature increases. It also means that when the crystallization temperature increases, bigger crystals are formed. However, as it is more difficult for the nuclei to reach the (bigger) critical size, the number of crystals is smaller.

Differential scanning calorimetry and important models

Differential scanning calorimetry (DSC) is a technique used to detect and analyze thermal events or transition occurring in a material during a temperature scan (non-isothermal sequence) or during time (isothermal sequence). This technique can be used to study the thermal transitions of a polymer, meaning the changes occurring when heating or cooling a polymer. It measures the differences in heat exchange between the analyzed sample and a reference. The crystallization phenomenon is observed in the form of an exothermic peak while the melting is observed in the form of an endothermic peak (Figure 23-A). Both crystallization and melting of the polymer are first-order transitions. This means that when the melting temperature is reached, the temperature of the polymer will not increase until the melt of all the crystal domains. Consequently, the degree of crystallinity of the polymer can be deduced by measuring the area under the melting peak.

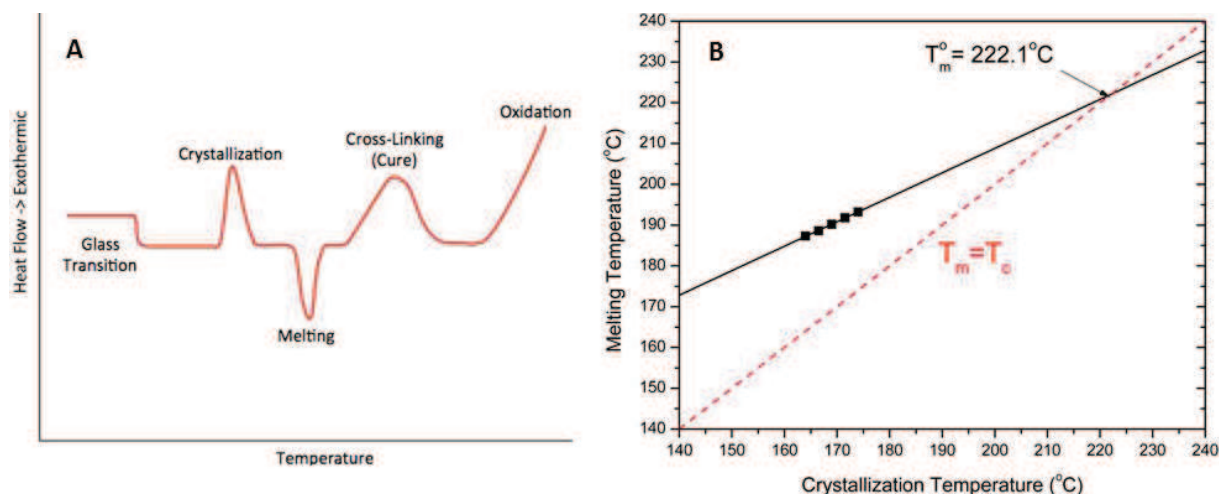


Figure 23: A) DSC curve and different endothermic and exothermic transitions, B) Determination of the melting temperature of the perfect crystal, extracted from (Tsanaktsis et al. 2015)

Several other parameters can also be extracted from DSC tests. A publication has recently reported the impact of cellulose nanocrystals on the isothermal crystallization kinetics of poly(ϵ -caprolactone) (Siqueira et al. 2011) thanks to Hoffman-Weeks, Avrami and Arrhenius equations⁸.

The Hoffman-Weeks method (Hoffman and Weeks 1962) allows the measurement of the equilibrium melting temperature T_m° , which is defined as the melting temperature of an infinite crystal size. This value is obtained by plotting the melting temperature value as a function of the crystallization temperature. The intersection between this line and the $y=x$ line gives the equilibrium melting temperature (Figure 23-B). The Hoffman-Weeks model (Table 10) allows then the calculation of the stability parameter, ϕ , and the thickening coefficient, γ . The stability parameter ϕ varies from 0 to 1 and the lowest value corresponds to the most stable crystals. The thickening coefficient represents the ratio of the lamellar thickness to the lamellar thickness of the critical nucleus.

The Avrami model describes phase transformations (or changes of state) in solids, at constant temperature. This model supposes a random nucleation with a growth identical in each direction. The Avrami coefficient n is supposed to be between 1 and 4 and it reflects the nature of the polymer transformation into crystal. The Avrami coefficient is also linked to the degree of crystallinity and the relative crystallinity (Table 11). Finally, there is an equation expressing the temperature dependence of reaction rates, which allows in particular the calculation of the minimum amount of energy necessary to form crystals (activation energy).

Table 10: Important models for the description of polymer crystallization mechanisms

Model	Parameter	Name
Hoffman and Weeks: $T_m^\circ - T_m = \phi \cdot (T_m^\circ - T_c)$ $\gamma = 1/\phi$	T_m° (°C)	Melting temperature of the perfect crystal (infinite crystal size)
	ϕ	Stability parameter
	γ	Thickening coefficient
Arrhenius equation: $\frac{1}{n} (\ln k) = \ln k_0 - \frac{\Delta E_a}{RT_c}$	k_0	Temperature-dependent pre-exponential factor
	ΔE_a (KJ/mol)	Total activation energy
	R (J/mol.K)	Universal gas constant
Avrami equation: $1 - X_t = \exp(-k(t)^n)$	X_t (%)	Relative crystallinity
	t (min)	Crystallization time
	K (min ⁻¹)	Crystallization rate
	n	Avrami exponent

⁸ These equations will be used to study the crystallization kinetics of CNC-reinforced PVOH in **Chapter II.2**.

Crystallization of CNC reinforced polymers

Previous researches have already observed some changes in polymer crystallization due to the introduction of CNCS. CNCs, due to their anchoring effect, are known to act as a very good nucleating agent. They indeed promote a heterogeneous crystallization of polyvinyl alcohol as confirmed by the literature studies (Rescignano et al. 2014). However, the influence of CNCs on the degree of crystallinity of the polymer is highly dependent on polymer properties (such as the molecular weight) and interactions with the filler. A study of nanocomposite films composed of tunicin nanocrystals in poly(oxyethylene) matrix has shown that the degree of crystallinity was constant up to 10 wt-% CNC and decreased for higher nanocrystal contents (Azizi Samir et al. 2004). It was also the case for CNCs in polylactic acid matrix (Pandey et al. 2010). A study also proved that the degree of crystallinity of PVOH increases with nanocrystal loading (Uddin et al. 2011). It was also observed that the dimensions of CNC have a stronger impact on the crystallinity of poly(butylene adipate-co-terephthalate) than its volume fraction (Mariano et al. 2016)). Researchers also noticed that the addition of CNCs increases the rate of crystallization of poly(ϵ -caprolactone) (Siqueira et al. 2011).

4.2. Use of nanocellulose in paper industry: context

The use of nanocellulose as additive in papermaking is a wide source of interest since the beginning of the 2000's as both CNFs and CNCs present similar composition than paper, but their exceptional properties at the nanoscale confer paper quality enhancement (Campano et al. 2018). One of the main reasons for the expansion of nanocellulose in paper industry is the up-scale production of both cellulose nanofibrils and nanocrystals and breakthrough to decrease the costs, accessibility and homogeneity of these materials.

There are two approaches for the use of nanocellulose in paper: put the nanocellulose in the bulk material, or at the surface. Nanocellulose can be used as a wet or dry strength additive, to enhance barrier properties in food packaging, to improve paper gloss, to reduce paper basis weight or to develop functionalized papers (Osong et al. 2016). If the use of cellulose nanofibrils in paper industry has been widely studied in reviews (Bardet and Bras 2014; Brodin et al. 2014; Boufi et al. 2016; Osong et al. 2016), the use of cellulose nanocrystals is still more challenging. This is due to the smaller dimensions (mainly in the length) that prevent the use of CNC in the wet-end part of the process without very low retention in the paper bulk. For these reasons, the use of CNC is often limited as filler in polymer matrix for coating or impregnation steps, for barrier properties or in printing applications.

The use of nanocellulose, and in particular cellulose nanofibrils, combines two advantages for paper-making industries: (i) the possibility to increase the paper performance with (ii) a material which can be easily produced in papermaking facilities already familiar with fiber fibrillation. Pilot trials are already performed by papermaking industries such as UPM, Stora enso, GL&V Company (University of Maine) or Paperlogic, especially with introduction of cellulose nanofibrils produced by their own facilities and mixed with the paper pulp with different content. For example, GL&V Company at the University of Maine studied the addition of 1 to 7% of CNF in the paper pulp and showed an increase in internal bond of 6.9% (with 1% CNF) to 28.4% (with 5% CNF), an improvement of almost 400% of Gurley porosity and a decrease in roughness of about 10% (with 5% CNF) (Cowles 2016). Higher contents up to 15% were tested at a pilot scale and reported by Paperlogic (Fein 2016; Reverdy 2017).

4.3. Bulk improvement of papers

The introduction of nanocellulose in paper bulk has so far been considered with cellulose nanofibrils only. This part consequently does not mention the use of cellulose nanocrystals in bulk.

Since a long time, refining process has been a common step in papermaking industries to increase fiber flexibility, enhance swelling ability, fibrillation, and hence increase the H-bonding potential. The refining is proved to enhance paper mechanical properties and highly refined fibers are already used in high added value papers (such as banknotes). Refining is also known to confer

particular optical properties such as transparency, as it is the case for tracing papers. The use of cellulose nanofibrils in paper bulk is just amplifying these characteristics already observed with fines (Taipale et al. 2010). Cellulose nanofibrils present indeed higher specific surface/lower dimensions which confer them higher bonding and functionalization abilities. Figure 24 synthesizes the different strategies relative with the bulk insertion of CNFs.

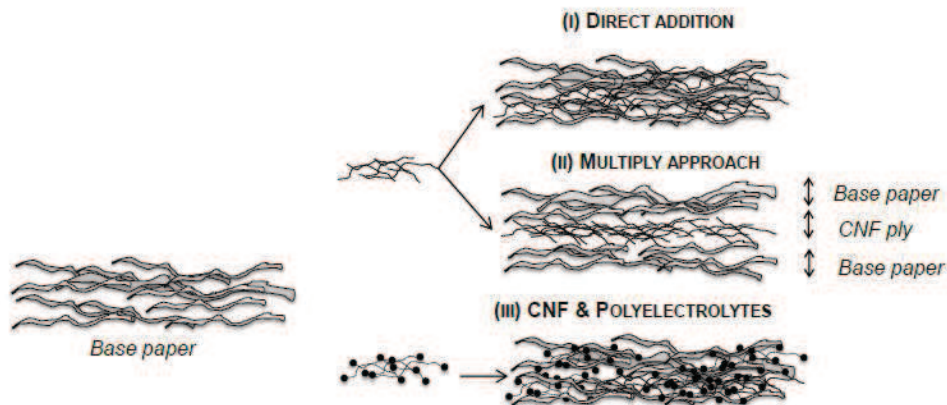


Figure 24: Different strategy for the use of cellulose nanofibrils in paper bulk, extracted from (Bardet and Bras 2014)

Direct addition of CNFs in the bulk. The direct addition is generally applied to enhance the (dry and wet) mechanical resistance of a paper sheet due to the increase of H-bonding brought by the cellulose nanofibrils (Madani et al. 2011; Hassan et al. 2011). For example, Madani et al. reported an increase of 25% in the tensile index and 170% in the strain at break by addition of 10% of CNF in the pulp. A direct benefit of the CNF introduction is also the possibility to decrease the basis weight while keeping the same mechanical properties: 60 g/m² paper without CNF and 41 g/m² with 10% CNF have showed similar tensile strengths (Hamann 2011). Consequently, lightweight materials can be produced. Another benefit is the possibility to increase the filler content from 30% to 50% while maintaining the paper strength (Torvinen et al. 2011), with addition of only 5% CNF. This is important for papermakers as fillers/pigments are essential for brightness or opacity.

Introduction of cellulose nanofibrils also allows decreasing the degree of fiber refining without losing mechanical properties (González et al. 2012). Effect of adding to a bagasse pulp different amounts of CNF on the tensile strength (wet and dry), tear resistance, burst strength, opacity and porosity of paper sheets has also been studied (Hassan et al. 2011). Finally, this increase of mechanical properties can also be an advantage for recycled papers. Indeed, Delgado-Aguilar et al. (Delgado-Aguilar et al. 2015) explained that the deinking and recycling of paper such as newspapers raise the problematic of decrease of strength. Today, the solution to avoid this is to refine the pulp to obtain more fibrillation. They have proved that only 1.5 wt% of CNF was necessary to achieve higher tensile strength and stiffness than paper from refined pulp with similar freeness and water retention value.

It is well-known that the price of cellulose nanofibrils is still higher than the price of other usual strengthening agents (CMC, starch,...). However, this can be balanced by the fact that paper saving costs can result (reduction of basis weight, increase of filler content, decrease of refining), and that the up-scaled progress of CNF producers decreases their cost and increases their accessibility in large volumes.

Due to the small dimensions and increase of bonding with fibers, the introduction of CNF in paper bulk also results in a decrease of the paper porosity. This densification results in a paper smoothness (Hassan et al. 2011) and in the reduction of air permeability (Hii et al. 2012) but in turn also leads to an increase of water vapor transmission rate (WVTR), and an increase of Cobb value up to 60% (Hamann 2011). Furthermore, issues with dewatering or drainage rate during paper process have also been reported (Hii et al. 2012; Rantanen and Maloney 2013) due to water retention brought by hydrogen bonding within the small capillary interstices of the fibrous network. It is possible to overcome these dewatering problems by carefully adjusting the ratio of CNF and polyelectrolytes as mentioned in a following section.

Multiply approach⁹. This approach no longer consists in the mixture between fibers and CNFs, but in the formation of an entire layer of CNF which can be surrounded or not by fiber layers. This approach has rarely been studied in scientific papers and only few examples can be found (Table 11). However, patents from Stora Enso or Akso Nobel (Wildlock and Heijnesson-Hulten 2007; Heiskanen and Backfolk 2017) have raised these strategies. The use of cellulose nanofibers in multiply approach is especially used in paperboard industry to increase bonds between two panels. For example, the invention of Akso Nobel relates to a method of producing a laminate paper product comprising two or more layers, with the addition of a CNF layer in an amount from about 0.05 to 50 wt%.

As the direct approach, the multiply with CNF is known to improve the mechanical properties (Mörseburg and Chinga-Carrasco 2009) but present also issues of drainage affecting press and drying sections. Furthermore, this strategy is often limited due to the difficult retention of CNFs in the fibrous material which presents an open structure. Morseburg and Chinga-Carrasco (2009) studied the effect of CNF addition in a multilayer thermomechanical paper sheet formation together with clays addition in the pulp. Clays usually deteriorate the mechanical strength of paper as it disturbs the interfibrillar hydrogen bonding network. They showed that placing CNF in the center of the layered sheet and clays at the top with TMP pulp was beneficial for mechanical properties.

CNF and polyelectrolytes. In previous studies, CNFs were used alone. A second generation of scientific publications and patents has highlighted the combination of CNF with polyelectrolytes. These polyelectrolytes can be strengthening agents (such as polyamidoamine-epichlorohydrin (PAE) (Ahola et al. 2007), cationic polymers (Manninen et al. 2011) or anionic polymers (CMCs), retention and flocculation agents, sizing agents (AKD,(Missoum et al. 2013)), or optical brightening agents. In

⁹ This approach will be followed in this PhD project and a more detailed literature is proposed in **Chapter III.4**.

addition to increase targeted properties, the addition of polyelectrolytes also allows decreasing the CNF amount and overcoming the drainage issues brought by CNF (Taipale et al. 2010). It also promotes additional dimensional stability as proved by Manninen et al. (Manninen et al. 2011): both hygroexpansion and drying shrinkage were decreased with the addition of cationic starch and the combination of CNF and starch produced a sheet with improved dimensional stability and strength properties. Furthermore, the addition of 5 to 50% of hydrophobized CNF by a patented AKD based emulsion process in paper handsheet was performed by Missoum et al. (2013a). With this hydrophobization on the nanofibrillar material they could improve air permeance and mechanical strength at the same time. They get also internal sizing, meaning less water absorption of the material, giving competitive value with industrial product.

Table 11: Properties achieved with the introduction of cellulose nanofibrils in the bulk paper

CNF content		Objectives and main results
Direct addition	0 – 30%	<ul style="list-style-type: none"> ▪ Improve wet & dry resistance (Hassan et al. 2011) ▪ Increase of 20% tensile index and 170% strain at break, effect of CNF quality (Madani et al. 2011) ▪ Increasing filler content from 30% to 50% (Torvinen et al. 2011) ▪ Increase of paper strength with 1% CNF, no decrease of drainage time (Djafari Petroudy et al. 2014) ▪ Reduction of drainage rate but increase of tensile strength and optical properties, increase of the air resistance (Hii et al. 2012) ▪ Decrease of fiber beating without decreasing mechanical properties (González et al. 2012, 2013) ▪ Impact of CNF on dewatering during press step (Rantanen and Maloney 2013) ▪ Better dispersion of CNC/CNF, optimization of the pulping conditions (time, retention system, dispersant agents) (Campano et al. 2018)
Multiply approach	0 – 10%	<ul style="list-style-type: none"> ▪ Increase of tensile strength and tensile stiffness (Wildlock and Heijnesson-Hulten 2007) ▪ Increase bonds between each ply of a multiply (Heiskanen and Backfolk 2017) ▪ Increase of strength and optical properties with CNF between TMP pulp (Mörseburg and Chinga-Carrasco 2009)
CNF and polyelectrolyte systems	0 – 30%	<ul style="list-style-type: none"> ▪ Maintaining of drainage rate and increase of paper strength (Taipale et al. 2010) ▪ Improve dimensional stability and tensile strength (Manninen et al. 2011) ▪ Increase wet tensile index (Ahola et al. 2007) ▪ Increase of Young's modulus of 72% and breaking length of 51% (Missoum et al. 2013)

In their study, Taipale et al. (2010), showed that at constant parameters, CNF increased strength but also time of drainage. However, by modifying the process conditions such as polyelectrolytes, pH, salt concentration it is possible to enhance the strength without affecting the drainability. Researchers from UPM-Kymene (Kajanto and Kosonen, 2012) came into a similar conclusion by proving that CNF addition by one or two percents and simultaneous addition of cationic starch do not affect the dewatering process and enhance air barrier and mechanical properties which was calculated as a possible decrease of 8 g/m² of basis weight. It has been found that the fiber defibrillation process influence the paper dewatering properties and an optimum combination of strength and dewatering was obtained by one pass through a microfluidizer (further passes decrease dewatering and do not improve strength) (Rantanen et al. 2015). Moreover, some authors showed that an in-situ precipitation of calcium carbonate on the surface of CNF overcomes the lack of dewatering performance of CNF on high filler content (70%) biocomposites containing

CNF (Rantanen and Maloney 2015). This research team developed a continuous pilot scale forming method suitable for CNF and other composite wood materials (Pirttiniemi et al. 2014).

4.4. Surface coatings

Most of the time in order to improve barriers, printing or add functional properties (Antimicrobial, hydrophobic paper), nanocellulose can be introduced in paper surface treatments thanks to different processes of coating or impregnation. If the bulk insertion is mainly limited to cellulose nanofibrils, the surface addition concerns both cellulose nanocrystals and nanofibrils and has several assets for paper and packaging applications (Hubbe et al. 2017). Because of the high viscosity of these materials which form a strong gel at low dry content (1% for CNFs, 10% for CNCs), the deposited quantity is often small. However, some researchers have also proposed the coating of paper with 100% cellulose nanofibrils (Syverud and Stenius 2009; Hult et al. 2010; Lavoine and Desloges 2014) and very recently, with 100% cellulose nanocrystals (Gicquel et al. 2017). In coating, CNFs and CNCs are assumed to fill the voids of the structure. This has consequences on surface porosity, roughness, optical properties, barrier properties and mechanical properties. The different strategies for nanocellulose-based paper coating are synthesized in Figure 25.

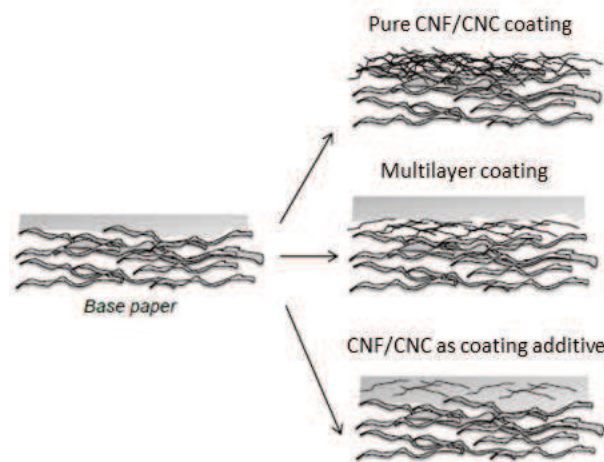


Figure 25: Different strategy for the use of cellulose nanofibrils and nanocrystals in surface treatment of a paper, adapted from (Bardet and Bras 2014)

4.4.1. Pure CNF/CNC coating in one or multilayer application

Due to the high viscosity of both cellulose nanofibril and cellulose nanocrystal suspensions at low solid content and price of these materials, this strategy has rarely been investigated. Recent progress for reducing production cost and market availability of these materials has led some researchers to consider this strategy. In the publication of Gicquel (Gicquel et al. 2017), different numbers of CNC layers were deposited with bar coating to decrease the air permeability and increase the grease resistance. Optical properties were also targeted, with the increase of gloss. The coating

of a cardboard with CNC has also allowed the deposition of electronic inks for printed electronic application, ink also composed with a mixture of silver and CNC (Hoeng et al. 2017). Indeed, printing process often requires smooth and closed surface to prevent the ink to penetrate into the paper (Reverdy 2017). This is particularly true for printing electronic where conductive properties are dependent on the formation of continuous lines.

Coating with 100% cellulose nanofibrils has been among the first strategies. Different coating methods can be used such as filtration via sheet former, bar coating, size press, spray coating or slot die. The key parameters of this strategy are (i) the quantity of CNF deposited at the surface and (ii) the homogeneity of this layer. These points have been source of challenge since the first deposition of a CNF layer on a paper in 2009 (Syverud and Stenius 2009) as it strongly affects the final paper properties.

Homogeneous layer. In 2009, 1 wt% of CNF suspension was deposited onto paper using dynamic sheet former with a coat weight between 2 and 8 g/m² (Syverud and Stenius 2009). The mechanical properties of the sheet were improved (increase by 28 % regarding the tensile strength) and the air permeability decreased drastically compared to the initial sheet. However, due to high viscosity of this material, heterogeneities of CNF layers were observed. Decrease of air permeability by 98% was also observed by (Hult et al. 2010), unfortunately this study also reported a very high oxygen permeability explained by a non-homogeneous CNF coating. Homogeneity has consequently been a recurrent issue for the coating of 100% CNF layers. This problem has been overcome by Aulin (Aulin et al. 2010) who managed to obtain homogeneous CNF layers (up to 2 g/m²) with a rod coater, leading to low air permeability but also good oil resistance.

CNF amount/Influence of coating process. Classical coating methods such as bar coating do not permit high coating thickness in one pass as CNF suspensions are usually containing very low dry matter contents (0.8 to 2wt%) (Aulin et al., 2010). Since 2010, a large panel of coating processes have been tested. (Beneventi et al. 2014) used the spray coating technique to deposit nanocellulose on paper and reported a decrease of air permeability. The same year, a publication from Lavoine (Lavoine and Desloges 2014) compared the impact of bar coating vs size press processes on resulting mechanical and barrier properties of the paper. She proved that the air barrier and the bending stiffness were considerably improved (+ 90% and +50% respectively) especially when bar coating was used, corresponding to an amount of 7 g/m² of CNF. Size press was not able to considerably improve the paper properties due to the difficulty to deposit large amounts of CNF (4 g/m² after ten passes in the size press). Lately, bar coating has also been used by Afra et al (Afra et al. 2016) who has reported that CNF coating improves surface smoothness, surface strength, tensile strength, stiffness and air resistance of paper. They proved in particular that for the same coat weight, a double coating layer applied at low solids (1.5%) performed better than a single coating layer at high solid content (3%). Recently, Kumar (Kumar et al. 2017), coated a CNF suspension using a pilot scale slot die coater on a paper with a roll-to-roll process and assessed the barrier properties. They showed that 1g/m² was sufficient to improve air, heptane, water vapor, grease and oil barrier, while reducing the WVTR

value of almost 85% and reached values suitable for packaging requirements. Dip and spin coating of CNF on porous cellulose substrate have also been compared (Herrera et al. 2016). They proved that dip coating (deposition of thick layer) is more suitable for substrate with large pore size while spin coating (deposition of thin layer) is more suitable for substrate with small pore size. In another study, Herrera (Herrera et al. 2017) also used dip coating to apply multilayers of nanocellulose on a porous paper in order to improve barrier and mechanical properties for paper packaging applications.

Requirements for good coatability. To increase the coatability and final coating quality, different strategies have been reported such as the addition of CMC (Mousavi et al. 2017), the increase of CNF degree of fibrillation, and the the substrate quality (Ridgway and Gane 2012; Kumar et al. 2017). Kumar studies show in particular that smooth but porous and highly hydrophilic substrate is an optimal.

4.4.2. CNF/CNC as coating additive

Cellulose nanofibrils

In some cases, nanocellulose is not the main component of the coating but can also be used (i) as reinforcement in polymeric matrix (nanocomposite), (ii) as a binder for particles stabilization and allowing efficient dispersion (Bardet et al. 2013), (iii) as a pigment. In these cases, mechanical and barrier properties are still targeted as well as optical properties and printability.

To increase the paper **printing properties**, Hamada (Hamada and Bousfield 2010) proposed two strategies to improve flexographic printability of a 90 g/m² uncoated paper: the replacement by CNF of the pigment or the replacement of the binder in a coating composed of clay pigments and PVOH binder. They reached an increase of 25% of the print density when CNF replaced the PVOH binder. This blend of CNF and PVOH has been patented by Stora enso (Heiskanen and Backfolk 2017) and Kemira (Malmborg et al. 2013). A mixture of CNF and inorganic pigments has also been patented by Omya (Gane et al. 2014). Other works have reported the combination of CNF and AKD, CNF holding the inkjet pigments at the surface while AKD acting as a barrier to liquid penetration in fine papers (Luu et al. 2011). CNF as a filler in combination with inorganic pigments (clays or kaolin) was also mentioned to promote smooth and flexible substrate for printed electronic application (Torvinen et al. 2012)

Mixtures of CNF and PVOH have also been studied by Guezennec (Guezennec 2012) who showed that including CNF in a PVOH suspension for paperboard coating limits the blistering effect of PVOH layer during drying. As a consequence, 5wt% of CNF provides better water vapor **barrier properties** and oxygen barrier properties compared to conventional coating.

Other properties of CNF have been reported such as the decrease of dusting and linting propensity of newspaper (Song et al. 2010) by coating a mixture of anionic starch and CNF.

Cellulose nanocrystals

If cellulose nanocrystals are rarely used alone as a coating on a cellulosic substrate, their use as slurry is quite rare too and only few examples are reported in the literature. In the publication of El-Wakil (El-Wakil et al. 2015), cellulose nanocrystals and titanium dioxide were reported to improve mechanical and water barrier properties as a coating for active food packaging. In this study, gluten-based films containing CNC and titanium dioxide were coated on unbleached kraft paper, and showed interesting antimicrobial properties. Another publication studies the influence of acid hydrolysis (sulfuric acid vs ammonium persulfate) on resulting coating on flexible-food packaging (Mascheroni et al. 2016). However, in this case, coating was applied on plastic films (PET) and not on a paper substrate.

However, the addition of a small amount of CNC to a polymer matrix to increase mechanical or barrier properties has been widely studied as nanocomposite films and many reviews already exist to relate the advantage for mechanical and barrier properties (Siró and Plackett 2010; Moon et al. 2011; Mariano et al. 2014; Oksman et al. 2016). All these performances of nanocomposites represent as many opportunities for paper industries. Recently, interest of cellulose nanocrystals for banknote application has been raised with a recent patent from Oberthur (Le Berre et al. 2015) which proposed to use cellulose nanocrystals inside banknote varnish to improve soil resistance as well as hydrophobic and oleophobic properties, and thus guarantee printing quality. Iridescence properties of cellulose nanocrystals have also attracted the attention of specialty paper industries. Bardet et al. (Bardet et al. 2015) have created iridescent pigments from cellulose nanocrystals from CNC liquid-crystalline suspensions and appropriate dry grinding. Authors targeted an application in paper anticounterfeiting features.

The use of nanocellulose in association with a polymeric matrix strongly depends of one parameter: the percolation threshold. Indeed, when nanocellulose is used as reinforcement within a continuous polymeric matrix, many studies have reported a maximum in strength at a certain level of reinforcement followed by a decline in strength for higher nanocellulose contents (Zimmerman 2004, Martinez-Sanz 2013c, Rafieian and simonsen 2014). The optimum point is often said to be associated with a percolation threshold, i.e. the proportion of CNF or CNC that is just sufficient to fill the volume with an interconnecting structure (Dufresne 2008; Moon et al. 2011). For higher contents, agglomeration phenomena are responsible of a decrease of strength.

Following these observations, Table 12 synthesizes the current opportunities regarding the use of CNF or CNC as a paper coating material.

Table 12: CNF and CNC properties when added in a surface treatment of a paper

Content	Cellulose nanofibrils	Cellulose nanocrystals
Pure coating 0 – 8 g/m ²	<ul style="list-style-type: none"> ▪ Oil resistance (Aulin et al. 2010) ▪ Air barrier (Syverud and Stenius 2009; Lavoine and Desloges 2014; Beneventi et al. 2014; Afra et al. 2016) ▪ (Syverud and Stenius 2009) ▪ Surface smoothness, (Afra et al. 2016) ▪ Surface strength (Syverud and Stenius 2009; Afra et al. 2016) ▪ +50% bending stiffness with 7g/m² CNF (Lavoine and Desloges 2014) ▪ Air, heptane, vapor, grease and oil barrier (Kumar et al. 2017) 	<ul style="list-style-type: none"> ▪ Decrease of air permeability and increase of grease resistance (Gicquel et al. 2017) ▪ Use of CNC for increase substrate properties of a cardboard for printed electronic application with an inked also containing CNC (Hoeng et al. 2017)
CNF/CNC as a coating additive 0.05 – 50 wt%	<ul style="list-style-type: none"> ▪ CNF and TiO₂ for increase of opacity (Bardet et al. 2013) ▪ Increase of printing properties (Hamada and Bousfield 2010; Luu et al. 2011) ▪ CNF for dispersion of inorganic pigments (Gane et al. 2014) ▪ Increase of barrier properties (Guezennec 2012) ▪ Decrease of dusting and linting of newspapers (Song et al. 2010) ▪ Increase of smoothness and flexibility for electronic printing application (Torvinen et al. 2012) 	<ul style="list-style-type: none"> ▪ CNC as iridescent pigment (Bardet et al. 2015) ▪ CNC in varnish for banknote soil resistance and oil resistance (Le Berre et al. 2015) ▪ CNC for improving mechanical and water barrier properties as a coating for active food packaging (El-Wakil et al. 2015)

4.5. Synthesis of nanocellulose strengths and weaknesses in paper industry and application for dog-ears and crumpling limitation

Cellulose nanofibrils and cellulose nanocrystals are promising materials for paper, cardboard and packaging applications with many positive impacts in bulk or in surface treatment (Figure 26). They are indeed expected to replace petroleum based materials (strengthening agents, latex,...) especially in coating which is mainly represented by plastic materials. However, to be fully competitive with existing products in the market, nanocellulose has to meet some requirements such as (i) competitive cost and (ii) easy processability. As already explained, new breakthrough in the production of CNFs and CNCs have reduced the price and allows up-scale production, but it still exists cheaper alternatives on the market. Furthermore, a large range of different qualities of cellulose nanofibrils exist in the market as this material is strongly process-dependant (Syverud et al. 2011; Kumar et al. 2017), and not always fully characterized. This is important as different properties of CNF will symmetrically lead to different paper properties. Furthermore, high viscosity at low dry content may lock some industrial development. Another issue is the hygroscopic character of nanocellulose: the uptake of moisture from atmosphere tends to be one of the most intractable problems associated in particular with the conservation of barrier properties (Hubbe et al. 2017). Some progresses have already been addressed to prevent this water uptake holding great promises (Vartiainen et al. 2016). The Figure 26 shows the advantages and the challenges still pending in paper industry for bulk addition or surface treatment.

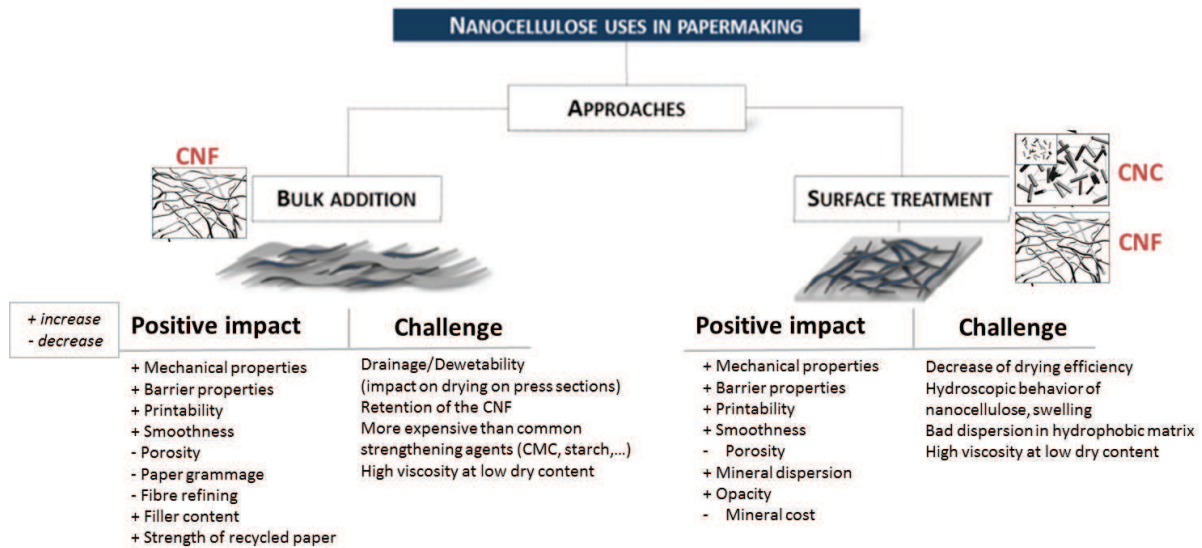


Figure 26: Use of nanocellulose in papermaking industry, adapted from (Reverdy 2017)

Finally, as paper production is an online process, future challenge will be the upgrading of existing products (grinders, homogenizers, microfluidizers,...) in online procedures and characterization with online quality control.

In this project, two strategies will be implemented in order to increase banknote substrate quality: (i) introduction of CNC within the PVOH matrix in the impregnation bath and (ii) a multilayer design with insertion of a CNF layer between the two cotton fiber layers. Cellulose nanocrystals reinforcement in the PVOH bath are expected to increase the strength of this layer and create a resistance to dog-ears, while the introduction of the CNF layer is expected to create a flexible and entangled network resisting to crumpling. No other scientific publication never reported the use of cellulose nanofibrils and cellulose nanocrystals for dog-ears and crumpling limitation in a paper application.

Conclusion

This **chapter I** introduces the general context (paper industry), the main raw materials (cellulose nanofibrils and cellulose nanocrystals) and the targeted applications (crumpling and dog-ears limitation) of this PhD project.

This work has the objective to limit banknote defects caused by manual handling: dog-ears and crumpling. The first one is the second reason of banknote destruction in sorting centers behind soil. No data still exists for the crumpling as there is no sensor in sorting centers to detect it, but this defect leads to circulation of banknote below the quality requirements and can easily result in a lack of mechanical properties, or “limp” banknotes. In both cases, dog-ears and crumpling reduce the banknote lifetime and cause large economic troubles. Nevertheless, no viable solution exists for now to prevent them. More generally, paper crumpling and folding events involve complex mechanisms and their understanding or limitation remain rarely investigated.

These last years, cellulose nanofibrils and cellulose nanocrystals have raised the scientific interest in paper-making industry. Thanks to the research advances and the up-scaling of nanocellulose producers, CNC and CNF are now available in large quantities and the increase of patent numbers proves the current interest for these natural materials with outstanding properties. Nowadays, the use of nanocellulose in paper and packaging industries is making the leap to massive industrialisation, targeting both high added value application markets and large volumes.

Nanocellulose already succeeds in improving the mechanical and barrier properties of paper for various applications. However, up to our knowledge, no publication mentions the use of nanocellulose for paper crumpling and folding limitation. This project consequently proposes innovative strategies for the improvement of banknote substrate with cellulose based products.

Challenges.

The main original feature of this project is to study how CNCs and CNFs contribute in improving banknote substrate quality and resistance under dog-ears or to crumpling deformation. This study will be divided into 4 chapters (Figure 27). **Chapter I** was dedicated to the literature review. The next chapter (**chapter II**) focuses on the decrease of dog-ears defect. In this chapter, CNCs are introduced in the PVOH impregnation bath. Indeed, CNCs are well known for their reinforcing effect and their use for nanocomposites. This chapter investigates the influence of the impregnation process and drying on CNC-reinforced PVOH properties and their resulting impact on the paper dog-ears resistance. On the other hand, CNFs are known to form a strong, cohesive, flexible and entangled network thanks to their large aspect ratio and high bonding ability. In **chapter III**, a CNF layer is introduced between the two fiber layers classically composing the banknote substrate. The behavior of this layer will be analyzed independently under the form of a nanopaper, and within the paper to quantify its impact on crumpling resistance. Finally, **Chapter IV** concludes this project by the combination of the two strategies for the production of a performant material

resistant to both dog-ears and crumpling. An up-scaling is then proposed with pilot and even industrial scale trials and their characterizations.

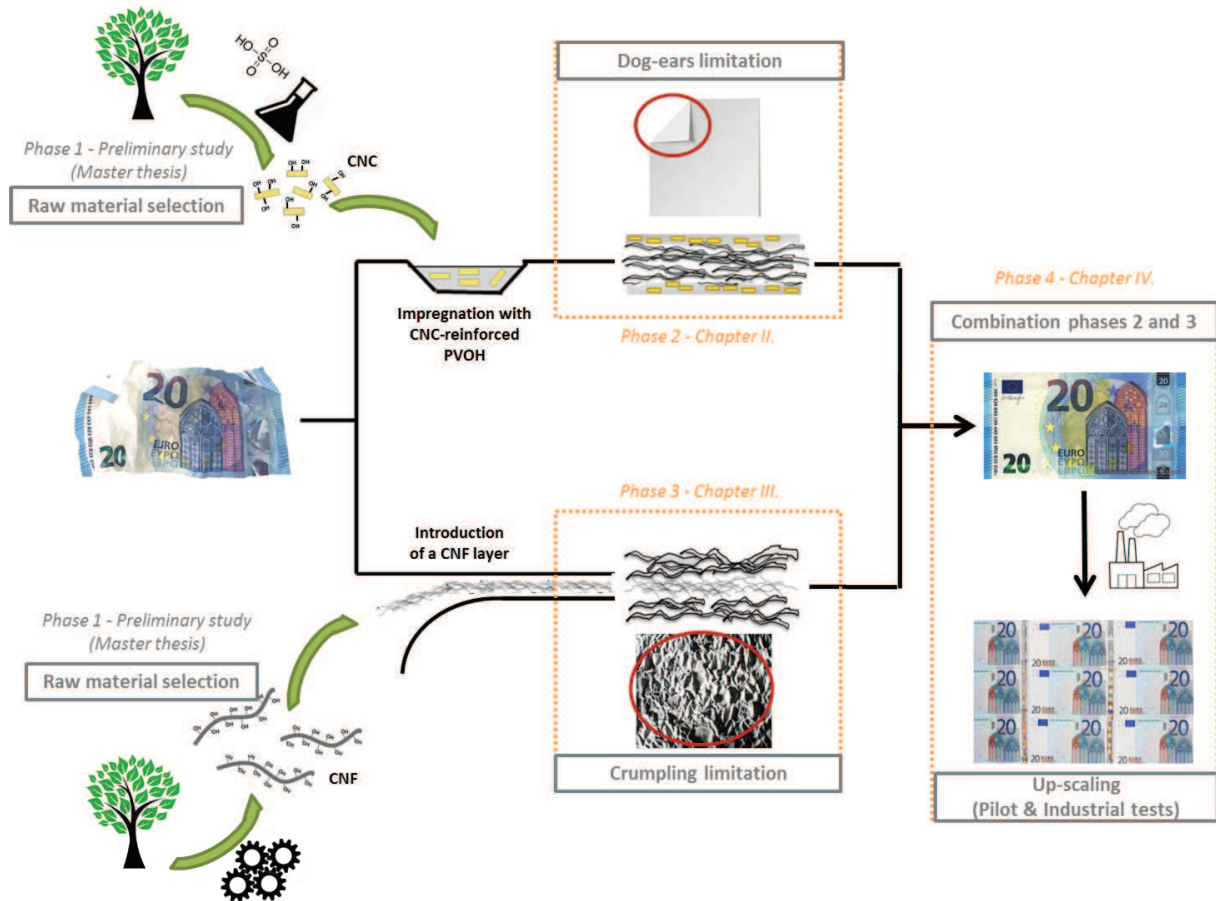


Figure 27: General overview of the project

References

- Abdul Khalil HPS, Davoudpour Y, Islam MN, et al (2014) Production and modification of nanofibrillated cellulose using various mechanical processes: A review. *Carbohydr Polym* 99:649–665. doi: 10.1016/j.carbpol.2013.08.069
- Abidi N, Hequet E, Tarimala S (2007) Functionalization of Cotton Fabric with Vinyltrimethoxysilane. *Text Res J* 77:668–674. doi: 10.1177/0040517507080621
- Abitbol T, Rivkin A, Cao Y, et al (2016) Nanocellulose, a tiny fiber with huge applications. *Curr Opin Biotechnol* 39:76–88. doi: 10.1016/j.copbio.2016.01.002
- Afra E, Mohammadnejad S, Saraeyan A (2016) Cellulose nanofibils as coating material and its effects on paper properties. *Prog Org Coat Complete*:455–460. doi: 10.1016/j.porgcoat.2016.09.018
- Ago M, Okajima K, Jakes JE, et al (2012) Lignin-based electrospun nanofibers reinforced with cellulose nanocrystals. *Biomacromolecules* 13:918–926. doi: 10.1021/bm201828g
- Ahola S, Österberg M, Laine J (2007) Cellulose nanofibrils—adsorption with poly(amideamine) epichlorohydrin studied by QCM-D and application as a paper strength additive. *Cellulose* 15:303–314. doi: 10.1007/s10570-007-9167-3
- Aloui H, Khwaldia K, Hamdi M, et al (2016) Synergistic effect of halloysite and cellulose nanocrystals on the functional properties of PVA based nanocomposites. *ACS Sustain Chem Eng* 4:794–800. doi: 10.1021/acssuschemeng.5b00806
- Andresen CA, Hansen A, Schmittbuhl J (2007) Ridge network in crumpled paper. *Phys Rev E Stat Nonlin Soft Matter Phys* 76:026108. doi: 10.1103/PhysRevE.76.026108
- Araki J, Kuga S (2001) Effect of Trace Electrolyte on Liquid Crystal Type of Cellulose Microcrystals. *Langmuir* 17:4493–4496. doi: 10.1021/la0102455
- Armentano I, Dottori M, Fortunati E, et al (2010) Biodegradable polymer matrix nanocomposites for tissue engineering: A review. *Polym Degrad Stab* 95:2126–2146. doi: 10.1016/j.polymdegradstab.2010.06.007
- Aulin C, Gällstedt M, Lindström T (2010) Oxygen and oil barrier properties of microfibrillated cellulose films and coatings. *Cellulose* 17:559–574. doi: 10.1007/s10570-009-9393-y
- Ávila Ramírez JA, Fortunati E, Kenny JM, et al (2017) Simple citric acid-catalyzed surface esterification of cellulose nanocrystals. *Carbohydr Polym* 157:1358–1364. doi: 10.1016/j.carbpol.2016.11.008
- Azizi Samir MAS, Alloin F, Sanchez J-Y, Dufresne A (2004) Cellulose nanocrystals reinforced poly(oxyethylene). *Polymer* 45:4149–4157. doi: 10.1016/j.polymer.2004.03.094
- Bai Y-X, Li Y-F (2006) Preparation and characterization of crosslinked porous cellulose beads. *Carbohydr Polym* 64:402–407. doi: 10.1016/j.carbpol.2005.12.009
- Bajpai P (2016) *Pulp and Paper Industry: Nanotechnology in Forest Industry*. Elsevier. ISBN: 978-0-12-811102-4
- Balankin AS, Silva IC, Martínez OA, Huerta OS (2007) Scaling properties of randomly folded plastic sheets. *Phys Rev E* 75:051117. doi: 10.1103/PhysRevE.75.051117
- Bardet R (2006) *Nanocelluloses as Potential Materials for Speciality Papers*. PhD thesis. Université Grenoble Alpes
- Bardet R, Belgacem MN, Bras J (2013) Different strategies for obtaining high opacity films of MFC with TiO₂ pigments. *Cellulose* 20:3025–3037. doi: 10.1007/s10570-013-0025-1
- Bardet R, Bras J (2014) Cellulose Nanofibers and Their Use in Paper Industry. In: *Handbook of Green Materials*. World Scientific, Chapter 13, pp 207–232.
- Bardet R, Roussel F, Coindeau S, et al (2015) Engineered pigments based on iridescent cellulose nanocrystal films. *Carbohydr Polym* 122:367–375. doi: 10.1016/j.carbpol.2014.10.020

- Beck S, Bouchard J, Berry R (2011) Controlling the Reflection Wavelength of Iridescent Solid Films of Nanocrystalline Cellulose. *Biomacromolecules* 12:167–172. doi: 10.1021/bm1010905
- Ben Amar M, Pomeau Y (1997) Crumpled paper. *Proc R Soc Math Phys Eng Sci* 453:729–755. doi: 10.1098/rspa.1997.0041
- Ben Azouz K, Ramires EC, Fonteyne WV den, et al (2012) Simple Method for the Melt Extrusion of a Cellulose Nanocrystal Reinforced Hydrophobic Polymer. *ACS Macro Lett* 1:236–240. doi: 10.1021/mz2001737
- Beneventi D, Chaussy D, Curtil D, et al (2014) Highly Porous Paper Loading with Microfibrillated Cellulose by Spray Coating on Wet Substrates. *Ind Eng Chem Res* 53:10982–10989. doi: 10.1021/ie500955x
- Bharimalla AK, Deshmukh SP, Patil PG, Vigneshwaran N (2015) Energy Efficient Manufacturing of Nanocellulose by Chemo- and Bio-Mechanical Processes: A Review. *World J Nano Sci Eng* 05:204. doi: 10.4236/wjnse.2015.54021
- Blair DL, Kudrolli A (2005) Geometry of Crumpled Paper. *Phys Rev Lett* 94:166107. doi: 10.1103/PhysRevLett.94.166107
- Bolaski W, Gallatin JC (1962) Enzymatic conversion of cellulosic fibers. *Hammermill Massachusetts Paper*. US3041246A
- Bondeson D, Oksman K (2007) Dispersion and characteristics of surfactant modified cellulose whiskers nanocomposites: Composite Interfaces: Vol 14, No 7-9. *Compos Interfaces* 14:617–630. doi: 10.1163/156855407782106519
- Börjesson M, Westman G (2015) Crystalline Nanocellulose — Preparation, Modification, and Properties. *Cellul - Fundam Asp Curr Trends*. doi: 10.5772/61899
- Boué L, Adda-Bedia M, Boudaoud A, et al (2006) Spiral Patterns in the Packing of Flexible Structures. *Phys Rev Lett* 97:166104. doi: 10.1103/PhysRevLett.97.166104
- Boufi S, González I, Delgado-Aguilar M, et al (2016) Nanofibrillated cellulose as an additive in papermaking process: A review. *Carbohydr Polym* 154:151–166. doi: 10.1016/j.carbpol.2016.07.117
- Brandrup J, Immergut EH, Grulke EA (1999) *Polymer Handbook*, 4th edition. Collection Wiley-Interscience.
- Brinchi L, Cotana F, Fortunati E, Kenny JM (2013) Production of nanocrystalline cellulose from lignocellulosic biomass: Technology and applications. *Carbohydr Polym* 94:154–169. doi: 10.1016/j.carbpol.2013.01.033
- Brodin FW, Gregersen OW, Syverud K (2014) Cellulose nanofibrils: Challenges and possibilities as a paper additive or coating material—A review. *Nord Pulp Pap Res J* 29:156–166. doi: 10.3183/NPPRJ-2014-29-01-p156-166
- Campano C, Merayo N, Balea A, et al (2018) Mechanical and chemical dispersion of nanocelluloses to improve their reinforcing effect on recycled paper. *Cellulose* 25:269–280. doi: 10.1007/s10570-017-1552-y
- Carvalho RA, Santos TA, Azevedo VM de, et al (2018) Bio-nanocomposites for food packaging applications: effect of cellulose nanofibers on morphological, mechanical, optical and barrier properties. *Polym Int* 67:386–392. doi: 10.1002/pi.5518
- Cassidy J, Doublet P (1993) Security paper, in particular for use as a passport flyleaf
- Cepi (2017) Key statistics 2016. www.cepi.org. Consulted in May 2018.
- Cervin NT, Andersson L, Ng JBS, et al (2013) Lightweight and strong cellulose materials made from aqueous foams stabilized by nanofibrillated cellulose. *Biomacromolecules* 14:503–511. doi: 10.1021/bm301755u
- Charreau H, L. Foresti M, Vazquez A (2013) Nanocellulose Patents Trends: A Comprehensive Review on Patents on Cellulose Nanocrystals, Microfibrillated and Bacterial Cellulose. *Recent Pat Nanotechnol* 7:56–80. doi: 10.2174/187221013804484854
- Chen D, Lawton D, Thompson MR, Liu Q (2012) Biocomposites reinforced with cellulose nanocrystals derived from potato peel waste. *Carbohydr Polym* 90:709–716. doi: 10.1016/j.carbpol.2012.06.002
- Chen L, Lai C, Marchewka R, et al (2016) Use of CdS quantum dot-functionalized cellulose nanocrystal films for anti-counterfeiting applications. *Nanoscale* 8:13288–13296. doi: 10.1039/C6NR03039D

- Cheng Q, Wang S, Rials TG, Lee S-H (2007) Physical and mechanical properties of polyvinyl alcohol and polypropylene composite materials reinforced with fibril aggregates isolated from regenerated cellulose fibers. *Cellulose* 14:593–602. doi: 10.1007/s10570-007-9141-0
- Cherian BM, Leão AL, De Souza SF, et al (2011) Cellulose nanocomposites with nanofibres isolated from pineapple leaf fibers for medical applications. *Carbohydr Polym* 86:1790–1798. doi: 10.1016/j.carbpol.2011.07.009
- Chiellini E, Corti A, D'Antone S, Solaro R (2003) Biodegradation of poly (vinyl alcohol) based materials. *Prog Polym Sci* 28:963–1014. doi: 10.1016/S0079-6700(02)00149-1
- Chindawong C, Johannsmann D (2014) An anisotropic ink based on crystalline nanocellulose: Potential applications in security printing. *J Appl Polym Sci* 131:. doi: 10.1002/app.41063
- Choo K, Ching YC, Chuah CH, et al (2016) Preparation and characterization of polyvinyl alcohol-chitosan composite films reinforced with cellulose nanofiber. *Materials* 9:E644. doi: 10.3390/ma9080644
- Coste G (2004) Histoire et évolution de la machine à papier. In: Cerig - Grenoble INP Pagora. <http://cerig.pagora.grenoble-inp.fr/histoire-metiers/machine-a-papier>
- Cowles D (2016) The Application of CNF to improve Paper Properties. TAPPI Nano Int Conf Nanotechnol Renew Mater Grenoble Fr
- De France KJ, Hoare T, Cranston ED (2017) Review of Hydrogels and Aerogels Containing Nanocellulose. *Chem Mater* 29:4609–4631. doi: 10.1021/acs.chemmater.7b00531
- Deboeuf S, Katzav E, Boudaoud A, et al (2013) Comparative Study of Crumpling and Folding of Thin Sheets. *Phys Rev Lett* 110:104301. doi: 10.1103/PhysRevLett.110.104301
- Deinhammer H, Ladi A (2017) Modelling euro banknote quality in circulation. *Eur Cent Bank Publ*. doi: 10.2866/02309
- Delgado-Aguilar M, González I, Pèlach MA, et al (2015) Improvement of deinked old newspaper/old magazine pulp suspensions by means of nanofibrillated cellulose addition. *Cellulose* 22:789–802. doi: 10.1007/s10570-014-0473-2
- Demirbas A (2007) Progress and recent trends in biofuels. *Prog Energy Combust Sci* 33:1–18. doi: 10.1016/j.pecs.2006.06.001
- Ding B, Kim H-Y, Lee S-C, et al (2002) Preparation and characterization of a nanoscale poly(vinyl alcohol) fiber aggregate produced by an electrospinning method. *J Polym Sci Part B Polym Phys* 40:1261–1268. doi: 10.1002/polb.10191
- Djafari Petroudy SR, Syverud K, Chinga-Carrasco G, et al (2014) Effects of bagasse microfibrillated cellulose and cationic polyacrylamide on key properties of bagasse paper. *Carbohydr Polym* 99:311–318. doi: 10.1016/j.carbpol.2013.07.073
- Dufresne A (2017) Nanocellulose: From Nature to High Performance Tailored Materials. Walter de Gruyter GmbH & Co KG
- Dufresne A (2013) Nanocellulose: a new ageless bionanomaterial. *Mater Today* 16:220–227. doi: 10.1016/j.mattod.2013.06.004
- Dufresne A (2010) Processing of polymer nanocomposites reinforced with polysaccharide nanocrystals. *Mol Basel Switz* 15:4111–4128. doi: 10.3390/molecules15064111
- Dufresne A (2008) Polysaccharide nano crystal reinforced nanocomposites. *Can J Chem* 86:484–494. doi: 10.1139/v07-152
- Dufresne A, Cavaille J-Y, Vignon MR, others (1997) Mechanical behavior of sheets prepared from sugar beet cellulose microfibrils. *J Appl Polym Sci* 64:1185–1194. doi: 10.1002/(SICI)1097-4628(19970509)64:6
- Dufresne A, Dupeyre D, Vignon MR (2000) Cellulose microfibrils from potato tuber cells: Processing and characterization of starch–cellulose microfibril composites. *J Appl Polym Sci* 76:2080–2092. doi: 10.1002/(SICI)1097-4628(20000628)76:14<2080::AID-APP12>3.0.CO;2-U
- Dufresne A, Thomas S, Pothan LA (2013) *Biopolymer Nanocomposites: Processing, Properties, and Applications*, Wiley

- Ehrenstein GW, Theriault RP (2000) Polymeric materials: structure, properties, applications
- El Miri N, Abdelouahdi K, Zahouily M, et al (2015) Bio-nanocomposite films based on cellulose nanocrystals filled polyvinyl alcohol/chitosan polymer blend. *J Appl Polym Sci* 132:n/a-n/a. doi: 10.1002/app.42004
- El-Wakil NA, Hassan EA, Abou-Zeid RE, Dufresne A (2015) Development of wheat gluten/nanocellulose/titanium dioxide nanocomposites for active food packaging. *Carbohydr Polym* 124:337–346. doi: 10.1016/j.carbpol.2015.01.076
- Favier V, Canova GR, Cavallé JY, et al (1995) Nanocomposite materials from latex and cellulose whiskers. *Polym Adv Technol* 6:351–355. doi: 10.1002/pat.1995.220060514
- Fein K (2016) Cellulose Nanofibrils addition to paper for improvement of barrier properties. TAPPI Nano Int Conf Nanotechnology Renew Mater Grenoble Fr
- Fortunati E, Luzi F, Puglia D, et al (2013a) Ternary PVA nanocomposites containing cellulose nanocrystals from different sources and silver particles: Part II. *Carbohydr Polym* 97:837–848. doi: 10.1016/j.carbpol.2013.05.015
- Fortunati E, Puglia D, Luzi F, et al (2013b) Binary PVA bio-nanocomposites containing cellulose nanocrystals extracted from different natural sources: Part I. *Carbohydr Polym* 97:825–836. doi: 10.1016/j.carbpol.2013.03.075
- Francis KC, Blanch JE, Magleby SP, Howell LL (2013) Origami-like creases in sheet materials for compliant mechanism design. *Mech Sci* 4:371–380. doi: 10.5194/ms-4-371-2013
- Frick JG, Andrews BK, Reid JD (1960) Effects of cross-linkage in wrinkle-resistant cotton fabrics. *Text Res J* 30:495–504. doi: 10.1177/004051756003000704
- Future Markets, Inc (2017) The Global Market for Nanocellulose 2017-2027.
- Gagliardi DD, Gruntfest IJ (1950) Creasing and Creaseproofing of Textiles. *Text Res J* 20:180–188. doi: 10.1177/004051755002000306
- Gane PAC, Schoelkopf J, Gantenbein D, Schenker M (2014) Process for the production of nano-fibrillar cellulose gels. Omya International. US8871056B2
- Garaeva GF, Spiridonova RR, Kochnev AM, Samuilov YD (2012) Radical polymerization of vinyl acetate in individual and mixed solvagens. *Russ J Gen Chem* 82:1834–1837. doi: 10.1134/S1070363212110187
- Gicquel E (2017) Development of stimuli-responsive cellulose nanocrystals hydrogels for smart applications. PhD thesis, Université Grenoble Alpes
- Gicquel E, Martin C, Garrido Yanez J, Bras J (2017) Cellulose nanocrystals as new bio-based coating layer for improving fiber-based mechanical and barrier properties. *J Mater Sci* 52:3048–3061. doi: 10.1007/s10853-016-0589-x
- Giese M, Blusch LK, Khan MK, MacLachlan MJ (2015) Functional Materials from Cellulose-Derived Liquid-Crystal Templates. *Angew Chem Int Ed* 54:2888–2910. doi: 10.1002/anie.201407141
- Gioia F, Dureisseix D, Motro R, Maurin B (2012) Design and Analysis of a Foldable/Unfoldable Corrugated Architectural Curved Envelop. *J Mech Des* 134:031003. doi: 10.1115/1.4005601
- Gjerde E (2008) *Origami Tessellations: Awe-Inspiring Geometric Designs*, A K Peters/CRC Press. ISBN: 978-1-56881-451-3
- González I, Boufi S, Pèlach MA, et al (2012) Nanofibrillated cellulose as paper additive in eucalyptus pulps. *BioResources* 7:5167–5180. Doi: 10.15376/biores.7.4.5167-5180
- González I, Vilaseca F, Alcalá M, et al (2013) Effect of the combination of biobeating and NFC on the physico-mechanical properties of paper. *Cellulose* 20:1425–1435. doi: 10.1007/s10570-013-9927-1
- Gonzalez JS, Ludueña LN, Ponce A, Alvarez VA (2014) Poly(vinyl alcohol)/cellulose nanowhiskers nanocomposite hydrogels for potential wound dressings. *Mater Sci Eng C Mater Biol Appl* 34:54–61. doi: 10.1016/j.msec.2013.10.006

- Guezennec C (2012) Développement de nouveaux matériaux d'emballage à partir de micro- et nano-fibrilles de cellulose. Phd thesis, Université de Grenoble
- Guo R, Ma X, Hu C, Jiang Z (2007) Novel PVA–silica nanocomposite membrane for pervaporative dehydration of ethylene glycol aqueous solution. *Polymer* 48:2939–2945. doi: 10.1016/j.polymer.2007.03.035
- Guyot C, Bacquet G, Schwob J (1992) Folding resistance of magazine papers. *Tappi Proc 1992 Coat Conf* 255–268
- Habibi M, Adda-Bedia M, Bonn D (2017) Effect of the material properties on the crumpling of a thin sheet. *Soft Matter* 13:4029–4034. doi: 10.1039/C6SM02817A
- Habibi Y (2014) Key advances in the chemical modification of nanocelluloses. *Chem Soc Rev* 43:1519–1542. doi: 10.1039/C3CS60204D
- Habibi Y, Dufresne A (2008) Highly Filled Bionanocomposites from Functionalized Polysaccharide Nanocrystals. *Biomacromolecules* 9:1974–1980. doi: 10.1021/bm8001717
- Habibi Y, Lucia LA, Rojas OJ (2010) Cellulose Nanocrystals: Chemistry, Self-Assembly, and Applications. *Chem Rev* 110:3479–3500. doi: 10.1021/cr900339w
- Hamada I, Bousfield DW (2010) Nano-fibrillated cellulose as a coating agent to improve print quality of synthetic fiber sheets. *TAPPI Adv Coat Fundam Symp*
- Hamann L (2011) Wet-end applications of NFC. *SUNPAP Workshop*. Espoo, Finland
- Hanaor DAH, Flores Johnson EA, Wang S, et al (2017) Mechanical properties in crumple-formed paper derived materials subjected to compression. *Heliyon* 3:. doi: 10.1016/j.heliyon.2017.e00329
- Hasan A, Waibhaw G, Tiwari S, et al (2017) Fabrication and characterization of chitosan, polyvinylpyrrolidone, and cellulose nanowhiskers nanocomposite films for wound healing drug delivery application. *J Biomed Mater Res A* 105:2391–2404. doi: 10.1002/jbm.a.36097
- Hassan EA, Hassan ML, Oksman K (2011) Improving Bagasse Pulp Paper Sheet Properties with Microfibrillated Cellulose Isolated from Xylanase-Treated Bagasse. *Wood Fiber Sci* 43:76–82. Doi: 10.1177/0021998312453189
- Heiskanen I, Backfolk K (2017) A process for the production of a composition comprising fibrillated cellulose and a composition. *Stora Enso*. EP2569483B1
- Henriksson M, Berglund LA, Isaksson P, et al (2008) Cellulose Nanopaper Structures of High Toughness. *Biomacromolecules* 9:1579–1585. doi: 10.1021/bm800038n
- Henriksson M, Henriksson G, Berglund LA, Lindström T (2007) An environmentally friendly method for enzyme-assisted preparation of microfibrillated cellulose (MFC) nanofibers. *Eur Polym J* 43:3434–3441. doi: 10.1016/j.eurpolymj.2007.05.038
- Herrera MA, Mathew AP, Oksman K (2017) Barrier and mechanical properties of plasticized and cross-linked nanocellulose coatings for paper packaging applications. *Cellulose* 24:3969–3980. doi: 10.1007/s10570-017-1405-8
- Herrera MA, Sirviö JA, Mathew AP, Oksman K (2016) Environmental friendly and sustainable gas barrier on porous materials: Nanocellulose coatings prepared using spin- and dip-coating. *Mater Des* 93:19–25. doi: 10.1016/j.matdes.2015.12.127
- Hii C, Gregersen ØW, Chinga-Carrasco G, Eriksen Ø (2012) The effect of MFC on the pressability and paper properties of TMP and GCC based sheets. *Nord Pulp Pap Res J* 27:388–396. doi: 10.3183/NPPRJ-2012-27-02-p388-396
- Hoeng F, Bras J, Gicquel E, et al (2017) Inkjet printing of nanocellulose–silver ink onto nanocellulose coated cardboard. *RSC Adv* 7:15372–15381. doi: 10.1039/C6RA23667G
- Hoeng F, Denneulin A, Bras J (2016) Use of nanocellulose in printed electronics: a review. *Nanoscale* 8:13131–13154. doi: 10.1039/C6NR03054H

- Hoffman JD, Weeks JJ (1962) Melting process and the equilibrium melting temperature of polychlorotrifluoroethylene. *J Res Natl Bur Stand A* 66:13–28
- Huang J, Lyu S, Fu F, et al (2017) Green preparation of a cellulose nanocrystals/polyvinyl alcohol composite superhydrophobic coating. *RSC Adv* 7:20152–20159. doi: 10.1039/c6ra27663f
- Hubbe MA, Ferrer A, Tyagi P, et al (2017) Nanocellulose in Thin Films, Coatings, and Plies for Packaging Applications: A Review. *BioResources* 12:2143–2233. doi: 10.15376/biores.12.1.2143-2233
- Hult E-L, Iotti M, Lenes M (2010) Efficient approach to high barrier packaging using microfibrillar cellulose and shellac. *Cellulose* 17:575–586. doi: 10.1007/s10570-010-9408-8
- Kaboorani A, Riedl B, Blanchet P, et al (2012) Nanocrystalline cellulose (NCC): A renewable nano-material for polyvinyl acetate (PVA) adhesive. *Eur Polym J* 48:1829–1837. doi: 10.1016/j.eurpolymj.2012.08.008
- Kalashnikova I, Bizot H, Cathala B, Capron I (2011) New Pickering Emulsions Stabilized by Bacterial Cellulose Nanocrystals. *Langmuir* 27:7471–7479. doi: 10.1021/la200971f
- Kamal MR, Khoshkava V (2015) Effect of cellulose nanocrystals (CNC) on rheological and mechanical properties and crystallization behavior of PLA/CNC nanocomposites. *Carbohydr Polym* 123:105–114. doi: 10.1016/j.carbpol.2015.01.012
- Kangas (2014) Characterization of fibrillated celluloses. A short review and evaluation of characteristics with a combination of methods. *Nord Pulp Pap Res J* 29:129–143. doi: 10.3183/NPPRJ-2014-29-01-p129-143
- Klemm D, Heublein B, Fink H-P, Bohn A (2005) Cellulose: Fascinating Biopolymer and Sustainable Raw Material. *Angew Chem Int Ed* 44:3358–3393. doi: 10.1002/anie.200460587
- Klemm D, Kramer F, Moritz S, et al (2011) Nanocelluloses: a new family of nature-based materials. *Angew Chem Int Ed Engl* 50:5438–5466. doi: 10.1002/anie.201001273
- Kolakovic R, Peltonen L, Laukkanen A, et al (2012) Nanofibrillar cellulose films for controlled drug delivery. *Eur J Pharm Biopharm* 82:308–315. doi: 10.1016/j.ejpb.2012.06.011
- Kumar A, Negi YS, Choudhary V, Bhardwaj NK (2016) Fabrication of poly (vinyl alcohol)/ovalbumin/cellulose nanocrystals/nanohydroxyapatite based biocomposite scaffolds. *Int J Polym Mater Polym Biomater* 65:191–201. doi: 10.1080/00914037.2015.1099102
- Kumar V, Ottesen V, Syverud K, et al (2017) Coatability of Cellulose Nanofibril Suspensions: Role of Rheology and Water Retention. *BioResources* 12:7656–7679. doi: 10.15376/biores.12.4.7656-7679
- Lam YL, Kan CW, Yuen CWM (2010) Wrinkle-resistant finishing of cotton fabric with BTCA—the effect of co-catalyst. *Text Res J* 81:0040517510380777. doi: 10.1177/0040517510380777
- Lavoine N, Bergström L (2017) Nanocellulose-based foams and aerogels: processing, properties, and applications. *J Mater Chem A* 5:16105–16117. doi: 10.1039/C7TA02807E
- Lavoine N, Desloges I (2014) Impact of different coating processes of microfibrillated cellulose on the mechanical and barrier properties of paper. *J Mater Sci* 49:2879–2893. doi: 10.1007/s10853-013-7995-0
- Le Berre M, Gillot J, Borde X (2015) Process for the surface treatment of a security document and associated security document. *Oberthur Fiduciaire*. WO2015091873 A1
- Lee T-J, Lee D-J, Seo J-H, et al (2018) Preventing Discoloration of Poly(vinyl alcohol)-Coated Paper Hydrophobized by Gas Grafting with Palmitoyl Chloride. *ACS Sustain Chem Eng* 6:1702–1707. doi: 10.1021/acssuschemeng.7b02925
- Lee WJ, Clancy AJ, Kontturi E, et al (2016) Strong and stiff: high-performance cellulose nanocrystal/poly (vinyl alcohol) composite fibers. *ACS Appl Mater Interfaces* 8:31500–31504. doi: 10.1021/acsami.6b11578
- Li L, Chan C-M, Li J-X, et al (1999) A Direct Observation of the Formation of Nuclei and the Development of Lamellae in Polymer Spherulites. *Macromolecules* 32:8240–8242. doi: 10.1021/ma991251z

- Liimatainen H, Visanko M, Sirviö JA, et al (2012) Enhancement of the nanofibrillation of wood cellulose through sequential periodate-chlorite oxidation. *Biomacromolecules* 13:1592–1597. doi: 10.1021/bm300319m
- Ljungberg N, Bonini C, Bortolussi F, et al (2005) New Nanocomposite Materials Reinforced with Cellulose Whiskers in Atactic Polypropylene: Effect of Surface and Dispersion Characteristics. *Biomacromolecules* 6:New nanocomposite materials reinforced with cellulose whiskers in atactic polypropylene: effect of surface and dispersion characteristics. doi: 10.1021/bm050222v
- Lobkovsky AE, Witten TA (1997) Properties of ridges in elastic membranes. *Phys Rev E* 55:1577–1589. doi: 10.1103/PhysRevE.55.1577
- Lu B a. I, Ping QU, Yuan G a. O, et al (2011) Pervaporation Properties and Characterization of Poly(vinyl alcohol)/Cellulose Nanocrystal Composite Membranes. *Chem J Chin Univeristies* 32:984–989. ISSN: 0251-0790
- Luu WT, Bousfield DW, Kettle J (2011) Application of nano-fibrillated cellulose as a paper surface treatment for inkjet printing. *Pap Conf*
- Madani A, Kiiskinen H, Olson J, Martinez DM (2011) Fractionation of microfibrillated cellulose and its effects on tensile index and elongation of paper. *Nord Pulp Pap Res J* 26:306–311. doi: 10.3183/NPPRJ-2011-26-03-p306-311
- Malmberg K, Heijnesson-Hulten AM, Sandström J (2013) Cellulosic barrier composition comprising anionic polymer. Akzo Nobel Chemicals International. US13697540
- Mandal A, Chakrabarty D (2014) Studies on the mechanical, thermal, morphological and barrier properties of nanocomposites based on poly(vinyl alcohol) and nanocellulose from sugarcane bagasse. *J Ind Eng Chem* 20:462–473. doi: 10.1016/j.jiec.2013.05.003
- Manninen M, Kajanto I, Happonen J, Paltakari J (2011) The effect of microfibrillated cellulose addition on drying shrinkage and dimensional stability of wood-free paper. *Nord Pulp Pap Res J* 26:297–305. ISSN: 0283-2631
- Mariano M, Chirat C, El Kissi N, Dufresne A (2016) Impact of cellulose nanocrystal aspect ratio on crystallization and reinforcement of poly(butylene adipate-co-terephthalate). *J Polym Sci Part B Polym Phys* 54:2284–2297. doi: 10.1002/polb.24139
- Mariano M, El Kissi N, Dufresne A (2014) Cellulose nanocrystals and related nanocomposites: Review of some properties and challenges. *J Polym Sci Part B Polym Phys* 52:791–806. doi: 10.1002/polb.23490
- Martoia F, Cochereau T, Dumont PJJ, et al (2016) Cellulose nanofibril foams: Links between ice-templating conditions, microstructures and mechanical properties. *Mater Des* 104:376–391. doi: 10.1016/j.matdes.2016.04.088
- Mascheroni E, Rampazzo R, Ortenzi MA, et al (2016) Comparison of cellulose nanocrystals obtained by sulfuric acid hydrolysis and ammonium persulfate, to be used as coating on flexible food-packaging materials. *Cellulose* 23:779–793. doi: 10.1007/s10570-015-0853-2
- Meree CE, Schueneman GT, Meredith JC, Shofner ML (2016) Rheological behavior of highly loaded cellulose nanocrystal/poly (vinyl alcohol) composite suspensions. *Cellulose* 23:3001–3012. doi: 10.1007/s10570-016-1003-1
- Missoum K, Martoia F, Belgacem MN, Bras J (2013) Effect of chemically modified nanofibrillated cellulose addition on the properties of fiber-based materials. *Ind Crops Prod* 48:98–105. doi: 10.1016/j.indcrop.2013.04.013
- Montes S, Carrasco PM, Ruiz V, et al (2015) Synergistic reinforcement of poly (vinyl alcohol) nanocomposites with cellulose nanocrystal-stabilized graphene. *Compos Sci Technol* 117:26–31. doi: 10.1016/j.compscitech.2015.05.018
- Moon RJ, Martini A, Nairn J, et al (2011) Cellulose nanomaterials review: structure, properties and nanocomposites. *Chem Soc Rev* 40:3941–3994. doi: 10.1039/C0CS00108B
- Mörseburg K, Chinga-Carrasco G (2009) Assessing the combined benefits of clay and nanofibrillated cellulose in layered TMP-based sheets. *Cellulose* 16:795–806. doi: 10.1007/s10570-009-9290-4
- Mousavi SMM, Afra E, Tajvidi M, et al (2017) Cellulose nanofiber/carboxymethyl cellulose blends as an efficient coating to improve the structure and barrier properties of paperboard. *Cellulose* 24:3001–3014. doi: 10.1007/s10570-017-1299-5

- Myers S, Lee L-B, Loo L, et al (2014) Crystallizable Block Copolymers: Earlier projects. In: Princet. Chem. Biol. Eng. <https://www.princeton.edu/cbe/people/faculty/register/group/research/completed-projects/crystallization-early/>. Accessed 25 Jan 2018
- Naderi A, Lindström T, Sundström J (2014) Carboxymethylated nanofibrillated cellulose: rheological studies. *Cellulose* 21:1561–1571. doi: 10.1007/s10570-014-0192-8
- Nagalakshmaiah M (2016) Melt processing of cellulose nanocrystals : thermal, mechanical and rheological properties of polymer nanocomposites. Phd thesis, Université Grenoble Alpes
- Narain R, Pfaff T, O'Brien JF (2013) Folding and crumpling adaptive sheets. *ACM Trans Graph* 32:1. doi: 10.1145/2461912.2462010
- Natterodt JC, Shirole A, Sapkota J, et al (2018) Polymer nanocomposites with cellulose nanocrystals made by co-precipitation. *J Appl Polym Sci* 134:45648. doi: 10.1002/app.45648
- Nechyporchuk O, Belgacem MN, Bras J (2014) Production of cellulose nanofibrils: A review of recent advances. *Ind Crops Prod* 93:2–25. doi: 10.1016/j.indcrop.2016.02.016
- Noshirvani N, Ghanbarzadeh B, Fasihi H, Almasi H (2016) Starch–PVA nanocomposite film incorporated with cellulose nanocrystals and MMT: a comparative study. *Int J Food Eng* 12:37–48. doi: 10.1515/ijfe-2015-0145
- Noshirvani N, Hong W, Ghanbarzadeh B, et al (2018) Study of cellulose nanocrystal doped starch-polyvinyl alcohol bionanocomposite films. *Int J Biol Macromol* 107:2065–2074. doi: 10.1016/j.ijbiomac.2017.10.083
- Oksman K, Aitomäki Y, Mathew AP, et al (2016) Review of the recent developments in cellulose nanocomposite processing. *Compos Part Appl Sci Manuf* 83:2–18. doi: 10.1016/j.compositesa.2015.10.041
- Oksman K, Mathew AP, Bismark A, et al (2014) Self- and direct-assembling of bionanomaterials. In: *Handbook of Green Materials*. Volume 3. p 1124. ISBN: 978-981-4566-45-2
- Olszewska A, Eronen P, Johansson L-S, et al (2011) The behaviour of cationic NanoFibrillar Cellulose in aqueous media. *Cellulose* 18:1213. doi: 10.1007/s10570-011-9577-0
- Osong SH, Norgren S, Engstrand P (2016) Processing of wood-based microfibrillated cellulose and nanofibrillated cellulose, and applications relating to papermaking: a review. *Cellulose* 23:93–123. doi: 10.1007/s10570-015-0798-5
- O'Sullivan AC (1997) The structure slowly unravels. *Cellulose* 4:173–207. doi: 10.1023/A:1018431705579
- Ouzas A, Niinivaara E, Cranston ED, Dubé MA (2018) In Situ Semibatch Emulsion Polymerization of 2-Ethyl Hexyl Acrylate/n-Butyl Acrylate/Methyl Methacrylate/Cellulose Nanocrystal Nanocomposites for Adhesive Applications. *Macromol React Eng* 0:1700068. doi: 10.1002/mren.201700068
- Pääkkö M, Ankerfors M, Kosonen H, et al (2007) Enzymatic Hydrolysis Combined with Mechanical Shearing and High-Pressure Homogenization for Nanoscale Cellulose Fibrils and Strong Gels. *Biomacromolecules* 8:1934–1941. doi: 10.1021/bm061215p
- Paiva MC, Zhou B, Fernando KAS, et al (2004) Mechanical and morphological characterization of polymer–carbon nanocomposites from functionalized carbon nanotubes. *Carbon* 42:2849–2854. doi: 10.1016/j.carbon.2004.06.031
- Panaitescu DM, Donescu D, Bercu C, et al (2007) Polymer composites with cellulose microfibrils. *Polym Eng Sci* 47:1228–1234. doi: 10.1002/pen.20803
- Pandey JK, Lee CS, Ahn S-H (2010) Preparation and properties of bio-nanoreinforced composites from biodegradable polymer matrix and cellulose whiskers. *J Appl Polym Sci* 115:2493–2501. doi: 10.1002/app.31205
- Pearson NG, Howland P (2008) Paper including watermarks and/or embossings. De la Rue International. US10496686
- Pennings AJ (1980) Polymer crystallization. *J Cryst Growth* 48:574–581. doi: 10.1016/0022-0248(80)90268-7

- Pereira ALS, do Nascimento DM, Morais JPS, et al (2014) Improvement of polyvinyl alcohol properties by adding nanocrystalline cellulose isolated from banana pseudostems. *Carbohydr Polym* 112:165–172. doi: 10.1016/j.carbpol.2014.05.090
- Peresin MS, Habibi Y, Vesterinen A-H, et al (2010a) Effect of Moisture on Electrospun Nanofiber Composites of Poly(vinyl alcohol) and Cellulose Nanocrystals. *Biomacromolecules* 11:2471–2477. doi: 10.1021/bm1006689
- Peresin MS, Habibi Y, Zoppe JO, et al (2010b) Nanofiber Composites of Polyvinyl Alcohol and Cellulose Nanocrystals: Manufacture and Characterization. *Biomacromolecules* 11:674–681. doi: 10.1021/bm901254n
- Peresin MS, Vesterinen A-H, Habibi Y, et al (2014) Crosslinked PVA nanofibers reinforced with cellulose nanocrystals: Water interactions and thermomechanical properties. *J Appl Polym Sci* 131:40334. Doi: 10.1002/app.40334
- Pérez J, Muñoz-Dorado J, de la Rubia T, Martínez J (2002) Biodegradation and biological treatments of cellulose, hemicellulose and lignin: an overview. *Int Microbiol Off J Span Soc Microbiol* 5:53–63. doi: 10.1007/s10123-002-0062-3
- Pirttiniemi J, Rantanen J, Kuosmanen P, Maloney T, (2014), Development of a Microfibrillated Cellulose Composite Web Forming Method, 2014 TAPPI International Conference on Nanotechnology for Renewable Materials, Vancouver (Canada)
- Popescu M-C (2017) Structure and sorption properties of CNC reinforced PVA films. *Int J Biol Macromol* 101:783–790. doi: 10.1016/j.ijbiomac.2017.03.168
- Pradier C, Cavoret J, Dureisseix D, et al (2016) An Experimental Study and Model Determination of the Mechanical Stiffness of Paper Folds. *J Mech Des* 138:041401. doi: 10.1115/1.4032629
- Pukánszky B, Mudra I, Staniek P (1997) Relation of crystalline structure and mechanical properties of nucleated polypropylene. *J Vinyl Addit Technol* 3:53–57. doi: 10.1002/vnl.10165
- Qing Y, Sabo R, Zhu JY, et al (2013) A comparative study of cellulose nanofibrils disintegrated via multiple processing approaches. *Carbohydr Polym* 97:226–234. doi: 10.1016/j.carbpol.2013.04.086
- Qua EH, Hornsby PR, Sharma HS, et al (2009) Preparation and characterization of poly (vinyl alcohol) nanocomposites made from cellulose nanofibers. *J Appl Polym Sci* 113:2238–2247. doi: 10.1002/app.30116
- Rånby BG, Ribí E (1950) Über den Feinbau der Zellulose. *Experientia* 6:12–14. doi: 10.1007/BF02154044
- Rantanen J, Maloney TC (2013) Press dewatering and nip rewetting of paper containing nano-and microfibril cellulose. *Nord Pulp Pap Res J* 28:582–587. doi: 10.3183/NPPRJ-2013-28-04-p582-587
- Rantanen J, Dimic-Misic K, Kuusisto J, Maloney TC (2015) The effect of micro and microfibrillated cellulose water uptake on high filler content composite paper properties and furnish dewatering. *Cellulose* 22:4003–4015. doi: 10.1007/s10570-015-0777-x
- Rantanen J, Maloney TC (2015) Consolidation and dewatering of a microfibrillated cellulose fiber composite paper in wet pressing. *Eur Polym J* 68:585–591. doi: 10.1016/j.eurpolymj.2015.03.045
- Rescignano N, Fortunati E, Montesano S, et al (2014) PVA bio-nanocomposites: A new take-off using cellulose nanocrystals and PLGA nanoparticles. *Carbohydr Polym* 99:47–58. doi: 10.1016/j.carbpol.2013.08.061
- Reverdy C (2017) Industrial applications of functional nanocelluloses. PhD thesis. Université Grenoble Alpes
- Revol J-F, Bradford H, Giasson J, et al (1992) Helicoidal self-ordering of cellulose microfibrils in aqueous suspension. *Int J Biol Macromol* 14:170–172. doi: 10.1016/S0141-8130(05)80008-X
- Ridgway CJ, Gane PAC (2012) Constructing NFC-pigment composite surface treatment for enhanced paper stiffness and surface properties. *Cellulose* 19:547–560. doi: 10.1007/s10570-011-9634-8
- Rohmer S, Merat A, Floderer V, Copinet A (2013) Geometric and topological modelling of 3d crumpled structures. 19th Int Conf Eng Des

- Rol F, Karakashov B, Nechporchuk O, et al (2017) Pilot-Scale Twin Screw Extrusion and Chemical Pretreatment as an Energy-Efficient Method for the Production of Nanofibrillated Cellulose at High Solid Content. *ACS Sustain Chem Eng* 5:6524–6531. doi: 10.1021/acssuschemeng.7b00630
- Roohani M, Habibi Y, Belgacem NM, et al (2008) Cellulose whiskers reinforced polyvinyl alcohol copolymers nanocomposites. *Eur Polym J* 44:2489–2498. doi: 10.1016/j.eurpolymj.2008.05.024
- Rouhi M, Razavi SH, Mousavi SM (2017) Optimization of crosslinked poly (vinyl alcohol) nanocomposite films for mechanical properties. *Mater Sci Eng C* 71:1052–1063. doi: 10.1016/j.msec.2016.11.135
- Saito T, Kimura S, Nishiyama Y, Isogai A (2007) Cellulose Nanofibers Prepared by TEMPO-Mediated Oxidation of Native Cellulose. *Biomacromolecules* 8:2485–2491. doi: 10.1021/bm0703970
- Saito T, Nishiyama Y, Putaux J-L, et al (2006) Homogeneous suspensions of individualized microfibrils from TEMPO-catalyzed oxidation of native cellulose. *Biomacromolecules* 7:1687–1691. doi: 10.1021/bm060154s
- Salas C, Nypelö T, Rodriguez-Abreu C, et al (2014) Nanocellulose properties and applications in colloids and interfaces. *Curr Opin Colloid Interface Sci* 19:383–396. doi: 10.1016/j.cocis.2014.10.003
- Salehpour S, Rafieian F, Jonoobi M, Oksman K (2018) Effects of molding temperature, pressure and time on polyvinyl alcohol nanocomposites properties produced by freeze drying technique. *Ind Crops Prod* 121:1–9. doi: 10.1016/j.indcrop.2018.04.079
- Sarrazin P Sheet of wrinkle-resistant paper. Arjowiggins Security. WO2013093872 (A1)
- Schyr B, Pasche S, Voirin G, et al (2014) Biosensors Based on Porous Cellulose Nanocrystal–Poly(vinyl Alcohol) Scaffolds. *ACS Appl Mater Interfaces* 6:12674–12683. doi: 10.1021/am502670u
- Sehaqui H (2011) Nanofiber networks, aerogels and biocomposites based on nanofibrillated cellulose from wood. PhD thesis. KTH Royal Institute of Technology
- Sehaqui H, Salajková M, Zhou Q, Berglund LA (2010) Mechanical performance tailoring of tough ultra-high porosity foams prepared from cellulose I nanofiber suspensions. *Soft Matter* 6:1824–1832. doi: 10.1039/B927505C
- Sharma RK (2011) Knowledge management in textile industry of Punjab. PhD thesis. Punjabi Univeristy
- Silvério HA, Neto WPF, Dantas NO, Pasquini D (2013) Extraction and characterization of cellulose nanocrystals from corncob for application as reinforcing agent in nanocomposites. *Ind Crops Prod* 44:427–436. doi: 10.1016/j.indcrop.2012.10.014
- Siqueira G, Frascini C, Bras J, et al (2011) Impact of the nature and shape of cellulosic nanoparticles on the isothermal crystallization kinetics of poly(ϵ -caprolactone). *Eur Polym J* 47:2216–2227. doi: 10.1016/j.eurpolymj.2011.09.014
- Siró I, Plackett D (2010) Microfibrillated cellulose and new nanocomposite materials: a review. *Cellulose* 17:459–494. doi: 10.1007/s10570-010-9405-y
- Siró I, Plackett D, Hedenqvist M, et al (2011) Highly transparent films from carboxymethylated microfibrillated cellulose: The effect of multiple homogenization steps on key properties. *J Appl Polym Sci* 119:2652–2660. doi: 10.1002/app.32831
- Sirviö JA, Honkaniemi S, Visanko M, Liimatainen H (2015) Composite Films of Poly(vinyl alcohol) and Bifunctional Cross-linking Cellulose Nanocrystals. *ACS Appl Mater Interfaces* 7:19691–19699. doi: 10.1021/acsami.5b04879
- Sjostrom E (1981) *Wood Chemistry: Fundamentals and Applications*. Gulf Professional Publishing. ISBN: 978-0-08-092589-9
- Smithers Pira (2017) *The future of Speciality Papers to 2022 Market report*
- Somerville C, Bauer S, Brininstool G, et al (2004) Toward a Systems Approach to Understanding Plant Cell Walls. *Science* 306:2206–2211. doi: 10.1126/science.1102765
- Song H, Ankefors M, Hoc M, Lindström T (2010) Reduction of the linting and dusting propensity of newspaper using starch and microfibrillated cellulose. *Nord Pulp Pap Res J* 25:495–504. doi: 10.3183/NPPRJ-2010-25-04-p495-504

- Song M, Yu H, Gu J, et al (2018) Chemical cross-linked polyvinyl alcohol/cellulose nanocrystal composite films with high structural stability by spraying Fenton reagent as initiator. *Int J Biol Macromol* 113:171–178. doi: 10.1016/j.ijbiomac.2018.02.117
- Song T, Tanpichai S, Oksman K (2016) Cross-linked polyvinyl alcohol (PVA) foams reinforced with cellulose nanocrystals (CNCs). *Cellulose* 23:1925–1938. doi: 10.1007/s10570-016-0925-y
- Spence KL, Venditti RA, Rojas OJ, et al (2011) A comparative study of energy consumption and physical properties of microfibrillated cellulose produced by different processing methods. *Cellulose* 18:1097–1111. doi: 10.1007/s10570-011-9533-z
- Spoljaric S, Salminen A, Luong ND, Seppälä J (2014) Stable, self-healing hydrogels from nanofibrillated cellulose, poly(vinyl alcohol) and borax via reversible crosslinking. *Eur Polym J* 56:105–117. doi: 10.1016/j.eurpolymj.2014.03.009
- Sultan E, Boudaoud A (2006) Statistics of Crumpled Paper. *Phys Rev Lett* 96:. doi: 10.1103/PhysRevLett.96.136103
- Sunasee R, Hemraz UD, Ckless K (2016) Cellulose nanocrystals: a versatile nanoplatform for emerging biomedical applications. *Expert Opin Drug Deliv* 13:1243–1256. doi: 10.1080/17425247.2016.1182491
- Syverud K, Chinga-Carrasco G, Toledo J, Toledo PG (2011) A comparative study of Eucalyptus and Pinus radiata pulp fibres as raw materials for production of cellulose nanofibrils. *Carbohydr Polym* 84:1033–1038. doi: 10.1016/j.carbpol.2010.12.066
- Syverud K, Stenius P (2009) Strength and barrier properties of MFC films. *Cellulose* 16:75–85. doi: 10.1007/s10570-008-9244-2
- Taipale T, Österberg M, Nykänen A, et al (2010) Effect of microfibrillated cellulose and fines on the drainage of kraft pulp suspension and paper strength. *Cellulose* 17:1005–1020. doi: 10.1007/s10570-010-9431-9
- Tallinen T, Aström JA, Timonen J (2009) The effect of plasticity in crumpling of thin sheets. *Nat Mater* 8:25–29. doi: 10.1038/nmat2343
- Tang X, Alavi S (2011) Recent advances in starch, polyvinyl alcohol based polymer blends, nanocomposites and their biodegradability. *Carbohydr Polym* 85:7–16. doi: 10.1016/j.carbpol.2011.01.030
- Taniguchi T, Okamura K (1998) New films produced from microfibrillated natural fibres. *Polym Int* 47:291–294. doi: 10.1002/(SICI)1097-0126
- Tanpichai S, Oksman K (2018) Crosslinked poly(vinyl alcohol) composite films with cellulose nanocrystals: Mechanical and thermal properties. *J Appl Polym Sci* 135:n/a-n/a. doi: 10.1002/app.45710
- Tanpichai S, Oksman K (2016) Cross-linked nanocomposite hydrogels based on cellulose nanocrystals and PVA: mechanical properties and creep recovery. *Compos Part Appl Sci Manuf* 88:226–233. doi: 10.1016/j.compositesa.2016.06.002
- Tejado A, Alam MN, Antal M, et al (2012) Energy requirements for the disintegration of cellulose fibers into cellulose nanofibers. *Cellulose* 19:831–842. doi: 10.1007/s10570-012-9694-4
- Torvinen K, Helin T, Kiiskinen H, et al (2011) Nanofibrillated cellulose as a strength additive in filler-rich SC paper. *TAPPI Int Conf Nanotechnol Renew Mater Arlingt on USA*
- Torvinen K, Sievänen J, Hjelt T, Hellén E (2012) Smooth and flexible filler-nanocellulose composite structure for printed electronics applications. *Cellulose* 19:821–829. doi: 10.1007/s10570-012-9677-5
- Tretinnikov ON, Zagorskaya SA (2012) Determination of the degree of crystallinity of poly(vinyl alcohol) by FTIR spectroscopy. *J Appl Spectrosc* 79:521–526. doi: 10.1007/s10812-012-9634-y
- Tsanaktsis V, Terzopoulou Z, Exarhopoulos S, et al (2015) Sustainable, eco-friendly polyesters synthesized from renewable resources: preparation and thermal characteristics of poly(dimethyl-propylene furanoate). *Polym Chem* 6:8284–8296. doi: 10.1039/C5PY01367D
- Turbak AF, Snyder FW, Sandberg KR (1983) Microfibrillated cellulose, a new cellulose product: properties, uses, and commercial potential. *J Appl Polym Sci* 37:815–827. doi: OSTI ID: 5062478

- Uddin AJ, Araki J, Gotoh Y (2011) Extremely oriented tunicin whiskers in poly(vinyl alcohol) nanocomposites. *Polym Int* 60:1230–1239. doi: 10.1002/pi.3067
- Uddin AJ, Fujie M, Sembo S, Gotoh Y (2012) Outstanding reinforcing effect of highly oriented chitin whiskers in PVA nanocomposites. *Carbohydr Polym* 87:799–805. doi: 10.1016/j.carbpol.2011.08.071
- Vardanyan V, Poaty B, Chauve G, et al (2014) Mechanical properties of UV-waterborne varnishes reinforced by cellulose nanocrystals. *J Coat Technol Res* 11:841–852. doi: 10.1007/s11998-014-9598-3
- Varshney VK, Naithani S (2011) Chemical Functionalization of Cellulose Derived from Nonconventional Sources. In: *Cellulose Fibers: Bio- and Nano-Polymer Composites*. Springer, Berlin, Heidelberg, pp 43–60
- Vartiainen J, Shen Y, Kaljunen T, et al (2016) Bio-based multilayer barrier films by extrusion, dispersion coating and atomic layer deposition. *J Appl Polym Sci* 133:n/a-n/a. doi: 10.1002/app.42260
- Vliegenthart GA, Gompper G (2006) Forced crumpling of self-avoiding elastic sheets. *Nat Mater* 5:216–221. doi: 10.1038/nmat1581
- Voronova MI, Surov OV, Guseinov SS, et al (2015) Thermal stability of polyvinyl alcohol/nanocrystalline cellulose composites. *Carbohydr Polym* 130:440–447. doi: 10.1016/j.carbpol.2015.05.032
- Wildlock Y, Heijnesson-Hulten A (2007) Method of producing a paper product. Kemira. US20100024998A1
- Xia QS, Boyce MC, Parks DM (2002) A constitutive model for the anisotropic elastic–plastic deformation of paper and paperboard. *Int J Solids Struct* 39:4053–4071. doi: 10.1016/S0020-7683(02)00238-X
- Xu M, Li W, Ma C, et al (2018) Multifunctional Chiral Nematic Cellulose Nanocrystals/Glycerol Structural Colored Nanocomposites for Intelligent Responsive Films, Photonic Inks and Iridescent Coatings. *J Mater Chem C*. doi: 10.1039/C8TC01321G
- Xu X, Yang Y-Q, Xing Y-Y, et al (2013) Properties of novel polyvinyl alcohol/cellulose nanocrystals/silver nanoparticles blend membranes. *Carbohydr Polym* 98:1573–1577. doi: 10.1016/j.carbpol.2013.07.065
- Zhang J, Jiang N, Dang Z, et al (2008) Oxidation and sulfonation of cellulose. *Cellulose* 15:489. doi: 10.1007/s10570-007-9193-1
- Zhang W, He X, Li C, et al (2014) High performance poly (vinyl alcohol)/cellulose nanocrystals nanocomposites manufactured by injection molding. *Cellulose* 21:485–494. doi: 10.1007/s10570-013-0141-y
- Zhou C, Chu R, Wu R, Wu Q (2011) Electrospun Polyethylene Oxide/Cellulose Nanocrystal Composite Nanofibrous Mats with Homogeneous and Heterogeneous Microstructures. *Biomacromolecules* 12:2617–2625. doi: 10.1021/bm200401p
- Zhou L, He H, Jiang C, et al (2017) Cellulose nanocrystals from cotton stalk for reinforcement of poly(vinyl alcohol) composites. *Cellul Chem Technol* 51:109–119. doi: no data

Chapter II

Introduction of cellulose nanocrystals in polyvinyl alcohol matrix for dog- ears limitation

Table of content chapter II

1. Extension of buckling-based metrology to thick cellulose nanocrystal-reinforced polyvinyl alcohol coatings.....	101
1.1. Introduction.....	101
1.2. Materials and methods	104
1.2.1. Methods	104
1.2.2. Methods	104
1.2.3. SIEBIMM experiments	105
1.3. Results and discussion.....	109
1.3.1. Extension of SIEBIMM method to micrometer-thick nanocomposite coatings..	109
1.3.2. Influence of CNCs on the Young’s modulus of thick PVOH/CNC coatings	113
1.3.3. Influence of coating parameters on the Young’s modulus PVOH/CNC coating..	116
1.4. Conclusions.....	119
2. Impregnation of paper with cellulose nanocrystal-reinforced PVOH: synergistic effect of infrared drying and CNC content on polymer crystallinity.....	121
2.1. Introduction.....	121
2.2. Materials and methods	123
2.2.1. Materials.....	123
2.2.2. Methods	123
2.3. Results and discussion.....	127
2.3.1. Paper structure and penetration of the composite during the impregnation process.....	127
2.3.2. Influence of CNC on drying mechanisms.....	131
2.3.3. Effect of CNC on PVOH crystallization	136
2.4. Conclusions.....	144
3. Use of cellulose nanocrystals in a polyvinyl alcohol matrix to decrease banknotes dog-ears defect.....	145
3.1. Introduction.....	145
3.2. Materials and methods	147
3.2.1. Materials.....	147
3.2.2. Methods	148
3.3. Results and discussion.....	155

Part I: Influence of cellulose nanocrystals on ply formation and recovery from bending deformations	155
3.3.1. Step 1: resistance of the material to the creation of the ply: impact of cellulose nanocrystals.....	155
3.3.2. Step 2: recovering of the paper from bending deformation: dog-ears resistance	158
3.3.3. Step 3: Resistance after folding.....	160
Part II: Research of key parameters for improving the paper elastic angle recovery	163
3.3.4. Influence of paper drying parameter	163
3.3.5. Influence of the nanocellulosic material	167
3.3.6. Influence of the matrix molecular weight of PVOH.....	170
3.4. General conclusion	172
References	173
Supplementary data	179

Chapter II: Introduction of cellulose nanocrystals in polyvinyl alcohol matrix for dog-ears limitation

Introduction

Chapter I allowed us to highlight the context of the project and its main challenges. Chapter II focuses on the improvement of banknote dog-ears resistance thanks to the introduction of CNCs in the PVOH impregnation bath (Figure 1-A). This chapter is divided into 3 parts (Figure 1-B) and is ordered from fundamental studies to applied results.

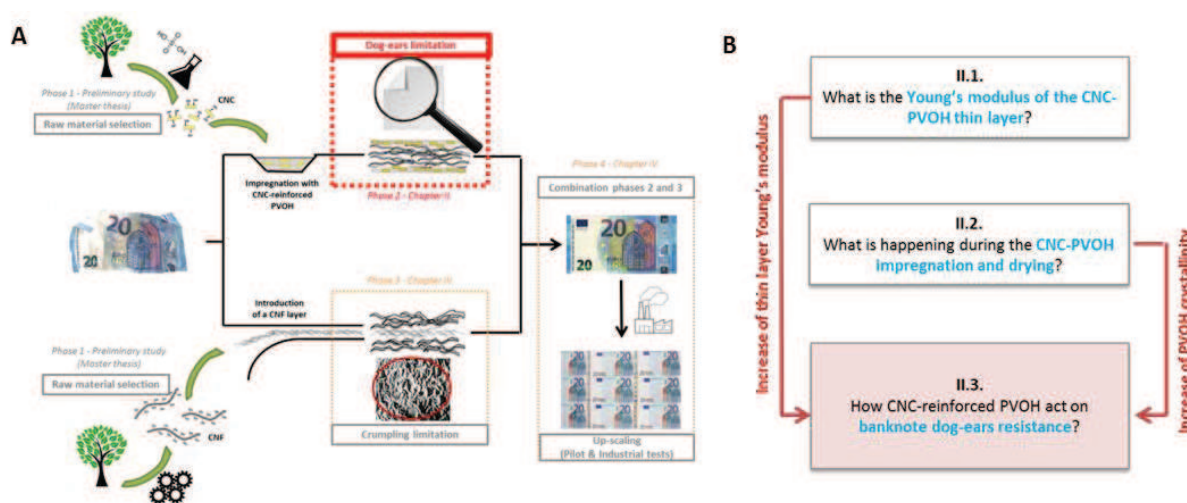


Figure 1: A) PhD overview of the different chapters and B) Details for chapter II

After impregnation and drying of the paper, a thin PVOH-CNC composite layer is deposited onto the paper. The Young's modulus of this layer is difficult to characterize due to its low thickness, and this property is also strongly correlated to the way of deposition of the layer on the substrate. However the classical methods for measuring the Young's modulus of composite materials are mostly developed for free-standing films. **Chapter II.1.** proposes to use buckling metrology for studying the impact of CNCs in the PVOH matrix as a coating layer. This method is used for the characterization of micrometric paper coating for the first time. This fundamental study investigates also the influence of the deposition process (bar coating or impregnation) and surrounding humidity on the Young's modulus of the resulting layer. ***This work is submitted in Langmuir and was presented at ACS conference (USA) in March 2018.***

Chapter II.2. investigates more deeply the process of paper impregnation with CNC reinforced PVOH. This study describes the final structure of the material after impregnation and reports how the presence of CNCs, the drying conditions and the PVOH crystallization synergistically impact the final paper properties. ***This work is submitted in ACS applied materials & Interfaces.***

Results of Chapter II.1 and Chapter II.2. are then used to explain how the presence of CNCs successfully impact the dog-ears resistance of banknote in **Chapter II.3**. In this last section, the dog-ears phenomenon is divided into three different steps which are the creation of the fold, the elastic angle recovery after folding and the resistance of the paper after a fold. The chapter describes the influence of CNCs on each step. Finally, Chapter II.3. ends with the identification of the key parameters linked to the dog-ears resistance and proposes protocol adaptations for an optimization of the results. ***This part was patented.***

1. Extension of buckling-based metrology to thick cellulose nanocrystal-reinforced polyvinyl alcohol coatings

*This work is adapted from J. Desmaisons, E. Niinivaara, E. D. Cranston, A. Dufresne, J. Bras, Extension of buckling-based metrology to thick cellulose nanocrystal-reinforced polyvinyl alcohol coatings”, Submitted in **Langmuir**.*

1.1. Introduction

Cellulose is the most important structural component in plants and is highly abundant, biodegradable and biocompatible. Acid hydrolysis of natural cellulose can be implemented to breakdown the disordered regions of the polymer to produce highly crystalline nanoparticles that are insoluble in water. These particles, cellulose nanocrystals (CNCs), are rod-like in shape and range from 5 to 20 nm in cross-section and a few hundred nanometers in length, depending on the raw material and hydrolysis conditions used (Dufresne 2017). The high crystallinity (and stiffness) of CNCs provides them with a specific Young’s modulus similar to that of Kevlar® and steel (between 100 and 160 GPa in the axial direction) (Eichhorn 2011; Dufresne 2017). The impressive mechanical properties offered by the nanoscale and low-density material, in addition to the non-abrasive and easily processable nature of cellulosic materials in general (Azizi Samir et al. 2005), explain the great interest in CNCs as reinforcing agents in polymer nanocomposites.

CNCs have been successfully used to reinforce several polymer matrices, whereby their hydrophilic nature provides them especially good compatibility with hydrophilic polymers. This has led to nanocomposites with excellent dispersion of CNCs, particularly in water-soluble and hydrophilic polymer matrices (Mariano et al. 2014). As an example, the water solubility and hydrogen bonding capacity of polyvinyl alcohol (PVOH) has given rise to PVOH/CNC nanocomposites being among the first studied polysaccharide nanocomposites. These composites utilize the film forming abilities, mechanical strength, flexibility and long-term thermal stability of PVOH (Roohani et al. 2008; Mandal and Chakrabarty 2014; Sirviö et al. 2015). Initial research efforts into PVOH/CNC nanocomposites focused on films obtained by solvent casting, and many of these studies reported an increase in mechanical properties upon the addition of CNCs to PVOH (Roohani et al. 2008; Chen et al. 2012; Pereira et al. 2014). PVOH/CNC nanocomposite films have also been studied for their barrier properties (Sirviö et al. 2015) and as biomimetic, stimuli responsive materials for medical implants (Stone et al. 2011; Jorfi et al. 2013). In addition to solvent cast films, recent literature has reported coatings as one promising application for water-based nanocellulose/polymer formulations such as PVOH/CNC composites (Brodin et al. 2014; Hubbe et al. 2017).

While solvent casting is a slow, isotropic process that results in the formation of free-standing films, coating involves the controlled deposition of thin layers, usually in the micrometer range, onto the surface of a substrate (e.g. paper or plastic films), often providing additional

properties to the substrate material. The literature reports various techniques for the deposition of nanocellulosic coatings, such as impregnation (Amini et al. 2016), bar coating (Gicquel et al. 2017), spray coating (Beneventi et al. 2014; Huang et al. 2017), and dip coating (Herrera et al. 2017). Regardless of the coating technique, however, CNC doped coatings have caught the interest of the food packaging industry due to their ability to improve both the barrier and mechanical properties of plastic films (Mascheroni et al. 2016) or porous substrates (El-Wakil et al. 2015; Herrera et al. 2017).

Characterizing the mechanical properties of coatings is not possible using conventional methods such as dynamic mechanical analysis, three-point bending tests, and classic tensile tests, as these methods are only applicable to free-standing films. Nevertheless, it has been observed that processing parameters (support, speed, formulation viscosity, coating device, and drying process) have a strong impact on nanocellulose organization and consequently on the subsequent properties of nanocellulosic composites (Hoeger et al. 2011; Lavoine and Desloges 2014). For example, drying plays a key role in the final material properties of composite coatings, and we can easily suggest that the impact of drying is more significant for thin layers than for thick free-standing films. To circumvent the need for free-standing films, this work uses a buckling-based metrology to understand the reinforcing effect of CNCs in a PVOH matrix applied as a coating layer.

The basic principle of this buckling-based metrology is to measure the way in which a thin, rigid film wrinkles when the soft substrate upon which it is coated is compressed. The buckling instability, defined as the balance between the energy required to bend the stiff film and the energy required to deform the soft underlying substrate, leads to a minimum wrinkle wavelength, which minimizes the total strain energy in the system (Stafford et al. 2004). The wavelength of the wrinkles depends on the properties of both the substrate and the film, and creates a unique buckling pattern; this phenomenon was observed previously by Biot, who modeled the bending of an infinite beam on an elastic substrate (Biot 1937). Later, Bowden et al. observed ordered structures in metal thin films (gold) deposited on polydimethylsiloxane (PDMS) (Bowden et al. 1998). Bowden's work also established a mathematical formula linking the buckling wavelength to the Young's modulus of the film, which takes into account the thickness of the film, Young's modulus of the substrate and the Poisson's ratios of both the film and the substrate. This formula was later used by Stafford who, for the first time, implemented this buckling-based metrology with polymeric materials (Stafford et al. 2004), introducing strain-induced elastic buckling instability for mechanical measurements (SIEBIMM). Recently, the SIEBIMM method was used to determine the Young's modulus of multilayer thin-film composites containing starch (Johansson and Wågberg 2012), cellulose nanofibrils (CNFs) (Cranston et al. 2011; Azzam et al. 2017), and CNCs (Kan and Cranston 2013; Martin 2015) demonstrating its applicability to a variety of polymer-nanoparticle systems.

Using the SIEBIMM method, the Young's modulus of supported thin films has been characterized for film thicknesses ranging from nanometers up to 1.7 μm (Kan and Cranston 2013). However, coatings are usually several to tens of micrometers thick, and the upper limit for the SIEBIMM method in terms of thickness remains unclear. The work presented here first explores the

adaptability of the SIEBIMM method to characterize the modulus of micrometer-thick coatings, after which this extension of the SIEBIMM method is used to calculate the influence of CNCs in a PVOH matrix as a model nanocomposite coating. The final undertaking is to understand the effects of the coating process, deposition technique (oriented or not), drying and environmental humidity (Figure 1) on the mechanical properties of PVOH/CNC coatings.

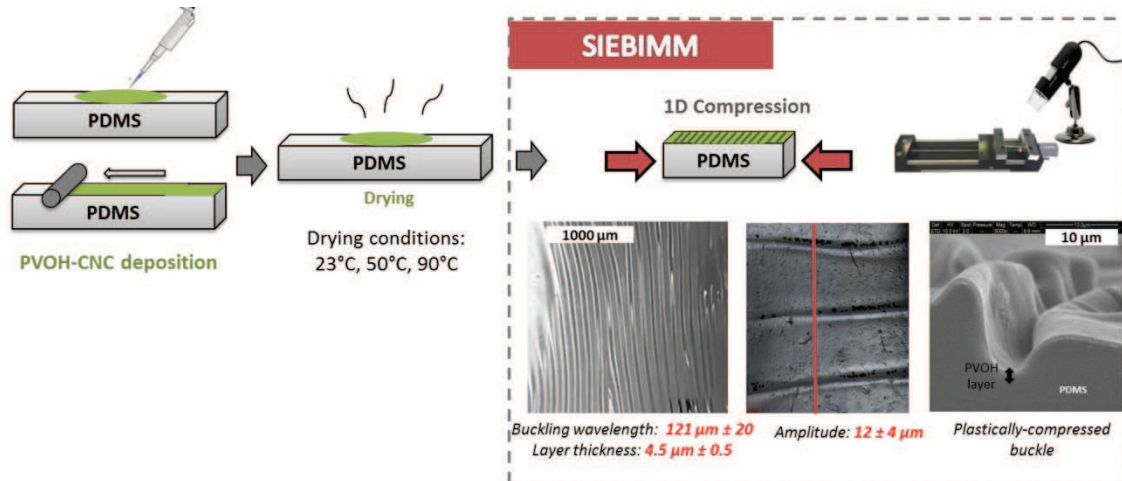


Figure 1: Buckling of micrometer-thick nanocomposite coatings. The buckling wavelength has been captured using a USB optical microscope (image sensor 5 M pixels, magnification ratio 10x to 300x), the amplitude using an optical profilometer, and the plastically compressed buckle was measured by SEM.

1.2. Materials and methods

Unless otherwise noted, all water used was distilled water.

1.2.1. Methods

Cellulose nanocrystals (CNCs). CNCs were purchased from the University of Maine (produced by the USDA Forest Products Laboratory) and had a length of 136 nm (± 50), and a cross-section of 11 nm (± 5). The dimensions were measured using an atomic force microscope (AFM) in tapping mode with a silica coated cantilever (OTESPA[®] 300 KHz – 42 N/m, Bruker, USA). The S content is 200 $\mu\text{mol}\cdot\text{g}^{-1}$. The sodium was used. The CNC suspension was delivered at 12 wt% and was diluted to 10^{-4} wt% followed by high-shear homogenization (Ultraturrax[®], IKA) and drops of the suspension were deposited on mica substrates and dried overnight at room temperature for AFM imaging. Scan sizes of $3.3 \times 3.3 \mu\text{m}^2$ were performed and the length and cross-section (height) were averaged from three separate images, with 50 measurements per image ($N=150$).

Polyvinyl alcohol (PVOH). The PVOH used was a mixture of a high molecular weight PVOH (Mw) (Mowiol[®] 28-99 145000 g/mol) and a low Mw PVOH (Mowiol[®] 6-98 (47 000 g/mol), all purchased from Sigma Aldrich. The 5 wt% PVOH stock solution was prepared by mechanically mixing Mowiol[®] 28/99 and Mowiol[®] 6/98 (2:1 by mass, respectively) and dissolving said polymer mixture into water whilst heating with constant stirring. The temperature of the mixture was maintained at 90 °C for minimum 2 h, ensuring the complete dissolution of PVOH. The solution was then stored at room temperature.

Polydimethylsiloxane (PDMS). PDMS was purchased from Sigma Aldrich (Sylgard[®] 184, 10 g clip-pack). The Sylgard elastomer kit was comprised of a base and a curing agent.

1.2.2. Methods

PDMS preparation. PDMS substrates were prepared by mixing the base and the curing reagent using a mass ratio of 10:1, respectively. The mixture was vigorously mixed by hand for 10 min to obtain a homogeneous mixture, and then kept under vacuum for at least 1 hour to remove any trapped air. The PDMS was cast into a rectangular metallic mold (5 cm \times 5 cm), previously polished to avoid defects on the surface, and subjected to vacuum for an additional 30 min. Finally, the PDMS was cured at 100 °C for 1 h. After cooling, the 4 mm thick PDMS was cut into 5 cm \times 1 cm strips and rinsed with water and ethanol. The thickness of the PDMS strips was measured using a caliper.

Dynamic mechanical analysis (DMA). The Young's modulus of the PDMS was determined using DMA (RSA3, TA instruments). PDMS samples with dimensions of 1 cm \times 3 cm (4 mm thick) were compressed using a compression rate of 0.6 mm/min and a preload of 1 N, with a 15 mm gap between the clamps. The Young's modulus varied between 4.5 and 6.8 MPa, depending on the batch of PDMS – the exact Young's modulus measured by DMA for each PDMS batch was used in the respective calculations. These values of Young's modulus are in the same range of values than

reported in literature (Cranston et al. 2011; Kan and Cranston 2013; Martin 2015). A Poisson's ratio of 0.5, a typical value for elastomeric materials, was assumed for PDMS.

Casting PVOH coatings. PVOH films with a 50 g/m² basis weight were prepared by solvent casting from aqueous solution. The 5 wt% stock solution of PVOH was cooled in a polytetrafluoroethylene mold and dried at 23 °C and 50 %RH for one week.

Tensile tests for PVOH films. Tensile tests (Instron 5965) were performed on cast PVOH films (5 cm × 1.5 cm) using a crosshead speed of 10 mm/min. Each film was conditioned at 23 °C and 50 %RH for at least 48 hours before testing and 5 repeats were performed on three separate films.

PVOH/CNC mixture. The addition of CNCs into the PVOH solution was carried out by heating the previously prepared 5 wt% PVOH stock solution to 60°C and adding the required volume of water and mass of CNCs to obtain a total solids content of 5 wt% and a PVOH/CNC mass ratio of 90:10. The PVOH/CNC suspension was mechanically stirred for 1 h at 60°C after which it was exposed to an ultrasonic dispersive energy of 5 kJ/g of dry CNC, using a 250 Watt (or 250 J/s) sonication probe (Sonifier S-250A, Branson, USA) at 50% of its maximum energy.

Percolation threshold. The percolation threshold was calculated using the equation $\Phi_d = \frac{0.7}{f}$ (Dufresne 2017), where Φ_d is the volumetric percolation threshold and f the aspect ratio. The aspect ratio is obtained by dividing the CNC length by its cross-section. The weight percolation threshold was calculated using equation (1):

$$\Phi_m = \Phi_d \frac{\rho_c}{\Phi_d \rho_c + \rho_e (1 - \Phi_d)} \quad (1)$$

Where Φ_m is the weight percolation threshold, ρ_c and ρ_e are the density of cellulose (1.54 g/cm³) and PVOH (1.29 g/cm³, extracted from the security data sheet of Sigma Aldrich), respectively.

1.2.3. SIEBIMM experiments

Coating PVOH/CNC nanocomposites on PDMS. Prior to coating, a corona treatment (4 passes under 300 mA, Calvatron SG-2) was performed on the PDMS substrate in order to increase its surface energy, and hence promote better adhesion between the PVOH/CNC coating and the substrate. Before deposition of the coating on to the PDMS, the 5 wt% PVOH solution and PVOH-CNC mixture, were diluted to a range of concentrations from 0.01 wt% to 2.5 wt% to produce different coating thicknesses. Two coating deposition methods were tested: (i) solvent casting and (ii) classical bar coating. For the solvent casting deposition, 300 μ L of the diluted suspension was deposited onto the corona treated PDMS with a micropipette. For the bar coating deposition, strips of PDMS were placed in a rectangular plate 4 mm deep and a smooth metallic bar was used to spread the suspension over the substrate surface.

Drying of coatings on PDMS. Unless otherwise noted, the coated PDMS samples were dried under ambient conditions (50 %RH and 23°C) for two days. Other drying protocols were also performed to

determine the effect of drying temperature on Young's modulus of the coating. Therefore, select samples were dried in an oven at 50 °C for 4 h or at 90°C for 3 h.

Buckling measurements under ambient conditions (SIEBIMM). After deposition of the coating onto the PDMS and subsequent drying, the samples were conditioned at 23°C and 50 %RH overnight prior to performing buckling measurements. For these measurements, the coated PDMS substrates were fixed with screw clamps to a homebuilt compression apparatus, and compressed at 1 mm/min to a final compression strain of 5%. Experiments were carried out in a climate controlled room (23°C and 50 %RH). The Young's modulus of each coating was calculated using the following equation (2):

$$E_f = 3E_s \frac{(1 - \nu_f^2)}{(1 - \nu_s^2)} \left(\frac{\lambda}{2\pi d_f} \right)^3 \quad (2)$$

Where E_f is the Young's Modulus of the PVOH/CNC coating, λ is the wavelength of the periodic wrinkles induced in the coating upon buckling (measured by USB optical microscopy, focus range from 10 mm to 500 mm, image sensor 5 M pixels, magnification ratio 10x to 300x), E_s is the Young's Modulus of the PDMS substrate, ν_s the Poisson's ratio of the substrate, ν_f the Poisson's ratio of the coating, and d_f the coating thickness. It should be noted that Equation 2 has numerous conditions: i) it is only valid for sinusoidal waveforms, and low applied compression strain ($\epsilon \ll 10\%$), ii) the elastic modulus of the layer must be much higher than the substrate, iii) the width of the coating layer must be significantly greater than its thickness, iv) the amplitude of the wave pattern must be smaller than the wavelength, and v) the substrate thickness must be much greater than the layer thickness (Stafford et al. 2004).

Buckling measurements at different relative humidities. Buckling experiments were performed at different relative humidities by placing the samples, the compression apparatus and the USB microscope into a glovebox (AtmosBag, Sigma Aldrich). Nitrogen gas was passed through the glovebox to achieve humidities of 0 %RH or 20 %RH, and a saturated NaCl solution was used to induce 98 %RH. The samples were conditioned in their selected environment overnight before measuring the buckling wavelength using the homebuilt compression apparatus mentioned earlier.

Average Young's modulus. In sections 3.2 and 3.3 of the Results and Discussion, an average Young's modulus is reported. The data representing the buckling wavelength as a function of coating thickness was submitted to a linear regression analysis in order to smooth out the thickness values. The thickness values adjusted with this linear regression were then used for the calculation of the Young's modulus. The standard deviation of the Young's modulus value obtained after linear regression was calculated using the LINEST function in Microsoft Excel 2010.

Coating thickness. Coating thickness is a sensitive parameter, and small variations can induce significant fluctuations in the Young's modulus calculations. Two separate methods were used to measure coating thickness as a function of humidity. Spectroscopic ellipsometry (SE) was used to measure the coating thickness in ambient humidity (40-55 %RH) and at 0% RH. The values obtained

for coating thickness through SE were also compared to those obtained by scanning electron microscopy (SEM), carried out at 0 %RH. Both SE and SEM provided the same coating thicknesses regardless of relative humidity (ambient or 0%RH). Consequently, an average between the SE and SEM values was used. A more detailed description of each of these two methods can be found below.

Scanning Electron Microscopy. SEM imaging of coated slices of PDMS (carefully cut to size with a razor blade) was performed using a ESEM in EDT mode (Quanta 200©, FEI, Japan) at a working distance of 10 mm with 10 keV and a spot size of 3.5. Prior to imaging, the samples were gold sputter coated (5 nm thick gold coating). At least 5 images were taken per magnification. ImageJ software was then used to determine the coating thickness. A minimum of 20 analyses were performed for each image (N=100).

Spectroscopic Ellipsometry (SE). To accurately measure the difference in thickness between 0 %RH and ambient humidity (40-55 %RH), a M-2000UTM variable angle spectroscopic ellipsometer (J.A. Woollam Co., Inc, Lincoln, NE) was used, with wavelengths between 250 and 1680 nm, and incident angles of 55-75 °, with 5 ° increments. CompleteEase® software was used to determine the thicknesses of the nanocomposite coatings, using a classic Cauchy model to fit the raw ellipsometric data, assuming the PVOH/CNC coating was a transparent film.

Wavelength and amplitude measurement. The wavelengths and amplitudes of the buckled coatings were measured using an optical profilometer (InfiniteFocus, Alicona) with a vertical resolution of 1.6 µm and a lateral resolution of 5.8 µm. Images of 2.2 mm x 7.5 mm were taken for said analysis.

Differential scanning calorimetry (DSC). DSC analyses were carried out using a TA DSC Q100. Two kinds of samples were tested; 1. Neat PVOH and PVOH/CNC films cast in a polytetrafluoroethylene mold (ca. 42 µm thick) and 2. Neat PVOH or PVOH/CNC coatings carefully peeled from the PDMS substrate after deposition by solvent casting and drying under ambient conditions (resulting film thickness was ca. 16 µm). The neat PVOH coating was also submitted to an annealing treatment at 80°C and 105°C for 120 min, to artificially change its crystallinity. DSC measurements were done by linearly heating 8 ± 2 mg samples with a linear ramp of 10 °C/min from room temperature to 250°C, in order to obtain complete melting of the PVOH crystals. Cellulose nanocrystals have a good thermal stability until 250°C as reported in literature (Reid et al. 2017). The experiments were performed under a N₂ blanket, and a minimum of 3 repetitions were carried out. The heat of fusion (ΔH_m) was obtained from the DSC curves and was used to determine the degree of crystallinity (X_c) of the sample based on its relationship to the theoretical crystalline heat of fusion (ΔH^o_m) for completely crystalline PVOH, using the following equation (3):

$$X_c = \frac{\Delta H_m}{\Delta H^o_m \times (1-wf)} \times 100 \quad (3)$$

Where ΔH_m° = is the enthalpy of fusion for completely crystalline PVOH (161 J/g) (Uddin et al. 2012), and w_f is the weight fraction of the cellulosic filler, CNCs in this case, which is used to normalize the enthalpy in regard to the fraction of PVOH in the sample.

Saxs experiments. This experiment was performed by Senechal et al. 2010 but it was not published. Films were prepared by solvent casting on Teflon mold of PVOH/CNC with a ratio 96:4 regarding amount of PVOH and CNC respectively. The solid content was 20% and the drying was performed in an oven at 35°C for 24h. The same mixture was also coated on a PE paper using bar coating deposition and drying under IR light. SAXS diagrams were obtained using PVOH as background on the SIMaP rotating anode SAXS setup.

1.3. Results and discussion

1.3.1. Extension of SIEBIMM method to micrometer-thick nanocomposite coatings

PVOH films were solvent cast on to corona treated PDMS substrates to obtain coatings with thicknesses ranging from 67 nm to 40 μm . These coatings were used as a model system (i.e. without nanoparticles) to assess the suitability of the SIEBIMM method to characterize thicker (above 1.7 μm) coatings, which is the upper limit reported in literature (Kan and Cranston 2013). Upon unidirectional compression (at 5% compression strain), coatings below a thickness of 35 μm buckled reproducibly, giving sinusoidal wave patterns as shown in Figure 2 A B and C. However, an increase in thickness beyond this point resulted in an increase in the rigidity of the coated layer and it became harder to both compress the material and to obtain a homogeneous buckling pattern (Figure 2-D). Furthermore, for coating thicknesses below 35 μm , the amplitude of the wrinkles (as observed through optical profilometry (Figure 2 inset values) were smaller than their wavelength as required by the SIEBIMM model.

One obstacle in assessing the suitability of the SIEBIMM method with micrometer-thick coatings is ensuring that films buckle throughout their entire thickness. As shown by the SEM image in Figure 1, for coating thicknesses up to 35 μm , this is indeed the case. In fact, even after plastic deformation, SEM images showed a complete buckling of the neat PVOH coating. This SEM image also revealed sufficient adhesion between the coating and the substrate to avoid delamination or relaxation of the buckled patterns for PVOH coatings up to 35 μm thick. Furthermore, when coatings were “over” compressed from 5% to 25% compression strain, each sample maintained a constant buckling wavelength, confirming good adhesion to the PDMS substrate regardless of coating thickness. Finally, no cracking of the layer was observed (even for coatings thicker than 35 μm).

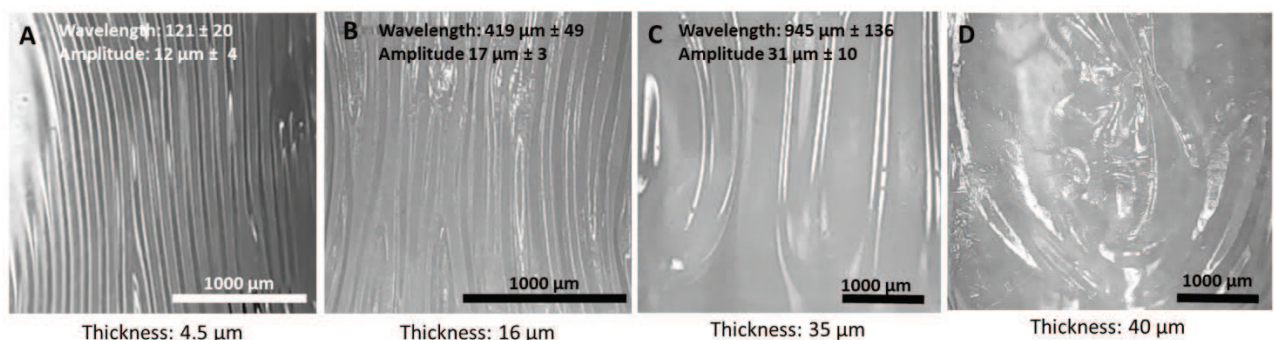


Figure 2: Buckling patterns as observed through optical microscopy for elastically compressed PVOH coatings on PDMS substrates with different thicknesses. Wavelength and amplitude values are provided in the inset, and measured by digital analysis of microscopy images and optical profilometry, respectively.

Coatings of varying thicknesses were elastically compressed (i.e., to a compressive strain of 5%), and the buckling wavelengths were measured as reported in Figure 3-A. A linear correlation was

seen between the wrinkle wavelength and the PVOH coating thickness for films of 67 nm to 35 μm in thickness (regression coefficient $R^2 = 0.9996$). This correlation of wavelength with thickness agrees with that originally demonstrated by Bowden et al. (Bowden et al. 1998), as well as subsequent users of buckling-based metrologies. In Figure 3-B, the standard deviation (absolute dispersion) and coefficient of variation (relative dispersion) of the buckling wavelengths are reported as a function of PVOH thickness. Absolute dispersion increases linearly with an increase in thickness, implying that sample heterogeneities increase with increasing thickness. Relative dispersion, on the other hand, shows a different trend; beyond a thickness of 1 μm , the coefficients of variation lie between 10 and 20% whereas the nanometer thick coatings show higher values due to the resolution limitations of the microscopes used (optical microscope and SEM). Regardless, the plateau in the coefficient of variation (at ca. 15%) indicates an acceptable set of data for buckling wavelength up to a coating thickness of 35 μm .

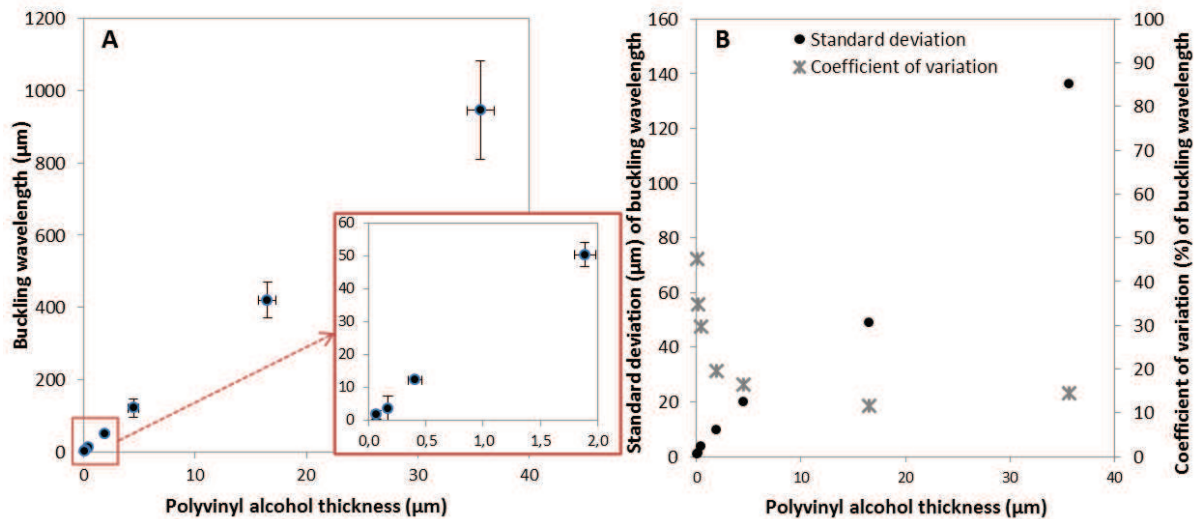


Figure 3: A) Buckling wavelength for PVOH coatings (measured at 50 %RH) with different thicknesses prepared on PDMS by casting and drying at ambient temperature and B) absolute and relative dispersion of buckling wavelength values as a function of coating thickness.

The elastic moduli for the PVOH coatings are represented in the box plot below (Figure 4-A) where the red cross represents the average value, and the horizontal line the median value. The lower and upper limits of the boxes are the first and third quartiles, respectively (50 % of the central data lies between these two limits; 25 % above and 25% below). For each box, any data located below or above the lower and upper ends of the chart whiskers, respectively, can be considered as outliers. The average values for the Young's modulus of the PVOH coatings are all between 1.2 and 2.5 GPa regardless of thickness. For PVOH thicknesses between 60 nm and 4.4 μm , the Young's moduli exhibit some anomalies, however, these are no longer present in the coatings with thicknesses between 4.4 to 35.6 μm . Furthermore, at the largest thicknesses, the average and median values for Young's moduli are equal and variability is low. These results further confirm the fact that the variations are due more so to the lack of resolution in the microscopy techniques at the

nanoscale, and are not a reflection of the adaptability of the SIEBIMM method to micrometer-thick coatings.

An analysis of variance (ANOVA) test was performed in order to determine whether coating thickness has a significant impact on elastic modulus. For each film thickness, between 20 and 90 values of buckling wavelength were measured and as many Young's moduli were calculated. Two hypotheses were formulated: the null hypothesis states that there is no influence of thickness on Young's modulus and the alternative hypothesis states that the thickness is an explicative value for the Young's modulus. The bar chart of standardized coefficients, beta, (Figure 4B) is used to visually compare the relative impact of the thickness; the higher the absolute value of the coefficient, the more significant the effect of thickness on Young's modulus. Furthermore, when the confidence interval spans $x=0$, the difference between each group of values is considered insignificant. The group of values obtained with the lowest thickness were considered as a reference. Note that except for the second group, all the other groups of data showed statistically insignificant differences. As such, we conclude that the values of Young's modulus obtained for the thickest ($35 \mu\text{m}$) and the thinnest (60 nm) coatings are not significantly different.

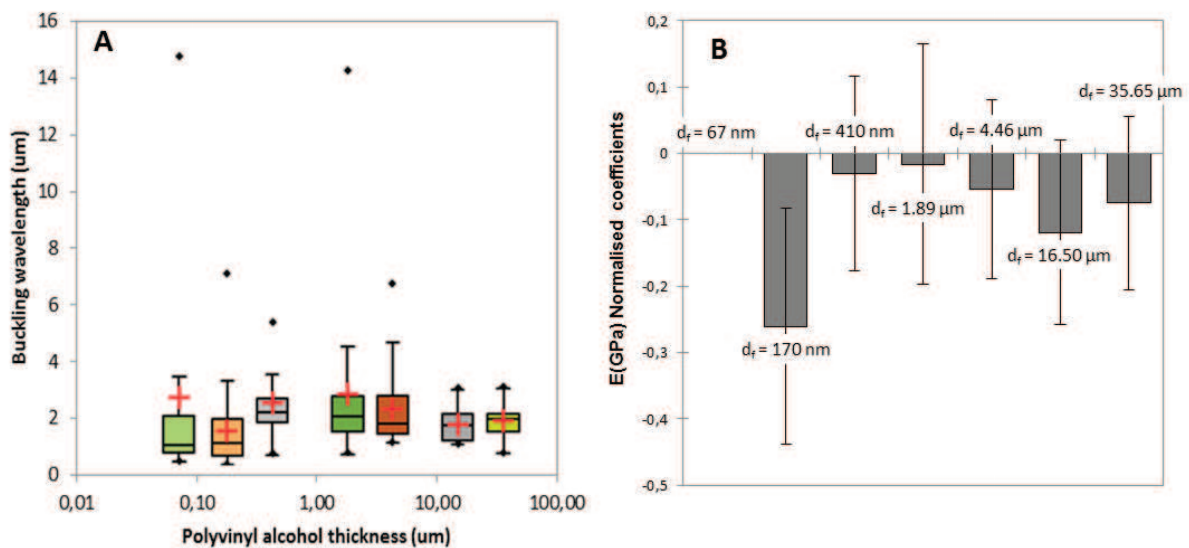


Figure 4: A) Box plot showing the Young's moduli for PVOH coatings calculated from SIEBIMM measurements at 50 %RH, B) Standardized coefficients (95% confidence interval). ANOVA study where explicative variable is thickness (from SEM), measured variable is Young's modulus, E (GPa)

The average Young's modulus for PVOH coatings from all of the sets of data (independent of thickness) with propagated error is $1.9 \pm 2.2 \text{ GPa}$. To overcome the high sensitivity of the model to sample heterogeneities, a linear regression between wavelength and thickness values was performed as shown in Figure 5. With this adjustment in the wavelength, a constant Young's modulus of $1.61 \pm 0.1 \text{ GPa}$ was obtained, which correlates well with a solvent cast PVOH film measured by more traditional tensile testing ($1.2 \pm 0.3 \text{ GPa}$).

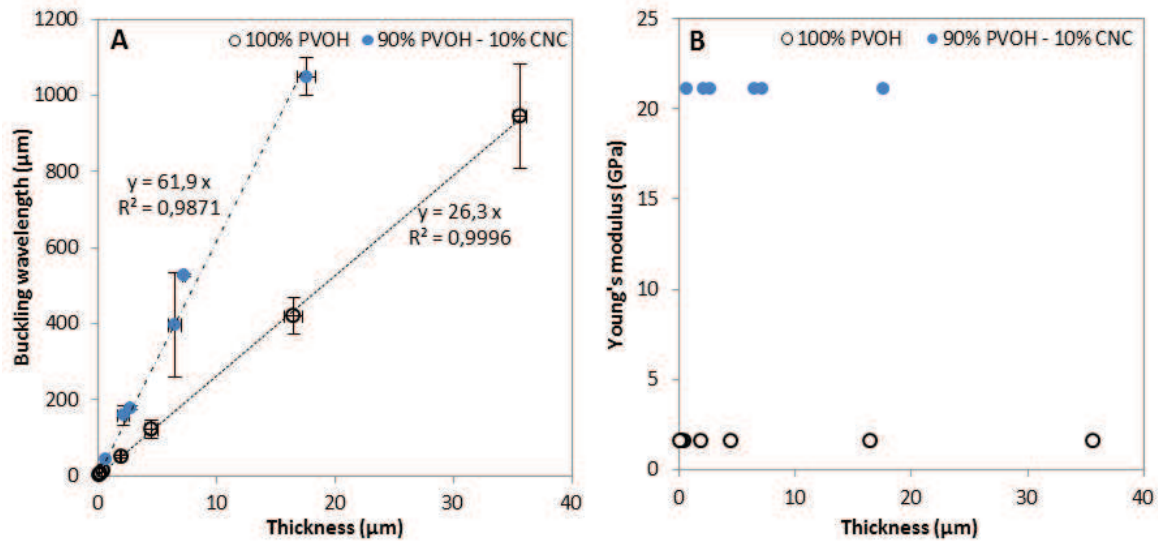


Figure 5: Comparison of PVOH coatings without (open circles) and with (filled blue circles) CNCs: A) buckling wavelength (measured at 50% RH) as a function of coating thickness showing linear regression analysis, and B) Young's moduli calculated from linear fits.

In the literature, the SIEBIMM method has been used to calculate the Young's modulus of layer-by-layer (LbL) deposited nanocellulose-based composites on PDMS (Cranston et al. 2011; Kan and Cranston 2013; Martin 2015). The LbL method allows for the deposition of homogeneous layers with tailored roughnesses and thicknesses between a few nanometers to 1.7 μm . These conditions are particularly well adapted for buckling metrology where even small changes in film thickness, or buckling wavelengths, induce significant variations in the calculated Young's modulus. In this work, the difficulty comes from the casting deposition of thicker coating and with a more heterogeneous process. A clear thickness limitation was established here. Accordingly, the results allow us to conclude that, for coating thicknesses up to 35 μm , (i) a sinusoidal waveform is observed, (ii) the amplitude of the wave pattern is smaller than the wavelength, and (iii) the adhesion between the coating and the substrate is good and did not exhibit cracking.

The remaining condition for the SIEBIMM method states that the substrate must be significantly thicker than its coating (Stafford et al. 2004). This condition, however, proved to be the most questionable. Here, the thickness ratio between the 4 cm thick PDMS substrate and the PVOH coating was 4×10^9 for nanometer-thick coatings and 4×10^6 for micrometer-thick coatings. Despite the large range of ratio between substrate and coating thicknesses, this study confirmed both experimentally and statistically that the calculated Young's modulus was not in fact influenced by the coating thickness, up to 35 μm . However, to prevent sample heterogeneities causing significant variation in Young's moduli, film thickness and buckling wavelength must be measured at the exact same location on the sample. Furthermore, using at least three different PVOH thicknesses in the micrometer range and fitting a linear trend to the plot of buckling wavelength versus coating thickness allows for the most reliable values and a decreased standard deviation.

1.3.2. Influence of CNCs on the Young's modulus of thick PVOH/CNC coatings

CNCs were added to PVOH at a ratio of 10:90 wt%, respectively, and as with the neat PVOH system, six different coating thicknesses ranging from 600 nm to 17.5 μm were solvent cast onto a PDMS substrate. As in the previous section, buckling was performed under ambient conditions (23°C, 50 %RH). Figure 5A shows the linear relationship between the buckling wavelength and coating thickness for PVOH/CNC composite coatings which is the same trend but with a steeper slope than for the neat PVOH coatings. Calculations of the average Young's modulus revealed that the addition of 10 wt% CNCs led to a sharp increase in the elastic modulus of the PVOH coating - from 1.6 ± 0.1 GPa for the neat PVOH to 21 ± 2 GPa for the PVOH/CNC composite. This increase can be explained through three phenomena: (i) the homogeneous dispersion of CNCs in the PVOH due to the high compatibility between the matrix (PVOH) and the filler (CNCs) (Dufresne 2008; Habibi et al. 2010), (ii) the high stiffness of the CNCs (reinforcement effect) and (iii) the increase in PVOH crystallinity due to the addition of CNCs. These contributions are discussed further below.

Reinforcing effect of CNCs. Typically reported modulus values for CNCs lie between 100 and 160 GPa in the axial direction, and between 10 and 50 GPa in the transverse direction (Moon et al. 2011). The broad range in moduli reported is due to the fact that the Young's modulus of CNCs strongly depends on the technique by which it is measured, along with the properties of the cellulosic material such as the source, crystal structure, anisotropy, degree of crystallinity and defects (Eichhorn 2011; Moon et al. 2011). Nevertheless, the high elastic modulus of CNCs allows them to act as a reinforcing element when they are introduced to soft polymer matrices. Additionally, due to their high aspect ratio, and tendency to form interparticle hydrogen bonds (Favier et al. 1995) and strong van der Waals bonds (Berg et al. 2007), CNCs can form a percolating network at fairly low loadings. The percolation threshold of CNCs by weight, calculated from Equation 1 using their dimensions, is 7 wt%, meaning that percolation should be reached in these PVOH/CNC systems containing 90 wt% PVOH and 10 wt% CNCs, assuming the CNCs are well-dispersed.

In the literature, different models are proposed to predict the Young's modulus of CNC-reinforced polymer composites (Eichhorn 2011; Moon et al. 2011; Xu et al. 2013; Abitbol et al. 2014; Reid et al. 2018). The Halpin Kardos model is a semi-empirical model that considers short oriented fibers encased in a matrix (Halpin and Kardos 1972). In this case, interactions between fibers are not taken into consideration. Consequently, this model is especially accurate for short fibers in isotropic composites (such as CNC-reinforced polymers) whose filler-filler interactions are negligible. On the other hand, the Ouali model is based on the percolation theory and is an extension of the phenomenological series-parallel model proposed by Takayanagi (Ouali et al. 1991). This model highlights the importance of filler-filler interactions and is accurate for composites with high filler content.

Table 1: Comparison between elastic modulus of CNC-reinforced PVOH composites calculated from Halpin-Kardos and Ouali models, and elastic modulus obtained from SIEBIMM experiments

Model	Halpin-Kardos model	Ouali model	SIEBIMM
Description	Model based on non-percolating network	Model based on percolation theory	Experimental result from buckling metrology
Equations	$E_{ } = E_m \frac{1 + \eta_{ }\zeta\phi_i}{1 - \eta_{ }\phi_i}$ $E_T = E_m \frac{1 + 2\eta_T\zeta\phi_i}{1 - \eta_T\phi_i}$ $E_c = 0.184E_{ } + 0.816E_T$ <p style="text-align: center;"><u>Where</u></p> $\eta_{ } = \frac{\frac{E_f}{E_m} - 1}{\frac{E_f}{E_m} + \zeta} \text{ and } \eta_T = \frac{\frac{E_f}{E_m} - 1}{\frac{E_f}{E_m} + 2}$	$E_c = \frac{(1-2\Psi + \Psi\phi_f)E_mE_f + (1-\phi_f)\Psi E_f^2}{(1-\phi_f)E_f + (\phi_f - \Psi)E_m}$ <p style="text-align: center;"><u>Where</u></p> $\Psi = 0 \text{ if } \phi_f \leq \phi_c$ $\Psi = \phi_f \left(\frac{\phi_f - \phi_c}{1 - \phi_c} \right)^b \text{ if } \phi_f > \phi_c$	$E_f = 3E_s \frac{(1 - \nu_f^2)}{(1 - \nu_s^2)} \left(\frac{\lambda}{2\pi d_f} \right)^3$
Composite coating			
Young's modulus (E _c)	2.4 GPa	4.4 GPa	21.4 ± 2.0 GPa

The Young's modulus predicted from the Halpin Kardos model is the lowest of the three models, as given in Table 1, where $E_{||}$ and E_T are the longitudinal and transverse elastic moduli of a unidirectional composite, respectively, E_m is the Young's modulus of the matrix (given a value of 1.6 GPa, as reported beforehand), E_f is the Young's modulus of the filler (given a value of 150 GPa (Mariano et al. 2014)), and E_c is the Young's modulus of the composite. Furthermore, ζ is a shape factor that considers the filler geometry, (here, $\zeta = 2L/W$ where L is the CNC length and W is the CNC width), and ϕ_i is the volume fraction of the filler. The Young's modulus from the Ouali model is also given in Table 1, where the subscripts f and m refer to the filler and matrix phases, respectively, ϕ_f is the volume fraction of the filler, ϕ_c is the critical percolation threshold based on $\phi_c = 0.7 / (L/W)$ (Dufresne 2017), and b is the critical percolation exponent (where b is 0.4 for a three dimensional network (Takayanagi et al. 1964; Ouali et al. 1991). Finally, Ψ is the volume fraction of the percolating filler network.

The Ouali model highlights that percolation improves the mechanical properties of a composite. Indeed, the Young's modulus of the PVOH/CNC composite calculated from the Ouali model (4.4 GPa) is almost double in comparison to that of the non-percolating model (2.4 GPa). However, percolation alone is not sufficient to explain the 21 ± 2 GPa elastic modulus obtained using the SIEBIMM method upon the addition of 10 wt% CNCs. This high value of elastic modulus confirms the compatibility between the CNCs and the PVOH matrix, which results in pronounced interfacial interactions and good dispersion of the CNCs in the polymer matrix. In literature, the good dispersion of CNCs in a PVOH matrix has been observed using AFM tapping mode on dried films (Paralikar et al. 2008). The dispersion of CNC in a PVOH-chitosan matrix was also correlated with their effectiveness in improving the properties of bio-nanocomposite films (El Miri et al. 2015). Moreover, there is another phenomenon at play, which drastically impacts the mechanical properties: the increase in PVOH crystallinity with the addition of CNCs.

Increase of PVOH crystallinity. At the nanoscale, coating thickness may have an impact on polymer crystallinity. Several studies have demonstrated an increase in crystallinity with an increase in film thickness (up to 870 nm) as a result of higher vertical growth of the polymer crystals and greater possibility for nuclei survival (Ritala et al. 1994; Kim et al. 2000; Chang et al. 2002). However, at micrometer scale, it can be presumed that the coating thickness may not impact the crystallinity to the same degree. Indeed, using DSC we found a similar value of 22% for the degree of crystallinity for PVOH coatings that were 42 and 16 μm thick (both samples were solvent cast onto PDMS substrate and dried under ambient conditions of 23°C, 50%RH). Conversely, however, the drying and annealing steps of the coating preparation were shown to have a strong impact on crystallinity. To highlight the effect of PVOH crystallinity on the Young's modulus of the coatings, Figure 6 shows a linear increase in the Young's modulus of PVOH (measured by SIEBIMM) with increasing crystallinity, where crystallinity was controlled through different annealing treatments at either 80 or 105 °C for 2 hours. This shows that an increase in the matrix crystallinity results in an increase in the mechanical properties of the composite.

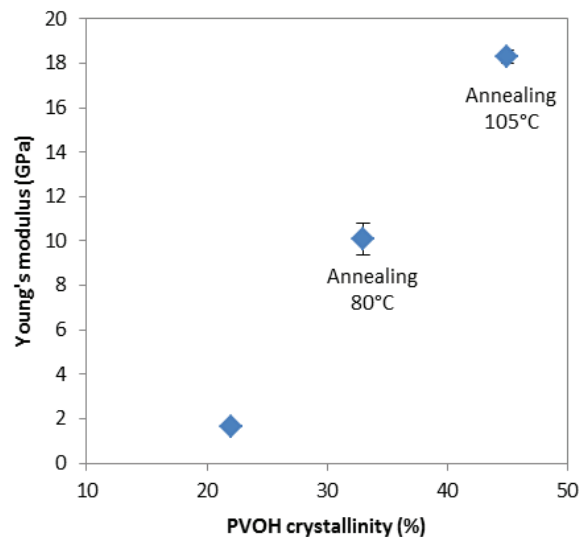


Figure 6: Average Young's modulus for PVOH coatings (measured by SIEBIMM) as a function of PVOH crystallinity (measured by DSC) controlled through annealing heat treatments at 80 and 150 °C.

The addition of CNCs to the PVOH matrix also had an effect on the polymer crystallization. In such systems, CNCs plays the well-known role of nucleating agent as previously shown in several other polymer matrices (Gray 2008; Siqueira et al. 2011), as well as in PVOH (Rescignano et al. 2014). Up to their percolation threshold, increasing the CNC content increases PVOH crystallinity. However, there is a threshold beyond which an excess of CNCs can hinder macromolecular chain crystallization (Siqueira et al. 2011). Here, with the addition of 10 wt% CNCs, the crystallinity of solvent cast PVOH films increased from 22% to 38%. We can consequently argue that the large increase in elastic modulus brought by the introduction of CNCs is partially due to the reinforcement effect of CNCs, and partially due to the increase in PVOH crystallinity.

It is worth noting that no previous work has reported such high Young's moduli for CNC-reinforced PVOH materials – values are usually in the range of several GPa (Paralikar et al. 2008; Mandal and Chakrabarty 2014; Sirviö et al. 2015). However, the literature does not report mechanical properties of PVOH coatings measured by SIEBIMM, and as mentioned earlier, a comparison of absolute elastic moduli determined by different techniques on materials prepared in different ways is challenging. Furthermore, for PVOH-based materials characterization is often performed on thicker (free standing) samples. As such, we believe that this work demonstrates that SIEBIMM is a quantitative tool (to compare relative values) to assess the impact of the reinforcing additive on PVOH coatings, as discussed above, as well as the parameters of the coating process, as discussed in the next section.

1.3.3. Influence of coating parameters on the Young's modulus PVOH/CNC coating

The processing method of a nanocomposite material governs its resulting mechanical properties (Dufresne 2008). The purpose of this section is to show how the SIEBIMM method can be used to determine the influence of each processing step on the mechanical properties of micrometer-thick coatings. The formation of a continuous network and the orientation of the nanocrystals are two key parameters for the elastic modulus properties. In addition to which, processing speed, solution viscosity, orientation and drying have a strong impact on CNC orientation/distribution and consequently on the mechanical properties of the coating.

Bar coating vs solvent casting deposition. Both neat and CNC-reinforced PVOH was deposited onto PDMS substrates, either by solvent casting or bar coating to compare the effect of deposition method on the Young's modulus of the coating. Figure 7A shows the linear relationship between buckling wavelength and thickness after bar coating for thicknesses ranging between 350 nm and 9.4 μm . A clear difference can be seen between the neat PVOH and the CNC reinforced samples, in addition to which, a steeper slope in the linear relationship is evident in comparison to that reported for the solvent casting deposition method, as shown in Figure 5A. Figure 7B reports the Young's moduli as a function of the CNC content and method of deposition. It appears that (i) the addition of CNCs increases the elastic modulus in both cases and (ii) higher values are obtained with bar coating. Due to the synergistic effect of the orientation and mechanical properties of the CNCs, along with their high affinity for the hydrophilic PVOH matrix, an average elastic modulus as high as 73.8 GPa can be obtained for a bar-coated PVOH/CNC coating containing 10 wt% CNCs.

The underlying difference between the two coating techniques is the orientation of the CNCs within the resulting composite. Where solvent casting results in an isotropic deposition, the bar coating process forces the CNCs to align in the direction of coating, leading to an orientation of the CNCs as measured by small angle x-ray scattering (Figure 8). Indeed, previous studies have already reported the alignment of CNCs as a result of shear stress (Hoeger et al. 2011; Abitbol et al. 2014).

The high Young's modulus values seen for PVOH/CNC coatings prepared by bar coating is most likely explained by the CNC orientation but also by the fact that the compression of the samples

during testing was performed along the axial direction, and consequently in the same direction as the assumed orientation of the CNCs. Other phenomena also participate to increase the Young's modulus, even in the neat PVOH coatings; i.e., the drying mechanism of a droplet onto PDMS - the so-called "coffee ring effect" (Deegan et al. 2000) – is very different than that occurring in a thin film. Interestingly, however, no differences in the degree of crystallinity were observed regardless of deposition technique.

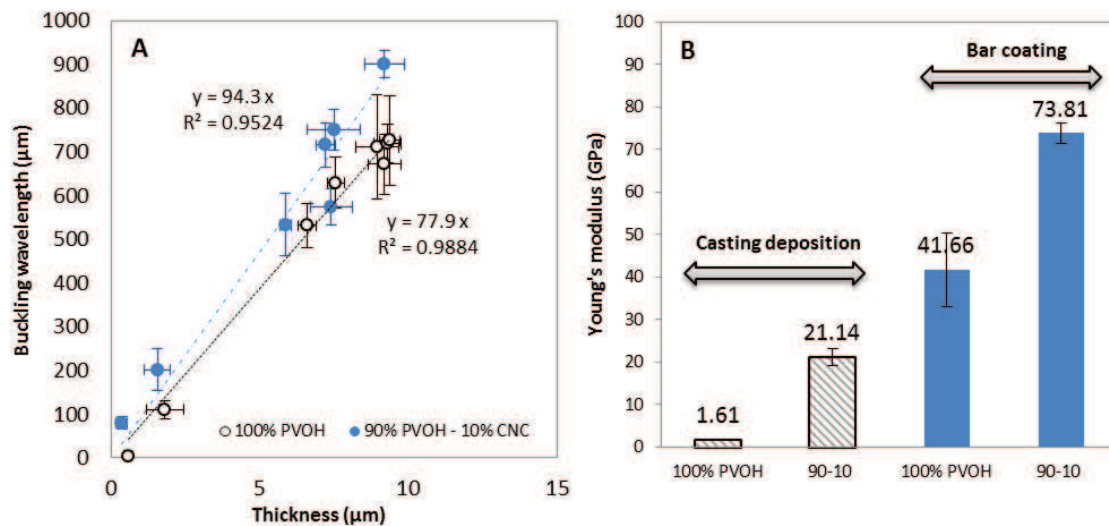


Figure 7: A) Buckling wavelength at 50 %RH as a function of film thickness for bar coated samples comparing neat PVOH (open circles) and 90% PVOH-10% CNC nanocomposite (filled blue circles) coatings, and B) Young's modulus comparing casting and bar coating deposition methods, for neat and 10 wt% CNC-reinforced PVOH.

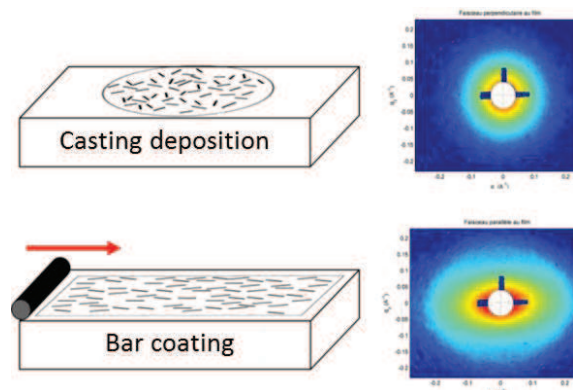


Figure 8: Orientational order of CNCs in PVOH matrix as a function of the coating method as interpreted using SAXS data (SAXS images adapted from Senechal et al. 2010.)

Influence of drying temperature and humidity on mechanical properties of coatings.

The drying step of coating preparation is another processing parameter which can lead to variations in the mechanical properties. Due to the lack of readily available techniques, the effect of drying on the Young's modulus of a coated layer has not previously been studied despite the

potential implications to paper and packaging applications. As such, the effects of drying on neat and CNC-reinforced solvent cast PVOH coatings were assessed at three different temperatures (23°C, 50°C and 90°C for respectively 24 h, 4 h and 1 h). Figure 9A shows an increase in the Young's modulus (measured by SIEBIMM) with increasing drying temperature for both coatings, while still showing the positive impact of CNC reinforcement on the mechanical properties. This increase in Young's modulus with increasing drying temperature can be explained by an increase in the degree of crystallinity of PVOH as reported in **Chapter II.2**.

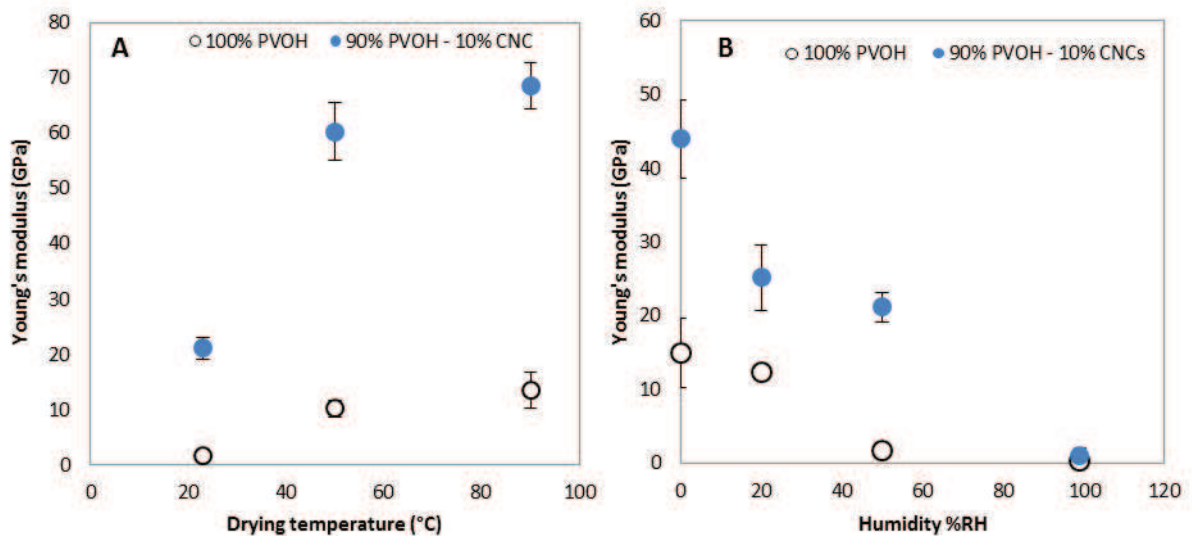


Figure 9: Young's modulus for neat PVOH and PVOH/CNC coatings (determined using the SIEBIMM method) as a function of A) drying temperature of the coating (at 50 %RH) and B) the relative humidity during the measurement.

The results reported above are for buckling experiments carried out at a constant relative humidity of 50 %RH. Subsequently, we investigated the effect of humidity on neat PVOH and CNC-reinforced PVOH coatings solvent cast on PDMS and dried under ambient conditions (23°C and 50 %RH). Buckling was performed at four different relative humidities of 0, 20, 50 and 98 %RH. As shown in Figure 9B, the Young's modulus of the coatings were highly dependent on relative humidity: the higher the relative humidity, the lower the Young's modulus, and a maximum value of 44 ± 5 and 15 ± 5 GPa were obtained for the neat PVOH and CNC-reinforced coatings at 0 %RH, respectively. As the calculation of elastic modulus with SIEBIMM is highly dependent on film thickness, the influence of humidity on the thickness of the coatings was determined through SE measurements carried out at 0, 35, 40 and 50 % RH. Results showed that coating thickness was not affected by relative humidity, and as such, the thickness of the coating was assumed constant at 98% RH as well. Furthermore, the Poisson's ratio of the coating and the PDMS was assumed to be independent of humidity.

It appears from the humidity testing results that the PVOH/CNC composite coatings are more sensitive to water than neat PVOH (as shown by the steeper slope for coatings with CNCs in Figure

9B). More specifically, the CNC-reinforced PVOH coating showed an increase of 0.4 GPa in Young's modulus per unit decrease in relative humidity, whereas the corresponding increase for neat PVOH was only 0.1 GPa. This result is expected given the humidity sensitivity of both PVOH and hydrophilic natural fibers (and CNCs) which is known to decrease their reinforcing abilities under high humidity and wet conditions. Previously, PVOH has been studied for its utilization in humidity sensors, as it has an inherent ability to both absorb and desorb atmospheric moisture, and readily change its moisture content (Yang and Chen 1998; Chen and Kao 2006). In the PVOH/CNC systems here, both water and PVOH interfere with the cellulose-cellulose van der Waals interactions, and hydrogen bonds are replaced with cellulose-water hydrogen bonds. This distinct dependence of the Young's modulus on humidity measured using the SIEBIMM method has also been observed for CNC-polyethylenimine (PEI) composites (Kan and Cranston 2013) and CNC-xyloglucan composites (Martin 2015). In both cases, the elastic modulus decreased linearly with increasing relative humidity. Kan and Cranston predicted an increase of 0.3 GPa per unit decrease in relative humidity for the CNC-PEI system, which is in direct agreement to the trend found here.

1.4. Conclusions

This work investigated the adaptability of the buckling-based metrology SIEBIMM to determine the Young's modulus of micrometer-thick nanocomposite coatings. Young's moduli could be determined for PVOH coatings of up to 35 μm thick, whilst still meeting all of the conditions set forth by the model. However, small thickness variations induced significant fluctuations in the calculated Young's moduli, which suffer from the heterogeneities of thicker coatings. Consequently, a few notes of caution should be considered: first, the coating thickness and the buckling wavelength must be measured on the same spot on the sample, and secondly, it is recommended to carry out buckling experiments using a minimum of three coating thicknesses such that a linear regression analysis of the data can be performed to minimize the error.

The SIEBIMM method was also used to characterize the influence of both adding CNCs as a reinforcing agent for PVOH coatings, and the coating process parameters (i.e., isotropic or oriented deposition, drying temperature, humidity) on the Young's modulus. Results showed a strong increase in modulus with the introduction of 10 wt% CNCs into the PVOH coating, due to the synergistic effect between CNC reinforcement and the successive increase in PVOH crystallinity. A constant Young's modulus of 21 ± 2 GPa was obtained for solvent cast coatings of PVOH/CNC on PDMS ranging from 600 nm to 17.5 μm in thickness. An increase in Young's modulus was also observed when the CNC orientation (by bar coating) and drying temperature were increased. Measurement of Young's modulus obviously depends on several parameters such as cellulose source (crystal structure and degree of crystallinity), measurement technique, material protocol, possible defects and environmental conditions (Kan and Cranston 2013). The values reported here for CNC-reinforced PVOH coatings were higher than those reported in the literature from other experimental

techniques. However, the SIEBIMM method for micrometer-thick coatings should be considered as an easy and powerful tool to measure the impact of additives and process parameters on mechanical properties such that the performance and potential applications of nanocomposite coatings can be fully assessed.

2. Impregnation of paper with cellulose nanocrystal-reinforced PVOH: synergistic effect of infrared drying and CNC content on polymer crystallinity

*This article is adapted from J. Desmaisons, M. Rueff, J. Bras, A. Dufresne, "Impregnation of paper with cellulose nanocrystal (CNC)-reinforced PVOH: synergistic effect of infrared drying and CNC content on crystallinity" Submitted in **Journal of Material Science**.*

2.1. Introduction

During paper impregnation with polymer solutions and the subsequent drying process, complex phenomena are involved that determine the final properties of the paper. Understanding these steps allows the manufacturing of materials with tailored properties such as barrier properties, stiffness, or dog-ear resistance. Dog-ears refer to flapped corners appearing on paper sheets. One reason for this complexity is the synergistic effect between independent parameters (material structure, polymer solution concentration, presence of filler, drying temperature, and polymer thermal properties) which become very critical for a key parameter: the crystallinity of the impregnated semi-crystalline polymer.

Polyvinyl alcohol (PVOH) is a water soluble semi-crystalline polymer commonly used in the paper industry. The crystallization of PVOH is a process associated with the partial local alignment of the polymer chains. This process results in the formation of folded chain lamellae, forming larger spheroidal structures known as spherulites. It is well-known that the properties of a semi-crystalline polymer depend on its degree of crystallinity but also on its crystalline structure (Pukánszky et al. 1997). It has been found for example that the yield stress of polypropylene is a function of the spherulite size (Way et al. 1974; Karger-Kocsis 1989) and a correlation has also been observed between its crystalline structure and its fracture resistance (Karger-Kocsis 1989). However, this "crystalline structure" is in fact a set of several parameters such as the crystalline form, lamella dimensions, crystallite size, spherulite size, and degree of crystallinity, which all affect the mechanical properties simultaneously and change as a function of the crystallization conditions. It has been nonetheless found that the most important parameters determining the stiffness of polymers are lamella thickness and degree of crystallinity, and a mathematical equation has been proposed for calculating the Young's modulus of polypropylene by analyzing the crystallization exotherms (Pukánszky et al. 1997). The effect of crystallinity parameters on the Young's modulus is consequently no longer under debate. In parallel, the relationship between Young's modulus and elastic recovery for nanocomposite coatings has been reported (Musil et al. 2002). The elastic recovery of such coatings can be directly linked to the dog-ear resistance of impregnated paper. Such a relationship has never been studied, to our knowledge.

Thanks to their very high Young's modulus (about 140 GPa), cellulose nanocrystals (CNCs) have been tested since the mid-1990s as reinforcing agents in polymer matrices for a large range of composite applications such as automotive, construction, membranes, adhesives, and sensors (Mariano et al. 2014). Because of their small dimensions and resulting retention issues, the use of CNCs in papermaking is often limited and only a few papers address the introduction of CNC for paper coating or impregnation alone (Gicquel et al. 2017) or in slurry (El-Wakil et al. 2015; Mascheroni et al. 2016). The addition of small amounts of CNC to a polymer matrix has shown improvement of the polymer film's mechanical and barrier properties in multiple examples (Paralikar et al. 2008; Roohani et al. 2008; Siqueira et al. 2009; Oksman et al. 2016; Espino-Pérez et al. 2018). Furthermore, CNCs play the role of reinforcing agent but can also impact the crystallization of the polymeric matrix when using a semi-crystalline polymer. It is known for example that the presence of CNCs decreases the activation energy for crystallization and hence dramatically accelerates the crystallization kinetics, as has been shown for example for polycaprolactone (Siqueira et al., 2011) or polypropylene (Gray, 2008). It appears that CNCs act as "nucleating agents", i.e., they favor the germination process. CNCs are also known to induce heterogeneous crystallization and crystal growth in two dimensions. Furthermore, the shape of the nanoparticles, their specific surface area, and their surface chemistry can also impact the crystallization of polymers such as polycaprolactone (Siqueira et al. 2011).

In parallel, it is well known that the crystallization temperature is a key factor influencing polymer crystallization. From the glass transition to the melting temperature, when the crystallization temperature increases, the critical nucleus size becomes bigger and it leads to the formation of a smaller number of larger crystals. Crystal growth becomes dominant over its nucleation. The drying temperature of the paper after impregnation with a water soluble polymer-CNC suspension is thus important, as polymer crystallization occurs during this step. The temperature to consider is the actual temperature at the surface of the paper during drying, which may differ from the set temperature and also depends on the type of drying process used (radiative vs. conductive). To our knowledge, there is no published study focusing on the crystallization of water soluble polymers impregnated into paper and its relationship with drying conditions and CNC filler content.

Therefore this study aims to understand the crystallization of PVOH during the paper impregnation process, when the polymeric matrix is reinforced with CNCs and submitted to different drying treatments. First, the impact of CNCs on the drying kinetics of the PVOH layer will be studied, followed by the impact of both CNCs and drying conditions on PVOH crystallization (Figure 1). The first part of the study defines the paper material structure after impregnation and penetration of the PVOH/CNC composite. The second part deals with a comparison between two drying modes: drying under infra-red radiation or in an oven, and focuses on the modeling of heat flow during infra-red treatment. The contribution of CNCs to the drying kinetics is also investigated. Finally, the third part studies the crystallization process of PVOH at the end of the impregnation process, influenced by the presence of CNCs and the drying conditions used.

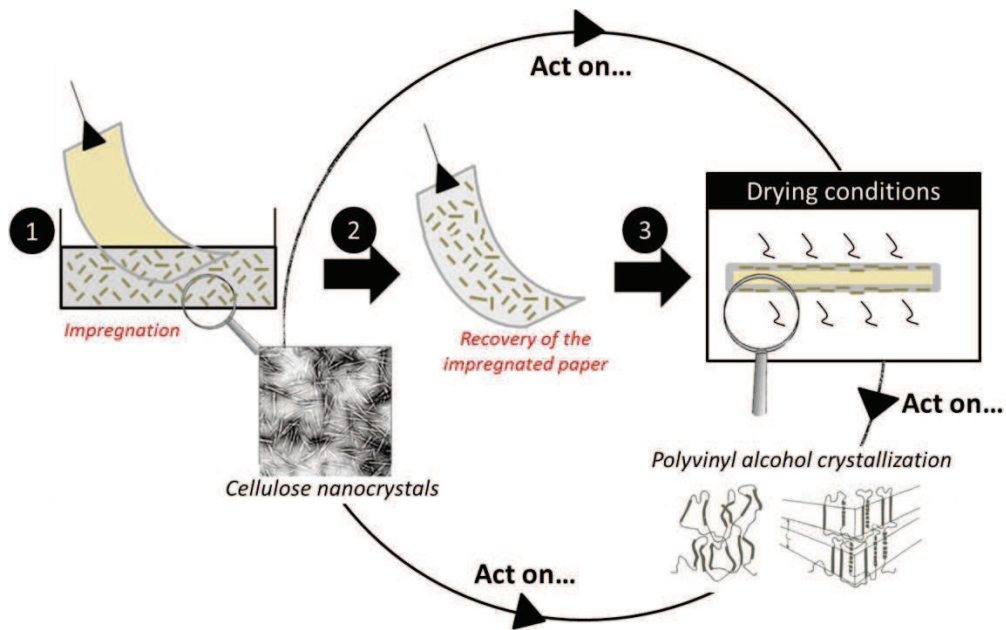


Figure 1: Effect of CNCs and drying on PVOH crystallinity during the paper impregnation process

2.2. Materials and methods

2.2.1. Materials

Paper substrate was kindly supply by the paper company partner. The fibers used for the paper consisted of 100 wt% cotton (60°SR). TiO₂ anatase, strengthening agent polyamidoamine epichlorohydrin (PAE) and anionic polymer carboxymethylcellulose (CMC) were used as additives in the pulp slurry in confidential amounts. Two layers with basis weights of 20 g.m⁻² (first layer) and 60 g.m⁻² (second layer) were combined to form the resulting semi-finished paper product, which has a final basis weight of 80.8 ± 2.4 g.m⁻².

The PVOH used in this study was a mixture of Mowiol 28-99 (Mw = 145,000 g.mol⁻¹, acetyl content 0.2-1%) and Mowiol 6-98 (Mw = 47,000 g.mol⁻¹, acetyl content 1.1-1.9%), bought from Sigma Aldrich. Commercial CNC extracted from wood pulp was purchased from the University of Maine as a 12 wt% CNC suspension. The nano-rods have a length of 136 nm (± 43), and a width of 11 nm (± 2). Their detailed characterization is available elsewhere (Gicquel et al. 2017).

2.2.2. Methods

PVOH-CNC formulation. Mowiol 28-99 and Mowiol 6-98 were mechanically mixed in a weight ratio of 2:1, respectively, and added to water with a final PVOH concentration of 5 wt%. When the temperature reached 90 °C, the suspension was mechanically stirred for at least 2 h, until the PVOH was completely dissolved. To introduce CNC into the PVOH solution, the previously prepared PVOH mixture was heated at 60 °C, then the desired quantities of water and CNC suspension were added to

obtain several CNC/PVOH ratios (wt%). Water was then added to obtain a 5 wt% total solid concentration. The suspension was mechanically stirred for 1 h, then the suspension was exposed to an ultrasonic dispersive energy of 5 kJ.g^{-1} of dry CNC using a 250 W (or 250 J.s^{-1}) sonication probe (Sonifier S-250A, Branson, USA) at 50% of maximum energy and at room temperature with an ice bath.

Impregnation and drying protocol. Paper substrates with $15 \text{ cm} \times 10 \text{ cm}$ dimensions were immersed in a hot impregnation bath ($60 \text{ }^\circ\text{C}$) containing the mixture of PVOH and CNC for 20 s. Then the impregnated paper was placed on a Teflon plate and the overflow was removed with one pass of a 1 kg Teflon roll. The sample was placed in an oven with air convection and dried at $115 \text{ }^\circ\text{C}$ for 3 min. During drying the sample was maintained under tension between two metal frames. When specified in the text, other drying processes were tested by extending the drying time or by using infrared lamps. Infrared drying was performed with 2,500 W long-wave IR lamps. As it is possible to dry only one side with IR lamps with our equipment, two passes were performed by turning the paper over between two drying steps. Each drying step lasted 60 s.

Modeling of infrared drying in short-wave IR dryer. To model the heat transfer during infrared drying, experiments were set up on a short-wave ($2 \times 1,000 \text{ W}$ tubes) electrical infrared dryer (234 V) (Figure 2). Impregnated paper ($14 \text{ cm} \times 17 \text{ cm}$) was placed on a frame directly attached to a balance (PE 360 from Mettler, precision 1 mg) during drying to measure the weight of evaporated water. In parallel, thin T-type thermocouples, manufactured in the laboratory with $75 \text{ }\mu\text{m}$ insulated wires from Omega (United Kingdom), were fixed on each side of the paper to measure the surface temperature of the sample. It is worth noting that the thermocouples were not protected against incident light and an error factor should be taken into account.

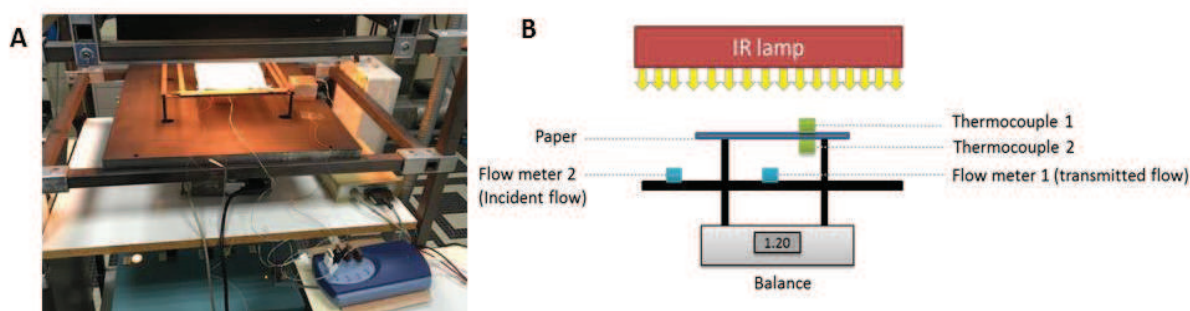


Figure 2: Experimental set up to determine the heat transfer occurring during short-IR drying, A) Actual set up and B) outline

Two heat flux meters (CapTec, Lilles, France) were also used: one under the paper to measure the heat flux below the sample during drying, and the other placed on an external corner to measure the incident heat flux. The position of the lamps was 22 cm above the paper and the maximal incident flux density was 4.8 kW.m^{-2} . A correction factor k was used to take into consideration the difference of solid angle radiation between the central fluxmeter and the external fluxmeter. The signals from the thermocouples and fluxmeters were recorded and converted into physical values using a TC08

thermocouple data logger and Picolog software (Pico technology, United Kingdom). The evaporation flux density was obtained after smoothing and derivation of the weight as a function of time using an Excel macro. The temperature values were also smoothed and derivatized as a function of time with the same macro.

Differential scanning calorimetry (DSC). DSC analyses were carried out with TA DSC Q100 equipment. As mentioned at the end of the Introduction, DSC measurement were performed using neat PVOH and CNC-reinforced PVOH films obtained by casting/evaporation, whose crystallinity can differ from that of impregnated PVOH solutions on paper. This is related to the impossibility of characterizing the impregnated papers. Nevertheless, the study remains comparative even if it is not directly quantitative. Samples with a weight of 8 ± 2 mg were analyzed with different heating rates (as shown in Table 1) under a N₂ atmosphere. Measurements were performed at least in duplicate. The heat of fusion ΔH_m was obtained from DSC curves and used to determine the degree of crystallinity (X_c) of the sample by its relationship with the theoretical 100% crystalline heat of fusion (ΔH_m°), using equation (1):

$$X_c = \frac{\Delta H_m}{\Delta H_m^\circ \times (1-w_f)} \times 100 \quad (1)$$

where $\Delta H_m^\circ = 161 \text{ J.g}^{-1}$ is the enthalpy of fusion for 100% crystalline PVOH,¹⁶ and w_f is the weight fraction of the cellulosic filler, here CNC, included to normalize the enthalpy according to the polymer content in the sample.

Table 1: Description of the DSC sequences performed.

Classical ramp	Variation of crystallization temperature	Influence of convective and radiative drying on PVOH crystallization	
		Convective	Radiative
Heating scan: 10°C.min ⁻¹ Start: -50°C Stop: 250 °C	Erasing thermal history: 1: Heating scan 100°C.min ⁻¹ from RT to 237°C 2: Isotherm for 15 min Fast cooling to crystallization temperature Tc: Cooling scan 100°C.min ⁻¹ to Tc Isotherm for 15 min Melting: Heating scan 10°C.min ⁻¹ to 250°C	Erasing thermal history: 1: Heating scan 100°C.min ⁻¹ from RT to 237°C 2: Isotherm for 15 min Temperature in impregnation bath: 3: Heating scan 100°C.min ⁻¹ to 60°C 4: Isotherm for 15 min Conductive drying: 5: Cooling scan 100°C.min ⁻¹ to 47°C 6: Isotherm for 0.67 min 7: Heating scan 82°C.min ⁻¹ to 115°C 8: Isotherm for 0.50 min Melting: 9: Heating scan 10°C.min ⁻¹ to 250°C	Erasing thermal history: 1: Heating scan 100°C.min ⁻¹ from RT to 237°C 2: Isotherm for 15 min Temperature in impregnation bath: 3: Heating scan 100°C.min ⁻¹ to 60°C 4: Isotherm for 15 min Radiative drying: 5: Heating scan 100°C.min ⁻¹ to 200°C 6: Isotherm for 2 min Melting: 7: Heating scan 10°C.min ⁻¹ to 250°C

Modeling of crystallization kinetics. The heat flow measured during the crystallization exotherm and melting endotherm was extracted from DSC experiments and analyzed using TA Universal analysis software. The melting temperature was recorded at the maximum of the melting endotherm peak. The degree of crystallinity (X_c) of the samples was determined from the heat of fusion (Eq. 1). The Avrami parameters (n , k) as well as the relative crystallinity X_r (%) and the crystallization half-time ($t_{1/2}$) were extracted using the Avrami plug-in developed by Lorenzo (Lorenzo et al. 2007). All fits were performed for a relative volumetric conversion ranging from 3% to 20%, considering a crystal density for PVOH of 1.35 g.cm^{-3} and an amorphous density of 1.26 g.cm^{-3} .

Scanning Electron Microscopy. SEM observations were performed with ESEM (Quanta 200©, FEI, Japan) on paper cross-section and surface after gold sputter coating of 5 nm, with a tension of 10 keV, a spot size of 3.5 nm, in EDT mode. The working distance was 10 mm. At least 10 images were recorded for each sample and the most representative were selected.

CNC grafting with fluorescent agent. A commercial fluorescent agent (Tinopal CBS, BASF, Germany) was used. This fluorescent agent consists of a 27 wt% solution of 4,4'-distyrylbiphenyl sodium sulfonate salt (DSPB) with a molecular weight of 562 g.mol^{-1} . For the preparation of 15 g CNC (dry content), a dilute solution of DSPB was prepared by adding 0.250 g of pure solution to 45 g of water. Then, 0.5 g of the diluted solution was added to the 0.5 wt% CNC suspension and stirred for 15 min in a flask wrapped with aluminum foil to prevent photolysis of DSPB. The CNC was dialyzed against distilled water for at least one week, until no more fluorescence was detected in the washing water.

Optical microscopy of cross-sections with paper inclusion. Inclusion resin was prepared from a mixture of dibutyl phthalate and epichlorohydrin, called "Araldite M". An 11 g quantity of araldite was mixed with 12 g of dodecenyl succinic anhydride (DDSA) and 0.6 g of benzyl dimethyl amine (BDMA). After stirring, the resin was degassed under vacuum for 2 h. The resin was then poured into individual molds $0.7 \text{ cm} \times 1.5 \text{ cm}$ containing paper samples. The resin was then again degassed under vacuum for 5 h. Finally, polymerization of the resin was performed in an oven at $60 \text{ }^\circ\text{C}$ for 48 h. Tough resin blocks with embedded paper were recovered. A microtome was used to cut paper slices $7 \text{ }\mu\text{m}$ thick. These slices were observed with an optical microscope (Zeiss Axio Vert.A1, Germany). DSPB (fluorescent agent) absorbs in the UV spectral range (absorption wavelength 351 nm) and emits strong blue fluorescence (emission wavelength 425 nm). The reflector was chosen for an excitation wavelength ranging between 325 and 375 nm. Images were analyzed using AxioVision Release 4.8 and ImageJ software.

Zero-span Breaking length L_{r0} (km). The breaking length of paper was measured using a joined-clamp tensile device (Pulmac TS-100, USA) following the ISO:15361 method. Samples had a width of 15 mm and a length of 5 cm. All samples were stored in a conditioned room ($23 \text{ }^\circ\text{C}$, 50% RH) for at least 48 h before testing and 10 duplicates were performed to obtain average values. Wet samples were immersed for 1 min in water and pressed between two blotter papers to remove the excess water. The breaking length L_{r0} (km) was calculated using the following equation (2):

$$Lr_0 = \frac{F}{l.g.BW} \quad (2),$$

where F is the force at break (kgf), l is the sample width (0.015 m), g is the gravitational constant (9.8 m.s⁻²) and BW is the basis weight (g.m⁻²).

2.3. Results and discussion

Note: a positive influence of CNC-PVOH impregnation on paper stiffness and elastic angle recovery was reported and patented earlier in this project (Bras et al. 2017). This study reports on our fundamental understanding of the changes in material properties occurring during the impregnation and drying steps responsible for the final folding resistance of the paper.

2.3.1. Paper structure and penetration of the composite during the impregnation process

When a plastic film such as polyethylene terephthalate (PET) or polylactic acid (PLA) is dipped in an impregnation bath, it results in a multilayer material with three distinct zones, as there is no penetration of the substrate by the impregnating agent. This multilayer structure has already been observed in the literature for a coating of CNC on PET film, resulting in a coated layer thickness of 450 ± 50 nm, observed by SEM (Mascheroni et al. 2016). When a fibrous material such as paper is impregnated, the resulting material is much more complex and disordered due to the porosity of the paper, which can lead to different degrees of penetration of the coating into the paper. This penetration strongly depends on the paper structure (porosity, sizing), the solution concentration, and its viscosity, but also on the impregnation process and speed. Consequently, it is always difficult to predict the final structure. In the literature, CNC has rarely been studied as coating reinforcement for paper, and studies which proposed such applications did not mention the final paper structure (El-Wakil et al. 2015).

A model to define the paper structure after impregnation is its division into 3 zones: two PVOH-CNC layers, two PVOH-CNC-fiber composite layers, and a central fiber layer (Figure 3B). Finally, if the coating penetrates the bulk, fibers can become surrounded by the PVOH/CNC mixture (Figure 3C) and induce individual fiber reinforcement. All these possible structures can affect both the drying (surface drying or deep drying) and the final mechanical properties of the material. Indeed, mechanical laws are not the same for multilayers, composite or porous materials.

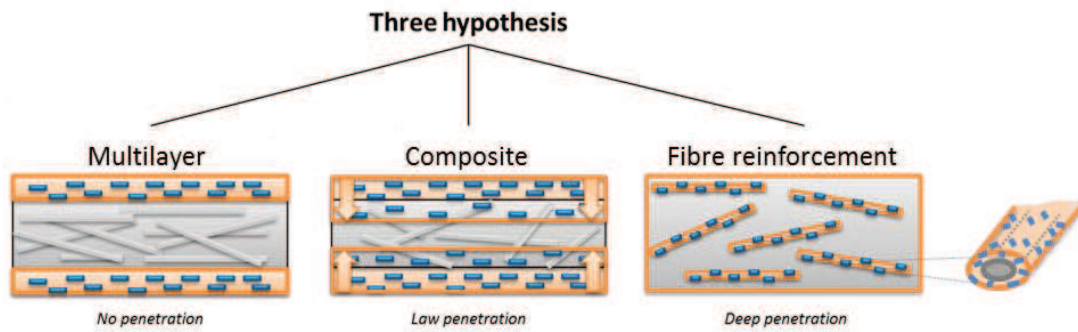


Figure 3: Penetration of PVOH/CNC after paper impregnation: three different models

Paper was impregnated with neat PVOH or 10 wt% CNC-reinforced PVOH composite. SEM images of paper cross-sections before and after impregnation were not accurate enough to detect the presence of CNCs and consequently do not provide clues about their location. However, observation of the surface shows coverage of the fibers after impregnation with either neat PVOH or 10 wt% CNC-reinforced PVOH (Figures 4A and 4B, respectively). Thickness measurement of the paper impregnated with neat PVOH or 10 wt% CNC-reinforced PVOH shows an experimental value of $3.4 \pm 0.4 \mu\text{m}$ for the layer thickness, which is $2 \mu\text{m}$ below the theoretical value obtained by calculation from basis weight (BW) and layer density (ρ) (thickness = $\frac{BW}{\rho}$). As this difference is not due to paper swelling (since the same values were obtained for theoretical and experimental thickness for a paper impregnated with water), it could be due to penetration of the coating. Furthermore, we can still distinguish the fiber surface once it is impregnated, meaning that the multilayer organization as reported for plastic films cannot be considered.

To confirm this result, penetration of CNCs was followed by grafting a fluorescent agent to the surface of the nanoparticles. After impregnation and paper inclusion, observations with polarized optical microscopy show fluorescence not only at the surface but deep inside the material (Figures 4C and 4D). To better visualize the fluorescent agent, images with inverted colors are presented in Figures 4E and 4F.

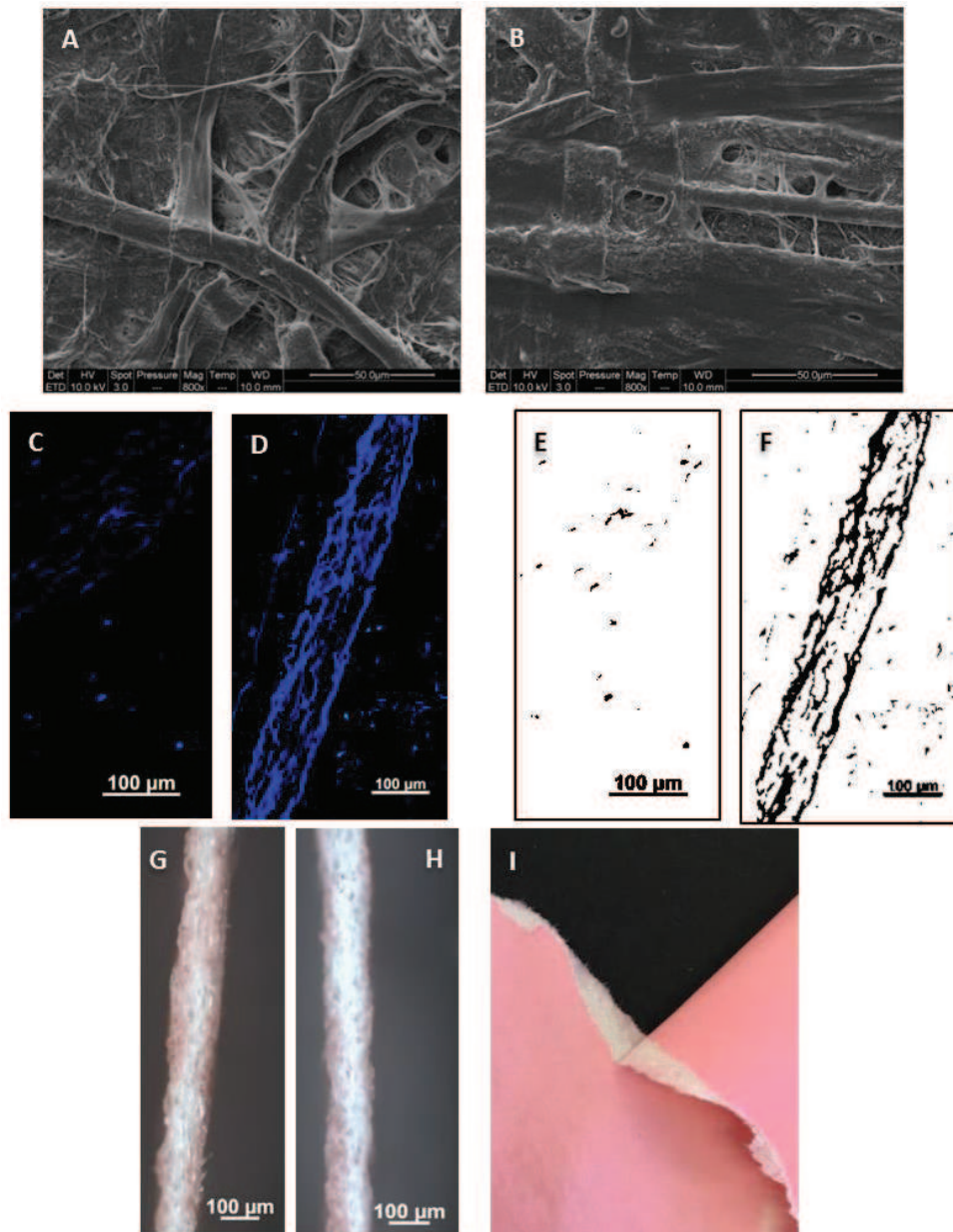


Figure 4: SEM images of the paper surface: (A) uncoated paper and (B) paper impregnated with neat PVOH. Optical micrographs of paper inclusion impregnated with (C,E) neat PVOH and (D,F) 10 wt% fluorescent CNC reinforced PVOH (C and D corresponds to real colors, and E and F to inverted colors). Optical micrographs of paper impregnated with (G) neat PVOH and (H) 10 wt% fluorescent CNC reinforced PVOH with addition of a red water dye in the impregnation bath. (I) Torn paper impregnated with red colored water impregnation bath.

The water pathway in the paper sheet during the impregnation process was also followed using a red azoic dye soluble in water (Figures 4G and 4H). Using ImageJ software, the penetration of water in paper was determined when impregnating with water, or a solution of 5 wt% PVOH or 10 wt% CNC-reinforced PVOH. The following results are described as a function of the total thickness of the paper. The water penetration for paper impregnated with only water was $70\% \pm 2$. This is confirmed in Figure 4I which shows that no dye is present in the middle of the paper once torn, confirming the partial penetration of water with our process. The solution penetration when using neat PVOH was very similar with a value of $60\% \pm 3$. The slight difference might be due to the slight

difference in viscosity between water and PVOH solution. In the case of impregnation with 10 wt% CNC-reinforced PVOH composite, the water penetration was exactly the same as for neat PVOH, which is consistent with the fact that the addition of CNCs does not change the viscosity of PVOH and therefore its penetration. These results rule out the possibility of the multilayer model and attest to significant penetration into the material. Furthermore, it can be seen that the penetration is asymmetric: this can be due to the asymmetric structure of the paper and asymmetric drying performed in this case with infrared lamps.

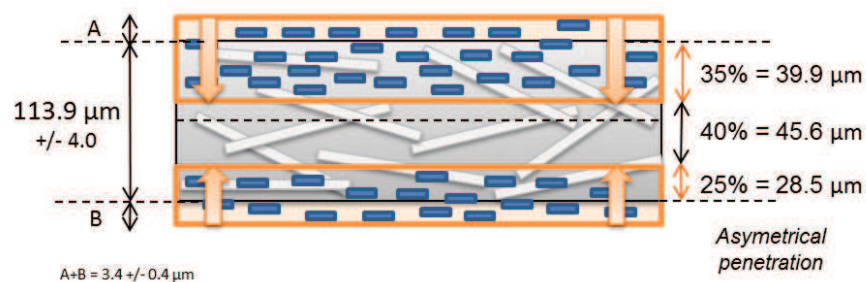


Figure 5: Penetration of PVOH or CNC-PVOH composite after paper impregnation.

Figure 5 summarizes the possible structure of the impregnated paper. One question is still pending: do we have any individual fiber coating? To know if the penetration also leads to fiber reinforcement, tensile tests with joined clamps were performed on the paper before and after impregnation with water, neat PVOH or CNC-reinforced PVOH, to determine the breaking length value L_{r0} . This test is characteristic of fiber strength, and the wet results are independent of the impacts of drying and of fiber interconnection. It appears in Figure 6 that similar results are obtained before and after paper impregnation with water, PVOH or CNC-PVOH composite. In other words, no fiber reinforcement appears with impregnation of neat PVOH or CNC-reinforced PVOH. Furthermore, SEM images of fibers at the breaking area show similar morphologies and do not show any appearance of a coating layer around the fiber. The model of fiber reinforcement can consequently be excluded. It should also be mentioned that other experiments were carried out to improve the visualization of the final material, such as X-ray nanotomography and cartography of chemical elements inside the material (X-ray microanalysis of grafted CNCs), and introduction of a micro-robot to measure the bending force of a single fiber inside the SEM device. However, these experiments did not lead to successful results and did not allow us to make any conclusions.

Consequently, the final impregnated paper has a complex structure with a composite part containing fibers, PVOH and CNCs, and a neutral layer with only fibers. This neutral layer represents only 40% (in volume) of the whole material. Furthermore, physical tests of the impregnated papers showed similar fiber strength before and after paper impregnation, meaning that no fiber reinforcement occurs.

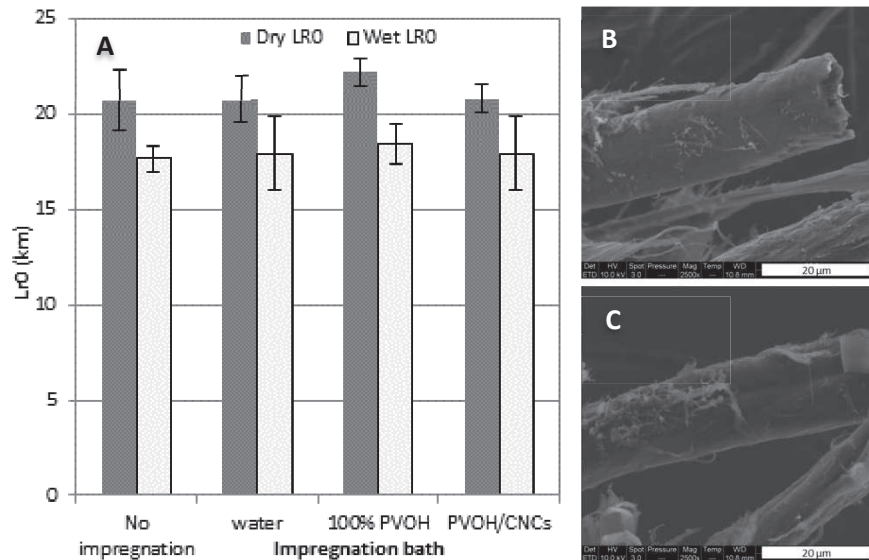


Figure 6: (A) Breaking length (Lr0/km) with joined clamps for dry samples and wet samples; SEM images of fibers at the breaking point for (B) the uncoated paper and (C) the paper impregnated with 10 wt% CNC reinforced PVOH.

2.3.2. Influence of CNC on drying mechanisms

After impregnation and penetration of the coating, the usual drying process for the paper is in an oven for 3 min at 115 °C (lab-scale process). By testing different drying conditions and measuring the paper's dog-ear resistance, it appeared that a significant improvement was obtained for a paper dried for 2 min with long-wave IR drying. This part deals with understanding (i) the difference between convective and IR drying conditions and (ii) how CNCs impact the drying kinetics.

Long-wave infrared drying vs. convective drying temperature measurement

The heat transfer process differs between convective drying and radiative drying and this could affect the paper drying kinetics. Most of all, the energy inputs are not in the same range and are far higher for infrared. Moreover, the temperature of the paper surface significantly differs between these two drying conditions. Thermocouples were fixed on the paper surface to follow the paper temperature during classical convective drying of 3 min at 115 °C (Figure 7A) and during 2 min infrared drying (Figure 7B). The temperature of air inside the oven regulated at 115 °C oscillates between 114 °C and 116 °C when the oven is empty. When the paper is drying, the air temperature 10 cm from the paper surface averages 115 °C (Figure 7A). However, the thermocouple fixed directly on the paper surface shows 4 different phases. First, there is a warm-up period where the temperature of the test piece increases until a given temperature (here 47 °C). Secondly, the temperature remains constant and isothermal drying takes place, during 100 s here. For convective drying (dispersion drying), a hot air flow is used to bring heat and remove water: heat is transferred to the product to evaporate liquid, and mass is transferred as a vapor into the surrounding gas. At the surface, a thin film of stagnant air is present. As evaporation is an endothermic phenomenon, the temperature at the paper surface is always lower than the temperature of the air and equilibrium is

established between the rate of diffusion of water through the boundary layer and the heat transport of the air flow. During the third period, the temperature at the paper surface increases until reaching that of air (here 115 °C) at a rate of about 80 °C.min⁻¹. Once the paper is completely dried, its surface temperature is equal to that of the air. Consequently, during a 3 min drying process in an oven at 115 °C, the paper surface is actually at 115 °C for less than 40 s. It was found that this temperature evolution was exactly the same regardless of the impregnation bath formulation (neat PVOH or 10 wt% CNC-reinforced PVOH).

In the case of infrared drying, the evolution of temperature at the paper surface is completely different: 200 °C is reached within only 10 s of drying and maintained during the whole drying process (Figure 7B). Slight differences of a few degrees can be expected between the top and bottom surfaces, but this is accounted for because the thermocouple measuring the paper surface temperature at the top is in front of the incident light, and the value is consequently slightly over-estimated. We can thus only conclude that the real paper surface temperature at the top is between 180 °C and 200 °C, which is still a very high temperature. In this case, heat transfer takes place by coupling between the infrared radiation and OH groups from the water, and evaporation can be very fast. Such a difference in temperature at the surface of paper between convective and infrared drying has already been observed in previous studies for other applications (Denneulin et al. 2011; Le Corre et al. 2012) and values obtained in this study agree with these previous observations.

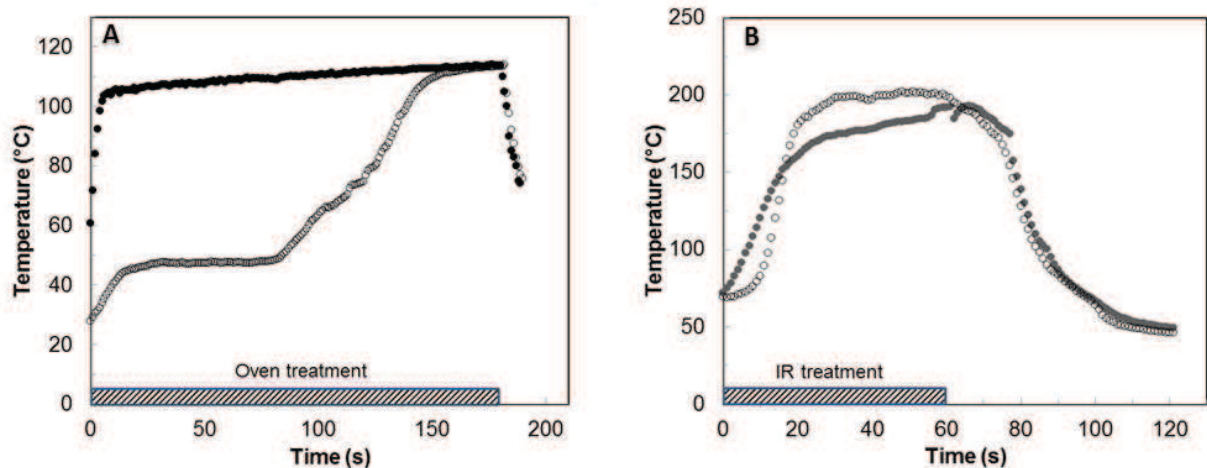


Figure 7: A) Evolution of the temperature in the oven (●) and at the surface of the paper (○) impregnated with neat PVOH, when applying 3 min convective drying (oven drying) at 115°C, B) Evolution of the temperature at the surface of the paper (below (●) and above (○)) impregnated with neat PVOH, when applying 1 min long-wave IR drying (2500 W). This drying was carried out twice (1 min for each side of the paper).

Influence of CNC on the short-wave infra-red drying mechanism

It is worth noting that exceptionally, this modeling was performed using short-wave IR-drying instead of long-wave IR drying as reported in the other parts of the study. Long-wave IR drying achieved better paper physical properties, but this equipment did not allow the simultaneous measurement of paper weight, paper surface temperature, and heat flux as was possible with the short-wave IR equipment.

After impregnation, the paper was dried with short-wave infrared equipment. To understand how CNCs act on the drying kinetics, the heat flux density under IR drying was calculated using the equations shown in Table 2. Thermocouples were fixed on the paper surface to follow the paper temperature during drying (solid line in Figure 8) and three different phases were observed. First, a heating phase is observed during which the temperature of the sample increases up to a given temperature (here 60 °C). Secondly, the temperature remains constant and isothermal drying takes place, during 1 min here. Once the paper is completely dried, a third period is observed where the temperature at the paper surface increases.

Table 2: Modeling of drying mechanisms.

Main equations	Parameter references
$\phi_{IR}(t) = \phi_{abs}(t) + \phi_{refl}(t) + \phi_{tr}(t)$	t: time (sec)
$\phi_{abs}(t) = \phi^*_{abs}(t) + \phi_{conv}(t) + \phi_{rad}(t)$	T: temperature (°C)
$\phi^*_{abs}(t) = \phi_{evap}(t) + \phi_{heat}(t)$	Cp : Heat capacity (kJ/kg.K)
$\phi_{evap}(t) = \frac{-dm(t)}{A dt} \times \Delta H_{evap}[T(t)]$	“w” = water
$\phi_{heat}(t) = \frac{m.Cp}{A} \times \frac{dT}{dt}$	“p” = paper
$m.Cp = \frac{mw(t).Cpw+mp.Cpp}{A}$	Cp _p = 1,3 KJ/kg.K
	Cp _w = 4,18 KJ/kg.K
	m: mass
	ΔH _{evap} (T) : heat of vaporization, which is a function of temperature
	A: area of the test piece
	φ _{IR} (t) (kW.m ⁻²) : Incident heat flux density
	φ _{abs} (t) (kW.m ⁻²) : Absorbed heat flux density
	φ _{refl} (t) (kW.m ⁻²) : Reflected heat flux density
	φ _{tr} (t) (kW.m ⁻²) : Transmitted heat flux density
	φ* _{abs} (t)(kW.m ⁻²) : Apparent absorbed heat flux density
	φ _{conv} (t) (kW.m ⁻²) : Heat flux density due to the convective heat exchange between the test piece and the surrounding air
	φ _{rad} (t) (kW.m ⁻²) : Heat flux density due to the radiation heat loss between the test piece and the surrounding
	φ _{evap} (t) (kW.m ⁻²) : Heat flux density corresponding to evaporation
	φ _{heat} (t) (kW.m ⁻²) : Heat flux density corresponding to the increase of temperature of the material

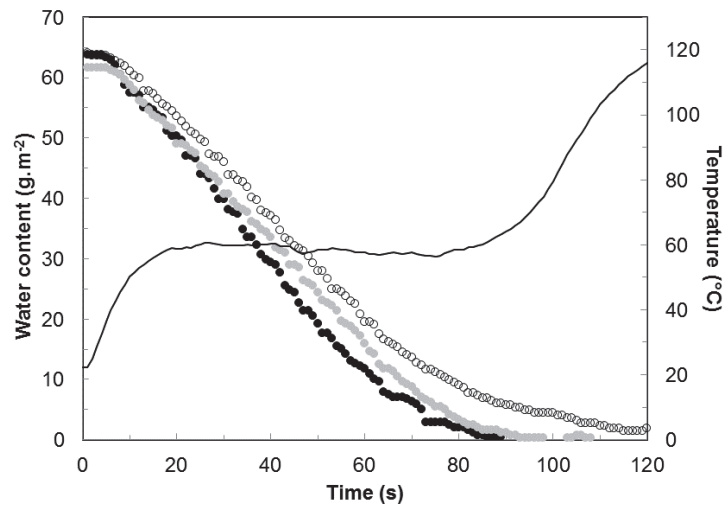


Figure 8: Influence of impregnation bath on water evaporation: Evolution of the water content during IR drying at 234 V as a function of time for paper impregnated with water (●), neat PVOH (○), and 10 wt% CNC reinforced PVOH (●), and evolution of paper surface temperature as a function of time (-).

During IR drying, the energy emitted by the lamps (ϕ_{IR}), or incident heat flux, is equal to the sum of the energy absorbed by the paper (ϕ_{abs}), the energy reflected by the paper (ϕ_{refl}) and the energy transmitted through the paper (ϕ_{tr}). This incident heat flux is measured as the total transmitted heat flux without paper.

The apparent absorbed heat flux is the sum of the heat flux needed for the evaporation of water (ϕ_{evap}) and the flux density responsible for the increase of temperature of the paper (ϕ_{heat}). Slight but significant differences can be observed in Figure 8 when the paper is impregnated with neat PVOH (open circles) or CNC-reinforced PVOH (grey circles). The introduction of CNC tends to accelerate the evaporation of water. A possible explanation could be that PVOH starts to boil during drying and forms a skin at the surface, thus hindering water evaporation. Assuming this hypothesis, CNCs could reduce this skin effect and hence promote the evaporation of water.

The evolution of the evaporation rate as a function of paper moisture content also shows slight differences between the paper impregnated with neat PVOH and the paper impregnated with CNC-reinforced PVOH composite (Figure 9). At the end of the drying process, the presence of CNCs speeds up the evaporation, which is consistent with the water evaporation acceleration observed when adding CNC (Figure 8). This might be due to their high specific surface area which increases the exchange surface. Recent PhD studies showed similar results (Guezennec 2012; Raynaud 2017), but cellulose nanofibrils (CNFs) were used instead of CNCs. Indeed, Raynaud (Raynaud 2017) reported faster PVOH solution drying (cast in Teflon mold) under infrared heating when CNFs were added into the solution. This study also reported a more homogeneous heat distribution at the beginning of the drying step induced by nanofibrils and mentioned a limited skin effect during fast PVOH drying when adding CNFs.

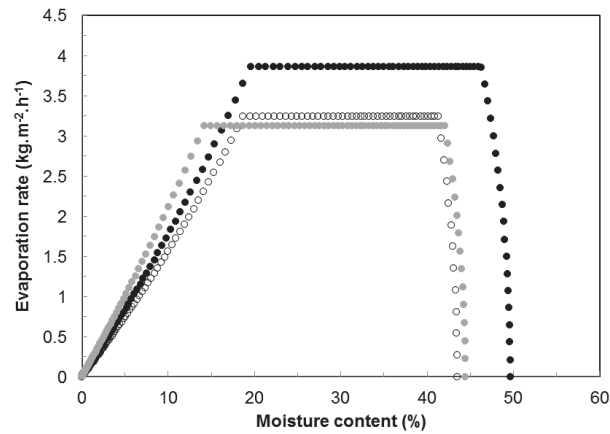


Figure 9: Evaporation rate during IR drying for paper impregnated with water (●), neat PVOH (○), and 10 wt% CNC reinforced PVOH composite (◌).

To deepen understanding of this phenomenon, each heat flux (absorbed, reflected, and transmitted) was calculated and analyzed separately. It should be noted here that the heat flux sensor placed below the sample measured the heat flux not only transmitted through the sample but also the heat flux irradiated by the sample on the sensor surface because the surfaces are not both at the same temperature. Therefore, this value is expected to vary slightly during the experiment as the temperature changes, but its order of magnitude can be evaluated at between 0.4 and 0.5 kW.m⁻². This term (ϕ_{rad}) as well as the convective heat exchange between the sample and the surrounding air (ϕ_{conv}) has been neglected. This assumption does not impact the following comments as it consists of a comparison between samples dried under the same conditions. Figure 10 presents the results obtained during paper drying after impregnation with neat PVOH (panel A) or 10 wt% CNC-reinforced PVOH (panel B). The incident flux is the same in both cases (same IR drying conditions). The transmitted flux is also similar with and without nanocrystals. However, differences appear for the absorbed flux at half of the drying stage: the absorbed flux is higher in the presence of nanoparticles (as indicated by the vertical lines in Figure 10A and B, and the black arrow in Figure 10A). This increase of absorbed flux at the end of the drying process in the presence of CNCs could explain the increase in evaporation rate for a given time. In both Figures 10A and 10B, the reflected flux density tends to increase after about 60 s of drying: the paper reflects the IR radiation more when it is dried, and this time of 60 s effectively coincides with a moisture content of the paper lower than 10%.

To conclude this discussion of drying mechanisms, it can be assumed that neat PVOH coating creates a skin effect which slows down the kinetics of water evaporation. This skin effect is slightly reduced when adding CNCs, i.e. evaporation is slightly faster, and differences appear at the end of the drying process where the absorbed flow is higher. In addition, CNCs do not impact the transmitted flow or the reflected flow. CNC can therefore be considered as a dielectric potential which might be more sensitive to IR and absorb more IR intensity. It is worth noting that the differences observed remain low, but could be enhanced by changing the IR wavelength/conditions.

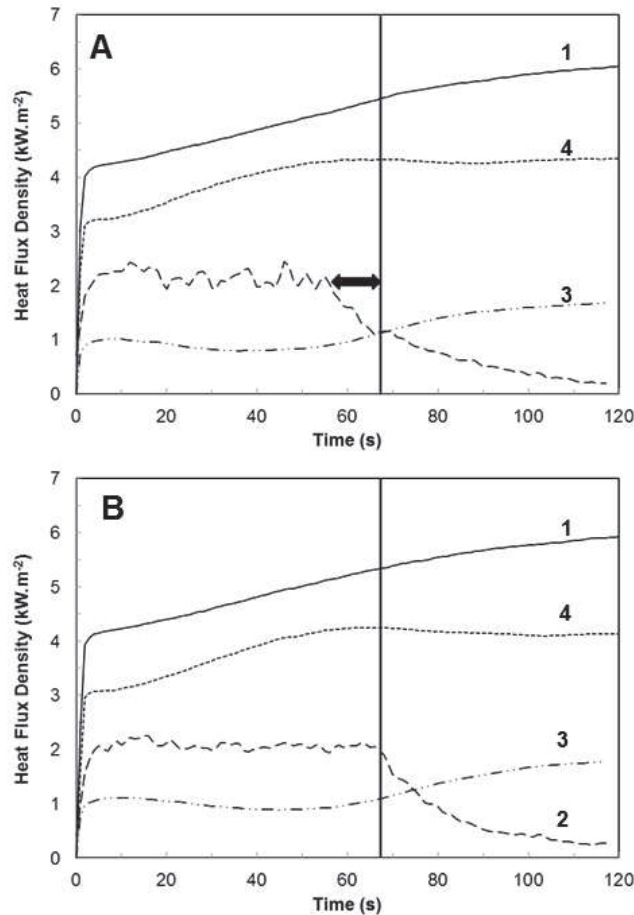


Figure 10: Heat flux density measured during drying for paper impregnated with (a) neat PVOH and (b) 10 wt% CNC-reinforced PVOH composite: incident (1), absorbed (2), transmitted (3) and absorbed + reflected (4) heat flux density. The vertical lines in Figs. 10a and 10b, and the black arrow in Fig. 10a indicate the difference between the two samples at half of the drying stage.

2.3.3. Effect of CNC on PVOH crystallization

After its impregnation on paper, the polymer passes from a liquid state to a solid state during the isothermal drying process and crystallization occurs at this stage. Crystals with various molecular chain orientations and sizes are formed. Under quiescent conditions, most often in very dilute solutions, crystalline lamellae or "single" crystals are formed. Lamellar thickness is controlled by nucleation and growth conditions. Electron microscopy (Hannay 1976) and other techniques (Peppas and Hansen 1982; Shan and Lickfield 2007) have shown that crystallization (growth) proceeds outward from a primary center (a nucleation site) until growth stops or slows down to an imperceptible level at very low supersaturation levels. Crystallization from more concentrated solutions or from the super-cooled molten state produces spherulites (polycrystalline spherical arrays). These arrays are formed by radiating platelets of lamellae (often splayed or branched) in which the polymer chains are also folded to varying degrees, depending upon the molecular weight of the polymer and experimental crystallization conditions. The chains are usually oriented tangentially to their growth direction.

The previous section showed that CNCs impact the drying of the impregnated layer. The influence of both CNCs and drying conditions on PVOH crystallization will now be investigated. Indeed, it is well known that nucleating agents or additives can have an effect on crystallization behavior (Gachter and Muller 1985), and that crystal growth is extremely temperature-sensitive and nucleation-controlled (Sadler 1987). Due to its hydroxyl groups, the crystallinity of PVOH is originally low as the formation of ordered macromolecular structures hinders its crystallization. However, it is possible to increase the polymer crystallinity by performing a second thermal treatment, also called an "annealing treatment".

At this stage it is worth remembering that the study on PVOH crystallization by DSC was carried out with polymer films (39 μm thick) and not coated papers, for practical issues. DSC measurements carried out on PVOH films with or without a thermal treatment at 150 $^{\circ}\text{C}$ confirmed that the degree of crystallinity of PVOH increases from 25% to 45% upon thermal treatment. In addition, an increase in the elastic angle recovery after folding (dog-ears resistance) from $63.2^{\circ} \pm 5.4$ to $83.4^{\circ} \pm 7.5$ has been observed by this simple annealing treatment. The investigation in the following section was carried out in order to show and explain the increase of PVOH crystallinity that we observe when we introduce CNCs in the polymer matrix.

Nucleating effect

The degree of crystallinity X_c of PVOH was determined for neat PVOH and CNC-reinforced PVOH from the melting endotherm and for different crystallization temperatures (Table 3). The results show an increase in the degree of crystallinity when adding the cellulosic nanoparticles. CNCs, due to their anchoring effect, act as very good nucleating agents. They indeed promote a heterogeneous crystallization of PVOH as confirmed elsewhere (Rescignano et al. 2014). From Table 3 it is also possible to see that the melting temperature (T_m) increases when the crystallization temperature (T_c) increases. When T_c increases, thicker crystals can form and consequently, the thermal energy needed for melting these bigger crystals increases. This phenomenon is attributed to the critical nucleus size, which is higher for higher T_c values. For a higher T_c , it is more difficult to form a nucleus (and consequently, a smaller number of crystals is expected) but growth is easier because of amorphous chain mobility.

Table 3: Degree of crystallinity (X_c) and melting temperature (T_m) determined by DSC for neat PVOH and 10 wt% CNC reinforced PVOH, after isothermal crystallization performed at different crystallization temperatures (T_c).

T_c ($^{\circ}\text{C}$)	Net PVOH		90 wt-% PVOH - 10 wt-% CNC	
	X_c (%)	T_m ($^{\circ}\text{C}$)	X_c (%)	T_m ($^{\circ}\text{C}$)
150	20	198.6	25	216.3
175	22	215.7	29	217.2
190	20	222.0	31	217.6
195	25	221.3	34	224.3
197	32	225.9	35	226.6
200	39	227.5	47	226.0

The degree of crystallinity of PVOH was found to increase as a function of CNC content until reaching an optimum around 10 wt% CNC (Figure 11). For higher CNC contents, the crystallinity starts to decrease. This optimal CNC content (10 wt%) corresponding to the highest crystallization has been observed previously for other polymer matrices. For tunicin CNC reinforced poly(oxyethylene), it was reported that the degree of crystallinity was constant up to 10 wt% CNC and decreased for higher contents (Azizi Samir et al. 2004). Similar results were observed for CNC-reinforced polylactic acid (Pandey et al. 2010). Increased crystallinity of PVOH upon adding CNC was also reported (Uddin et al. 2011). It was also observed that the dimensions of CNC have a stronger impact on the crystallinity of poly(butylene adipate-co-terephthalate) than its volume fraction (Mariano et al. 2016). This optimal CNC content can be explained by the percolation approach. According to the average length (136 nm) and width (11 nm) of CNCs used in this study, their percolation threshold can be estimated at around 6 vol% corresponding to about 7 wt%, assuming $1.3 \text{ g}\cdot\text{cm}^{-3}$ and $1.6 \text{ g}\cdot\text{cm}^{-3}$ for the densities of PVOH and crystalline cellulose, respectively. Therefore, for 10 wt% CNC the percolation threshold is reached, meaning that the nanoparticles can connect to form a percolating network. When a denser network forms it prevents the growth of polymer spherulites and consequently hinders the transport of polymer segments for crystallization. Moreover, addition of additional CNC above the percolation threshold can also lead to CNC aggregation, which can also hinder crystallization.

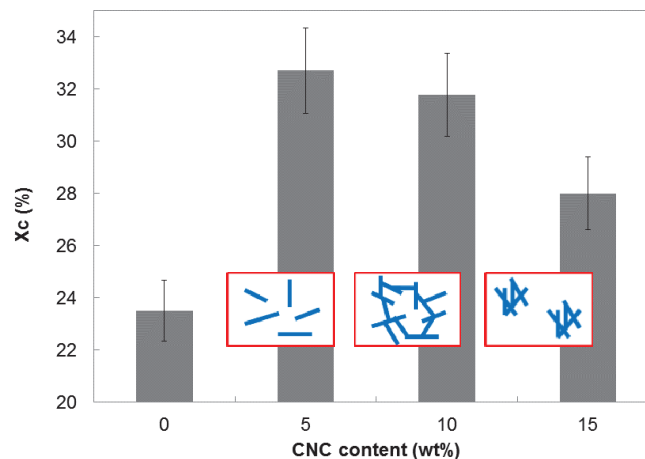


Figure 11: Evolution of the degree of crystallinity (X_c) for PVOH as a function of CNC content (simple heating scan).

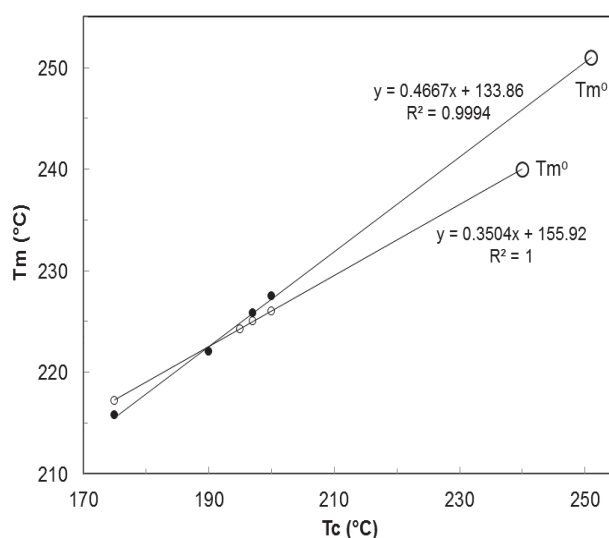
Crystal growth - Impact of CNCs on isothermal crystallization kinetics

The equilibrium melting temperature T_m° is defined as the melting temperature of an infinite size crystal. The T_m° of PVOH was evaluated using the Hoffman-Weeks method (Hoffman and Weeks 1962) for crystallization temperatures ranging between 175 and 200 °C (Figure 12). These results are to be taken with caution as this method is usually performed with a high number of data points, and so the results will only be considered qualitative. Data linearization and extrapolation were used to determine both the stability parameter (ϕ) and T_m° value based on the least square method (Hoffman and Weeks 1962; Nishi and Wang 1975) following equations 3 and 4:

$$T_m^0 - T_m = \phi \cdot (T_m^0 - T_c) \quad (3)$$

$$\gamma = 1/\phi \quad (4)$$

The thickening coefficient (γ), representing the ratio of the lamellar thickness to the lamellar thickness of the critical nucleus, was calculated from the stability parameter. The stability parameter (ϕ) varies from 0 to 1 and the lowest value corresponds to the most stable crystals. Results collected in Figure 12 show that with 10 wt% CNCs in PVOH matrix, the obtained equilibrium melting temperature ($T_m^0 = 240$ °C) is lower than the equilibrium melting temperature for neat PVOH ($T_m^0 = 251$ °C). This decrease in T_m^0 value imparted by CNC can be explained by the hindrance to crystallization introduced by the nanoparticles. A lower equilibrium melting temperature is also associated with a thinner lamellae thickness.



Sample	T_m (°C)	ϕ	γ
Neat PVOH	251	0.47	2.14
10 wt% CNC reinforced PVOH	240	0.35	2.86

Figure 12: Evolution of the melting point (T_m) as a function of crystallization temperature (T_c) for neat PVOH (●) and 10 wt% CNC-reinforced PVOH composite (○): determination of the equilibrium melting temperature (T_m^0), thickening coefficient (γ) and stability parameter (ϕ).

Figure 12 also shows the values obtained for the stability parameter (ϕ) and the thickening coefficient (γ) and also shows the difference with introduction of CNCs. The thickening coefficient corresponds to the ratio of the lamellar thickness to the nucleus critical size. As mentioned above, thinner lamellae thicknesses appear with the introduction of CNCs. An increase of this thickening coefficient can be explained by a predominant decrease of the critical nucleus size, which is consistent with the CNC nucleation effect.

We can then conclude that the presence of CNC promotes the reduction of the critical nucleus size, leading to an easier nucleation and a higher amount of crystals (responsible for an increase of degree of crystallinity), but with smaller lamellae.

Impact of CNCs on bulk crystallization kinetics

To further investigate the effect of CNCs on PVOH crystallization, the isothermal crystallization kinetics were analyzed using the Avrami equation (Table 4) where X_t is the relative degree of crystallinity, t the crystallization time, k the crystallization rate constant (min^{-1}) and n the Avrami exponent. The two latter parameters combine the contribution of both nucleation and growth. The crystallization kinetics are generally well characterized when the activation energy E_c , the Avrami exponent n , and the crystallization rate k are determined (Mehta et al. 2004). Avrami parameters describe the change of state in solids for a constant temperature, and are particularly useful for the description of crystallization kinetics. These parameters can be calculated assuming that nucleation occurs randomly and uniformly and that growth is similar in all directions. The Avrami coefficient n depends on the nucleation type and growth geometry, and its value ranges between 1 and 4. It indicates in particular if the crystal growth is one-dimensional, two-dimensional or three-dimensional. A value of 4 is classically obtained for a sporadic and three-dimensional growth while a value of 3 is obtained for instantaneous three-dimensional growth or two-dimensional and sporadic growth (Hafsaoui 2013). A value of 2 can reveal two-dimensional crystallization growth with a heterogeneous type of nucleation (Siqueira et al. 2011), and a value of 1 is characteristic of one-dimensional crystal growth.

Table 4: Study of crystallization kinetics, equations, parameters and results.

	Parameter	Neat PVOH	10 wt% CNC/PVOH	
Avrami equation $1 - X_t = \exp(-kt^n)$	X_t (%)	Relative crystallinity		
	t (min)	Crystallization time		
	k (min^{-1})	Crystallization rate		
	n	Avrami exponent		
Arrhenius equation $\frac{1}{n}(\ln k) = \ln k_0 - \frac{\Delta E_a}{RTc}$	k_0	Temperature-dependent pre-exponential factor	2.886	2.347
	ΔE_a ($\text{kJ}\cdot\text{mol}^{-1}$)	Total activation energy	1.216	0.875
	R ($\text{J}\cdot\text{mol}^{-1}\cdot\text{K}^{-1}$)	Universal gas constant	8.314	8.314

In the literature, n values ranging from 0.67 to 1.52 have been obtained for PVOH and for crystallization temperatures in the range 142-192 °C (Peppas and Hansen 1982), revealing that the crystallization of PVOH is one-dimensional. However, these values strongly depend on the molecular weight of the polymer. In the present study, n values ranging from 1.85 to 2.27 were obtained for PVOH after isothermal crystallization at temperatures of 115 °C – 215 °C (Figure 13-B), revealing that the crystallization of PVOH is one-dimensional for crystallization temperatures below 200 °C. For higher crystallization temperatures, a two-dimensional crystallization growth with a heterogeneous

type of nucleation was observed. It highlights the strong effect of temperature on the crystalline structure that will be studied in more detail in the next section. Another point that should be noted is the influence of CNC. The presence of the nanoparticles slightly increases the value of n regardless of the crystallization temperature (Figure 13B).

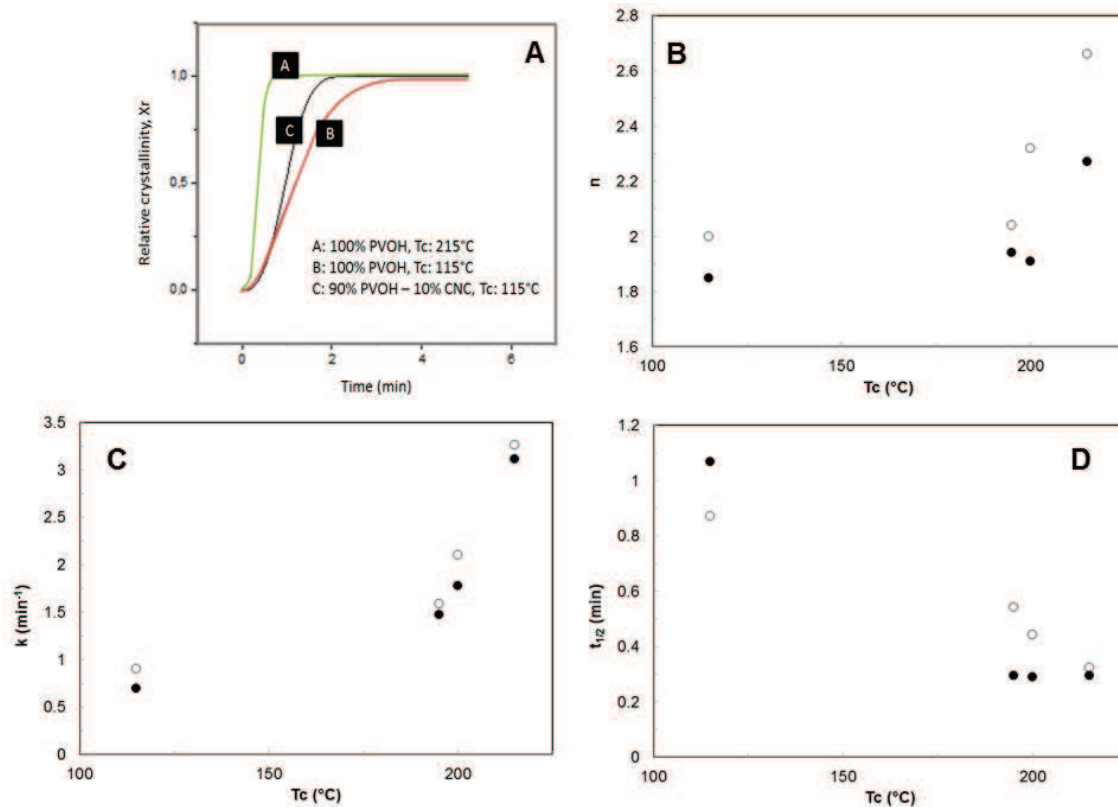


Figure 13: PVOH crystallization kinetics: evolution of A) the relative crystallinity (X_r) vs. time for neat PVOH crystallized at 215°C (A) or 115°C (B), and 10 wt% CNC reinforced PVOH composite crystallized at 115°C (C); evolution of the B) Avrami exponent (n), C) crystallization rate (k), and D) crystallization half-time ($t_{1/2}$) vs. crystallization temperature (T_c) for neat PVOH (●) and 10 wt% CNC-reinforced PVOH composite (○).

The coefficient k corresponds to the rate constant (min^{-1}) and gives information about the growth of PVOH crystallites. First, we can see that its value increases when the crystallization temperature increases (Figure 13-C). The transition from an amorphous to a crystalline phase is therefore faster. This result is consistent with the evolution of the relative crystallinity for neat PVOH (Figure 13-A) where an acceleration of the crystallization kinetics between $T_c = 115^\circ\text{C}$ and $T_c = 215^\circ\text{C}$ is clearly observed. This result agrees with the literature (Mehta et al. 2004). Furthermore, slightly higher k values are observed for the composite (Figure 13-C) meaning that the nanoparticle promotes a faster crystallization; this is also confirmed by comparing the evolution of the relative crystallinity at 115°C with or without CNCs (Figure 13-A). An increase in the rate of crystallization when adding cellulose nanofiller has also been observed for poly(ϵ -caprolactone) (Siqueira et al. 2011).

To summarize the effect of adding 10 wt% CNC to PVOH on its crystallization:

- CNCs act as nucleating agents for PVOH; they favor germination and promote heterogeneous crystallization.
- The phenomenon leads to a decrease in activation energy for the bulk crystallization of the matrix (from 1.216 to 0.875 kJ.mol⁻¹, as calculated from the Arrhenius equation) (Table 3).
- The crystallization rate slightly increases and the transition from amorphous to crystalline phase is faster.
- The growth of the crystal, with or without CNCs, is two-dimensional.
- The resulting degree of crystallinity of the matrix is higher for the composite.

This increase in matrix crystallinity is probably responsible for the observed increase in the Young's modulus of the coating layer and plays a key role in the design of paper with tailored mechanical properties.

The PVOH used in this study is a mixture consisting of 2/3 long-chain PVOH (Mowiol 28-99) and 1/3 short-chain PVOH (Mowiol 6-98). A simple heating scan (10 °C.min⁻¹) was performed by DSC from -50 °C to 250 °C to determine its thermal characteristics and more specifically the melting endotherm. Figure 14 shows the DSC traces for both Mowiol 28-99 and Mowiol 6-98. It can be seen that the degree of crystallinity is slightly higher for short-chain PVOH than for long-chain PVOH. It is indeed well known that an increase in the molecular weight limits the ability of the polymer to crystallize because of more entanglements, resulting in a lower degree of crystallinity. The melting points also differ between the two PVOHs, corresponding to two different populations of crystals in the case of long- ($T_m = 231$ °C) or short-chain PVOH ($T_m = 228$ °C) (Figure 14). The PVOH mixture exhibits an intermediate melting point value ($T_m = 229$ °C).

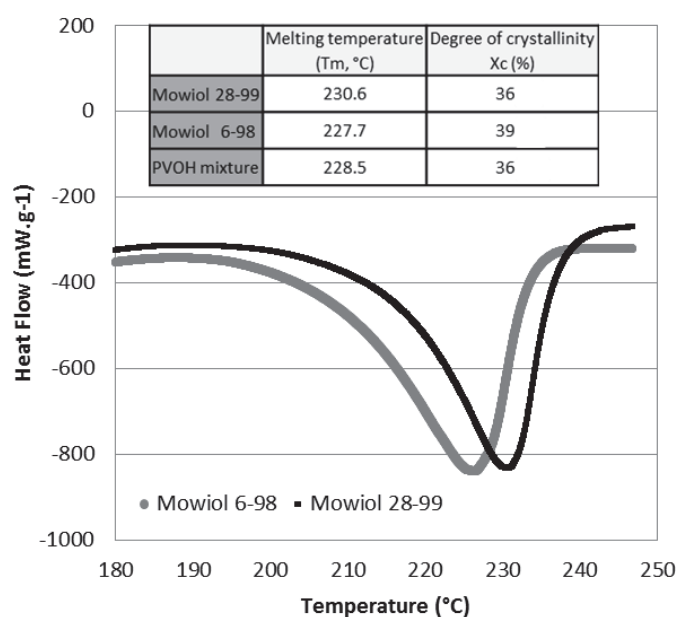


Figure 14: Melting endotherm, melting point (T_m) and degree of crystallinity (X_c) for short- (Mowiol 6-98) (●) and long-chain PVOH (Mowiol 28-99) (○), and mixture (2/3 Mowiol 28-99 and 1/3 Mowiol 6-98) (Δ).

The relative crystallinity of PVOH with and without CNCs was determined by performing isothermal crystallization at different temperatures (from 175 °C to 215 °C). For both neat PVOH and 10 wt% CNC-reinforced PVOH composite, a single melting endotherm was observed at 227 °C when using a crystallization temperature up to 200 °C. This thermal event corresponds to the melting of short-chain PVOH (Mowiol 6-98, $M_w = 47,000 \text{ g}\cdot\text{mol}^{-1}$) as shown in Figure 14. For crystallization temperatures higher than 200 °C, a second melting endotherm appears (Figure 15) at 235 °C. It corresponds to the melting of long-chain PVOH (Mowiol 28-99, $M_w = 145,000 \text{ g}\cdot\text{mol}^{-1}$) as shown in Figure 14. In other words, from a crystallization temperature of 200 °C, a second population of crystals emerges corresponding to the crystallization of long-chain PVOH.

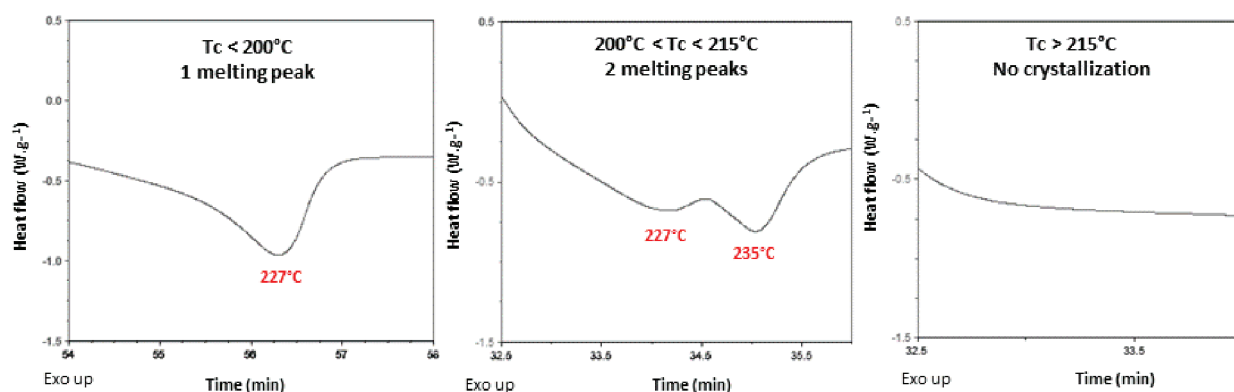


Figure 15: DSC thermograms for neat PVOH at different crystallization temperatures.

Convective vs. radiative drying

Heat transfer differs between convective drying and radiative drying and this could impact the paper drying kinetics. In particular, the energy input is not in the same range and it is far higher for infrared. The evolution of the temperature for impregnated paper dried under convective conditions (3 min in an oven at 115 °C) or under radiative conditions (2 min long-wave IR drying at 200 °C - 1 min on each side) are reported in Figures 7-A and B. These two different thermal treatments lead to dramatically different temperature changes. For traditional convective drying, the temperature does not exceed 120 °C, and therefore only one crystal population can form from the crystallization of short-chain PVOH, whereas for long-wave IR drying, a second crystal population starts to appear due to the crystallization of long-chain PVOH. Therefore, a higher degree of crystallinity can be expected for PVOH with radiative drying.

Specific DSC experiments were performed in order to simulate these drying conditions of the paper surface and thus measure the degree of crystallinity reached for PVOH in each case (Table 1). It appears that the degree of crystallinity obtained under the same thermal conditions as convective drying is effectively much lower than the degree of crystallinity obtained with IR drying (Figure 16), with or without CNC. Moreover, the presence of CNCs increases the crystallinity independently of the drying method for the reasons explained in the previous section.

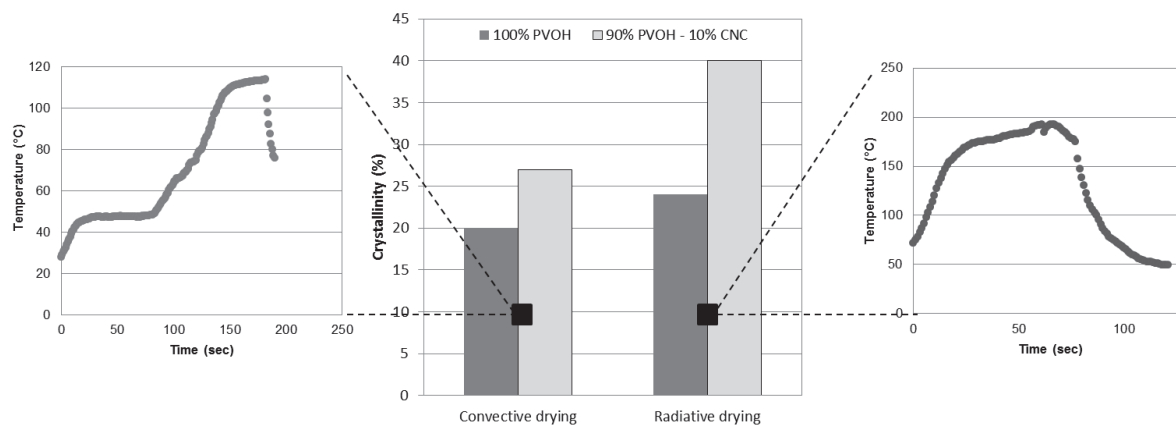


Figure 16: Degree of crystallinity for neat (black) and 10 wt% CNC-reinforced PVOH (crosshatched) after convective drying or infrared drying. The evolution of the temperature at the surface of the paper as a function of time during convective drying (left) or radiative IR drying (right) is also reported.

2.4. Conclusions

The purpose of this study was to elucidate the influence of CNCs on drying kinetics and the impact of both CNCs and temperature on PVOH crystallinity. It has been shown that CNCs tend to reduce the skin effect during infrared drying of an impregnated paper and slightly accelerate the evaporation of water at the end of the drying process. Due to the difficulty of characterizing the crystallization phenomena on the impregnated paper, the crystallinity study was performed on solvent cast films. However, these results can explain the impressive Young's modulus observed with buckling metrology adapted in the precedent study (**Chapter II.1.**) to characterize micron thick coatings. The results from these films allowed us to understand that CNCs act as nucleating agents for PVOH (decreasing the activation energy) and favor an increase in the degree of crystallinity up to a 10 wt% filling in the matrix, corresponding to the percolation threshold. Moreover, it was shown that the crystallization of PVOH strongly depends on the temperature. A temperature of 200 °C promotes the crystallization of both long- and short-chain PVOH and is also the starting temperature for two-dimensional crystal growth, while a crystallization temperature lower than 200 °C promotes one-dimensional crystal growth and the crystallization of short-chain PVOH only.

This study did not focus on crystal morphology as the point was only to explain the increase of PVOH degree of crystallinity and only used DSC equipment. However, to go further, it would be interesting to study this morphology thanks to polarized optical microscopy, TEM or AFM. Furthermore, the degree of crystallinity of PVOH could be studied in further details using WAXS or SAXS techniques.

3. Use of cellulose nanocrystals in a polyvinyl alcohol matrix to decrease banknotes dog-ears defect

These results have been used to apply for the patent “Use of cellulose on a paper product”, EP3228744 A1, Julien Bras, Alain Dufresne, Johanna Desmaisons, Gilles Roberty, Marion Lutsche, 2016

3.1. Introduction

Because of the high quantity of handling, the banknote average lifetime is between a few months and 3 years, depending on the banknote denomination and the country habits and weather. Some defects particularly impact this duration and increase the number of unfit banknotes in sorting centers. In 2009, 33 billion banknotes were sorted within the Eurosystem and 5.4 billion were destroyed because they did not meet the quality requirements. The first reason of unfit banknotes is soil, the second one is the flapped corners also called “dog-ears”, responsible for 10% of destroyed banknotes (i.e. about 500 million banknotes or 432 tons banknotes). With a cost of 15 cents per banknote production, the economic loss due to dog-ears can reach high values, between 70 and 90 millions of euro. The first consequence of dog-ears is the increase of thickness in the area of the folded corner, which complicates automatic transportation of banknotes in sorting machines and can cause paper jams. The dog ears corners of a paper product can also be easily separated by tear from the paper product. Dog-ears can also weaken the barrier layer of banknotes and favor penetration of soil. Finally, it can also cause storing problems as the banknotes are stored in boxes with specific heights in order to store a specific number of banknotes. Other problems can also prevent proper operation of automatic proceedings: a banknote can be caught in another one, or the fold can cover security features.

Mechanical information about thin paper behavior during folding and unfolding process are lacking (Pradier et al. 2016). Fundamental approaches and publications are still limited as well as the understanding of phenomena involved in spite of several applications such as envelope or corrugated boards, meaning that the secrecy of such industry is the main reason of such low level of publication. Nevertheless, some solutions have already been proposed to reduce dog-ears defect. The first alternative has proposed to use special paper structure like round corners (Cassidy et al. 1993). This suggestion had the advantage to reduce paper jam in automatic transportation of banknotes, but completely changes banknote design and requires adaptations in sorting machines. A second alternative which has been patented (Pearson and Howland 2008) was corners reinforcement by watermarks. However, such a localized reinforcement of the corner regions by forming watermarks requires a complex adaptation of the paper manufacturing process. Another patented solution has been the impregnation of the substrate with an aqueous solution containing hydroxylated polymeric binder (Sarrazin 2013). This method is not selective and highly polymer demanding with adaptation

of paper machine in both impregnation and drying sections. Consequently, no satisfying method exists for now.

Some countries, for example Canada or New Zealand, have decided to use synthetic polymer (polypropylene) banknotes to reduce defects such as crumpling, tearing or dog-ears. Nevertheless, Euro strategy is to keep paper substrate. The challenge for banknote substrate is consequently to compete with high-performance products and state-of-the-art science by using nature-based materials. Nanocellulose, whose interest, patents and publications are exponentially increasing, can answer these high quality requirements. These nanomaterials indeed combine advantages of cellulose (abundancy, biodegradability, low toxicity) and nano-scale features (high specific area and mechanical properties, high aspect ratio). Extracted mainly by acid hydrolysis of the fiber, cellulose nanocrystals have recently proved their efficiency in nanocomposite reinforcement thanks to good dispersion properties in hydrophilic matrices, Young's Modulus comparable to Kevlar, and various grafting possibilities arising from hydroxyl groups. However, if the use of cellulose nanofibrils in paper industry is nowadays widely developed (Bardet and Bras 2014); (Brodin et al. 2014), utilization of CNCs in paper industry is still uncommon. Cellulose nanocrystals dimensions strongly limit their use in the bulk of paper (low retention), and only coating or impregnation processes are for now possible (Gicquel et al. 2017).

Interest of nanocellulose for banknote application has been very recently raised with a recent patent from Oberthur (Le Berre et al. 2015) proposing to use cellulose nanocrystals inside banknote varnish to improve soil resistance as well as hydrophobic and oleophobic properties, and thus guarantee printing quality. This solution doesn't concern dog-ears recovery but proposed for the first time the use of CNCs in a varnish for banknote application. This study proposes to include cellulose nanocrystals in the impregnation bath to limit dog-ears defect on paper substrate. As in everyday life, a paper can be manually folded in large possibilities of direction and intensities, the folding process is hard to control and repeat and only few studies have tried to explain the mechanisms involved. The first part of this study proposes to understand the influence of cellulose nanocrystals in the paper dog-ears limitation. The dog-ears phenomenon has been divided in three steps: the creation of the fold, the angle recovery of the folded corner and the resistance of the paper after the ply (Figure 1). A dog-ears resistant material would be a material with a reduction of both the ability to fold after a bending deformation and the ability to return in the initial plane state after a fold without creating irreversible paper weakness. Finally, a second part proposes to identify the key parameters responsible for a better elastic angle recovery after folding and an optimization of the results through variation of drying process, nanocellulosic material and matrix molecular weight and cross-linking.

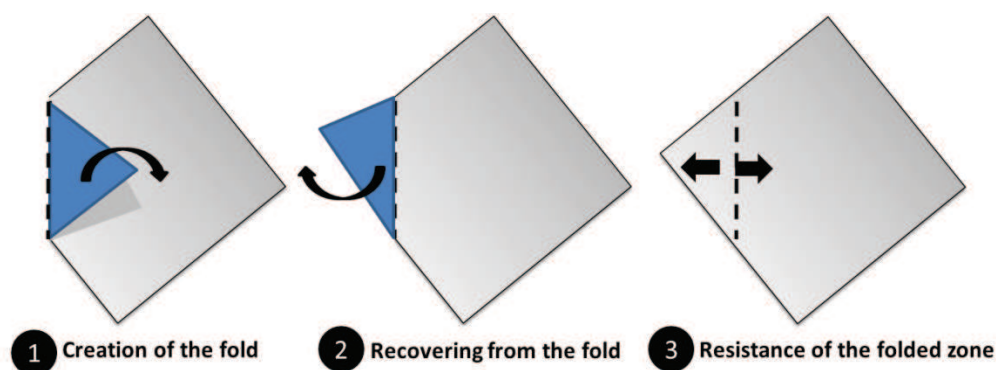


Figure 1: Description of the three successive steps for characterizing the fold mechanism

3.2. Materials and methods

3.2.1. Materials

Nanocellulosic materials. When not specified, CNCs were purchased from the University of Maine (produced by the USDA Forest Products Laboratory) and have a length of 136 nm (± 50), and a height of 11 nm (± 5). The dimensions were measured using Atomic Force Microscopy (AFM) imaging, in tapping mode using silica coated cantilever (OTESPA[®] 300 KHz – 42 N/m, Bruker, USA). Scans of 3.3 x 3.3 μm^2 were performed and the average length and width were averaged from 3 different images, with 50 measurements in one image. The suspension was delivered at 12 wt%. If specifically reported, three other commercial sources of CNCs have been used from Melodea (solid content 3 wt%), Blue Goose (solid content 2 wt%) and CelluForce (dry powder).

Three kinds of cellulose nanofibrils were also tested: (i) anionic cellulose nanofibrils (1% w/w) bought from Betullium[®] and with a carboxylic content of 1300 $\mu\text{mol/g}$, (ii) enzymatic cellulose nanofibrils (2% w/w) bought from CTP and produced from bisulfite Domsjö pulp (softwood) after enzymatic pretreatment (using a cellulase solution mainly composed of endoglucanase), one pass at 1000 bar followed by 4 passes at 1500 bar in a Homogenizer GEA Panther, with a carboxylic content of 5.4 $\mu\text{mol/g}$ and (iii) cationic CNF obtained by ultrafine friction grinder supermasscolloider and pretreatment with epoxypropyltrimethyl ammonium chloride (EPTMAC) and having a trimethylammonium chloride content of 930 $\mu\text{mol/g}$. This last source is not a commercial supply and protocol will be described.

Polyvinyl alcohol (PVOH). The PVOH used in all experiments was a mixture between a high molecular weight PVOH (Mowiol 28-99, 145 000 g/mol, 0.2-1% acetyl content) and a low molecular weight PVOH (Mowiol 6-98, 47 000 g/mol, 1.1 – 1.9% acetyl content), all bought from Sigma Aldrich. The weight mixture ratio was respectively 2:1 and the solid content of the solution before dilution was 5 wt% in water. Two other PVOH were used, only when specifically mentioned in the text: 100% long

chain PVOH (Mowiol 28-99) and 100% short chain PVOH (Mowiol 4-98, 27 000 g/mol, 1.1 – 1.9% acetyl content). These PVOH were also bought from Sigma Aldrich and prepared at 5wt% in water.

Banknote substrate was kindly supply by *Banque De France*. It corresponds to Velin paper produced at Vic le Comte papermaking, before impregnation in PVOH bath. This Velin paper was produced on a pilot paper machine running around 2 m/min. The fibers used for the paper consist of 100 wt-% cotton (60°SR). TiO₂ Anatase (5 wt-%) was used as additive and acidic dies were added into the pulp slurry. In addition to TiO₂ the paper pulp also includes 2.7 wt.-% wet strength agent polyamideamine epichlorohydrin (PAE) and 3-6 wt-% anionic polymer carboxymethylcellulose (CMC). Two layers with basis weights of about 20 g.m⁻² (first layer) and around 60 g/m² (second layer) are combined to form the resulting semi-finished paper product, which has a final basis weight of 80.8 ± 2.4 g.m⁻².

Other materials. Poly acrylic acid (PAA) was bought from Sigma-Aldrich with an average molecular weight of 1800 g.mol⁻¹ (Tg: 106°C). 2,2,6,6-Tetramethyl-1-piperidinyloxy (TEMPO) 98%, sodium bromide (NaBr), sodium hypochlorite (NaClO, 12 wt%), were also purchased from Sigma-Aldrich and used as received.

3.2.2. Methods

Dispersion of dry CNC powder from CelluForce. The dispersion procedure has been extracted from CelluForce NCC™ Dispersion Guide. The right amount of CNCs was weighted to make a suspension of 1 liter at 5wt%. A beaker of 2 liters has been used to ensure an efficient stirring at the top of the suspension. Water was first introduced into the beaker, and stirring has been performed with a long and large magnetic stir bar. The speed has been adjusted such that the vortex formed was large enough to reach the tip of the stir bar. Finally, CNCs were added progressively into the deionized water, avoiding the addition directly into the heart of the vortex to prevent splashing and avoiding also the addition onto the walls of the beaker. An increase of viscosity of the suspension was observed and indicates a good dispersion of CNCs. The dispersion lasted for at least 1hour, and the stirring speed was continuously increased to keep the same vortex intensity.

Polyvinyl alcohol (PVOH) solution. The right amount of PVOH has been weighted to make a solution at 5 wt%. Classically, Mowiol 28-99 and Mowiol 6-98 were used in a ratio of 2:1, but other tests have been performed with Mowiol 28-99 alone or Mowiol 4-98 alone. First, the water was introduced in a round bottom flask, heated at 90°C and stirred mechanically. When the temperature of water has reached 90°C, dry PVOH was added progressively. Both mixing and heating were maintained until the complete dissolution of PVOH in water, taking in average 3 hours.

PVOH-CNC mixture. To introduce cellulose nanocrystals into the PVOH solution, the previously prepared PVOH mixture was first heated at 60°C. Then, the needed quantities of water and nanocrystals were added to obtain 5% w/w total concentration and the required weight ratio PVOH/CNC. If not specified in the text, the weight ratio of PVOH and CNC was respectively 90:10. The

suspension was then mechanically stirred during 1 hour at 60°C. Then, this suspension was exposed to an ultrasonic dispersive energy of 5 kJ/g of dry CNC using a 250 Watt (or 250 J/s) sonication probe (Sonifier S-250A, Branson, USA) at 50% of maximum energy.

Impregnation protocol. Before impregnation, the PVOH (with or without CNCs) solution has been heated at 60°C, and this temperature was kept during the whole impregnation process. Velin paper with 15cm x 10cm dimensions was immersed in the warm impregnation bath containing the mixture of PVOH and CNCs for 20 s. Then, the impregnated paper was placed on a Teflon plate and the overflow was removed with one pass of a 1kg Teflon roll. Finally, the sample was placed between two metallic frames to prevent shrinkage and dried in an oven with air convection at 115°C for 3 min. When specified in the text, other drying processes have been tested by extending the drying time to 10 minutes or by using Infra-Red lamps.

Infra-red drying after impregnation. Infrared drying of paper was performed with 2500W long wave IR lamps. During drying, the paper sample were maintained by a metallic frame to prevent shrinkage. As it is possible to dry only one side at a time, samples were turned at the middle time of the drying (“Symmetric drying”). Other tests have been performed without turning the paper sample (“Asymmetric drying”). Different drying durations were tested: 2 minutes and 4 minutes. If not specified in the text, the IR drying was 2 minutes and symmetric drying was used.

Dewatering during IR drying. the amount of water removed during IR drying has been calculated by taking paper samples at different time during drying, put them in closed plastic bags to maintain their water content constant, and weight them immediately with a precision balance.

TEMPO-mediated oxidation of CNCs TEMPO-mediated oxidation of CNC was performed following a procedure previously described in the literature (Habibi et al. 2006). About 3 g of CNC was dispersed by an ultrasonic probe treatment (5 min, 20 kHz) in 200 ml of water. TEMPO (88.55 mg, 0.567 mM) and NaBr (972 mg, 9.44 mM) were dissolved in 100 ml of deionized water and slowly added to the CNC suspension. A 12 wt% NaClO suspension (18 g, 29 mM) was then added dropwise to the suspension to start oxidation. pH of the suspension was maintained around 10–10.5 by the addition of 0.25 M NaOH solution while stirring the suspension for 3 h. Reaction was then quenched by the addition of ethanol (10 ml), and the resulting CNCs were washed with distilled water at least three times by centrifugation (10,000 rpm, 30 min) and put in dialysis against distilled water at least for one week until neutral pH was obtained.

Charge content (carboxylic groups). The charge density of oxidized CNCs was determined by classical conductimetric titration. About 15 mg of CNC was put into 50 ml of distilled water and treated with an ultrasonic dispersive energy of 5 kJ/g of dry CNC using a 250 Watt (or 250 J/s) sonication probe (Sonifier S-250A, Branson, USA) at 50% of maximum energy. pH of the suspension was adjusted to 2 by adding HCl 0.1 M to allow carboxylate groups to be in their protonated form. The suspension was then titrated against 0.1 ml increment of NaOH 0.01 M.

Cationic cellulose nanofibrils. Cationic CNFs were prepared from eucalyptus pulp (Cenibra, Brazil). In this case, cellulose fibers were suspended in water at a solid content of 2 wt% and refined at 80 °SH using disk beater in accordance with standard ISO 5267-1. Then, the suspension was filtered until a solid concentration of 40 wt%. The suspension of fibers at 40 wt% was then mixed with water (40g CNF dry content and 449g water). Then, a sodium hydroxide solution (NaOH, 29.6 g at 3.7 wt%) was added drop by drop to the cellulose suspension. The mixture was then heated at 65°C and kept under mixing for 30 min. Then, epoxypropyltrimethyl ammonium chloride (EPTMAC, 132.2 g corresponding to 4 mol/mol_{AGU}) was added. This mixture was kept at a temperature of 65°C for 5 additional hours. At the end of the reaction the pH was neutralized thanks to a few drops of hydrochloric acid (HCl 1 M). The pretreated suspension was then filtered using a Buchner and washed with distilled water. Finally, the pretreated cellulose suspensions at 2wt% were fibrillated using an ultrafine friction grinder supermasscolloider (Model MKZA6-2, Disk model MKG-C 80, Masuko Sangyo Co., Ltd, Japan) working at 2500 rpm, in recirculation for 2.5 h.

Charge content (trimethylammonium chloride groups). The number of trimethylammonium chloride groups was estimated by conductimetric titration of chloride ions with AgNO₃(aq, assuming the presence of one chloride counterion per trimethylammonium chloride group. 0.4 g of dry fiber in 200 mL of water were titrated with 0.06 M AgNO₃ by adding approximately 0.5 mL in 30 seconds intervals.

Elastic angle recovery. Paper samples were cut in square samples of 5cmx5cm. Then, samples were placed in a standardized position on a flat surface in such a way that the folding line created by the dog ear was orthogonal and in the same plane as the focus direction of the camera measuring the angle. This position changes as a function of the angle considered (Figure 2). The dog-ear was formed by folding back the corner of the paper to the mark which is located at 26mm of the corner and at an angle of 45°, without creating further pressure on the folding line. Two other angles have been tested (20° and 70°) but results are only mentioned in Supporting Information 2. Then, weights were placed on the folded corner such that the folded line concurs with the diameter of the round weight. Different pressures between 0.1 and 1.2 kPa have been applied by changing the weight. After removal of the weight and stabilization time of 120 s, picture of the angle recovery was taken thanks to a camera (72 dpi resolution). Pictures were then analyzed thanks to ImageJ software and the elastic angle recovery has been considered as the average of at least 10 different samples. Samples have been conditioned at 23°C and 50 %RH for at least 48h before testing and measurements were performed in the same conditions.

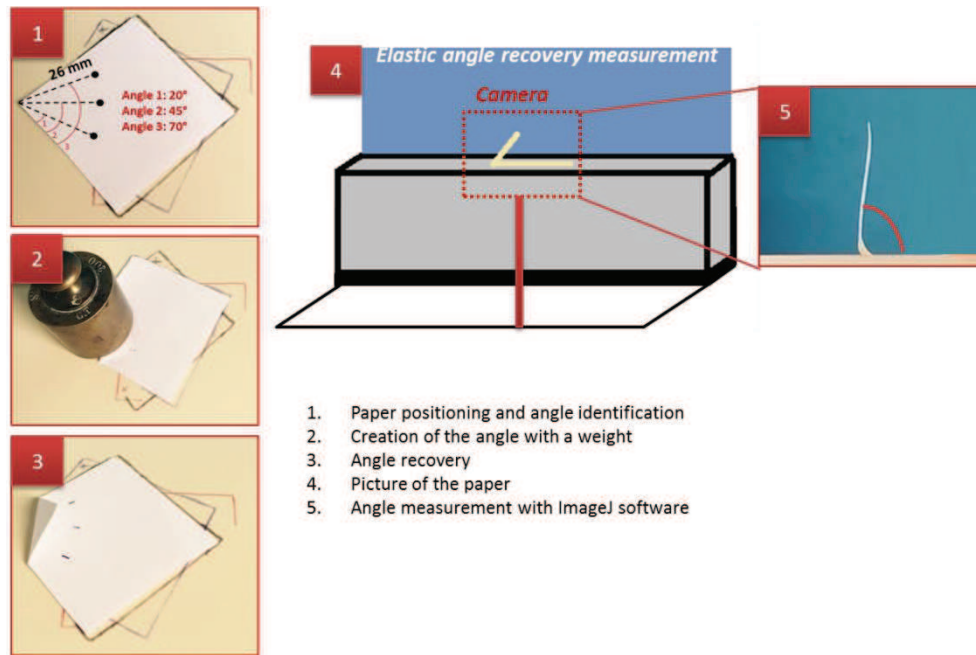


Figure 2: Method for measuring the elastic angle recovery

Force angle recovery. This test has been implemented to measure the force of the paper recovery after folding. Paper with 3cmx3cm dimensions has been folded in exactly the same way as the procedure described in “Elastic angle recovery” protocol (Angle 2 45°, and 0.6 kPa pressure). The paper is then quickly taped on the transparent plastic support (Figure 3) while manually maintaining the folded paper. After a time corresponding to 7 seconds after the removal of the weight on the folded paper corner, the paper was released. This paper encounters the force captor (1000 mN, Swema®, Sweden) after an opening angle of 45°. The force angle recovery has been considered as the average of 10 different samples. Samples have been conditioned at 23°C and 50 %RH for at least 48h before testing and measurements were performed in the same room.

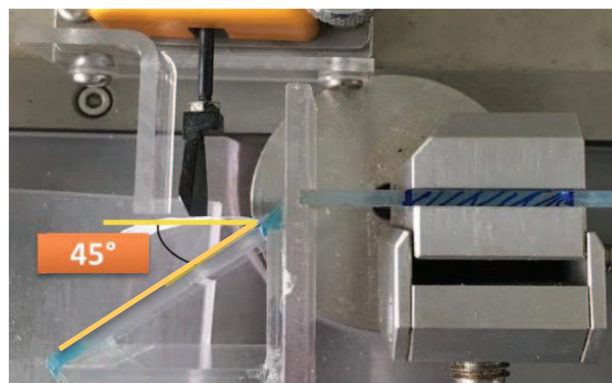


Figure 3: Measurement of the paper force angle recovery

Tensile tests on folded papers and crack propagation. The tensile properties were measured with a vertical extensometer (Instron 5965), with a speed of 10 mm/min and a gap between the jaws of 10 cm. The width of paper samples was 45 mm. Basis weights have been measured using 10x10 cm²

surfaces and thickness were measured with Lhomargy micrometer with an average of 3 points on each paper strip, and these values were reported to the tensile test software BlueHill. The tensile tests have been performed on folded samples. To create the fold, each paper strip has been folded in two identical parts, and a rectangular weight of 1 kg fitting exactly with the dimensions of the folded paper was deposited for 10 seconds. Different numbers of folds have been performed by repeating the same procedure and manually stretching the paper in a linear plane between each repetition. To study the crack propagation occurring at the fold, a notch of 1 cm has been performed by scissors before the tensile test. Each value was averaged on at least 5 samples. Samples have been conditioned at 23°C and 50 %RH for at least 48h before testing and measurements were performed in the same room.

Film casting. Films consisting of 100% PVOH or 90 wt% PVOH and 10 wt% CNCs with 50 g/m² basis weight were produced by classic solvent-casting. The PVOH solution with or without CNCs has been cooled in a Teflon mold with a concentration of 5 wt% and let dried at 23°C and 50% RH for one week.

Dynamical mechanical analysis (DMA). Mechanical characterization of impregnated papers or cast films has been performed at room temperature by dynamic mechanical analysis (DMA). The dynamic frequency sweep test was performed in the linear range, with 0.05% displacement, from 50 Hz to 0.05 Hz, with 10 points per decade. $\tan(\delta)$, or tangent of the loss angle, corresponding to the ratio between loss modulus and storage modulus, was directly extracted from the mechanical curves. This parameter corresponds to the ability to dissipate energy in the material; if $\tan(\delta)=0$ the material is considered as perfectly elastic, if $\tan(\delta)=\infty$, the material is considered as totally viscous. Samples have been previously conditioned at 23°C and 50 %RH for at least 48h.

Bending rigidity B (mN.mm). Bending rigidity of impregnated papers was measured with a Büchel stiffness tester (Büchel Van Der Korput®, Netherlands). Paper samples were cut with a length of 7cm and a width of 3.8 cm, corresponding to the standard TAPPI 5605. The test length has been set at 25mm (distance between the captor and the jaw) and a force captor of 5000 mN was used. Samples have been conditioned at 23°C and 50 %RH for at least 48h and measurements were performed in the same room.

Hinge index (N.mm). The folding behavior has been modeled as a hinge joint with a torsional spring, as described by Pradier et al (Pradier et al. 2016). The movement was expected to be sufficiently slow to discard viscous effect, and the experiment was based on static equilibrium. The aim was to observe the rigid movement of two faces linked by a simple straight fold (Figure 4). The criteria for designing the testing device were as follows: a possible broad range for the folding angle, a sufficient control precision for small loads (to test somehow low basis weight papers), and a uniform loading of the fold along its length. A paper sample (1.5 cm x 5 cm) with a single fold was prepared by splitting the paper into two identical parts in the direction of the length. The loads applied were 405 mg and 810 mg. The opening angle of the sample for each weight was measured by taking a picture and perform an image analysis (ImageJ®, NIMH, USA). The torque applied to the fold was estimated with

the assumption that the boundary hinge is perfect. The load was applied at $L_p = 2.5$ cm of the fold. When neglecting the face bending, the torque (N.mm) was given by: $t = m.g.L_p.\cos(\alpha/2)$, where m is the loading weight, g is the gravity, and α is the opening angle. Samples have been conditioned at 23°C and 50 %RH for at least 48h and measurements were performed in the same conditions.

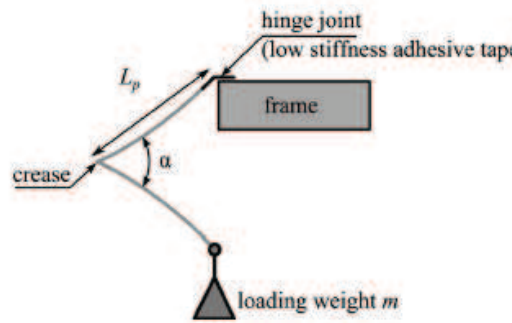


Figure 4: Experimental design for determination of the opening angle under loading (Pradier et al., 2016)

AFM. Dimensions of CNCs and CNFs have been extracted from AFM pictures (Dimension Icon®, Bruker, USA). The suspensions diluted at 10^{-4} wt% were beforehand dropped on mica plates and let dried overnight. Scans of $3 \times 3 \mu\text{m}^2$ were taken in tapping mode using silica coated cantilever (OTESPA®, 300 KHz, - 42 N/m, Bruker, USA). At least 4 images per sample were obtained and 50 measurements were realized by sample.

Percolation threshold. The percolation threshold of cellulose nanocrystals has been calculated following equation (1) and (2):

$$\Phi_{\text{vol}}(\%) = \frac{0.7}{L/D} \quad (1)$$

$$\Phi_{\text{wt}}(\%) = \Phi_{\text{vol}} \cdot \frac{\rho_c}{\Phi_{\text{vol}} \cdot \rho_c + \rho_s (1 - \Phi_{\text{vol}})} \quad (2)$$

With Φ_{vol} (%) the volume percolation threshold, Φ_{wt} (%) the weight percolation threshold, L (nm) the nanoparticle length, D (nm) the nanoparticle, ρ_c the density of cellulose (1.54 g/cm^3) and ρ_s the density of the solvent. The percolation threshold is reached in the dry state for CNC in the PVOH matrix, consequently ρ_s is considered as the density of PVOH (1.29 g/cm^3 extracted from the security data sheet of Sigma Aldrich). All the values reported in this study are the percolation threshold in weight concentration.

Cross-linking with poly acrylic acid (PAA). PAA and water have been added to the PVOH solution such that to obtain a final concentration of 5wt% and a weight ratio PVOH:PAA of 8:2. Another suspension has been prepared, containing PVOH, CNC and PAA. In this case, the weight ratio of these components has been respectively 8:1:1. The mixtures have been then stirred mechanically for 1 hour at 60°C and kept at 60°C for the paper impregnation. After impregnation, the paper has been

dried in an oven or by infra-red, and an additional curing treatment of 10 minutes at 140°C has been performed.

CNC sulfate charge (Zeta potential). The z-potential of CNCs in water (0.01 wt%) was determined using an electrophoretic mobility zeta-meter (Zetasizer 2000 Particle Sizer, Malvern Instruments). The instrument measures electrophoretic light scattering of a 35 mW solid state laser beam at a 660 nm wavelength, and all reported values were an average of 5 measurements.

Surface desulfation of CNCs. The desulfation of H₂SO₄-CNC was performed with a treatment of OSO₃H under alkaline condition (Figure 5), as described in the literature (Hasani et al. 2008; Lin and Dufresne 2014). In the procedure, 50 mL of different concentrations of NaOH solution (0.5 mol/L and 2 mol/L) were added to 100 mL of CNC aqueous suspension (2wt%) and each mixture was stirred at 60°C for 1 hour in the case of 0.5 mol/L NaOH, and 3 hours in the case of 2mol/L NaOH. During reaction, the cellulose nanocrystals tend to aggregate because of the removal of surface sulfate groups. Resulting CNCs were washed with distilled water at least three times by centrifugation (10,000 rpm, 30 min) and put in dialysis against distilled water at least for one week until neutral pH was obtained.

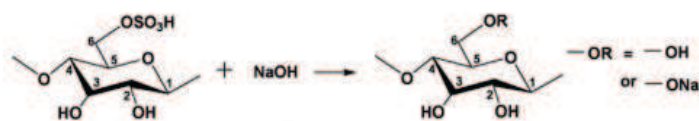


Figure 5: desulfation procedure of sulfuric acid hydrolyzed CNCs

3.3. Results and discussion

Part I: Influence of cellulose nanocrystals on ply formation and recovery from bending deformations

A preliminary work (Supplementary data 1) has shown that the presence of CNCs in PVOH matrix does not impact the viscosity of the suspension, as the final solid content of the mixture is already very dilute (5 wt%). From Chapter II.2., it is known that the paper resulting from the impregnation step is a composite material. It is composed of extremal thin layers consisting of PVOH/CNC nanocomposite (3.4 μm), followed by asymmetric layers of fibers penetrated with the impregnated mixture (28 and 40 μm). Finally, a deep layer of 45 μm is composed of only fibers without penetration of the suspension (Figure 6). If we focus on the thin micrometric layers only composed of PVOH and CNCs, it has also been shown using buckling metrology that the addition of 10wt% cellulose nanocrystals results in an impressive increase of the layer Young's modulus (from 1.6 to 21 GPa) due to the synergistic effect of the reinforcing ability of CNCs and the increase of the matrix crystallinity from 22% to 32%. The increase of the Young's modulus is also correlated to lower energy dissipation in the material. Consequently, the material becomes more elastic. This point is determinant when folds are created because plastic damages are by definition irreversible, and an increase of the material elasticity is synonymous to an increase of the reversibility of the stress. As said in introduction, the dog ears phenomenon can be divided in 3 successive mechanical steps: 1) ply creation, 2) Recovery from bending, and 3) resistance after the fold. This part 1 will present the influence of CNC on each step.

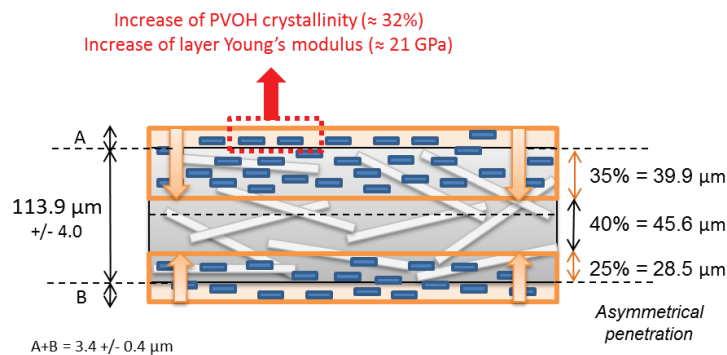


Figure 6: Structure of the paper after impregnation

3.3.1. Step 1: resistance of the material to the creation of the ply: impact of cellulose nanocrystals

The folding mechanism can be observed at different scales. At the microscopic scale, the fold creates a compression on the fibers localized inside the bending zone and a tensile stress on the fibers localized at the outside of the bend. It results in plastic damages. At the macroscopic scale, the

fold creates a decrease in thickness and stiffness along the axis of the fold (Francis et al. 2013) and the fold can be modeled as a hinge-like behavior where the paper is assimilated to a thin plate and the fold to a mechanical joint (Francis et al. 2013; Pradier et al. 2016).

(i) Influence of cellulose nanocrystals on the fold at the microscopic scale.

The internal friction factor $\text{Tan}(\delta)$, measuring the damping properties, has been measured for PVOH films containing different amount of CNCs and on papers impregnated with CNC and PVOH. Tests were performed for different frequencies, at room temperature and in the linear range. To be as close as possible to the reality, the test should be performed at the frequency corresponding to the speed at which the banknote is folded in circulation. As this frequency is not easily simulated and presents a lot of variations, a range of frequencies were tested. $\text{Tan}(\delta)$ represents the ratio between the loss modulus (energy dissipated) and the storage modulus (elastic portion) of the material. It characterizes hence the ability of this material to dissipate energy: the less is $\text{tan}(\delta)$ value, the higher is the elasticity of the material. When the loss modulus is greater than the storage modulus ($\text{tan}(\delta) > 1$) viscous liquid character is dominant. If it is the contrary ($\text{tan}(\delta) < 1$), elastic solid character is dominant. In these experiments, all samples present elastic solid behavior. Furthermore, It appears that the $\text{tan}(\delta)$ value for a film containing 10 wt% CNCs is 1/3 lower than its value for a film only composed of PVOH (Figure 7-A), meaning a higher amount of elasticity. Same experiments were performed directly on impregnated papers (Figure 7-B), and present different conclusions as a function of the frequency used. If the frequency is lower than 2 Hz or higher than 17 Hz, same values are obtained. However, between 2 and 17 Hz, it appears that the amount of elasticity of the material is higher with 10 wt% CNCs in the impregnation bath.

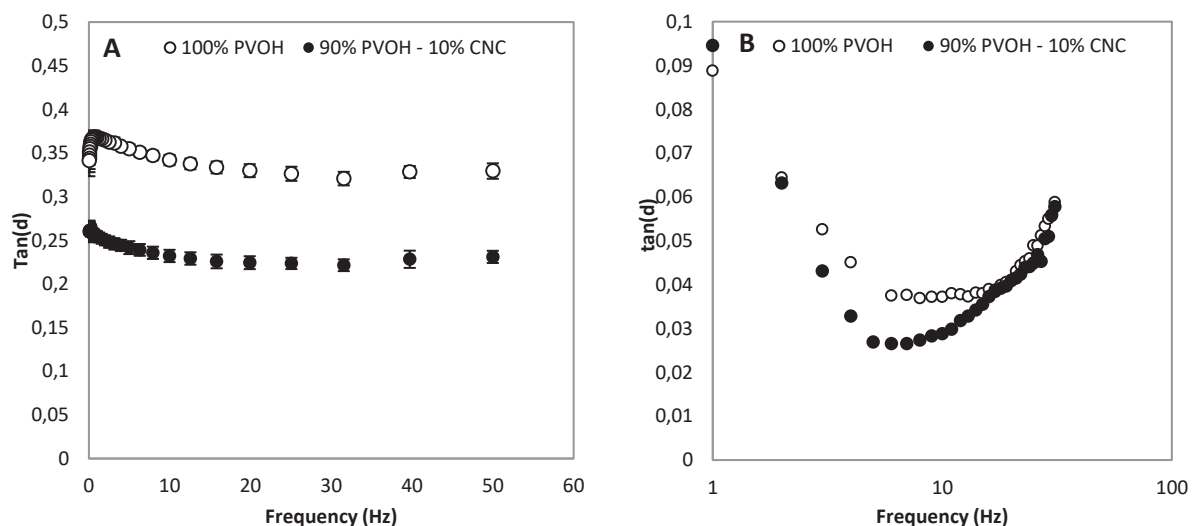


Figure 7: $\text{Tan}(\delta)$ as a function of frequency for A) cast films and B) papers impregnated with PVOH with and without CNCs, after drying for 3 minutes at 115°C

Damping property of nanocellulose containing composites have been investigated in literature as a function of the temperature for characterizing thermal behavior (Gong et al. 2011) or

as a function of the frequency for characterizing mechanical behavior (Park et al. 2013). Indeed, this value provides useful indication about the changes in the molecular mobility of the polymer matrix induced by the nanofiller inclusion. A lot of studies reported the decrease of $\tan(\delta)$ with increasing amount of nanocellulose (Gong et al. 2011; Boufi et al. 2013). In composite materials, the loss factor might be analyzed in terms of the contribution of the filler, the polymer matrix, and the interphase pondered by their corresponding volume fractions. Furthermore, decrease of $\tan(\delta)$ value is associated to higher material stiffness (Dufresne et al. 2013).

We know from the previous study (**Chapter II.2.**) that no reinforcement effect of the fiber is induced by the penetration of the PVOH/CNC suspension into the paper. Consequently, no change occurs at the fiber level. However, $\tan(\delta)$ values show that changes occur on the whole material. The differences of paper elasticity are only explained by the thin layer at the top of the paper. Cellulose nanocrystals act as a nucleating agent in polyvinyl alcohol, and PVOH crystallization results in the formation of smaller crystals but in higher quantities. Thus, the crystallinity of the PVOH layer is increased when adding 10% cellulose nanocrystals. Furthermore, crystalline regions are responsible for tenacity, high modulus of elasticity and resistance towards bending, and play consequently a key role in paper dog-ears resistance as the layer bears part of the stress during the bending deformation. In other words, it is more difficult to create a fold thanks to this micrometric layer of CNC-reinforced PVOH.

(ii) Influence of cellulose nanocrystals on the fold at the macroscopic scale.

To characterize the “foldability” of the paper, or the resistance of the paper to be irreversibly folded, two parameters characteristic of the fold can be calculated: the hinge index (or ability for a material to rotate around a hinge) and the force needed to create a fold.

At the macroscopic scale, the fold behavior relies on a macroscopic local hinge with a torsional spring. The aim of the hinge index is to observe the rigid movement of the two paper faces linked by the straight fold. When measuring the hinge index on papers impregnated with PVOH or PVO-CNC and classically dried for 3 minutes at 115°C, no significant differences appeared (results not shown). However, if the papers are dried with infrared, the hinge index increases with the addition of 10 wt% CNCs (Figure 8), proving that cellulose nanocrystals favor the rotation of a paper along the fold without damages. The impact of temperature has been studied in further details and will be discussed in the following part.

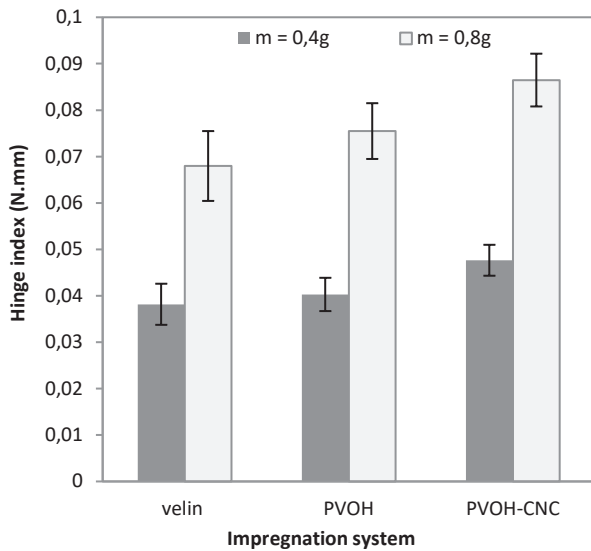


Figure 8: Hinge index of paper dried with infra-red drying (1 minute for each side), containing or not 10 wt% cellulose nanocrystals

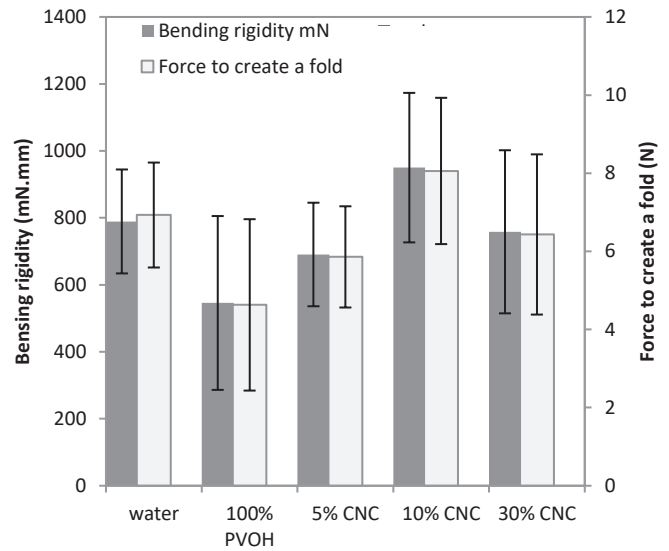


Figure 9: Bending stiffness of papers impregnated with water or PVOH containing different amount of CNCs (wt%)

The bending rigidity B (N.mm) as well as the force necessary to create a fold ($F(N) = \frac{B}{thickness}$) are represented in Figure 9. Even if standard deviations are high, the trends are sufficient to conclude that (i) impregnation with PVOH decreases the folding resistance if we compare with an impregnation with water, and (ii) the introduction of CNCs up to 10 wt% increases the bending rigidity and, hence, the force needed to create the fold which passes from about 4 N to 8 N. If more than 10wt% of CNCs is added in the PVOH matrix, the bending rigidity and the force needed to create the fold start to decrease. This optimum at 10wt% can be explained by the percolation threshold reached by the nanocrystals and has been observed in a wide range of characterization tests like PVOH crystallinity and CNC-PVOH mechanical properties (see **chapter II.2.**).

3.3.2. Step 2: recovering of the paper from bending deformation: dog-ears resistance

Cellulose nanocrystals in a right amount corresponding to the percolation threshold can increase the Young's modulus of the thin layer, the elasticity of the whole material, the bending rigidity and the force needed to create a fold. Hence, these nanocrystals create a resistance to the apparition of dog-ears. However, they do not prevent them completely. Another parameter which is important to test is the elastic angle recovery once the paper corner is folded, or the ability for the paper to return to its initial plane shape after a fold. Indeed, this property would avoid some issues in sorting centers like the increase of paper thickness, the banknotes caught in another one, the covering of security feature, or the packaging problems. The objective is to reach an angle recovery higher than 90°. A preliminary study (Supplementary data 2) studied the influence of angle orientation (20°, 45° and 70°) and demonstrated that the folding behavior does not exhibit a

dependency on its orientation. That is why only results performed with an angle of 45° are reported. Furthermore, Supplementary data 2 also reports the angle recovery after folding as a function of time and shows that the angle position is stabilized after 120 s. Consequently, the angle position reported in the following results is reported after 120 s of stabilization.

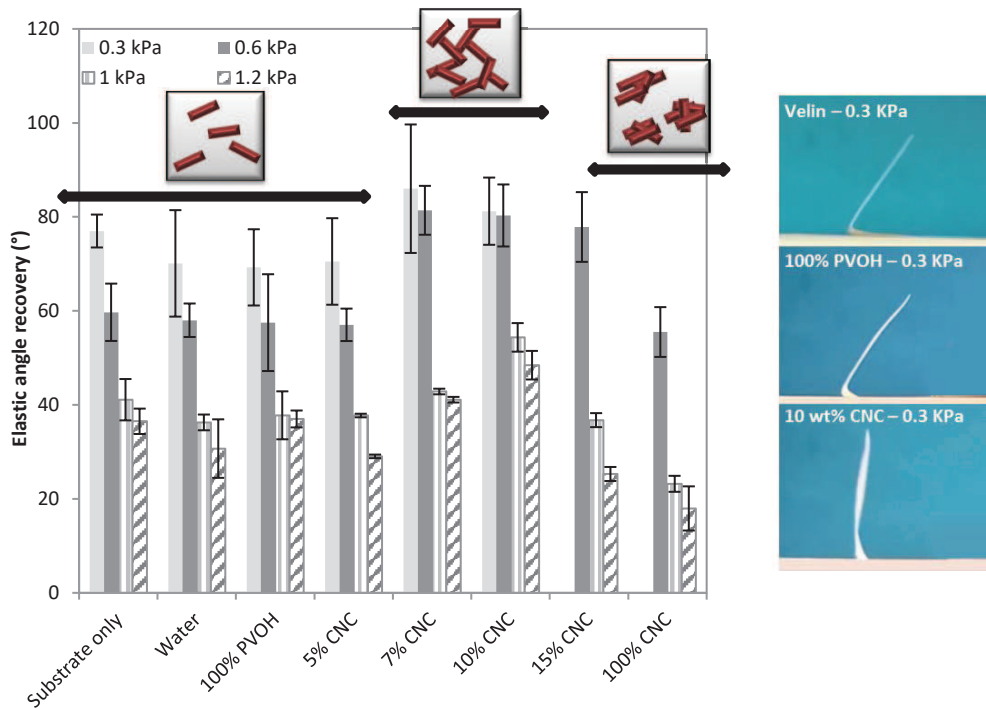


Figure 10: Elastic recovery after folding of banknote substrate impregnated with water or different PVOH/CNC composites, for different pressures on folded corner

The elastic angle recovery of paper impregnated with PVOH and different amounts of CNCs is shown in Figure 10. Different pressures have been applied on the folded corners, from 0.3 kPa (100g) to 1.2 kPa (1Kg). When the pressure increases, the elastic angle recovery decreases drastically. Whatever the pressure, only slight differences happen between the substrate (Velin paper), the substrate impregnated with water and the substrate impregnated with PVOH only. When adding 5wt% CNCs, still nothing happens. The quantity of CNCs is indeed too small. However, a significant jump of the value occurs from 5wt% to 7wt% of CNCs and an optimum is reached between 7wt% and 10 wt%, depending on the pressure applied. As already explained, this high increase of properties is brought by the formation of a network between the CNCs inside the PVOH matrix. Several measurements converged to this optimum and impart reliability on the results (Figure 11). Considering the standard deviation and the slight differences between these two points, 10 wt% CNCs has been considered in the whole study as the better amount for decreasing the dog-ears defect. Furthermore, the most representative pressure to simulate a manual handling of banknotes is assumed to be 0.6 kPa (200g) (intermediate pressure) and it is also at this pressure that the higher gaps are observed. That is why, if not specified, the elastic angle recovery is always measured for this pressure.

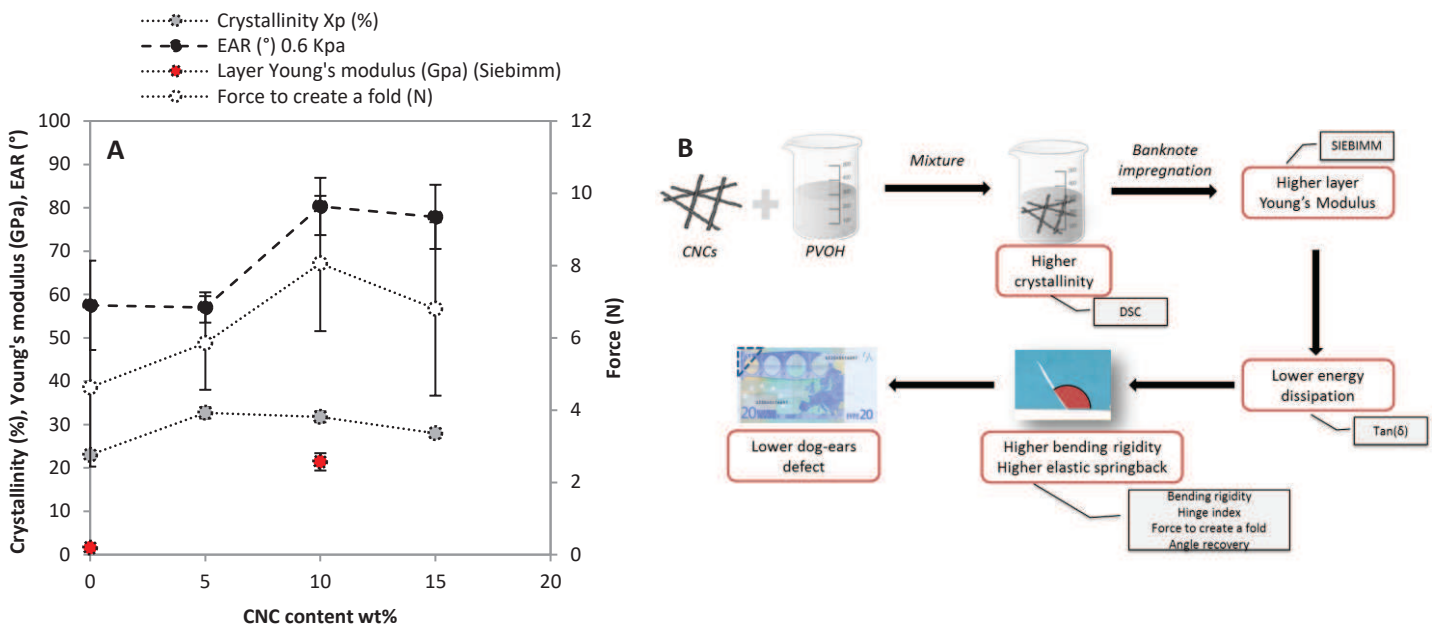


Figure 11: Link between different phenomena explaining the decrease of dog-ears defect with 10 wt% CNCs in PVOH matrix, A) Mean values and B) Causal connections. EAR = Elastic angle recovery. Crystallinity and Buckling Young's modulus extracted from chapters II.1. and II.2.

The force of the angle recovery has also been measured. For classical papers dried in oven after impregnation, no significant impact of CNCs was observed. Indeed, paper impregnated with PVOH showed a force recovery of 18.4 ± 4.6 and the paper impregnated with addition of 10wt% CNCs showed a force recovery of 15.7 ± 4.7 . However, if the papers are dried with Infra-red, an increase of 34% is observed with the addition of 10 wt% CNCs as a force recovery of 31.1 ± 5.6 mN has been obtained in comparison with 20.3 ± 5.9 mN for the PVOH only. These results show the importance of the drying treatment which enhances the properties of the neat PVOH but also the impact of CNCs. Drying effect has been widely studied in part II.

3.3.3. Step 3: Resistance after folding

When a folded paper is flattened in the initial plane structure, irreversible damages remain due to plastic deformation occurring during the fold. The fibers located at the exterior of the fold are stretched while the fibers located at the inside of the fold are compressed. The additional stress is imparted to H-bonds of the fibers, and some are broken. This phenomenon creates a weak zone with both fiber damages and fiber-bonds damages, also visible by the decrease of thickness (Figure 12). The intensity of these damages is mainly relative to the paper structure such as porosity, fiber length or refining. To measure the impact of repetitive folds on the paper, mechanical properties, i.e. tensile tests have been performed on paper samples folded 1 time, 5 times or 10 times. Another aspect of the dog-ears issue is that the folded corner can be pulled out from the banknote. The tear

propagation has consequently also been studied by carrying out tensile tests on folded papers having a small tear at the fold location.

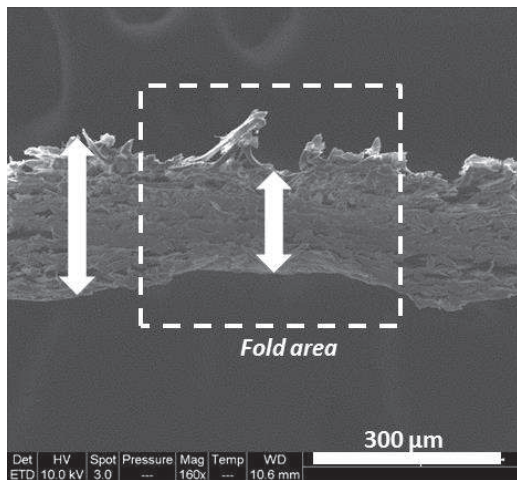


Figure 12: Decrease of paper thickness in the fold area.

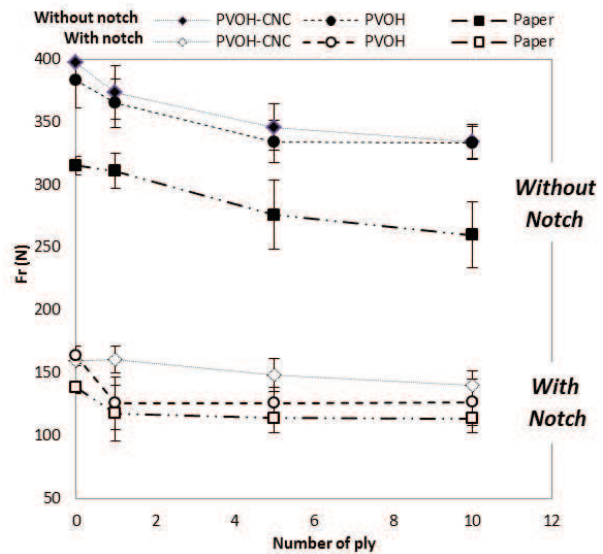


Figure 13: Paper resistance after folding, classic tensile test and study of tear propagation (tensile test on samples with a notch). The legend mentions the reference paper, a paper impregnated with 100% PVOH and a paper impregnated with 90 wt% PVOH and 10 wt% CNCs

Figure 13 compares the resistance of the ply zone after folding for the Velin paper, the velin impregnated with 100% PVOH and the velin impregnated with 90 wt% PVOH and 10 wt% CNCs. Classical tensile tests (without notch) does not show any significant impact of the CNCs in the impregnation bath as both impregnated papers present close mechanical properties. In each case, these mechanical properties decrease when increasing the number of plies. With only one ply, only 20% of the papers crack at the fold area, while 100% of the folded papers crack at the fold area already after 5 plies.

What is more interesting is the influence of CNCs on the paper crack propagation. In this case, all the cracks are performed at the fold area due to the presence of the notch. It appears on the graph that a significant increase of mechanical properties is induced by the presence of the cellulose nanoparticles. Figure 13 presents the breaking force, but the same conclusions are observable for Young's modulus and breaking length. The difference is higher when only one ply is performed, and tends to decrease with the increase of folding repetition. This decrease can be interpreted by the damage of the thin impregnated layer due to successive folds.

Conclusion on Part 1

Introduction of CNCs in the PVOH matrix has shown a beneficial impact in each step of the folding mechanism. First, CNCs limit the creation of the fold by increasing the elasticity of the material ($\tan(\delta)$) and the bending rigidity. The force needed to create the fold is also increased. Furthermore, CNCs also increase the elastic angle recovery after a fold, reinforce the bending zone and slow down the crack propagation which can occur at the fold location. It is worth also remembering that these effects are obtained for 10wt% of CNCs in a layer of 5 g.m^{-2} . The final content of CNCs in the whole paper material is subsequently very low, only 0.6%. However, despite the fact that these results are highly encouraging, they barely reach the angle recovery value targeted at 90° . In the next section, different parameters such as the paper drying, the surface chemistry of CNC, and different nanocellulosic materials or polymeric matrices are tested to optimize these EAR values.

Part II: Research of key parameters for improving the paper elastic angle recovery

The correlation between crystallinity, layer Young's modulus and their influence on dog-ears resistance has been shown in the previous part. With 10 wt% CNCs in the PVOH matrix, an increase of the elastic angle recovery from $57.5^\circ \pm 10.3$ to 85.4 ± 8.2 has been obtained. Despite this interesting improvement, it remains below an elastic recovery of 90° which has been targeted. In this section, different studies have been performed aiming to (i) identify the key parameters and (ii) optimize the elastic angle recovery after folding.

3.3.4. Influence of paper drying parameter

Test of different drying processes.

It is well known that thermal treatments on some polymeric material like PVOH induce changes in its crystallinity: this is the so called annealing effect. As a preliminary test, an additional thermal treatment has been performed on a dried PVOH-impregnated paper. As the glass transition of PVOH occurs at 32°C and the melting point at 214°C , a temperature in between (150°C) has been chosen to induce an increase of crystallinity of PVOH. DSC tests on PVOH films having experienced or not the thermal treatment confirmed that PVOH crystallinity passes from 25% to 45% with the thermal treatment. In parallel, an increase in elastic angle recovery of paper from $63.2 \pm 5.4^\circ$ to $83.4 \pm 7.5^\circ$ has been observed by this simple annealing effect.

Another possibility for changing the PVOH crystallinity is to act directly on the paper drying step. Three different dryings have been considered: the classical convective drying (3 minutes at 115°C), a longer convective drying (15 minutes at 115°C) or a drying with infra-red (2 minutes at 2500W). In the previous study (**Chapter II.2.**), the evolution of the temperature at the paper surface during IR drying and the influence of this drying on PVOH crystallization (coupled with the influence of CNCs) have been explained. It appears that crystallization at 200°C favors the crystallization of both short and long PVOH chains, and the resulting crystallinity value is higher than with convective drying at lower temperatures. As CNCs also impact the CNC crystallization, the combination of IR drying and presence of CNC allows reaching a degree of crystallinity of 40%.

By taking a look on the $\tan(\delta)$ values of these papers, it can be seen that the paper dried with infra-red drying present the lowest energy dissipation, synonym of higher elasticity (Figure 14). More interesting, this influence is confirmed by the elastic angle recovery value. Indeed, a value higher than 100° is reached thanks to an impregnation of 90 wt% PVOH and 10 wt% CNCs and the infra-red drying, which is above the targeted value of 90° .

The longer convective drying (15 min at 115°C) only increases the elastic angle recovery value in the case of water and PVOH impregnation, but it remains lower than the one obtained with a classical drying and 10 wt% CNCs. We can consequently not consider an increase of drying time as a

replacement of the CNCs. This increase of time also does not impact the angle recovery in the presence of CNCs. On the other hand, IR drying increases the elastic angle recovery for both PVOH alone and PVOH with 10 wt% CNCs.

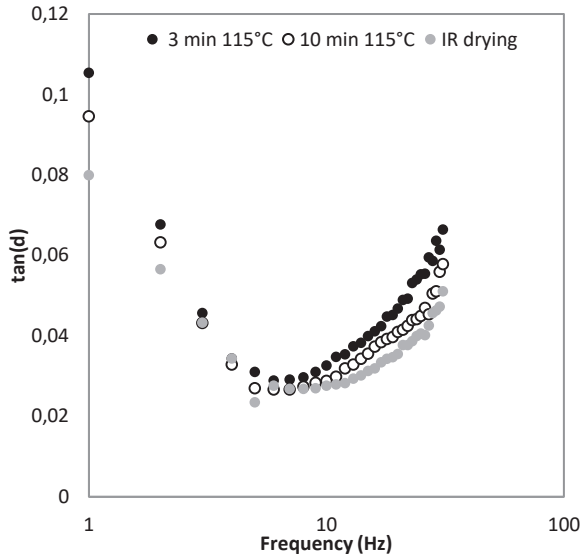


Figure 14: $\tan(\delta)$ vs. frequency for paper impregnated with 90 wt% PVOH and 10wt% CNC, after different drying processes

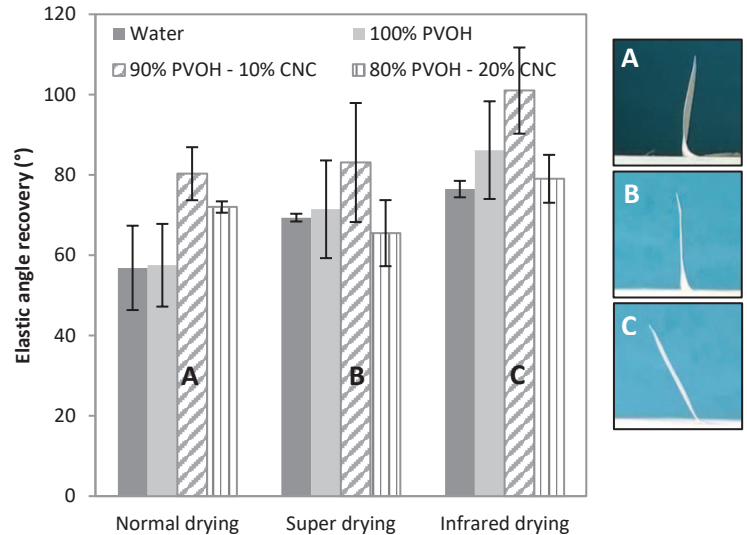


Figure 15: Influence of drying process on paper elastic angle recovery after folding. Normal drying = 3 minutes at 115°C, Super drying = 15 minutes at 115°C, IR drying = 2 minutes with 2500W Long-wave infra red

Optimization of IR drying.

In the first experiments, the IR drying was performed with a 2500W lamp positioned at 20 cm from the sample. As this system only allow for drying one face, 1 minute drying was applied to the paper, after what the paper sample was returned and dried for another 1 minute. This drying method has been called “symmetric”. Then, another drying process has been tested by drying 2 minutes continuously without returning the paper. This drying has been called “asymmetric”. Elastic angle recovery of the impregnated paper has finally been measured on each side of the paper (Front side and back side) to check the influence of drying asymmetry. Other tests have also been performed by increasing the time of drying and move the position of the lamps.

Influence of drying time. Results in Figure 16 (A and B) show that the elastic angle recovery value for impregnated paper dried 2 minutes or 4 minutes are in the same range. This can be explained by the fact that two minutes are sufficient to evaporate the whole amount of water in the paper (Figure 16-C). Consequently, it is not necessary to double the drying time. As a comparison, increasing the duration of the convective drying (115°C) from 3 minutes to 15 minutes did not change either the values of elastic angle recovery.

Influence of drying asymmetry. The paper surface temperature has been measured during drying under IR-2500W with one thermocouple on each side of the paper. As the drier is composed of only one IR lamp at the top, a slight difference of temperature occurs between each paper side. As

described in Chapter II.2., the front side of the paper is on average at 200°C (slightly overestimated because of radiation) while the back side of the paper is on average at 180°C. Figure 16-A and B show the elastic angle recovery value after symmetric drying (paper returned at the middle time of the drying) and asymmetric drying (no change of paper position). When the paper is impregnated with PVOH only, the elastic angle recovery measured on front side (recto) and back side (verso) are very close whatever the drying time and symmetry. However, if we take a look on the paper impregnated with PVOH-CNC and dried for 2 minutes, a slight difference appears between paper front side and backside. This difference remains unchanged when the 2 minutes-drying is symmetric or not and it tends to disappear with the increase of drying time to 4 minutes.

As the kinetics of water evaporation is slightly faster in the presence of CNCs, the difference of angle recovery between front side and back side after 2 min IR drying cannot be explained by a lack of drying. As the main difference between 100% PVOH impregnation and PVOH/CNC impregnation are related to a difference in PVOH crystallization, we can assume that in the presence of CNCs, 4 minutes drying promote a higher crystallization homogeneity than with only 2 minutes drying.

Note: The Velin paper is not symmetric as it is composed of two cotton fiber layers, one at 60 g/m² and the other one at 25 g/m². For the tests, “front-side” is considered with the 60 g/m² layer at the top. However, no difference in elastic angle recovery value has been noticed between each side of the Velin paper and we consequently assume that differences observed are only imparted by the drying process.

Distance between IR lamp and paper. Finally, the lamp position has been changed in order to be closer or further than the paper surface (Figure 16-D). Not surprisingly, the most the lamps are closed to the paper surface, the higher is the resulting paper elastic angle recovery. However, the difference is rather small and can be linked to small variation in paper surface temperature. When not specified, all the experiments were performed with the lamps at 20 cm from the paper surface.

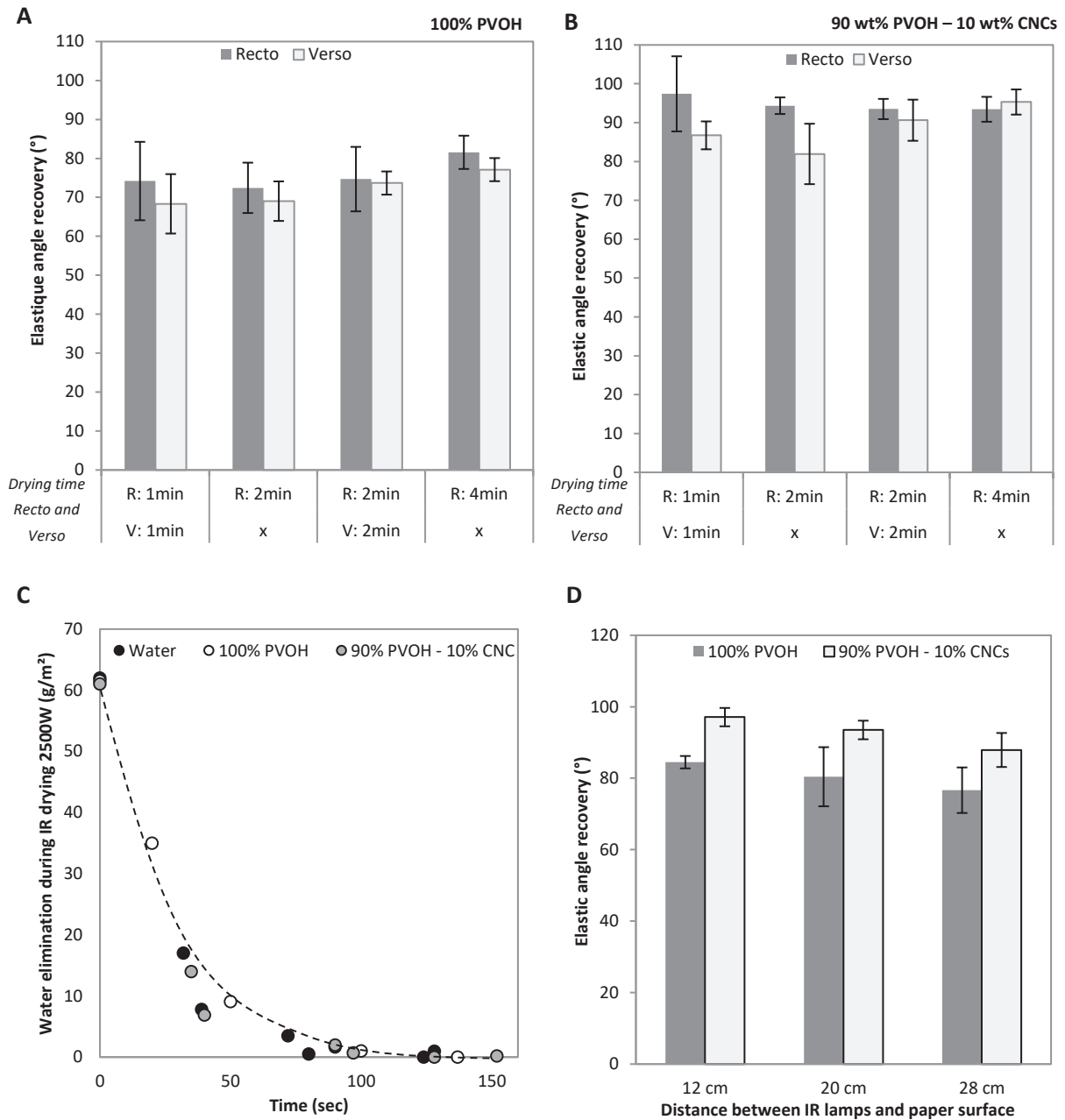


Figure 16: Optimization of IR drying with A) elastic angle recovery of paper impregnated with 100%, B) elastic angle recovery of paper impregnated with 90 wt% PVOH and 10 wt% CNC, C) water evaporation kinetics during IR drying and D) influence of IR lamp position. All these experiments were performed with long-wave 2500W IR lamp.

3.3.5. Influence of the nanocellulosic material

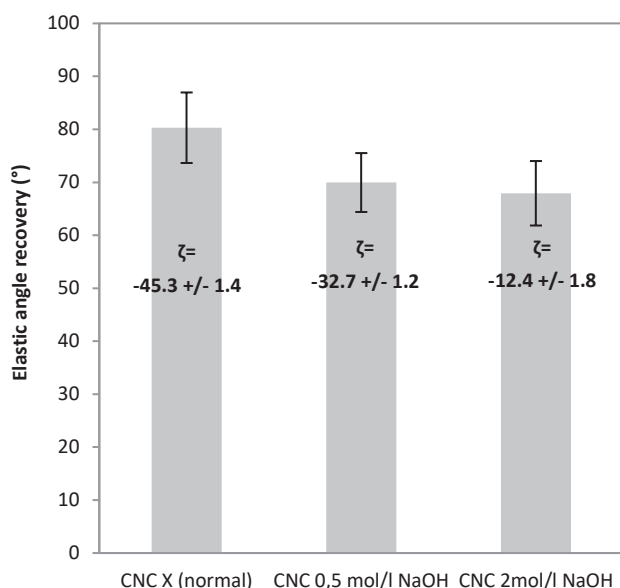


Figure 17: Influence of CNC desulfation on paper elastic angle recovery.

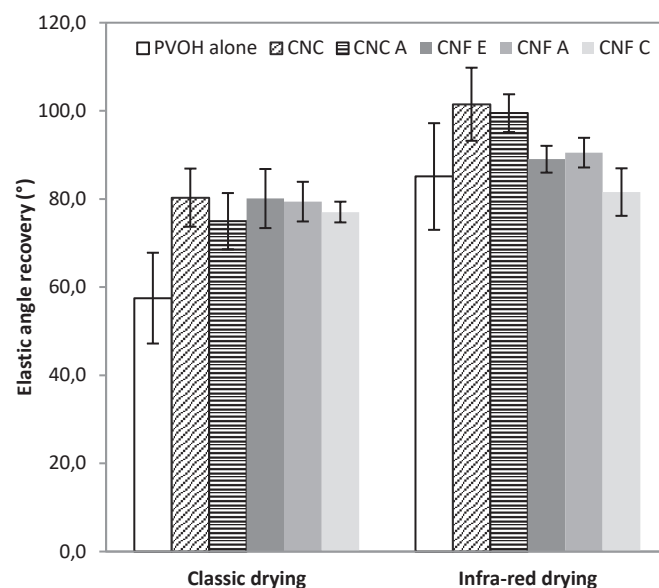


Figure 18: Influence of nanocellulosic material on paper elastic angle recovery. Cellulose nanocrystals (CNC) and cellulose nanofibrils (CNF) are added at 10 wt% in the PVOH matrix. A=Anionic, E= Enzymatic, C= Cationic

Influence of sulfate content on CNCs. Cellulose nanocrystals are obtained after acid hydrolysis of the cellulose fibers. If this acid hydrolysis is performed with sulfuric acid, an esterification reaction occurs between the acid and cellulose molecules and leads to covalent coupling of half sulfate ester groups on the surface of CNCs (Lin and Dufresne 2014). These negative sulfate groups influence the dispersion and physical properties of the nanocrystals. Some changes in sulfate group (OSO_3^-) content could change the dispersion and surface interactions between CNCs and PVOH, and hence changes the resulting mechanical properties.

Commercial CNCs have been desulfated thanks to an alkaline treatment, with different concentrations of sodium hydroxyde (0.5 mol.L^{-1} and 2 mol.L^{-1}). It first appeared that desulfated CNCs tend to aggregate more easily. Indeed, the removal of sulfate ester groups on the surface of CNC reduces their colloidal stability in aqueous medium. The removal of sulfate groups has been confirmed thanks to the decrease of the zeta potential value (Figure 17). Finally, CNCs with gradient sulfate content have been mixed with polyvinyl alcohol, impregnated on paper, and dried with the convective drying. Figure 17 shows that the elastic angle recovery of these papers is affected by the decrease of sulfate groups on the CNC surface, with a loss of 10°C between the commercial CNC and the same CNC desulfated with 0.5 mol.L^{-1} NaOH. This loss can be explained by a lower dispersion of the CNCs in the PVOH matrix.

The sulfate content of CNCs mainly depends on the hydrolysis conditions. Nowadays, it exists on the market a large bench of different CNCs with different dimensions, crystallinity and surface

chemistry. Knowing the differences between these nanoparticles is essential for the up-scaling of a material with tunable properties, and especially in the case of this study where the correlation between sulfate groups and the dog-ears resistance has just been experimentally reported.

Comparison between different CNC sources. Due to the recent availability of CNC at industrial scale from several producers, characterization and differentiation of these materials has become a key challenge in order to select the better source for each application. A benchmarking of commercial CNCs obtained by sulfuric acid hydrolysis has been recently performed (Reid et al. 2017) and it confirms the variability of this product. Four different commercial sources of CNCs have been compared: CNCs from the University of Maine, from CelluForce, from Melodea and from Blue Goose. Table 2 synthesizes their dimensions, surface chemistry, crystallinity, and it also reports the value of elastic angle recovery for a paper impregnated with 10 wt% of these nanocrystals in 90 wt% PVOH matrix. Two groups of values stand out: high angle recovery values are obtained for CNCs from the University of Maine and lower values are obtained for CNCs from Melodea and CelluForce. The lower value obtained for CNCs from Melodea can be explained by the low sulfate content at the CNC surface. However, this parameter is not sufficient to explain the low value obtained with CNC from CelluForce, as the sulfate content is close to the one of CNC from the University of Maine. Other parameters which can be influent are the aspect ratio (and consequently, the percolation threshold) and the fabrication process.

Table 2: Comparison between commercial CNCs from different producers. L= Length, W= Width *source: (Reid et al. 2017). Angle recovery performed with 0.6 kPa. Measures with 10wt% CNC and 90 wt% PVOH.

	Process	Dimensions (nm)	Aspect ratio	Percolation threshold (wt%)	Crystallinity	Sulfate content R-OSO ₃ H mmol/kg	Elastic angle recovery (°) 10 wt% CNC
University of Maine – Forest product lab	Sulfuric acid hydrolysis from dissolving pulp	L: 136 (+/- 43) W: 11 (+/-2)	12.4 ± 7.5	7	80.3% (+ Cell II)	340*	80.3 (+/- 6.6)
Blue Goose	Transition-metal-catalyzed oxidative method, variety of biomass source*	L: 150 (+/- 50) W: 11.5 (+/- 2.5)	13.0 ± 9.5	6	83%	(carboxyl functional groups)	78.5 (+/- 8.8)
Melodea	Acid hydrolysis from bleached pulp, flax or hems fibers Presence of salt.	L: 217 (+/- 89) W: 12,5 (+/- 3,4)	17,3 ± 16.3	5	-	12.5 (+/- 0.5)	66.4 (8.1)
CelluForce	Sulfuric acid hydrolysis from bleached kraft pulp	L: 183 (+/- 88)* W: 6 (+/- 2)*	30.5 ± 37.3	3	90%	250*	69.7 +/- 9.4

As the dimensions of CNCs are heterogeneous (high standard deviation), the aspect ratio value is consequently too imprecise to make distinctions between these CNCs. The percolation threshold is based on this aspect ratio and the values reported here only consider the average value

but not the huge standard deviation. We can still notice that the average percolation threshold of CNC from CelluForce is lower (3 wt%) and a use of 10 wt% of these CNCs could lead to aggregates and damage the resulting physical properties. Furthermore, CelluForce has been bought as a dry powder while CNC from the University of Maine has been delivered under the form of a suspension at 12 wt%. It is possible that CNC from CelluForce were not enough dispersed when diluted in water, even if no characterization tests have allowed us to conclude on that point.

Use of anionic CNC. Cellulose nanocrystals present high quantity of hydroxyl groups on their surface. This property allows for the grafting of anionic charges thanks to chemical post-treatments. TEMPO-mediated oxidation is known for introducing carboxylate groups on cellulose surface. CNCs with a charge density of $1100 \pm 26 \mu\text{mol.g}^{-1}$ have been obtained, indicating a strong oxidation of CNCs. For CNC, introduction of such negatively charged groups has the effect of increasing suspension stability, thanks to the formation of repulsive forces (Montanari et al. 2005; Hoeng et al. 2015). Furthermore, the carboxylic groups can react with the hydroxyl groups of the PVOH: an esterification process happens and leads to cross-linking of PVOH. Papers have been impregnated with 90wt% PVOH and 10wt% of anionic CNCs. Elastic angle recovery measurement after folding has not shown any improvement of its value compared with classical CNCs whatever the drying process (Figure 18).

Replacement of cellulose nanocrystals by cellulose nanofibrils. From the same plant fiber, two different kinds of nanocellulose can be obtained: cellulose nanocrystals and cellulose nanofibrils. Cellulose nanofibrils are long filaments with micrometric length and diameter ranging from 20 to 40 nm obtained after bio-chemical pretreatment and mechanical shearing, with both amorphous and crystalline domains (Dufresne 2017). Due to the very high aspect ratio of this material, low percolation threshold is expected (< 1 wt%). However, it is difficult to estimate a percolation threshold for flexible filaments that can fold on themselves.

As a first test, without taking into account these differences in percolation threshold, 10wt% of CNFs have been added to the PVOH matrix. Three different kinds of CNF have been used: CNF pretreated with enzymes ("CNF E"), CNF tempo-oxidized ("CNF A") and CNF grafted with cationic groups ("CNF C"). Results in Figure 18 do not show any difference in angle recovery of paper impregnated with PVOH/CNF whatever the surface chemistry of the CNF and whatever the paper drying. More interesting, with the classical drying (3 minutes at 115°C), an increase in the angle recovery from 57 to 80° is observed if we compare with the neat PVOH impregnation. These results are competitive with the one obtained with CNCs. In a second step, different amounts of CNFs have been tested (1, 5, 10 and 15 wt%) (Results not shown). It appears that same results were obtained whatever the CNF content (and after a paper drying of 3 minutes at 115°C). This observation is consistent with the fact that the percolation threshold of CNF is lower than 1wt%. Consequently, an advantage of using CNF is consequently the possibility to decrease the amount of nanomaterial into the impregnation bath. Scientific publications already investigated the ability of CNF to be used as reinforcement for polyvinyl alcohol or PEO matrix and proved that CNF is an excellent reinforcement

comparable to cellulose nanocrystals (Lu et al. 2008; Xu et al. 2013) thanks to the strong fiber-matrix interfacial bonding and large aspect ratio of the fibers.

However, the use of CNFs is an interesting candidate as a replacement of CNCs only in the case of classical drying. Indeed, no increase of angle recovery value has been observed after a classical drying or after an infra-red drying as it was the case for CNCs. From 1 wt% to 15 wt% of CNF in PVOH, same elastic angle recovery values were obtained after classic paper drying or after infra-red drying. This can be explained by the fact that CNC impact more the PVOH crystallization than CNF. Scientific publications are controversial on this subject, and different conclusions are found as a function of the matrix and type of nanocellulose. If both CNF (Suryanegara et al. 2009) and CNC (Uddin et al. 2011) seems to act as nucleating agent, the crystallinity of matrix reinforced with nanocellulose are often higher with CNC than with CNF. Siqueira et al. confirmed that the crystallinity of the Poly(ϵ -caprolactone) increases more with CNCs than with CNFs (Siqueira et al. 2011), and the same conclusion was reported for PEO matrix (Xu et al. 2013). Finally, the entanglements and percolations of CNF also results in higher probability of fiber agglomeration compared to CNCs and a lower dispersion which could happen during impregnation process can also results in damaged properties.

To conclude, if an infra-red drying can be implemented in the industrial process, the use of CNCs allows for higher results in elastic angle recovery. However, if industrial constraints enjoin a convective drying at lower temperatures, the use of cellulose nanofibrils as a replacement of cellulose nanocrystals could be considered. Up to now, up-scaling (pilot tests) and patent only concern cellulose nanocrystals. Furthermore, the first part of this study has reported that the dog-ears resistance should be divided into different aspects and the impact of cellulose nanofibrils on the creation of the ply of resistance after folding remains unknown.

3.3.6. Influence of the matrix molecular weight of PVOH

In the literature, the effect of CNCs on PVOH matrix gives rise to contradictory results. Some researchers show an increase in mechanical properties thanks to the addition of CNCs with an optimum reached for different CNC/PVOH ratios (Pereira et al. 2014; Gonzalez et al. 2014; Mandal and Chakrabarty 2014) while other researchers did not observe any influence of CNCs (Fortunati et al. 2013). These heterogeneous results can be explained by the difference of raw materials (CNC percolation threshold) and protocols (dispersion of CNCs in the matrix, humidity level, thickness and drying procedure). PVOH molecular weight and recrystallization possibility are also key factors which determine the properties of the final nanocomposite and, consequently, the properties of the resulting impregnated papers. Martin et al. (Martin et al. 1972) showed long time ago that molecular weight of a polymer can affect its mechanical properties and more recent studies show for example that an increase in the polyvinyl alcohol molecular weight leads to an increase in tensile, adhesive

strength and water resistance while a decrease of molecular weight leads to an increase in flexibility (Tang and Alavi 2011).

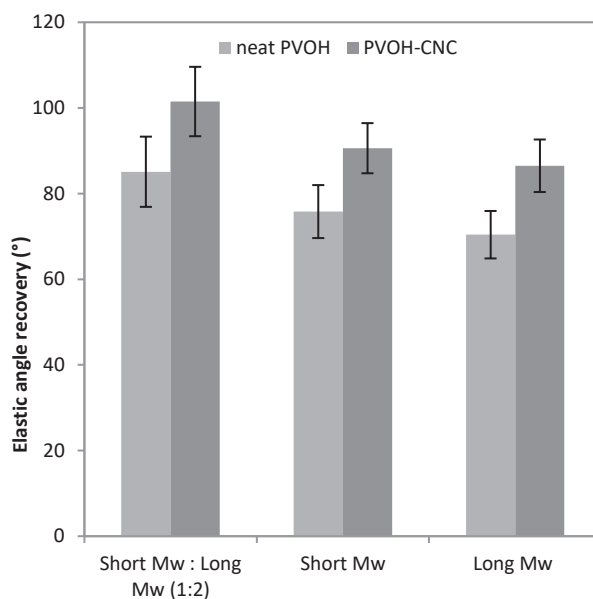


Figure 19: Elastic angle recovery for papers impregnated with different PVOH molecular weight (MW), with and without the presence of 10 wt% CNCs, and dried 2 minutes under infra-red

Figure 19 shows the elastic angle recovery of papers impregnated with PVOH of different molecular weights, with and without CNCs. The RESIST mixture used for all the study is a mixture composed of 2/3 long PVOH chains and 1/3 short PVOH chains. This mixture has been compared with only long-chain PVOH ($145000 \text{ g.mol}^{-1}$) or only short-chain PVOH (27000 g.mol^{-1}). Study of PVOH crystallization (**Chapter II.2.**) has shown that the crystallinity of PVOH is slightly higher for the short-chain PVOH with 39.7% against 36.5% for both mixture and long-chain PVOH. It is indeed well known that when the molecular weight increases, the polymer has more difficulties to crystallize because of more important chain entanglements which can hinder the polymer crystallization. Moreover, an increase of molecular weight can also be linked to an increase of viscosity (Fox and Flory 1950), and hence to a decrease of PVOH deposition. However, as the final content of the impregnation bath is very dilute (5wt%), this parameter should not be determinant. As expected, long-chain PVOH gives rise to paper with slightly lower elastic angle recovery than with short-chain PVOH.

However, the impregnation with short chain PVOH gives rise to lower elastic angle recovery values than the impregnation with the mixture, even if the crystallinity is higher. The PVOH degree of crystallinity is consequently not the only parameter to take into account. It is worth noting that same viscosity was observed and same amount of PVOH was deposited on the paper. To better explain the results obtained with the PVOH mixture, mechanical properties of a PVOH layer composed by the mixture or low molecular weight PVOH should be performed thanks to the Siebimm test (**Chapter II.1.**). The full understanding of PVOH matrix influence on paper elastic angle recovery is a perspective of this work.

3.4. General conclusion

It is well known in the field of paper products, that a paper may be intentionally or unintentionally folded down during its use and form corner folds, also known in banknote industry as “Dog-ears”. To increase the dog-ears resistance of banknotes, the strategy of this work consists in the impregnation of banknote substrate with CNC-reinforced PVOH. In a first part, the dog-ears resistance has been studied through three different mechanisms: the creation of the fold, the fold recovery and the resistance of the paper after the fold. Different ratios of CNCs have been tested and 10 wt% CNCs in 90 wt% PVOH appeared to give the most satisfying results in the three steps of the dog-ears. These results can be correlated to the nucleating effect of CNCs which tends to increase the PVOH crystallinity and results in a paper top layer with reinforced mechanical properties. In the second part, different parameters such as drying, nanocellulosic material, PVOH molecular weight and cross-linking have been studied in order to reach an elastic angle recovery higher than 90°. Infra-red drying allowed exceeding this target with success. The drying temperature, and hence temperature of PVOH crystallization, has indeed a significant impact on the degree of crystallinity. As the crystalline regions are responsible for tenacity, high modulus of elasticity and resistance towards bending, they also impact the dog-ears resistance. Change in matrix molecular weight did not give satisfying results. However, the choice of the nanocellulosic material, and especially the CNC sulfate content, appeared to be, with the drying treatment, one of the most determining factors. Finally, two options could industrially answer the need of banknote dog-ears resistance. The better is obtained with a paper impregnated with 10 wt% CNCs from the University of Maine in 90 wt% PVOH and dried 2 minutes with a 2500-W long wave infra-red. With a convective drying, an increase of dog-ears resistance has also been observed with a same amount of CNCs, but in this case the replacement of CNC material by CNF could be a cost-saving alternative for competitive results. These very positive results have recently been patented (Bras et al. 2016) and performed in pilot and industrial scales in Banque De France facilities (**Chapter IV.1.**).

References

- Abitbol T, Prevo BG, Galli C, et al (2014) Comparison of nanocrystalline cellulose and fumed silica in latex coatings. *Green Mater* 2:206–221. doi: 10.1680/gmat.14.00017
- Amini E, Azadfallah M, Layeghi M, Talaei-Hassanloui R (2016) Silver-nanoparticle-impregnated cellulose nanofibre coating for packaging paper. *Cellulose* 23:557–570. doi: 10.1007/s10570-015-0846-1
- Azizi Samir MAS, Alloin F, Dufresne A (2005) Review of Recent Research into Cellulosic Whiskers, Their Properties and Their Application in Nanocomposite Field. *Biomacromolecules* 6:612–626. doi: 10.1021/bm0493685
- Azizi Samir MAS, Alloin F, Sanchez J-Y, Dufresne A (2004) Cellulose nanocrystals reinforced poly(oxyethylene). *Polymer* 45:4149–4157. doi: 10.1016/j.polymer.2004.03.094
- Azzam F, Chaunier L, Moreau C, et al (2017) Relationship between Young's Modulus and Film Architecture in Cellulose Nanofibril-Based Multilayered Thin Films. *Langmuir* 33:4138–4145. doi: 10.1021/acs.langmuir.7b00049
- Bardet R, Bras J (2014) Cellulose Nanofibres and Their Use in Paper Industry. In: *Handbook of Green Materials*. World Scientific, Chapter 13, pp 207–232.
- Beneventi D, Chaussy D, Curtil D, et al (2014) Highly Porous Paper Loading with Microfibrillated Cellulose by Spray Coating on Wet Substrates. *Ind Eng Chem Res* 53:10982–10989. doi: 10.1021/ie500955x
- Berg O van den, Schroeter M, Capadona JR, Weder C (2007) Nanocomposites based on cellulose whiskers and (semi)conducting conjugated polymers. *J Mater Chem* 17:2746–2753. doi: 10.1039/B700878C
- Biot MA (1937) Bending of an infinite beam on an elastic foundation. *J Appl Mech* A 1-7. ISSN : 0021-8936
- Boufi S, Kaddami H, Dufresne A (2013) Mechanical Performance and Transparency of Nanocellulose Reinforced Polymer Nanocomposites. *Macromol Mater Eng* 299:560–568. doi: 10.1002/mame.201300232
- Bowden N, Brittain S, Evans AG, et al (1998) Spontaneous formation of ordered structures in thin films of metals supported on an elastomeric polymer. *Nature* 393:146. doi: 10.1038/30193
- Bras J, Dufresne A, Desmaisons J, Roberty G, Lutsche M (2017) Use of nano cellulose on a paper product. *European Central Bank* EP3228744 A1
- Brodin FW, Gregersen OW, Syverud K (2014) Cellulose nanofibrils: Challenges and possibilities as a paper additive or coating material—A review. *Nord Pulp Pap Res J* 29:156–166. doi: 10.3183/NPPRJ-2014-29-01-p156-166
- Cassidy J, Doublet P (1993) Security paper, in particular for use as a passport flyleaf. *Arjo Wiggins SA* EP0599675A1
- Chang JF, Kuo HH, Leu IC, Hon MH (2002) The effects of thickness and operation temperature on ZnO:Al thin film CO gas sensor. *Sens Actuators B Chem* 84:258–264. doi: 10.1016/S0925-4005(02)00034-5
- Chen D, Lawton D, Thompson MR, Liu Q (2012) Biocomposites reinforced with cellulose nanocrystals derived from potato peel waste. *Carbohydr Polym* 90:709–716. doi: 10.1016/j.carbpol.2012.06.002
- Chen Y-T, Kao HL (2006) Humidity sensors made on polyvinyl-alcohol film coated SAW devices. *Inst Eng Technol Electron Lett* 42:948–949. Doi: 10.1049/el:20061216
- Cranston ED, Eita M, Johansson E, et al (2011) Determination of Young's Modulus for Nanofibrillated Cellulose Multilayer Thin Films Using Buckling Mechanics. *Biomacromolecules* 12:961–969. doi: 10.1021/bm101330w
- Deegan RD, bakajin O, Dupont TF, et al (2000) Contact line deposits in an evaporating drop. *Phys Rev E* 62:756-765. Doi:10.1103/PhysRevE.62.756

Chapter II References

- Denneulin A, Blayo A, Neuman C, Bras J (2011) Infra-red assisted sintering of inkjet printed silver tracks on paper substrates. *J Nanoparticle Res* 13:3815–3823. doi: 10.1007/s11051-011-0306-2
- Dufresne A (2008) Polysaccharide nano crystal reinforced nanocomposites. *Can J Chem* 86:484–494. doi: 10.1139/v07-152
- Dufresne A (2017) *Nanocellulose: From Nature to High Performance Tailored Materials*. Walter de Gruyter GmbH & Co KG
- Dufresne A, Thomas S, Pothan LA (2013) *Biopolymer Nanocomposites: Processing, Properties, and Applications*, Wiley
- Eichhorn SJ (2011) Cellulose nanowhiskers: promising materials for advanced applications. *Soft Matter* 7:303–315. doi: 10.1039/C0SM00142B
- El Miri N, Abdelouahdi K, Zahouily M, Fihri A, Barakat A, Solhy A, El Achaby M (2015) Bio-nanocomposite films based on cellulose nanocrystals filled polyvinyl alcohol/chitosan polymer blend. *J. Appl. Polym. Sci.* 132(22):1-13. doi: 10.1002/app.42004
- El-Wakil NA, Hassan EA, Abou-Zeid RE, Dufresne A (2015) Development of wheat gluten/nanocellulose/titanium dioxide nanocomposites for active food packaging. *Carbohydr Polym* 124:337–346. doi: 10.1016/j.carbpol.2015.01.076
- Espino-Pérez E, Bras J, Almeida G, et al (2018) Designed cellulose nanocrystal surface properties for improving barrier properties in polylactide nanocomposites. *Carbohydr Polym* 183:267–277. doi: 10.1016/j.carbpol.2017.12.005
- Favier V, Canova GR, Cavallé JY, et al (1995) Nanocomposite materials from latex and cellulose whiskers. *Polym Adv Technol* 6:351–355. doi: 10.1002/pat.1995.220060514
- Fortunati E, Puglia D, Luzi F, et al (2013) Binary PVA bio-nanocomposites containing cellulose nanocrystals extracted from different natural sources: Part I. *Carbohydr Polym* 97:825–836. doi: 10.1016/j.carbpol.2013.03.075
- Fox TG, Flory PJ (1950) Second-Order Transition Temperatures and Related Properties of Polystyrene. I. Influence of Molecular Weight. *J Appl Phys* 21:581–591. doi: 10.1063/1.1699711
- Francis KC, Blanch JE, Magleby SP, Howell LL (2013) Origami-like creases in sheet materials for compliant mechanism design. *Mech Sci* 4:371–380. doi: 10.5194/ms-4-371-2013
- Gachter R, Muller H (1985) *Plastics Additives Handbook Stabilizers Processing Aids Plasticizers Fillers Reinforcements Colorants for Thermoplastics* - AbeBooks, Carl Hanser Verlag
- Gicquel E, Martin C, Garrido Yanez J, Bras J (2017) Cellulose nanocrystals as new bio-based coating layer for improving fibre-based mechanical and barrier properties. *J Mater Sci* 52:3048–3061. doi: 10.1007/s10853-016-0589-x
- Gong G, Pyo J, Mathew AP, Oksman K (2011) Tensile behavior, morphology and viscoelastic analysis of cellulose nanofibre-reinforced (CNF) polyvinyl acetate (PVAc). *Compos Part Appl Sci Manuf* 42:1275–1282. doi: 10.1016/j.compositesa.2011.05.009
- Gonzalez JS, Ludueña LN, Ponce A, Alvarez VA (2014) Poly(vinyl alcohol)/cellulose nanowhiskers nanocomposite hydrogels for potential wound dressings. *Mater Sci Eng C Mater Biol Appl* 34:54–61. doi: 10.1016/j.msec.2013.10.006
- Gray DG (2008) Transcrystallization of polypropylene at cellulose nanocrystal surfaces. *Cellulose* 15:297–301. doi: 10.1007/s10570-007-9176-2
- Guezennec C (2012) *Développement de nouveaux matériaux d’emballage à partir de micro- et nano-fibrilles de cellulose*. Phd thesis, Université de Grenoble
- Habibi Y, Chanzy H, Vignon MR (2006) TEMPO-mediated surface oxidation of cellulose whiskers. *Cellulose* 13:679–687. doi: 10.1007/s10570-006-9075-y
- Habibi Y, Lucia LA, Rojas OJ (2010) Cellulose Nanocrystals: Chemistry, Self-Assembly, and Applications. *Chem Rev* 110:3479–3500. doi: 10.1021/cr900339w

Chapter II References

- Hafsaoui SL (2013) Etude et modélisation de la stabilité thermique et des propriétés des polyamides au cours du rotomoulage. Phd thesis, Ecole nationale supérieure d'arts et métiers - ENSAM
- Halpin J c., Kardos J I. (1972) Moduli of Crystalline Polymers Employing Composite Theory. *J Appl Phys* 43:2235–2241. doi: 10.1063/1.1661482
- Hannay N (ed) (1976) *Treatise on Solid State Chemistry: Volume 3 Crystalline and Noncrystalline Solids*. Springer US. ISBN: 978-1-4684-2666-3
- Hasani M, Cranston ED, Westman G, Gray DG (2008) Cationic surface functionalization of cellulose nanocrystals. *Soft Matter* 4:2238–2244. doi: 10.1039/B806789A
- Herrera MA, Mathew AP, Oksman K (2017) Barrier and mechanical properties of plasticized and cross-linked nanocellulose coatings for paper packaging applications. *Cellulose* 24:3969–3980. doi: 10.1007/s10570-017-1405-8
- Hoeger I, Rojas OJ, Efimenko K, et al (2011) Ultrathin film coatings of aligned cellulose nanocrystals from a convective-shear assembly system and their surface mechanical properties. *Soft Matter* 7:1957–1967. doi: 10.1039/C0SM01113D
- Hoeng F, Denneulin A, Neuman C, Bras J (2015) Charge density modification of carboxylated cellulose nanocrystals for stable silver nanoparticles suspension preparation. *J Nanoparticle Res* 17:244. doi: 10.1007/s11051-015-3044-z
- Hoffman JD, Weeks JJ (1962) Melting process and the equilibrium melting temperature of polychlorotrifluoroethylene. *J Res Natl Bur Stand A* 66:13–28. doi: 10.1.1.465.6222
- Huang J, Lyu S, Fu F, et al (2017) Green preparation of a cellulose nanocrystals/polyvinyl alcohol composite superhydrophobic coating. *RSC Adv* 7:20152–20159. doi: 10.1039/c6ra27663f
- Hubbe MA, Ferrer A, Tyagi P, et al (2017) Nanocellulose in Thin Films, Coatings, and Plies for Packaging Applications: A Review. *BioResources* 12:2143–2233. doi: 10.15376/biores.12.1.2143-2233
- Jalal Uddin A, Araki J, Gotoh Y (2011) Extremely oriented tunicin whiskers in poly(vinyl alcohol) nanocomposites. *Polym Int* 60:1230–1239. doi: 10.1002/pi.3067
- Johansson E, Wågberg L (2012) Tailoring the mechanical properties of starch-containing layer-by-layer films. *Colloids Surf Physicochem Eng Asp* 394:14–22. doi: 10.1016/j.colsurfa.2011.11.017
- Jorfi M, Roberts MN, Foster EJ, Weder C (2013) Physiologically Responsive, Mechanically Adaptive Bio-Nanocomposites for Biomedical Applications. *ACS Appl. Mater. Interfaces* 5(4):1517-1526. doi: 10.1021/am303160j
- Kan KHM, Cranston ED (2013) Mechanical testing of thin film nanocellulose composites using buckling mechanics. *Tappi J* 12(4):9–17
- Karger-Kocsis J (1989) Chapter 6 - Microstructure and Fracture Mechanical Performance of Short-Fibre Reinforced Thermoplastics. In: Friedrich K (ed) *Composite Materials Series*. Elsevier, pp 189–247
- Kim H, Horwitz JS, Kushto G, et al (2000) Effect of film thickness on the properties of indium tin oxide thin films. *J Appl Phys* 88:6021–6025. doi: 10.1063/1.1318368
- Lavoine N, Desloges I (2014) Impact of different coating processes of microfibrillated cellulose on the mechanical and barrier properties of paper. *J Mater Sci* 49:2879–2893. doi: 10.1007/s10853-013-7995-0
- Le Berre M, Gillot J, Borde X (2015) Process for the surface treatment of a security document and associated security document. Oberthur Fiduciaire. WO2015091873 A1
- Le Corre D, Bras J, Choisnard L, Dufresne A (2012) Optimization of the batch preparation of starch nanocrystals to reach daily time-scale. *Starch* 64:489–496. doi: 10.1002/star.201100145
- Lin N, Dufresne A (2014) Surface chemistry, morphological analysis and properties of cellulose nanocrystals with graded sulfation degrees. *Nanoscale* 6:5384–5393. doi: 10.1039/C3NR06761K

Chapter II References

- Lorenzo AT, Arnal ML, Albuerne J, Müller AJ (2007) DSC isothermal polymer crystallization kinetics measurements and the use of the Avrami equation to fit the data: Guidelines to avoid common problems. *Polym Test* 26:222–231. doi: 10.1016/j.polymertesting.2006.10.005
- Lu J, Wang T, Drzal LT (2008) Preparation and properties of microfibrillated cellulose polyvinyl alcohol composite materials. *Compos Part Appl Sci Manuf* 39:738–746. doi: 10.1016/j.compositesa.2008.02.003
- Mandal A, Chakrabarty D (2014) Studies on the mechanical, thermal, morphological and barrier properties of nanocomposites based on poly(vinyl alcohol) and nanocellulose from sugarcane bagasse. *J Ind Eng Chem* 20:462–473. doi: 10.1016/j.jiec.2013.05.003
- Mariano M, Chirat C, El Kissi N, Dufresne A (2016) Impact of cellulose nanocrystal aspect ratio on crystallization and reinforcement of poly(butylene adipate-co-terephthalate). *J Polym Sci Part B Polym Phys* 54:2284–2297. doi: 10.1002/polb.24139
- Mariano M, El Kissi N, Dufresne A (2014) Cellulose nanocrystals and related nanocomposites: Review of some properties and challenges. *J Polym Sci Part B Polym Phys* 52:791–806. doi: 10.1002/polb.23490
- Martin C (2015) Films multicouches à base de nanocristaux de cellulose : relation entre structure et propriétés mécaniques et/ou optiques. PhD thesis University Grenoble Alpes
- Martin JR, Johnson JF, Cooper AR (1972) Mechanical Properties of Polymers: The Influence of Molecular Weight and Molecular Weight Distribution. *J Macromol Sci Part C* 8:57–199. doi: 10.1080/15321797208068169
- Mascheroni E, Rampazzo R, Ortenzi MA, et al (2016) Comparison of cellulose nanocrystals obtained by sulfuric acid hydrolysis and ammonium persulfate, to be used as coating on flexible food-packaging materials. *Cellulose* 23:779–793. doi: 10.1007/s10570-015-0853-2
- Mehta N, Agarwal P, Kumar A (2004) A study of the crystallization kinetics in Se₆₈Ge₂₂Pb₁₀ chalcogenide glass. *Indian J. Eng. Mater. Sci.* 11(6):511–515
- Montanari S, Roumani M, Heux L, Vignon M (2005) Topochemistry of Carboxylated Cellulose Nanocrystals Resulting from TEMPO-Mediated Oxidation. *Macromolecules* 38:. doi: 10.1021/ma048396c
- Moon RJ, Martini A, Nairn J, et al (2011) Cellulose nanomaterials review: structure, properties and nanocomposites. *Chem Soc Rev* 40:3941–3994. doi: 10.1039/C0CS00108B
- Musil J, Kunc F, Zeman H, Polakova H (2002) Relationships between hardness, Young's modulus and elastic recovery in hard nanocomposite coatings. *Surf Coat Technol* 154:304–313. doi: 10.1016/S0257-8972(01)01714-5
- Nechporchuk O, Belgacem MN, Pignon F (2014) Rheological properties of micro-/nanofibrillated cellulose suspensions: Wall-slip and shear banding phenomena. *Carbohydr Polym* 112:432–439. doi: 10.1016/j.carbpol.2014.05.092
- Nelson K, Retsina T, Pytkkanen V, et al (2015) Nanocellulose production using lignosulfonic acid. API Intellectual Property Holding. US20160237173A1
- Nishi T, Wang TT (1975) Melting point depression and kinetic effects of cooling on crystallization in poly (vinylidene fluoride)-poly (methyl methacrylate) mixtures. *Macromolecules* 8(6):909–915. doi: 10.1021/ma60048a040
- Oksman K, Aitomäki Y, Mathew AP, et al (2016) Review of the recent developments in cellulose nanocomposite processing. *Compos Part Appl Sci Manuf* 83:2–18. doi: 10.1016/j.compositesa.2015.10.041
- Ouali N, Cavaillé JY, Perez J (1991) Elastic, viscoelastic and plastic behavior of multiphase polymer blends. *Plast Rubber Compos Process Appl* 16:55–60. doi: 0959-8111/91/\$03.50
- Pandey JK, Lee CS, Ahn S-H (2010) Preparation and properties of bio-nanoreinforced composites from biodegradable polymer matrix and cellulose whiskers. *J Appl Polym Sci* 115:2493–2501. doi: 10.1002/app.31205

Chapter II References

- Paralikar SA, Simonsen J, Lombardi J (2008) Poly(vinyl alcohol)/cellulose nanocrystal barrier membranes. *J Membr Sci* 320:248–258. doi: 10.1016/j.memsci.2008.04.009
- Park SH, Lee SG, Kim SH (2013) The use of a nanocellulose-reinforced polyacrylonitrile precursor for the production of carbon fibres. *J Mater Sci* 48:6952–6959. doi: 10.1007/s10853-013-7503-6
- Pearson NG, Howland P (2008) Paper including watermarks and/or embossings. De la Rue International. US7399513B2
- Peppas NA, Hansen PJ (1982) Crystallization kinetics of poly(vinyl alcohol). *J Appl Polym Sci* 27:4787–4797. doi: 10.1002/app.1982.070271223
- Pereira ALS, do Nascimento DM, Morais JPS, et al (2014) Improvement of polyvinyl alcohol properties by adding nanocrystalline cellulose isolated from banana pseudostems. *Carbohydr Polym* 112:165–172. doi: 10.1016/j.carbpol.2014.05.090
- Pradier C, Cavoret J, Dureisseix D, et al (2016) An Experimental Study and Model Determination of the Mechanical Stiffness of Paper Folds. *J Mech Des* 138:041401. doi: 10.1115/1.4032629
- Pukánszky B, Mudra I, Staniek P (1997) Relation of crystalline structure and mechanical properties of nucleated polypropylene. *J Vinyl Addit Technol* 3:53–57. doi: 10.1002/vnl.10165
- Raynaud S (2017) Développement de nouveaux matériaux barrières utilisant des microfibrilles de cellulose. PhD thesis Université Grenoble Alpes
- Reid MS, Stimpson TC, Niinivaara E, et al (2018) Comparing Soft Semicrystalline Polymer Nanocomposites Reinforced with Cellulose Nanocrystals and Fumed Silica. *Ind Eng Chem Res* 57:220–230. doi: 10.1021/acs.iecr.7b03836
- Reid MS, Villalobos M, Cranston ED (2017) Benchmarking Cellulose Nanocrystals: From the Laboratory to Industrial Production. *Langmuir* 33:1583–1598. doi: 10.1021/acs.langmuir.6b03765
- Rescignano N, Fortunati E, Montesano S, et al (2014) PVA bio-nanocomposites: A new take-off using cellulose nanocrystals and PLGA nanoparticles. *Carbohydr Polym* 99:47–58. doi: 10.1016/j.carbpol.2013.08.061
- Ritala M, Leskelä M, Niinistö L, et al (1994) Development of crystallinity and morphology in hafnium dioxide thin films grown by atomic layer epitaxy. *Thin Solid Films* 250:72–80. doi: 10.1016/0040-6090(94)90168-6
- Roohani M, Habibi Y, Belgacem NM, et al (2008) Cellulose whiskers reinforced polyvinyl alcohol copolymers nanocomposites. *Eur Polym J* 44:2489–2498. doi: 10.1016/j.eurpolymj.2008.05.024
- Sadler DM (1987) New explanation for chain folding in polymers. *Nature* 326:174–177. doi: 10.1038/326174a0
- Sarrazin P (2013) Sheet of Wrinkle-Resistant Paper. Arjowiggins Security. WO2013093872 (A1)
- Senechal T, De Geiser F, De Boissieu M, Bras J (2010) Study of cellulose whiskers orientation in nanocomposites for barrier packaging. 6th Int Conf Nanostructured Polym Nanocomposites Madrid (Spain)
- Shan H, Lickfield GC (2007) Crystallization Kinetics Study of Polyethylene. *Int J Polym Anal Charact* 12:327–338. doi: 10.1080/10236660701355345
- Siqueira G, Bras J, Dufresne A (2009) Cellulose Whiskers versus Microfibrils: Influence of the Nature of the Nanoparticle and its Surface Functionalization on the Thermal and Mechanical Properties of Nanocomposites. *Biomacromolecules* 10:425–432. doi: 10.1021/bm801193d
- Siqueira G, Fraschini C, Bras J, et al (2011) Impact of the nature and shape of cellulosic nanoparticles on the isothermal crystallization kinetics of poly(ϵ -caprolactone). *Eur Polym J* 47:2216–2227. doi: 10.1016/j.eurpolymj.2011.09.014
- Sirviö JA, Honkaniemi S, Visanko M, Liimatainen H (2015) Composite Films of Poly(vinyl alcohol) and Bifunctional Cross-linking Cellulose Nanocrystals. *ACS Appl Mater Interfaces* 7:19691–19699. doi: 10.1021/acsami.5b04879

Chapter II References

- Stafford CM, Harrison C, Beers KL, et al (2004) A buckling-based metrology for measuring the elastic moduli of polymeric thin films. *Nat Mater* 3:545–550. doi: 10.1038/nmat1175
- Stone DA, Wanasekara ND, Jones DH, et al (2011) All-Organic, Stimuli-Responsive Polymer Composites with Electrospun Fibre Fillers. 1(1): 80-83 doi: 10.1021/mz200049v
- Suryanegara L, Nakagaito AN, Yano H (2009) The effect of crystallization of PLA on the thermal and mechanical properties of microfibrillated cellulose-reinforced PLA composites. *Compos Sci Technol* 69:1187–1192. doi: 10.1016/j.compscitech.2009.02.022
- Takayanagi M, Uemura S, Minami S (1964) Application of equivalent model method to dynamic rheo-optical properties of crystalline polymer. *J Polym Sci Part C Polym Symp* 5:113–122. doi: 10.1002/polc.5070050111
- Tang X, Alavi S (2011) Recent advances in starch, polyvinyl alcohol based polymer blends, nanocomposites and their biodegradability. *Carbohydr Polym* 85:7–16. doi: 10.1016/j.carbpol.2011.01.030
- Uddin AJ, Araki J, Gotoh Y (2011) Extremely oriented tunicin whiskers in poly(vinyl alcohol) nanocomposites. *Polym Int* 60:1230–1239. doi: 10.1002/pi.3067
- Uddin AJ, Fujie M, Sembo S, Gotoh Y (2012) Outstanding reinforcing effect of highly oriented chitin whiskers in PVA nanocomposites. *Carbohydr Polym* 87:799–805. doi: 10.1016/j.carbpol.2011.08.071
- Way JL, Atkinson JR, Nutting J (1974) The effect of spherulite size on the fracture morphology of polypropylene. *J Mater Sci* 9:293–299. doi: 10.1007/BF00550954
- Xu X, Liu F, Jiang L, et al (2013) Cellulose Nanocrystals vs. Cellulose Nanofibrils: A Comparative Study on Their Microstructures and Effects as Polymer Reinforcing Agents. *ACS Appl Mater Interfaces* 5:2999–3009. doi: 10.1021/am302624t
- Yang M-R, Chen K-S (1998) Humidity sensors using polyvinyl alcohol mixed with electrolytes. *Sens Actuators B Chem* 49:240–247. doi: 10.1016/S0925-4005(98)00134-8

Supplementary data

Chapter II.3. Use of cellulose nanocrystals in a polyvinyl alcohol matrix to decrease banknotes dog-ears defect

1. Impregnation process of CNC-reinforced PVOH

Nanocelluloses are well known for their gel-like behavior and high viscosity at low solid content and low shear rate. This property is especially observable with cellulose nanofibrils because of their high aspect ratio and highly entangled network. Although cellulose nanocrystals do not form entangled network, their dimensions, their CNC-CNC H-bonding and their anionic charge also result in a colloidal stable gel structure when the percolation threshold is reached. This particular property makes nanocelluloses good thickening agent in cosmetics or food (Nelson et al 2015), but it can create issues in papermaking process like coating, size-press or impregnation. Indeed it is well known that different viscosity can change suspension pick-up mass, its penetration in porous paper and its drying behavior. For these reasons, the impregnation bath viscosity has been checked for different formula. Figure SD1A shows the evolution of the viscosity as a function of the shear rate for impregnation bath containing PVOH and different ratio of CNCs. All curves are in the same range of viscosity at low shear rate: this can be explained by the low dry content (5 wt%) of the suspensions, and consequently low amount of cellulose nanocrystals, not sufficient to significantly increase the viscosity.

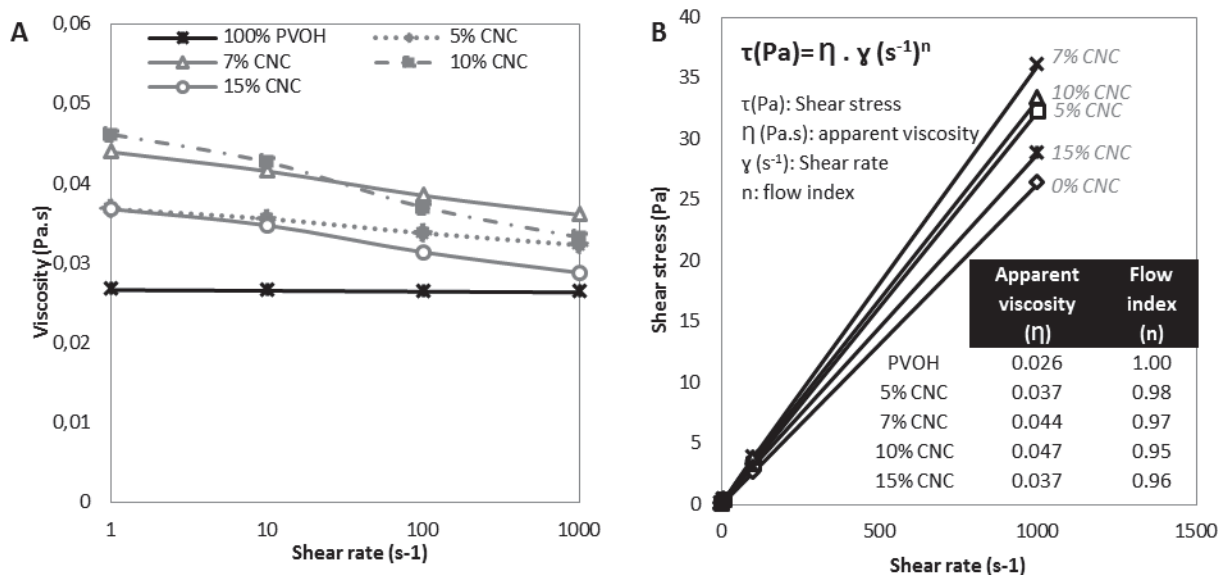


Figure SD1: A) Viscosity measurement for impregnation bath containing 0-5-7-10-15 wt% CNCs in PVOH matrix, and with a total solid content of 5 wt%, and B) Ostwald-de-Waele relationship

Furthermore, if PVOH solutions show Newtonian behavior (viscosity independent of shear rate), the addition of cellulose nanocrystals promote a slightly shear thinning behavior which increases with the increase in CNC content. Indeed, the viscosity decreases with the increase of shear

rate, and the flow index passes from $\eta=1.00$ (100% PVOH) to $\eta=0.95$ (10% CNC) (Figure SD1-B). This phenomenon has already been identified in previous literature results (Nechyporchuk et al. 2014) and does not disturb the impregnation process, as also demonstrated by pilot test and industrial tests results (See Chapter IV).

The choice of the impregnation protocol has to be carefully defined as it will strongly act on final paper properties. The challenge is to be as close as possible to the industrial process while transposing an on-line paper production to a lab-scale and discontinuous process. To be comparable to Banque de France impregnation procedure, the PVOH-CNC mixture is first heated at 60°C and kept at this temperature during all the impregnation process. The Velin paper is then soaked in this bath for a determined time. Figure SD2 shows the evolution of PVOH/CNC mass absorption on the Velin paper as a function of the impregnation time. It appears that the quantity of PVOH/CNC deposited on the paper increases during the first 20 seconds of impregnation and thereafter reaches a plateau around 6.5 g.m⁻². It can also be noticed that the quantities impregnated are slightly the same with and without the introduction of CNCs in the PVOH matrix. This can be explained by the viscosity value which remains the same. Pilot-scale impregnation of PVOH containing 0-5-10 or 20 w/w% CNCs on multilayer substrate also shows same mass absorptions: 4.4 ± 1.0 g.m⁻² were impregnated with 100%PVOH solution, 5.9 ± 1.4 g.m⁻² with 10% CNCs, and 4.4 ± 1.2 g.m⁻² with 20% CNCs.

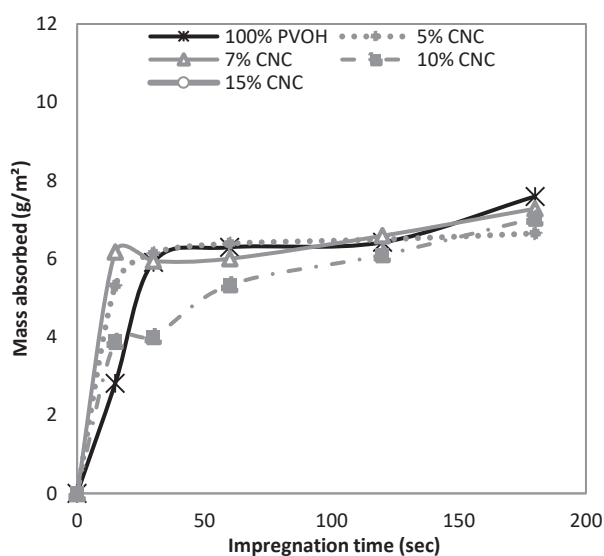


Figure SD2: Impregnation of banknote substrate (velin) with a PVOH matrix containing different amount of CNCs (wt%), and with a total solid content of 5 wt%

Overflow removal step. At lab-scale, the impregnated paper is pressed between a Teflon plate and a Teflon roll while at industrial scale the impregnated paper is pressed between two rolls. The drying is also difficult to reproduce. Classical drying for lab-scale has been performed in an oven at 115°C, with the paper maintained under tension on a metallic frame. This drying step has appeared to be a key parameter for the final paper properties, and especially for the dog-ears resistance. More details are given in **chapter II.2**.

2. Elastic angle recovery measurement

As the occurrence of dog-ears on banknote results from several and random handling, it is particularly difficult to define a relevant protocol reflecting the real life while being a reproducible and quantitative method. The paper elastic angle recovery has been measured as a principal criterion for determining the dog-ears resistance. This method has been implemented in the case of this study and different parameters were preliminary tested. First, the folded angle was performed with different weights corresponding to different pressures between 0.5 and 1.2 kPa (Table SD1). Indeed, dog-ears on banknotes can result from handling with different intensities. The influence of these pressures is detailed in the Results and Discussion part.

Table SD1: Different pressures applied for creating dog-ears

Pressure (kPa)	Force (N)	Weight (g)
0.3	0.981	100
0.6	1.962	200
1.0	5.886	600
1.2	9.810	1000

Furthermore, the angle recovery is a dynamic phenomenon and it can be also interesting to study not only the final recovery value but the speed of recovery. Evolution of these angles with time has been studied by taking pictures after 5, 10, 20, 30 and 120 seconds (Figure SD3). It can be seen that stabilization occurs faster for Velin paper and Velin impregnated with 100% PVOH while the angle recovery of Velin impregnated with 90wt% PVOH and 10wt% CNCs continues to increase. To simplify the results, only results at 120s are mentioned in this study. The speed of recovery can also be correlated with the force of recovery, whose results are presented in R&D part. Finally, different angles have been tested: 20°, 45° and 70° (Figure SD4). Similar results have been obtained whatever the angle, proving that the folding angle has no influence. This conclusion has also been reported in the literature by (Pradier et al. 2016) who proved that the folding behavior does not exhibit such a dependency on its orientation. In this study, only results at 45° are mentioned.

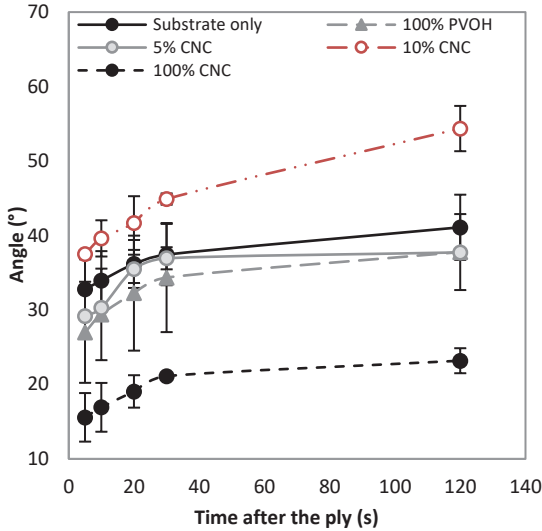


Figure SD3: Elastic recovery after folding with 1 kPa pressure, for different recovery time. Percentages of CNCs represent the ratio of CNCs in PVOH matrix.

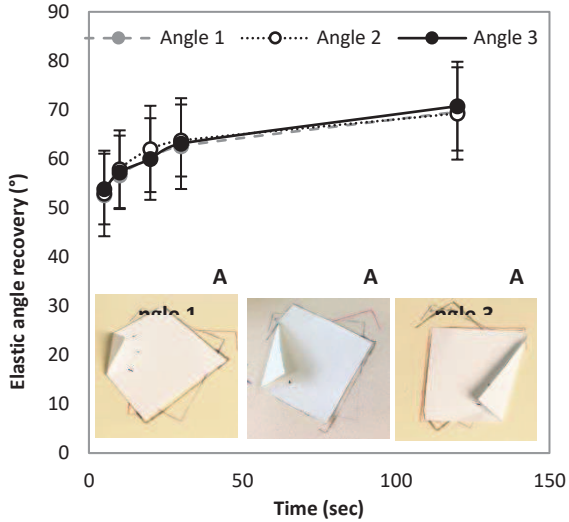


Figure SD4 Influence of the angle direction on resulting elastic angle recovery, paper impregnated with 100% PVOH and folding with 0.3 kPa.

Chapter III

Design of a multilayer material containing cellulose nanofibrils for crumpling limitation

Chapter

III

Table of content chapter III

1. A new quality index for benchmarking of different cellulose nanofibrils	189
1.1. Introduction.....	189
1.2. Materials and methods	192
1.2.1. Materials.....	192
1.2.2. Preparation of cellulose nanofibrils	192
1.2.3. Characterization	193
1.3. Results and discussions	195
1.3.1. Selection of analyses of CNF suspensions	195
1.3.2. Proposition of quality index	199
1.3.3. Influence of energy consumption on quality index.....	202
1.3.4. Influence of pulp source and preparation for CNF production	203
1.3.5. Comparative analysis of different commercial cellulose nanofibrils	206
1.3.6. Proposition of a simplified quality index, Q.I.*	208
1.4. Conclusion	209
2. Hybrid nanopaper of cellulose nanofibrils and PET microfibers with high tear and crumpling resistance	211
2.1. Introduction.....	211
2.2. Materials and methods	213
2.2.1. Materials.....	213
2.2.2. Methods	213
2.2.3. CNF characterization	214
2.3. Results and discussion.....	216
2.3.1. Nanocellulose characterization	216
2.3.2. Structural properties of nanopapers containing PET fibers	216
2.3.3. Mechanical properties of nanopaper containing PET	219
2.3.4. Crumpling resistance	224
2.4. Conclusions.....	227
3. Influence of pretreatment and degree of defibrillation on cellulose nanofibril cryogel properties and strategies to introduce a porous CNF layer inside a papermaking process	229
3.1. Introduction.....	229
3.2. Materials and methods	232

3.2.1.	Materials.....	232
3.2.2.	Methods	232
3.3.	Results and discussions	236
3.3.1.	Effect of mechanical treatment on cryogels and mechanical properties	236
3.3.2.	Effect of CNF pre-treatment on cryogel structural and mechanical properties	239
3.3.3.	Different strategies to prepare porous cellulose nanofibrils material for introduction in a paper 241	
3.3.3.1.	Classical cryogels crushed with cutting mills.....	241
3.3.3.2.	Cross-linking with polyamide amine epichlorohydrin resin	242
3.4.	Conclusions.....	245
4.	Introduction of cellulose nanofibril as a paper middle layer: three strategies for crumpling limitation and tear-resistant material	247
4.1.	Introduction.....	247
4.2.	Materials and methods	250
4.2.1.	Materials.....	250
4.2.2.	Methods	250
4.2.3.	Crumpling characterizations.....	253
4.3.	Results and discussion	256
4.3.1.	Material configuration and modeling of CNF layer inside the material.....	256
4.3.2.	Interest of a CNF layer for crumpling limitation (strategy 1)	257
4.3.3.	Mixture of CNF with additives for CNF-bonding reduction (strategy 2)	264
4.3.4.	Introduction of porous CNF beads in a paper middle layer for crumpling limitation in tear resistance (strategy 3).....	267
4.4.	Conclusions.....	269
	References.....	271
	Supplementary data	281

Chapter III: Design of a multilayer material containing cellulose nanofibrils for crumpling limitation

Introduction

Chapter II reported one of the strategies of the project, consisting in introducing CNCs in the PVOH impregnation bath in order to improve the banknote dog-ears resistance. Chapter III focuses now on the second strategy, relating to the limitation of banknote crumpling thanks to the introducing of a CNF layer inside the material (Figure 1-A). This chapter is divided into 4 parts (Figure 1-B). The first three studies are dedicated to fundamental research in order to be used in the 4th part which reports the applied results.

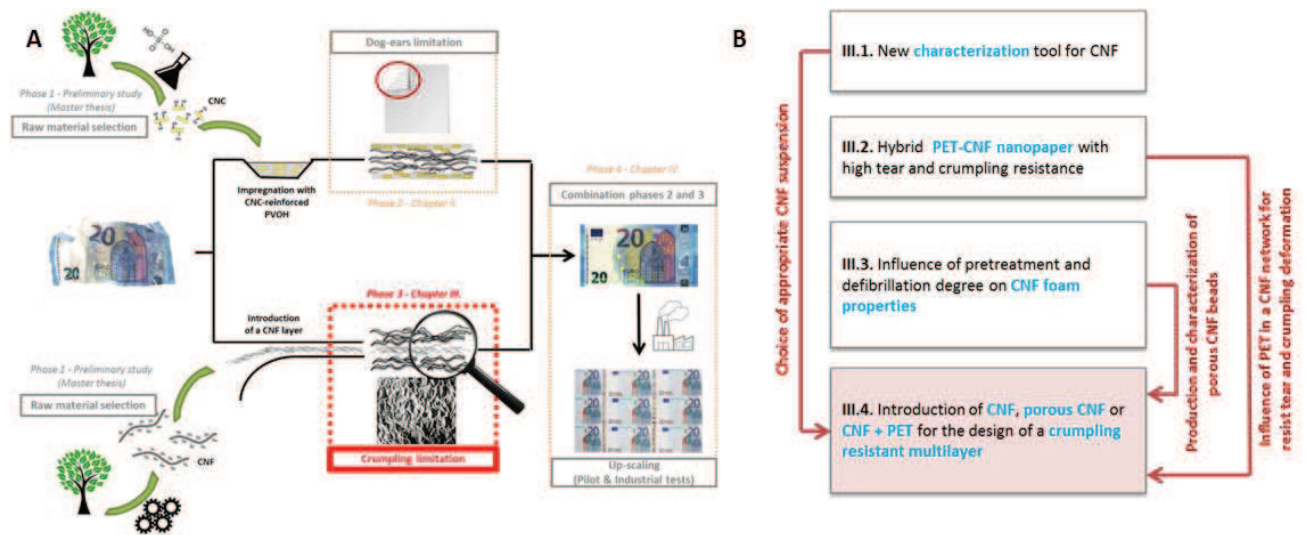


Figure 1: A) PhD overview of the different chapters and B) Details for chapter III

Chapter III.1. proposes a new characterization tool for CNFs: the quality index. In a preliminary study not reported in this manuscript (phase 1), it has been proved that CNF could successfully be produced at large scale from cotton or from eucalyptus with bio-chemical pretreatments and Masuko super-grinding. Consequently, if CNFs successfully improve the banknote crumpling resistance, ECB would have the choice between a commercial supply or an own production. However, due to the variety of bio-chemical pretreatments and high-shear mechanical treatments, it exists on the market a wide range of CNF suspensions with different morphological, physical and chemical properties. Furthermore, the variability of these properties leads inevitably to various results for the targeted application. In parallel, there is still a lack of characterization tool to differentiate the CNF suspensions. **Chapter III.1.** proposes a new method, based on a multi-scale analysis, for establishing a ranking of CNF suspensions and comparing the CNFs produced in our lab with the CNFs present on the market. This tool will also be used in Chapter III.4. to identify the suspensions which successfully contribute to improve the crumpling resistance. ***This work has been***

published in Carbohydrate Polymers and presented at TAPPI nano conference (Canada) in June 2017.

The multilayer paper thought for **Chapter III** is composed of two external layers of refined fibers and an intermediate thin CNF layer. CNFs are expected to form a cohesive entangled network inside the paper which helps to resist the crumpling deformation. However, the creation of a very dense layer could also act as a weak point for the tear propagation, which is known to suffer from highly bonded area. In order to take advantage of the CNF network for resisting the crumpling deformation while producing a material resistant to tear deformation, other strategies have raised. First, CNF has been mixed with small amounts of PET fibers in order to decrease the cohesion of the CNF network and benefit from the tear and crumpling resistance properties of these synthetic fibers. Secondly, no additives were added but the porosity of the CNF layer was increased thanks to the production of CNF foams or porous beads.

Chapter III.2. investigates the impact of PET fibers on CNF network tear, crumpling and mechanical properties. In this work, the CNF layer was taken out of the paper and modeled under the form of hybrid nanopapers containing CNF and PET. ***This work is submitted to Cellulose and was presented at TAPPI nano conference (USA) in June 2018. Please note that for confidentiality reasons, no paper application was mentioned in this work.***

Chapter III.3. proposes a fundamental understanding of CNF foams preparation and properties, as a function of the CNF pretreatment and mechanical treatment. Furthermore, this work also investigates the possible way for an up-scalable introduction of porous CNF inside a paper-making process. ***The first part was performed in collaboration with Université Bretagne Sud (Lorient, France), and was presented at ICC conference (Japan) in October 2017. Please note that for confidentiality reasons, this collaboration targeted the production of CNF foams for thermal insulation application.***

Finally, **Chapter III.4.** is a gathering of all the precedent studies for the production of a crumpling-resistant multilayer paper. In this part, CNFs are introduced (i) as a classical suspension (ii) mixed with PET or (iii) in a porous form between two layers of refined fibers, thanks to a dynamical hand-sheet former. A structural analysis of this multilayer will be performed and the impact of the CNF network on the crumpling and tear resistance properties will be reported. ***A patent relative with this part is in submission process.***

1. A new quality index for benchmarking of different cellulose nanofibrils

This section is adapted from the publication “J. Desmaisons, E. Boutonnet, M. Rueff, A. Dufresne, J. Bras (2017) – A new quality index for benchmarking of different cellulose nanofibrils, Carbohydrates Polymers 174:318-329”. This part was also presented in an oral presentation in TAPPI international conference (2017).

1.1. Introduction

In a context wherein modern society is demanding high-performance bio-based materials, cellulose nanofibrils (CNFs) are considered to be a promising solution, as confirmed by the exponential increase in the number of patents and publications on the topic. Indeed, in SciFinder, using descriptors like cellulose nanofibrils (CNF), microfibrillated cellulose (MFC), cellulose nanocrystals (CNCs) and nanowhiskers, 61 publications have been published in 2001 against more than 1000 in 2015. Indeed, at the nanoscale, these cellulose fibrils combine the advantages of cellulose renewability, biodegradability, and non-toxicity with a high surface area, high aspect ratio, and a large amount of hydroxyl groups. This leads to impressive mechanical properties, either individually or as a network (Dufresne, 2012); (Oksman et al., 2016), but also provides a wide variety of possible surface functionalization (Missoum et al. 2013). The results are encouraging in various areas of application such as nanocomposites (Mariano et al. 2014; Oksman et al., 2016; Siró & Plackett, 2010), biomedical (Jorfi & Foster, 2015; Lin & Dufresne, 2014), cosmetic and emulsions (Ullah, Santos, & Khan, 2016), paper reinforcement (Bardet et al. 2014; Brodin 2014; Osong et al. 2016), barrier packaging (Lavoine et al.2012), and batteries and electronic components (Hoeng, et al. 2016). Furthermore, it is anticipated that the world market of nanocellulose products will reach 250 million dollars by 2019 (Marketsandmarkets.com, 2015).

Beyond the technological requirements, feasibility and economic aspects are also important for developing such new materials. The production of CNFs is still a subject of optimization, as the high-energy consumption of the fibrillation process is still a barrier for large-scale industrialization. Since 2007, the application of pre-treatments has reduced the energy from about 30,000 kWh/t (Siró, et al. 2011; Spence et al.2011) to less than 2,000 kWh/t (Saito et al. 2007; Tejado et al. 2012) and has unlocked large-scale production. Currently, CNFs are classically extracted from the fiber by combining enzymatic (Henriksson et al. 2007) or chemical pre-treatments (Saito et al. 2007) and mechanical treatments (microfluidization (Zimmermann, Pöhler, & Geiger, 2004), super-grinding (Abe et al. 2007), or homogenization (Nakagaito & Yano, 2004)). Recent reviews detail many possibilities for CNF production (Abdul Khalil et al. 2014; Nechyporchuk et al. 2014) and, in practice, a large number of treatment combinations is possible. With the same starting fibers, tens of distinct CNF suspensions may be produced, inducing a large number of different characteristics. Siqueira et al. were among the first to demonstrate the large differences in quality with small differences in processing and asked for further classification to describe several CNF grades (Siqueira et al. 2010). Furthermore, the

obtained nanofibril suspension is in reality a multiscale and complex material containing fibers (millimeter scale), poorly fibrillated fibers (micrometer scale), nanofibrils (diameters less than 100 nm), and sometimes even soluble oligomers in water. Finally, all of these possibilities are magnified by the use of different vegetable sources and initial fiber properties (García et al. 2017; Jonoobi, et al. 2015). In parallel, the industrial interest and the number of patents are increasing: there are 220 patents reported on nanocellulose in 2015, against 11 in 2000 (SciFinder data, CNF, MFC, and CNC descriptors). Furthermore, new products using CNFs are gradually being proposed for the market.

Taking into consideration all of these parameters, the situation is the following: nanocellulose potentially sparks new industrial expectations for a wide range of applications. However, a large variety of grade qualities is possible and available. It would then be necessary to have clear distinctions between all of the proposed nanocellulose grades, thus helping to choose the most appropriate one. Nevertheless, a comparison of all nanofibril suspensions is difficult. The high heterogeneities have for a long time created debates even in nomenclature. Sometimes called “fibril aggregates” (Cheng et al. 2007), “cellulose microfibrils” (Dufresne et al. 1997), “microfibrillated cellulose” (Turbak et al.1983), or “cellulose nanofibrils” (Henriksson et al. 2008), a nanocellulose suspension is, in reality, all of these at the same time. The Technical Association of the Pulp and Paper Industry (TAPPI) has proposed standard terms to describe nanocellulose materials (TAPPI WI 3021) based on the size and aspect ratio. During the last decade, great progress has been made on characterization tools. A recent state-of-the-art study (Kangas et al., 2014) proposed tens of analytical methods based on the amount of nanomaterials, particle size distribution, rheology, morphology, crystallinity, mechanical properties, and surface chemistry. However, even if the combination of these methods can lead to an accurate representation of the suspension, such a list of analyses generally requires some expensive, complex, and time-consuming devices, but also needs expertise and does not allow for comparisons.

It consequently becomes essential to have more easily applicable and powerful comparison methods to control the quality of the different grades available. These methods should also permit the reproducibility of the manufacturing process for conformity and quality assessment. Most of the time, the comparison of CNF production in the literature only relies on a single criterion comparison such as nanofibril dimensions, neglecting the higher-scale part of the suspension. Recently, the determination of a “degree of fibrillation” (Oksman et al. 2009), “fibrillation degree” (Chinga-Carrasco et al. 2013), or “yield of fibrillation” (Benhamou et al. 2014; Besbes et al. 2011; Chaker et al. 2013) has been proposed to express the quality of a nanofibril suspension. Some studies have also focused on nanofibril suspension comparisons by multi-criteria approaches (Moser et al. 2015; Qing et al. 2013), but they still do not present a clear definition or normalization method. The fibrillation degree can be likened to the water retention value (WRV), as the WRV increases due to an increase in surface area (Carrillo et al. 2014; Hoeger et al. 2013; Nechyporchuk et al, 2014). More and more, the so-called “yield of fibrillation” is determined through nanoparticle isolation, thanks to centrifugation steps (Ahola et al. 2007; Benhamou et al. 2014; Besbes et al. 2011; Chaker et al. 2013; Moser et al. 2015; Naderi et al. 2015). The capacity of CNFs to transmit or scatter visible light can also

be related to the fibrillation degree (Nechyporchuk et al. 2014), both in suspensions (Besbes et al. 2011; Saito et al. 2006) or films (Qing et al. 2013). Dynamic light scattering, light transmittance analysis, ultraviolet-visible (UV-vis) spectrophotometry, or turbidity measurements are often used to compare CNF quality (Iwamoto et al. 2008; Moser et al. 2015). All of these studies have the advantage of proposing a multifactor analysis. However, the danger of using exclusively optical methods is the inescapable subjectivity, as only small areas containing nanofibrils are characterized, excluding poorly fibrillated “microfibers.” Such assessments on CNFs are performed at the laboratory scale on a specific suspension using a high-level microscopy tool that is difficult to implement in a production mill. A publication by Chinga-Carrasco (Chinga-Carrasco et al. 2013) focused particularly on the comparison of optical methods for determining the CNF defibrillation degree and, in this case, interesting methods have been proposed, such as using an image scanner that allows for the characterization of nanoparticles, as well as the residual fibers. Such a system appears to be promising for the evaluation of CNF quality in online processes. Finally, other studies have focused on mechanical fractionation (Tanaka et al. 2012), degree of polymerization, and viscosity (Syverud et al. 2011). Based on all these methods, it is possible to compare two or more nanofibril suspension levels and select the best. However, to date, all the proposed methods result in a qualitative ranking, and even if multi-tests are performed, no synthesizing method exists and the suspensions are ultimately compared test by test.

This publication proposes a multifactor CNF “Quality Index” (Q.I.) based on a quantitative ranking, as well as a simplified version easily adopted by any researcher or industry. The final objective is to obtain a unique value combining a panel of characterizations representative of the three scales of CNF materials. This quality index could ease the monitoring of nanocellulose production, both at the lab scale and industrial scale, in terms of CNF quality control. To promote its feasibility and widespread usage, only simple and standard equipments have been used. Furthermore, the potential to link the energy consumption to the CNF quality index could lead to treatment optimization and money savings. Another objective of this quality index is to allow for a benchmarking of CNF suspensions available on the market and to guide the CNF consumer toward the most appropriate suspension regarding the application. Finally, this method can also be used to optimize processing by varying production parameters and observing the ensuing CNF quality. As such, after the relevant tests of the method, the differences between CNFs from dried or never-dried pulp are exposed.

1.2. Materials and methods

1.2.1. Materials

Commercial cellulose nanofibrils. Commercial suspensions of nanofibrils were purchased or kindly supplied from the current market. The nanofibril suspensions came from different locales and were extracted from different plant sources with different mechanical disintegration processes such as homogenization, microfluidization, and super-grinding. For confidentiality reasons and material transfer agreements, some company names are not mentioned and the different suspensions will be labeled CNF-1, CNF-2, (...), CNF-13. More information is available in supplementary data.

1.2.2. Preparation of cellulose nanofibrils

Pulps. CNF were also produced at the laboratory scale from cotton pulp, eucalyptus pulp, and a mixture of maple and aspen pulp. Cotton pulp has been kindly supplied at a 3.4 wt% concentration by a company (confidential, France). Eucalyptus was purchased as dry kraft pulp from Brazil and the hemicellulose content was 15%. Then, a mixture of maple and aspen kraft pulp was kindly supplied by TEMBEC company in both never-dried conditions and dry sheets, with a hemicellulose content of 8% (commercial name: Biofloc 92).

Disintegration process. The pulps were first refined to obtain a fibrillation degree (in Shopper Riegler) between 60 and 70°SR using a beater (PFI, Metrotec, France). Then, an enzymatic pretreatment using a cellulose solution mainly composed of endoglucanase (FiberCare® Cellulase 4890 ECU/g enzyme solution) was performed with a concentration of 300 ECU/g of cellulose. 200 g of refined pulp were introduced at 2 wt% in a reactor pre-heated at 50°C with a 200 rpm rotation speed. A pH of 5 was set by introducing an acetate buffer composed of acetic acid and sodium trihydrate. Once the temperature (50°C) and pH (5) stabilized, an enzyme solution was poured into the reactor and left for a reaction time of 2 h. To stop the enzymatic activity, the reactor was heated to 80°C for 10 min, then cooled to 25°C. Finally, the suspension was recovered, filtered in a Buchner funnel using a nylon sieve with a hole diameter of 1 µm, and washed with deionized water in order to eliminate sugars created during the reaction. The cellulose pulp was finally diluted to 2 wt%. These pretreated fibers were then passed through an ultrafine friction grinder (Model MKZA6-2, Disk model MKG-C 80, Masuko Sangyo Co., Ltd, Japan) working at 2500 rpm, in recirculation for 2.5 h, to obtain the CNF suspension. Samples were recovered every 30 min to follow the evolution of the suspension properties.

Energy measurement. The energy consumption is linked to the duration of the super-grinding treatment. A three-phase wattmeter introduced on the Masuko device directly measured the total active power. The variations in power were carefully recorded during the 2.5 h duration of the treatment at the rate of one measurement per minute. By multiplying the power by the time interval, a specific energy in kWh/t was obtained. The time, “t = 0”, corresponds to the beginning of

the super-grinding treatment, after refining and enzymatic treatment. The measured energy does not include energy from the disintegration of the pulp (refining).

1.2.3. Characterization

Preparation of films. CNF films, also called “nanopapers,” were prepared with a sheet former (Rapid Kothen, ISO 5269-2) from 2 g of CNFs (dry content) diluted to 0.5% in deionized water. First, the suspension was filtered under vacuum at –600 mbar during a specific time until removal of water supernatant. After this time, the filtration is extended for five additional minutes. Then, the sheet was dried under vacuum at 85°C between (from interior to exterior) two nylon sieves (one on each side) to prevent adherence and two cardboards (one on each side) for 20 min. All films were stored for 48 h in a conditioned room at 23°C and 50% RH before characterization.

Macroscopic size (μm^2) and homogeneity (%). The microscopic part of the suspension was characterized using an optical microscope (Zeiss Axio Vert.A1, Germany). The CNF suspension was previously diluted to 0.1 wt%, stirred for 10 minutes with Ultra Turrax (IKA® T-25), and plunged for five minutes in an ultrasonic bath to foster dispersion. Pictures were taken at 10× magnification in a window of 2584x1936 pixels and analyzed with Fiji software. All the particles have to be correctly dispersed and do not present any entanglement or superposition. Images were transformed to 8-byte format and thresholded. Then, using the “analyze particles” mode, the average size of the visible particles was extracted (“macroscopic size”) corresponding to average surface of the particle. More precisely, the software counts the number of total particles and sums the surface of each element. The macro-size is obtained by divided the total surface by the number of particles. Six images by sample were considered. The homogeneity was calculated by comparing the number of visible particles smaller than 5 μm , those ranging from 5 to 10 μm , and those larger than 10 μm . The more the particle size is comprised in the same class of dimensions, the higher is the homogeneity (regardless the class). These two tests do not characterize the nanoscale regions of the suspensions, but rather the microscale regions. Indeed, a nanofibril suspension is in reality composed of nano-, micro-, and macro-dimensions, and it would be limiting to avoid the characterization of larger dimensions.

Nanosized fraction (%). This protocol is adapted from Naderi et al. (Naderi et al. 2015), and consists in the determination of the nanoscale particle quantity in the suspension by a gravimetric method. CNF suspensions were beforehand diluted to 0.02 wt% to be below networking concentration and were then centrifuged at 1000 g for 15 min to remove the largest components. The concentrations before and after centrifugation (in the supernatant part) were measured and the nano-sized fraction of the suspension was calculated using the following equation (1):

$$NF(w/w\%) = \frac{C_{ac}}{C_{bc}} \times 100 \quad (1)$$

Where C_{ac} and C_{bc} correspond to the mass concentration after and before centrifugation, respectively. $NF(\%)$ corresponds not only to both CNFs and nanofibril aggregates, but also to larger, coarser entities that have resistance to the phase separation through the centrifugal force.

Turbidity (NTU). The turbidity of the CNF suspensions was measured with a portable turbidimeter (Aqualytic, AL-250, wave-length 860 nm), on a CNF suspension that was beforehand diluted to 0.1 wt% and stirred for 10 min with Ultra Turrax (IKA® T-25). This test measures the scattered light at an angle of 90° to the incident light and is directly linked to the shape, size, and refractive index of the suspended matter. The unity NTU refers to Nephelometric Turbidity Units. If the suspension is only composed of nanoscale materials, the turbidity value is close to zero. However, the presence of poorly fibrillated fibers in the suspension results in an increase of the turbidity.

Mechanical properties. The tensile properties were measured with a vertical extensometer (Instron 5965), following the standard NF Q03-004. Basis weights have been measured using a surface of 65x50mm² and thickness were measured thanks to two equipments: SEM and Lhomargy micrometer. These values were then reported into the tensile device to obtain the Young's Modulus. The grips have been selected to limit slipping of samples. Tensile tests were performed at 10 mm/min. The dimensions of the samples were 10 cm for the length and 15 mm for the width. The Young's modulus value is directly linked to CNF interactions, surface area, and dimensions. For each sample, three measurements were carried out for samples from at least three different nanopapers; the minimal number of repetitions was 9 and the average value was used for further calculations.

Transmittance at 550 nm (%). The transmittance of the CNF films was measured for a wavelength of 550 nm using a UV-spectrophotometer (Shimadzu Manufacturing Inc., USA) in photometric mode. This test is directly linked to the CNF dimensions, surface area, and interactions, as nanoparticles with strong interactions (so CNF films with low density) are expected to reduce the number of air/solid interfaces and consequently reduce the change in the refractive index of the material, allowing for a higher light transmittance. For each sample, five measurements were performed for samples from at least three different nanopapers: the minimal number of repetitions was 15.

Tear resistance (mN). The tear resistance was measured using a tear tester (Noviprofiber, Elmendorf pendulum 4000mN, France). Samples were cut at (65 × 50) mm² dimensions, and the measurement corresponds to the force (mN) needed for tear propagation after a primer. Similar to the other tests performed on the films, this test is characteristic of CNF interactions and dimensions; the more homogeneous the fibers are at the nanoscale, the more cohesive the material will be, without an air/solid interface that can restrict the tear propagation. This will result in small tear resistance values. For each sample, three measurements were carried out for samples from at least 3 different nanopapers: the minimal number of repetitions was nine.

Porosity (%). The porosity was calculated from the film basis weight (g/m²) and its thickness (μm), using the following equation (2):

$$P(\%) = 1 - \frac{BW}{e \times \rho_c} \quad (2)$$

where BW is the basis weight (kg/m^2), e is the thickness (m), and ρ_c is the density of cellulose, taken as 1540 kg/m^3 . In this test, the more homogeneous the fibers are at the nanoscale, the more cohesive the material will be, and the lower the porosity. At least five replicates were performed.

1.3. Results and discussions

1.3.1. Selection of analyses of CNF suspensions

One of the main reasons for the cautious industrialization of CNFs over the last decade is the production cost. Since its first production in 1983 by Turbak et al. (Turbak et al. 1983), various pre-treatments (mechanical or chemical) and mechanical treatments have been studied in order to find those that are most energy efficient. The morphology, aspect ratio, and degree of crystallinity of CNFs are mainly determined by two factors: the cellulose source and, especially, the extraction method, which may bring about irreversible changes in the fibers. At least seven potential pre-treatments and nine mechanical treatments exist today (Nechyporchuk et al. 2014). This corresponds to a minimum of 63 possible combinations for the same plant source. To completely switch from research to industrialization, strong and reliable methods that allow for differentiation of all these suspensions have to be developed.

The characterization of nanoparticles often requires state-of-the-art technologies based on various scientific techniques such as optical, physical, mechanical, and rheological methods, with each analysis giving information on the suspension from a different perspective. Today, there is no unique device permitting one to identify the totality of nanofibril properties, which is also one of the reasons to explain why industrial production and its monitoring are still a challenge. Table 1 (adapted from Kangas et al., 2014) synthesizes the different characterization tools developed over the last decade to analyze different cellulosic nanomaterial aspects. Most of the time, these characterizations require expensive specialized equipment (e.g., atomic force microscopy (AFM) or dynamic light scattering) which are rarely present in industry. Moreover, the utilization of these tools is often linked to special training and expertise and can be time-consuming for sample preparation or data acquisition. All these factors are key issues for CNF production in industry where low cost, convenience, and quick results are expected. From Table 1, eight methods have been identified to answer to these criteria: The fractionation by gravitation, transmittance at 550 nm, turbidity, Brookfield viscosity, optical microscopy, mechanical properties of the nanopaper using tensile tests, tear resistance of the nanopaper, and porosity of the nanopaper calculated from the basis weight and thickness.

It was first decided to perform eight characterizations on CNFs in order to represent all the aspects of the CNF suspensions. Table 2 synthesizes the analysis in the case of CNFs produced from

eucalyptus fiber pre-refined at 70°SR and subjected to an enzymatic pre-treatment, followed by a super-grinding mechanical process. Half of the tests were performed directly on the suspension (“direct tests”) and the others were performed after the transformation of the suspension into a nanopaper (“indirect tests”). From optical microscope analyses, it is possible to extract information about the macroscale parts of the suspension. The first parameter gives the particle size heterogeneity of the suspension and the second one lists the average size of this macroscale part: the lower the value, the higher the mechanical disintegration of the fibers. The characterization of the nanoscale part is performed with two other direct tests: the turbidity and nanosized fraction. Indirect tests give further information about CNF interactions, surface area, and dimensions, and also give redundant information with the direct tests. For each test, the average value was converted into a grade. Finally, it was found that the CNF suspension could be represented with a unique quality index ($Q.I. = 75.0 \pm 5.7$), representative of the multifactorial analysis detailed below.

Table 1: Existing analysis tools for cellulose nanofibrils (The two first columns are adapted from Kangas et al.; 2014)

Property	Characterization method	Device cost /Availability in industry	Expertise requirement	Time-consuming
Amount of nanomaterials	▪ Mechanical fractionation by combination of sieves and membranes (Tanaka, 2012)	Classic equipments	High	High
	▪ Fractionation by centrifugation or gravimetry (Ahola et al.2008; Besbes et al. 2011; Moser et al. 2015; Naderi et al. 2015)	Classic equipment	Low	Medium
	▪ Field/tube fractionation (Haapala et al.2013)	Expensive	High	High
Average particle size/size distribution	▪ Light scattering measurement (Moser et al. 2015)	Expensive	High	Low
	▪ Transmittance at 550nm (UV-spectroscopy) (Chinga-Carrasco et al. 2013; Moser et al. 2015)	Classic equipment	Low	Low
	▪ Turbidity (Chinga-Carrasco et al. 2013)	Classic equipment	Low	Low
	▪ Microscopy (SEM, TEM, AFM)	Expensive	High	High
Rheology (viscosity, yield stress, gel point, aspect ratio)	▪ Rheometers (cone/plate or plate/plate geometry) (Pääkkö et al. 2007)	Classic equipment	High	High
	▪ Brookfield viscosity (Moser et al. 2015)	Classic equipment	Low	Low
	▪ Couette rheometer	Expensive	High	High
Visual aspect	▪ Optical Microscope (Oksman et al. 2009)	Classic equipment	Low	Low
	▪ Scanning electron microscope (SEM) (Chinga-Carrasco et al. 2013)	Expensive	High	High
	▪ Transmission electron microscope (TEM) (Qing et al. 2013)	Expensive	High	High
	▪ Atomic force microscopy (AFM)	Expensive	High	High
Crystallinity	▪ X-ray diffraction (XRD) (Iwamoto et al. 2008; Qing et al. 2013)	Expensive	Medium	Low
Water retention	▪ WRV (Carrillo et al. 2014; Hoeger et al. 2013)	Classic equipment	Low	Medium
Degree of polymerization	▪ Viscosity measurement in Cuem solution (Moser et al. 2015; Qing et al. 2013)	Medium	Medium	Low
Specific surface area	▪ X-ray scattering (SAXS) (Leppänen et al. 2010)	Expensive	High	High
	▪ N2 adsorption (BET) (Pääkkö et al. 2007)	Expensive	High	High
Surface charge and chemistry	▪ Conductimetric titration (Saito et al. 2007)	Classic equipment	Low	High
	▪ Polyelectrolyte (PE) titration (Junka et al. 2013)	Classic equipment	Medium	Low
	▪ Zeta potential (Eronen et al. 2012)	Expensive	High	Low
	▪ X-ray photoelectron spectroscopy (XPS)	Expensive	High	Low
	▪ Fourier Transform Infrared (Johansson et al. 2011)	Classic equipment	Medium	Low
	▪ Spectroscopy (FT-IR) (Saito et al. 2006)	Classic equipment	High	Low
Mechanical properties (on nanopapers)	▪ Strength properties on nanopapers, Instron (Qing et al. 2013)	Classic equipment	Low	Low
	▪ Visco-elastic properties of nanopapers (Dynamic mechanical analysis, DMA)	Expensive	High	Low
	▪ Tear resistance	Classic equipment	Low	Low
Network density (on nanopapers)	▪ Air permeability (Vase de Mariotte, Bendsen)	Classic equipment	Low	Medium
	▪ Porosity (calculation from basis weight and thickness) (Qing et al. 2013)	Classic equipments	Low	Low
	▪ Transparency (Haze meter) (Syverud et al. 2011)	Expensive	Low	Low

Table 2: Analysis of a cellulose nanofibril suspension (*CNF obtained after refining and enzymatic treatment of eucalyptus pulp, and super-grinding defibrillation)

Characterization	Direct/indirect	Information	Value for R-Euca-CNF*	Mark /10	Q.I. and Q.I.*
Average size of microparticles (μm^2)	Direct (On suspension)	Characterization of the macro-part	$5.9 \mu\text{m}^2 \pm 1.0$	8.1	Complete modeling Q.I. = 75.0 ± 5.7
Homogeneity(%)			$42.6 \% \pm 5.0$	7.7	
Nanosized fraction (%)		Quantity of particles at nanoscale	$67.5\% \pm 13.5$	6.7	
Turbidity (NTU)			Dimensions	$242.2 \text{ NTU} \pm 4.5$	8.6
Transmittance at 550nm (%)	Indirect (On nanopaper)	Interactions, surface area, dimensions	$4.21\% \pm 0.42$	5.1	
Tear resistance (mN)			$38 \text{ mN} \pm 8$	7.6	
Young's Modulus (GPa)			11.2 ± 0.6	9.8	
Porosity (%)			$33.4\% \pm 3.3$	6.1	

1.3.2. Proposition of quality index

The first important step for a quality index proposition is defining the quality requirements. CNFs can possess different dimensions, surface chemistries, and morphologies. They are composed of various structural components: nanofibrils (nanoscale), poorly fibrillated fibers (micrometer scale), and fibers (millimeter scale) resulting from incomplete defibrillation during mechanical shearing. The ideal suspension would be composed of only nanoscale components. This nanoscale part is responsible for the high specific surface area, and consequently, the high H-bonding potential resulting in a highly cohesive material with interesting mechanical properties and with various possibilities for surface functionalization. In other words, the major potential of CNFs depends on the nanoscale dimensions. It has been proposed in the literature that the degree of fibrillation can be defined as the disintegration of cellulose fibers into its natural nano-components (Chinga-Carrasco et al. 2013). In our publication, the notion of quality will be defined as qualifying a homogeneous suspension in terms of both dispersion and size distribution, with nanometric dimensions. The direct consequences are the formation of a viscous gel due to entanglements and the formation of a highly bonded network, possibly transformed into a transparent nanopaper (due to a low porosity), with a high Young's modulus, but a low tear resistance (due to the ease with which the tear may propagate in cohesive media).

The second step is the determination of the scope of application. The purpose of this present method is to be applicable and reproducible in each laboratory and industrial setting, regardless the production quantity or high-level equipment available. There is consequently a compromise to find between the use of accurate but expensive and time-consuming devices and the use of common devices that are more easily accessible. In this study, the use of eight criteria overcomes the lack of advanced technology. Another part of this study will demonstrate the possibility of reducing these criteria to only four parameters. Furthermore, the most powerful equipments for characterizing nano-elements (like AFM or transmission electron microscopy (TEM)) give direct information about nanofibril morphology and properties, but they focus only on nanoscale regions and consequently miss information.

A unique quality index will be derived from the eight criteria that were selected to give a representative image of the CNF suspension. The final idea is to have an equation that automatically determines the quality index by just entering the test results (Figure 1).

First of all, cellulose nanofibrils have been produced with a super grinder and samples were taken every 20 minutes during three hours. This first step has been repeated for different vegetable source and allows us to detect the general trend of each property. Then, for each test, a database was established by gathering results from the literature, tests on commercial CNF suspensions, and tests on laboratory-produced CNF suspensions. This database has a minimum of 20 values corresponding to a large range of suspension qualities, ranging from the starting pulp to cellulose filaments and poorly defibrillated cellulose using laboratory equipment without pretreatments to

highly defibrillated cellulose with strong pretreatment and mechanical shearing, and commercial suspensions. By combining the trends obtained and the values in the database, correspondence tables were then established for each test (Figure 2), associating a value with a mark out of 10 based on the database and our last 20 years of expertise. For example, the associated mark for a turbidity of 300 NTU is 8/10. Then, the mark relative to the interval of value has been plotted. By fitting the trend curves to these plots, each characterization test has been associated with a single equation allowing for the conversion of the raw data into a mark.

The quality index is defined as the weighted sum of the marks (3) to linearly convert each isolated equation into a single equation containing eight coefficients (4). The weighting coefficients have been chosen so that the total weight is ten. Different combinations and values of coefficients (1, 2 and 3) have been tested to find the most discriminant quality index. Finally, the two highest coefficients have been assigned to the parameters that create the highest disparity in final quality index.

$$Q.I. = 2 * \text{Nanosized fraction mark} + 2 * \text{Turbidity mark} + 1 * \text{Young's Modulus mark} + 1 * \text{Porosity mark} + 1 * \text{Transmittance mark} + 1 * \text{Tear resistance mark} + 1 * \text{Macro size mark} + 1 * \text{Homogeneity mark} \quad (3)$$

$$Q.I. = 0.20x_1 + (-0.02x_2) - 0.035x_3^2 + 1.27x_3 - 0.16x_4 + 1.65\ln(x_5) - 3.59\ln(x_6) - 2.67\ln(x_7) + 0.18x_8 + 69.6 \quad (4)$$

with x_1 representing the nanosized fraction (%), x_2 the turbidity (NTU), x_3 the Young's modulus (GPa), x_4 the porosity (%), x_5 the transmittance at 550 nm (%), x_6 the tear resistance (mN), x_7 the macro-size (μm^2), and x_8 the macroscopic homogeneity (%).

This quality index has been validated for several CNF grades and is a new tool to monitor their production. The following examples use the quality index, first to provide a validation of the method and, second, to confirm its potential applications.

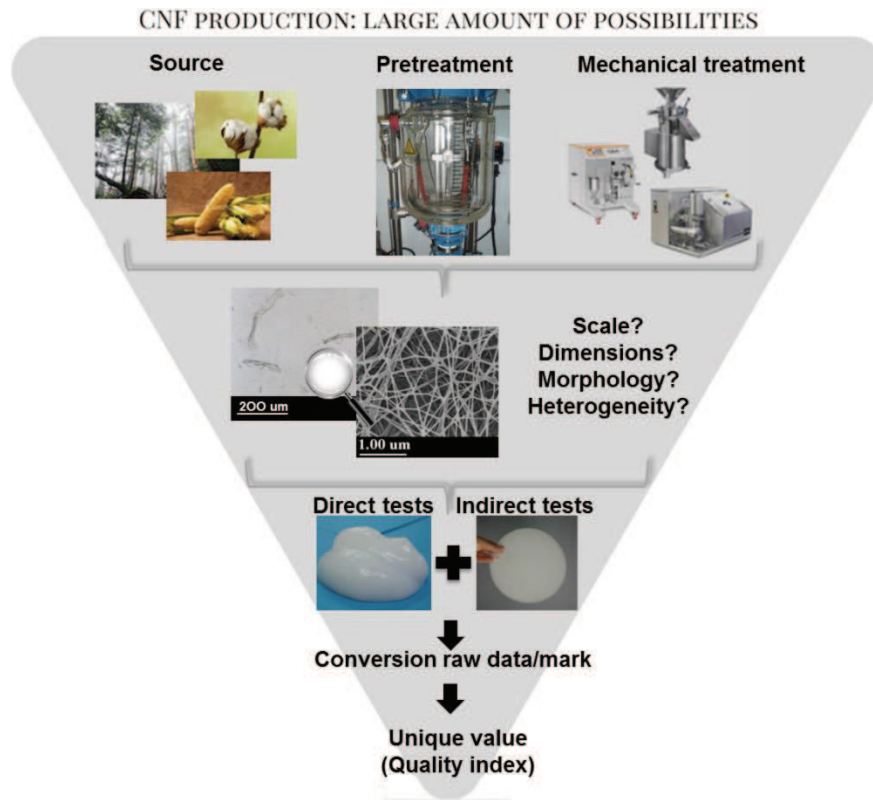


Figure 1: Quality index determination: general scheme

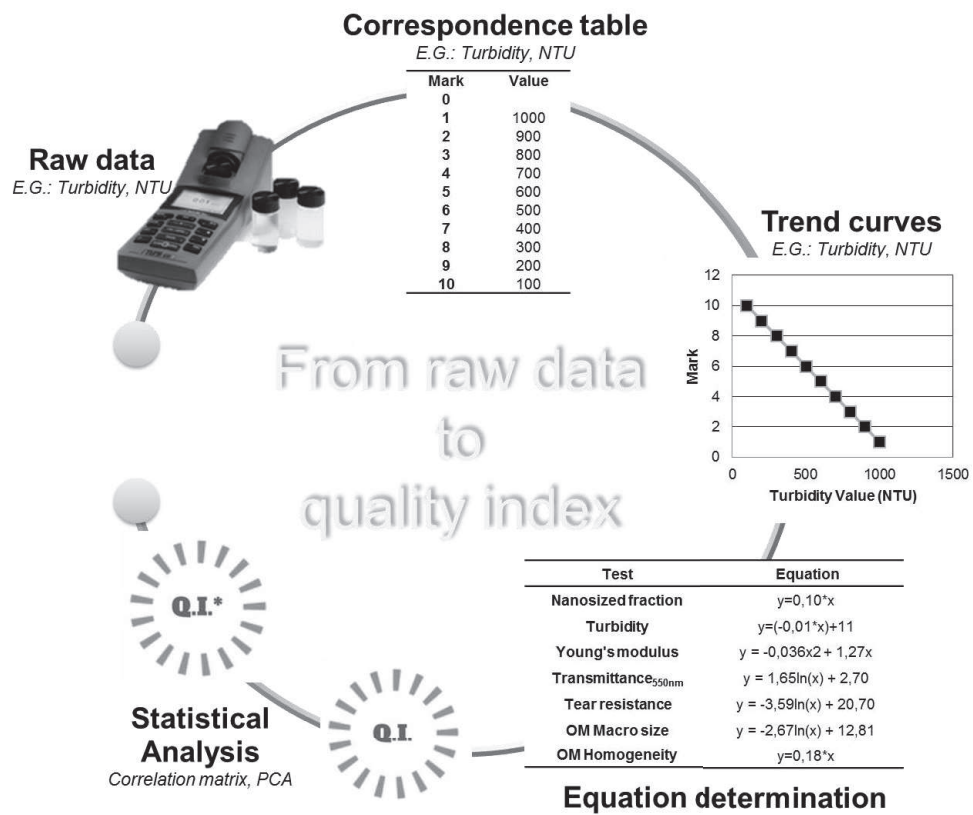


Figure 2: Conversion of experimental values into quality index

1.3.3. Influence of energy consumption on quality index

In order to make CNFs commercially competitive, low-cost sources as well as energy-efficient processes are required. Since 2008, it is well known that using pretreatments reduces the energy demand of mechanical processes from 20,000–30,000 kWh/t to 1,000 kWh/t. If energy efficiency is a key parameter in CNF production, its control and optimization is rarely industrially investigated due to a lack of characterization. The present study proposes to use this quality index to link defibrillation quality with energy consumption. The data collected provide comparative values, as energy depends on the power and dimensions of the equipment used (in our case, a Supermasscolloider). Consequently, the energy values in kWh/t here are higher than what can be expected industrially.

Two nanofibril suspensions have been produced starting from two pulps with different hemicellulose contents: an eucalyptus kraft pulp and a kraft pulp from aspen and maple. Figure 3 shows the evolution of the quality index as a function of the energy consumption, corresponding to different treatment durations in the Masuko super-grinder. The time “t = 0” corresponds to the beginning of the super-grinding treatment, after the refining and enzymatic treatments. The influence of the hemicellulose content will be commented on in greater detail in the next section, but it is worth noting here that the two curves have different values but the same trend. Figure 3 shows a strong evolution of the quality index from 0 to 5,000 kWh/t followed by stabilization. This means that the beginning of the mechanical treatment is determinant for defibrillating the large fibers, until an optimum point from which superior defibrillation becomes difficult and highly energy consuming. For eucalyptus CNFs, the quality index passes from 68.3 (\pm 4.5) to 75 (\pm 5.7), for an increase of 5,267 kWh/t. In other words, 42% of the total energy is consumed for an increase of 9% in the quality index. Considering a rate of 0.15 €/kWh, almost 800 €/t could be economized. A similar trend is observed with the lower hemicellulose content source: by stopping the treatment after a consumption of 4,000 kWh/t instead of running until 12,000 kWh/t, 63% of the total energy consumption could be saved for a difference of 10% in the quality index. Still, considering a rate of 0.15 €/kWh, 1,100 € could be saved. Considering these values, a producer can strike a balance between energy efficiency and the necessary CNF quality. These two examples also confirm the possible utilization of the quality index to monitor energy consumption.

The same study can be performed with industrial equipments: A similar curve would be obtained and each producer can estimate the minimal energy consumption to reach quality index stabilization. Some projects with company partners are in progress (confidential). The purpose is to favor the control of industrial quality while helping to decrease the production cost. Indeed, it is worth wondering if a small quality increase justifies a large economic loss. The final answer belongs to the intended application: the just compromise between quality and price has to be determined.

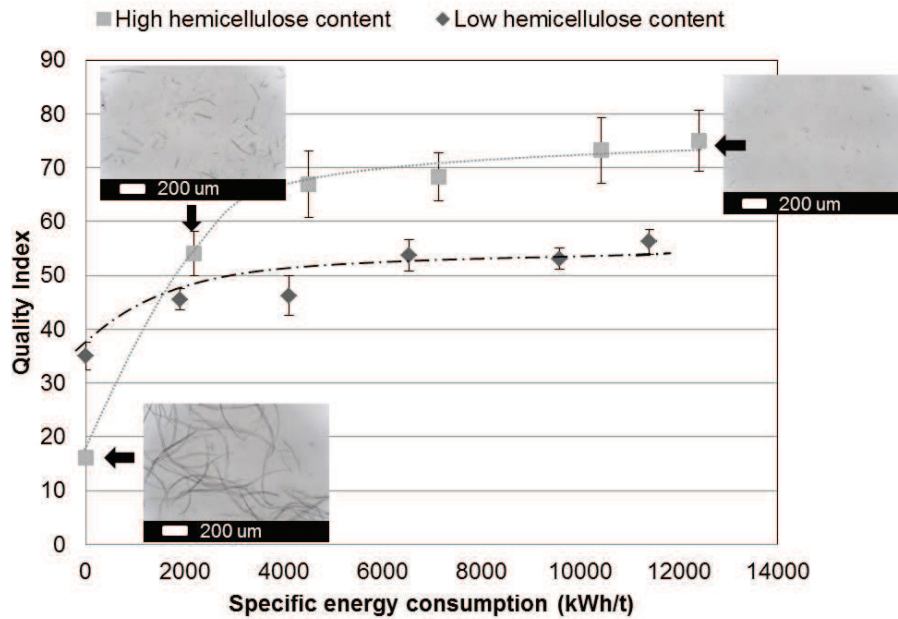


Figure 3: Link between quality index and energy consumption during super-grinding process, for CNF with high hemicellulose content (from eucalyptus and CNF) and medium hemicellulose content (commercial pulp). The pulp is beforehand refined and pretreated with enzymes

1.3.4. Influence of pulp source and preparation for CNF production

From a single plant source, a wide range of CNF suspensions can be produced by varying the pretreatments (chemical and/or mechanical), mechanical shearing, and post-treatments (chemical and/or mechanical). Traditionally, CNF suspensions are produced from bleached pulp being presented in the form of either dry sheets or suspension. It has been shown in the literature that this drying step of the pulp induces irreversible changes and will influence the defibrillation process as well as all the treatments applied beforehand on the pulp, such as pre-refining (Balea et al. 2017). Finally, beyond the pulp treatment, the hemicellulose content will significantly change the disintegration ability and nanoparticle quality (Iwamoto et al. 2008). This section illustrates all these phenomena for the production of CNFs through quality index characterization.

It is already known from the literature that the drying of pulp induces changes in the fiber morphology and deteriorates the fiber and final paper properties (Weise et al. 1996). These deteriorations are mainly due to irreversible structural changes in the fibers (Oksanen et al. 1997) occurring during the hornification phenomenon: when the fibers are dried, the removal of water brings adjacent microfibrils into close contact and hydrogen bonds are formed between them (García et al. 2002). This results in the loss of fiber conformability and swelling capacity, which hinders the bonding potential of the fibers and reduces the strength properties. A publication by Iwamoto et al. (Iwamoto et al. 2008) has investigated the impact of once-dried and never-dried pulps with different amounts of hemicellulose in defibrillation using a similar grinding treatment. In this publication, the

degree of fibrillation was evaluated by scanning electron microscopy (SEM) observations of the fibrillated pulps and light transmittance measurements of the fibrillated pulp/acrylic resin composites. This publication has highlighted experimentally the better facility for never-dried pulp to defibrillate after a grinding treatment based on the final CNF dimensions obtained. The idea is to check if the same trend is observed with the quality index to confirm the consistency of the method and to provide further proof of the pulp-drying influence on defibrillation with a multi-criteria and quantitative approach.

Figure 4 confirms that CNFs obtained from never-dried pulp possess a better quality index than those produced from dried pulp. The quality index obtained with never-dried pulp at 4,000 kWh/t is reached at 12,000 kWh/t when using dried pulp: the energy consumption is therefore multiplied by three. Considering a rate of 0.15 €/kWh, the economic loss is 1,202 kWh/t. Furthermore, the quality index obtained with never-dried pulp is never achieved with dried pulp.

The same comparisons were performed with CNF suspensions produced from different pulps with different hemicellulose contents, and with or without pre-refining. Three different sources have been used: cotton, a commercial mixture of aspen and maple, and a commercial product from eucalyptus. First, it can be noticed that pulp with a higher hemicellulose content (eucalyptus) seems to better defibrillate than both medium hemicellulose content and low hemicellulose content (cotton), as a higher quality index is obtained. CNFs obtained from refined cotton have a quality index of 47.4 ± 3.4 compared to 75 ± 5.7 for CNFs obtained from refined eucalyptus. Eucalyptus is composed of shorter fibers than cotton and has a higher hemicellulose content which facilitates disintegration and can reduce energy input (Tonoli et al. 2012). Indeed, a clear correlation was found between the hemicellulose content and the ease of cell wall delamination. Hemicellulose plays an important role in regulating nanofibril aggregation through hydrogen bonding. Assuming that hemicellulose is tightly attached to the cellulose microfibrils via multiple hydrogen bonds, thereby physically filling the gap between the cellulose microfibrils, the hemicellulose will act as a physical barrier, inhibiting the likelihood of microfibril aggregation (Chaker et al. 2013). The presence of carboxylic groups in hemicellulose is another parameter likely to facilitate the delamination of the fibers through electrostatic repulsion forces. However, we should be careful with this conclusion. Indeed, it is worth noting that a direct comparison is only possible if the same source and starting fiber shapes are used in all experiments with different amount of same hemicelluloses. Such experiments are very long to be designed and need physico-chemical expertise and processes.

Finally, the influence of refining before fiber defibrillation is also highlighted. Refining is well known in the paper industry to induce hydration, fibrillation, and fiber cutting. Refining thus affects the fiber structure and improves the bonding. It also increases the surface charges (Gharehkhani et al. 2015). All these parameters lead to an easier defibrillation and decrease the subsequent energy necessary during mechanical disintegration. It is shown in Figure 4 that, with this pretreatment, the quality index for CNFs obtained with enzymatic and super-grinding treatments passes from 62.2 ± 6 to 75 ± 5.7 , corresponding to an evolution of 17%.

These last results confirm the importance of the pulp treatment before defibrillation; starting pre-treatment and mechanical shearing on never-dried pulp allows for a better final quality index with lower energy consumption. Furthermore, this quality index method also underlines the importance of the starting raw material; it is demonstrated that it is easier to obtain better CNF quality with eucalyptus pulp. Moreover, this quality index has to be linked with economic considerations to obtain a whole comparison in the selection of raw materials. For example, in addition to possessing a better quality index, eucalyptus is a fast-growing species with good fiber quality and relatively cheap market price, which leads to a better candidate than cotton for CNF production.

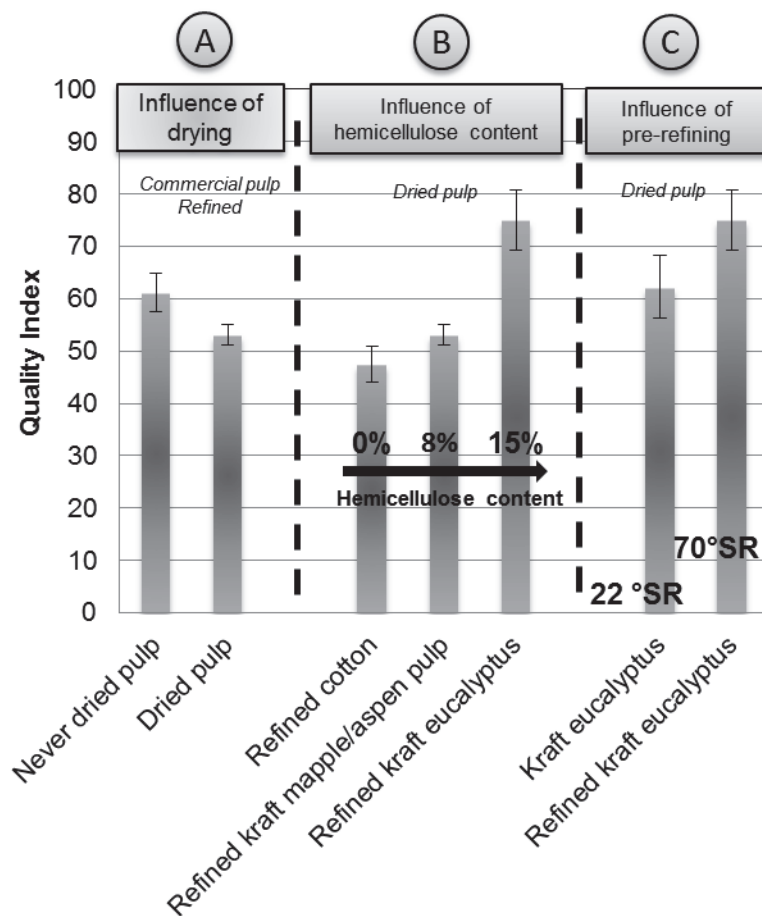


Figure 4: Influence of pulp drying (Dried or Never Dried), pulp refining and hemicellulose content on Quality Index

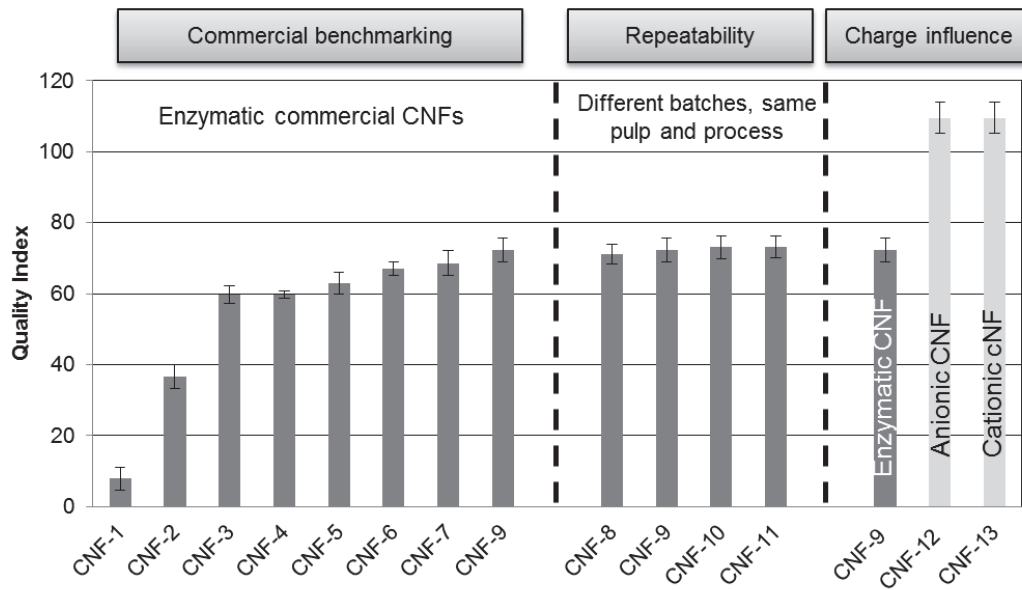


Figure 5: Comparative analysis of A) Commercial CNF B) CNF produced from different pulps with enzymatic and super-grinding treatment

1.3.5. Comparative analysis of different commercial cellulose nanofibrils

Thanks to the very recent upscaling of nanocellulose manufacturing and the increasing amount of commercial grades available, the application of nanocellulose in the end-user industries is currently undergoing a revolutionary change driven by increasing petroleum prices and the high-energy intensity in the production of chemicals and synthetic polymers (Nanocellulose Market, 2016). Furthermore, the continuous discovery of the large potential of these nanomaterials contributes to extending the range and fields of application. To be situated in this international market, market studies propose values and volumes of nanocellulose production regarding field of application, type of nanocellulose (cellulose nanocrystals, CNFs, nanocomposites), and localization. However, these studies do not take into consideration the final CNF properties and quality, as no universal method exists for establishing such a benchmark.

Based on the quality index method, one of the first benchmarkings between different commercial sources has been implemented (Figure 5). All these suspensions are sold on the market as CNFs and come from different locales and plant sources. Four suspensions are particularly remarkable for their extreme values: CNF-1, CNF-2, CNF-12, and CNF-13. Additionally, other similarities can be noticed: CNF-3 through CNF-5 share similar quality index values, as well as CNF-6 through CNF-9. A further analysis would be to target a quality index value as a function of the field of application, as CNFs for the paper industry do not have to share the same performance as is necessary for biomedical applications.

CNF-8 through CNF-11 correspond to different CNF batches, but were produced under the same conditions by the same supplier. One of the possible applications of the quality index is also to allow a producer to check the reproducibility of its production. In this example, almost the same quality

index has been calculated for the four batches. This is a way to prove the efficiency of the process for this industry, and at the same time, it is a way to prove the relevancy of the quality index, as values obtained are coherent.

Until now in this study, all the suspensions considered were initially pre-treated with enzymes. However, three pretreatments are usually considered: enzymatic treatment (Henriksson et al. 2007), anionic treatment with the famous TEMPO-mediated oxidation (Saito et al., 2006), and cationic treatment (Hasani et al. 2008). Today, chemically grafted CNFs are also available on the market. These functionalized nanocellulose products have the particularity to be platforms for large possibilities of surface modification through various chemistries (Habibi et al. 2014) and represent a growing interest for highly sophisticated applications such as biomedical or antibacterial applications. Such chemical pretreatments also have the advantage of easing the defibrillation process by creating repulsion between the fibers, consequently weakening the structure. This leads to a decrease in energy consumption for the production of a higher CNF quality. It is consequently not surprising that the quality index obtained with an anionic treatment reaches a quality index of 110 ± 4.3 , while the better commercial enzymatic CNFs tested were just 73.1 ± 3.1 . It should be noted, however, that the quality index method has been initially developed considering only enzymatic suspensions. The introduction of surface charges can impart different behaviors for some tests performed on CNF suspension, such as the turbidity measurement and the nanosized fraction. An optimized quality index relevant for functionalized CNFs should be developed. A similar comment is possible for hybrid CNFs with mineral filler available on the market (e.g. Fiberlean[®], Imerys). Such CNFs cannot be analyzed with a quality index. The method is, for now, restricted to suspensions without additives, as any filler which would influence the tests, such as turbidity or light transmittance, would distort the results.

To conclude, this comparative analysis tends to allow the consumer to choose the appropriate CNF suspension regarding his or her necessity of quality and considering the cost requirements. It also allows industries and researchers to compare their production to the market. Quality index scores can also serve as a reference or target for a producer. A higher discrimination of the commercial sources would further help the benchmarking, as several sources present a similar range of quality index values. Moreover, it is worth noting that we have chosen to present in this paper the most general method possible. As specific applications need sometimes specific selective properties, optimized and adapted quality index can be developed as a function of the field of application. These points take part of improvement tracks. Eight measurements might also take too long, and that is why a simplified Q.I. (Q.I.*) is proposed in the following section.

1.3.6. Proposition of a simplified quality index, Q.I.*

The final purpose of the quality index method is to propose an easy and fast method to characterize the dispersion and size homogeneity, at nanoscale dimensions, of a CNF suspension. A multi-criteria approach based on eight tests has been considered in order to overlook as little as possible regarding the suspension properties, but neglecting rapidity concerns. Furthermore, characterization with eight tests can bring redundancy and two different tests can lead to similar interpretations. To allow for a faster determination of a quality index and to limit the number of required criteria, a simplified version has been proposed through the use of statistical analysis by limiting the number of required parameters.

A correlation matrix of the eight parameters selected for the quality index has been established (correlation matrix is presented in absolute values in supplementary data). This matrix studies the intensity of links existing between the variables and consequently brings out the correlation between two different parameters. The closer the correlation coefficient is to one, the more the criteria are correlated. Beyond 0.6, the parameters are considered dependent, and this dependence is even stronger beyond 0.7.

Transparency marks show a strong correlation with four other parameters (turbidity, tear resistance, Young's modulus, and porosity). It is similar for tear resistance marks which are correlated with porosity, Young's modulus, macroscopic size, and homogeneity. Then, porosity and Young's modulus both present three correlations. To limit the number of required parameters for quality index determination, parameters presenting a high redundancy with the others could be removed from the equation.

To complete this study, a principal component analysis (PCA) has been performed. This method is used to convert a set of observations of possibly correlated variables into a set of values of linearly uncorrelated variables called principal components (Jain & Shandliya, 2013). The number of principal components is less than or equal to the number of original variables. This method allows for the reduction in the number of variables and makes the information less redundant. By combining matrix correlation results with PCA results, four parameters among the eight have been selected: nanosized fraction, turbidity, Young's modulus, and macro-size. An equation for a simplified Quality Index (Q.I.*) has been thus defined (6). In this case again, the weighting coefficients have been chosen so that the total weight is ten. The two highest coefficients have been assigned to the parameters that create the highest disparity in final quality index in order to be discriminant (5).

$$Q.I.* = 3*Nanosized\ fraction\ mark + 3*Turbidity\ mark + 2*Young's\ Modulus\ mark + 2*Macro\ size\ mark \quad (5)$$

$$Q.I.* = 0.30x_1 + (-0.03x_2) - 0.071x_3^2 + 2.54x_3 - 5.35\ln(x_7) + 59.9 \quad (6)$$

with x_1 representing the nanosize fraction (%), x_2 the turbidity (NTU), x_3 the Young's modulus (GPa), and x_7 the macro-size (μm^2).

Figure 6 represents the comparison between the classical quality index and simplified quality index for commercial-source benchmarking (A) and for energy consumption study of CNFs produced from refined eucalyptus after an enzymatic treatment (B). This graph confirms the relevance of the correlation matrix and PCA study: the choice of these four parameters for the simplified quality index gives similar trends than the classic quality index with eight parameters and similar values. It is now up to the final user to decide between the complete and more precise Quality Index (Q.I.) or the faster, simplified Quality Index (Q.I.*).

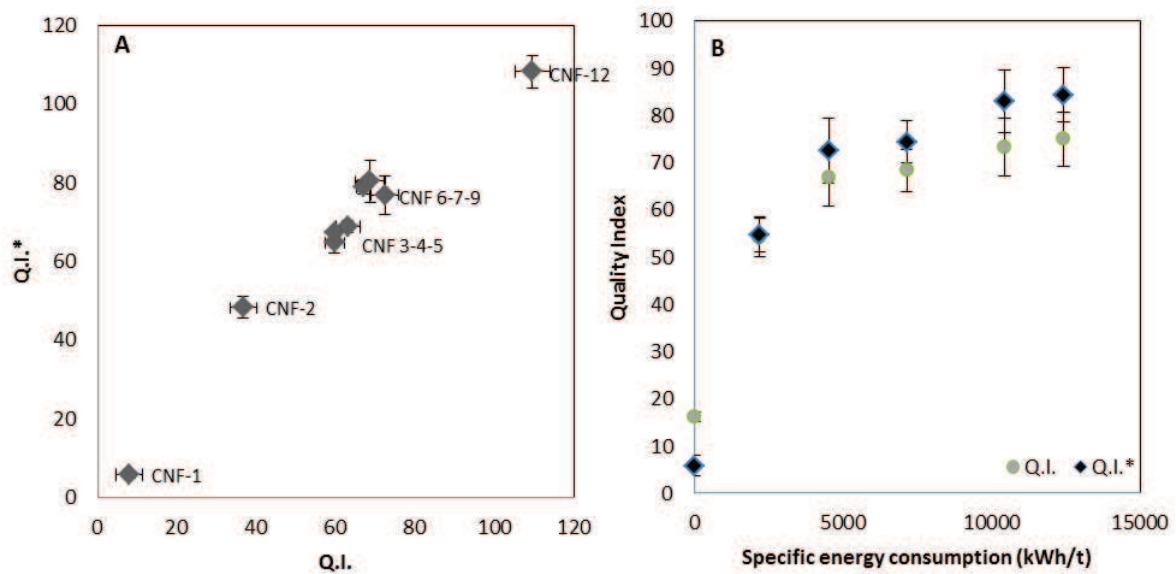


Figure 6: Comparison of classical vs simplified Quality Index A) for commercial sources B) for CNF produced from eucalyptus pulp refined, pretreated with enzyme and submitted to different super-grinding treatment.

1.4. Conclusion

This study proposed a multi-criteria method to characterize CNF suspensions and establish a quality ranking. Two equations were proposed, one based on eight tests (Q.I.) and a simplified version based on only four tests (Q.I.*). In each case, the user only has to enter the raw values of the test to obtain a final and single grade called the “quality index.” This quality index has been used in several examples to evaluate the loss in energy consumption via mechanical treatment, to make comparisons between commercial and laboratory sources of CNFs, and to highlight the influence of pulp pre-refining, hemicellulose content, and drying on the defibrillation process. These analyses prove the interest and robustness of this first quality index proposed for CNFs.

Some challenges still exist and open the door to optimization of the method. Increasing the discrimination in the quality index values would allow for a more accurate ranking, for example, in the comparison of commercial sources.

It has been chosen in this paper to stay general and compare all the suspensions with the same criteria. However, a specific quality index might be designed if wet-end paper addition, cosmetic emulsion, or transparent printed electronic applications are targeted, as each application has its own selective properties. Optimization and adaptation of the quality index to specific industrial concerns are currently in progress in different projects. However, the simplified quality index as presented can already be the first universal index for characterizing CNFs in industry.

2. Hybrid nanopaper of cellulose nanofibrils and PET microfibers with high tear and crumpling resistance

This section is submitted in Cellulose journal “J. Desmaysons, E. Gustafsson, A. Dufresne, J. bras (2018) – submitted”. This work was also presented in an oral presentation in TAPPI international conference 2018.

2.1. Introduction

Due to its abundancy, renewability and interesting mechanical properties, cellulose is an attractive polymer offering potential solutions to the global demand of environmental friendly materials as alternatives to petroleum-based materials. The hierarchical structure of natural cellulose fibers used in traditional products such as paper and board or textile, can be deconstructed using a top-down strategy in order to obtain nanometer scale materials with amplified properties (Dufresne 2017). After pretreatment of native cellulose, using enzymes (Pääkkö et al. 2007; Henriksson et al. 2007) or by chemical surface functionalization (Saito et al. 2006; Odabas et al. 2016) in order to weaken the structure, a high-shearing mechanical treatment is applied to transform the cellulose fiber suspension into a heterogeneous suspension composed of defibrillated fibers from micro to nanoscale, called microfibrillated cellulose (MFC) or more recently cellulose nanofibrils (CNF) (Kim et al. 2015; Nechyporchuk et al. 2016). Known since the early 1980's, such pretreatments and new mechanical fibrillation have allowed multiple developments over the past 10 years and positioned CNF as one of the most promising sustainable building blocks for mechanical and functional high performance materials as shown by recent and numerous reviews (Mariano et al. 2014; Hoeng et al. 2016; Lavoine and Bergström 2017; De France et al. 2017; Benítez and Walther 2017). In this regard, in addition to its use in suspensions or emulsions, several CNF materials have emerged with a large potential of applications, e.g for use as reinforcement within a polymer matrix (nanocomposite), but also as a matrix with organic or inorganic fillers (hybrid nanopaper), or as such (pure nanopaper).

Due to their high aspect ratio and flexibility, CNFs can entangle and form films by solvent casting, or nanopapers by vacuum filtration using a procedure similar to classical wood fiber paper making (Henriksson et al. 2008). Pure nanopapers (composed only of CNF) are widely known for their mechanical properties, optical transparency, low thermal expansion and oxygen barrier characteristics (Henriksson et al. 2008; Nogi Masaya et al. 2009; Sehaqui et al. 2011; Lavoine et al. 2012; Benítez and Walther 2017). Consequently, nanopapers have been considered as promising green and efficient material for use in electronic devices (Zhu et al. 2014; Hoeng et al. 2016; Zhou et al. 2016), batteries (Sheng et al. 2017), barrier films for food packaging (Yu et al. 2014) or filtration membranes for water purification (Mautner et al. 2015; Voisin et al. 2017). Today, barrier and mechanical properties of such nanopapers as a function of structural and environmental parameters (degree of polymerization, fibril length, porosity, counter-ions, orientation, humidity) are well known (Benítez and Walther 2017). Young's modulus (13.2 GPa), tensile strength (214 MPa), and strain to failure (10%) are classical values reported for high quality CNFs (Sehaqui et al. 2011). However, due

to the large hydrogen bonding and high surface area (50-150 m²/g), these nanopapers are strongly cohesive with low range of porosities (between 13% and 25%), resulting in very low tear-resistance and cracking under deformation such as crumpling. Such drawbacks limit their use in some applications when handling or machine automation is necessary. Furthermore, the hydrophilic nature of CNFs results in a loss of mechanical strength and durability in water or at high moisture environment (Wang et al. 2018). By improving these particular properties, CNF nanopaper could target new applications or increase their competitiveness as, for example, nanopaper-based membranes for water purification and filtering. Recently proof of concept of CNF use in liquid filtration has been demonstrated (Mautner et al. 2015), and further research in water filtration membranes is expected to focus on hybrid membranes where nanocelluloses are used in combination with other (nano)particles to improve pore structure and mechanical stability (Voisin et al. 2017).

The principal problem comes from the fact that the best mechanical properties are correlated with the high surface area, hydrogen bonding and low material porosity, which are characteristic of CNF but in contradiction with tear and cracking resistance under strong deformation such as crumpling. However, the tear resistance issue is rarely studied and only one recent publication reports the negative impact of CNF pretreatments in tear resistance. The same study reports a slight increase in cross directional tear resistance in oriented nanopapers prepared using a dynamic sheet former (Djafari Petroudy et al. 2017). In regular paper, the tear resistance is an important characteristic for daily handled paper, such as wrapping papers and it is also important for papers submitted to industrial constraints such as papers for bottle labels.

To enhance the general properties of CNF nanopapers, two strategies stand out: chemical modification of CNF nanopapers (Fukuzumi et al. 2009; Trovatti et al. 2018) or the use of inorganic fillers to obtain hybrid nanopapers. The main drawbacks of chemical modification are the low efficiency and hazardous time-consuming processes which hinder the commercial production (Wang et al. 2018). On the other hand, the strategy of hybrid nanopapers has been widely developed thanks to the fast and easy procedure. Literature often reports the use of CNF as a matrix with introduction of nanoclay to enhance nanopaper thermal and mechanical properties (Yong et al. 2018), to induce gas barrier properties (Liu et al. 2011; Wu et al. 2012; Bardet et al. 2015) or to quickly produce large and flat hybrid nanopapers (Sehaqui et al. 2010). The use of nanocellulose as a matrix has also been reported for example with Graphene or silicate for increased stiffness and toughness (Malho et al. 2012; Wu et al. 2014), with carbon nanotubes for increased surface conductivity and printability (Koga et al. 2013), with talc for barrier properties (Liimatainen et al. 2013), and with introduction of residual lignin to enhance wet strength (Wang et al. 2018). However, to our knowledge, no study has proposed a hybrid nanopaper solution for designing tear and crumple resistant material.

The aim of this study was to produce hybrid nanopaper of CNF reinforced with polyethylene terephthalate (PET), in order to increase the tear resistance and limit crumpling of nanopapers, in dry

and wet states. Such a nanopaper could improve efficiency of, for example, filter membranes in aqueous media or dry materials that need to be handled such as packaging films. PET is a synthetic fiber well known for its resistance to deformation, resistance to crumpling and good dimensional stability giving it interesting applications in textiles (McAdam and McClelland 2002), but also in tissue engineering (Wei et al. 2007) and in non-woven materials for filtration (Dotti et al. 2007). CNF has previously been used to improve the strength and modify the porosity of highly porous PET membranes for air particle filtration. (Sim and Youn 2016). However, its use as filler for a CNF matrix in hybrid nanopapers is an innovative strategy.

2.2. Materials and methods

2.2.1. Materials

Commercial CNFs were purchased from the Pulp and Paper Research and Technical Center (CTP), Grenoble, France. They are produced from bisulfite Domsjö pulp (softwood) after enzymatic pretreatment (using a cellulase solution mainly composed of endoglucanase), one pass at 1000 bar followed by 4 passes at 1500 bar in a Homogenizer GEA Panther. The CNF suspension was delivered at 2% w/w concentration and has a hemicellulose content of about 5%.

Polyethylene terephthalate (PET) microfibers with a diameter of 15 μm and cut to a length of 6 mm were kindly supplied by Alhstrom Brignoux (Dacron[®], type 205NSD). The Dtex of these synthetic fibers is 1.7.

2.2.2. Methods

Nanopaper preparation. CNF suspension was mixed with PET fibers at 95:5, 90:10, 80:20 and 60:40 weight ratios respectively based on the dry weight of CNF/PET. The mixture was then diluted to 0.5% solid content in deionized water and stirred mechanically for at least 2 hours before use. CNF nanopapers were prepared using a handsheet former (Rapid Kothen, ISO 5269-2) from 2 g of CNFs (dry content) diluted to 0.5% in deionized water. The suspension was filtered on a 1 μm nylon sieve under vacuum at -600 mbar during one minute until the removal of water supernatant. Then, the sheet was dried under vacuum at 85°C between two 1 μm nylon sieves sandwiched between two round shape cardboards for 20 min. Hybrid nanopapers were produced with exactly the same protocol from CNF-PET suspension diluted to 0.5% in deionized water. The final nanopapers had a target basis weight of 60 g/m^2 . All the nanopapers were stored for 48 h in a conditioned room at 23°C and 50% RH before any characterization.

2.2.3. CNF characterization

Quality Index. The CNF suspension (without PET) was characterized using the Quality index method (Desmaisons et al. 2017). Following the method, four tests were performed on the suspension (macroscopic size and homogeneity determined by optical microscope, nanosized fraction and turbidity) and four tests were performed on the resulting nanopaper (Young's modulus, transmittance at 550 nm, tear resistance and porosity). Each test was performed following exactly the same protocols as described in the Quality Index publication. The resulting quality index was calculated using equation (1):

$$Q.I. = 0.20x_1 + (-0.02x_2) - 0.035x_3^2 + 1.27x_3 - 0.16x_4 + 1.65\ln(x_5) - 3.59\ln(x_6) - 2.67\ln(x_7) + 0.18x_8 + 69.6 \quad (1)$$

where x_1 is the nanosized fraction (%), x_2 the turbidity (NTU), x_3 the Young's modulus (GPa), x_4 the porosity (%), x_5 the transmittance at 550 nm (%), x_6 the tear resistance (mN), x_7 the macro-size (μm^2), and x_8 the macroscopic homogeneity (%).

Optical microscopy. The macroscopic particle size of the CNF in suspension was characterized using an optical microscope (Zeiss Axio Vert.A1, Germany). The suspension was diluted to 0.1 wt%, stirred for 10 min using an Ultra Turrax (IKA® T-25), and immersed for 5 min in an ultrasonic bath ensure good dispersion. Images were taken at 10× magnification and analyzed with Fiji software. Images were transformed to 8-byte format, thresholded and analyzed using the “analyze particles” mode. The average size of the visible particles (“macroscopic size”) was reported as the average surface area of the particle.

Atomic force microscopy (AFM). AFM (Nanoscope III®, Bruker) was used to characterize the CNF dimensions. The CNF suspension was first diluted to 1×10^{-4} wt% and dispersed with a high-shear homogenizer (Ultraturrax®, IKA). Then, a drop of this diluted suspension was deposited on a mica substrate and dried overnight at room temperature. AFM images were acquired in tapping mode with a silicon cantilever (OTESPA®, IKA) at different locations. The resulting images were subjected to 1st order polynomial flattening to reduce the effects of curve and tilt. A total of five images with a scan size of $3.3 \mu\text{m} \times 3.3 \mu\text{m}$ were acquired and the most representative was used to quantify fibril dimensions. At least 50 measurements of diameters were performed on each image.

Nanopaper porosity (%). The porosity of the nanopapers was calculated using equation 2:

$$P(\%) = \left(1 - \frac{\rho}{a \times \rho_{CNF} + b \times \rho_{PET}}\right) \times 100 \quad (2)$$

where ρ is the apparent density calculated from the volume and weight of tensile test strips, $\rho_{CNF}=1.54$, $\rho_{PET}=1.38$ and a and b are the weight fractions of CNF and PET, respectively.

Tensile tests. The tensile properties were measured with a vertical extensometer (Instron 5965), following the standard NF Q03-004. The basis weight was calculated from the mass of each 150 mm x 15 mm test strip and the thickness of each strip was measured using a Lhomargy micrometer. Tensile

tests were performed at 10 mm/min with a gauge length of 100 mm and four repeats were performed per sample.

Tear resistance. The tear resistance was measured using a Noviprofiber tear tester (Elmendorf, France) equipped with a 4000mN pendulum. The instrument measures the out of plane force needed to tear a sample and two types of measurements were performed; tear resistance after initiation by the cut of a primer and tear resistance without use of any primer. The former gives the force needed to sustain a tear once the crack is formed, whereas the latter gives the force needed to initiate the crack. The dimensions of the test specimens were $65 \times 50 \text{ mm}^2$ and four samples were tested for each PET/CNF combination. The tear resistance for wet samples was measured after soaking test specimens for 2 minutes in water followed by blotting of the surfaces to remove excess water. The reported values of the tear index were normalized by the basis weight of the dry test specimens.

Dry crumpling (Balloon test). Hybrid nanopapers were cut into square samples ($6.7 \times 6.7 \text{ cm}^2$). In a typical measurement, a sample was carefully placed in a balloon made out of thick rubber, without creasing the sample, and the balloon was thereafter inflated and deflated rapidly in a controlled and automatic manner with custom-built apparatus to mimic hand crumpling. Two cycles of inflating/deflating were performed after which the sample was carefully removed and kept without further manual handling. Three repeats were performed for each sample type. Pictures of the crumpled samples were taken with a digital camera (PENTAX) with a resolution of 72 dpi. The photos were analyzed by a panel of 5 persons. Each person gave a grade between 0 (worst samples) and 5 (nanopaper without any crumpling or tear damage after balloon test). These grades were averaged to obtain the “crumpling resistance index”.

Wet crumpling (Balloon test). The same protocol was performed on wet hybrid nanopapers, immersed for 5 seconds or 1 minute in water before testing. Excess water was removed by gentle pressing between blotting papers before inserting the sample into the balloon. The water content in the wet samples was determined gravimetrically from soaked and gently blotted samples and calculated in relation to the bone dry weight of the samples.

Scanning electron microscopy (SEM). Nanopaper slices were cut with a razor blade. SEM was performed with ESEM (Quanta 200©, FEI, Japan) on nanopapers slices after carbon sputter coating of 5 nm, with a tension of 10 keV, a spot size of 3.5, in EDT mode. The working distance was 10 mm. At least 5 pictures by samples were performed and the most representative were selected.

Air Permeability. The Gurley air permeability, measuring the time in seconds required to press 100 mL of air through a 6.45 cm^2 circular sample area using a pressure differential of 1.22 kPa, was performed on a Gurley-Hill SPS Tester (USA) following TAPPI standard T460. The sample dimensions were 50mm x 50mm and the reported values were averaged over three measurements.

2.3. Results and discussion

2.3.1. Nanocellulose characterization

Cellulose nanofibrils (CNF) were characterized using Quality Index and a grade of 72 was obtained. This value is among the best values reported in our recent benchmarking study testing 11 commercial grades of enzymatic CNF (Desmaisons et al. 2017). The quality index characterization takes into account the properties of the suspension as well as the properties of the resulting nanopapers, and includes particle dimensions at multiple length scales. Figure 1a shows that the nanosized fraction (73.2 % of the total dry material) is composed of elemental fibrils with an average diameter of 20 ± 6 nm and a length of 3.0 ± 1.7 μm . The remaining material is composed of micrometer sized fibrils or poorly refined fibers on a millimeter scale. The optical microscopy (Figure 1b) gives an overview of the macroscopic fraction of the suspension. The average surface area of the particles in the macroscopic fraction (> 1 μm) was $6 \mu\text{m}^2 \pm 1$, and these fiber fragments appeared predominantly in a flocculated structure, which is often the case for CNF extracted with enzymatic pre-treatment and mechanical disintegration (Nechyporchuk et al. 2016b). The good quality of the suspension was confirmed by the gel-like behavior of the suspension at low solid content (Figure 1c). The high aspect ratio and the high specific surface area of the nanofibrils results in interconnections even at low concentrations. These interconnections combine with the hygroscopic nature of cellulose result in suspension with high viscosity (Nechyporchuk et al. 2016b).

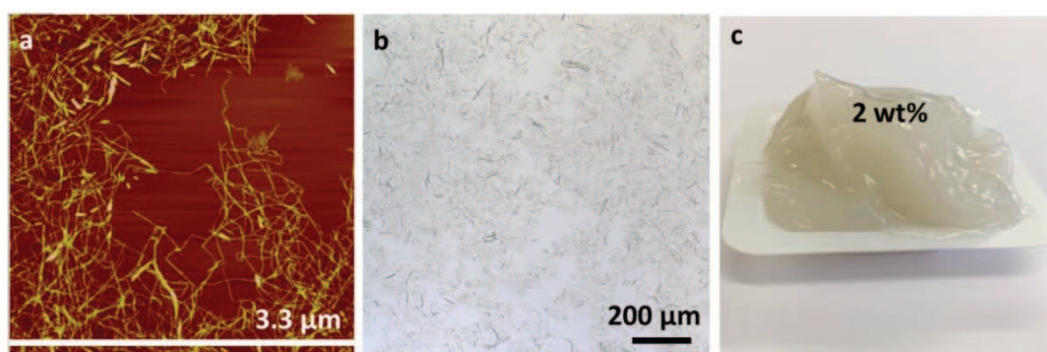


Figure 1: Analysis of the CNF suspension with a) AFM, b) Optical microscope and c) picture of the gel at 2 wt%.

2.3.2. Structural properties of nanopapers containing PET fibers

The vacuum filtration methodology to produce nanopaper using a Rapid Kothen type equipment is analogous of that used to produce handsheets from traditional wood pulp. However, due to the nano-dimensions of CNF, the structural, mechanical and physical properties are completely different. Cellulose nanofibrils, once filtered and dried, have the particularity to form highly cohesive materials known for their low porosity (González et al. 2014). In this work hybrid nanopapers were produced by incorporating 5-40% PET fibers into the CNF suspension. Figure 2 shows cross-sectional SEM images of nanopapers containing 5-40% PET. All 4 samples have the same solids content targeting a basis weight of 60 g/m^2 . Incorporation of the large PET fibers ($15 \mu\text{m}$ in diameter and 6 mm long) had

a strong effect on the thickness of the films, and drastically changed the density and porosity of the material. The images show that the PET fibers were evenly distributed in the z-direction, which can be attributed to the relatively fast filtration speed, preventing settling of the PET fibers which have a lower density and dispersibility in the suspension than CNF. The presence of PET fibers also resulted in the formation of a lamellar film structure where sheets of dense CNF films form around the network of PET fibers.

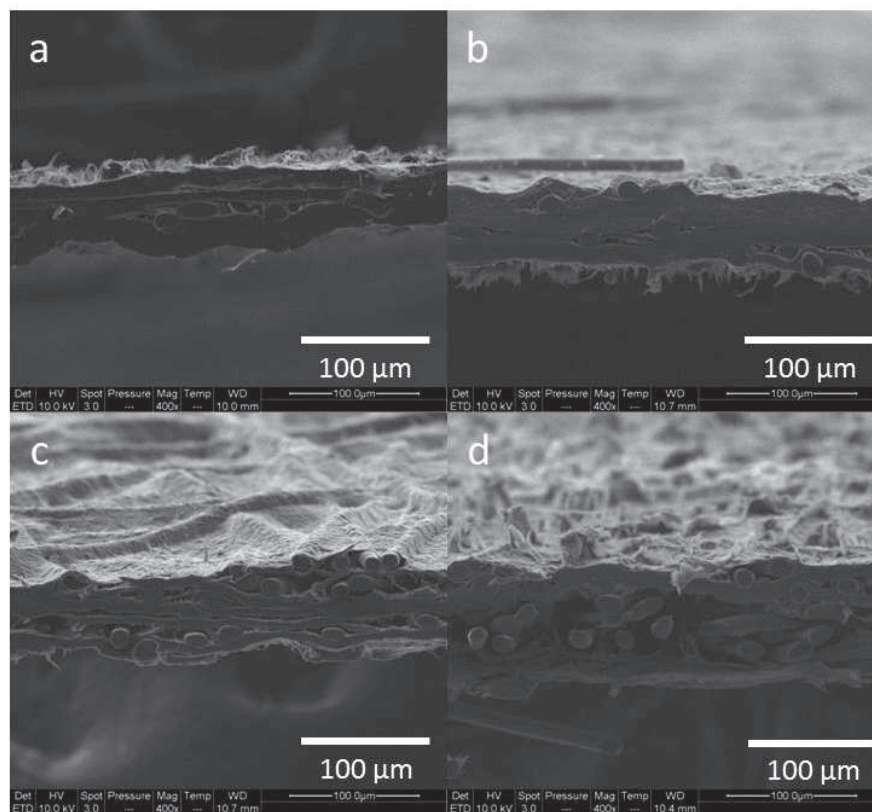


Figure 2. Cross-sectional SEM images of nanopapers with a) 5% PET, b) 10% PET, c) 20% PET and d) 40% PET.

The increased thickness of the nanopapers containing larger fractions of PET fibers can be seen in Figure 3a. The thickness was measured using a micrometer and displays a linear increase as a function of PET content. The results in Figure 3b further show that there was a strong correlation between the nanopaper porosity and the content of long and large PET fibers, allowing for the porosity to be tuned between 30% for the all CNF nanopapers to 70% for the nanopapers containing 40% PET. As a result the density of the sheets ranged between 1.15 g/cm³ for nanopapers made from 100% CNF and 0.4 g/cm³ for containing 40% PET fibers.

Previously reported methods to increase the porosity of nanopaper from 13% to up to 86% are much more complicated and include solvents with different polarities (Henriksson et al. 2008), applying supercritical drying (Sehaqui et al. 2011) or forcing flocculation of the CNFs prior to the nanopaper formation (Benítez et al. 2013; Mautner et al. 2015). Such tailoring in porosity can be very useful and is often targeted for nanopaper-based filtration membranes but also for scaffold materials

with high specific surface area. However, in general, an increase in porosity reduces strongly the Young's modulus, yield strength and tensile strength.

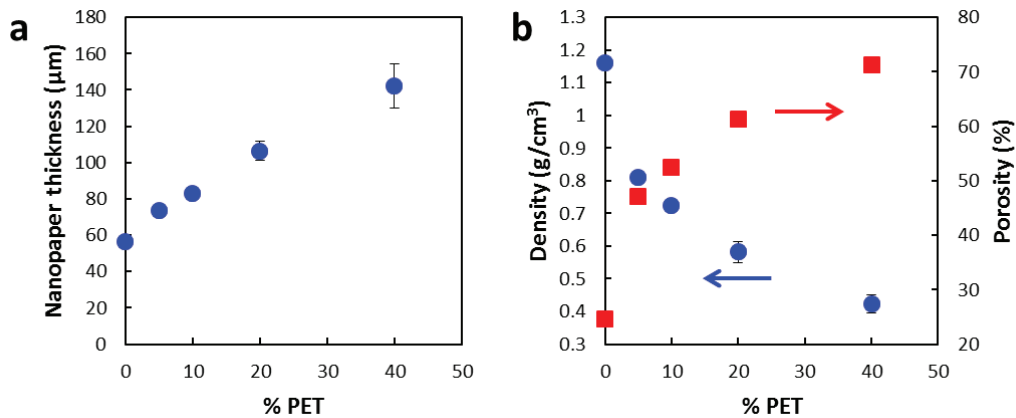


Figure 3. a) Thickness and b) density and porosity as a function of PET content in CNF/PET nanpaper.

The air permeability of the CNF/PET sheets was evaluated using Gurley air permeability which measures in seconds the amount of time it takes to press 100 mL air through the film. A low value corresponds to high permeability. Figure 4 shows as expected that the increased porosity also increases the permeability of the nanpaper and reduces its barrier properties. The lamellar structure observed in the SEM images in Figure 2 indicates that the large pores created by the PET fibers are mainly oriented in the x-y plane. Despite this there was a near exponential increase of the air permeability with increasing PET content.

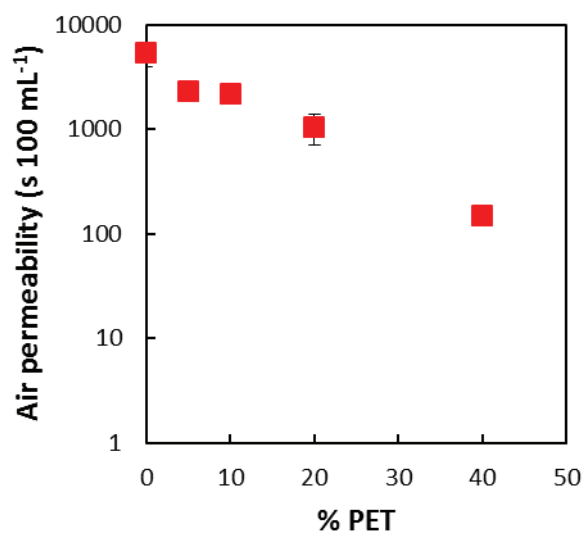


Figure 4. Gurley air permeability as a function of PET content in CNF/PET nanpaper

2.3.3. Mechanical properties of nanopaper containing PET

Tensile properties

The unique mechanical properties of dry nanopapers, mainly due to the strong inter-fibril hydrogen bonds which act as cross links, are well known. High strength and stiffness values of CNF nanopapers have been reported in literature (Sehaqui et al. 2011; González et al. 2014). Wet tensile strength is also an important property in many applications such as food packaging or filter membranes used in humid conditions. It has already been reported in literature that wet tensile strength of nanopapers is about 13 times higher than wet tensile strength of paper sheets made from the original pulp fibers (Hassan et al. 2012). However, wet tensile strength of wet nanopapers or membranes produced with CNF in comparison with the dry materials are still far below the dry properties (Karim et al. 2016). Very recently, researchers have propose the use of lignin-containing CNFs from tobacco stalk and managed to obtain a nanopaper wet tensile strength of 83 MPa, which was at this time the highest value reported in literature (Wang et al. 2018) but was still 3 times lower than the dry tensile strength values reported at 255 MPa.

The stress-strain curves for dry or wet nanopapers containing different amount of PET can be seen in Figure 5. For dry films (Figure 5a), the elastic modulus, stress at break and strain at break decreased with increasing amount of PET. For wet films (Figure 5b), soaked in water for 2 minutes, elastic modulus and stress at break decreased with increasing PET content whereas there was a slight increase in strain at break due to the plasticizing-like effect of water up to 20% PET content where the cohesion in the wet film was too low. Water “plasticizes” the film by swelling it and breaking hydrogen bonds so that the fibrils can slide slightly before they break. We can however notice that strain to failure values were much lower than classical values obtained in literature (around 10%) (Henriksson et al. 2008). Such differences can be explained by differences in drying procedures (temperature, time), in raw nanomaterials (different type of CNF), and in tensile measurement protocol.

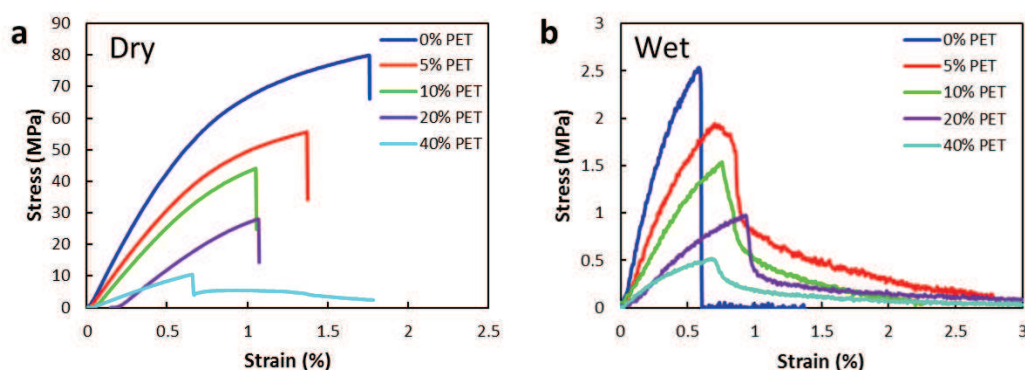


Figure 5. a) Tensile stress-strain curves for dry nanopaper containing 0-40% PET fibers and b) stress-strain curves for PET/CNF nanopapers soaked in water for 2 minutes.

The tensile properties are summarized in Figure 6. Not surprisingly, the wet mechanical properties of the hybrid nanopapers are far below the dry properties. Furthermore, as reported in the previous graph (Figure 5), there is a near linear decrease in stress at break and Young's modulus for both wet and dry samples with the increase of PET content. We have shown above that introduction of PET has a large effect on the density of the sheets. It is well known that density has a large influence on the mechanical properties of a porous material. Lower density means a lower bonded area and therefore a weaker material with more air in the cross section. Even though we expect the sheet like structure of CNF in the films with high PET content to be strongly bonded, the introduction of PET creates a layered structure with weak bonds between the layers, giving a less stiff material that also breaks under lower stress. The PET fibers work as spacers and create a porous sandwich-like structure in the thin CNF films. Furthermore, it is well known in non-woven industry that these synthetic fibers also have low compatibility with cellulose and do not form hydrogen bonds, creating weak interfaces within the nanopaper, further lowering the mechanical properties (Sim and Youn 2016).

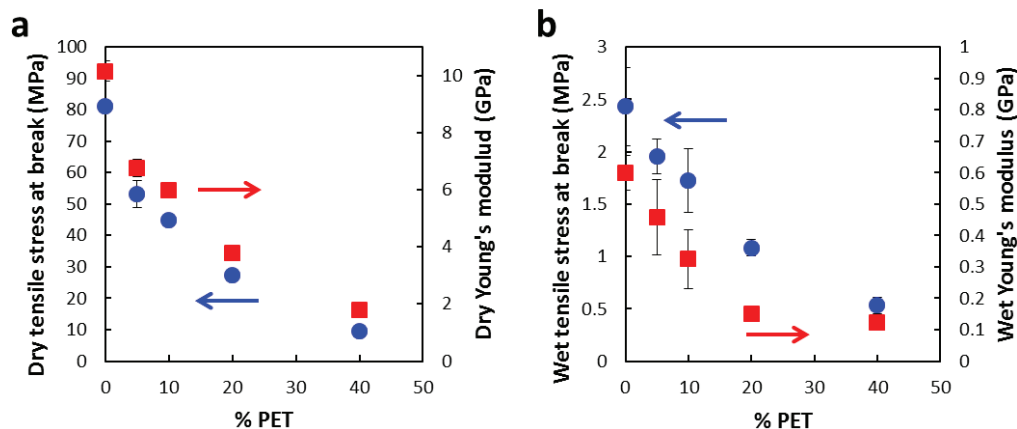


Figure 6. Stress at break and Young's modulus for a) dry nanopapers and b) wet nanopapers as a function of PET fiber content in the nanopaper.

To highlight the effect of sheet density on the dry mechanical properties of hybrid nanopapers, the results reported in Figure 6a were plotted as a function of density for 5, 10, 20 and 40 wt% PET in the CNF matrix. Figure 7 displays a strong linear correlation between density and both stress at break and Young's modulus of dry nanopapers, showing that the main contributor to the loss of mechanical properties is the overall lowering of density of the sheets containing PET fibers. The PET fibers introduced into the nanopaper are strong and stiff, but since the interactions between PET fibers and CNF lack the strong contribution of hydrogen bonding and the interactions between adjacent PET fibers are weak when processing far below the melting point of PET, an increasing fraction of PET fibers in the hybrid nanopaper reduces the mechanical properties.

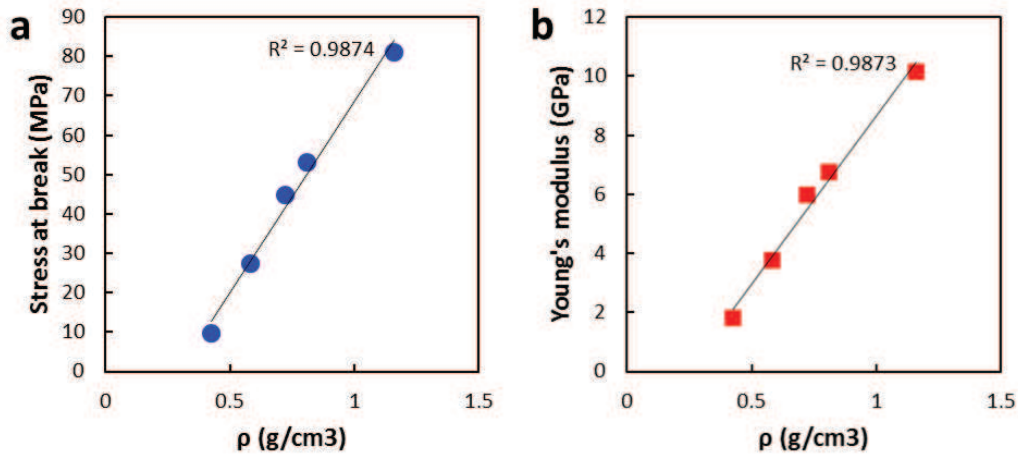


Figure 7. a) Stress at break and b) Young's modulus as a function of density for PET containing CNF nanopapers. A lower density corresponds to a higher PET content.

Tear resistance

Tear resistance of hybrid nanopapers, as a function of PET content, is reported in Figure 8 for dry and wet nanopapers. The results in Figure 8a were obtained by initiating the crack using a notch and are consequently more representative of the tear propagation. This test corresponds to the standard characterization method for fibrous materials. On the other hand, results in Figure 8b were obtained without initiation with a notch and are in this case representative of both the minimal force required to create the tear as well as the tear propagation. The first method has rarely been investigated in nanopaper characterization and the second one has, to our knowledge, never been. In both cases, increasing amount of PET within the CNF nanopaper led to a strong increase in dry tear resistance. In other words, PET fibers act both on tear initiation and tear propagation. A 10 % PET fiber content improved the dry tear resistance by an order of magnitude from 0.9 to 8.4 mN m²/g. This tear index is similar to that of regular copy paper which has a tear index of 6-8 mN m²/g depending on the tearing direction of the anisotropic paper. At 40% PET content the nanopapers had a notch initiated tear index of 21 mN m²/g and a tear index without the use of a notch of 50 mN m²/g, both a 20-fold increase compared to the all CNF nanopaper. However, as reported in figure 5, this strong increase came at the cost of severely deteriorated mechanical properties. The strong positive impact of PET microfibrils on the tear resistance of CNF nanopapers is the opposite of that of polylactic acid (PLA) microfibrils combined with CNF recently reported by Robles et al (Robles et al. 2018). It was reported that the PLA fibers bind poorly to the CNF and additionally the tensile strength of PLA is significantly lower than that of PET making rupture of PLA fibers more likely. This shows the importance of the mechanical properties of the long fiber fraction for improving the tear resistance. Additionally the PLA fibers were fibrillated which improves the bonding but further weakens the fibers.

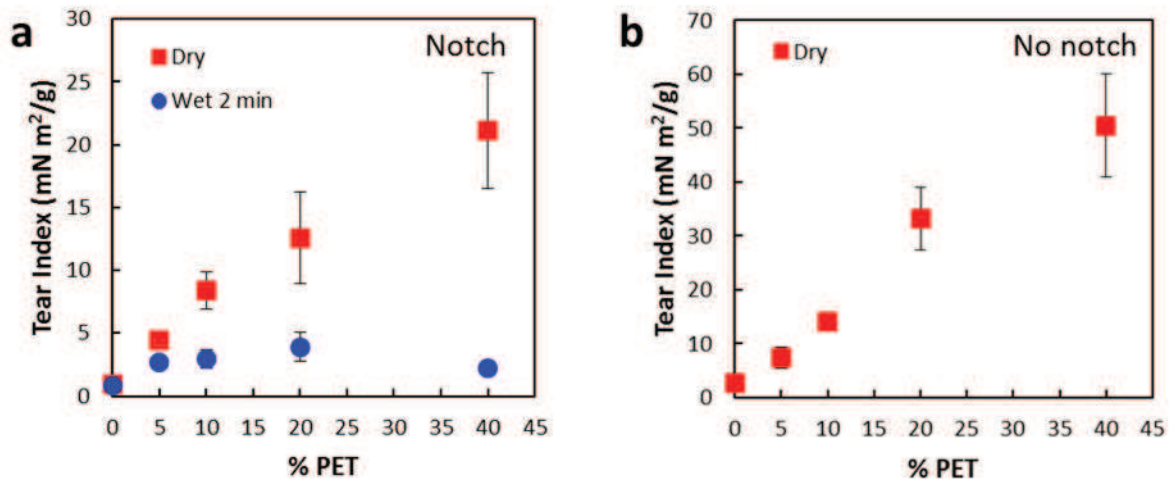


Figure 8. Tear resistance normalized by basis weight for dry and wet nanopapers as a function of PET content, a) with notch initiation, b) without notch initiation

Tear is a complex phenomenon to explain. It has been reported that tear resistance in fibrous material depends on the total number of fibers participating in the tear, the strength of the individual fibers and the number and strength of the fiber-fiber joints (Brandon 1981). Furthermore, the tear mechanisms principally involves two phenomena: pulling fibers out of the material or rupturing the fibers (Hassan et al. 2015), and the first phenomenon is preponderant on the second.

Nanocellulose has previously been added to unrefined fiber pulp from 2 up to 10 wt% and it has been shown to improve the tear resistance of the resulting paper by improving the fiber-fiber contact area and thus the total strength of the fiber-fiber bonds (Brucato 1986; Hassan et al. 2011; González et al. 2012; Petroudy et al. 2017). However, the tear resistance of a nanopaper is much lower than the one of a paper. Weak tear resistance is a common issue for nanocellulose films due to the rapid crack propagation in the dense brittle films once the defect is formed. Furthermore, the diameter of these nanofibrils is widely lower than the diameter of classical fibers, and consequently the rupture of these nanomaterials is enhanced.

Although few publications mention the tear phenomenon in nanopaper, some analogies can be made with highly refined papers, where mechanical treatment has created large fibrillation at the cost of decreasing fiber length and weakened individual fibers. In 1981, Brucato et al. explained that a paper with a high quantity of fiber bonds as a result of a high degree of refining will have greater tensile strength and bursting strength but lower tear resistance than a paper having only moderately bonded fibers (Brucato 1986). The well bonded paper transmits applied stress directly to the propagation point of a tear so that the paper tears more easily. On the other hand, a moderately bonded paper will tend to distribute the applied stress to areas adjacent to the tear propagation point as well as to the propagation point so that it has more resistance to tear as recently studied in detail in a PhD thesis (Krasnoshlyk 2017).

Introduction of long and thick PET microfibers in the CNF matrix in this work resulted in the formation of a network of strong and long fibers with an individual fiber width on the μm scale within the brittle network of nanofibrils. The first probable failure across the tear crack of this hybrid network is fiber pull-out due to the strength of the individual PET fibers and the weak bonding between PET and CNF. Because of the length of the PET fibers this requires a lot of energy which results in an increased tear resistance. Furthermore, structural analysis showed that introduction of PET fibers tends to decrease the cohesion of the CNF network and hence to increase the porosity. This increase in porosity, until an optimum point, can also play a role in limitation of tear propagation as it increases the number of solid/air interfaces and contributes to limit the tear propagation. However, there is today no literature data proving the direct influence between porosity and tear propagation regarding nanopaper materials.

In order to separate the effect of the increased porosity from that of the PET network, nanopapers from 100% CNF with different porosities were produced by introducing different amount of ethanol in the aqueous solvent prior to vacuum filtration. Nanopapers with higher porosity had larger tear index (Figure 9) showing that it is possible to improve the tear index of nanopapers even without PET fibers addition. However, when comparing similar porosities it is clear that the effect of introducing PET clearly outweighs that of only increasing the porosity. At 52% porosity the all CNF sheet had a tear index of $0.85 \text{ mN m}^2/\text{g}$ whereas the sheet containing 20% PET which has a similar porosity had a tear index multiply by more than 10, with a value of $12.5 \text{ mN m}^2/\text{g}$.

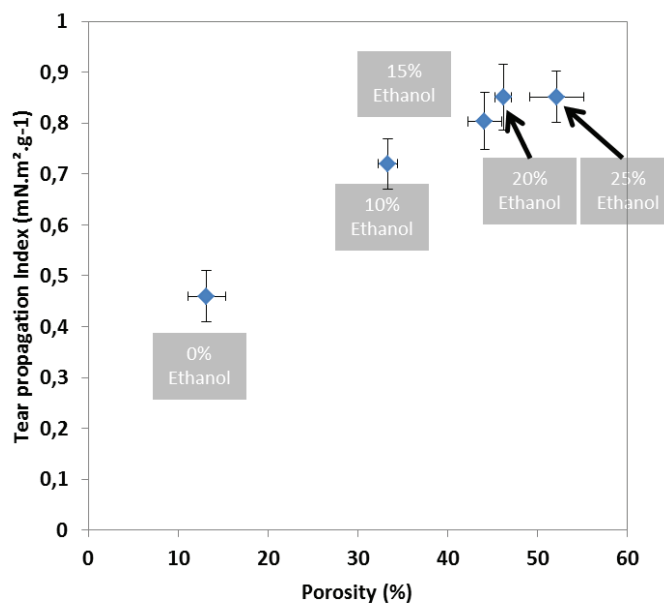


Figure 9: Tear index as a function of porosity for nanopapers prepared from aqueous suspensions containing 0-25 v/v % ethanol. The porosity increased with increasing ethanol concentration.

Finally, wet tear resistance is also reported in Figure 8a. The wet tear resistance increased after introduction of PET, but with limited effect above 10% PET addition. For wet sheets, the effect of higher PET addition was limited by increased swelling of the more porous sheets, leading to breaking of the lower amount of interfibril hydrogen bonds with global loss of mechanical properties as a result.

2.3.4. Crumpling resistance

The final property that was evaluated for the CNF/PET sheets was the crumpling resistance, which is a measure of how well the nanopaper can resist being crumpled without being teared and cracked. The crumpling process induces a network of wrinkles that fold the initial material into a smaller structure. From elasticity theory, we know that thin elastic plates have two modes of deformation: (i) bending, which involves curving the plates, and (ii) stretching, which changes the distances on the plate. Bending is much less expensive energetically than stretching, and is consequently the first mechanism of deformation during material crumpling. When the deformation exceed the elastic area, the expensive stretching energy will appear under the form of permanent wrinkle pattern (Sultan and Boudaoud 2006). The process is irreversible as the energy is accumulated in small regions leading to localized plastic deformation, and enhanced with the material slenderness. The crumpling resistance of sheet-like materials depends also on elasto-plastic properties of the raw material (Tallinen et al. 2009) and the resulting crumpling pattern also strongly depends on the crumpling process or way of compaction.

Nanopapers are usually brittle materials which do not resist such complex crumpling deformation, and, up to our knowledge, this property has never been investigated in the literature. However, the demonstration of crumpling resistant nanopapers could allow this material to better resist manual or automatic deformation and be useful in many applications such as food packaging or filtration membranes.

The crumpling behavior of the hybrid PET/CNF nanopaper was evaluated for both dry samples and samples soaked in water for 5 and 60 seconds. Figure 10a shows a set of pictures of 67x67 mm nanopaper samples subjected to two cycles of crumpling using a “balloon test”, where the sample is placed in a rubber balloon which is inflated and collapsed cyclically to simulate hand crumpling. A crumpling resistance index has been visually attributed to these papers and reported as a function of the PET content (Figure 10b). The value 0 has been attributed to the less crumpling resistant samples and conversely, a value of 5 has been associated to a perfectly crumpling resistant paper.

Crumpling of dry samples

As expected, the brittle all CNF nanopapers shattered and only a powder was left to analyze. That is why no photo of the sheet is available. Introduction of the interpenetrating network of long elastic PET fibers, observed in Figure 2, prevented the sheet from catastrophic failure and strongly

improved the recovery of the dry crumpled sheets. For the samples containing 5% and 10% PET, there were still some cracks in the samples. Above 10% PET there were no cracks and tears and the samples remained intact after 2 cycles of crumpling. The number of sharp folds and large creases also decreased as a result of the incorporation of the interpenetrating network of long elastic PET fibers. If the use of PET as hybrid nanopaper is still rare, PET fibers are well known in the textile industry for their ability to reduce textile shrinking and crumpling. These fibers present high tensile strength (around 150 MPa) and flexural strength (around 221 MPa) (RTP Imagineering plastics) which promotes resistance under bending and stretching, the two mechanisms involved in crumpling.

Crumpling of wet samples

PET also prevented the wet samples from complete disintegration. Even if the crumpling resistance index remains lower in wet state than in dry state, the fact that CNF nanopapers can be crumpled in a wet state is already by itself a novel property. An optimum was observed at 10% PET for both 5 seconds and 60 seconds of wetting (Figure 10b). The rapid decline in the mechanical properties of the wet samples with increasing PET content in Figure 6 as well as the plateau of the wet tear index in Figure 8a suggest that the cohesion of wet sheets containing more than 10% PET was too weak to utilize the crumpling resistance of the PET network.

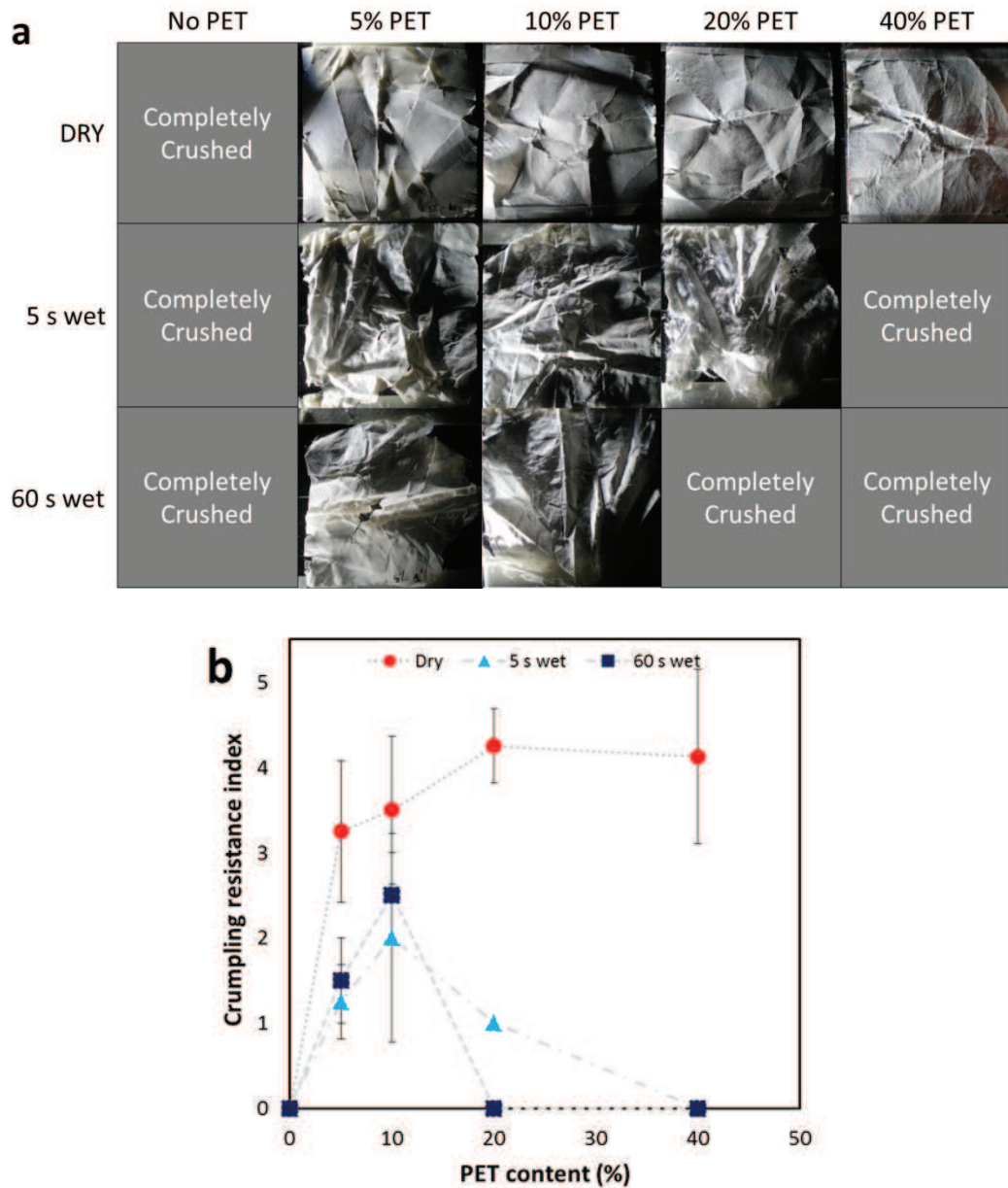


Figure 10. a) pictures of crumpled nanopapers (No photos were taken for the samples that were completely pulverized during the compression cycles in the balloon) and b) crumpling resistance index as a function of PET content

Table 1 shows moisture content in the sheets as a function of PET content and wetting conditions. PET fibers have low wettability because of their low surface energy (Gotoh and Kikuchi 2005). However, for both 5 s and 60 s wetting, a small but clear jump in the water content can be seen with the increase in PET ratio. More precisely, the differences appear from a PET content of 10 wt%. This shows that the more porous sheets absorb more water and thus are more sensitive to swelling and breaking of the inter-fibrillar hydrogen bonds which hold the sheets together. Adding 10 wt% PET in the nanopaper results in an increase in porosity from 20% to 48% as reported in Figure 2. Furthermore, for a given water content the higher porosity also gives water access to a higher surface area more rapidly which speeds up the swelling of the sheet.

Table 1. Moisture content in CNF/PET nanopapers, at 50% RH and after being soaked in water for 5 s or 60 s.

PET content (%)	50% RH (% water)	5 s wet (% water)	60 s wet (% water)
0	6.4	35.4	40.4
5	5.6	35.2	41.2
10	6.2	35.8	40.9
20	5.8	39.7	42.3
40	4.7	41.6	44.7

This increase in water content and accessibility due to the presence of 10wt% PET or more explain that wet crumpling values decrease after reaching an optimum at this same ratio. The same optimum was already observed for wet tear resistance, where a stabilization of the values happened with 10 wt% PET. In parallel, considering the important standard deviation, the values of dry crumpling resistance index for 10wt% PET are also close to the optimum value obtained for 20 wt%, meaning that 10 wt% PET could successfully increase dry and wet crumpling values of the hybrid-nanopapers. These results show that the simple addition of 10% PET fiber in nanopaper will strongly limit their tear and allow resistance to dry and wet crumpling.

2.4. Conclusions

PET microfibers were successfully incorporated in CNF nanopapers with good dispersion in the x-y plane as well as in the z-plane. The changes in the sheet morphology can be used to tune the porosity between 30% and 70% for sheets containing from 0 to 40 wt% PET. This loss in density resulted in a linear decrease of stress at break and Young's modulus and an exponential increase of air permeability with increasing amounts of PET. However, very interesting results were obtained regarding tear resistance and crumpling resistance. Due to the length and strength of the fibers, incorporation of PET fibers greatly improved the dry and wet tear resistance initiation (performed without notch) and propagation (performed with notch). Incorporation of 10 wt% PET fibers increased the dry tear resistance with notch by a factor of 10 while still maintaining most of the mechanical properties. It was also possible to improve the wet tear resistance by a factor of 4 with

limited effect above 10% PET addition. Furthermore, PET fibers make it possible the crumpling of nanopaper that previously was so brittle and had so poor tear resistance that it shattered from the deformation. Finally, incorporation of PET fibers also allows for crumpling of wet samples. However, above a content of 10 wt% PET, the cohesion in the wet sheet was too low to transfer the stress and the sheet failed. Consequently, there is an optimum at 10 wt% of PET for 90 wt% CNF which allows the best wet crumpling resistance and wet tear resistance. This work proposed for the first time hybrid nanopapers resistant to tear and crumpling deformations in dry and wet states which could find new applications for water filtration membranes or food packaging films. As a perspective, other tests will be performed by changing PET for cellulosic fillers, and other tests such as water permeability or oxygen permeability could be performed in order to go further in the application of such hybrid materials membranes.

3. Influence of pretreatment and degree of defibrillation on cellulose nanofibril cryogel properties and strategies to introduce a porous CNF layer inside a papermaking process

This study was performed in collaboration with another laboratory (LIMATB, Lorient) and was presented in an oral international conference at the 4th International Cellulose Conference (ICC 2017, Fukuoka, Japan).

3.1. Introduction

Because of their high aspect ratio and their abundant H-bonding capability, cellulose nanofibrils (CNFs) form an entangled network that behaves as a highly viscous gel in water, even at low solid content. When diluted in water, filtered and dried, these CNFs form a dense, transparent and highly cohesive film also called “nanopaper”. On the other hand, if the CNF gel retains its entangled network structure, and replacing water with air, a high specific surface area skeleton is formed and called “foam”, “cryogel” or “aerogel”. An aerogel is characterized by its high porosity (> 90%) and pore size ranging from 2 nm to 50 nm, while foam or cryogels are usually material with high porosity (>50%) but with pore sizes higher than 50 nm (Lavoine and Bergström 2017). The preparation process also helps for distinguishing aerogel obtained by supercritical drying vs cryogel or foam obtained by freeze-drying. Unfortunately, first publications about this porous cellulose structure were not so precise in terminology and the name “aerogel” tends to be over-used. In this publication, the term “cryogel” will be employed to refer to freeze-dried materials. Whatever they are, these materials are characterized by a low density ranging from 10 to 1000 kg.m⁻³ (Martoia et al. 2016). The combination of high porosity and extremely small pores provides cryogels with outstanding properties: extremely low density, high surface area, and low thermal conductivity. This material is particularly studied for heat or sound insulation (Thapliyal and Singh 2014), in biomedical applications as drug delivery systems or scaffolds for tissues (Stergar and Maver 2016), or in depolluting systems as highly adsorbing material or purifying membranes (Korhonen et al. 2011). Due to their weak structure or their highly energy- and time-consuming batch preparation process, no application was reported up to now in papermaking industry.

Aerogels are most of the time inorganic (such as silica-based aerogels) (Gesser and Goswami 1989). However, recent researches have been performed to develop bio-sourced and innovative porous materials from cellulose (Fischer et al. 2006; Liebner et al. 2008; Karadagli et al. 2015; Buchtová and Budtova 2016) and more recently, from nanocellulose (Sehaqui 2011; Lavoine and Bergström 2017; Jiang and Hsieh 2017). The reasons for this interest are the combination of their renewability and biocompatibility with an ultralow density, tunable porous architecture with outstanding mechanical properties of nanocellulose which compensate the lack of mechanical properties brought by the extremal porosity.

Choice of spray-freeze drying. The name “aerogel” usually refers to the CO₂ supercritical drying process: this method is based on bringing the liquid to the supercritical fluid phase by raising the

pressure and temperature above the critical point of the liquid so that, after depressurization, the fluid passes to the gas phase (Sehaqui 2011). Another classical method to produce CNF porous materials, “cryogel” or “foam”, is freeze-drying where CNF suspensions are frozen (in a freezer or dipped in liquid nitrogen) and sublimated under specific temperature and pressure conditions to change ice to air. This process results in an anisotropic morphology with aligned fibrils in the direction of the ice crystal growth, also called “2D sheet-like morphology”. Recently, researchers have proposed another way to produce cryogels with micro-porosity and 3D-structure: the spray-freeze drying (Jiménez-Saelices et al. 2017). In this case, a first layer of CNF suspension is sprayed in a mold and then frozen at -80°C , repeatedly until the whole filling of the mold, and finally the ice is sublimated by freeze-drying. It results an isotropic morphology, or “3D-fibril nanostructured skeleton morphology”. The 2D morphology gives rise to cryogel with a macroporosity while the 3-D structure favors nano and microporosity (from few tens of nanometers to few microns) (Figure 1).

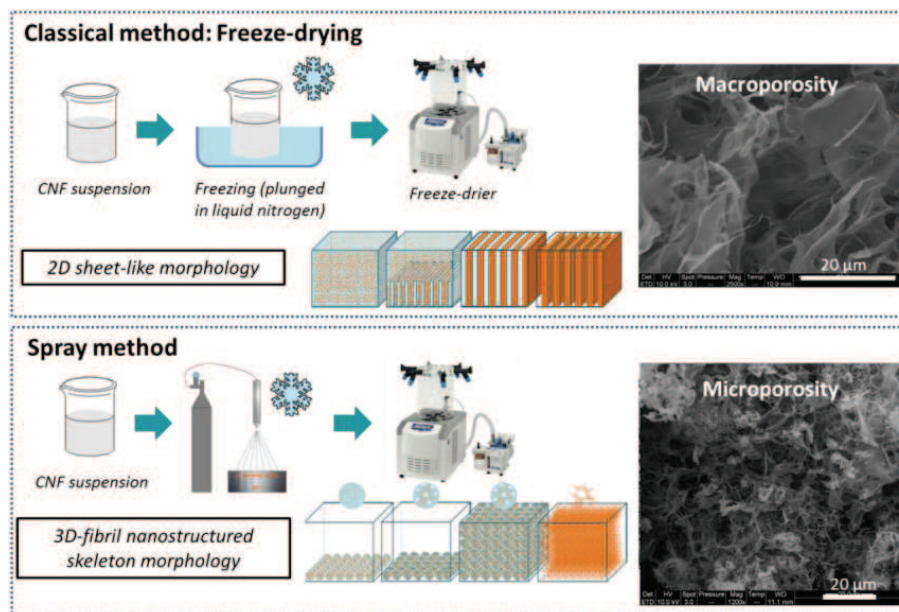


Figure 1: Difference between classical freeze drying method (or freeze-casting) and spray Freeze-drying method, adapted from (Jiménez-Saelices et al. 2017)

Influence of CNF pre-treatment and mechanical treatment on resulting cryogel properties. From previous chapters, it has been demonstrated that cellulose nanofibrils are a complex and multi-scale material whose properties depends on their production process. Studies on CNF aerogels, cryogels or foams already report the effect of bulk density (kobayashi et al 2014, rudaz et al 2014, sehaqui et al 2010), mixture between fiber and nanofiber (Seantier et al. 2016), ice templating and microstructure conditions (Martoia et al. 2016b) but have never investigated the impact of bio-chemical pre-treatment or even mechanical treatment of CNFs on the resulting cryogel properties. In this work, cellulose nanofibrils were produced from eucalyptus fibers after refining, biochemical pretreatment and super-grinding treatment. By varying the pretreatment or duration of the mechanical treatment, different qualities of CNF were produced with different morphologies and surface chemistry. This work proposes to understand the effect of these parameters on the structural and mechanical

properties of the sprayed-freeze dried cryogels (Figure 2). Cryogels have an unusual combination of high porosity and small pore size, making characterization of its porosity by conventional techniques (mercury intrusion, nitrogen adsorption/desorption) very difficult (Thapliyal and Singh 2014). All these techniques are based on the application of capillary pressures on the cryogel network, which may cause large volumetric compressions, leading to incorrect values for pore size and volume (Patel et al. 2009). The measurement of thermal conductivity is a non-damaging method and has been used in this study as a performance index: the lowest thermal conductivity (λ) is obtained for the better ratio between solid conduction limitation and gas convection limitation, and thus is characteristic of a homogeneous micro porosity structure.

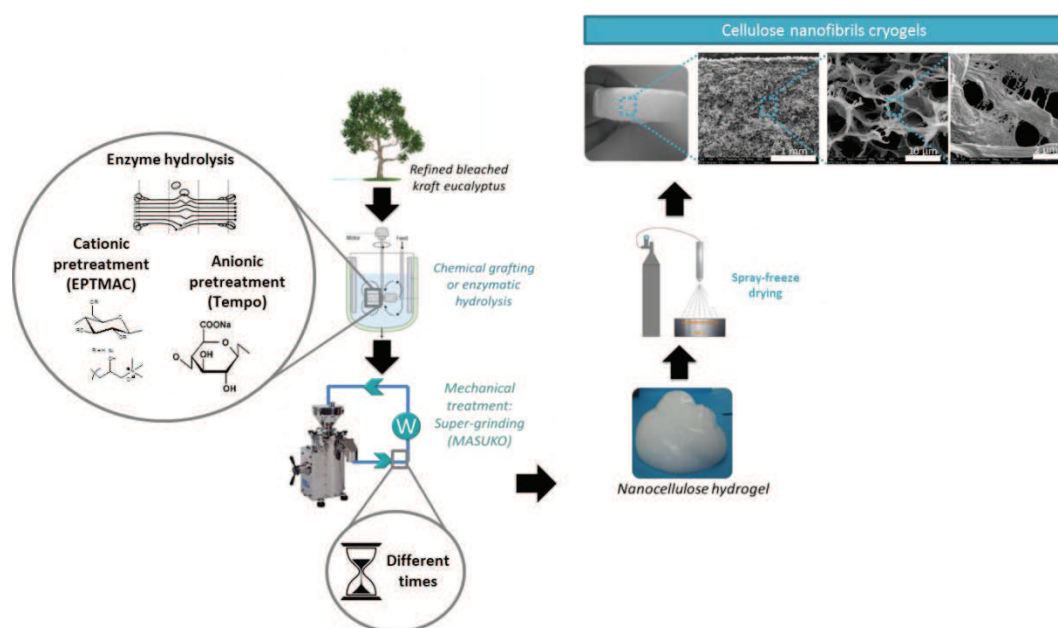


Figure 2: Effect of CNF pretreatment and mechanical treatment time on freeze-dried cryogels structural and physical properties

Application of cryogel beads stable in water for paper application. Cellulose nanofibrils are nowadays used under hydrogel form in paper process in multiply approach or in blend (Bardet and Bras 2014). However, the embedding of cellulose nanofibrils under cryogel form in a paper process has, to our knowledge, never been reported. To make possible the integration of CNF cryogels in the paper machine, one idea would be to spray them directly at the interface of the two cotton fiber layers. To meet these conditions, CNFs cryogels should be produced in the form of micrometric, water-resistant beads. The final purpose of this work is consequently to obtain a CNF cryogel powder that will keep its structure when mixed with water in order to be sprayed in a paper making process. For this purpose, experiments have been conducted trying to produce cryogel beads keeping their porous structure in water following different strategies (grinding, use of cross-linkers).

3.2. Materials and methods

3.2.1. Materials

Commercial nanocellulose. Commercial enzymatic CNF was purchased from the Pulp and Paper Research and Technical Center (CTP), Grenoble, France. They are produced from bisulfite domsjö pulp (softwood) after enzymatic pretreatment (using a cellulase solution mainly composed of endoglucanase), one pass at 1000 bar followed by 4 passes at 1500 bar in a Homogenizer. The CNF suspension was delivered at 2% w/w concentration. TEMPO-oxidized CNFs (called “anionic CNFs”) were purchased from Betullium® with an initial concentration of 4.8 wt% and a charge content of 1274 $\mu\text{mol.g}^{-1}$.

Eucalyptus pulp. Eucalyptus was purchased as dry kraft pulp from Cenibra, Brazil, and the hemicellulose content was 15%.

Other chemicals. Acetone (95%, Chimie Plus); Ethanol (96%, Acros Organic) ; FiberCare® Cellulase (4890 ECU/g), Octylamine (99%, 0.782 g/mL at 25 °C, Sigma Aldrich), Oxy-TEMPO (2,2,6,6-tetramethylpiperidine-1-oxyl) (98%, Sigma Aldrich), Sodium acetate trihydrate (ReagentPlus®, >99,7%), Sodium chloride (>99%, Sigma Aldrich, France), Sodium Hydroxyde (ACS reagent, >97,0%, Sigma Aldrich), Tert-Butanol (ACS reagent, >99%, Sigma Aldrich), Trimethyl(tetradecyl)ammonium bromide (99%, Sigma Aldrich, TTAB), 2,3-epoxypropyltrimethylammonium chloride (151.63 g/mol, 1.13 g/ml at 20°C, EPTMAC, Sigma Aldrich), Sodium Periodate (NaIO₄, 99.8%, Sigma Aldrich), Sodium Alginate (Sigma Aldrich), Calcium Chloride (Acros Organic).

3.2.2. Methods

Preparation and characterization of cellulose nanofibrils.

The pulps were first refined to obtain a fibrillation degree (in Shopper Riegler) between 60 and 70°SR using a beater (PFI, Metrotec, France). Then, an enzymatic pretreatment using a cellulase solution mainly composed of endoglucanase (FiberCare® Cellulase 4890 ECU/g enzyme solution) was performed with a concentration of 300 ECU/g of cellulose. 200 g of refined pulp were introduced at 2 wt% in a reactor pre-heated at 50°C with a 200 rpm rotation speed. A pH of 5 was set by introducing an acetate buffer composed of acetic acid and sodium trihydrate. Once the temperature (50°C) and pH (5) stabilized, an enzyme solution was poured into the reactor and left for a reaction time of 2 h. To stop the enzymatic activity, the reactor was heated to 80°C for 10 min, then cooled to 25°C. Finally, the suspension was recovered, filtered in a Buchner funnel using a nylon sieve with a hole diameter of 1 μm , and washed with deionized water in order to eliminate sugars created during the reaction. The cellulose pulp was finally diluted to 2 wt%. These pretreated fibers were then passed through an ultrafine friction grinder supermasscolloider (Model MKZA6-2, Disk model MKG-C 80, Masuko Sangyo Co., Ltd, Japan) working at 2500 rpm, in recirculation for different times (30min, 1h30 or 2h30), to obtain different grades of CNF suspension.

For the energy measurement during the mechanical treatment as well as characterization of the CNFs, methodology and characterizations refer to Quality index (**Chapter III.1.**). The eight tests involved in the quality index have been performed following the material and methods described in this study.

Cationic cellulose nanofibrils. Cationic CNFs were also prepared from eucalyptus pulp. In this case, cellulose fibers were suspended in water at a solid content of 2 wt% and refined at 80 °SR using disk beater in accordance with standard ISO 5267-1. Then, the suspension was filtered until reaching a solid concentration of 40 wt%. The fiber suspension at 40 wt% was then mixed with water (40 g CNF dry content and 449 g water). Then, a sodium hydroxide solution (NaOH, 29.6 g at 3.7 wt%) was added dropwise to the cellulose suspension. The mixture was then heated at 65°C and kept stirring for 30 min. Then, epoxypropyltrimethyl ammonium chloride (EPTMAC, 132.2 g corresponding to 4 mol/mol_{AGU}) was added. This mixture was kept at a temperature of 65°C for 5 additional hours. At the end of the reaction the pH was neutralized thanks to a few drops of hydrochloric acid (HCl 1 M). The pretreated suspension was then filtered using a Buchner and washed with distilled water. Finally, the pretreated cellulose suspensions at 2wt% were fibrillated using an ultrafine friction grinder supermasscolloider (Model MKZA6-2, Disk model MKG-C 80, Masuko Sangyo Co., Ltd, Japan) working at 2500 rpm, in recirculation for 2.5 h.

Quality Index. The enzymatic CNF suspensions produced after different mechanical treatment durations were characterized using Quality index (Desmaisons et al. 2017). According to the method, 4 tests were performed on the suspension (Macroscopic size and homogeneity determined by optical microscopy, nanosized fraction and turbidity) and 4 tests were performed on the resulting nanopaper (Young's modulus, transmittance at 550 nm, tear resistance and porosity). Each test was performed following exactly the same protocols as described in **Chapter III.1.** The protocol for making the nanopaper is also the same described in **Chapter III.1.** and **Chapter III.2.** The resulting quality index was determined from Equation (1):

$$Q.I. = 0.20x_1 + (-0.02x_2) - 0.035x_3^2 + 1.27x_3 - 0.16x_4 + 1.65\ln(x_5) - 3.59\ln(x_6) - 2.67\ln(x_7) + 0.18x_8 + 69.6 \quad (1)$$

with x_1 representing the nanosized fraction (%), x_2 the turbidity (NTU), x_3 the Young's modulus (GPa), x_4 the porosity (%), x_5 the transmittance at 550 nm (%), x_6 the tear resistance (mN), x_7 the macro-size (μm^2), and x_8 the macroscopic homogeneity (%).

Atomic force microscopy (AFM). AFM (Nanoscope III®, Bruker) was used to characterize CNF dimensions. The suspension was first diluted to 10^{-4} wt% and dispersed with a high-shear homogenizer (Ultraturrax®, IKA). Then, a drop of this diluted suspension was deposited on mica substrates and dried overnight at room temperature. The AFM pictures were taken in tapping mode with a silicon cantilever (OTESPA®, IKA) at different locations. Resulting images were subjected to 1st order polynomial flattening to reduce the effects of bowing and tilt. 5 images were taken at the same

magnification and the most representative was reported in this study. At least 50 diameter measurements were taken by image.

Preparation of spray-freeze cryogels (sections 3.1. and 3.2.). Cryogels were produced by spraying 1 wt% CNF suspensions on aluminium molds (2cmx2cm). After spraying a layer, the cryogel was frozen at -80°C for 5 minutes. Then, another CNF layer was sprayed, and this step was repeated until the complete filling of the mold. After what, these sprayed structures were freeze-dried for 3 days at 1 mBar and -20°C. For the effect of mechanical treatment duration, cryogels were produced with cellulose nanofibrils made from laboratory following the previously mentioned procedure.

Preparation of freeze-cast cryogels (section 3.3.1.). Cryogels were prepared using 1 wt% aqueous CNF suspensions characterized by different types of pre-treatment. The initial suspension was stirred for 10 s with an Ultra-turrax to ensure that all nanofibrils were well dispersed. Then, TEMPO-oxidized CNFs, cationic CNFs and enzymatic CNFs were cast into molds 3 cm on diameter and 2 cm in height and dipped into liquid nitrogen until the suspensions were completely frozen. Then, the different suspensions were put into the freeze-dryer for 3 days under the following conditions: pressure inside the chamber of 1mBar and temperature of -20°C.

Cryogels crushing. Cryogels were put into a cutting mill (Reitsh®, SM 100) for 2 hours in order to obtain porous powders. The sieve used was a Reitsh® reference 10241485, with a hole width of 0.75 mm.

Preparation of cross-linked CNF cryogel beads. This processing method was quite similar to Zhang's work (Zhang et al., 2017). First, a 5 wt% polyamide amine epichlorohydrin (PAE) solution was prepared from the initial 13 wt% solution by adding water in proportion. After that TEMPO-oxidized CNF (CNF-) at an initial concentration of 1.7 wt% was mixed with PAE resin varying total final concentration, e.g. 0.1, 0.6, 1.5 wt% as well as varying CNF-/PAE ratio (w%), e.g. 99/1, 98/2, 90/10. Then the different suspensions were stirred with an Ultra-turrax for 2 min at a speed rate of 6000 tr.min⁻¹ to ensure the dispersion of all components. The suspension was then introduced dropwise into liquid nitrogen using a syringe in order to form CNF frozen-beads. After that the frozen beads were freeze-dried for 19 hours at a pressure of 1 mBar and a temperature of -20°C. Finally, the CNF bead cryogels were placed into an oven for 3 hours at 120°C to obtain crosslinked cryogel spheres thanks to the wet-strength resin.

Characterization of the cryogels

Insulating properties. The thermal conductivity, λ , of the sample was measured using the hot strip technique. The hot strip technique consists of a homemade device (Université Bretagne Sud) made of a two-cavity isothermal aluminum case, one containing polyurethane foam, while the other contains the sample to be characterized (Figure 3). These two cavities are symmetrically positioned with respect to a strip that is electrically isolated from the case. Two electrodes provide the electrical power supply to the strip and two thermocouples measure the temperature of both the strip and the case while the temperature of the case is kept constant by a cooling circuit. The tests were

performed at atmospheric pressure in a temperature and humidity controlled room (23°C, 50% RH). At least five samples per formulation were tested.

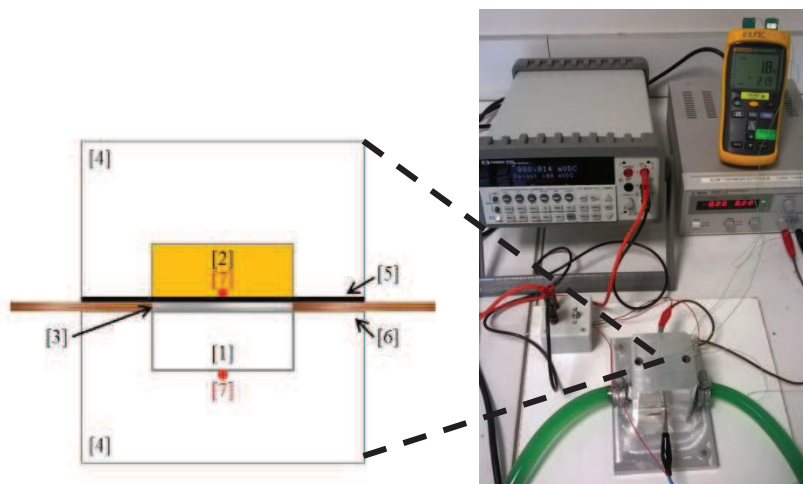


Figure 3: Hot strip device, (1) sample, (2) polyurethane foam, (3) strip NiCr, (4) isothermal aluminum case, (5) electrical insulator, (6) electrodes (copper), (7) thermocouples

Density and porosity. For spray freeze-dried and freeze cast cryogels, the density (kg/m^3) was determined by measuring the weight and volume of each individual. The weight was measured using an analytical balance while the dimensions were determined by image analysis on Fiji Software. For the cryogel beads, the weight was averaged on 10 beads while the volume was determined by employing Fiji Software and average beads diameter, also on 10 samples.

The cryogel porosity (P) was calculated using the density of the cryogel (ρ_{cryogel}) and density of cellulose ($\rho_{\text{cellulose}} = 1.54 \text{ g/cm}^3$) using eq. 1.

$$P(\%) = \left(1 - \frac{\rho_{\text{cryogel}}}{\rho_{\text{cellulose}}}\right) * 100 \quad (1)$$

Compression tests. Compression experiments were performed with DMA (RSA3, TA instruments) using the tensile/compression test. The cryogels were placed between two parallel plates and the tests were performed at room temperature. Elastic compression (storage modulus E') was determined with a frequency of 1 Hz and displacement of 0.05 mm. Change in humidity have been performed by adding a humidity controlled chamber around the DMA apparatus, with 30 min stabilization for each different humidity.

Re-dispersion kinetics into water. Re-dispersion kinetics into water was performed for cellulose bead cryogels by immersing them into petri dish filled with water. A DSLR camera (Nikon D300s) was used to measure the swelling over time by image analysis using Fiji Software. Photos were taken at constant time intervals, i.e. dry state, wet state, 1, 2, 3, 18 and 24 hours. The volume of each bead was measured at least 3 times for each time interval.

Brunauer–Emmett–Teller (BET) Analysis. The BET surface area was determined by N_2 adsorption and desorption using a Quantachrome (NOVA 1200e) gas adsorption analyzer. Samples were first

degassed at 105°C for 15h prior to the analysis to remove any trace of water followed by BET analysis at -196°C.

Scanning Electron Microscopy (SEM). SEM (Quanta 200©, FEI, Japan) was used to analyze the porous materials after sample cut with a razor lame. At least 5 pictures at the same magnification were recorded. Image-J software was then used to perform the pore size measurements and average was used based on a minimum of 50 measurements.

3.3. Results and discussions

3.3.1. Effect of mechanical treatment on cryogels and mechanical properties

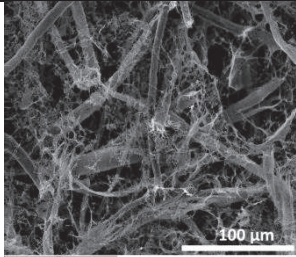
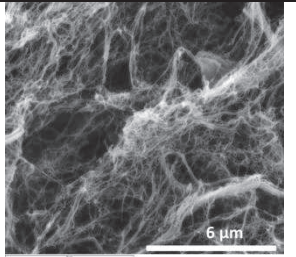
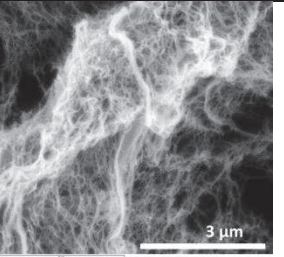
Cryogel structure. Physical and morphological properties of cryogels depend on two sets of parameters: (i) those describing the intrinsic properties of the constitutive material (here, the cellulose nanofibrils) and (ii) those describing the structure of the cryogel (open or closed pores, pore size or orientation, density) (Sehaqui 2011).

(i) The different mechanical treatment times led to cellulose nanofibrils with different quality index (Desmaisons et al. 2017) from 54.1 (± 1.3) to 75.0 (± 0.6) (Table 2). When the mechanical treatment time increased, the CNF quality index increased until an optimum point followed by a stabilization occurring between 1h30 and 2h30 of ultrafine friction grinding treatment. After 30 min, the suspension was a highly heterogeneous mixture containing a large quantity of poorly defibrillated fibers and only 22% of nanoscale fibrils. The resulting cryogel was consequently a material containing both poorly defibrillated fibers and cellulose nanofibrils. This situation can be compared to cryogels produced from a mixture of fiber and cellulose nanofibrils (Seantier et al. 2016). Large fibers appear on SEM pictures (Table 2) surrounded by fibrils in a heterogeneous mixture. By increasing the time in the super-grinder, the nanosized fraction increased up to 68% meaning that the nano fraction of the suspension became preponderant, CNFs dimensions measured with AFM decreased and SEM pictures showed the disappearance of coarse fibers.

(ii) In parallel, micro and macro pore sizes of the cryogels produced from these materials were significantly reduced. The addition of nanoscale fibrils fills the large pores and creates additional bonding which also reduces the average pore size. As the density of the cryogel decreases, we can assume that the cryogel produced with CNF_{2h30} has a higher number of smaller pores than the cryogels produced with CNF_{30min}. These results were confirmed by the increase of the specific surface area (from 22 ± 2 to $63 \pm 4 \text{ m}^2 \cdot \text{g}^{-1}$) with the increase of CNF defibrillation time. From SEM images, it can be observed that cryogels produced with CNF_{30min} have a large range of pore size from nanometer to micrometer scale, while for the cryogels produced from CNF_{1h}, the porosity distribution remains at the nanometer scale. Furthermore, in this last case, the cryogel structure is more open with smaller pore sizes made by individual CNFs.

SEM imaging gives only approximate dimensions of the pores and the sample preparation is a local and damaging method for this highly sensitive material. Such characterizations were consequently combine with the measurement of thermal properties, which allowed us to conclude more precisely about the quality and homogeneity of the close pores in the cryogels, in the total 3D structure, without damaging it. Indeed, the best insulating properties are obtained for the cryogels minimizing the solid conduction (characteristic of a large number of small pores) and the gas convection (characteristic of a small number of large pores). A material is insulating if its thermal conductivity λ is below 100 mW/(m.K). However, what is really challenging is the preparation of super-insulating materials, with a thermal conductivity below the thermal conductivity of air ($\lambda_{air} = 25$ mW/(m.K) (Seantier et al. 2016). Due to the large pore distribution and heterogeneity of the material composed of both fibers and nanofibrils, cryogels prepared from CNF_{30min} did not reach these super insulating properties. However, the thermal conductivity λ of cryogels produced with high quality CNF (CNF_{1h30} and CNF_{2h30}) appeared to be competitive with super insulating materials with λ value around 26 mW/(m.K). These results confirm the presence of closed pores whose dimension distribution decreases with the increase of CNF mechanical treatment time.

Table 2: Structural properties of CNF produced after different mechanical treatment time and their resulting cryogel characterizations

	CNF _{30min}	CNF _{1h30}	CNF _{2h30}
CNF suspension			
Energy consumption (KWh/t)	2194	7144	12411
Quality Index	54.1 (\pm 1.3)	68.3 (\pm 0.9)	75.0 (\pm 0.6)
Dimensions (nm) (AFM)	Too heterogeneous	Length : 1168.9 (\pm 222.9) Width : 39.7 (\pm 9.8)	Length : 1125.3 (+/- 502.8) Width : 28.6 (\pm 9.9)
Nanosized fraction	21.7 (\pm 4.4)	52.0 (\pm 10.4)	67.5 (\pm 13.5)
Suspension turbidity (NTU)	302.0 (\pm 7.5)	345.0 (\pm 8.2)	242.2 (\pm 0.5)
Spray-frozen cryogels			
SEM			
Pore size distribution (SEM) [min, max] and average value (nm)	[371 to 5144] 2187	[108 to 800] 367	[61 to 919] 241
Thermal conductivity (mW/m.K)	35.0 (\pm 4.5)	26.5 (\pm 2.6)	25.7 (\pm 2.3)
Cryogel density (kg/m ³)	30.3	23.0	23.6
Specific surface (m ² /g) (BET)	22 (\pm 2)	57 (\pm 2)	63 (\pm 4)

Cryogels mechanical properties. Cryogel morphology and physical properties are directly correlated. For the same reasons, mechanical properties of the cryogel will depend on the constitutive material and on the pore dimensions and structure. The increase in CNF quality when increasing the duration

of mechanical treatment tends to increase the mechanical properties of the resulting material. Indeed, the Young's modulus of fibers classically ranges from 4 GPa (Coir) to 13 GPa (Cotton) while the Young's modulus of CNFs is usually around 65 to 120 GPa (Dufresne 2017)). However, the decrease in cryogel density when increasing the duration of the mechanical treatment has an opposite consequence as a decrease in density is associated with a loss of mechanical properties. Furthermore, Weber et al. demonstrated that the density has the greatest effect on the physical properties among all the other mentioned parameters (Weber et al. 2000).

Figure 4 shows the evolution of the compression storage modulus as a function of humidity. The compression stress-strain curve usually displays three distinct regions, the initial elastic region at low stress, followed by a wide collapse plateau and finally a densification region. The young's modulus is determined from the slope of the elastic zone, and elastic compression is consequently a good indicator of cryogel mechanical properties.

Due to their large pore volume, many cryogels which have good insulating properties have low mechanical properties (Seantier et al. 2016). Not surprisingly, results showed that cryogels which present the highest thermal properties were also associated with lowest mechanical properties from ambient to higher humidity. Furthermore, the increase in humidity decreases the mechanical properties of the cryogels: this is due to the introduction of water inside the material and decrease of bonding. It can also be observed that high quality CNFs (CNF_{2h30}) produce cryogels more sensitive to humidity than cryogels produced with lower CNF quality (CNF_{1h30} or CNF_{30min}). The higher surface area and the easier exchange with humidity can explain this phenomenon. Nevertheless, if using these cryogels at ambient humidity, the storage modulus remain between 300 and 500 kPa which are classical values compared with other values obtained in the literature (Lavoine and Bergström 2017).

Furthermore, as the final purpose is to grind these cryogels in order to obtain a powder which retains its porous structure, the best option would be (i) a homogeneous structure with small pore distribution and (ii) good mechanical properties to support the grinding process. For this last point, if we consider a cryogel grinding under ambient humidity, the differences of cryogels storage modulus (i.e. rigidity) are not significant to impact the grinding process.

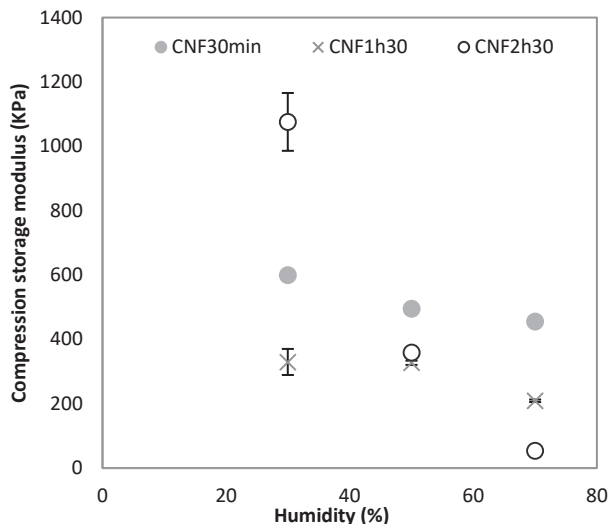


Figure 4: Compression properties of cryogels produced by spray and freeze-drying from CNF with different durations of mechanical treatment in Masuko super-grinder

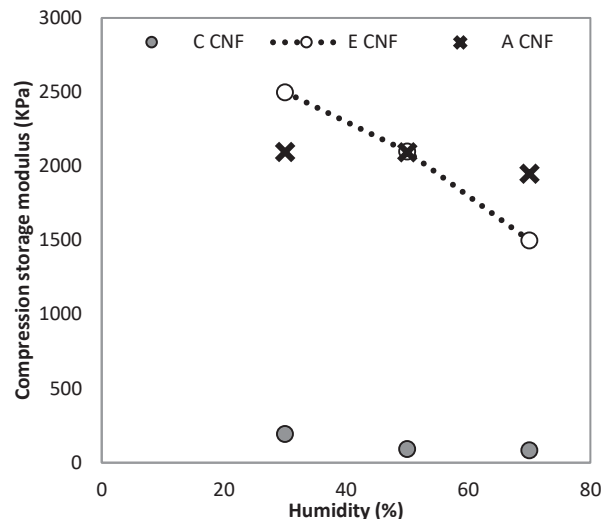


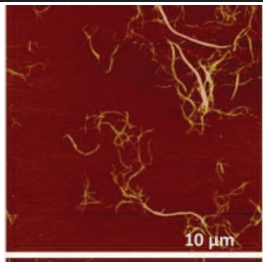
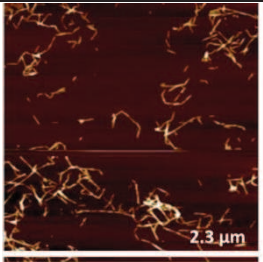
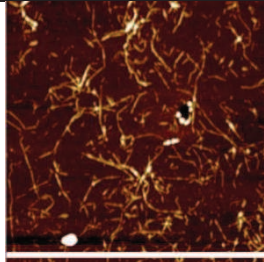
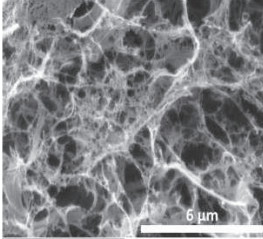
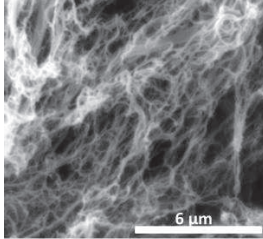
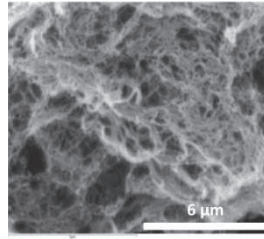
Figure 5: Compression properties of cryogels produced by spray and freeze-drying, from CNF with different pretreatments (E = enzymatic, A = anionic, C = cationic)

3.3.2. Effect of CNF pre-treatment on cryogel structural and mechanical properties

Cryogel structure. The effect of the CNF surface chemistry was also studied by comparing foams prepared with anionic, cationic or enzymatic cellulose nanofibrils. In this case, commercial suspensions were used and results are synthesized in Table 3. The specific surface area of these cryogels shows significant differences: $79 \pm 3 \text{ m}^2 \cdot \text{g}^{-1}$ was reached when cationic charges are present on the CNF surface against $39 \pm 1 \text{ m}^2 \cdot \text{g}^{-1}$ for classical enzymatic CNF. However, SEM pictures show similar structure and just slightly lower pore size with cationic cryogels. Increase of specific surface with the cationic charges can be linked to the electrostatic repulsion introduced by cationic groups, increasing the CNF dispersion.

By measuring the insulating properties, results showed a decrease in thermal conductivity with introduction of repulsive charges, with better results obtain for the cationic cryogel. For comparison, the values reported for cryogels prepared by freeze drying from cellulose fibers are around 0.029-0.030 W/(m.K) (Nguyen et al. 2014), which is close to silica aerogels (0.026 W/(m.K)) or wool aerogels (0.03-0.04 W/(m.K)) (Sequeira et al.). In the case of CNF pretreated with cationic groups, a value of $20.2 \pm 0.5 \text{ mW/m.K}$ has been obtained which is not far from the lowest value of 18 mW/m.K obtained in the literature for anionic CNF cryogel (Wicklein et al. 2015). The super-insulating properties obtained are synonym of high amount of close mesopores homogeneously distributed. These super-insulating properties can be linked to the good CNF quality, the electrostatic charge, the 3D-porous structure (linked to spray-freeze drying) and the freezing temperature (-80°C) allowing the better ratio between ice nucleation and growth of ice crystal.

Table 3: Structural properties of CNF obtained after different pretreatments and their resulting cryogels

	Enzymatic CNF	Anionic CNF	Cationic CNF
CNF suspension			
Dimensions (nm) (AFM)	Length : 776,2 (\pm 27,8) Width : 16,6 (\pm 4,3)	Length : 279,4 (\pm 211,7) Width : 14,7 (\pm 2,7)	Length : 835,9 (\pm 43,7) Width : 26,4 (\pm 3,6)
Charge content	(Carboxylic content) 5,4 μ mol/g	(Carboxylic content): 1274 μ mol/g	(ammonium content): 930 μ mol/g
AFM picture			
Spray-frozen cryogels			
SEM			
Average pore size (SEM) (nm)	300 \pm 61	293 \pm 57	220 \pm 42
Thermal conductivity (mW/m.K)	29.7 \pm 1.6	26.4 \pm 2.3	20.2 \pm 0.5
cryogel density (kg/m ³)	20.9	19.2	35.7
Specific surface (m ² /g) (BET)	39 \pm 1	No data	79 \pm 3

Cryogels mechanical properties. As already observed in the previous section, the better insulating properties (characteristic of 3D structure of mesopores homogeneously distributed) are correlated with lowest mechanical properties (Figure 5). Whatever the humidity, cryogel prepared with cationic CNF present lower compression modulus than enzymatic and anionic CNF. In this case, the difference is preponderant as there is a factor of 10 between cationic values and anionic values. At ambient humidity, similar mechanical properties were obtained for anionic or enzymatic cryogels. Anionic cryogels are surprisingly less sensitive to humidity than enzymatic cryogels and present more stable properties when changing humidity. Usually, anionic CNF are more sensitive to water. Furthermore, the maximal humidity studied was only 70 %RH. At higher amount of humidity it is possible than anionic CNF mechanical properties fall lower than enzymatic CNF mechanical properties.

Conclusion

The quality of cellulose nanofibrils (associated with an extensive mechanical treatment) and the surface chemistry (addition of repulsive charges) results in an open structure with small pore size distribution characterized by good to excellent insulating properties. However, this particular structure is also synonym of lower compression modulus. The mechanical treatment is not

significantly impacting this loss, but the surface chemistry can lead to an important gap when cationic charges are present at the surface of CNF. Anionic CNFs are a promising candidate as they present interesting cryogel structure and competitive mechanical properties, without being a lot damaged by the surrounded humidity (Table 4). The use of cross-linker, as it will be mentioned in the next section, can also help to improve these mechanical properties while keeping the good 3D-structure.

Table 4: Comparison of cryogels produced with different quality of CNF (different mechanical treatment time) or cryogels produced with CNF with various bio-chemical pretreatment. 1=Bad, 2=Medium, 3=Good

Mechanical treatment time	Homogeneous morphology and low size distribution	Thermal properties	Mechanical properties at ambient humidity	Influence of humidity
30min	1	1	3	2
1h30	2	2	3	2
2h30	3	2	3	1
Bio-chemical pretreatment	1=Bad, 2=Medium, 3=Good			
Enzymatic CNF	2	1	3	1
Anionic CNF	2	2	3	3
Cationic CNF	3	3	1	3

3.3.3. Different strategies to prepare porous cellulose nanofibrils material for introduction in a paper

The strategy to reduce the crumpling damage on banknote consists in introducing a CNF layer between the two refined cotton layers. When the CNFs form a film, the high density and cohesion unfortunately enhance the tear propagation, which is another current issue for banknotes. To overcome this effect, the idea is to associate the strong mechanical properties and resistance to deformation of CNFs with a highly porous structure hindering the tear propagation. Introduction of a cryogel as a middle layer is not possible within a papermaking process. However, the production of a cryogel powder which keeps its porous structure in water could be realized and sprayed in the intermediate layer without interrupting the papermaking process. Following studies have consequently been performed, targeting (i) the production of beads or powder (ii) with porous structure and (iii) keeping its structure when diluted in water, in order to be sprayed. The first strategy proposes to crush the freeze-dried cryogels with cutting mills, and the second strategy proposes to produce cross-linked beads with PAE.

3.3.3.1. Classical cryogels crushed with cutting mills

Enzymatic, cationic and anionic cryogels obtained after freeze casting (not spray freeze drying in this case) were crushed in a cutting mill to obtain porous powders. From SEM pictures (Figure 6-A), it appears that the CNF cryogels have kept their porous structure after the cutting mill treatment (similar results are obtained for enzymatic, anionic and cationic cryogels). Then, these powders have

been soaked into water for 3 days in order to test their water resistance ability (Figure 6-B). Whatever the pretreatment used, none of the cryogels has kept its structure: all samples have swollen and returned to the initial gel structure of CNF suspensions. This behavior can be explained by the fact that CNFs have a large number of hydroxyl groups on their surface. Therefore, they have a hydrophilic character and when dispersed into water, hydrogen bonds between water molecules and hydroxyl groups are formed and re-disperse the cryogels. This phenomenon is even enhanced by the presence of repulsive charges which enhance colloidal stability and so their dispersion in water.

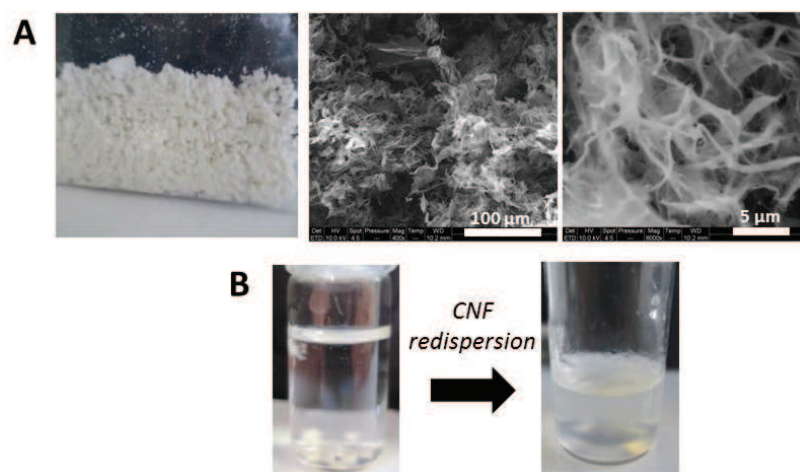


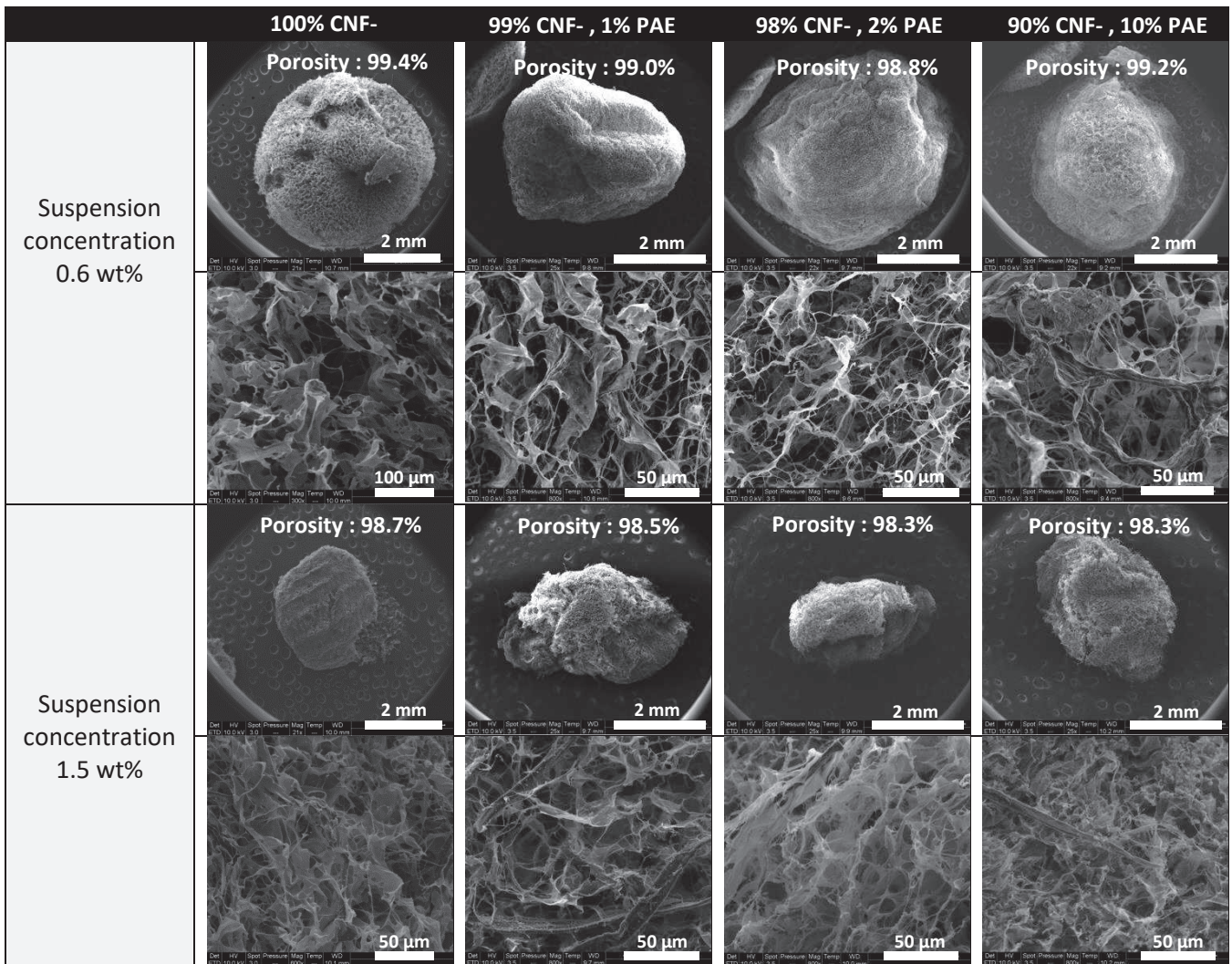
Figure 6: A) Enzymatic cryogel powder after crushing in cutting mill and B) Introduction of the powder into water

3.3.3.2. Cross-linking with polyamide amine epichlorohydrin resin

One limitation of native cellulose based cryogels, foams or aerogels is their tendency to disassemble and redispense in water. Chemical cross linking or post treatments can be used to yield stable cryogel capable to keep their initial shape in water medium (Kettunen et al. 2011; Jiang and Hsieh 2014). Polyamide amine epichlorohydrin resin (PAE) is an effective papermaking cross-linking agent, commercially available, and well-known to increase the wet strength properties of cross-linked cellulosic materials, including aerogels (Roy et al. 2009; Zhang et al. 2012). TEMPO-oxidized CNFs (anionic CNFs) and PAE were coupled to provide wet strength to the cryogel beads thanks to the ability of PAE to form covalent ester bonds between carboxyl groups of cellulose and azetidinium groups of PAE. There is also a secondary mechanism of self-cross linking of PAE groups that form a water insoluble network during the curing process (Obokata et al.; Ahola et al. 2007).

Anionic CNF and PAE were mixed together with different ratios and different final concentrations (0.1 wt%, 0.6 wt%, 1.5 wt%). To avoid damaging caused by the cutting-mill treatment, PAE/CNF were dropped into liquid nitrogen to directly form beads and then freeze-dried. Afterwards, the cross-linking reaction was thermally induced in an oven at 120°C for 3h.

Table 3: Porous beads produced by freeze-drying with different ratios of anionic CNF and PAE, for two concentrations



Cryogel beads structure as a function of final concentration and PAE/CNF ratio. By observing the effect of the concentration on the ability to form porous beads, it appears that a concentration of 0.1 wt% was not high enough to form consistent spheres. The non-ability to form spheres at low concentration comes from the fact that under a critical concentration the amount of cellulose nanofibrils is not high enough to form a network and results into the loss of the mechanical integrity of the cellulose cryogel beads (Martoia et al. 2016a). However, porous beads have been produced at 0.6 wt% or 1.5 wt%, with porosity values between 98% and 99% (Table 5).

Stability in water. Thanks to PAE cross-linking, the porous beads do not disassemble when soaked in water. The re-dispersion kinetics was evaluated by soaking cryogel beads into water and measuring the swelling behavior of these beads over time. PAE resin is a widely used agent in paper industry for preparing wet strengthened papers (Siqueira 2012). Therefore, it was expected through this test to highlight the effect of the PAE resin on the ability of the cryogel beads to keep their integrity when dipped in water. Figure 7 shows that the swelling behavior of the cryogel beads is composed of three major steps. When the beads are dipped into water they expand quickly until reaching a size

depending on the CNF/PAE ratio. Then, the volume of the CNF beads decreases and finally reaches a plateau where the swelling rate remains stable. After being soaked, the water easily diffused into the cryogel matrix through the pores. Then, shrinkage of the beads occurs resulting in a slow decrease in the slope before reaching a plateau after 3 hours into water. Therefore, the PAE resin is able to keep the integrity of the cryogel beads and plays its role of wet strength agent from 1 wt% to 10 wt%. It can be noticed that the CNF beads containing 2 wt% PAE present the most stable structure into water with a final expansion in volume of only 2%. This particular ratio also corresponds to the higher mechanical properties as explained in the following section.

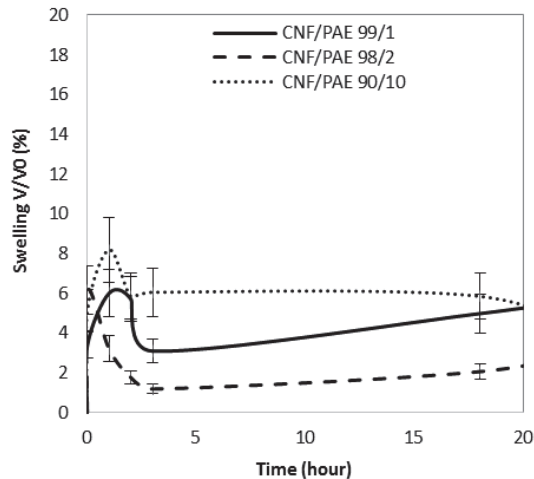


Figure 7: Swelling behavior for the CNF porous beads when dipped into water for 24h. The reference without PAE is not represented as the cryogel beads from anionic CNF are redispersed into water.

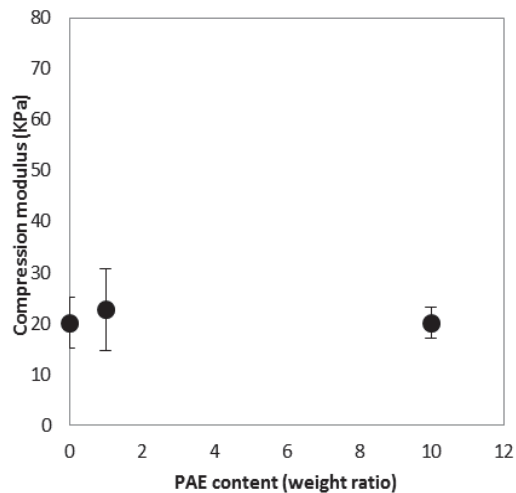


Figure 8: Evaluation of the mechanical properties for the cryogels produced by casting and freeze-drying at a concentration of 0.6 wt%

Mechanical properties. The mechanical properties of the CNF/PAE cryogels at a total concentration of 0.6 wt% have been evaluated through compression test (Figure 8). It should be noticed that the compression tests were actually not carried out on the beads but were performed on model samples obtained by freeze-drying. Lower values than the one obtained for spray-freeze dried cryogels were obtained and this highlights the important effect of the cryogel process on the resulting properties. However, the same compressive storage modulus was obtained whatever the PAE content. This result is not surprising as PAE is known to be a wet strength cross-linker but is rarely investigated for the dry properties. We can nevertheless mention a recent publication which showed that cross-linking of CNF with PAE improves by 150% the dry strength when compared to non-cross-linked CNF films (Sharma and Deng 2016). No other examples were found.

As the better results of stability into water were obtained for 2 wt% PAE, this ratio should be considered as the most promising solution. Furthermore, if too much PAE cross-linker is used, some studies reported non-biodegradable and non-recyclable issues (Su et al. 2012). Thus, it is important to use as small amount of PAE as possible.

As a perspective, experiments could be performed to produce porous beads with lower dimensions. This can be achieved by spraying the CNF/PAE suspension into liquid nitrogen before

freeze-drying. Another possibility is to produce cryogel mattresses and crush them after by cutting mill, as previous experiments have reported that the porosity is preserved. Further experiments are in progress to study the actual cross-linking between PAE and CNFs (FTIR).

Finally, to be completely up-scalable and adaptable in a papermaking process, solutions should be found to produce ultra-porous CNF beads/powders without the use of freeze-drying step, which is highly time- and energy-demanding. A preliminary study was performed in order to find a more sustainable way for cryogel powder production. The principal results as well as the main conclusions are described in **Supporting information 1**. Among the different strategies, only one has led to promising results: introduction of CNF as a middle layer in 25 wt% alcohol and 75 wt% water. However, lower porosity is obtained with this method in comparison with a classical cryogel process and this method requires the use of organic solvent. Some challenges still remain in this part to produce high quantity of CNF cryogels powder with higher porosity and without freeze-drying.

3.4. Conclusions

Cellulose nanofibrils are a complex and heterogeneous material whose properties depend on many factors such as the source, the production process or the surface charge. The structural and mechanical properties of CNF cryogels strongly depend on the CNF quality. It appears that the increase in the duration of the super-grinding treatment favors the decrease of cryogel pore size as demonstrated by BET values, SEM images and thermal insulating properties. Mechanical properties of these cryogels remain in the same range of values for mechanical treatment times from 30 min to 2h30 when compression is performed at ambient humidity, but the increase in CNF disintegration time also increases the sensibility to humidity of the cryogel. Introduction of surface charge using anionic or cationic pretreatment has also led to more homogeneous cryogel structure with smaller pore size. Extremely low values of thermal conductivity have been obtained for cryogel produced with cationic CNF, synonymous of close and meso-pores inside the cryogel. However, as mechanical properties tend to decrease with the decrease in pore size distribution, cationic cryogels present lower compressive modulus than anionic or enzymatic cryogels. Anionic cryogels appear to be the best compromise in terms of homogeneous porous structure and compressive modulus under various humidities. Finally, the use of CNF cryogels has been considered in a papermaking process for the first time. Cross-linking with PAE and grinding lead to porous water-resistant CNF beads, and introduction by spraying as a paper middle layer can be adapted. Next perspective concerns the optimization of water-stable CNF beads production (in term of process and characterization), and the development of a process avoiding the freeze-drying step as reported by preliminary results in supporting information of this document.

4. Introduction of cellulose nanofibril as a paper middle layer: three strategies for crumpling limitation and tear-resistant material

This study is inspired from J. Bras, A. Dufresne, J. Desmaisons, G. Roberty, M. Lutsche, G. Mosele, « Use of nano cellulose to decrease crumpling of paper », patent application in submission

4.1. Introduction

The situation concerning crumpled banknotes is complex. First, the crumpled banknotes can be put back in circulation even if they do not meet the visual quality requirements because of no detection of the defect. Otherwise, crumpling can increase banknotes local thickness and promote packaging and delivery troubles. Indeed, at the end of the sorting machine, fit banknotes are packaged. If the thickness increases, the number of banknote in the packaging is reduced, creating significant economic troubles. Moreover, a phenomenon called “spring effect” can appear, increasing the needed tension to maintain banknotes in their packaging box. Furthermore, crumpling defects can perturb the sorting procedure, resulting in rejected banknote. These rejected banknotes are afterward expensive to treat as they require a manual and individual sorting. Finally, crumpled banknotes in circulation are weakened and wrinkled areas can be easily teared. In the worst cases, a loss of mechanical properties leads to the circulation of limp banknotes.

For these reasons, there is a double challenge associated to crumpled banknotes: (i) develop quantitative methods to characterize the crumpling, and (ii) reduce the crumpling and spring effect phenomena. Such issue is much more studied in the textile field where some methods exist based on artificial crumpling and determination of mechanical properties after crumpling. Chemical cross-linking of cellulose with anti-creasing agent (Frick et al. 1960; Abidi et al. 2007; Lam et al. 2010) is the most popular method for improving the wrinkle resistance of textiles. Satisfactory dimensional stability and crease resistance can be achieved. Today, the most promising formaldehyde-free cross-linking agent for cotton cellulose is 1,2,3,4-butanetetracarboxylic acid (BTCA) (Lam et al. 2010). In paper industry, crumpling is rarely characterized and remains still unknown. Nowadays, some scientists have tried to propose modeling for paper crumpling (Deboeuf et al. 2013; Narain et al. 2013; Habibi et al. 2017), and some companies are trying to reduce this phenomenon, especially in security paper applications. For example, a recent patent proposes the use of a polymeric binder for wrinkle-resistant papers (Sarrazin and Security 2012). National bureau of standards (Carson and Merle 1946) described a device and a method allowing to crumple a paper with reproducibility. This procedure (used by central banks) is followed by visual classification with different categories of crumpled banknotes from acceptable banknotes to limp banknotes. During our study, a quantitative method based on image analysis has been proposed to replace such qualitative analysis.

Cellulose nanofibrils (CNFs) present some interesting properties with respect to papermaking, such as a high aspect ratio, a large specific surface area, and the ability to form a cross-linked network with pseudo-plastic behavior already in very dilute aqueous suspensions (Petroudy et al. 2017). Today, paper and board industry represents 21% of nanocellulose market and is the second area of application behind composites (Future Markets, Inc 2017). However, this interest for nanocellulose in paper industry is very recent in terms of publications and patents (Bardet and Bras 2014; Brodin et al. 2014). The opportunity to develop new breakthrough in papermaking industry is still attractive whatever their use as additives in bulk or coating formula or as 100% coating or middle layer formula. The use of CNF has emerged especially thanks to their outstanding potential in increasing wet and dry strength, decreasing the paper porosity and improving barrier properties (Taipale et al. 2010; Hassan et al. 2011; González et al. 2012; Aspler et al. 2013). Thanks to these particular properties, the use of CNF has been reported in food packaging (Abdul Khalil et al. 2016), in transparent and conductive papers (Razaq et al. 2011; Hu et al. 2013), in paper for flexible electronic device (Zheng et al. 2013) and recently in banknote (Le Berre et al. 2015). However, up to our knowledge, the correlation between CNF and crumpling resistance has never been reported. That is why the first part of this study will focus on the ability of CNF as a paper middle layer to form a strong and flexible network and limit the apparition of crumpling (Figure 1, strategy 1).

To obtain an efficient final product, it is important that the introduction of CNF, in favor of a gain of crumpling, does not reduce the other banknote mechanical properties. Especially, it is known that the tear strength is inversely correlated with high tensile strength and dense materials (Wistara and Young 1999). The nano-dimensions and large hydrogen bonding of CNF lead to extremely cohesive and dense layers. These properties are used for the creation of transparent films with good barrier properties, but have the counterpart to strongly affect the tear strength (See **Chapter III.2.**). To take advantage of the mechanical properties of the CNFs while guarantee good tear resistance properties, two other strategies have been considered. The second part of this study will focus on the addition of polyethylene terephthalate (PET) in the CNF layer (Figure 1, strategy 2) or in the use of CNF in a porous form ("CNF cryogel") mixed with the classical CNF suspension (Figure 1, strategy 3). The use of PET microfibers with high mechanical properties is already well known for its crumpling resistance in textile and tissue engineering (McAdam and McClelland 2002; Wei et al. 2007). The efficiency of PET as additive in hybrid nanopapers has already been proved regarding crumpling and tear resistance (See **Chapter III.2.**). On the other hand, the use of CNF cryogel whose porosity ranges from 50 to 99.9% could achieve the same increase of air/solid interfaces while avoiding the use of inorganic filler. It is worth noting that the use of CNF cryogel in a papermaking process has never been considered due to the difficulty for up-scaling its preparation process and the extremely brittle structure of this material. However, another part of this manuscript has been dedicated to the production of CNF beads stable in water and efficient for spraying in a papermachine (See **chapter III.3.**). These CNF porous beads will be now used in this multilayer application, mixed with the CNF suspension with different ratios.

Consequently, this study proposes three strategies (shown in Figure 1) to limit paper crumpling by using cellulose nanofibrils. Some results of this work have been used for a patent application (in submission process).

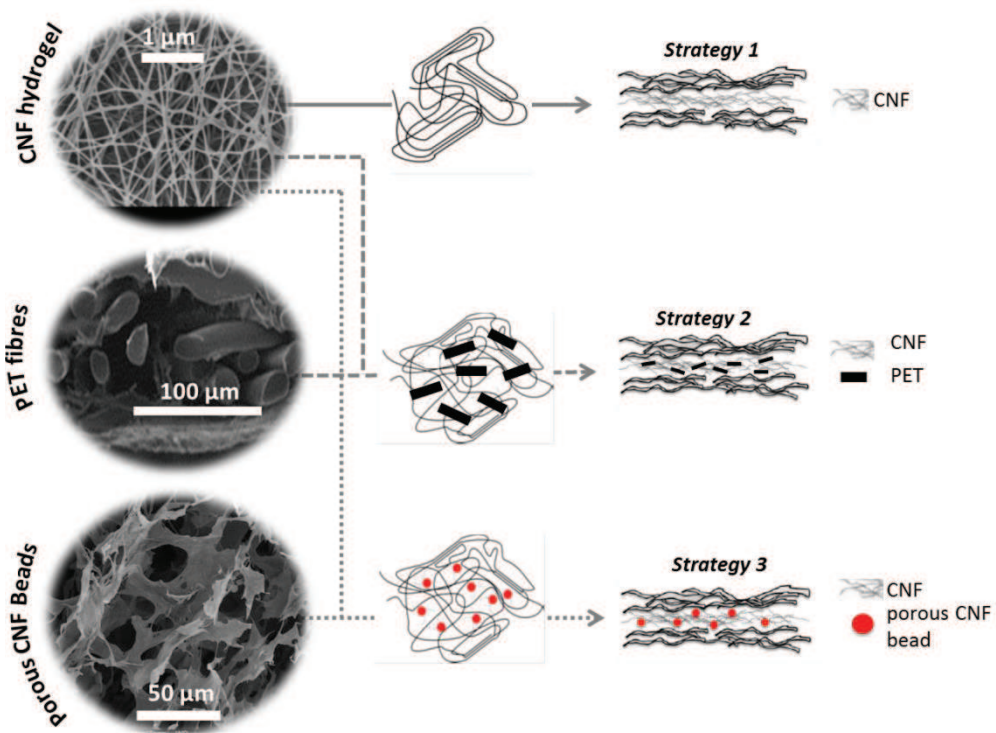


Figure 1: Three strategies for obtain crumpling resistant paper thanks to the introduction of a CNF layer inside two fiber layers

4.2. Materials and methods

4.2.1. Materials

Nanocellulosic material. Commercial CNFs (“Com-CNF”) were purchased from the Pulp and Paper Research and Technical Center (CTP), Grenoble, France. They are produced from bisulfite Domsjö pulp (softwood) after enzymatic pretreatment (using a cellulase solution mainly composed of endoglucanase), one pass at 1000 bar followed by 4 passes at 1500 bar in a Homogenizer. The CNF suspension was delivered at 2% w/w concentration and has a hemicellulose content of 5%. CNF have also been produced from eucalyptus (“Euca-CNF”) after a refining step to 65 SR°, a similar enzymatic pretreatment and an ultrafine friction grinder supermasscolloider (Model MKZA6-2, Disk model MKG-C 80, Masuko Sangyo Co., Ltd, Japan). The detail protocols are described below. Two functionalized CNF were also used: a TEMPO-oxidized CNF suspension (“Anionic CNF”), bought from Betulium (Espoo, Finland) with an initial concentration of 4.8 wt% and a charge content (carboxylic content) of 1274 $\mu\text{mol/g}$, and a cationic CNF suspension (“Cationic CNF”), with a charge content (quaternary ammonium content) of 930 $\mu\text{mol/g}$, whose protocol has been described in **Chapter III.2.**

Pulps. All the laboratory tests on dynamical handsheet former were performed with eucalyptus pulp, purchased as dry kraft pulp from Cenibra, Brazil, with a hemicellulose content of 15%. If no other precision, this pulp was refined at 65 °SR. Cotton pulp for pilot tests has been kindly supplied at a 3.4 wt% concentration and at 65 °SR by a company (confidential, France).

Others. Polyethylene terephthalate (PET) microfibers with a diameter of 15 μm and cut to a length of 6 mm were kindly supplied by Alhstrom Brignoux (Dacron®, type 205NSD). The Dtex of these synthetic fibers is 1.7. Acetic acid (ACS reagent, >99.7%), Sodium acetate trihydrate (ReagentPlus®, >99.7%) were bought from Sigma Aldrich. FiberCare® Cellulase (4890 ECU/g) was kindly supplied by Novozymes. Other additives were tested for this work but results will not be presented: Titanium dioxide PRETIOX (grade AVO1L, anatase, PRECOLOR), Glass fibers (Saint Gobain, 5 μm +/- 2.9 diameter) and Glass beads (1mm diameter, Dutsher). 4,4'-distyrylbiphenyl sodium sulfonate salt (DSPB) was supplied by Tinopal CBS, BASF, Germany.

4.2.2. Methods

Eucalyptus pulp refining. The eucalyptus pulp was plunged for 48 hours in water and vigorously mixed with a Lhomargy system for 10 minutes. The refining step was then performed with a PFI mill apparatus (Beater PFI, NPFI-02 model, Techlab system), following the standard ISO 5264-2. A pulp sample of 30 g at 10 w% consistency was beaten between a roll with 33 bars and the smooth interior of the hammer configurable number of rotations. The two fiber layers constitutive of the multilayer were refined at 65 °SR.

Enzymatic treatment. The enzymatic treatment was performed with FiberCare® Cellulase 4890 ECU/g enzyme solution, with a ratio of 300 ECU/g cellulose, and diluted to 13% in deionized water.

This protocol is already described in **Chapter III.2. Experimental part, preparation and characterization of cellulose nanofibrils.**

Masuko treatment. After refining and enzymatic treatment, the pretreated fibers were passed through an ultrafine friction grinder (Model MKZA6-2, Disk model MKG-C 80, Masuko Sangyo Co., Ltd, Japan) working at 2500 rpm, in recirculation for 2.5 h, to obtain the CNF suspension (“Euca-CNF”). The final quality index of the suspension was 75 (See **Chapter III.1.**). Samples were also recovered every 30 min to follow the evolution of the suspension properties. These samples with lower mechanical treatment time were only used in Figure 8.

Preparation of multilayered papers. Multilayer papers have been prepared with a dynamic sheet former (EP Meca, France), consisting in spraying the fibrous suspension into a drum rotating at 1100 tour/min. The pump was fixed at 600 rpm. All the suspensions were diluted to 0.1 wt% before being projected through the flume. First, a wall of water was created on the rotating drum, and the first layer of refined eucalyptus fiber (65 °SR, 25 g/m²) was projected on this water to allow a more homogeneous repartition of the pulp. Then, a second layer of refined eucalyptus fibers (65 °SR, 60 g/m²) was projected. Finally, a scooping time of 30 seconds was applied to remove the water. The paper was then dried between two blotter papers and under constraint by contact with a hot cylinder for 10 minutes at 105°C. The final dimensions of the sheet are 88 cm x 22 cm and this bilayer composed of two layers of refined eucalyptus constitutes the reference material. The same protocol has been applied for the three-layer materials, with spraying of first a 20 g/m² of refined fibers, then a 5 g/m² of CNF with different quality indexes and with or without additives, and finally the 60 g/m² layer of refined fibers. All the dried papers were stored for at least 48 hours in conditioned room at 23°C and 50% RH before testing.

Mixture of CNF with PET. For the multilayer containing PET as additive, commercial CNF (Com-CNF) was mixed with PET fibers with 90:10, 80:20 and 60:40 weight ratios respectively. These mixtures were diluted to 0.1 wt% and stirred with a mechanical mixing for 2 hours before being sprayed as a layer of 5 g/m², following the previously described protocol .

Porous CNF beads and introduction in multilayer. Cryogels were prepared using 1 wt% aqueous suspensions of commercial CNF (Anionic CNF from Betulium®, 1274 µmol.g⁻¹) that has been cross-linked with a weight CNF/PAE ratio at 98/3 as protocol described in **Chapter III.3.**. The initial suspension was mixed 10 seconds with an Ultra-turrax to make sure that all nanofibrils were well dispersed. Then, CNF was cast into molds 3 cm in diameter and 2 cm height and dipped into liquid nitrogen until the suspension was completely frozen. Finally, the different suspensions were put into the freeze-dryer for 3 days under the following conditions: pressure inside the chamber of 1 mBar and a temperature of -20°C. After that the prepared CNF cryogels were put into a cutting mill (Reitsh®, SM 100) for 2 hours in order to obtain porous powders. The sieve used was a Reitsh® reference 10241485, with a hole width of 0.75 mm. This material has been fully characterized in a previous study (See **Chapter III.3.**). The powder was then mixed with CNF suspension in different

ratios, or used alone, and diluted at 0.1 wt%. The mixing was performed with a magnetic stirrer for 30 minutes. The suspension was then directly sprayed in the dynamic handsheet former.

Quality Index. The CNF suspensions were characterized according to the Quality Index method (**See Chapter III.1.**). Com-CNF corresponds to “CNF-9” of this publication. CNF prepared from eucalyptus correspond to the “high hemicellulose content” CNF, and the different quality indexes from this pulp were obtained for different time of mechanical treatments, corresponding to the different specific energy consumptions.

Grafting of CNF with a fluorescent agent. CNFs were grafted with a fluorescent agent (Tinopal CBS, BASF, Germany). This fluorescent agent is a 27 wt% solution of 4,4'-distyrylbiphenyl sodium sulfonate salt (DSPB) with a molar weight of 562 g/mol. For 15 g dry content of Com-CNF, a solution was prepared by diluting 0.250 g of pure DSPB solution into 45 g of water. Then, 0.5 g of this diluted solution was added to 0.1 wt% CNF suspension, and the mixture was stirred for 15 minutes in a flask wrapped in aluminum foil. The suspension has then been put in dialysis for one week against distilled water.

Optical microscopy in fluorescent mode. Paper slices of multilayers containing fluorescent CNF were cut with a razor blade and analyzed under optical microscope (Zeiss Actio Imager M1M, camera MRC5). DSPB absorbs in the UV spectral range (absorption wavelength: 351 nm) and emit strong blue fluorescence (emission wavelength: 425 nm). The fluorescence source (X-cite serie 120) was used in reflection mode. The reflector has been chosen for an excitation wavelength ranging between 325 and 375 nm. Images were analyzed using softwares AxioVision Release 4.8 and ImageJ and the most representative were selected.

Scanning Electron Microscopy (SEM). SEM was performed on paper slices and surfaces after gold sputter coating of 5nm, with a tension of 10 keV, a spot size of 3.5, in EDT mode. The working distance was fixed at 10 mm. At least 6 images were taken in slices and surfaces areas, and the most representatives were selected.

X-ray Nanotomography. This protocol is extracted from (Krasnoshlyk 2017). The X-ray source of 3SR laboratory (Hamamatsu Corporation L8121-03) sealed with a source tension between 40 and 150 kV and a current between 0 and 500 μ A was used. This source generates a polychromatic conic X-ray beam. The detector is a flat-panel (Varian PaxScan[®] 2520V) that measures the intensity of incident X-ray photons on an array of 1536x1920 pixels in either landscape or portrait modes. The distance between the X-ray source, the rotation axis and the detector defines the effective used pixel size, which was chosen to be 0.7 μ m. The reconstruction software DigiCT version 2.4.2 from Digisens was used. Quantitative image analysis of the paper structure were performed on the binarised images, to identify fiber and pore phases. For that, the grey level images were converted into black and white images by thresholding operation on ImageJ software. The critical value of thresholding was manually selected based on visual assessment.

Porosity and thickness measurement based on X-ray images. This method provides a quantitative analysis of the local thickness and porosity variation in thickness direction in paper samples. The analysis was performed on the binarised 3D X-ray images. Moreover, the binarised images were cropped in order to remove the clamps from the images. Those images were used to obtain the local thickness and porosity maps using a code developed in Matlab and fully explained in a recent PhD study (Krasnoshlyk 2017).

ANOVA test (statistical analysis). This statistical analysis was performed using Minitab software. An “Anova test with 1 factor” has been used to identify if the differences between the populations (here, crumpling values of different multilayers) are statistically significant. The null hypothesis has been defined as “there are no significant differences between the different multilayers”. The significance threshold has been defined at 0.05, indicating a risk of 5% that the model goes wrong.

Tear resistance. The tear resistance was measured by a tear tester (Noviprofiber, Elmendorf pendulum 16000 mN, France). Samples were cut at (65 × 50) mm² dimensions, and the measurement corresponds to the force (mN) needed for the tear propagation after a primer. At least 10 repeats were performed on samples beforehand conditioned in controlled room for 48 hours (23°C, 50% RH) and average was calculated.

4.2.3. Crumpling characterizations

NBS method. A crumpling device has been developed by the National Bureau of Standards (NBS). The NBS crumpling device consists in an apparatus for rolling the paper sample and a device in which the rolled paper is crumpled under a certain speed of compaction: 200 mm/min, 5 kN (Figure 2). In the usual procedure, there are four repetitions of this step, with rotation of 90° of the paper between each step (NBSx4). Tests have also been performed by only compressing one time the rolled paper (NBS x1). All the samples were conditioned at 23° C and 50 % RH for at least 48 hours before testing. The exact steps of crumpling are presented in supplementary data 2.

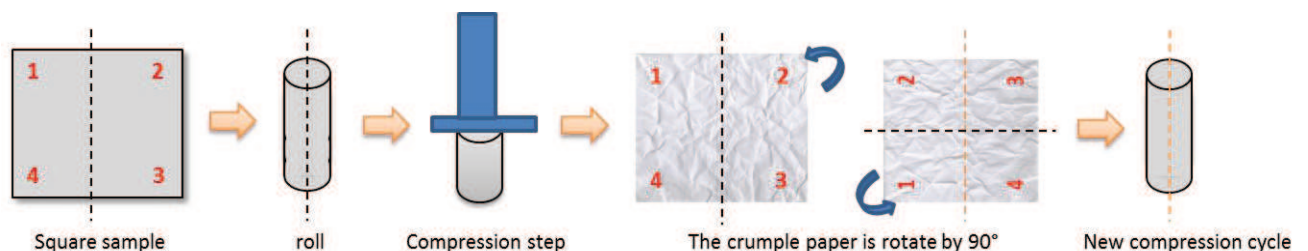


Figure 2: NBS method for artificial crumpling

Balloon test. The balloon test was developed by ECB and has been carried out at the Den Norske Bank (DNB), Amsterdam. Square samples (6.7x6.7 cm²) were cut. In a typical measurement, a dry

sample was carefully placed in a balloon made out of thick rubber, without creasing the sample, and the balloon was thereafter inflated and deflated rapidly in a controlled and automatic manner with custom-built apparatus to mimic hand crumpling (Figure 3). 15 cycles of inflating/deflating were performed after which the sample was carefully removed and kept without further manual handling. Seven duplicates were performed for each sample. The crumpling has then been quantified using image analysis.

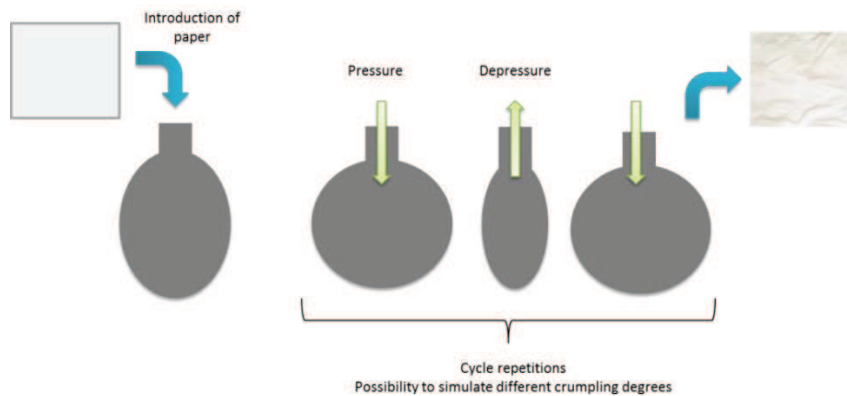


Figure 3: Balloon test method for artificial crumpling

Image analysis of crumpled papers. The image analysis was inspired by Arjowiggins security method (Sarrazin, 2012). First, square samples of 6.7 * 6.7 cm were created with the pre-mentioned methods (NBS or balloon test). Then, high-resolution images were taken of the crumpled samples and analyzed following this procedure:

- Lighting of the sample with raking light (LED source), set at 2 cm of the sample edge
- Sample photography with a digital camera (PENTAX) at 25 cm from the sample. Resolution of photography: 72 dpi.
- Analysis of the photography with ImageJ software. The image was first converted into 8 bit corresponding to 256 gray levels. Then, an operation of thresholding at 64 was performed. This thresholding converts into "0" (white color) all pixels having a value lower than 64 and to "255" (black color) the pixels having a higher value (Figure 4-B). The number of white and black pixels has been measured with "Analysis-Histogram" mode of ImageJ. Finally, the crumpling value (%) was obtained by dividing the quantity of black pixels by the quantity of white pixels. It is worth noting that lower crumpling values are linked to higher crumpling resistance, and the purpose of this work is consequently to decrease the crumpling value.

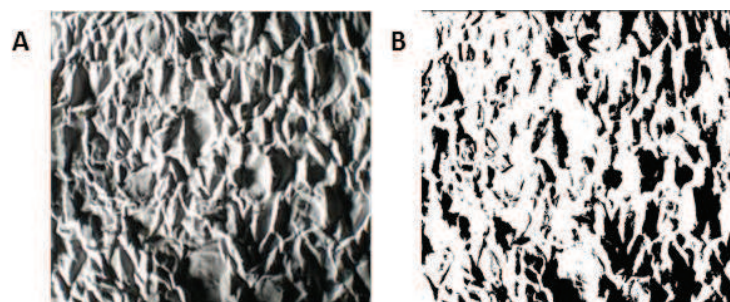


Figure 4: Crumpled paper A) before thresholding and B) after thresholding

Spring-effect. A spring-effect can be observed on stacked crumpled banknotes and has been measured as follow. First, 10 crumpled papers (crumpled with NBS x4) were stacked on a dynamic mechanical analysis device (DMA). The compression jaws of the DMA were then brought closer until the detection of a positive and non-zero pressure. The thickness of these 10 layers was directly measured as the gap between the DMA jaws and corresponds to “thickness before compression (mm)”, e_{bc} . Then, a pressure of 10 N (1 kg) was applied on the crumpled layers, the thickness of the layers under the constraint was read as distance between the jaws and corresponds to “thickness after compression (mm)”, e_{ac} . The spring effect was calculated as the difference between thickness before compression and after compression: Spring effect (mm) = $e_{bc} - e_{ac}$. At least 5 duplicate were produced.

Surface topography. Topographic measurements were carried out on the laser device 3Dstick sensor (Centre technique du papier, Grenoble, France). The principle is based on laser triangulation: the projected laser line is deformed by the relief of the object. Then, the profile was reconstituted by the camera. By moving the laser, it is possible to reconstitute a topographical model of the object. Waviness profiles have been extracted using the image analysis on Gwyddion software.

4.3. Results and discussion

Part I. Influence of a CNF layer in the paper crumpling mechanism

4.3.1. Material configuration and modeling of CNF layer inside the material

At lab scale, multilayers were produced using a dynamical handsheet former. Multilayers were also produced in Banque de France pilot machine, by incorporating a spray of cellulose nanofibrils within the two fiber layers produced by round-shape formers. Figure 5A show the theoretical structure of the material. Because of their nano-dimensions, the retention of cellulose nanofibrils in papermaking is generally limited and is difficult to control, which can then result in inefficient applications (Ridgway and Gane 2012; Afra et al. 2016). For this reason, it is important to check the real structure of the material, which can be a multilayer with three distinct layers (as expected) or a composite with CNF dispersed in the bulk material.

To get an idea of the CNF retention during the pilot tests (2015), the consumption of CNF in the spray device has been calculated. As expected, $4.8 \pm 0.2 \text{ g.m}^{-2}$ of the suspension has been consumed. In the meantime, a CNF layer of only $3.8 \pm 0.2 \text{ g.m}^{-2}$ has been measured on the final paper. We consequently know that almost 1 g.m^{-2} of the CNF has not been retained by the fibrous material. Indeed, a fibrous material, even refined, constitutes an open structure and the nano-part of the CNF suspension can easily go through or been lost by spray process. During lab tests, differences in basis weight with and without CNF layers allowed us to have similar conclusion as $3.7 \pm 0.9 \text{ g.m}^{-2}$ of CNF were present in the final paper.

To localize the CNFs inside the paper, several tests have been performed with mitigated success. SEM pictures of paper slices did not allow detecting the presence of CNF (Figure 5B). CNFs have then been grafted with a fluorescent agent and look under fluorescent light under optical microscopy (Figure 5C). In this case, the observation of the paper slice showed that CNFs are well concentrated in an intermediate layer and are not dispersed in the whole material. To obtain more precise information, nanotomography tests have been performed on these multilayers with a resolution (pixel size) of $0.7 \mu\text{m}$ (Figure 5D). Variation of porosity inside the paper as a function of the thickness has also been extracted from the nanotomography pictures (Figure 5E and F). Results were disappointing and did not show a decrease of porosity which would be induced by a CNF layer, as it was successfully achieved by Charfeddine (Charfeddine 2016). Furthermore, images extracted did not allow making differences between fiber fibrillation due to refining and cellulose nanofibrils. Consequently, only the microscope images combined with the calculation of CNF content inside the material allow us to conclude on a multilayer structure.

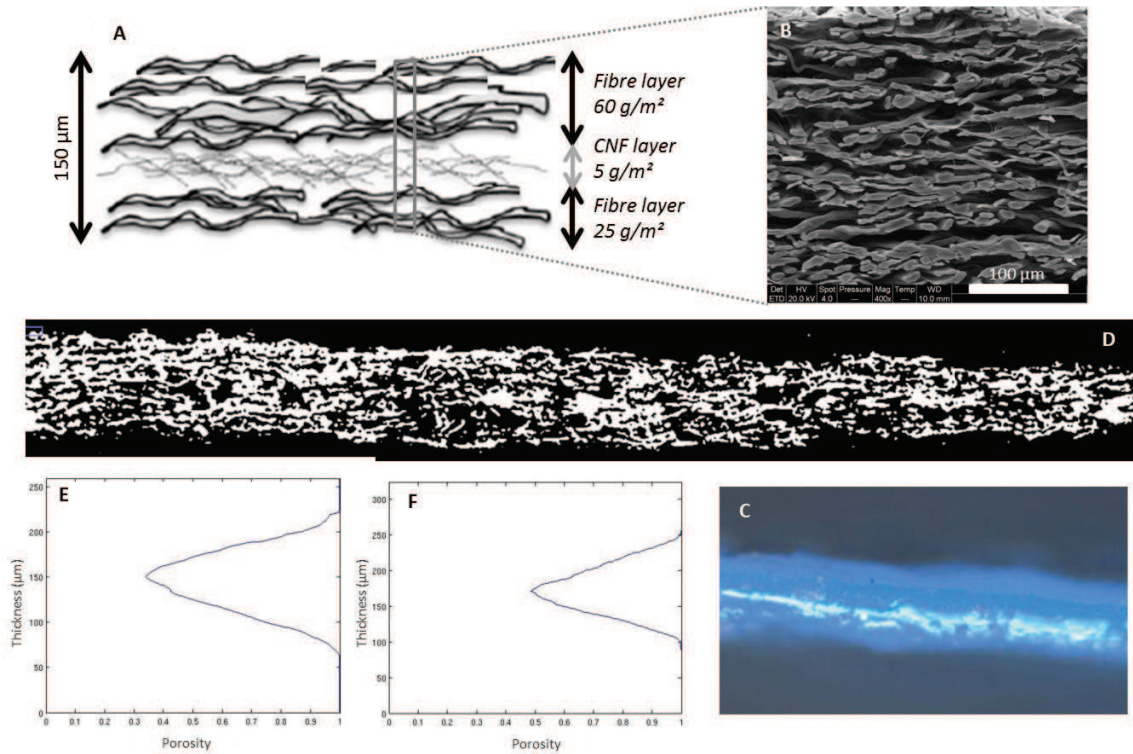


Figure 5: A) Preparation of the multilayer of analysis of the paper containing the CNF layer with B) SEM picture C) Optical microscopy and D) Nanotomography, and porosity profile as a function of the thickness for E) the reference bilayer and F) the multilayer with CNF

4.3.2. Interest of a CNF layer for crumpling limitation (strategy 1)

If the mass insertion of CNF has recently emerged from industries in bulk or coating applications, the correlation with crumpling resistance has never been studied in the literature. The interest of cellulose nanofibrils for crumpling deformation has consequently to be proved. Crumpling is a complex phenomenon involving plastic deformations, self-avoiding interactions and jamming effects (Ben Amar and Pomeau 1997) and whose explanations and modeling divide the scientific community (Habibi et al. 2017). Indeed, all these effects are very difficult to disentangle (Deboeuf et al. 2013; Habibi et al. 2017) and identifying the key parameters involved in crumpling deformation is already a source of debate. For example, some researchers suggest that the material properties have only a minor effect on crumpling (Balankin et al. 2007) and that key parameters are the finite bending rigidity and the self-avoidance property. In another hand, other researchers argue that crumpling can be visualized as successive events of folding (Deboeuf et al. 2013) and, as the folding behavior is strongly correlated to the material mechanical properties, it can be expected that a change in the material mechanical properties will also change the crumpling resistance. This last explanation has been favored in our study and the idea to associate CNF with crumpling resistance rose from the expectation that this strong and flexible network with impressive mechanical properties could

undergo the deformation without create damages on the paper. Supporting information reports explanations on crumpling protocols that will be used in the following section.

Influence of fiber defibrillation

The reference paper was composed of two fiber layers. Then, a third layer was added composed of fibers with different degrees of defibrillation. These different degrees of defibrillation were obtained by changing the time of high-shearing mechanical treatment, and resulting materials (from poorly defibrillated fibers to high quality CNF) were characterized using the Quality Index method (Desmaisons et al. 2017). Increasing the time of mechanical treatment increased the content of nanoscale material in the suspension and the resulting quality index. Figure 6 shows the crumpling values (NBS method) and spring-effect of multilayers as a function of the quality index of the intermediate layer. For a quality index from 16 (refined fiber without super-grinding treatment) to 54 (30 min of super-grinding treatment), same values of crumpling were obtained, meaning that there is no influence of poor defibrillation on crumpling. However, after this point, the crumpling value of the multilayer dramatically decreased. The crumpling was hence reduced by 18% with a quality index of 67, and the best values of crumpling resistance were obtained for CNF with a quality index between 68 and 74. Indeed, multilayer produced with a layer of CNF with a Q.I. of 68 reached a crumpling value of $35 \pm 4 \%$, against $51 \pm 8 \%$ for the refined fibers without super-grinding treatment. Exactly same trends were obtained for a crumpling with Balloon test instead of NBS, meaning that these results are not dependent on the crumpling process. Results converged toward a minimal quality index of 68 for the best impact of CNF on multilayer crumpling resistance. From this point and for all the following results, the CNF from eucalyptus were used with a super-grinding time treatment of 2h30, corresponding to a quality index of 75 ± 6 .

The spring effect gives another point of view of the crumpling phenomena, as it is dependent on the crumpling pattern but also on the paper stiffness after crumpling. Indeed, when a paper is crumpled, the interlaced fibers are disturbed, the bonds are loosened, and the structure becomes less compact. This loss of compaction and decrease of stiffness lead to a spring effect which is a real issue during the banknote package step at the end of the sorting machines. Results show that the increase of CNF quality index strongly decreases the spring-effect.

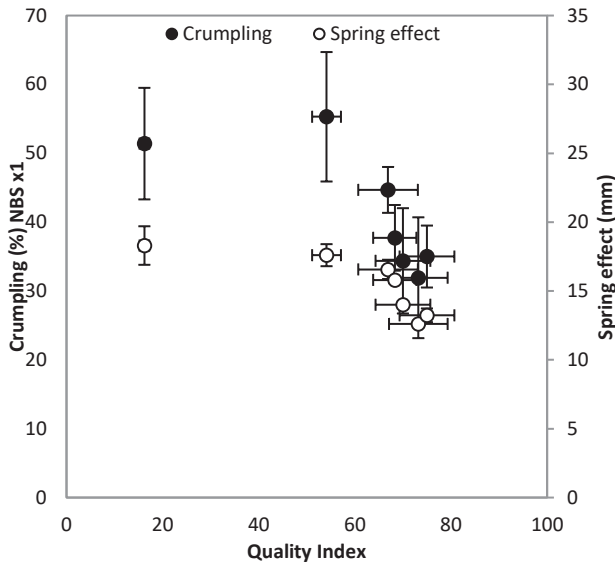


Figure 6: Crumpling (NBS x1) and spring effect of multilayers containing a layer of defibrillated eucalyptus fibers with different quality index

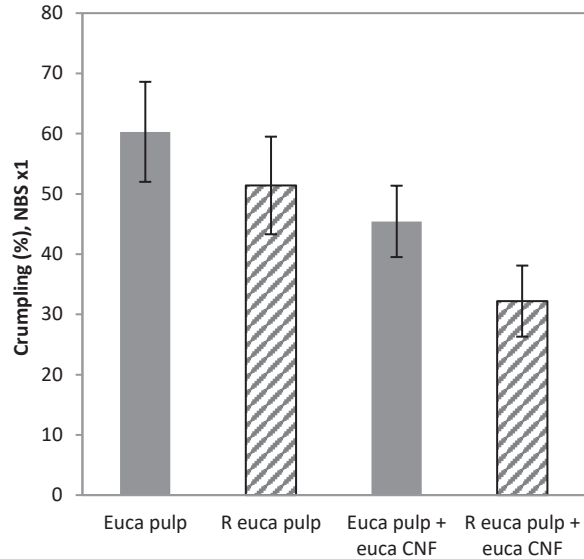


Figure 7: Crumpling value of multilayers composed of two layers of eucalyptus pulp (Euca pulp), two layers of refined eucalyptus pulp (R euca pulp), and these same multilayers with the addition of a CNF layer (Q.I. : 75)

If the use of CNF in the papermaking process is recent, the fiber defibrillation has been used for many times through refining process. This process results in fibers with lower size, swelled, fibrillated and hydrated. It is interesting to see in Figure 7 that the refining of external fiber layers (65 SR°) already play a role in decreasing the bilayer crumpling ability. This effect is strongly reinforced thanks to the addition of the CNF layer by passing from 51.4% to 32.3% of crumpling values.

Influence of CNF layer position

After this first very positive configuration, multilayers were produced by changing the expected localization of the intermediate layer. In the classical procedure, 5 g.m⁻² CNF layer are introduced between two fiber layers of 25 g.m⁻² and 60 g.m⁻². Two other configurations have been tested with reduction of this asymmetry: the CNF layer was introduced between two fiber layers of 50 g.m⁻² and 35 g.m⁻², and at the middle of the paper (between two fiber layers of 42.5 g.m⁻²). This change has induced different paper crumpling properties (Figure 8). The most the paper is asymmetric, the better is the crumpling resistance, with a decrease of crumpling by 30% between the classical configuration vs the CNF layer at the middle of the paper. Indeed, the asymmetry increases the stiffness of one side of the paper which avoids crumpling. This is in accordance with composite materials theories which proved that the bending and shear stiffness of material made from layers of several materials increases (i) with higher thickness of the layers having a higher elastic modulus and, more interesting, (ii) with higher distance from the neutral axis (Garuckas and Bareisis 2003). Exactly same trends have been observed for other intensity of crumpling (NBS x4 and balloon test). The fact that the change of expected location of CNF actually changes the paper crumpling resistance also confirms the theory of a multilayer material.

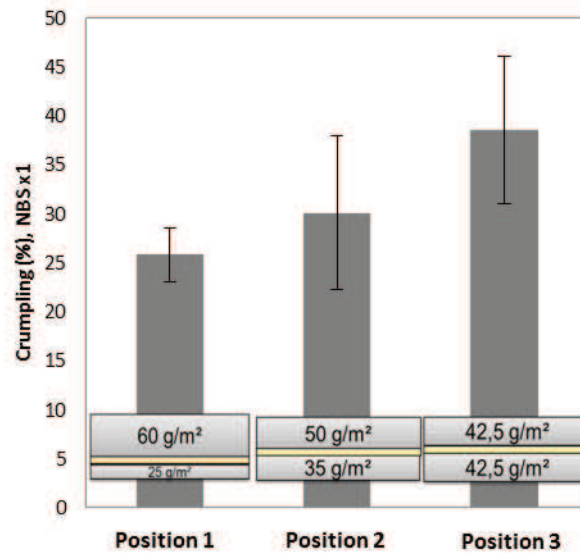


Figure 8: Multilayers prepared with different localization of the 5g/m² CNF layer

Influence of CNF source

It is well known that cellulose nanofibril properties strongly depend on the disintegration process, and in a second way on the biomass source (Nechyporchuk et al. 2016). Previous results (Figure 6) showed the influence of the mechanical treatment intensity for CNF from a same source (eucalyptus). Figure 9, in another hand, compare multilayers with CNF produced from different source and different mechanical treatment device: CNF produced from kraft pulp of eucalyptus (hardwood) by ultrafine grinding and a commercial CNF material produced from bisulphite pulp of spruce (softwood) and by homogenizer. This figure also shows the results for different crumpling processes: NBS x1, NBS x4, and balloon test. Whatever the crumpling method, a strong decrease of crumpling value was obtained thanks to the addition of the Eucalyptus-CNF layer, and the crumpling resistance is almost doubled. However, different results were obtained with the commercial CNF from softwood. In this last case, the increase of crumpling resistance was only observed for the balloon test crumpling and NBSx1, corresponding to the lightest crumpling intensities.

These two CNF suspensions have similar quality index: 72 ± 3 for the commercial source and 75 ± 6 for the CNF produced from eucalyptus, meaning that they have similar global morphological and physical properties. However, the CNFs were extracted from different sources, one hardwood and the other one softwood, meaning that they own different hemicellulose contents. The hemicellulose content for CNF from eucalyptus is 19% while the hemicellulose content for CNF from softwood is 5%. This hemicellulose content seems to play a positive key role in the crumpling resistance of the CNF network. Furthermore, in the same way as it exists a minimal force to create a fold (**Chapter II.3.**), it also exists a minimal force to create a crumpling pattern. This force is a power law dependence on the size of the crumpled object (which is a fixed parameter in our case), with a crumpling exponent depending on material properties (which change with the CNF introduction), but

also on compaction protocol and self-avoidance constraints (Deboeuf et al. 2013; Habibi et al. 2017). It is consequently normal that changing the compaction protocol lead to different results.

Despite the fact that better results were obtained with CNF produced from eucalyptus, the commercial CNF presents the advantage to strongly decrease the crumpling from the balloon test which is the most representative of the manual handling of banknotes. Furthermore, the spring effect is decreased whatever the CNF source, which is a positive conclusion and means that the improvement of crumpling resistance is not only based on the visual pattern but also on the layer rigidity.

The introduction of CNF had also the purpose to increase mechanical properties with a special attention to the tear resistance. Indeed, CNF films are well known for their poor tear properties due to their low porosity structure. Tear resistance of the multilayers have consequently been tested (Figure 9). The introduction of a commercial-CNF layer effectively decreases significantly the tear resistance of the material. To reach the same value as the reference bilayer and even gain additional tear resistance, another strategy consists in the reduction of the CNF layer density by decreasing CNF interaction with additives or by introduction of porous beads of CNF. These strategies will be reported in another part.

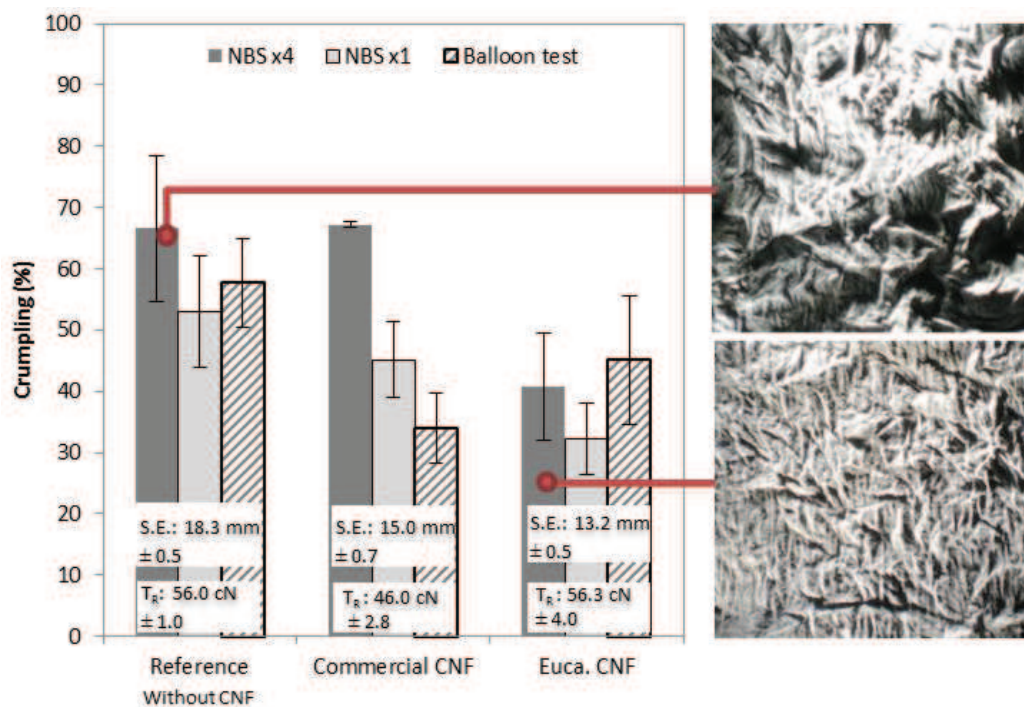


Figure 9: Multilayer made with an intermediate layer of commercial CNF or CNF produced from eucalyptus
Reference = bilayer, Tr = tear resistance, S.E. = spring effect

Influence of CNF functionalization

To check the influence of surface chemistry on resulting paper crumpling, two chemical pretreatments were tested: the grafting of anionic or cationic charge on the CNF surface. No

significant improvement of multilayer crumpling resistance was observed between introduction of classical CNFs and modified CNFs. Crumpling values of $32.2\% \pm 5.9$, $32.3\% \pm 5.0$ and $28.1\% \pm 7.2$ were obtained for respectively enzymatic CNF, anionic CNF and cationic CNF. Worst, the tear resistance has decreased. If we compare the dimensions of enzymatic nanofibrils vs grafted cellulose nanofibrils, the last ones present lower average length and average width. This decrease in dimensions is synonym of higher specific surface, and higher H-bonding. The presence of charge also improves the dispersion in water. It results in more cohesive network and damages the tear properties. As the paper crumpling is not improved thanks to chemical pretreatment on CNF and the paper tear resistance is decreased, this strategy will not be chosen for next experiments.

Statistical analysis

A lot of tests have been performed and still high standard deviations were obtained, with sometimes questions about repeatability. A statistical analysis of variance (ANOVA test) has been performed for all crumpling values to understand if the middle layer significantly influences the crumpling resistance. Three populations have been tested: reference bilayers (without CNF), multilayers with a commercial layer of CNF, and multilayers with a layer of CNF produced from refined eucalyptus. Two hypotheses were proposed: 1) there is no significant influence of the middle layer (“null hypothesis”) and 2) there is a significant influence of the middle layer (“alternative hypothesis”). The ANOVA test gives us three interesting parameters: the critical value F (value from which it is possible to refute the null hypothesis), the F value, and the probability P (which should be lower to 0.5 to refute the null hypothesis). The F value obtained was 16.0 for a critical value of 3.2, meaning that it is possible to refute the null hypothesis. Furthermore, a probability value of 0.00001 was obtained, which is far below the 0.5 limit. All these parameters combined, it is possible to conclude that the alternative hypothesis is true: there is a statistical and significant influence of the middle layer.

Conclusion

As a final experiment, a crumpling pattern has been designed by depositing diluted (0.02 wt%) refined eucalyptus fibers or cellulose nanofibrils produced from eucalyptus in a shrinkable polystyrene substrate (Figure 10). The substrate has then been shrunken in an isothermal vacuum oven at 135°C for 15 minutes. Different crumpling patterns were formed. In the case of the fiber layer, large and high peaks are formed while the structure with the CNF layer remains flatter and small peaks are formed. This last test combined with the previous results proves that, whatever the intensity of crumpling, a CNF network is more efficient than a fiber network to take up the stress and present lower visual deformations. When introduced in a paper, CNF with a quality index higher than 68 promotes a decrease of crumpling value up to 40%. As a consequence, the spring effect brought by the stack of crumpled banknote also decreases. However, the crumpling phenomenon strongly depends on the material properties (CNF source) and protocol of crumpling (NBSx1, NBSx4, or Balloon test). The use of CNF produced from eucalyptus has given satisfying results for all intensities of crumpling, while the use of commercial CNF has shown a strong decrease in crumpling only with

the Balloon test. Commercial CNFs are nonetheless interesting as (i) they have good results with the most representative test for banknote crumpling and (ii) they present the advantage to be commercially available with a local and high-scale production. That is why commercial CNF have been used for the following part.

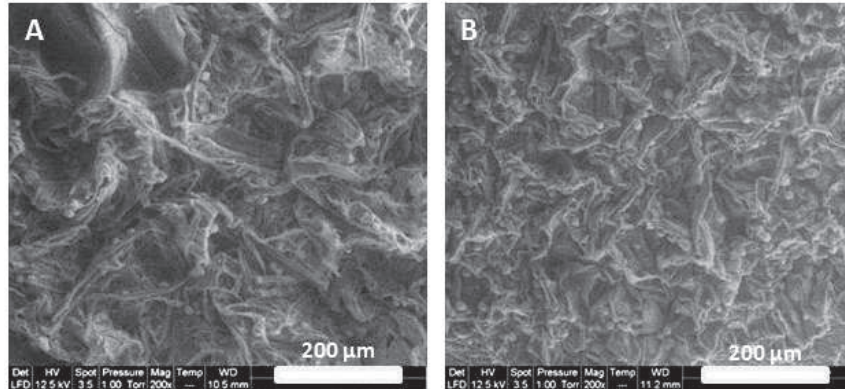


Figure 10: Crumpled pattern of shrunken PS substrate after deposition of A) Refined eucalyptus fibers and B) Cellulose nanofibrils from eucalyptus. SEM picture, low vacuum conditions.

Part II. Use of PET fiber or porous CNF beads to combine crumpling resistance and high tear resistance

The interesting impact of CNFs for paper crumpling limitation allow considering this nanomaterial for new potential applications in security paper or food packaging industry whose handling tend to damage the materials. Such positive result has been considered for patent application. However, a daily handled material (such as a banknote) is also a material which suffers from tear. The next part has reported that the successful increase of crumpling resistance with insertion of CNF in the paper is to the detriment of tear resistance. This part proposes two other strategies to keep (or increase) the crumpling resistance brought by the CNF network while increasing the paper tear resistance.

Only few researchers have studied the influence of CNF in paper tear resistance. Petroudy et al. have shown a favorable effect on tear resistance with the addition of less than 5 wt% CNF mixed with softwood pulp and an inverse effect from 5 to 10 wt% CNF. These results suggest that the role of CNF may include aspects of both conventional reinforcement and bonding agent. However, it is known that the increase of inter-fiber bonding sometimes can decrease the amount of energy dissipated during tearing of the paper (Wistara and Young 1999). The well bonded papers transmit applied stress directly to the propagation point of a tear so that the paper tears more easily. In our case, the multilayer structure is the worst scenario as it is not only creating additional bonding with fibers but it also creates a highly dense zone which could act as a weak area for tear propagation. Furthermore, the eucalyptus fibers are already strongly refined and do not suffer from a lack of bonding. When the degree of bonding is already high, the tear resistance is mostly determined by the fiber strength (Levlin 1998), and in this case the problem is that, due to the low dimensions, individual CNFs are more easily ruptured than individual fibers.

Two strategies have raised for keeping the crumpling resistance while increasing the tear resistance. The first one consists in adding synthetic fibers (PET) to (i) decrease the CNF layer cohesion and (ii) introduce micrometric fibers harder to pull out during tear. The other strategy consists in playing on CNF layer density without introduction of any additive.

4.3.3. Mixture of CNF with additives for CNF-bonding reduction (strategy 2)

Influence of PET additive in the CNF layer for crumpling and tear resistance.

PET microfibers were mixed with commercial CNF in different ratios. These mixtures containing both PET and CNF were then sprayed in the dynamical handsheet former between two fiber layers to produce a multilayer. Table 1 shows that the introduction of PET tends to decrease the crumpling value whatever the crumpling method. The lower crumpling value was obtained for the multilayer containing 5 g.m⁻² of 10 wt% PET-90wt-% CNF, and crumpling pattern difference is visible in Figure 11. Introduction of 10 wt% or 20 wt% PET in the CNF network also resulted in a strong

decrease in the spring effect. Finally, by looking at the tear resistance values which was the first targeted property, it appears that 10 wt-% PET was enough to make up the loss of tear strength brought by the CNF layer, and 20 wt-% PET strongly increased this property. However, there is an optimum value between 10 and 20% PET above which increasing the amount of PET is unfavorable for both crumpling, spring effect and tear resistance.

Table 1: Crumpling, spring effect and tear resistance of multilayers produced with a layer containing CNF and different ratios of PET

Multilayer	Crumpling			Spring effect (mm)	Tear resistance (cN)
	NBSx1	NBSx4	Balloon test		
Reference bilayer	53.0 ± 9.0	66.6 ± 11.9	57.7 ± 7.5	18.3 ± 0.5	56.0 ± 1.0
Wt-% content of PET in CNF layer					
0	45.1 ± 6.2	67.2 ± 0.5	33.4 ± 7.5	15.0 ± 0.7	46.0 ± 2.8
10	37.9 ± 5.5	37.1 ± 8.1	26.7 ± 11.5	8.4 ± 0.2	60.1 ± 1.8
20	41.0 ± 5.3	49.3 ± 5.2	21.3 ± 9.3	8.8 ± 0.2	69.4 ± 2.6
40	44.9 ± 7.0	31.1 ± 9.4	25.1 ± 7.4	13.8 ± 0.5	64.2 ± 1.9

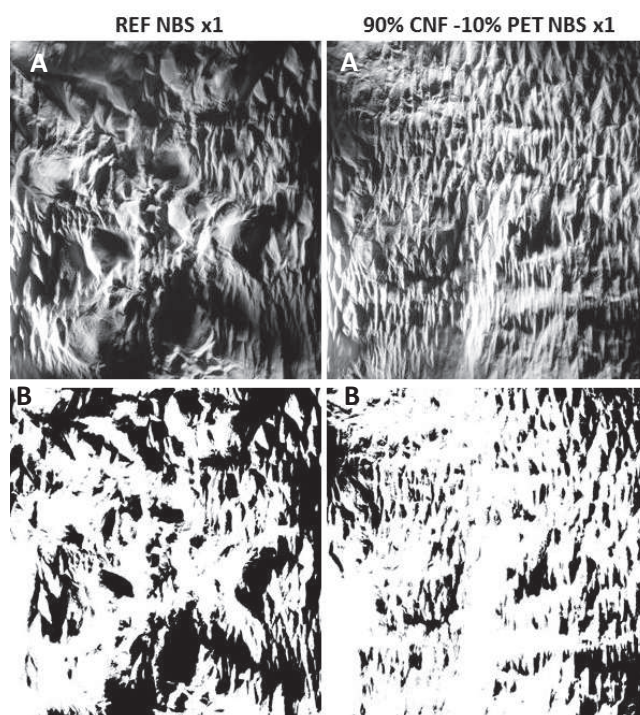


Figure 11: Crumpling images of reference bilayer of fibers and of multilayer containing a 5 g.m⁻² layer composed of 90 wt% CNF and 10 wt% PET, after A) binarisation and B) thresholding. Crumpling: NBSx1

Similar conclusions were observed in **Chapter III.2.**, which investigated the influence of PET in crumpling and tear resistance properties of hybrid nanopapers. It has been explained in this chapter that tear resistance in fibrous material depends on the total number of fibers participating in the

tear, the strength of the individual fibers and the number and strength of the fiber-fiber joints (Brandon 1981). Furthermore, the tear mechanisms principally involves two phenomena: pulling fibers out of the material or rupturing the fibers (Hassan et al. 2015), and the first phenomenon is preponderant on the second. Introduction of long and thick PET microfibers in the CNF matrix resulted in the formation of a network of strong and long fibers with an individual fiber width on the μm scale within the brittle network of nanofibrils. The first probable failure across the tear crack of this hybrid network is fiber pull-out due to the strength of the individual PET fibers and the weak bonding between PET and CNF. Because of the length of the PET fibers this requires a lot of energy which results in an increased tear resistance. Furthermore, structural analysis performed in the same work showed that introduction of PET fibers tends to decrease the cohesion of the CNF network and hence to increase the porosity. This increase in porosity, until an optimum point, can also play a role in limitation of tear propagation as it increases the number of solid/air interfaces and contributes to limit the tear propagation.

Furthermore, the presence of a large aromatic ring in the PET repeating unit gives the polymer notable stiffness and strength. This stiffness makes PET microfibers highly resistant to deformation, and they especially impart excellent resistance to crumpling in fabrics, that is why they are particularly used in industry with other fibers such as cotton to reinforce the inherent properties of these fibers while contributing to the ability of the fabric to recover from crumpling (Encyclopaedia Britannica, Inc. 2018).

However, above an optimum point between 10 wt% PET and 20 wt% PET, increasing the PET content damages both crumpling spring-effect and tear resistance. Indeed, a higher ratio of synthetic fibers, which does not form any bond with the CNFs, decreases the layer cohesion in such a way that there is an important loss of mechanical properties.

Conclusion.

The multilayer tear resistance has successfully been increased thanks to the mixing of 10% PET fibers with the CNF suspension, balancing the loss in tear strength induced by the CNF layer alone. This improvement can be linked to the individual strength and micrometric dimensions of PET synthetic fibers, and in a second time to the decrease in the CNF layer cohesion. Furthermore, stiff PET fibers have contributed to increase the crumpling resistance and the spring effect due to their high resistance to crumpling deformation. This method is fast and easily reproducible. However it requires the use of inorganic and synthetic filler. The next strategy consists in looking for an increase in layer porosity in order to increase the tear resistance, but by using exclusively CNF. For this reason, the CNF suspension will be mixed with porous CNF beads, or CNF “cryogels”.

4.3.4. Introduction of porous CNF beads in a paper middle layer for crumpling limitation in tear resistance (strategy 3)

The use of CNF as a porous material was investigated to decrease the layer cohesion and density responsible for tear propagation. Cross-linked CNF cryogels were beforehand produced by pouring the suspension into liquid nitrogen and sublimating water with a freeze-dryer. The cryogels were then crushed with knife milling to obtain porous CNF powder with porosity higher than 98%. Details on this porous powder are given in a previous study (See chapter III.3.). This powder was then mixed with CNF suspension in different ratios before spraying or directly sprayed in the multilayer.

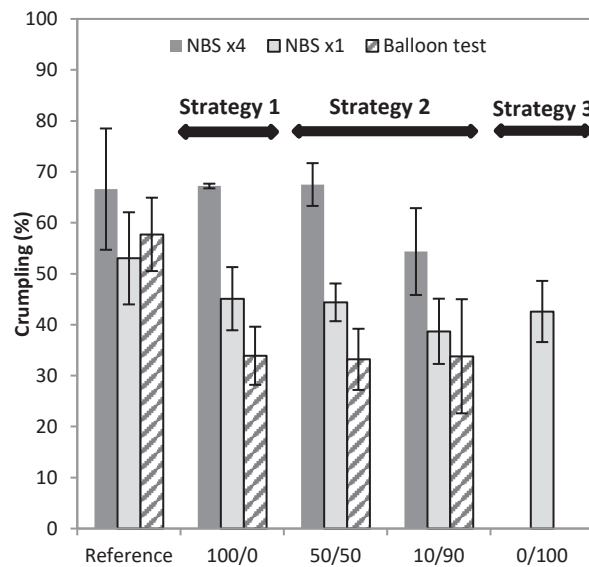


Figure 12: Crumpling of paper multilayers. The reference is composed of two fiber layers and the other samples have a CNF layer with various amount of porous CNF beads, CNF suspension/porous CNF powder

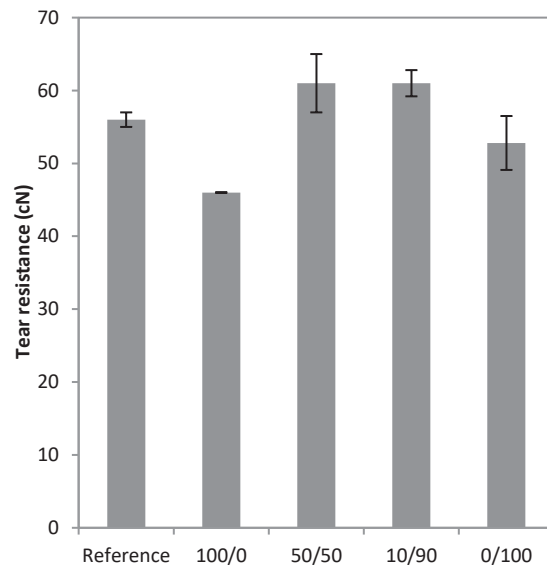


Figure 13: Tear resistance of paper multilayers. The reference is composed of two fiber layers and the other samples have a CNF layer with various amount of porous CNF beads, CNF/CNF beads

Different interpretations can be extracted from Figure 12 regarding the crumpling intensity. Taking the strongest crumpling (NBS x4) as baseline, corresponding to a repeated crumpling, the addition of CNF suspension (ratio 100/0) was not sufficient to obtain better crumpling resistance. However, if 10 wt% of CNF is mixed with 90 wt% CNF porous beads, a significant decrease is observed. This ratio also allows a slight decrease of the first crumpling pattern obtained with NBSx1. Regarding the Balloon test, satisfying results were already obtained with the classical spraying of CNF suspension and addition of CNF under porous form gives similar results. We can consequently conclude that the replacement of part of CNF suspension by porous CNF beads does not change the crumpling value for light intensity tests (NBS x1 and balloon test) and slightly increases the crumpling resistance for strong intensity test (NBS x4). No significant differences were obtained for spring-effect of multilayer containing CNF alone or with porous CNF beads.

On the other hand, the replacement of part of the CNF suspension by porous CNF beads has slightly contributed to increase the tear resistance value (Figure 13). The loss of tear strength

unfortunately brought by the CNF layer has been replaced by a slight gain as the tear resistance passed from $56.0 \text{ cN} \pm 1.0$ to $61.0 \text{ cN} \pm 1.8$ with a ratio 90/10 of CNF porous beads/CNF suspension. As a conclusion, if we compare with the reference bilayer, introducing a 5 g.m^{-2} layer composed of 10 wt% porous CNF beads and 90 wt% CNF represents an interesting solution to improve the crumpling properties whatever the crumpling intensity, while keeping (and even increasing) the tear resistance value of the paper, and avoiding the use of inorganic filler (Figure 14).

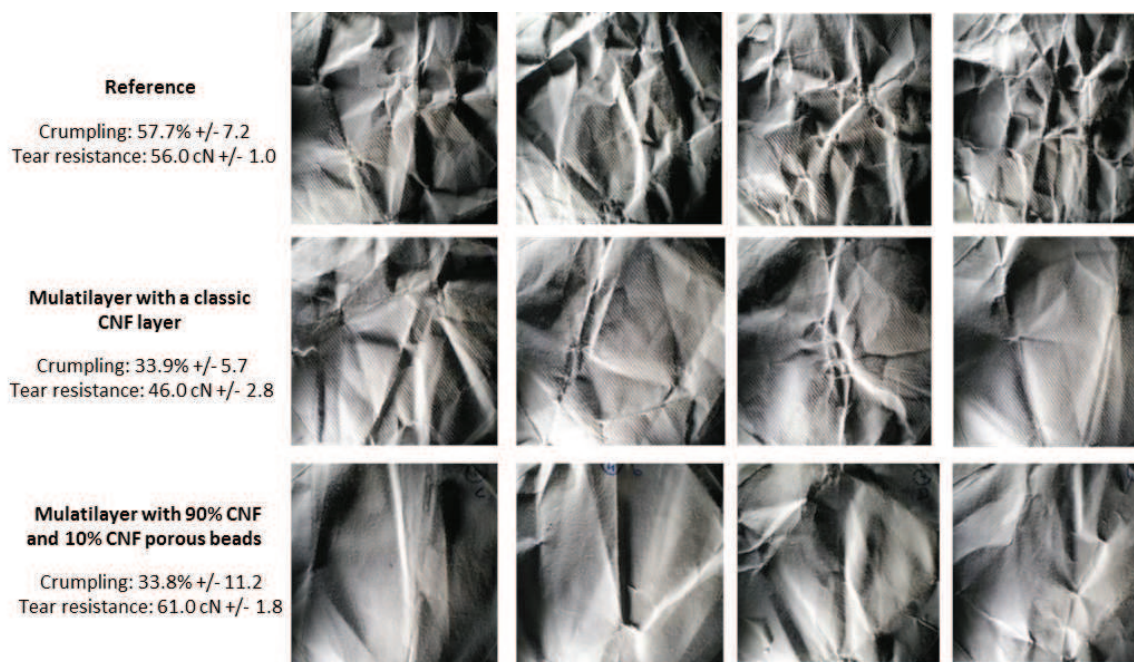


Figure 14: Crumpling images of multilayers with 4 duplicates by sample (crumpling with Balloon test)

CNF cryogels in literature are mainly produced under the form of porous mat for applications such as acoustic or thermal insulation (Thapliyal and Singh 2014; Jiménez-Saelices et al. 2017) or filtering medium for biomedical applications (Stergar and Maver 2016) and it is the first time that cryogels are considered for crumpling limitation in a papermaking process. However, the use of such a mat would be incompatible with a paper-making process as complex and time-consuming steps of freezing and drying are required. That is the reason why Chapter III.2. proposed different solution to produce CNF porous beads, stable in water in order to be sprayed in a papermaking process, and without the use of freeze-drying process. This strategy is innovative and proposes a biobased solution without resorting to synthetic additives. However, the production of porous CNF beads requires still some time and optimization. In parallel, the use of PET as additive is easy and fast to implement. Furthermore, for an intermediate layer composed by 90 wt% CNF and 10 wt% PET, the multilayer show the same increase in tear resistance than with porous beads and higher crumpling resistance for each crumpling intensity.

4.4. Conclusions

Paper crumpling has been characterized following different procedures, allowing to reproduce different intensities of crumpling and different behaviors, from the creation of the crumpling pattern (NBS x1), to a gentle and manual handling (Balloon test), until strong duplications of crumpling with high paper damage (NBS x4). The topography of the crumpling pattern has been studied thanks to image analysis, and the loss in mechanical properties brought by the loose of fiber bonds during crumpling has also been characterized through the spring effect, which is an important issue for banknote crumpling. Insertion of a CNF layer inside the two fiber layers constitutive of an original banknote has successfully managed to decrease the crumpling value up to 40% and the spring effect as synthesized in Table 2. However, key factors have been identified such as CNF quality index, CNF source, surface chemistry and location within the multilayer.

Furthermore, the presence of this highly cohesive network and high bonding between CNF and fibers have created a narrower zone of breakage for tear propagation instead of a distribution of the tearing event over a relatively large area within the multilayer. To compensate this loss in tear resistance, other strategies have been implemented. Mixing of CNF with 10 wt-% PET has succeeded in compensating the loss of tear resistance, and the final multilayer paper even presents higher tear strength. Furthermore, the use of this flexible fiber well known for its resistance to crumpling deformation has positively contributed to decrease the crumpling and spring effect of the multilayers. This strategy is also particularly interesting as it decreases the amount of expensive CNF for replacement by cheaper PET fibers. The final strategy has considered the use of a 100% cellulosic material, playing only with the material structure. As such, the CNF suspension was mixed with porous CNF beads obtained by freeze-drying and crushing. The same increase than PET additive was obtained for a layer containing 10 wt-% suspension CNF and 90wt% of porous CNF beads.

Table 2: Synthesis of results regarding crumpling limitation as a function of the three strategies considered. *NBS x4, euca CNF

Influence of ...	Best result	Advantage	Drawback
CNF from eucalyptus or commercial CNF (Strategy 1)	CNF from eucalyptus produced with super-grinding Minimal Q.I. : 68	Decrease in crumpling up to 40%* Decrease in spring effect by 28% Confirmation with statistical study (ANOVA)	Variation as a function of the crumpling protocol Decrease in tear resistance
CNF layer position	Asymmetrical position (usual)	x	x
CNF pretreatment	Enzymatic CNF (usual)	x	x
Mix of CNF with PET (strategy 2)	10% PET – 90% CNF	Strong additional decrease in crumpling (NBS x1, NBS x4 and balloon test) Decrease in spring effect by 55% Increase of tear resistance up to 60.1 cN +/- 1.8	Use of inorganic filler
Mix of CNF with porous CNF beads (strategy 3)	10% CNF – 90% porous CNF beads	Additional decrease in crumpling (NBS x4) Increase in tear resistance up to 61.0 cN +/- 1.8	Additional steps for the production of porous CNF beads

Final perspectives would be to use porous CNF beads without freeze-drying step and better control the stability of their porous structure when they are sprayed into water, as described in **Chapter III.3.** Pilot tests have been conducted in Banque De France with spraying of a CNF layer inside the two classical layers of a banknote papers (**See Chapter IV.1.**). Industrial tests are still in discussion and would give the opportunity to test the introduction of a CNF/PET layer.

References

- Abdul Khalil HPS, Davoudpour Y, Saurabh CK, et al (2016) A review on nanocellulosic fibres as new material for sustainable packaging: Process and applications. *Renew Sustain Energy Rev* 64:823–836. doi: 10.1016/j.rser.2016.06.072
- Abdul Khalil HPS, Davoudpour, Y., Islam, M. N., Mustapha, A., Sudesh, K., Dungani, R., & Jawaid, M. (2014). Production and modification of nanofibrillated cellulose using various mechanical processes: A review. *Carbohydrate Polymers*, 99, 649–665. <https://doi.org/10.1016/j.carbpol.2013.08.069>
- Abe, K., Iwamoto, S., & Yano, H. (2007). Obtaining cellulose nanofibres with a uniform width of 15 nm from wood. *Biomacromolecules*, 8(10), 3276–3278. doi: 10.1021/bm700624p
- Abidi N, Hequet E, Tarimala S (2007) Functionalization of Cotton Fabric with Vinyltrimethoxysilane. *Text Res J* 77:668–674. doi: 10.1177/0040517507080621
- Afra E, Mohammadnejad S, Saraeyan A (2016) Cellulose nanofibils as coating material and its effects on paper properties. *Prog Org Coat* 101:455–460. doi: 10.1016/j.porgcoat.2016.09.018
- Ahola S, Österberg M, Laine J (2007) Cellulose nanofibrils—adsorption with poly(amideamine) epichlorohydrin studied by QCM-D and application as a paper strength additive. *Cellulose* 15:303–314. doi: 10.1007/s10570-007-9167-3
- Aspler J, Bouchard J, Hamad W, et al (2013) Review of Nanocellulosic Products and Their Applications. In: Dufresne A, Thomas S, Pothen LA (eds) *Biopolymer Nanocomposites*. John Wiley & Sons, Inc., Hoboken, NJ, USA, pp 461–508. ISBN: 978-1-118-60995-8
- Balankin AS, Silva IC, Martínez OA, Huerta OS (2007) Scaling properties of randomly folded plastic sheets. *Phys Rev E* 75:051117. doi: 10.1103/PhysRevE.75.051117
- Balea, A., Merayo, N., De La Fuente, E., Negro, C., & Blanco, Á. (2017). Assessing the influence of refining, bleaching and TEMPO-mediated oxidation on the production of more sustainable cellulose nanofibres and their application as paper additives. *Industrial Crops and Products*, 97: 374–387. doi: 10.1016/j.indcrop.2016.12.050
- Bardet R, Reverdy C, Belgacem N, et al (2015) Substitution of nanoclay in high gas barrier films of cellulose nanofibrils with cellulose nanocrystals and thermal treatment. *Cellulose* 22:1227–1241. doi: 10.1007/s10570-015-0547-9
- Bardet, R., & Bras, J. (2014). Cellulose Nanofibres and Their Use in Paper Industry. In *Handbook of Green Materials* (pp. 207–232). World Scientific.
- Ben Amar M, Pomeau Y (1997) Crumpled paper. *Proc R Soc Math Phys Eng Sci* 453:729–755. doi: 10.1098/rspa.1997.0041
- Benhamou, K., Dufresne, A., Magnin, A., Mortha, G., & Kaddami, H. (2014). Control of size and viscoelastic properties of nanofibrillated cellulose from palm tree by varying the TEMPO-mediated oxidation time. *Carbohydrate Polymers*, 99, 74–83.
- Benítez AJ, Torres-Rendon J, Poutanen M, Walther A (2013) Humidity and Multiscale Structure Govern Mechanical Properties and Deformation Modes in Films of Native Cellulose Nanofibrils. *Biomacromolecules* 14:4497–4506. doi: 10.1021/bm401451m
- Benítez AJ, Walther A (2017) Cellulose nanofibril nanopapers and bioinspired nanocomposites: a review to understand the mechanical property space. *J Mater Chem A* 5:16003–16024. doi: 10.1039/C7TA02006F
- Besbes, I., Vilar, M. R., & Boufi, S. (2011). Nanofibrillated cellulose from alfa, eucalyptus and pine fibres: preparation, characteristics and reinforcing potential. *Carbohydrate Polymers*, 86(3), 1198–1206. doi: 10.1016/j.carbpol.2011.06.015

Chapter III References

- Binks BP (2002) Particles as surfactants—similarities and differences. *Curr Opin Colloid Interface Sci* 7:21–41. doi: 10.1016/S1359-0294(02)00008-0
- Brandon CE (1981) Properties of paper. In: Casey, J.P. (Ed.), *Pulp and paper, chemistry and Chemical Technology*, vol. 3. Wiley-VCH Verlag GmbH & Co, pp. 1715-1972. Casey, J.P. (Ed.), Weinheim
- Brodin FW, Gregersen OW, Syverud K (2014) Cellulose nanofibrils: Challenges and possibilities as a paper additive or coating material—A review. *Nord Pulp Pap Res J* 29:156–166. doi: 10.3183/NPPRJ-2014-29-01-p156-166
- Brucato A (1986) Method of making paper having improved tearing strength. Brooks Rand Ltd, US4609432A
- Buchtová N, Budtova T (2016) Cellulose aero-, cryo- and xerogels: towards understanding of morphology control. *Cellulose* 23:2585–2595. doi: 10.1007/s10570-016-0960-8
- Carrillo, C. A., Laine, J., & Rojas, O. J. (2014). Microemulsion systems for fibre deconstruction into cellulose nanofibrils. *ACS Applied Materials & Interfaces*, 6(24), 22622–22627. doi: 10.1021/am5067332
- Carson F. T., Merle B. Shaw (1946) Wearing quality of experimental currency-type papers. 36:256–257 National Bureau of Standard – US department of Commerce
- Cervin NT, Andersson L, Ng JBS, et al (2013b) Lightweight and strong cellulose materials made from aqueous foams stabilized by nanofibrillated cellulose. *Biomacromolecules* 14:503–511. doi: 10.1021/bm301755u
- Chaker, A., Alila, S., Mutjé, P., Vilar, M. R., & Boufi, S. (2013). Key role of the hemicellulose content and the cell morphology on the nanofibrillation effectiveness of cellulose pulps. *Cellulose*, 20(6), 2863–2875. doi: 10.1007/s10570-013-0036-y
- Charfeddine (2016) 3D synchrotron X-ray microtomography for paper structure characterization of z-structured paper by introducing micro nanofibrillated cellulose. *Nord Pulp Pap Res J* 31:219–224. doi: 10.3183/NPPRJ-2016-31-02-p219-224
- Cheng, Q., Wang, S., Rials, T. G., & Lee, S.-H. (2007). Physical and mechanical properties of polyvinyl alcohol and polypropylene composite materials reinforced with fibril aggregates isolated from regenerated cellulose fibres. *Cellulose*, 14(6), 593–602. doi: 10.1007/s10570-007-9141-0
- Chinga-Carrasco, G. (2013). Optical methods for the quantification of the fibrillation degree of bleached MFC materials. *Micron*, 48, 42–48. doi: 10.1016/j.micron.2013.02.005
- De France KJ, Hoare T, Cranston ED (2017) Review of Hydrogels and Aerogels Containing Nanocellulose. *Chem Mater* 29:4609–4631. doi: 10.1021/acs.chemmater.7b00531
- Deboeuf S, Katzav E, Boudaoud A, et al (2013) Comparative Study of Crumpling and Folding of Thin Sheets. *Phys Rev Lett* 110:104301. doi: 10.1103/PhysRevLett.110.104301
- Desmaisons J, Boutonnet E, Rueff M, et al (2017) A new quality index for benchmarking of different cellulose nanofibrils. *Carbohydr Polym* 174:318–329. doi: 10.1016/j.carbpol.2017.06.032
- Djafari Petroudy SR, Rasooly Garmaroody E, Rudi H (2017) Oriented Cellulose Nanopaper (OCNP) based on bagasse cellulose nanofibrils. *Carbohydr Polym* 157:1883–1891. doi: 10.1016/j.carbpol.2016.11.074
- Dotti F, Varesano A, Montarsolo A, et al (2007) Electrospun Porous Mats for High Efficiency Filtration. *J Ind Text* 37:151–162. doi: 10.1177/1528083707078133
- Dufresne A (2017) *Nanocellulose: From Nature to High Performance Tailored Materials* (Boston/Berlin). Walter de Gruyter GmbH & Co KG. Second edition.

Chapter III References

- Dufresne, A., Cavaille, J.-Y., Vignon, M. R., & others. (1997). Mechanical behavior of sheets prepared from sugar beet cellulose microfibrils. *Journal of Applied Polymer Science*, 64(6), 1185–1194. doi: 10.1002/(SICI)1097-4628(19970509)64:6
- Encyclopaedia Britannica, Inc. (2018) Polyethylene terephthalate, chemical compound
- Erlandsson J, López Durán V, Granberg H, et al (2016) Macro- and mesoporous nanocellulose beads for use in energy storage devices. *Appl Mater Today* 5:246–254. doi: 10.1016/j.apmt.2016.09.008
- Eronen, P., Laine, J., Ruokolainen, J., & Österberg, M. (2012). Comparison of multilayer formation between different cellulose nanofibrils and cationic polymers. *Journal of Colloid and Interface Science*, 373(1), 84–93. doi: 10.1016/j.jcis.2011.09.028
- Fischer F, Rigacci A, Pirard R, et al (2006) Cellulose-based aerogels. *Polymer* 47:7636–7645. doi: 10.1016/j.polymer.2006.09.004
- Frick JG, Andrews BK, Reid JD (1960) Effects of cross-linkage in wrinkle-resistant cotton fabrics. *Text Res J* 30:495–504. doi: 10.1177/004051756003000704
- Fukuzumi H, Saito T, Iwata T, et al (2009) Transparent and High Gas Barrier Films of Cellulose Nanofibres Prepared by TEMPO-Mediated Oxidation. *Biomacromolecules* 10:162–165. doi: 10.1021/bm801065u
- Future Markets, Inc (2017) The Global Market for Nanocellulose 2017-2027
- García, A., Labidi, J., Belgacem, M. N., & Bras, J. (2017). The nanocellulose biorefinery: woody versus herbaceous agricultural wastes for NCC production. *Cellulose*, 24(2):693-704. doi: 10.1007/s10570-016-1144-2
- García, O., Torres, A. L., Colom, J. F., Pastor, F. I. J., Díaz, P., & Vidal, T. (2002). Effect of cellulase-assisted refining on the properties of dried and never-dried eucalyptus pulp. *Cellulose*, 9(2), 115–125. doi: 10.1023/A:1020191622764
- Garuckas D, Bareisis J (2003) Influence of Different Factors on the Stiffness and Strength of Multilayer Composite Elements. *Mech Compos Mater* 39:153–164. doi: 10.1023/A:1023413529598
- Gesser HD, Goswami PC (1989) Aerogels and related porous materials. *Chem Rev* 89:765–788. doi: 10.1021/cr00094a003
- Gharehkhani, S., Sadeghinezhad, E., Kazi, S. N., Yarmand, H., Badarudin, A., Safaei, M. R., & Zubir, M. N. M. (2015). Basic effects of pulp refining on fibre properties—A review. *Carbohydrate Polymers*, 115, 785–803. doi: 10.1016/j.carbpol.2014.08.047
- González I, Alcalà M, Chinga-Carrasco G, et al (2014) From paper to nanopaper: evolution of mechanical and physical properties. *Cellulose* 21:2599–2609. doi: 10.1007/s10570-014-0341-0
- González I, Boufi S, Pèlach MA, et al (2012) Nanofibrillated cellulose as paper additive in eucalyptus pulps. *BioResources* 7:5167–5180. doi: 10.15376/biores.7.4.5167-5180
- Gotoh K, Kikuchi S (2005) Improvement of wettability and detergency of polymeric materials by excimer UV treatment. *Colloid Polym Sci* 283:1356–1360. doi: 10.1007/s00396-005-1308-3
- Haapala, A., Laitinen, O., Karinkanta, P., Liimatainen, H., & Niinimäki, J. (2013). Optical characterisation of size, shape and fibrillarity from microfibrillar and microcrystalline cellulose, and fine ground wood powder fractions. *Appita Journal* 66(4), 331-339. ISSN: 1038-6807
- Habibi M, Adda-Bedia M, Bonn D (2017) Effect of the material properties on the crumpling of a thin sheet. *Soft Matter* 13:4029–4034. doi: 10.1039/C6SM02817A

Chapter III References

- Habibi, Y. (2014). Key advances in the chemical modification of nanocelluloses. *Chem. Soc. Rev.*, 43(5), 1519–1542. <https://doi.org/10.1039/C3CS60204D>
- Hasani, M., Cranston, E. D., Westman, G., & Gray, D. G. (2008). Cationic surface functionalization of cellulose nanocrystals. *Soft Matter*, 4(11), 2238–2244. doi: 10.1039/B806789A
- Hassan EA, Hassan ML, Oksman K (2011) Improving Bagasse Pulp Paper Sheet Properties with Microfibrillated Cellulose Isolated from Xylanase-Treated Bagasse. *Wood Fibre Sci* 43:76–82. doi: 10.1177/0021998312453189
- Hassan ML, Bras J, Mauret E, et al (2015) Palm rachis microfibrillated cellulose and oxidized-microfibrillated cellulose for improving paper sheets properties of unbeaten softwood and bagasse pulps. *Ind Crops Prod* 64:9–15. doi: 10.1016/j.indcrop.2014.11.004
- Hassan ML, Mathew AP, Hassan EA, et al (2012) Nanofibres from bagasse and rice straw: process optimization and properties. *Wood Sci Technol* 46:193–205. doi: 10.1007/s00226-010-0373-z
- Henriksson, M., Berglund, L. A., Isaksson, P., Lindström, T., & Nishino, T. (2008). Cellulose Nanopaper Structures of High Toughness. *Biomacromolecules*, 9(6), 1579–1585. <https://doi.org/10.1021/bm800038n>
- Henriksson, M., Henriksson, G., Berglund, L. A., & Lindström, T. (2007). An environmentally friendly method for enzyme-assisted preparation of microfibrillated cellulose (MFC) nanofibres. *European Polymer Journal*, 43(8), 3434–3441. doi: 10.1016/j.eurpolymj.2007.05.038
- Hoeger, I. C., Nair, S. S., Ragauskas, A. J., Deng, Y., Rojas, O. J., & Zhu, J. Y. (2013). Mechanical deconstruction of lignocellulose cell walls and their enzymatic saccharification. *Cellulose*, 20(2), 807–818. doi: 10.1007/s10570-013-9867-9
- Hoeng F, Denneulin A, Bras J (2016) Use of nanocellulose in printed electronics: a review. *Nanoscale* 8:13131–13154. doi: 10.1039/C6NR03054H
- Hu L, Zheng G, Yao J, et al (2013) Transparent and conductive paper from nanocellulose fibres. *Energy Environ Sci* 6:513–518. doi: 10.1039/C2EE23635D
- Iwamoto, S., Abe, K., & Yano, H. (2008). The Effect of Hemicelluloses on Wood Pulp Nanofibrillation and Nanofibre Network Characteristics. *Biomacromolecules*, 9(3), 1022–1026. <https://doi.org/10.1021/bm701157n>
- Jain, P. M., & Shandliya, V. K. (2013). A survey paper on comparative study between Principal Component Analysis (PCA) and Exploratory Factor Analysis (EFA). *International Journal Of Computer Science And Applications*, pp. 415–424. ISSN: 0974-1011
- Jiang F, Hsieh Y-L (2014) Amphiphilic superabsorbent cellulose nanofibril aerogels. *J Mater Chem A* 2:6337–6342. doi: 10.1039/C4TA00743C
- Jiang F, Hsieh Y-L (2017) Cellulose Nanofibril Aerogels: Synergistic Improvement of Hydrophobicity, Strength, and Thermal Stability via Cross-Linking with Diisocyanate. *ACS Appl Mater Interfaces* 9:2825–2834. doi: 10.1021/acsami.6b13577
- Jiménez-Saelices C, Seantier B, Cathala B, Grohens Y (2017) Spray freeze-dried nanofibrillated cellulose aerogels with thermal superinsulating properties. *Carbohydr Polym* 157:105–113. doi: 10.1016/j.carbpol.2016.09.068
- Johansson, L.-S., Tammelin, T., Campbell, J. M., Setälä, H., & Österberg, M. (2011). Experimental evidence on medium driven cellulose surface adaptation demonstrated using nanofibrillated cellulose. *Soft Matter*, 7(22), 10917–10924. doi: 10.1039/C1SM06073B

Chapter III References

- Jonoobi, M., Oladi, R., Davoudpour, Y., Oksman, K., & Dufresne, A. (2015). Different preparation methods and properties of nanostructured cellulose from various natural resources and residues: a review, *Cellulose*, 22(2):935–969. doi: 10.1007/s10570-015-0551-0
- Jorfi, M., & Foster, E. J. (2015). Recent advances in nanocellulose for biomedical applications. *Journal of Applied Polymer Science*, 132(14):1-19 doi: 10.1002/app.41719
- Junka, K., Filpponen, I., Lindström, T., & Laine, J. (2013). Titrimetric methods for the determination of surface and total charge of functionalized nanofibrillated/microfibrillated cellulose (NFC/MFC). *Cellulose*, 20(6), 2887–2895. doi: 10.1007/s10570-013-0043-z
- Kangas. (2014). Characterization of fibrillated celluloses. A short review and evaluation of characteristics with a combination of methods. *Nordic Pulp and Paper Research Journal*, 29(01), 129–143. doi: 10.3183/NPPRJ-2014-29-01-p129-143
- Karadagli I, Schulz B, Schestakow M, et al (2015) Production of porous cellulose aerogel fibres by an extrusion process. *J Supercrit Fluids* 106:105–114. doi: 10.1016/j.supflu.2015.06.011
- Karim Z, Claudpierre S, Grahn M, et al (2016) Nanocellulose based functional membranes for water cleaning: Tailoring of mechanical properties, porosity and metal ion capture. *J Membr Sci* 514:418–428. doi: 10.1016/j.memsci.2016.05.018
- Kettunen M, Silvennoinen RJ, Houbenov N, et al (2011) Photoswitchable Superabsorbency Based on Nanocellulose Aerogels. *Adv Funct Mater* 21:510–517. doi: 10.1002/adfm.201001431
- Kim J-H, Shim BS, Kim HS, et al (2015) Review of nanocellulose for sustainable future materials. *Int J Precis Eng Manuf-Green Technol* 2:197–213. doi: 10.1007/s40684-015-0024-9
- Koga H, Saito T, Kitaoka T, et al (2013) Transparent, conductive, and printable composites consisting of TEMPO-oxidized nanocellulose and carbon nanotube. *Biomacromolecules* 14:1160–1165. doi: 10.1021/bm400075f
- Korhonen JT, Kettunen M, Ras RHA, Ikkala O (2011) Hydrophobic Nanocellulose Aerogels as Floating, Sustainable, Reusable, and Recyclable Oil Absorbents. *ACS Appl Mater Interfaces* 3:1813–1816. doi: 10.1021/am200475b
- Krasnoshlyk V (2017) Etude multi-échelles et multiphysiques des mécanismes de fissuration dans les matériaux à base de fibres naturelles. PhD thesis, University of Grenoble Alpes
- Lam YL, Kan CW, Yuen CWM (2010) Wrinkle-resistant finishing of cotton fabric with BTCA—the effect of co-catalyst. *Text Res J* 81:0040517510380777. doi: 10.1177/0040517510380777
- Lavoine N, Bergström L (2017) Nanocellulose-based foams and aerogels: processing, properties, and applications. *J Mater Chem A* 5:16105–16117. doi: 10.1039/C7TA02807E
- Lavoine N, Desloges I, Dufresne A, Bras J (2012) Microfibrillated cellulose – Its barrier properties and applications in cellulosic materials: A review. *Carbohydr Polym* 90:735–764. doi: 10.1016/j.carbpol.2012.05.026
- Le Berre M, Gillot J, Borde X (2015) Process for the surface treatment of a security document and associated security document. *Oberthur Fiduciaire WO2015091873 A1*
- Lemahieu L, Bras J, Tiquet P, et al (2011) Extrusion of Nanocellulose-Reinforced Nanocomposites Using the Dispersed Nano-Objects Protective Encapsulation (DOPE) Process. *Macromol Mater Eng* 296:984–991. doi: 10.1002/mame.201100015
- Levlin J-E (1998) *Papermaking Science and Technology, Book 17: Pulp and Paper Testing*, Fapet Oy. J.-E. Levlin, L. Söderhjelm (eds), Helsinki, Finland. ISBN: 9525216004

Chapter III References

- Liebner F, Potthast A, Rosenau T, et al (2008) Cellulose aerogels: Highly porous, ultra-lightweight materials. *Holzforschung* 62:. doi: 10.1515/HF.2008.051
- Liimatainen H, Ezekiel N, Sliz R, et al (2013) High-Strength Nanocellulose–Talc Hybrid Barrier Films. *ACS Appl Mater Interfaces* 5:13412–13418. doi: 10.1021/am4043273
- Lin, N., & Dufresne, A. (2014). Surface chemistry, morphological analysis and properties of cellulose nanocrystals with gradiented sulfation degrees. *Nanoscale*, 6(10), 5384–5393. doi: 10.1039/c3nr06761k
- Liu A, Walther A, Ikkala O, et al (2011) Clay Nanopaper with Tough Cellulose Nanofibre Matrix for Fire Retardancy and Gas Barrier Functions. *Biomacromolecules* 12:633–641. doi: 10.1021/bm101296z
- Malho J-M, Laaksonen P, Walther A, et al (2012) Facile Method for Stiff, Tough, and Strong Nanocomposites by Direct Exfoliation of Multilayered Graphene into Native Nanocellulose Matrix. *BIOMACROMOLECULES* 13:1093–1099. doi: 10.1021/bm2018189
- Mariano M, El Kissi N, Dufresne A (2014) Cellulose nanocrystals and related nanocomposites: Review of some properties and challenges. *J Polym Sci Part B Polym Phys* 52:791–806. doi: 10.1002/polb.23490
- Marketsandmarkets.com. (2015). Nanocellulose Market by Type (Cellulose nanocrystals, Cellulose nanofibrils, cellulose nanocomposites, and others), Application (Composites and Packaging, Paper and Paper Board, Biomedicine, Rheology Modifier, Flexible Electronics and Sensors, and Others), and Geography - Regional Trends & Forecast to 2019 (No. CH 3320).
- Martoia F, Cochereau T, Dumont PJJ, et al (2016) Cellulose nanofibril foams: Links between ice-templating conditions, microstructures and mechanical properties. *Mater Des* 104:376–391. doi: 10.1016/j.matdes.2016.04.088
- Mautner A, Lee K-Y, Tammelin T, et al (2015) Cellulose nanopapers as tight aqueous ultra-filtration membranes. *React Funct Polym* 86:209–214. doi: 10.1016/j.reactfunctpolym.2014.09.014
- McAdam R, McClelland J (2002) Sources of new product ideas and creativity practices in the UK textile industry. *Technovation* 22:113–121. doi: 10.1016/S0166-4972(01)00002-5
- Missoum, K., Belgacem, M., & Bras, J. (2013). Nanofibrillated Cellulose Surface Modification: A Review. *Materials*, 6(5), 1745–1766. doi: 10.3390/ma6051745
- Moser, C., Lindström, M. E., & Henriksson, G. (2015). Toward Industrially Feasible Methods for Following the Process of Manufacturing Cellulose Nanofibres. *BioResources*, 10(2), 2360–2375. doi: 10.15376/biores.10.2.2360-2375
- Naderi, A., Lindström, T., & Sundström, J. (2015). Repeated homogenization, a route for decreasing the energy consumption in the manufacturing process of carboxymethylated nanofibrillated cellulose, *Cellulose*, 22(2), 1147–1157. Doi: 10.1007/s10570-015-0576-4
- Nakagaito, A. N., & Yano, H. (2004). The effect of morphological changes from pulp fibre towards nano-scale fibrillated cellulose on the mechanical properties of high-strength plant fibre based composites. *Applied Physics A*, 78(4), 547–552. doi: 10.1007/s00339-003-2453-5
- Narain R, Pfaff T, O'Brien JF (2013) Folding and crumpling adaptive sheets. *ACM Trans Graph* 32:1. doi: 10.1145/2461912.2462010
- Nechporchuk O, Belgacem MN, Bras J (2014) Production of cellulose nanofibrils: A review of recent advances. *Ind Crops Prod* 93:2–25. doi: 10.1016/j.indcrop.2016.02.016

Chapter III References

Nechporchuk O, Belgacem MN, Pignon F (2016) Current Progress in Rheology of Cellulose Nanofibril Suspensions. *Biomacromolecules* 17:2311–2320. doi: 10.1021/acs.biomac.6b00668

Nguyen ST, Feng J, Ng SK, et al (2014) Advanced thermal insulation and absorption properties of recycled cellulose aerogels. *Colloids Surf Physicochem Eng Asp* 445:128–134. doi: 10.1016/j.colsurfa.2014.01.015

Nogi Masaya, Iwamoto Shinichiro, Nakagaito Antonio Norio, Yano Hiroyuki (2009) Optically Transparent Nanofibre Paper. *Adv Mater* 21:1595–1598. doi: 10.1002/adma.200803174

Obokata T, Yanagisawa M, Isogai A Characterization of polyamideamine-epichlorohydrin (PAE) resin: Roles of azetidinium groups and molecular mass of PAE in wet strength development of paper prepared with PAE. *J Appl Polym Sci* 97:2249–2255. doi: 10.1002/app.21893

Odabas N, Amer H, Bacher M, et al (2016) Properties of Cellulosic Material after Cationization in Different Solvents. *ACS Sustain Chem Eng* 4:2295–2301. doi: 10.1021/acssuschemeng.5b01752

Oksanen, T., Buchert, J., & Viikari, L. (1997). The Role of Hemicelluloses in the Hornification of Bleached Kraft Pulps. *Holzforschung*, 51(4), 355–360. <https://doi.org/10.1515/hfsg.1997.51.4.355>

Oksman, K., Aitomäki, Y., Mathew, A. P., Siqueira, G., Zhou, Q., Butylina, S., ... Hooshmand, S. (2016). Review of the recent developments in cellulose nanocomposite processing. *Composites Part A: Applied Science and Manufacturing*, 83:2–18. doi:10.1016/j.compositesa.2015.10.041

Oksman, K., Mathew, A. P., & Sain, M. (2009). Novel bionanocomposites: processing, properties and potential applications. *Plastics, Rubber and Composites*, 38(9–10), 396–405. doi: 10.1179/146580109X12540995045723

Osong, S. H., Norgren, S., & Engstrand, P. (2016). Processing of wood-based microfibrillated cellulose and nanofibrillated cellulose, and applications relating to papermaking: a review. *Cellulose*, 23(1), 93–123. doi: 10.1007/s10570-015-0798-5

Pääkkö, M., Ankerfors, M., Kosonen, H., Nykänen, A., Ahola, S., Österberg, M., Lindström, T. (2007). Enzymatic Hydrolysis Combined with Mechanical Shearing and High-Pressure Homogenization for Nanoscale Cellulose Fibrils and Strong Gels. *Biomacromolecules*, 8(6), 1934–1941. doi: 10.1021/bm061215p

Patel RP, Purohit NS, Suthar AM (2009) An overview of silica aerogels. *Int J ChemTech Res* 1:1052–1057. ISSN: 0974-4290

Petroudy SRD, Sheikhi P, Ghobadifar P (2017) Sugarcane Bagasse Paper Reinforced by Cellulose Nanofibre (CNF) and Bleached Softwood Kraft (BSWK) Pulp. *J Polym Environ* 25:203–213. doi: 10.1007/s10924-016-0800-9

Pickering SU (1907) Pickering Emulsions. *J Chem Soc Trans* 91:2001–2021. doi: 10.1039/CT9079102001

Qing, Y., Sabo, R., Zhu, J. Y., Agarwal, U., Cai, Z., & Wu, Y. (2013). A comparative study of cellulose nanofibrils disintegrated via multiple processing approaches. *Carbohydrate Polymers*, 97(1), 226–234. doi: 10.1016/j.carbpol.2013.04.086

Razaq A, Nyström G, Strømme M, et al (2011) High-Capacity Conductive Nanocellulose Paper Sheets for Electrochemically Controlled Extraction of DNA Oligomers. *PLOS ONE* 6:e29243. doi: 10.1371/journal.pone.0029243

Ridgway CJ, Gane PAC (2012) Constructing NFC-pigment composite surface treatment for enhanced paper stiffness and surface properties. *Cellulose* 19:547–560. doi: 10.1007/s10570-011-9634-8

Robles E, Kánnár A, Labidi J, Csóka L (2018) Assessment of physical properties of self-bonded composites made of cellulose nanofibrils and poly(lactic acid) microfibrils. *Cellulose* 25:3393–3405. doi: 10.1007/s10570-018-1822-3

Chapter III References

- Roohani M, Habibi Y, Belgacem NM, et al (2008) Cellulose whiskers reinforced polyvinyl alcohol copolymers nanocomposites. *Eur Polym J* 44:2489–2498. doi: 10.1016/j.eurpolymj.2008.05.024
- Roy D, Semsarilar M, Guthrie JT, Perrier S (2009) Cellulose modification by polymer grafting: a review. *Chem Soc Rev* 38:2046–2064. doi: 10.1039/B808639G
- RTP Imagineering plastics (r) RTP 1105 BLK Polyethylene Terephthalate (PET) Product Data Sheet - RTP Company. <http://web.rtpcompany.com/info/data/1100/RTP1105BLK.htm>. Accessed 22 May 2018
- Saito, T., Kimura, S., Nishiyama, Y., & Isogai, A. (2007). Cellulose Nanofibres Prepared by TEMPO-Mediated Oxidation of Native Cellulose. *Biomacromolecules*, 8(8), 2485–2491. doi : 10.1021/bm0703970
- Saito, T., Nishiyama, Y., Putaux, J.-L., Vignon, M., & Isogai, A. (2006). Homogeneous suspensions of individualized microfibrils from TEMPO-catalyzed oxidation of native cellulose. *Biomacromolecules*, 7(6), 1687–1691. doi: 10.1021/bm060154s
- Sarrazin P, Security A (2012) Sheet of wrinkle-resistant paper. Arjowiggins Security WO2013093872 (A1)
- Seantier B, Bendahou D, Bendahou A, et al (2016) Multi-scale cellulose based new bio-aerogel composites with thermal super-insulating and tunable mechanical properties. *Carbohydr Polym* 138:335–348. doi: 10.1016/j.carbpol.2015.11.032
- Sehaqui H (2011) Nanofibre networks, aerogels and biocomposites based on nanofibrillated cellulose from wood. PhD manuscript. KTH Royal Institute of Technology
- Sehaqui H, Liu A, Zhou Q, Berglund LA (2010) Fast Preparation Procedure for Large, Flat Cellulose and Cellulose/Inorganic Nanopaper Structures. *Biomacromolecules* 11:2195–2198. doi: 10.1021/bm100490s
- Sehaqui H, Zhou Q, Ikkala O, Berglund LA (2011) Strong and Tough Cellulose Nanopaper with High Specific Surface Area and Porosity. *Biomacromolecules* 12:3638–3644. doi: 10.1021/bm2008907
- Sequeira S, Evtuguin DV, Portugal I Preparation and properties of cellulose/silica hybrid composites. *Polym Compos* 30:1275–1282. doi: 10.1002/pc.20691
- Sharma S, Deng Y (2016) Dual Mechanism of Dry Strength Improvement of Cellulose Nanofibril Films by Polyamide-epichlorohydrin Resin Cross-Linking. *Ind Eng Chem Res* 55:11467–11474. doi: 10.1021/acs.iecr.6b02910
- Sheng J, Tong S, He Z, Yang R (2017) Recent developments of cellulose materials for lithium-ion battery separators. *Cellulose* 24:4103–4122. doi: 10.1007/s10570-017-1421-8
- Sim K, Youn HJ (2016) Preparation of porous sheets with high mechanical strength by the addition of cellulose nanofibrils. *Cellulose* 23:1383–1392. doi: 10.1007/s10570-016-0865-6
- Siqueira EJ (2012) Polyamidoamine epichlorohydrin-based papers : mechanisms of wet strength development and paper repulping. PhD thesis. University of Grenoble Alpes
- Siqueira, G., Tapin-Lingua, S., Bras, J., da Silva Perez, D., & Dufresne, A. (2010). Morphological investigation of nanoparticles obtained from combined mechanical shearing, and enzymatic and acid hydrolysis of sisal fibres. *Cellulose*, 17(6), 1147–1158. doi: 10.1007/s10570-010-9449-z
- Siró, I., & Plackett, D. (2010). Microfibrillated cellulose and new nanocomposite materials: a review. *Cellulose*, 17(3), 459–494. doi: 10.1007/s10570-010-9405-y

Chapter III References

- Siró, I., Plackett, D., Hedenqvist, M., Ankerfors, M., & Lindström, T. (2011). Highly transparent films from carboxymethylated microfibrillated cellulose: The effect of multiple homogenization steps on key properties. *Journal of Applied Polymer Science*, 119(5), 2652–2660. doi: 10.1002/app.32831
- Spence, K. L., Venditti, R. A., Rojas, O. J., Habibi, Y., & Pawlak, J. J. (2011). A comparative study of energy consumption and physical properties of microfibrillated cellulose produced by different processing methods. *Cellulose*, 18(4), 1097–1111. doi: 10.1007/s10570-011-9533-z
- Stergar J, Maver U (2016) Review of aerogel-based materials in biomedical applications. *J Sol-Gel Sci Technol* 77:738–752. doi: 10.1007/s10971-016-3968-5
- Stergar J, Maver U (2016) Review of aerogel-based materials in biomedical applications. *J Sol-Gel Sci Technol* 77:738–752. doi: 10.1007/s10971-016-3968-5
- Stuart AR, Amstad E, Gauckler LJ (2007) Colloidal Stabilization of Nanoparticles in Concentrated Suspensions. *Langmuir* 23:1081–1090. doi: 10.1021/la062042s
- Su J, Mosse WKJ, Sharman S, et al (2012) Paper strength development and recyclability with polyamideamine-epichlorohydrin (pae). *BioResources* 7:0913–0924. doi: 10.15376/biores.7.1.0913-0924
- Sultan E, Boudaoud A (2006) Statistics of Crumpled Paper. *Phys Rev Lett* 96(13):136103. doi: 10.1103/PhysRevLett.96.136103
- Syverud, K., Chinga-Carrasco, G., Toledo, J., & Toledo, P. G. (2011). A comparative study of Eucalyptus and Pinus radiata pulp fibres as raw materials for production of cellulose nanofibrils. *Carbohydrate Polymers*, 84(3), 1033–1038. doi: 10.1016/j.carbpol.2010.12.066
- Taipale T, Österberg M, Nykänen A, et al (2010) Effect of microfibrillated cellulose and fines on the drainage of kraft pulp suspension and paper strength. *Cellulose* 17:1005–1020. doi: 10.1007/s10570-010-9431-9
- Tallinen T, Aström JA, Timonen J (2009) The effect of plasticity in crumpling of thin sheets. *Nat Mater* 8:25–29. doi: 10.1038/nmat2343
- Tanaka. (2012). Nanocellulose characterization with mechanical fractionation. *Nordic Pulp and Paper Research Journal*, 27(04), 689–694. doi: 10.3183/NPPRJ-2012-27-04-p689-694
- Tejado, A., Alam, M. N., Antal, M., Yang, H., & Ven, T. G. M. van de. (2012). Energy requirements for the disintegration of cellulose fibres into cellulose nanofibres. *Cellulose*, 19(3), 831–842. <https://doi.org/10.1007/s10570-012-9694-4>
- Thapliyal PC, Singh K (2014) Aerogels as Promising Thermal Insulating Materials: An Overview. *J Mater* 2014:1–10. doi: 10.1155/2014/127049
- Tonoli, G. H. D., Teixeira, E. M., Corrêa, A. C., Marconcini, J. M., Caixeta, L. A., Pereira-da-Silva, M. A., & Mattoso, L. H. C. (2012). Cellulose micro/nanofibres from Eucalyptus kraft pulp: Preparation and properties. *Carbohydr Polym*, 89(1), 80–88. doi: 10.1016/j.carbpol.2012.02.052
- Trovatti E, Tang H, Hajian A, et al (2018) Enhancing strength and toughness of cellulose nanofibril network structures with an adhesive peptide. *Carbohydr Polym* 181:256–263. doi: 10.1016/j.carbpol.2017.10.073
- Turbak, A. F., Snyder, F. W., & Sandberg, K. R. (1983). Microfibrillated cellulose, a new cellulose product: properties, uses, and commercial potential. *J. Appl. Polym. Sci.: Appl. Polym. Symp.*; (United States); Journal Volume: 37; Conference: 9. cellulose conference, Syracuse, NY, USA
- Ullah, H., Santos, H. A., & Khan, T. (2016). Applications of bacterial cellulose in food, cosmetics and drug delivery. *Cellulose*, 23(4), 2291–2314. doi: 10.1007/s10570-016-0986-y

Chapter III References

- Voisin H, Bergström L, Liu P, Mathew AP (2017) Nanocellulose-Based Materials for Water Purification. *Nanomaterials* 7:37-57 doi: 10.3390/nano7030057
- Wang Q, Du H, Zhang F, et al (2018) Flexible cellulose nanopaper with high wet tensile strength, high toughness and tunable ultraviolet blocking ability fabricated from tobacco stalk via a sustainable method. *J Mater Chem A*. doi: 10.1039/C8TA01986J
- Weber H, De Grave I, Röhr E (2000) Foamed Plastics. In: Ullmann's Encyclopedia of Industrial Chemistry. Wiley-VCH Verlag GmbH & Co. KGaA
- Wei Q, Liu Y, Hou D, Huang F (2007) Dynamic wetting behavior of plasma treated PET fibres. *J Mater Process Technol* 194:89–92. doi: 10.1016/j.jmatprotec.2007.04.001
- Weise, U., Maloney, T., & Paulapuro, H. (1996). Quantification of water in different states of interaction with wood pulp fibres. *Cellulose*, 3(1), 189–202. doi: 10.1007/BF02228801
- Wicklein B, Kocjan A, Salazar-Alvarez G, et al (2015) Thermally insulating and fire-retardant lightweight anisotropic foams based on nanocellulose and graphene oxide. *Nat Nanotechnol* 10:277–283. doi: 10.1038/nnano.2014.248
- Wistara N, Young RA (1999) Properties and treatments of pulps from recycled paper. Part I. Physical and chemical properties of pulps. *Cellulose* 6:291–324. doi: 10.1023/A:1009221125962
- Wu C-N, Saito T, Fujisawa S, et al (2012) Ultrastrong and high gas-barrier nanocellulose/clay-layered composites. *Biomacromolecules* 13:1927–1932. doi: 10.1021/bm300465d
- Wu C-N, Yang Q, Takeuchi M, et al (2014) Highly tough and transparent layered composites of nanocellulose and synthetic silicate. *Nanoscale* 6:392–399. doi: 10.1039/C3NR04102F
- Yong C, Mei C, Guan M, et al (2018) A comparative study of different nanoclay-reinforced cellulose nanofibril biocomposites with enhanced thermal and mechanical properties. *Compos Interfaces* 25:301–315. doi: 10.1080/09276440.2018.1400271
- Yu H, Yan C, Yao J (2014) Fully biodegradable food packaging materials based on functionalized cellulose nanocrystals/poly(3-hydroxybutyrate-co-3-hydroxyvalerate) nanocomposites. *RSC Adv* 4:59792–59802. doi: 10.1039/C4RA12691B
- Zhang F, Ren H, Dou J, et al (2017) Cellulose Nanofibril Based-Aerogel Microreactors: A High Efficiency and Easy Recoverable W/O/W Membrane Separation System. *Sci Rep* 7:40096. doi: 10.1038/srep40096
- Zhang W, Zhang Y, Lu C, Deng Y (2012) Aerogels from crosslinked cellulose nano/micro-fibrils and their fast shape recovery property in water. *J Mater Chem* 22:11642–11650. doi: 10.1039/C2JM30688C
- Zheng G, Cui Y, Karabulut E, et al (2013) Nanostructured paper for flexible energy and electronic devices. *MRS Bull* 38:320–325. doi: 10.1557/mrs.2013.59
- Zhou L, Yang Z, Luo W, et al (2016) Thermally Conductive, Electrical Insulating, Optically Transparent Bi-Layer Nanopaper. *ACS Appl Mater Interfaces* 8:28838–28843. doi: 10.1021/acsami.6b09471
- Zhu H, Fang Z, Preston C, et al (2014) Transparent paper: fabrications, properties, and device applications. *Energy Environ Sci* 7:269–287. doi: 10.1039/C3EE43024C
- Zimmermann, T., Pöhler, E., & Geiger, T. (2004). Cellulose Fibrils for Polymer Reinforcement. *Advanced Engineering Materials*, 6(9), 754–761. doi: 10.1002/adem.200400097

Supplementary data

Chapter III.1. A new quality index for characterization of different cellulose nanofibrils

Table SD1: Commercial cellulose nanofibrils

Reference	Pre-treatment	Information and Supplier country
CNF-1	Enzymatic	Extracted from Iyocell, USA
CNF-2	Enzymatic	Canada
CNF-3	Enzymatic	Germany
CNF-4	Enzymatic	France
CNF-5	Enzymatic	Switzerland
CNF-6	Enzymatic	Norway (Booregard, Exilva product)
CNF-7	Enzymatic	USA (Maine University)
CNF-8	Enzymatic	France
CNF-9	Enzymatic	France
CNF-10	Enzymatic	France (Inofib)
CNF-11	Enzymatic	France (Inofib)
CNF-12	Anionic	Finland
CNF-13	Cationic	Finland

Table SD2: Correlation matrix between the eight parameters chosen for Quality Index measurement

	Macro. size	Homogeneity	Nanosized fraction	Turbidity	Transmittance	Tear resistance	Young's Modulus	Porosity
Macro. size	1.00							
Homogeneity	0.72	1.00						
Nanosized fraction	0.46	0.45	1.00					
Turbidity	0.44	0.38	0.56	1.00				
Transmittance	0.44	0.32	0.52	0.69	1.00			
Tear resistance	0.66	0.60	0.53	0.35	0.71	1.00		
Young's Modulus	0.60	0.45	0.45	0.45	0.71	0.71	1.00	
Porosity	0.52	0.35	0.59	0.41	0.74	0.67	0.83	1.00

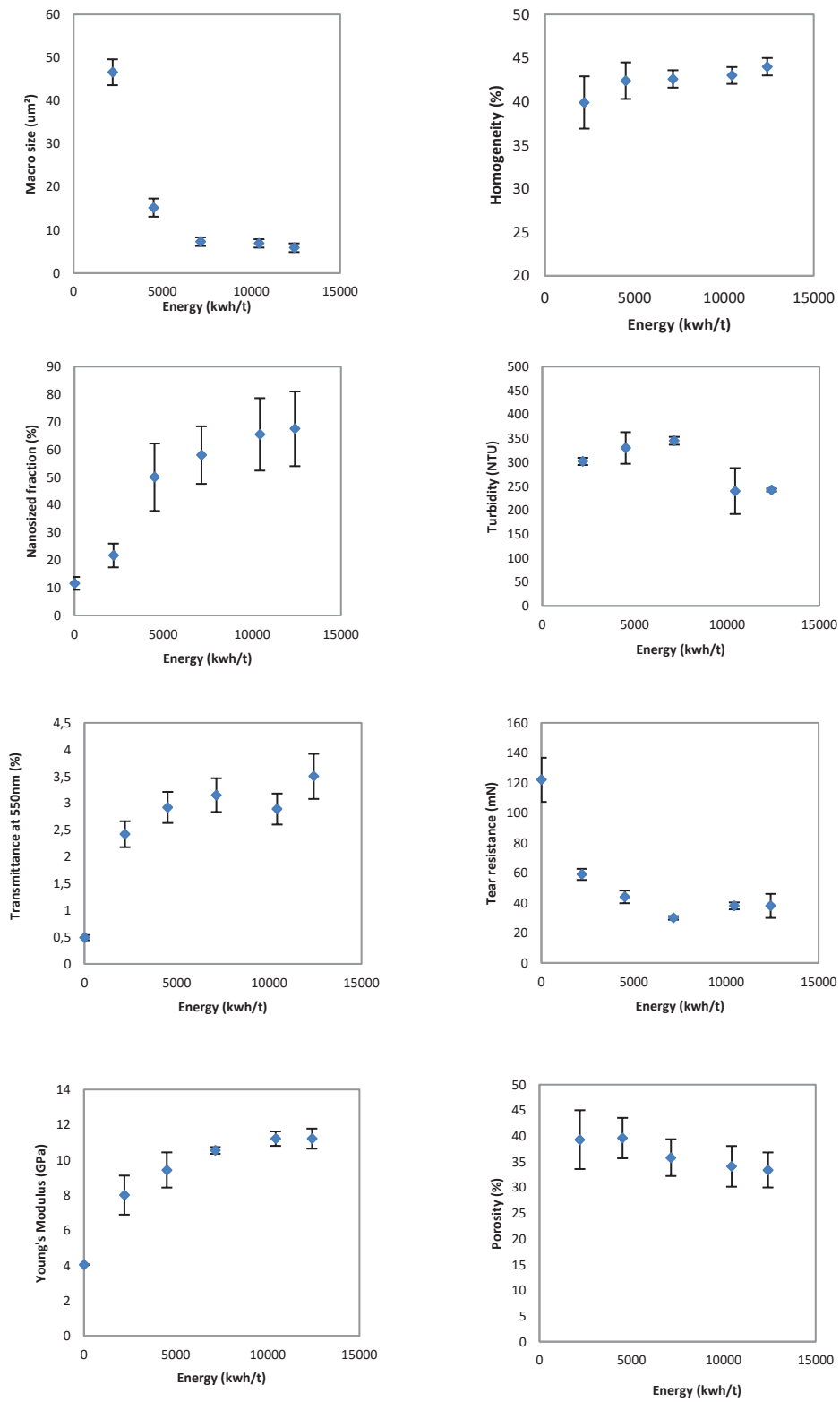


Figure SD1: Characterization values for each parameter as a function of the energy, for refined eucalyptus pretreated with enzymes

Chapter III.3: Influence of pretreatment and degree of defibrillation on cellulose nanofibril cryogel properties and strategies to introduce a porous CNF layer inside a papermaking process

In order to upscale the production of porous CNF cryogels and to make it suitable with a papermaking process, different strategies were proposed to avoid the use of freeze-drying.

1. Material and methods

Cross-linked nanofibrils cryogel beads using a superhydrophobic surface. Nanocellulose aerogel beads have been recently produced by Erlandsson (Erlandsson et al. 2016) through the use of a superhydrophobic surface and a cellulose cross-linker so-called alkyl ketene dimer (AKD). The processing method used was adapted from their work. First, 250 mL of enzymatic CNF suspension was prepared at a concentration of 1.4 wt% and 3.047 g of Sodium Periodate (NaIO_4), corresponding to a concentration of 0,057 M, was added to the dispersion. Thereafter, the suspension was mixed with AKD solution using an Ultra-turrax for 5 min at a speed rate of $10000 \text{ tr}\cdot\text{min}^{-1}$ to ensure a good dispersion. The mixture was then introduced into a syringe which allows depositing droplets manually on the superhydrophobic surface.

As part of this project, two superhydrophobic surfaces have been used: Polytetrafluoroethylene (PTFE) mold and coated surface with NeverWet®. The mold was then recovered with aluminum foil to prevent exposure to light and put in desiccator at controlled humidity containing saturated NaCl salt solution for 20h to oxidize CNF beads (Roohani et al. 2008). Indeed, NaCl solution was used to induce a humidity level of 75% and therefore it limits evaporation. After 20h, the beads formed were stored into freezer at -4°C until the whole structure was frozen and thereafter thawed under ambient conditions. The beads were then solvent-exchanged, first with ethanol 96% and then with acetone. Both solvents were changed 3 times with an incubation time of 15 min. Finally, the excess of acetone was removed carefully before being drying under ambient conditions.

Porous CNF membranes with alcohol and surfactant. 2 g of commercial enzymatic CNF were diluted at 0.5 wt%. Part of the water, from 0 to 50 wt%, was replaced by other solvents: ethanol, acetone or propanol. Trials were also made by adding in the 0.5% diluted CNF suspension (in water) a proportion of surfactant (TTAB) of 0.5, 1 or 2%. Then, the suspension was filtered under vacuum at -600 mbar for 2 min and dried under vacuum at 90°C between (from interior to exterior) two nylon sieves to prevent adherence, two cover sheets and two cardboards for 30 min.

Encapsulation process. The encapsulation method has been inspired by Lemahieu et al. (Lemahieu et al. 2011). Different CNF/alginate suspensions were prepared using two kinds of CNF (enzymatic or TEMPO-oxidized) and different ratios (Table SD3). The final concentration of each suspension was 2.5 wt% and was prepared by adding alginate powder into CNF suspension and mixed using an Ultra-turrax for 2 min at $8000 \text{ tr}\cdot\text{min}^{-1}$. The CNF/alginate suspension was then dropped into a 5 wt% CaCl_2 solution inducing the cross-linking of the alginate around the nanofibrils. The cross-linked beads were

filtered using a Büchner apparatus with a nylon cloth (pore size of 1 μ m) and dried overnight under ambient conditions.

Table SD3: Experimental design of CNF beads through encapsulation method

	CNF Type	CNF:aAlginate (wt: wt)	Ratio	Designation
Varying CNF type	Enzymatic	1:1.5	40/60	CNF/Alginate 40/60
	TEMPO-oxidized	1:1.5	40/60	CNF-/Alginate 40/60
Varying ratio	Enzymatic	1.25:1.25	50/50	CNF/Alginate 50/50
	Enzymatic	1.5:1	60/40	CNF/Alginate 60/40
	Enzymatic	1.75:0.75	70/30	CNF/Alginate 70/30

Octylamine process for cryogel preparation. This processing method was inspired by Cervin's work (Cervin et al. 2013). In order to produce CNF cryogels, two octylamine solutions were prepared with a concentration of 0.8 or 2.4 g/L at pH 9, in order to be able to neutralize one-third of the CNF charge and all the charges, respectively. TEMPO-oxidized CNF was used as the raw material and octylamine with a volume of 30 mL was added to the suspension. The dispersion was stirred sequentially with an Ultra-turrax for 3 min at 8000 tr.min⁻¹ and 3 min at 10000 tr.min⁻¹. Finally, the dispersion was stirred with a stainless steel milk beater for 10 min which induced the introduction of air bubbles at the water/cellulose interface. The excess of water was carefully removed using a syringe before drying the cryogel under ambient conditions for one week or overnight in an oven at 30°C.

2. Results and discussion: testing different strategies without freeze-drying

Porous membrane with surfactant or alcohol: Porous membranes have been produced by filtration of a CNF suspension containing different ratios (from 0% to 50%) of ethanol, propanol or acetone. Trials with addition up to 2% of TTAB surfactant have also been performed. The change of part of water by alcohol reduces the surface tension and consequently limits the natural cohesion of the material, resulting in a material with higher porosity. Moreover, alcohol reduces the boiling temperature of the mixture, the solvent is thus faster evaporated which tends to create porosity. Surfactants induce also a decrease in the surface tension of water by forming a nanolayer at the air/water interface. This nanolayer can then increase its surface in contact with air, creating water films that trap air, forming bubbles and thus foam through an external energy provided by stirring.

In Figure SD2, it appears that it exists a direct correlation between the porosity and the tear resistance value. Same trends and same optimum at 20% of alcohol are observed for porous membrane obtained with acetone or propanol. With CNF in 25% ethanol and 75% water, a porosity of 46.2% was obtained (against 13% for CNF in water) and the tear resistance value of the resulting porous film significantly increased (8 cN against 2.4 cN in water only). Results were even higher with 25% acetone (55% porosity) and 25% propanol (60% porosity), as shown in Figure SD3. This method presents the advantage to promote sufficient porosity to decrease the tear propagation and could be adapted in a paper-making process as the CNF could be introduced as a middle layer without specific requirements of drying. However, this assumes that the use of solvent is acceptable and the porosity increases.

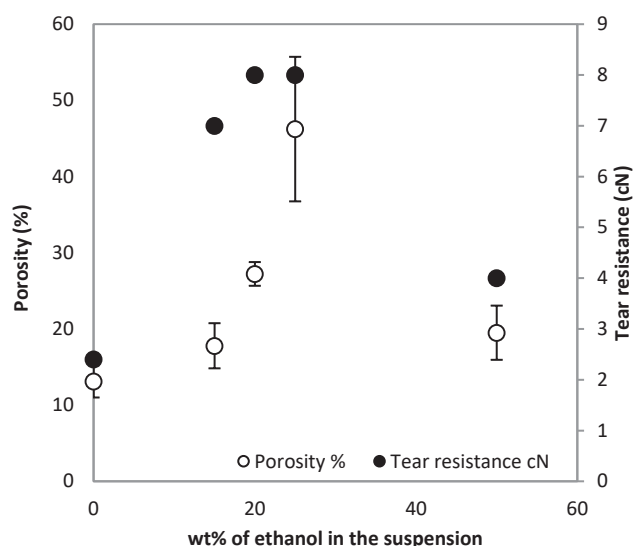


Figure SD2: Porosity and tear resistance for porous CNF membranes obtained by changing part of the aqueous phase by various quantities of ethanol

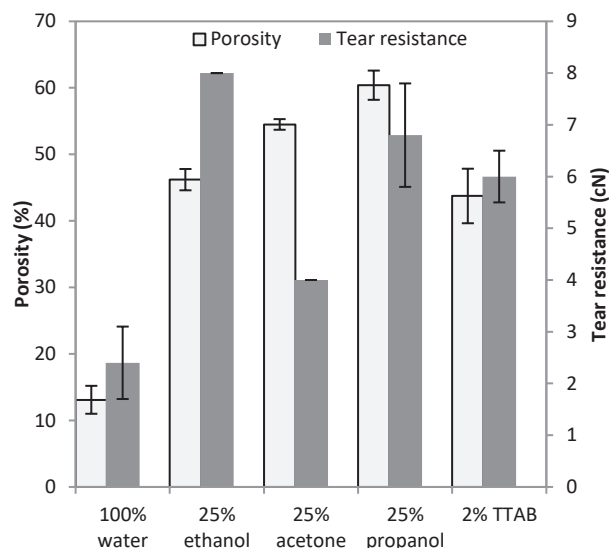


Figure SD3: Porosity and tear resistance for porous CNF membranes obtained by changing part of the aqueous phase with different alcohols or by addition of surfactant TTAB

Encapsulation process: In this method, alginate was used for its ability to form a small capsule when dropped into CaCl_2 . Alginate gelling results from bonding between carboxylic groups and ions, i.e. Ca^{2+} in the present case (Lemahieu et al. 2011). As a result, small CNF/alginate capsules were produced with different types of CNF, i.e. enzymatic CNF or TEMPO-oxidized CNF, as well as different CNF/alginate ratios at a concentration of 2.5 wt%. The obtained capsules were characterized in terms of density, porosity and morphology (SEM). It appears that dense beads were obtained with an extremely low porosity, far from a cryogel structure. One possible improvement would be to find a way to remove alginate while keeping the CNF structure inside. No successful method was found.

Pickering emulsion: Pickering emulsion technology has been used for more than a century to stabilize high-energy interfaces (Pickering 1907). Only recently, this concept has been exploited for the preparation of ultra-stable wet foams (Binks 2002), and for the production of a wide range of low-density, porous materials (Stuart et al. 2007). The present idea, as described by Cervin (Cervin et al. 2013), is to prepare CNF-stabilized cryogel through the use of octylamine. Indeed, octylamine has the ability to be absorbed onto anionic CNF surface and results in partially hydrophobic CNFs which can be used to form a thick entangled CNF layer onto the gas bubble after being foamed (Cervin et al. 2013; Lavoine et Bergström 2017). In addition, when the particles are partially hydrophobic, it is energetically favorable for them to attach to the gas-liquid interface and replace part of the high energy solid-liquid area by a lower energy solid-gas area. Coalescence is hindered by the steric repulsion between the attached particles and the particles form a layer at the interface that strongly resists shrinkage and expansion of bubbles.

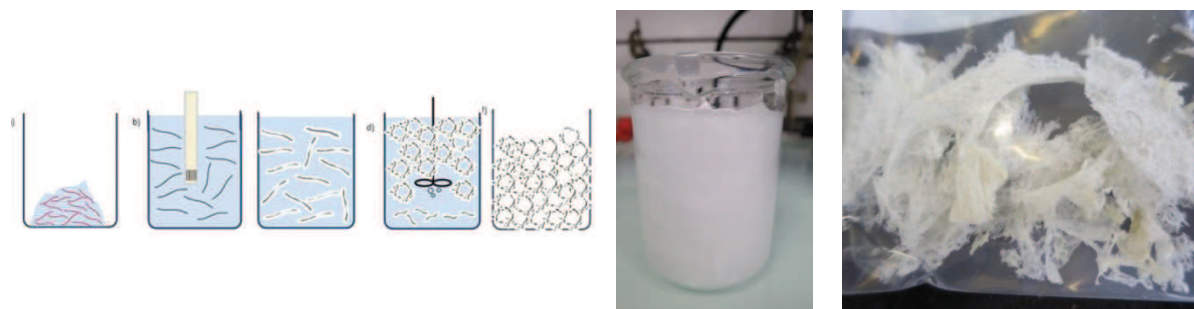


Figure SD4: A) Octylamine cryogel ratio 1:1 B) sheet-like structure obtained after cryogel drying C) paper coating with octylamine cryogel

Different octylamine/CNF ratios were tested: the amount of octylamine was chosen to be able to neutralize one-third (1:3) or the totality (1:1) of the anionic CNF charges. After foaming, the filtration and drying of the suspensions are also key points to obtain porous dried cryogels and require lot of precaution. The filtration step is indeed essential for removing the excess of water but can also break the wet cryogel structure if it is performed too quickly. Different drying conditions of the cryogels were also tested: drying under ambient conditions or in an oven at 30°C. Drying in the oven resulted in yellowed and shrank structure. Consequently, drying under ambient conditions has been selected.

Resulting materials were analyzed under optical microscopy and SEM and present a sheet-like structure as shown in Figure SD4 for both ratios of octylamine. This is the proof that the introduction of octylamine was not sufficient in our experiments for stabilizing the air-bubbles at the air/liquid interface as expected and reported by Cervin (Cervin et al. 2013). There are several issues with this method for an upscale use on a paper-making process. Indeed, the resulting cryogel has a brittle sheet-like structure which completely loses its porosity if crushed in a cutting mill. Furthermore, an online introduction of the wet cryogel between the two cotton layers is not conceivable as the filtration step and drying step require to be slow and with a lot of cautions.

Cross-linked cellulose nanofibrils cryogel beads using a superhydrophobic surface. An innovative way to obtain ultra-porous CNF beads has been developed recently by Erlandsson (Erlandsson et al. 2016). The particularity of this process is the deposition of CNF beads on a superhydrophobic surface. These beads consequently keep their spherical structure. Then, the beads are frozen and thereafter thawed to create the porous CNF network, and the water which is now localized on the external layer of the beads is then removed by solvent exchange with ethanol and acetone. Anionic CNFs were mixed with sodium periodate to increase the mechanical properties and wet stability of CNF cryogel beads. We have also worked as a preliminary study on cross-linked CNFs based on hydrazone cross-linking between aldehyde-functionalized CNFs and hydrazide-functionalized CNFs. The grafting of both CHO-CNFs and NHH₂-CNFs has been proved through conductometric titration and FTIR.

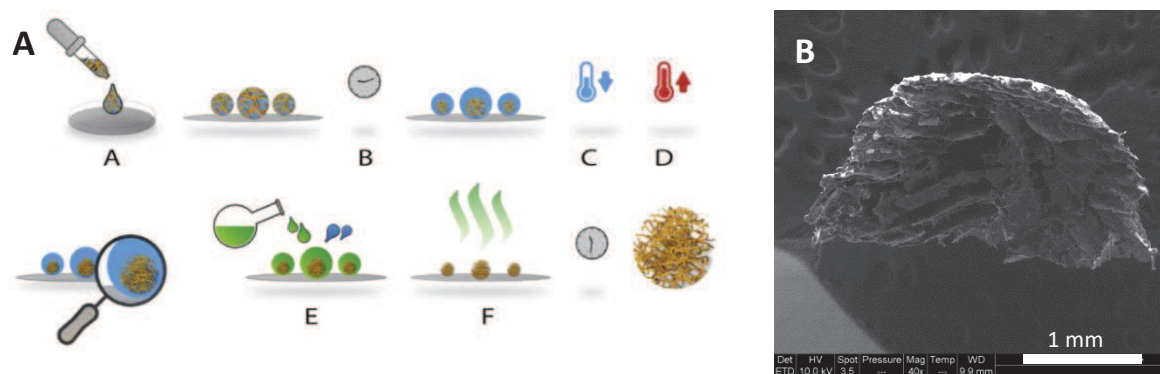


Figure SD5: A) Production of porous CNF beads using a super-hydrophobic surface (Erlandsson et al. 2016) and B) SEM picture of a porous bead obtained with this process

Mitigated results were obtained. Beads with big pores were produced when trials were performed bead by bead as shown in Figure SD5-FigureB. However, a very low reproducibility was achieved as 80% of the attempts resulted in porosity-free shrunk beads after the drying step. The treatment of CNF with periodate or with hydrazine cross-linked did not induce differences. Furthermore, the increase in beads amount is challenging as the beads deposited on a same hydrophobic surface automatically move and collapse. To overcome this problem, different sieves made of aluminum or cardboard, also treated with super-hydrophobic treatment, were produced and beads were introduced inside each cell. This strategy worked and allowed the simultaneous production of several beads but the same reproducibility issue was observed.

Furthermore, this method although avoiding freeze-drying presents incoherent steps with the paper-making process. Indeed, to be completely frozen, the CNF beads are placed overnight in a fridge (time-consuming). Furthermore, the solvent exchange step increases the number of handling and is not possible on an online process.

Conclusion

Advantages and drawbacks of each technique investigated are synthesized in Table SD4. Finally, only two methods appear to be promising for the use of cryogel as a middle layer in a paper-making process. The first one is to use cross-linked suspensions of anionic CNF with 2wt% PAE, spraying the suspension in liquid nitrogen to obtain a frozen powder and freeze-drying. This method allows the formation of ultra-porous powder (98-99% porosity) keeping its structure even when diluted into water during 20 hours. The main drawback remains the use of freeze-drying process which reduces the possibility of an online production. The second promising method is the dilution of the CNF suspension in 25% acetone or propanol. In this case, CNF with alcohol could be directly introduced as a middle layer in the paper-making process and the porosity would appear after the drying step. Despite the lower porosity obtained in the CNF film produced with alcohol (only 60% maximum), interesting increase in tear resistance was observed.

Table SD4: Comparison of processes to obtain a porous material adaptable to papermaking process, A) with and B) without the use of freeze-drying step

	Avoiding of freeze-drying	Advantages	Drawbacks	Final porosity (%)	Perspective
A					
Freeze-dried cryogels crushed with cutting mills	No	Production of a porous powder; Can be sprayed in papermachine process	No conservation of porous structure in water	<i>No data</i>	Rejected method
Porous beads cross-linked with PAE	No	Production of cryogel beads; Porous structure; Conservation of porous structure in water	Beads still too big to be sprayed; Use of liquid nitrogen; Time consuming	98-99%	Use a spray to obtain a powder
B					
Change of part of the aqueous phase with alcohol or addition of a surfactant	Yes	Production of porous films; Process adaptable to paper-making process	Use of solvent; Low final porosity	60%	Possibility to implement online
Encapsulation process	Yes	Green and fast process	Unsuccessful method Sheet-like structures;	No porosity	Rejected method
Pickering emulsions	Yes	Production of cryogels	Hazardous filtration and drying steps Low repeatability;	<i>No data</i>	Rejected method
Use of superhydrophobic surface	Yes	Production of cryogel beads; Large porosity	Lot of steps; Time consuming	<i>No data</i>	Rejected method

Chapter III.4: Introduction of cellulose nanofibril as a paper middle layer: three strategies for crumpling limitation and tear-resistant material

1) Choice of crumpling protocol and parallel with reality

While simple at a first glance, the paper crumpling is a complex phenomenon that depends on material parameters but also on the crumpling protocol (Habibi et al. 2017). This crumpling protocol is particularly hard to define and to reproduce at lab scale as banknotes are daily crumpled by hand, wallets and pockets, with different intensities and random movements. However, to be consistent, crumpled papers have to be compared with exactly the same crumpling conditions. Literature often reports compaction protocols based on the formation of a paper ball, but this method implies a manual handling and hence depends on the user. In this work, two principal methods were used to make a crumpling pattern with satisfying repeatability on paper samples: NBS and balloon tests. These two methods involve completely different movements and intensities and the challenge is to find which one is the most representative of reality.

Habibi et al. (2017) reported two main contributions to the crumpling force: the force needed for the creation of the first crumpling pattern, and the mechanical response of a crumpled paper submitted to additional crumpling deformation. Moreover, the force needed to crumple a paper for the first time is larger than for a paper that has already been crumpled before. For a banknote substrate which is daily manipulated, the main contribution of crumpling is due to the mechanical response of the crumpled network since most of the crease pattern has already been created. In this study, “NBS x1” can be considered as the crumpling test representative of the creation of a crumpling pattern while “NBS x4” is most representative of successive crumplings. The main differences for multilayer samples occur mainly at these two steps and that is the reason why they were kept in Results and Discussion section. Furthermore, beyond 4 crumpling repetitions, the paper becomes limp due to a strong decrease of its mechanical properties.

However, such crumpling seems very aggressive for paper and far from what happens in the daily life. That is why the papers have been crumpled with the balloon test. This test results in higher uncertainties than the other ones, as the position of the paper inside the balloon test during compression and decompression cycles is not controlled and can induce variations on the results. However, this method allows the crumpling with the lightest intensity and is the closer to what is happening in reality in pockets or wallets.

After the crumpling, an image analysis is performed to extract a crumpling value. This image analysis is sufficient to characterize multilayer papers produced at lab-scale. However, it does not allow the characterization of printed papers such as banknotes. Consequently, another method has been set up, based on surface topography and extraction of waviness profile (Figure SD6-A). It appears that the trends obtained with this test are exactly the same as the one obtained after image analysis whatever the sample (Figure SD6-B). Consequently, all these results performed using image analysis would be reproducible for banknote or any printed paper with surface topography test.

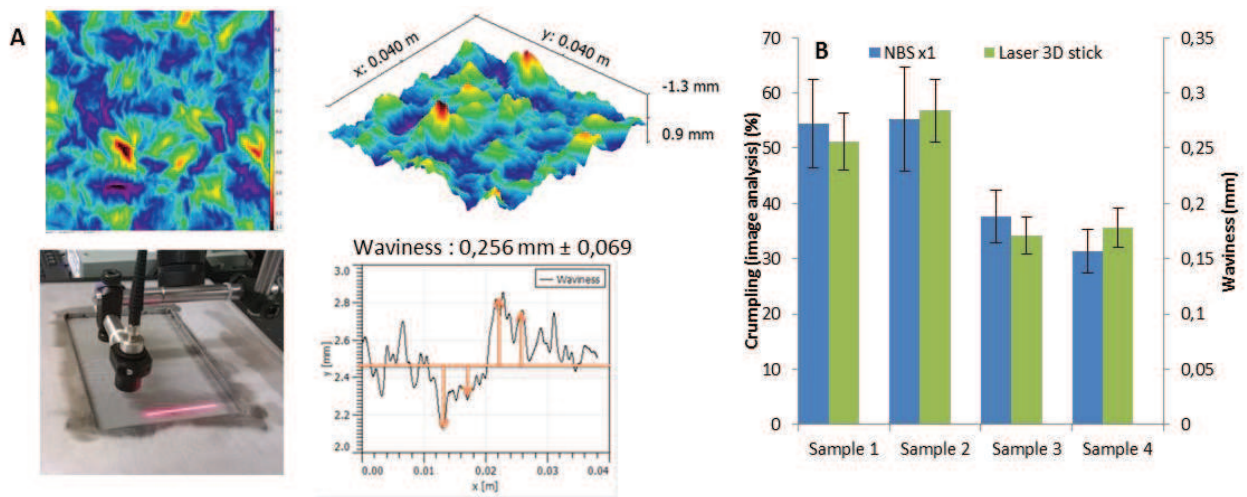


Figure SD6: A) Determination of waviness profile using Laser 3D stick sensor, after NBSx1 crumpling, B) comparison between image analysis and waviness profile

2) Exact steps of crumpling for national bureau of standard (NBS) method:

- 1) Cut a test sample of 67 x 67 mm. All features of the banknote / sample must be included
- 2) Mark a corner of the test sample.
- 3) Place the fork (1) into the sheath (2) by pulling the knob (5).
- 4) Insert the test sample through the slot (4) into the sheath (2) and between the two legs of the fork (1).
- 5) Roll the sample (3) into a cylinder by rotating the knob (5).
- 6) Move the fork (1) with the rolled sample (3) out of the sheath (2) by pushing the knob (5).
- 7) Take the rolled paper (3) from the fork (1).
- 8) Take the tube (6) with the cap (7) from the apparatus.
- 9) Close the cap (7).
- 10) Insert the rolled paper (3) into the tube (6).
- 11) Be sure that there is a piston (8) with the flat side up in the tube (9).
- 12) Place the tube (6) with the rolled paper (3) into the tube (9) over the piston (8). The flat side of the piston (8) is in contact with the rolled paper (3).
- 13) Press the cap (7) until the weight (10) is lifted.
- 14) Now the paper sample (3) has been crumpled.
- 15) Open the cap (7).
- 16) Press the tube (6) downwards, the paper sample (3) will be pushed out of the tube (6) by the piston (8).
- 17) Remove the crumpled paper (3) from the tube (6).

18) Straighten the sample by hand

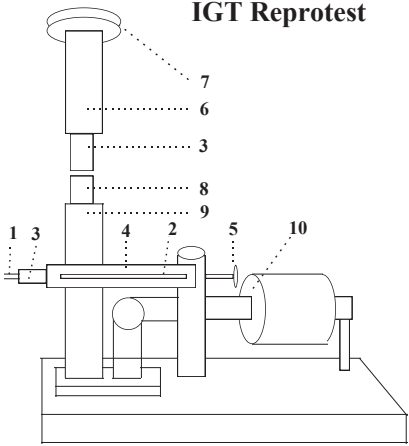


Figure SD7: NBS method device

Chapter IV

Scale-up and combination of the two strategies

Chapter

IV

Table of content chapter IV

Introduction.....	297
1. Project scale-up: pilot tests and industrial tests	299
1.1. Introduction.....	299
1.2. Materials and methods	300
1.2.1. Pilot tests.....	300
1.2.2. Industrial tests.....	302
1.2.3. Improvement track for industrial tests optimization	304
1.2.4. Characterization tools	305
1.3. Results and discussion.....	306
1.3.1. Pilot tests.....	306
1.3.2. Intdustrial tests.....	312
1.3.3. Improvement tracks for industrial tests.....	315
1.4. Conclusions.....	317
2. Combining of the two strategies: influence of CNC reinforced PVOH impregnation, CNF middle layer and banknote calendering on the whole paper properties	319
2.1. Introduction.....	319
2.2. Materials and methods	320
2.2.1. Materials.....	320
2.2.2. Methods	322
2.3. Results and discussion.....	324
2.3.1. Influence of CNC-reinforced PVOH impregnation on paper crumpling resistance.....	324
2.3.2. Influence of the CNF layer on paper foldability and crack propagation occurring after folding	326
2.4. Conclusions.....	332
References.....	333

Chapter IV: Scale-up and combination of the two strategies

Introduction

This PhD was performed in an industrial context, and was consequently an opportunity to combine fundamental research with the development and production of an innovative material. Previous chapters proposed two solutions to limit banknote dog-ears and crumpling, which are two classical defects occurring with banknote handling. These strategies were developed at the lab-scale and independently of each other, in order to explain the mechanisms involved and prove the efficiency of cellulose nanocrystals and cellulose nanofibrils for paper dog-ears and crumpling resistance. This last chapter proposes a transition from research to industrialization (Figure 1) and gathers the two different strategies.

In **chapter IV.1.**, a CNF layer has been innovatively sprayed between the two fiber layers constitutive of a banknote substrate, on a pilot paper machine (Banque De France, Chamalières). The papers have then been impregnated using a pilot coater machine with CNC-PVOH suspension. Then, the addition of CNCs in the PVOH matrix was tested at the industrial scale using real banknote paper machine (Banque de France, Vic-le-comte). This up-scaling allowed (i) testing the adaptability of lab processes with paper machine requirements and (ii) comparing the results obtained at the lab-scale with results obtained at pilot and then industrial scale.

Finally, **chapter IV.2.** proposes a combination of the two strategies and investigates the influence of CNCs and CNFs on collateral properties. This section reports the effect of impregnation with CNCs on paper crumpling and the impact of a CNF layer on paper dog-ears resistance.

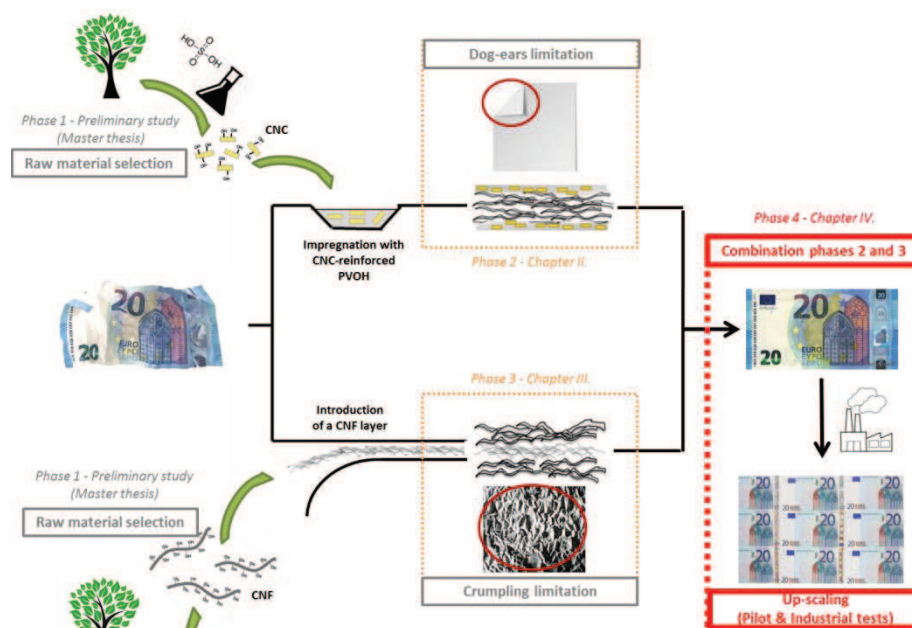


Figure 1: General overview of the project and chapter organization

1. Project scale-up: pilot tests and industrial tests

1.1. Introduction

The RESIST project started with the breakdown of the fiber into nano-elements to produce cellulose nanofibrils (CNFs) and cellulose nanocrystals (CNCs), and aimed to end with the construction of an innovative crumpling and dog-ears resistant banknote. In applied science, the transition from research to industry is essential but sometimes this gap takes years to be crossed. Indeed, lab-scale and industrial-scale do not suffer from the same requirements and constraints. If almost everything is possible at lab-scale, the up-scaling needs to take into account parameters such as the supplying feasibility, the adaptability with existing process and the economic impact.

Nanocellulose science has particularly suffers from this phenomenon. For a long time, the number of scientific publications has shown an exponential increase passing from 198 in 2010 to 1129 in 2017¹, proving the outstanding properties of this material for many applications. However, the increase of patents in pulp and paper industry has been more cautious due to the expensive cost, the difficulty for characterization, the low solid content of the suspensions and the lack of information regarding process issues (impact on drainage, problem of retention, viscosity and pumping difficulty) of this material. Nowadays, some of these problems have been overcome thanks to huge improvements on nanocellulose process, allowing its production in large quantity, at high solid content, with a close attention to the energetic consumption (Spence et al. 2011; Tejado et al. 2012; Rol et al. 2017). Years after their discovery in the 50's for cellulose nanocrystals (CNCs) and in the 80's for cellulose nanofibrils (CNF), their use in pulp and paper industry has become one of the most targeted application (Campano et al. 2018), with 51% of the volume industry demand for nanocellulose which will come from pulp and paper industry (Future Markets, Inc 2017).

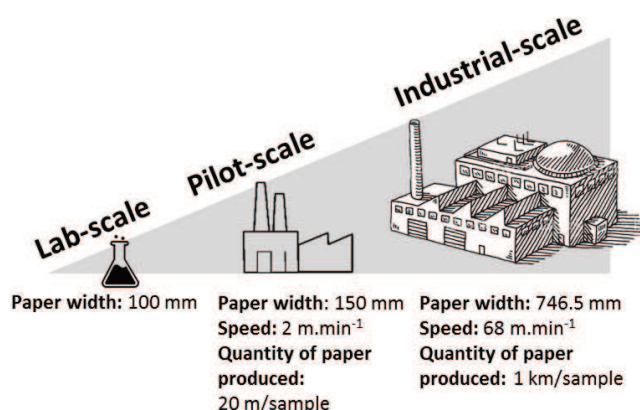


Figure 1: Up-scaling production of banknote paper containing nanocellulose

¹ Based on SciFinder research. Descriptors: Cellulose + CNF, Cellulose + MFC, Cellulose + NFC, Cellulose nanofibers, nanofibrillated cellulose, cellulose nanofibrils, Cellulose + CNC, Cellulose + NCC, Cellulose nanocrystals, Nanocrystalline cellulose, Cellulose nanowhiskers

At lab-scale, a new banknote structure has been developed. This banknote, classically composed of two refined cotton fiber layers, has been modified with (i) the insertion of a CNF layer between the fiber layers for crumpling limitation, and with (ii) the addition of CNCs in the PVOH impregnation bath for dog-ears limitation. Lab experiments showed enthusiastic results with 2 patent applications. The natural next step is now to check the validity of these results with higher volumes (Figure 1). Both CNF and CNC have been implemented using the pilot machine dedicated to banknote manufacturing in Banque De France facility. Later, the CNC reinforced PVOH strategy has also been tested on a real banknote paper machine, at industrial scale. This test was also the opportunity to test the impact of some of the post-treatments involved in the banknote manufacturing, such as part of the security feature step (deposition of the holographic tape).

1.2. Materials and methods

Due to confidentiality reasons, no pictures were allowed during pilot and industrial tests.

1.2.1. Pilot tests

Pilot tests were performed in October 2015 in Banque de France facility (Chamalières). It is worth noting that these pilot tests were performed at the beginning of the project and strategies were not fully optimized at this point.

Pulp. Refined cotton (65 °SR) without dye or security items was prepared from 11 kg dry sheets of cotton. Moreover, 5 wt.-% of TiO₂ Anatase and acidic dyes were added into the pulp slurry. In addition to TiO₂ the pulp also includes 2.7 wt.-% wet strength agent Polyamideamine epichlorohydrin (PAE) and 0.9 wt.-% anionic polymer carboxymethylcellulose (CMC). Cotton fibers have an average length of 603 µm and an average width of 27.5 µm.

Polyvinyl alcohol (PVOH). PVOH used was a confidential mixture of a high molecular weight PVOH and a low molecular weight PVOH. The weight ratio was respectively 2:1 and the solid content of the solution was 5 wt%.

Cellulose nanocrystals (CNCs). Commercial CNCs extracted from wood pulp were purchased from the University of Maine as a CNC suspension at 12 wt%. They have a length of 136 nm (+/- 50), and a width of 11 nm (+/-5), and a sulfate content of 340 mmol/kg. Their detailed characterization is available in (Gicquel et al. 2017).

PVOH-CNC formulation. Polyvinyl alcohol (PVOH) was previously cooked by Banque de France with a solid content of 5% and kept at a temperature of 60°C. Cellulose nanocrystals at 12wt% and water were added in order to obtain different ratios of CNC/PVOH (Table 1), while keeping a final solid content of 5%. The mixture has been mechanically stirred for 1 hour at 60°C before impregnation, and kept at this temperature during the trial.

Cellulose nanofibrils (CNFs). CNF suspensions were prepared at lab-scale from cotton dry sheets. This pulp was firstly soaked into water overnight before being refined at 65 °SR, pre-treated with enzymes and defibrillated with ultrafine friction grinder (Model MKZA6-2, Disk model MKG-C 80, Masuko Sangyo Co., Ltd, Japan) working at 2500 rpm, in recirculation for 2.5 h. The protocol is exactly the same as the one described in Chapter III.1. Experimental section, except that cotton pulp was used instead of eucalyptus pulp. The final solid content of the suspension was 2 wt%.

Mixture of CNF with additives. Cotton fibers have been refined at 65 °SH and pretreated with enzymes following the already described protocol. However, in this case, the pretreated pulp has been mixed with 20 wt% titanium dioxide “TiO₂” (PRETIOX®, grade AV01L, anatase) or 20 wt% glass fibers “GF” (confidential source) before being disintegrated in Masuko super-grinder. Titanium dioxide powder before disintegration consisted of spherical particles with an average diameter of 0.40 +/- 0.05 µm and glass fibers have an average diameter of 5 +/- 3 µm. These additives act as abrasive agents and allowed decreasing the duration of the mechanical treatment. For the same resulting CNF dimensions, CNF + TiO₂ has been mechanically treated during 30 minutes and CNF + GF 1 hour. The final solid content of the suspensions was 2 wt%.

Pilot paper machine description. The pilot paper machine runs at 2 m.min⁻¹ and the paper width is 250 mm. The pilot machine is composed of two round shape formers in order to produce a two layers paper, with a first layer of 30 g.m⁻² and a second layer of 60 g.m⁻². For the introduction of the CNF layer, a spray has been introduced between these two fiber layers. In this case, the two fiber layers had final basis weight of 25 g.m⁻² and 60 g.m⁻² and the CNF layer was pulverized for a theoretical final content of 5 g.m⁻². Another trial has been performed with a CNF layer of 10 g.m⁻² instead of 5 g.m⁻². The CNF layer was sprayed above the thinner fiber layer and recovered by the thicker one. The spray allowed a total CNF width layer of 180 mm, with a homogeneous width of 150 mm. The range of possible flow rate with this spray was between 15 and 40 L.h⁻¹, with an increase in droplet size induced by the increase in flow rate. The flow rate during our trials was estimated at 18.9 L.h⁻¹. Before spraying, a red dye was introduced in the CNF batch in order to check the homogeneity of the nanofibrils and their distribution within the final paper. The CNF suspension was sprayed at a solid content of 2 wt%. The pilot paper machine ran during 20 minutes for each paper sample.

Pilot coater description. The impregnation has been performed on a pilot coater independent of the pilot paper machine. The maximal speed of this pilot coater is 4 m.min⁻¹ but for the trial, 2 m.min⁻¹ was set. The final paper width was 250 mm and the impregnation time was 3.5 seconds. After impregnation, the paper went through convective driers with hot air at 115°C. The length of the drying section was 60 cm, corresponding to a drying time of 18 seconds. Finally, the paper crosses a soft calendaring section before being rolled and recovered. The final paper humidity, which is important to control in order to prevent shrinking and crumpling, was 6% RH.

Paper samples. 4 paper samples were produced from the pilot paper machine and 3 were produced with a deposition of 5 g.m^{-2} of different CNF suspensions (with or without additives). Then, different ratios of CNC/PVOH have been tested on the reference paper (bilayer without CNF), and two different impregnation bath have been tested on the 5 multilayers. Samples are synthesized in Table 1.

Table 1: samples preparation on pilot paper machine and pilot coater

Sample name	Pilot papermachine	Pilot coater
1.0	Two layers 60 and 30 g.m^{-2}	X
2.0	Two layers 60 and $25 \text{ g.m}^{-2} + 5 \text{ g.m}^{-2}$ CNF	X
3.0	Two layers 60 and $25 \text{ g.m}^{-2} + 5 \text{ g.m}^{-2}$ (80 wt% CNF – 20 wt% TiO ₂)	X
4.0	Two layers 60 and $25 \text{ g.m}^{-2} + 5 \text{ g.m}^{-2}$ (80 wt% CNF – 20 wt% GF)	X
1.1	Sample 1	100% PVOH
1.2	Sample 1	95 wt% PVOH – 5 wt% CNC
1.3	Sample 1	90 wt% PVOH – 10 wt% CNC
1.4	Sample 1	80 wt% PVOH – 20 wt% CNC
1.5	Sample 1	60 wt% PVOH – 40 wt% CNC
2.1	Sample 2	100% PVOH
2.4	Sample 2	80 wt% PVOH – 20 wt% CNC
3.1	Sample 3	100% PVOH
3.4	Sample 3	80 wt% PVOH – 20 wt% CNC
4.1	Sample 4	100% PVOH
4.4	Sample 4	80 wt% PVOH – 20 wt% CNC

1.2.2. Industrial tests

Industrial tests were performed on October 2017 in Banque de France paper machine facility (Europafi, Vic-Le-Comte). Contrary to pilot tests, only the impregnation strategy with CNC-reinforced PVOH has been tested at the industrial scale.

Pulp. Refined cotton (65 °SR) without dye or security items was prepared from 11 kg dry sheets of cotton. This pulp also contained TiO₂ (Anatase), wet strength agent (PAE) and CMC in confidential amounts. The cotton fibers had an average length of $603 \mu\text{m}$ and an average width of $27.5 \mu\text{m}$.

Polyvinyl alcohol (PVOH). PVOH used was a confidential mixture of a high molecular weight PVOH and a low molecular weight PVOH. The weight ratio was respectively 2:1 and the solid content of the solution was 4.5 wt%. For the trials, 1100 kg were cooked directly in Banque De France. Before the introduction of cellulose nanocrystals (CNCs), the PVOH temperature was set at 71°C.

Cellulose nanocrystals (CNCs). A dry CNC powder was bought from Celluforce (Canada). These nanocrystals have a length of $183 \pm 88 \mu\text{m}$ and a width of $6 \pm 2 \mu\text{m}$, and a sulfate content of 250 mmol.kg^{-1} (Reid et al. 2017). A CNC suspension of 5.55 kg in 128 kg of water was prepared following the dispersion protocol extracted from CelluForce NCC™ Dispersion Guide.

CelluForce NCC™ Dispersion Guide. This guide was used for the section “Dispersing large volumes of NCC powder to 10 wt% or lower”. The right amount of water has been first added in the container. Then, the CNCs were progressively added by avoiding the CNC powder to hit the inner wall of the container. The mixing was then started for 1 hour and the speed was progressively increased until the formation of a vortex.

PVOH-CNC formulation. After cooking of 1100 kg of 4.5 wt% PVOH, the CNC suspension was directly introduced and mechanically stirred for 1 hour. The final mixture was composed of 90 wt% PVOH and 10 wt% CNCs, with a solid content of 4.5 wt%. After the introduction of CNCs, the impregnation bath temperature decreased from 71°C to 62°C.

Paper machine description. More details are given in the bibliographic part, Chapter I. Since October 2017, a new paper machine manufactured by Allimand is effective, with a width of 2.55 m and a length of 100 m. However, these trials have been performed with the former paper machine and the following description corresponds to this one. This paper machine, running at 68 m.min⁻¹ and with a width of 746.5 mm, is composed of two round shape former which distribute the cotton fiber suspension. Two layers are formed: first, the thinner one of approximately 25 g.m⁻², and a thicker one of approximately 60 g.m⁻² containing also the watermark. After wet formation, these layers are dried by the press section, the hot cylinders and the air driers as described in Figure 2. These steps are followed by a coating section composed of an impregnation bath containing the polyvinyl alcohol (PVOH), in which are introduced the cellulose nanocrystals (CNCs). Finally, the impregnated paper is routed to another drying section composed of three air driers. In the two first ones, the temperature is generally regulated between 80 and 92°C, and the last one is not alimeted but keeps a temperature of approximately 66°C. After a soft calendering, the paper is recovered.

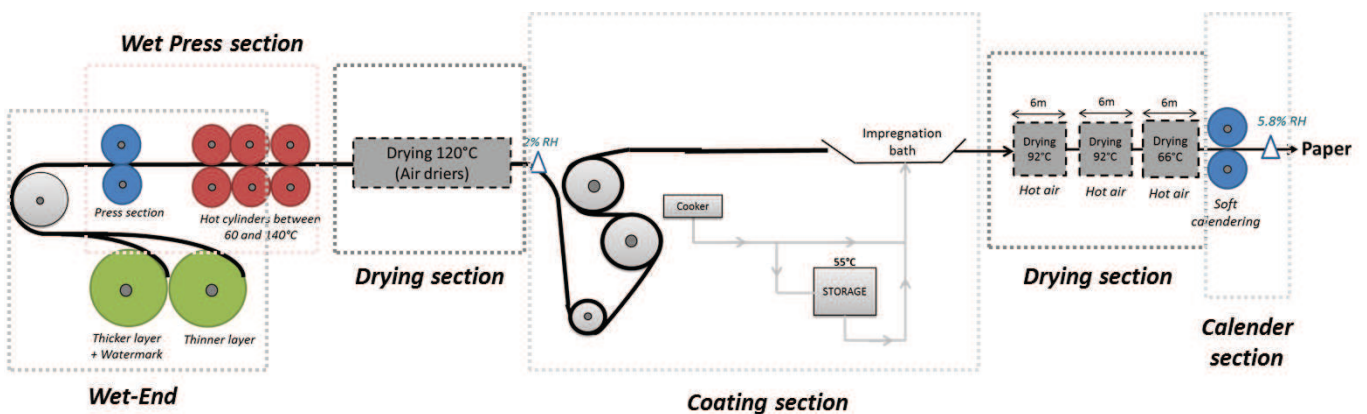


Figure 2: Overview of a banknote paper machine (described from Banque de France facility)

Security feature step. After the paper machine production, a security feature step consisting in the deposition of a hologram has been performed. The paper was subjected for few seconds to hot air (140°C), followed by a rapid contact with a hot surface (170°C). Then, the paper was cooled, before

being again heated by a rapid contact with a second hot surface (140°C). The paper was finally cooled and humidified. Then, a localized calendering was performed just on the holographic tape.

Paper samples. Paper samples were recovered after an impregnation bath of 100% PVOH, at the end of the paper machine (sample 1) and after the security feature step (sample 2). In this case, the two drier sections following the impregnation step were classically set at 92°C each (drying 1). Then, the impregnation bath was changed for the mixture containing 90 wt% PVOH and 10 wt% CNCs. With the same drying (drying 1), two paper samples were recovered after the paper machine production (sample 1') and after the security feature step (sample 2'). Finally, the temperature of the drying sections was increased to 105°C each (drying 2), and two other paper samples were recovered from this drying, one after the paper machine production (sample 1'') and one after the security feature step (sample 2''). To conclude, 6 different samples were analyzed. It is worth noting that, for time and feasibility reasons, the paper sample impregnated with only 100% PVOH and dried with drying 2 (105°C) was not performed.

1.2.3. Improvement track for industrial tests optimization

These trials were performed at lab-scale in Laboratory of Pulp and Paper Science (LGP2, Grenoble).

Polyvinyl alcohol (PVOH). PVOH used was a mixture of Mowiol 28/99 (31 000 g.mol⁻¹) and Mowiol 6/98 (47 000 g.mol⁻¹), bought from Sigma Aldrich.

Cellulose nanocrystals (CNCs). Cellulose nanocrystals from the University of Maine (12 wt%) or cellulose nanocrystals from Celluforce (dry powder) were used for these lab tests. Description was already mentioned in previous pilot test and industrial test sections.

Dispersion of dry CNC powder from CelluForce. The dispersion procedure has been extracted from CelluForce NCC™ Dispersion Guide. The right amount of CNCs was weighted to make a suspension of 1 liter at 5 wt%. A beaker of 2 liters has been used to ensure an efficient stirring at the top of the suspension. Water was first introduced into the beaker, and stirring has been performed with a long and large magnetic stir bar. The speed has been adjusted such that the vortex formed was large enough to reach the tip of the stir bar. Finally, CNCs were added progressively into the deionized water, avoiding the addition directly into the heart of the vortex to prevent splashing and avoiding also the addition onto the walls of the beaker. An increase of viscosity of the suspension was observed and indicates a good dispersion of CNCs. The dispersion lasted for at least 1 hour, and the stirring speed was continuously increased to keep the same vortex intensity.

PVOH-CNC formulation. Mowiol 28/99 and Mowiol 6/98 were mechanically mixed in a weight ratio of respectively 2:1, and put in water with a final PVOH concentration of 5 wt-%. When the temperature reached 90°C, the suspension was kept mechanically stirred during at least 2 hours, until complete dissolution of PVOH. To introduce CNCs into the PVOH solution, the previously

prepared PVOH mixture was heated at 60°C. Then, the desired quantity of water and nanocrystal suspension was added to have several ratios (wt%) of PVOH + CNC once dried. Water was then introduced to obtain a 5 wt-% total solid concentration. The suspension was mechanically stirred during 1 hour. Then, the suspension was exposed to an ultrasonic dispersive energy of 5 kJ/g of dry CNC using a 250 Watt (or 250 J/s) sonication probe (Sonifier S-250A, Branson, USA) at 50% of maximum energy and at room temperature with an ice bath.

Impregnation and drying protocol. Paper substrates with 15 cm x 10 cm dimensions were immersed in a warm impregnation bath (60°C) containing the mixture of PVOH and CNCs for 20 s. Then, the impregnated paper was placed on a Teflon plate and the overflow was removed with one pass of a 1 kg Teflon roll. Then, the sample was placed in an oven with air convection and dried at 115°C for 3 min. During drying the sample was maintained under tension between two metal frames. When specified in the text, other drying processes have been tested by extending the drying time or by using infra-red lamps. Infrared drying was performed with 2500 W long wave IR lamps. As it is possible to dry only one side with IR lamps with our equipment, two passes were performed by turning the paper between two drying steps. Each drying lasts 60 s.

1.2.4. Characterization tools

All the samples were stored in a conditioned room (23°C, 50% RH) for at least 48 hours before testing.

Brookfield viscosity (mPa.s). The viscosity of the CNF suspension used for pilot trials has been characterized using Brookfield rheometer (DV-E Viscometer, Brookfield Ametek®, United states). The suspension solid content was 2% and the viscosity has been measured at 100 rpm after a stabilization time of 10 minutes. This test has been repeated 5 times for each sample.

Elastic angle recovery. Details are given in Chapter II.3., experimental section, 2.2. “Methods”. The pressure applied in this study was 0.6 kPa, corresponding to a weight of 200 g. Additional information is also given in Chapter II.3. “Supporting Information 2”.

Crumpling. Pilot papers were crumpled using NBS x1 method. Details are given in Chapter III.4., experimental section, 2.3. “Crumpling characterization”. The resulting papers were then characterized by their waviness profile, also described in the same chapter.

Spring effect. Details are given in Chapter III.4., experimental section, 2.3. “Crumpling characterization”.

Double ply. The double ply test has been performed in machine direction orientation. Papers were cut with a length of 15 cm and a width of 15 mm, and tested in a double-ply device (Lorentzen &

Wettres®, Sweden), following the norm ISO 5626 1994 and with a weight of 600 g. For each samples, 10 duplicates were performed.

Tensile tests. The tensile properties were measured with a vertical extensometer (Instron 5965), following the standard NF Q03-004. Basis weights have been measured using a surface of 10x10 cm² and the thickness was measured with Lhomargy micrometer. These values were then reported into the tensile device to obtain the Young's Modulus, breaking length and breaking force. The grips have been selected to limit slipping of samples. Tensile tests were performed at 10 mm/min. The dimensions of the samples were 10 cm for the length and 15 mm for the width. For each samples, 10 duplicates were performed.

Tear resistance. The tear resistance was measured using a tear tester (Noviprofibre, Elmendorf pendulum 16000 mN, France). Samples were cut at (65 × 50) mm² dimensions, and the measurement corresponds to the force (mN) needed for tear propagation after a primer. For each samples, 10 duplicates were performed.

Scanning electron microscopy (SEM). SEM images were obtained for paper cross sections and surfaces after gold sputter coating of 5 nm, with a tension of 10 keV, a spot size of 3.5, in EDT mode. The working distance was fixed at 10 mm. At least 6 images were taken for cross section and surface, and the most representative were selected.

1.3. Results and discussion

1.3.1. Pilot tests

1.3.1.1. General observations during the trials

Introduction of the CNF layer.

The pilot paper machine of Banque de France is developed for the production of a two layer paper, corresponding to the banknote structure. There are consequently two round-shape formers producing first a thin layer (30 g.m⁻²) and then a thicker layer (60 g.m⁻²) of refined cotton. For this project, a spray device has been set up in order to introduce a CNF layer between the two fiber layers, with an expected basis weight of 5 g.m⁻². The main purpose of this CNF layer is the increase of crumpling resistance.

To be perfectly independent, one idea of the project was the direct production of CNF material from the Euro paper mills. A preliminary study (Phase 1) concluded to the feasibility of the production of CNF from the refined cotton pulp, with competitive properties comparing to commercial grades (also confirmed by the Quality Index, **Chapter III.1.**). That is why these tests have

been performed with CNF from cotton pulp. Three different CNF suspensions have been prepared: a classic one, a CNF suspension prepared with 20 wt% TiO₂, and a CNF suspension prepared with 20 wt% GF. These additives have been considered for two reasons. First, they act as abrasive agent during the mechanical disintegration step. A complementary study has proved that they significantly reduce the energy consumption necessary for the CNF production. This point is particularly important as a gain of energy is linked to a gain of cost, and the high energy consumption of CNF production is still one of their main drawbacks. Secondly, the introduction of additives is also a way to decrease the hydrogen bonding of the CNF layer, and consequently decrease the layer cohesion and tear propagation. Titanium dioxide has been especially used as it is already a constituent of the pulp slurry and promotes paper opacity. Glass fibers have been used as an alternative. Later in this project, polyethylene terephthalate (PET) has been considered as a promising additive, enhancing the crumpling resistance in dry and wet states and allowing better tear resistance. However, at the time of pilot tests (November 2015), this strategy was not yet investigated.

One of the main objectives of this pilot study was the evaluation of the process feasibility. The most critical points were the possibility to spray the CNF layer without (i) drainage issues and (ii) retention issues. The second objective was the confirmation of interesting results observed at lab-scale regarding the decrease of crumpling defects.

CNF suspensions were sprayed at 2 wt% solid content, corresponding to a viscosity of 150 mPa.S at 100 rpm. Despite this viscosity value, the suspension has been easily sprayed with a homogeneous distribution in width, as indicated by the red coloration used to localize CNF in the final material. However, especially when CNF was produced with TiO₂, some agglomerates were visually observed. A better CNF spraying would be achieved by dilution of the suspension, but this additional amount of water would risk impacting the drainage. In this case (CNF solid content 2%), no drainage issues were observed. Consequently, even if the viscosity slightly affects the spraying, this solution worked and allows the deposition of a CNF layer inside the paper without impacting the paper drying or any other process issues. For other tests, an optimization of the spray flow rate and nozzle diameter could limit CNF flocs.

Retention of CNF.

Because of their nano-dimensions, the retention of cellulose nanofibrils as wet end additive in papermaking is usually limited and difficult to control or calculate. Problems of retention can then result in inefficient CNF influence (Ridgway and Gane 2012; Afra et al. 2016). During pilot tests, the width of the paper machine was 250 mm while the width of sprayed CNF was 150 mm. The location of CNF is observable thanks to their coloration. Consequently, it is possible to know the basis weight of fiber layers only and the basis weight of the fiber layers containing the CNF layer for each sample. The difference between these two values is reported in Figure 3. At the same time, the CNF consumption is measured by weighting the quantity of CNF suspension before and after spraying.

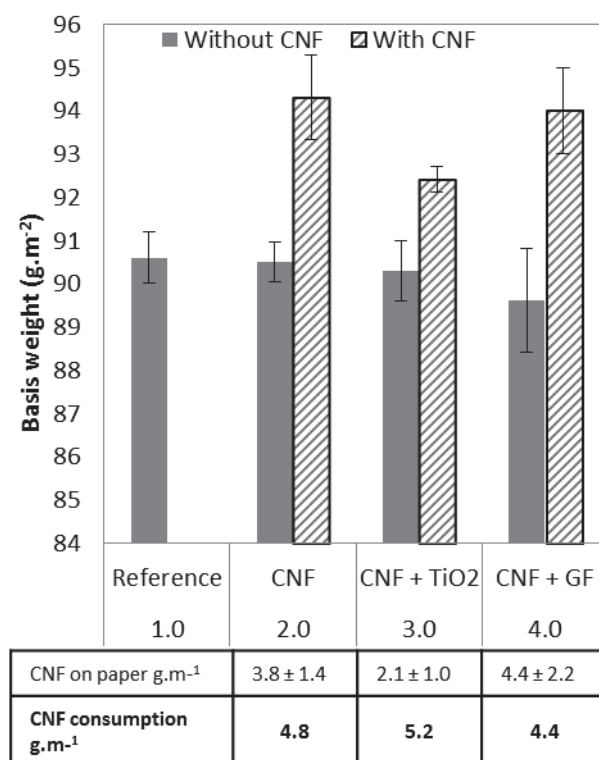


Figure 3: Basis weights of multilayers produced on pilot paper machine

The targeted quantity of CNF in samples 2, 3 and 4 was 5 g.m^{-2} . Figure 3 shows that the CNF consumption follows this objective for the spraying of CNF alone and CNF with TiO_2 and is slightly lower for the spraying of CNF containing glass fibers. The loss in this last case can be due to a system clogging because of higher dimensions of glass fibers.

Finally, by comparing the CNF consumption with the quantity of CNF present on the paper, it is possible to see that a part ranging from 1 to 3 g.m^{-2} of the nanomaterial, which is sprayed on the thinner fiber layer (20 g.m^{-2}), was not retained by the fibrous material and goes through the material porosity or around spray zone. This loss of material constitutes not only a loss in final paper properties but also an economic loss. However, for now, the only possible solution to obtain a 5 g.m^{-2} layer inside the paper is to increase the amount of sprayed CNF.

Introduction of CNC in the impregnation bath.

After the multilayer production, the paper reel was introduced in the pilot coater for impregnation. Beforehand, CNCs in suspension were added with different weight ratios in the PVOH bath and vigorously mixed using a mechanical stirrer. The final solid content was kept at 5% for each sample. After introduction of CNCs, foam was formed. This foam was eliminated by decreasing the mixing speed and no other issues were observed during the whole impregnation process, including the drying step. Whatever the CNC content in the PVOH, an impregnation of $5.1 \pm 0.7 \text{ g.m}^{-2}$ was achieved.

1.3.1.2. Final paper properties

General mechanical properties.

Cellulose nanofibrils, due to their nano-dimensions and their high bonding potential, are well known to decrease the paper porosity when they are mixed in a pulp slurry (Hassan et al. 2011). This can have disastrous consequences on the tear resistance, as the tear easily propagates with lower solid/air interfaces. Furthermore, CNFs are easily ruptured during tear deformation due to their low individual dimensions. In this case, they were introduced as a thin middle layer and this structure was confirmed in previous study (**Chapter III.4.**). Figure 4 shows that the CNF layer does not strongly impact the total multilayer density as only a slight increase is reported between the reference paper and the paper with CNF inside. This does not mean that the density is not high locally, and lab-studies have shown that these CNF layers can represent a weak point enhancing the tear propagation. In this case, no differences were reported for multilayer tear resistance in machine direction. The expected increase of property brought by the additives did not show relevant results. However, in cross direction, slight decreases of tear resistance were observed with sample 3.0 (containing CNF + GF) testifying the presence of weaker area in these cases.

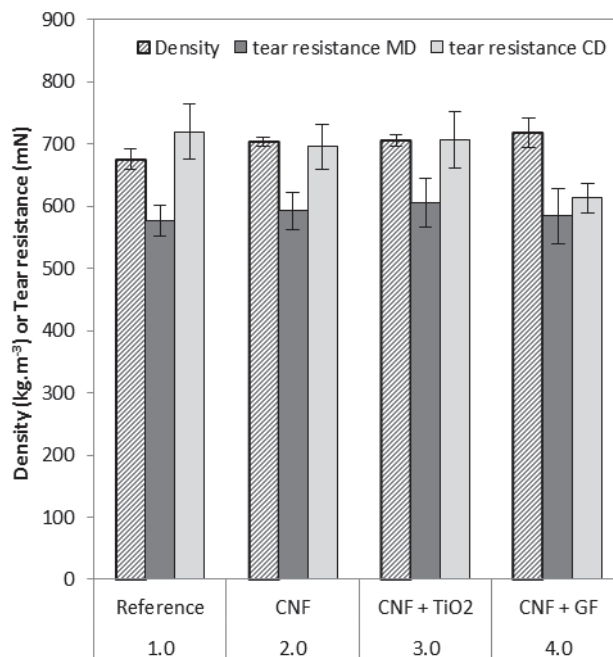


Figure 4: Density and tear resistance of multilayer produced from pilot test, without impregnation. MD = machine direction, CD = cross direction

Tensile tests and double-ply values of the multilayers are reported in Table 2. It appears that the introduction of the CNF layer (with or without additives) did not change any of these mechanical properties, except a slight increase of Young's modulus obtained with the introduction of CNF alone. After impregnation, the papers show better mechanical properties (both tensile properties and

double ply) and these results were not impacted by the introduction of CNCs in the impregnation bath, whatever the ratio.

To conclude, introduction of a CNF layer within the paper bulk and/or introduction of CNCs in the impregnation bath did not enhance nor damage the global mechanical properties.

Table 1: general mechanical properties (tensile properties and double ply) of multilayers produced from pilot tests. MD = machine direction, CD = cross direction.

	Reference	Introduction of CNF layer (with or without additives)	Impregnation with different ratios of CNC/PVOH
Fr (N)	MD: 126.5 ± 1.4 CD: 88.2 ± 0.8	MD: similar values CD: similar values	
E (Gpa)	MD: 5.7 ± 0.1 CD: 4.0 ± 0.1	MD: Slight increase with CNF (6.9 ± 1.9 for sample 2.0) CD: similar values	Increase of properties by $\approx 15\%$ with PVOH but no influence of CNCs
Lr (Km)	MD: 9.5 ± 0.1 CD: 6.6 ± 0.1	MD: similar values CD: similar values	
Double ply	MD: 1549 ± 257	MD: similar values	Increase of double ply number with PVOH but no influence of CNCs (1992 ± 551 for sample 1.3)

Reduction of crumpling and dog-ears.

Influence of CNCs on dog-ears limitation. At lab-scale, the introduction of cellulose nanocrystals with a ratio of 10 wt% in PVOH matrix has successfully contributed to increase the dog-ears resistance, and it has been confirmed with several parameters in **Chapter II.3**. Figure 5 presents the elastic angle recovery values of the pilot papers without impregnation and after impregnation with different ratios of CNCs. Similar results of elastic angle recovery after folding were obtained for banknote paper without impregnation and with impregnation of 100% PVOH. With introduction of CNCs, this value increases until an optimum obtained for 10 wt% CNCs. The same optimum was observed during lab experiments. Even if lower values of angle recovery were obtained compared to lab tests, these pilot tests confirm the same benefit of CNCs for dog-ears limitation. These interesting results as well as the confirmation of process feasibility at up-scale level have motivated the filing of a patent, accepted and published in 2017 (Bras et al. 2017).

Influence of the CNF layer on crumpling limitation. Preliminary studies at lab-scale have proved that the addition of a CNF layer within paper decreases both the crumpling and spring effect phenomena. To characterize the crumpling, three methods with different intensities were implemented (NBS x1, NBS x4, and balloon test) followed by an image analysis performed on thresholded pictures. In pilot tests, a dye was introduced in the CNF batch and disturbed this image analysis. For printed or colored papers, another characterization method has been performed based on a laser deformation by paper

relief and measuring the waviness profile. Moreover, it has been proved that this method gives exactly the same trends than crumpling values quantified by classical image analysis (**Chapter III.4.**). Figure 6 shows that the waviness profile of a paper after NBSx1 crumpling (intermediate intensity) is significantly decreased with the introduction of a CNF layer. Furthermore, the spring effect has been strongly decreased by more than 50%. These results have consequently confirmed the possibility to up-scale this strategy as (i) a CNF layer has been successfully sprayed into the two cotton fiber layers and (ii) results for the decrease of crumpling showed the same trends than for lab-tests. However, the results with additives showed mitigated results as both TiO₂ and GF increase the crumpling value and the spring effect compare to CNF addition alone.

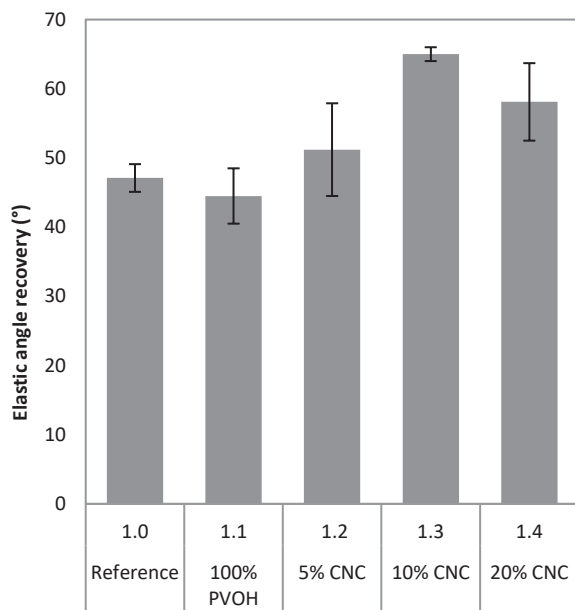


Figure 5: Elastic angle recovery of pilot banknote paper impregnated with different weight ratios of CNCs in the PVOH bath

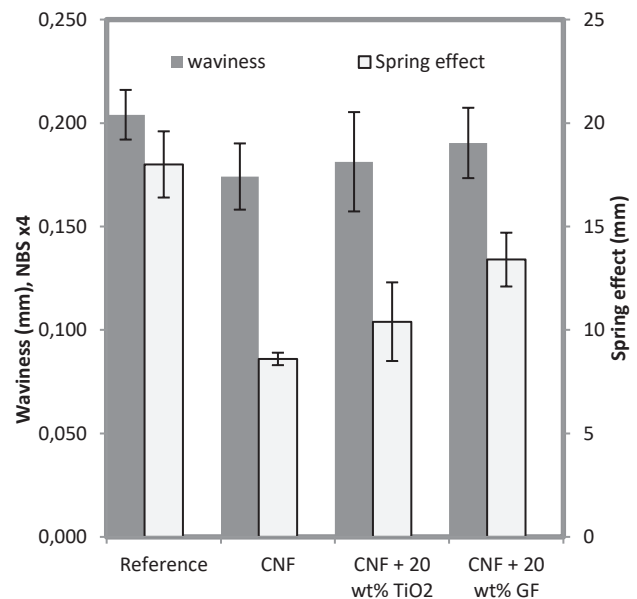


Figure 6: Waviness profile and spring effect of pilot papers after crumpling with NBS x4

1.3.1.3. Conclusion

The two strategies of the project for dog-ears and crumpling limitation have been up-scaled and confirmed using a spray system for CNF and by introducing CNC in the PVOH impregnation bath. First, the feasibility was proved as no paper process issues were observed during the trials, and the presence of the CNF layer within the paper was confirmed. Secondly, the introduction of the CNF layer without additives has contributed to limit the crumpling and the spring effect, and the introduction of 10 wt% CNCs in the impregnation bath has contributed to increase the elastic angle recovery after folding. In parallel, no change in general paper density was observed and the mechanical properties (tear resistance, tensile properties, double-ply) was not affected by this change of paper structure. These interesting results at both lab and pilot scales have motivated the desire to go one step further and perform industrial tests on banknote paper machine.

1.3.2. Industrial tests

1.3.2.1. General observations during the trials

Industrial tests with real banknote paper machine were performed at Banque de France Europafi (Vic le Comte). Only the CNC reinforced PVOH strategy was tested as the priority was the confirmation of the patent at industrial level. Furthermore, this strategy is easy and fast to implement, without changing any part of the paper machine process. Cellulose nanocrystals in large amount have been provided by Celluforce under the form of a dry powder. The CNC suspension has been prepared before the test, and added on site to the PVOH prepared by Banque de France in order to obtain 10 wt% CNC and 90 wt% PVOH. This mixture has been vigorously stirred, and, as observed in pilot tests, foam appeared. However, this foam disappeared with the decrease of stirring speed. No change in viscosity occurred with the introduction of CNCs in the PVOH as the mixture solid content was kept at 5%.

Lab tests have proved that the drying temperature after impregnation has a strong impact on the mechanical properties of resulting paper, and especially on dog-ears resistance (**Chapter II.3.**). For pilot tests, the drying temperature was set at 115°C and this is also the reason why lab tests classical temperatures were performed at 115°C. However, the best results were obtained with infrared drying, allowing reaching quickly temperatures of 200°C, and the resulting elastic angle recovery after folding was increased by 27%. On the industrial paper machine, the drying temperature is regulated to keep a final paper humidity of 5.8% RH, and was fixed at 92°C during the trial. An increase of this temperature is complicated to implement, as it can induce paper shrinking and, worst, paper break. However, as the best results of dog-ears limitation were obtained with the highest temperatures, temperatures of the driers were especially increased at 105°C for the need of the project. Despite the fact that such conditions are not a long term possible strategy, only small paper shrinkage (2 mm) was observed and, fortunately, no paper break.

For the record, paper samples were recovered (i) at the end of the paper machine process and (ii) after security feature steps, in order to study the impact of post-treatment on dog-ears properties (Figure 7).

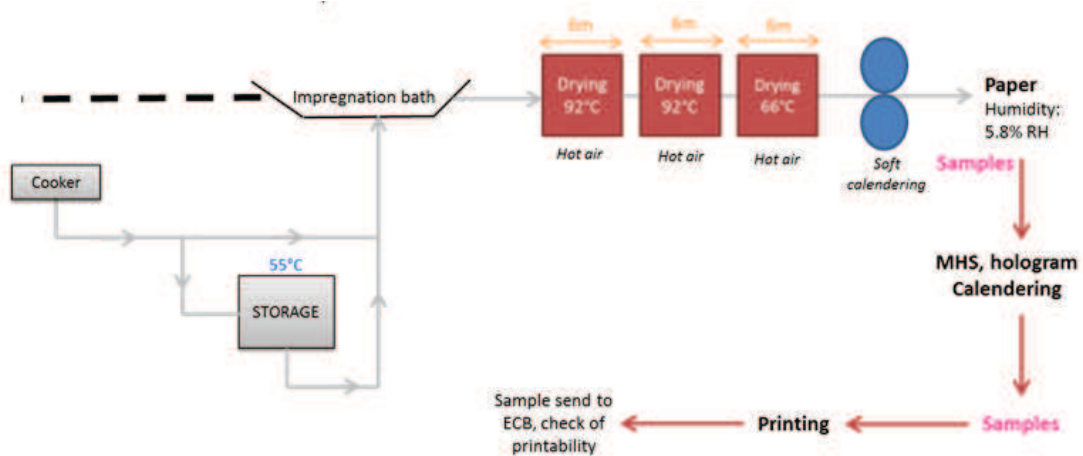


Figure 7: Impregnation of banknote paper with CNC-reinforced PVOH at Europafi facility

1.3.2.2. Final paper properties

General mechanical and structural properties.

Tensile tests and double-ply were performed on paper impregnated with PVOH or CNC reinforced PVOH, before and after the security feature step, and for 92°C or 105°C drying temperatures. All these samples presented equivalent basis weights, Young’s modulus, breaking strength, breaking length, and double-ply value. Furthermore, no change in paper structure occurred with introduction of CNC in the impregnation bath or with increase of drying temperature (Figure 8). In each case, the impregnated layers are not visible on paper slices, and the paper surfaces showed same partial fiber recovery.

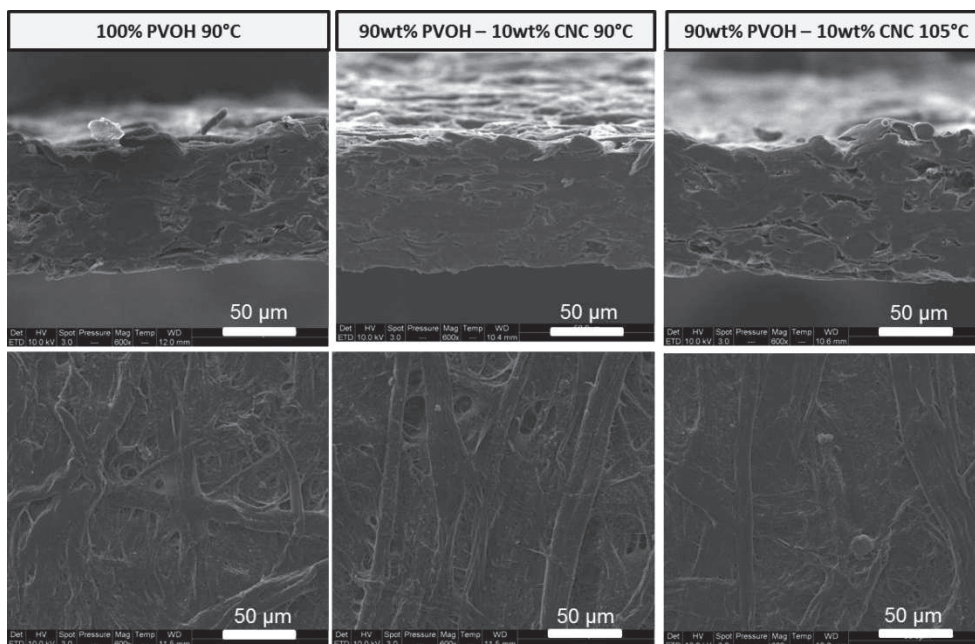


Figure 8: SEM images of industrial paper cross sections and surfaces after different impregnation baths and drying temperatures

Increase of banknote dog-ears resistance.

The elastic angle recovery of banknote papers impregnated with PVOH or CNC reinforced PVOH was calculated as shown in Figure 9. Classically, 2 minutes of stabilization are applied after the removal of the pressure on the folded angle. In this case, additional tests were performed by waiting 5 minutes. At the end of the paper machine (Figure 9-A), for a similar drying temperature of 92°C, the elastic angle recovery was unfortunately not increased by the addition of CNCs in the impregnation bath. The elastic angle recovery test has also been performed by duplicating the protocol twice on the same folding angle, in order to see if the influence of CNCs could appear after successive folding events. However, no better results were achieved. A slight increase of performance was observed with the increase of drying temperature from 92°C to 105°C confirming the impact of drying temperature on paper dog-ears behavior. However, as there is no reference for paper impregnated with 100% PVOH alone and dried at 105°C, it is not possible to conclude on the influence of CNCs in this case. These characterizations have been also performed with other pressure conditions (1.2 kPa instead of 0.6 kPa) and gave similar results.

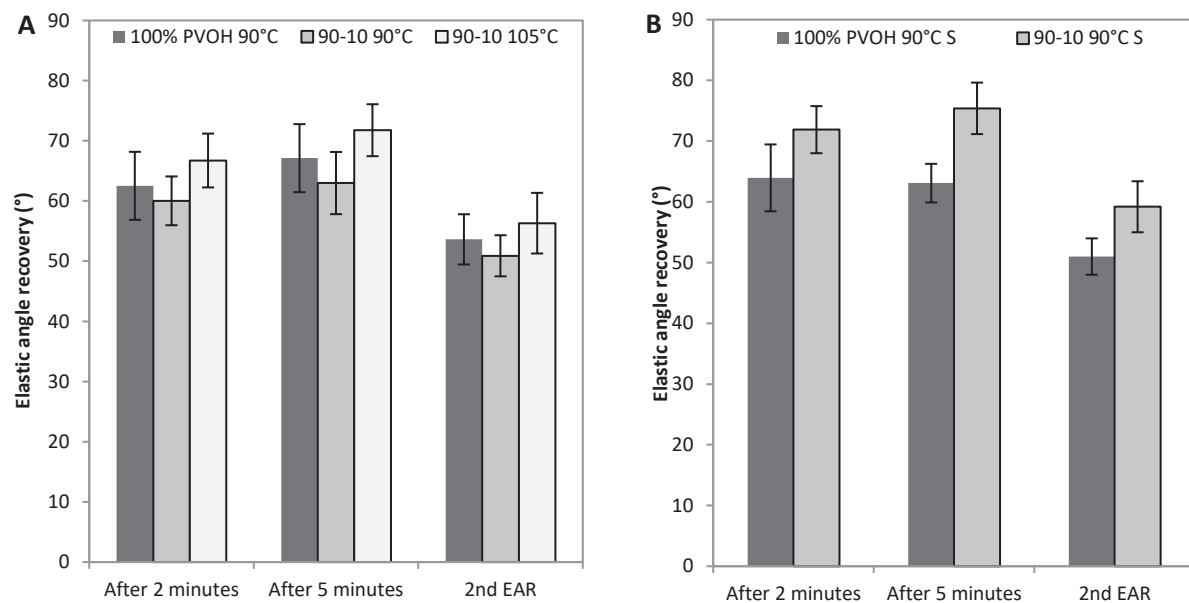


Figure 9: Elastic angle recovery (EAR) of papers from industrial test, after A) impregnation and drying at different temperatures and B) after the security feature step

Slightly different results were obtained after the security step (Figure 9-B). In this case, a small influence on paper elastic angle recovery after folding was observed after introduction of CNCs in the PVOH bath. This security step already includes thermal treatments (at 140°C and 170°C) which produce a fast annealing effect on paper surface. In any case, values of elastic angle recovery obtained remain below the one obtained at lab scale.

1.3.2.3. Conclusion

After the successful results obtained at lab and pilot scales, up-scaling at industrial level was not as good as expected (Figure 10) but confirms slight improvement, mainly after security step. This trial shows the influence of such post treatment. However, Figure 10 shows that the process conditions presented a lot of variations, such as different impregnation time, drying time, drying temperature and CNC source, and it is well known that change in paper process conditions lead to change in resulting paper properties. The next section tries to understand the reasons of these unexpected results and proposes solutions to implement for a second industrial trial.

	Lab scale	Pilot tests	Industrial test
EAR results (200g) *(depending on drying) ** drying at 90°C	Paper alone: 59.7 – 76.5* 100% PVOH: 67.1 – 80.4* 90-10: 74.0 – 97.5*	Paper alone: 47.1 ± 2.0 100% PVOH: 44.5° ± 4 90-10: 65° ± 1.0	Paper alone**: No value 100% PVOH**: 62.5 ± 5.6 (After security step: 63.9 ± 5.5) 90-10**: 60.0 ± 4.0 (After security step: 71.9 ± 3.9)
Impregnation time	20 seconds	3.5 sec	< 1 second
Coating concentration	5%	5%	4.5%
Drying time	Between 2 and 3 minutes	18 sec	10 sec
Drying temperature	115°C - IR	115°C	90°C or 105°C
CNC source	University of Maine	University of Maine	Celluforce

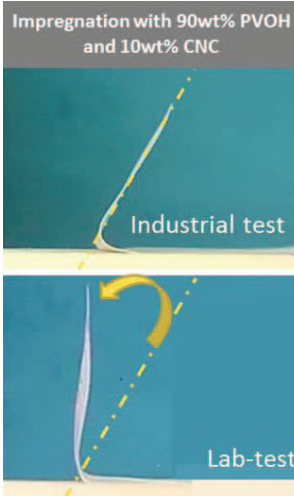


Figure 10: Comparison between lab, pilot and industrial scales in term of elastic angle recovery (EAR) results of papers and in terms of process conditions

1.3.3. Improvement tracks for industrial tests

1.3.3.1. Identification of impacting parameters

Factors which can explain the results of industrial tests have been identified in Figure 11. These factors, especially, target the main differences between lab test papers (whose CNCs strongly increased the dog-ears resistance) and papers produced at Europafi, in terms of:

- Raw material (change of CNC source)
- Paper machine process (change in paper tension)
- PVOH/CNC mixture (poor CNC dispersion, different percolation threshold due to change of CNC or incorrect ratio PVOH/CNC)
- Impregnation process (change of impregnation time and solid content, change in coating penetration in the paper, different overflow removal)
- Drying process (change in temperature and duration)
- Post treatment (soft calendaring of the paper after the drying section)

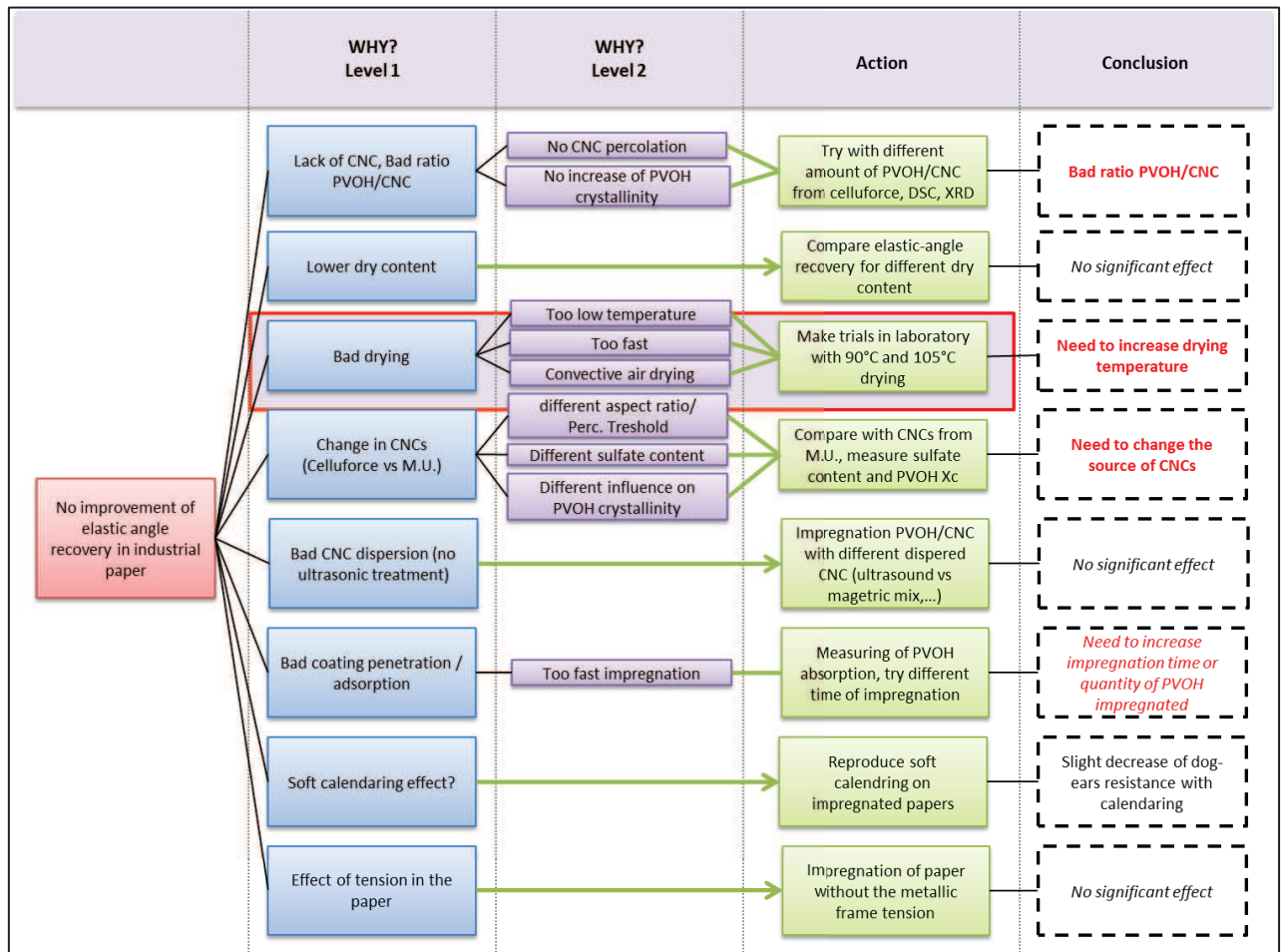


Figure 11: Causes and consequences matrix explaining the lack of paper dog-ears resistance observed after industrial tests

All the actions synthesized in Figure 11 have been investigated for each possible reasons. This helps separating each parameter into two categories: impacting or non-impacting parameters.

The change of solid content in the impregnation bath (5% in lab test vs 4.5% in industrial tests), as well as the difference in paper tension during impregnation appeared to be non-impacting parameters. The impact of calendaring on paper dog-ears resistance is mitigated. Only a slight decrease of dog-ears resistance has been observed with a soft-calendaring post treatment (50 kg/cm). However, the calendaring impact becomes more important with higher intensity (100 kg/cm) and can be responsible to important damage on paper dog-ears resistance.

On the other hand, the CNC source, the PVOH/CNC ratio, the drying conditions and the deposition of the PVOH-CNC layer on the paper appeared to strongly impact the paper elastic angle recovery after folding. CNCs from the University of Maine have been used for lab test while CNCs from Cellulforce, available in higher quantity and with competitive costs, have been chosen for the industrial tests. These two materials as well as their influence on dog-ears properties have been studied in a previous work (**Chapter II.3.**). Results showed that better results are obtained with CNC

from the University of Maine in comparison with CNC from Celluforce. CNCs from Celluforce present lower sulfate charge content, which has been proved to be an important parameter. Furthermore, the aspect ratio of CNC from the University of Maine and Celluforce is respectively 12.4 and 30.5, leading to a percolation threshold of respectively 7.2 and 2.9. It has been proved that the optimum of elastic angle recovery is obtained at the percolation threshold and a decrease of this property is observed with additional amounts of CNCs. Consequently, the amount of CNC from Celluforce during industrial test was not optimized. Furthermore, these CNCs have been received under dry powder form and they maybe suffer from a lack of dispersion during the suspension formulation and mixture with PVOH. However, trials at lab scale with ultrasonic probes to increase the CNC dispersion did not show any differences.

Furthermore, the duration of impregnation has been strongly reduced between lab and pilot tests (from 20 sec to less than 1 sec). Higher quantity of PVOH-CNC is deposited at lab-scale ($6.5 \text{ g.m}^{-2} \pm 0.6$) in comparison with industrial tests (2.2 g.m^{-2} , obtained after PVOH extraction by soxhlet). By changing the duration of impregnation at lab scale, it appears that a decrease of time is correlated to a decrease of resulting dog-ears properties. Finally, the drying temperature, among all the parameters, was the most impacting parameter as decreasing the temperature from 115°C to 105°C and then 92°C showed a drastically decrease of elastic angle recovery values even at lab scale.

1.3.3.2. Next steps

New industrial tests are in discussion for the end of this project (summer 2018). For now, some parameters are difficult to change, such as the CNC supply from Celluforce (allowing the high quantity necessary for the industrial tests), the duration of the impregnation bath and the drying temperature (which are process-dependent parameters). However, different CNC/PVOH ratios will be tested. To compensate the lack of temperature in the drying section after impregnation, the degree of crystallinity of PVOH will be artificially increased using a chemical component.

1.4. Conclusions

Trials at pilot and industrial test were key steps to learn more about (i) the banknote process and (ii) the possibility to implement new strategies with nanocellulose. Positive and negative conclusions are reported in the SWOT analysis (Table 3). Pilot tests have confirmed the possibility to spray a CNF layer between the two cotton fiber layers, and the possibility to introduce CNCs in the impregnation bath, without any process issues. Furthermore, the final multilayers have shown similar trends than lab experiments, with an increase in crumpling resistance with 5 g.m^{-2} CNF and an increase in dog-ears resistance with 10 wt% CNCs in 90 wt% PVOH. This pilot test was then extremely positive and confirms lab scale results. The trial at industrial scale also confirms the feasibility for the introduction of CNCs in the impregnation bath. However, this test was also the opportunity to point out many differences between lab and industrial experiments such as duration of impregnation, as well as duration and temperature of drying. These differences have unfortunately resulted in unsatisfying

paper dog-ears resistance. Nevertheless, the better understanding of the requirements and constraints allowed us to think about a better adaptation of the strategies in the banknote process and shows the strong influence of post treatment steps (such as security feature steps).

A second pilot test is already discussed and planned for summer 2018. In this new test, it is question to test the CNF-PET mixture as discussed in **Chapter III.2.** and **III.4.** and try different ratios of PVOH/CNC with CNC from Celluforce.

Table 2: SWOT analysis for the up-scaling of RESIST project

Strengths	Weaknesses
<ul style="list-style-type: none"> - Possibility to introduce a CNF layer by spray between the two fiber layers, and possibility to introduce CNCs in the PVOH matrix without causing process issues - Confirmation of lab results at pilot scale for both crumpling and dog-ears resistance - No damage of other paper properties (mechanical properties, double ply, tear resistance) 	<ul style="list-style-type: none"> - Difficulty for change the industrial paper machine parameters (increase of impregnation time, increase of drying temperature after impregnation bath) - Difficulty to implement the spray device on the industrial paper machine
Opportunities	Threats
<ul style="list-style-type: none"> - Availability of CNCs in large quantity and with competitive price - Possibility to produce large quantities of CNFs or to buy them from market - Possibility for patents 	<ul style="list-style-type: none"> - Difficulty to transfer the lab protocols into industrial paper machine

2. Combining of the two strategies: influence of CNC reinforced PVOH impregnation, CNF middle layer and banknote calendering on the whole paper properties

This work is a collaboration with 3SR laboratory (Grenoble, France) and especially with Victoria Krasnoshlyk, Sabine Rolland du Roscoat, and Pierre Dumont .

2.1. Introduction

In **chapters II** and **III**, two strategies were independently developed for increasing the resistance to dog-ears formation and crumpling of paper, which are both classical and costly problems associated with banknotes. The introduction of cellulose nanocrystals (CNCs) in the PVOH impregnation bath has boosted the paper surface rigidity due to the reinforcing effect of the CNCs and an increase in PVOH crystallinity. It has successfully conducted to higher dog-ears resistance. The introduction of cellulose nanofibrils (CNFs) between the two fiber layers of the paper has created an entangled, strongly cohesive and dense layer which contributed to limiting the crumpling deformation and spring effect if the paper. These two strategies were developed independently at lab-scale. However, the final objective was to develop a material combining the effect of CNCs and CNFs for the limitation of dog-ears and crumpling. In this chapter, papers were innovatively produced at pilot and industrial scale. During the pilot tests, papers were produced with and without the CNF layer, and then impregnated with different amounts of CNCs in the PVOH impregnation bath. Production of a paper combining the two strategies was an opportunity to test the influence of one over the other. When a new material is produced by changing its structure or components, not only the targeted properties need to be studied but also the overall properties of the material.

Crumpling and folding mechanisms are strongly correlated. They are both a result of irreversible plastic deformation due to a lack of material rigidity and elasticity. Furthermore, among the models proposed in the literature to describe the crumpling mechanisms, some researchers suggest that crumpling results from successive folding events (Deboeuf et al. 2013; Francis et al. 2013). Consequently, it is worth evaluating if the CNCs, which increase the dog-ears resistance, could also limit the crumpling, and inversely if the CNF layer which decreases crumpling could also limit the dog-ears.

The first part of this study is a short overview of the influence of paper impregnation with CNC reinforced PVOH on crumpling properties. Results are given for various crumpling methods and intensities (Balloon test, NBS x1, NBS x4) and spring effect. The second part was a collaboration with another laboratory (3SR, Grenoble) and investigates the influence of a CNF layer on paper foldability and crack propagation occurring after folding. During this collaboration, papers with different structures such as tracing paper (high density paper), bilayer paper and paper containing CNF were

compared. Elastic angle recovery tests were performed to complete this study and to give a closer look at the dog-ears phenomenon.

2.2. Materials and methods

2.2.1. Materials

2.2.1.1. Raw materials

Cellulose nanofibrils. Commercial CNF (“Com-CNF”) were purchased from the Pulp and Paper Research and Technical Center (CTP), Grenoble, France. They are produced from bisulfite Domsjö pulp (softwood) after enzymatic pretreatment during 2 h (using a cellulase solution mainly composed of endoglucanase), one pass at 1000 bar followed by 4 passes at 1500 rpm in a homogenizer. The CNF suspension was delivered at 2% w/w.

Cellulose nanocrystals. Commercial CNCs extracted from wood pulp were purchased from the University of Maine as a CNC suspension at 12 wt%, and have a length of 136 nm (+/- 50), and a width of 11 nm (+/-5). Their detailed characterization is available in (Gicquel et al. 2017).

Polyvinyl alcohol (PVOH). The PVOH used was a mixture of Mowiol 28/99 (31 000 g.mol⁻¹) and Mowiol 6/98 (47 000 g.mol⁻¹), bought from Sigma Aldrich.

2.2.1.2. Influence of the CNF layer on the dog-ears resistance of paper

Production of nanopapers. Nanopapers were prepared with a sheet former (Rapid Kothen, ISO 5269-2) from CNFs diluted to 0.5% in deionized water. The different basis weights were obtained by changing the dry content of CNF (between 0.5 g and 3 g). First, the suspension was filtered under vacuum at -600 mbar during a specific time until removal of water supernatant. After this time, the filtration is extended for five additional minutes. Then, the sheet was dried under vacuum at 85°C between (from interior to exterior) two nylon sieves (one on each side) to prevent adherence and two cardboards (one on each side) for 20 min. All films were stored for 48 h in a conditioned room at 23°C and 50% RH before characterization.

Production of multilayers with different CNF quantities. Multilayer papers have been prepared with a dynamic sheet former (EP Meca, France, Model FORM-PAGORA-RET), consisting in spraying the fibrous suspension into a drum rotating at 1100 tour/min. Details are given in Chapter III.4., experimental section, 2.2. “Methods”.

Reference paper. The reference paper was produced during pilot tests at Banque de France (Chamalières) and is composed of two fiber layers of refined cotton. The first layer has a basis weight of 30 g.m⁻² and the second one 60 g.m⁻², for a final basis weight of 90 g.m⁻². More details are given in Chapter IV.1. where pilot tests have been described, and this paper was labeled “Sample 1.0”.

Multilayer containing CNF. This paper was also produced during the pilot test by spraying a CNF layer of 5 g.m^{-2} between two fiber layers of 25 and 60 g.m^{-2} . More details are given in Chapter IV.1. where the pilot tests have been described, and this paper was labeled “Sample 2.0”.

Tracing paper. The tracing paper consists of highly fibrillated fibers from a chemical pulp and was bought from Clairefontaine®, France (“Tracing paper in roll 40/45 g, 0.750 x 20m”). Basis weight and thickness are presented in the Result and Discussion section. The homogeneous structure of the tracing paper comes from the high degree of refining inducing which enables a large number of fiber-fiber bonds. Due to the papermaking process, this paper has a bulk porosity below 1%, leading to a continuous microstructure (Krasnoshlyk 2017).

2.2.1.3. Influence of paper impregnation with CNC-reinforced PVOH on crumpling resistance

Velin paper. This banknote substrate was kindly supplied by Banque De France. It is equivalent to the Velin paper produced at Vic le Comte papermaking, before impregnation in the PVOH bath. This Velin paper was produced on a pilot paper machine running at around 2 m.min^{-1} . The fibers used for the paper consist of 100 wt-% cotton (60°SR). TiO₂ Anatase (5 wt-%) was used as additive and acidic dies were added into the pulp slurry. In addition to TiO₂ the paper pulp also includes 2.7 wt-% wet strength agent polyamideamine epichlorohydrin (PAE) and 0.9 wt-% anionic polymer carboxymethylcellulose (CMC). Two layers with basis weights of about 20 g.m^{-2} (first layer) and around 60 g.m^{-2} (second layer) are combined to form the resulting semi-finished paper product, which has a final basis weight of $80.8 \text{ g.m}^{-2} \pm 2.4$.

PVOH-CNC formulation. Details are given in Chapter II.2., experimental section, 2.2. “Methods”.

Impregnation of Velin. Details are given in chapter II.2., experimental section, 2.2. “Methods”. Only impregnation with 100% PVOH or 90 wt% PVOH/ 10 wt% CNC were tested, with a classical convective drying during 3 minutes at 115°C.

Pilot papers. These papers were produced during pilot tests as described in Chapter IV.1. For this part of the study, sample 1.0 (bilayer paper or “reference paper”) has been compared with sample 1.1 (bilayer paper impregnated with 100% PVOH) and sample 1.3 (bilayer paper impregnated with 90 wt% PVOH and 10 wt% CNC).

Industrial papers. These papers were produced during industrial tests as described in Chapter IV.1. Paper samples were coated by passing through an impregnation bath, at the end of the paper machine or after the security feature step as specified in Table 1. Two drying protocols were tested after impregnation: one at 92°C and a second one at 105°C. It is worth noting that, for time and feasibility reasons, the paper sample impregnated with only 100% PVOH and dried at 105°C was not produced.

Table 1: Paper samples during industrial tests

Sample name	Impregnation process	Sample recovery
PVOH 90°C	Paper impregnated with 100% PVOH and dried at 90°C	End of paper machine
PVOH 90°C S	Paper impregnated with 100% PVOH and dried at 90°C	After security step
90-10 90°C	Paper impregnated with 90wt% PVOH and 10 wt% CNC, and dried at 90°C	End of paper machine
90-10 90°C S	Paper impregnated with 90wt% PVOH and 10 wt% CNC, and dried at 90°C	After security step
90-10 105°C	Paper impregnated with 90wt% PVOH and 10 wt% CNC, and dried at 105°C	End of paper machine
90-10 105°C S	Paper impregnated with 90wt% PVOH and 10 wt% CNC, and dried at 105°C	After security step

2.2.2. Methods

All the papers were stored for at least 48h in a conditioned room (23°C, 50 %RH) before testing and experiments were performed in this conditioned room.

Curvature angle pictures. Paper samples with dimensions of 45mm x 130mm were cut in machine direction. Then, the paper was manually folded in two identical parts in the length direction without applying any manual pressure at the location of the fold. Weights tailored with exactly the same dimensions as half of the paper (45 mm x 65 mm) were then deposited on the folded paper. The first weight was 100 g, and a second one of 400 g could be added for a total weight of 500 g. Pictures were taken using a Pentax Optio® camera 30 seconds after the deposition of the weight and at a distance of 20 cm. At least 5 duplicates were performed.

Paper folding before tensile tests. Paper samples with dimensions of 45 mm x 130 mm were cut in machine direction, cross direction or with a 45° orientation. Then, papers were subjected to different numbers of folds before performing tensile tests to study the crack propagation for folded papers. These folds were performed by manually folding in two identical parts the paper in the length direction without applying any manual pressure at the location of the fold. Then, a weight of 1 kg tailored with 45 mm x 65 mm dimensions was applied for 5 seconds and removed. The folded paper was then completely manually opened to recover a flat conformation. These steps were repeated for a determined number of folds between 1 and 48.

Tensile tests. The tensile properties were measured with a vertical extensometer (Instron 5965), following the standard NF Q03-004. Basis weights were measured using a surface of 10x10 cm² and the thickness was measured using Lhomargy micrometer. These values were then reported into the tensile device software to obtain the Young's Modulus, breaking length and breaking force. The grips have been selected to limit slipping of samples. Tensile tests were performed at 10 mm.min⁻¹, with a gap of 10 cm between the grips. At least 10 duplicates were performed to obtain average values.

Zero-span breaking length L_r (km). The zero-span breaking length was measured using a joined-clamps tensile device (Pulmac TS-100, USA). Samples had a diameter of 15 mm and a length of 5 cm.

Wet samples were immersed for 1 min in water and pressed between two blotter papers to remove the excess water. A pressure was extracted in kgf/15 mm. The value of zero-span breaking length Lr_0 (km) was calculated using the equation (1):

$$Lr_0 = \frac{F}{l.g.G} \quad (1)$$

where F is the force (kgf), l the sample diameter (0.015 m), g the acceleration of gravity (9.8 m.s^{-2}) and G the basis weight (g.m^{-2}). At least 10 duplicates were performed to obtain average values.

Scanning Electron Microscopy (SEM). SEM was performed with ESEM (Quanta 200©, FEI, Japan) on paper cross sections and surfaces after gold sputter coating of 5 nm, with a tension of 10 keV in EDT mode. The working distance was 10 mm. At least 10 pictures per sample were obtained and the most representative were selected.

Elastic angle recovery of paper and nanopapers. Details are given in Chapter II.3., experimental section, 2.2. “Methods”. The pressure applied in this study was 0.6 kPa, corresponding to a weight of 200 g. Additional information is also given in Chapter II.3. “Supporting Information 2”.

Crumpling with Balloon test. Details are given in Chapter III.4., experimental section, 2.3. “Crumpling characterization”.

Crumpling with National Bureau of Standard (NBS) method. Details are given in Chapter III.4., experimental section, 2.3. “Crumpling characterization”.

Image analysis of crumpled samples. Details are given in Chapter III.4., experimental section, 2.3. “Crumpling characterization”.

Waviness profile. Details are given in Chapter III.4., experimental section, 2.3. “Crumpling characterization”.

Spring-effect. Details are given in Chapter III.4., experimental section, 2.3. “Crumpling characterization”.

2.3. Results and discussion

2.3.1. Influence of CNC-reinforced PVOH impregnation on paper crumpling resistance

Previous chapter have shown a strong impact of cellulose nanocrystals on the dog-ears resistance of paper (**Chapter II.3.**). CNCs enhance the paper elasticity and decrease the occurrence of a fold. Furthermore, CNCs promote a better elastic angle recovery after a fold and finally, they hinder the tear propagation after a fold. Paper crumpling is often considered as a pattern obtained after multiple folding events. Since incorporation of CNCs in PVOH decrease folding damages, they can also be expected to improve the crumpling resistance.

Banknote substrates were produced from lab, pilot and industrial tests. The crumpling resistance was measured using different crumpling methods with varying intensities (NBS and Balloon test) and spring effect. When Velin is impregnated with 100% PVOH at lab scale, a slight increase of the crumpling can be observed (Figure 1). Introduction of 10 wt% CNCs, which corresponds to the optimal ratio for obtaining dog-ears resistance, gives a decreased crumpling in comparison to paper impregnated with 100% PVOH and is similar with the value of Velin without impregnation. The same conclusions were reported for other crumpling intensity (NBS x1).

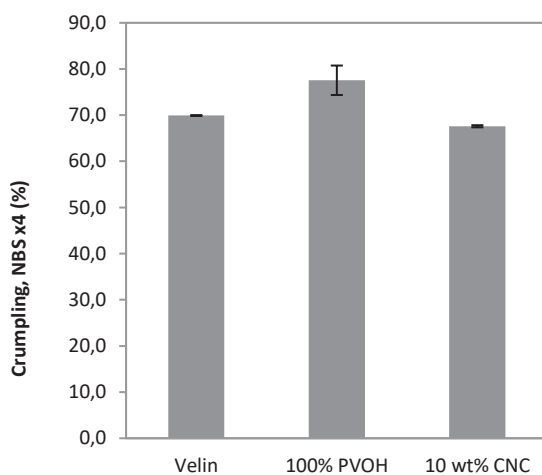


Figure 1: Velin impregnated at lab-scale with 100% PVOH or 90%wt PVOH and 10 wt% CNCs



Figure 2: Crumpling pattern of pilot papers after crumpling with Balloon-test

During pilot tests, papers were produced and impregnated in a PVOH bath containing different ratios of CNCs. Equivalent levels of crumpling were obtained for papers impregnated with 100% PVOH and papers impregnated with 90 wt% PVOH and 10 wt% CNCs for crumpling with NBS or with balloon tests. Figure 2 shows visually that similar crumpling patterns were obtained after impregnation with or without CNCs.

Papers produced at industrial scale and impregnated in a bath containing 90 wt% PVOH and 10 wt% CNCs and dried at 90°C were also subjected to crumpling deformation. Papers were coated at the end of the paper machine as well as after the security step. The results followed the same trend as in the lab experiments where an improvement of crumpling resistance was observed with the

addition of 10 wt% CNCs compared to PVOH only (Figure 3). This difference was also observed for spring effect values. The spring effect is correlated with the loss in mechanical properties caused by the fiber debonding during crumpling. The use of CNCs, which contribute to increase the layer Young's modulus from 1.6 to 21 GPa (See **Chapter II.1.**), provides a paper reinforcement sufficient to avoid this spring effect damage. It is worth noting that the increase of crumpling resistance with CNCs was observed for NBS x1 and NBS x4 crumpling methods. However, no difference was observed after crumpling with the gentler balloon test, meaning that the action of CNCs is variable and only has an impact at high crumpling strength. Furthermore, the application of a security step did not influence the crumpling results or spring effect.

In summary, the action of CNCs is preponderant for dog-ears resistance and slightly contributes to decrease the crumpling deformation pattern. Impregnation of paper with PVOH tends to reduce the crumpling resistance, and the introduction of CNCs compensates this loss. However, these results depend on the crumpling process and were not observed after Balloon-test crumpling, which is a better simulation of manual banknote handling. Even though the percolation threshold is reached at 10 wt% CNCs, there is no possibility of entanglements of the CNCs in contrast to cellulose nanofibrils for which the entanglements are a key property for the improved crumpling resistance.

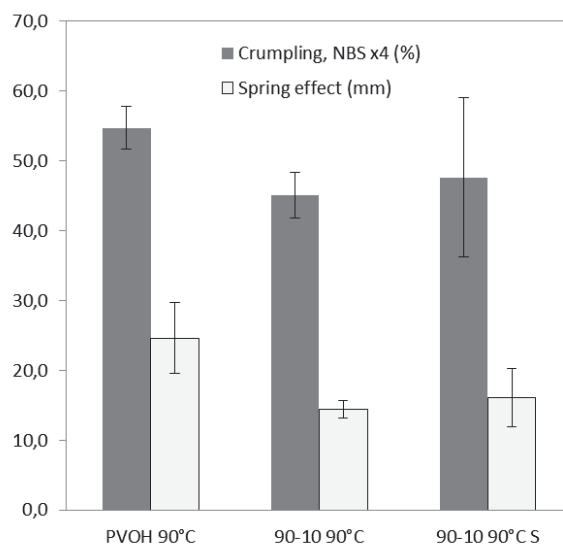


Figure 3: Crumpling tests and Spring-effect of paper produced from industrial tests and impregnated with 100% PVOH or 90 wt% PVOH – 10 wt% CNCs, dried at 90°C, and recovered before or after the security step.

2.3.2. Influence of the CNF layer on paper foldability and crack propagation occurring after folding

Paper folding induces deformations which exceed the elastic properties of the material and result in plastic deformation. This phenomenon can be reduced by increasing the material stiffness and paper elastic properties. In previous chapters, it has been shown that papers impregnated with CNC reinforced PVOH contain a stiff layer which reduces the formation of the fold, increases the elastic angle recovery after folding and limits the crack propagation after folding. This section studies the influence of the CNF layer on these three steps. In the case of CNF, it is no more about creating a strong thin layer at the surface but instead using an entangled network of CNF within the paper. Different papers were evaluated: a bilayer composed of refined fibers (reference material) and the same paper with a CNF layer inside (“Multilayer paper”). These papers present similar basis weight, thickness and density. In order to understand the influence of the paper structure on the fold mechanism, another paper with a different structure was also studied: a tracing paper. This tracing paper is composed of highly refined fibers and constitutes a cohesive and dense fiber network. Structural properties of these papers are shown in Table 2.

Table 2: Different paper tested for study of paper foldability and crack propagation occurring after folding

	Tracing paper	Reference	Multilayer with CNF
Basis weight (g.m ⁻²)	46.5 (+/- 0.2)	90.6 (+/- 0.6)	94.3 (+/- 1.0)
Thickness (μm)	44.5 (+/- 1.2)	134.1 (+/- 2.3)	134.0 (0.01)
Density (g.cm ³)	1042.7 (+/- 35.8)	675.6 (+/- 16.3)	703.7 (+/- 7.3)

2.3.2.1. Influence of the CNF layer on paper foldability and fold recovery

The curvature angle of folded papers under a mass of 100 g or 500 g, are higher for the paper containing the CNF layer (Figure 4-A). This fast and easy test is the first argument to show the bending resistance is improved by adding a CNF layer. This point is particularly important as the bending rigidity is the first parameter to prevent the creation of a fold (Barbier et al. 2006). However, the bending stiffness (mN) was measured and similar values were obtained for paper containing or not cellulose nanofibrils. Such result is difficult to explain but might be due to the fact that the reinforcement is inside the paper and not at the surface.

Spraying of different amounts of CNF were tested to study the impact of the layer basis weight on the paper curvature angle. A slight increase of this curvature angle appeared by increasing the CNF content from 2.5 g.m⁻² to 5 g.m⁻² but no improvement was observed with a CNF layer of 10 g.m⁻². The same optimum at 5 g.m⁻² has already been observed for crumpling resistance (**Chapter III.4.**) and can be explained by the fact that 5 g.m⁻² is sufficient to form a cohesive network inside the paper. Adding more CNF does not change the CNF network and consequently, does not change the resistance under deformation.

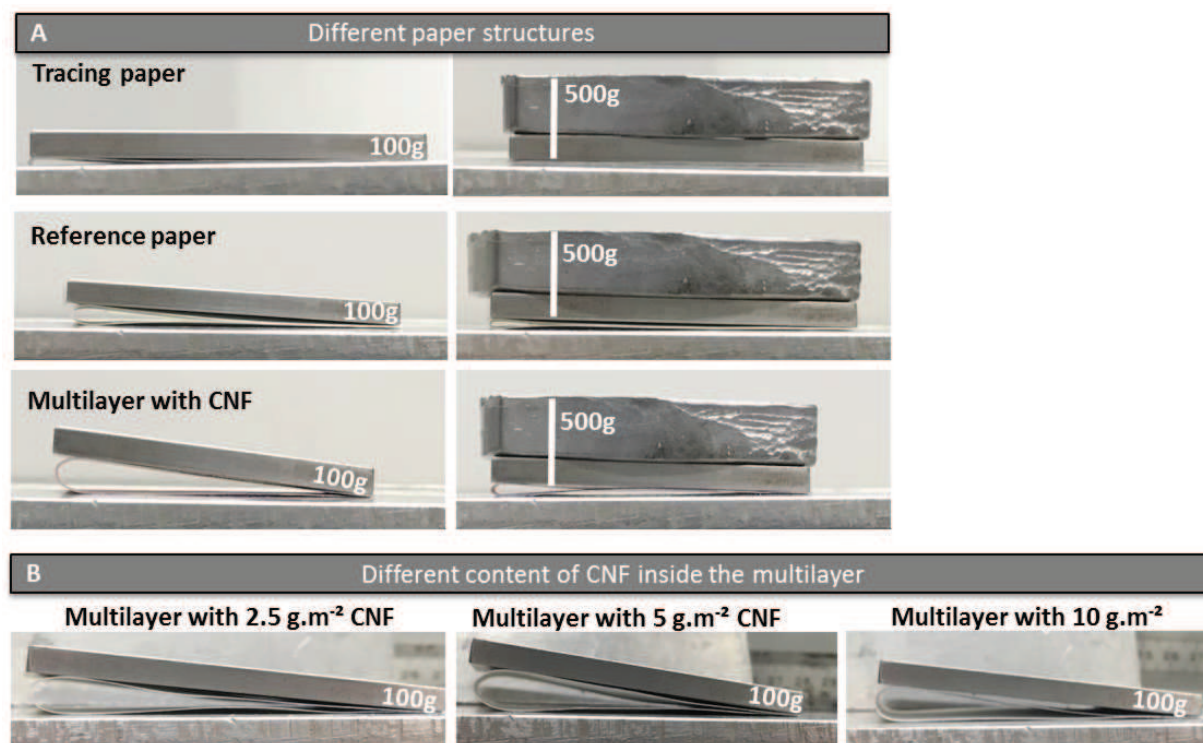


Figure 4: Curvature angle of folded paper with a weight of 100 g or 500 g

CNFs inside the multilayer form a cohesive layer which can be represented in the form of an individual nanopaper. This model was already used in **Chapter III.2**. To understand the behavior of CNFs submitted to fold deformation, the elastic angle recovery was measured on nanopapers produced with different basis weight. Results in Figure 5 show a linear relationship between the nanopaper basis weight and the elastic angle recovery. Furthermore, it can be observed that the tracing paper has a similar angle recovery to the nanopaper for an equivalent basis weight. The common points between nanopapers and tracing papers in comparison to classic fibrous materials are their higher density, smaller fiber dimensions, higher level of fibrillation and strong H-bonding, leading to dense and cohesive materials with superior mechanical properties compared with classical papers. Since nanopaper and tracing paper show similar folding deformation behavior, we can conclude that cohesion is likely to play a key role in elastic angle recovery after folding. From Figure 5, it is also possible to extrapolate the value of elastic angle recovery for a tracing paper at equal basis weight as the reference and multilayer papers, and hence only study the effect of the paper density.

By comparing the results of the three papers types in Figure 5, we can see that with equal basis weights, a huge increase in elastic angle recovery is observed when comparing the nanopaper (similar behavior than tracing paper) and the reference paper. When the CNF layer is introduced in the multilayer, the elastic angle recovery of the paper is also significantly increased. This result shows that the CNF layer transfers additional stress during folding deformation and influences the behavior of the whole paper, which behaves more like a high density paper.

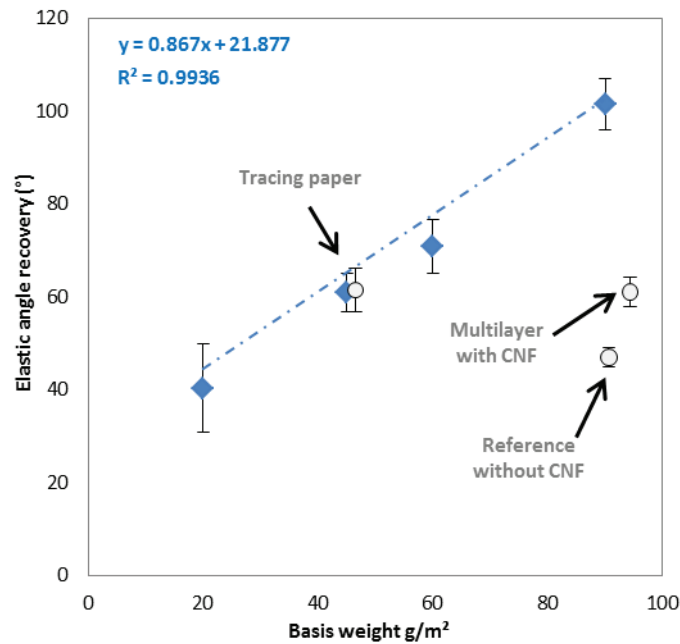


Figure 5: Elastic angle recovery after folding for nanopapers with different basis weights. As references, values for tracing paper, reference paper without CNF from pilot tests, and trilayer paper with CNF from pilot tests are also represented.

2.3.2.2. Influence of folding on paper mechanical properties

During the folding of paper, two possible modes of damages of the fiber network can occur: locally by breaking the fibers and/or on a network level by breaking the fiber bonds. Here the mechanical properties of papers after different numbers of plies have been studied. Classical Young's modulus and rupture force primarily give information about fiber-fiber bond damages, while energy at break, breaking length and wet LR_0 values (jointing-clamp tensile test) are more characteristic of the fiber damages.

Fiber damage vs fiber-bond damage. LR_0 values for papers were determined by performing jointing-clamp tensile test on wet samples, as a function of numbers of plies. By performing this tensile test on wet samples, the fiber bonding effect is removed and the results can be seen as measure of fiber break. No LR_0 difference was observed for the tracing paper subjected from 0 to 48 consecutive folds. In other words, repeated folding of this highly dense and refined network do not create additional fiber break. However, when performing classical tensile tests on tracing paper, the resulting mechanical properties (Fr , E , LR) were reduced when the number of folds increased. We can consequently conclude that folding a tracing paper mainly damages the fiber-fiber bonds and not the fibers themselves.

On the contrary, for the reference paper, a slight decrease of LR_0 was observed when comparing 0 ply ($17.6 \text{ km} \pm 0.3$) and 48 plies ($14.3 \text{ km} \pm 0.2$) as well as a decrease of classical tensile properties. In this case, the fold seems to damage both fibers and fiber-fiber bonds. Addition of a

CNF middle layer in this paper makes the behavior more similar to the tracing paper: no change in wet LR_0 was observed after 0 or 48 plies ($16.8 \text{ km} \pm 0.5$) and only classical tensile properties suffer from the repetitive folds. The introduction of the CNF layer seemingly not only changes the paper structure, it also prevents the fiber damage after a fold by creating a stiff area in the bulk of the paper. The general mechanical properties are improved and the loss of mechanical properties after repetitive folds is mainly induced by fiber-fiber bond damages.

Crack at the fold. One of the problems of dog-ears is the creation of a tear localized at the banknote corner. The effect of the number of folds on the crack formation was studied by inducing different numbers of plies on a paper, performing tensile tests, and observing from which number of folds the crack occurs at this fold (meaning that the damage is significant enough to tear the paper) (Figure 6). For the tracing paper, the folded zone became the weak point from the 6th fold while for the bilayer paper, the crack at the fold occurred from the 25th fold. This result is not surprising as the tear easily propagates in the dense structures, and the reference paper, even folded, presents a higher porosity than the tracing paper which is highly sensitive to tear. Furthermore lower basis weight of tracing paper might explain this point. When a CNF middle layer was introduced, the crack occurred at the ply from the 12th folds. The CNF layer is denser than the other fiber layers and the folds further emphasized these differences by compressing the paper structure around the fold. Nevertheless, general mechanical properties (Fr , R , Lr , energy at break) remain higher due to the CNF layer.

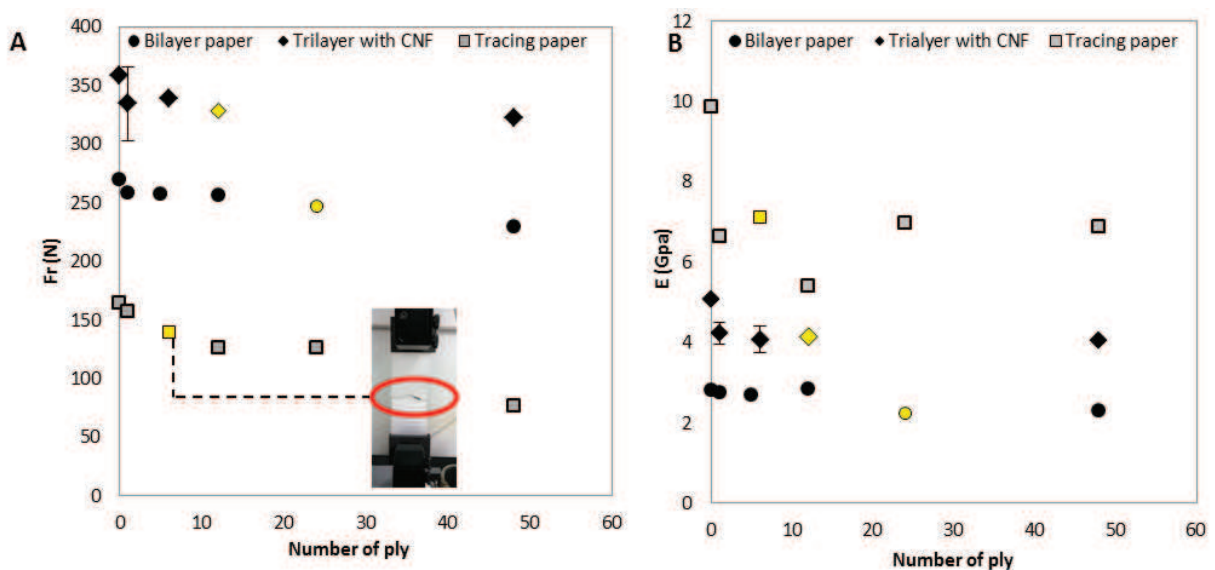


Figure 6: A) Breaking force and B) Young's modulus of folded papers for different number of folds. Tensile tests performed for samples in machine direction. From the yellow point, the crack occurs at the fold area.

Paper orientation. In previous experiments, the paper was cut in machine direction and folded in the middle in two identical parts. Other tests have been performed by folding samples taken in the cross direction, or $\pm 45^\circ$ directions. When the sample was cut in the machine direction, the largest decrease in mechanical properties (Fr and E) was observed after the first fold, after which the

properties only decreased slightly when the number of folds increased from 1 to 48 folds (Figure 6-A and B). The same trends were observed for papers cut in the cross direction or in $\pm 45^\circ$ directions. Consequently, the fold behavior is not influenced by the fiber orientation. This behavior was also observed for elastic angle recovery, which were similar in each direction. Furthermore, the literature also confirms this observation and argues that the physical phenomena involved (large strains, damage.) occur at a small scale (the paper thickness) and depend on the local paper composition close to the fold. The fold behavior is driven by the cross section along the fold line, with a complex process at this scale that may allow local fiber rotation (Pradier et al 2016). Consequently, the fraction of crossed fibers is a first order parameter, leading to a similar behavior independently of the fold direction. Fold orientation appears to have only a second-order influence.

Location of the CNF layer. In the standard case the CNF layer is introduced between two fiber layers of 60 and 20 g.m⁻². We have shown that changing the layer symmetry also changes the crumpling properties (**Chapter III.4.**). A more symmetric multilayer assembly, meaning that the CNF layer was closer to the middle of the sheet, resulted in a decrease of crumpling resistance. Similarly, when the CNF layer was closer to the middle of the paper, the loss of mechanical properties due to consecutive plies was increased. Figure 7 displays an SEM image of a multilayer paper containing CNF after a fold. From this micrograph, it seems that the change in paper structure during a fold is more pronounced closer to the paper surface and that the middle of the paper is not impacted by the deformation. That could explain why the CNF impact is higher when the CNF layer is asymmetrically introduced into the paper, since the CNF layer increases the rigidity of one side of the paper, which consequently better resists fiber-fiber break after a fold.

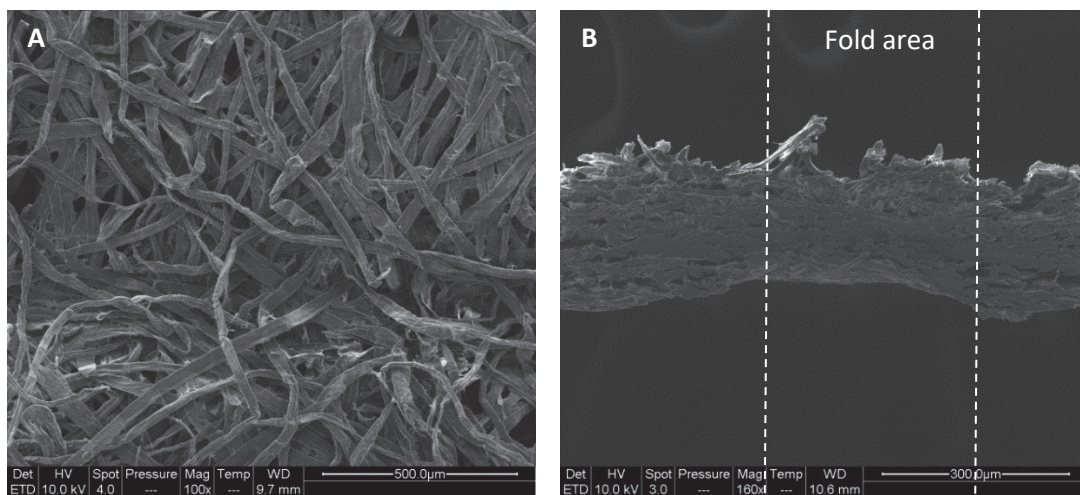


Figure 7: Paper structure after a fold A) Surface of a folded tracing paper and B) decrease of thickness in the fold area for the multilayer paper with CNF

2.3.2.3. Conclusion

The fold behavior has been characterized by (i) the curvature angle under different pressures (resistance to the creation of a fold), (ii) the elastic angle recovery after a fold and (iii) the mechanical

properties of folded papers after different numbers of plies. It has been shown that, when a CNF layer is introduced, the resistance to bending deformation is improved. Furthermore, the overall mechanical properties change. Introduction of a CNF layer gives mechanical behavior which is more similar to tracing paper. These observations suggest that it is the dense and cohesive CNF layer which governs the paper mechanical response after a fold. In tension, the crack statistically occurs more often at the location of the fold, but all the general mechanical properties remain increased thanks to the CNF layer. The CNF layer reduces the fiber break after a fold, promotes a higher elastic angle recovery and increases the overall mechanical properties of folded papers. This improvement is only possible with an asymmetric position of the CNF layer, as the fold impact is the most damaging close to paper surface and is reduced closer to the center of the sheet.

2.4. Conclusions

As a final conclusion, each strategy developed in this PhD manuscript was the most relevant for the targeted property (dog-ears or crumpling). However, in this chapter it has been demonstrated that the entangled CNF network interestingly contributes to increase the dog-ears resistance (Table 3). When a paper containing CNF is folded, the paper behaves similarly to a high-density paper, meaning that the action of the dense CNF layer of 5 g.m⁻² is the first resistance against the folding deformation. However, this contribution remains lower than the contribution of CNCs. On the other hand, the action of CNCs for increasing the crumpling resistance is less impacting and dependent on the crumpling method. Impregnation of a classic banknote by 100% PVOH reduced the crumpling resistance and the introduction of 10 wt% CNCs did offset this reduction. However, no significant improvement was reported in comparison with the non-impregnated substrate.

As a perspective, new tests are planned during the summer of 2018. These tests will give the opportunity to (i) optimize the test to obtain better results in dog-ears resistance (**Chapter IV.1.**) and (ii) introduce a CNF layer in order to evaluate the synergy between the two strategies on an industrial scale.

Table 3: Synthesis of dog-ears and crumpling resistance for different paper produced during pilot tests. *The CNF layer was introduced with a red pigment. Consequently, a classic image analysis was not possible and the crumpling was measured by waviness profile.

Paper sample	Elastic angle recovery (°)	Crumpling value (NBS x4)*	Tensile properties
Paper alone (1.0)	47.1 ± 2.0	Waviness profile(mm): 0.204 ± 0.012 Image analysis (%): 53.2 ± 4.2	-
Paper impregnated with 100% PVOH (1.1)	44.5° ± 4	Image analysis (%): 55.4 ± 6.2	Slight increase
Presence of 10wt% CNC in PVOH impregnation bath (1.3)	65° ± 1.0	Image analysis (%): 51.0 ± 5.3	No influence
Introduction of a CNF layer inside the paper (2.0)	61.1° ± 3.1	Waviness profile (mm): 0.174 ± 4.3	No influence
The two strategies combined	<i>No sample</i>	<i>No sample</i>	<i>No sample</i>

References

- Afra E, Mohammadnejad S, Saraeyan A (2016) Cellulose nanofibils as coating material and its effects on paper properties. *Prog Org Coat Complete*:455–460. doi: 10.1016/j.porgcoat.2016.09.018
- Barbier C, Larsson P-L, Östlund S (2006) On the effect of high anisotropy at folding of coated papers. *Compos Struct* 72:330–338. doi: 10.1016/j.compstruct.2005.01.003
- Bras J, Dufresne A, Desmaisons J, Roberty G, Lutsche M (2017) Use of nano cellulose on a paper product. European Central Bank. EP3228744 A1
- Campano C, Merayo N, Balea A, et al (2018) Mechanical and chemical dispersion of nanocelluloses to improve their reinforcing effect on recycled paper. *Cellulose* 25:269–280. doi: 10.1007/s10570-017-1552-y
- Deboeuf S, Katzav E, Boudaoud A, et al (2013) Comparative Study of Crumpling and Folding of Thin Sheets. *Phys Rev Lett* 110:104301. doi: 10.1103/PhysRevLett.110.104301
- Francis KC, Blanch JE, Magleby SP, Howell LL (2013) Origami-like creases in sheet materials for compliant mechanism design. *Mech Sci* 4:371–380. doi: 10.5194/ms-4-371-2013
- Future Markets, Inc (2017) The Global Market for Nanocellulose 2017-2027
- Gicquel E, Martin C, Garrido Yanez J, Bras J (2017) Cellulose nanocrystals as new bio-based coating layer for improving fiber-based mechanical and barrier properties. *J Mater Sci* 52:3048–3061. doi: 10.1007/s10853-016-0589-x
- Hassan EA, Hassan ML, Oksman K (2011) Improving Bagasse Pulp Paper Sheet Properties with Microfibrillated Cellulose Isolated from Xylanase-Treated Bagasse. *Wood Fiber Sci* 43:76–82
- Krasnoshlyk V (2017) Etude multi-échelles et multiphysiques des mécanismes de fissuration dans les matériaux à base de fibres naturelles. PhD Thesis Grenoble Alpes
- Narain R, Pfaff T, O'Brien JF (2013) Folding and crumpling adaptive sheets. *ACM Trans Graph* 32:1. doi: 10.1145/2461912.2462010
- Reid MS, Villalobos M, Cranston ED (2017) Benchmarking Cellulose Nanocrystals: From the Laboratory to Industrial Production. *Langmuir* 33:1583–1598. doi: 10.1021/acs.langmuir.6b03765
- Ridgway CJ, Gane PAC (2012) Constructing NFC-pigment composite surface treatment for enhanced paper stiffness and surface properties. *Cellulose* 19:547–560. doi: 10.1007/s10570-011-9634-8
- Rol F, Karakashov B, Nechyporchuk O, et al (2017) Pilot-Scale Twin Screw Extrusion and Chemical Pretreatment as an Energy-Efficient Method for the Production of Nanofibrillated Cellulose at High Solid Content. *ACS Sustain Chem Eng* 5:6524–6531. doi: 10.1021/acssuschemeng.7b00630
- Spence KL, Venditti RA, Rojas OJ, et al (2011) A comparative study of energy consumption and physical properties of microfibrillated cellulose produced by different processing methods. *Cellulose* 18:1097–1111. doi: 10.1007/s10570-011-9533-z
- Tejado A, Alam MN, Antal M, et al (2012) Energy requirements for the disintegration of cellulose fibers into cellulose nanofibers. *Cellulose* 19:831–842. doi: 10.1007/s10570-012-9694-4

General conclusions and perspectives

General conclusions and perspectives

The main objective of this PhD was the design of a new banknote substrate displaying improved resistance to dog-ears and crumpling deformations through the use of nanocellulose. Dog-ears and crumpling are classical defects resulting from daily handling of banknote and are responsible for many economic troubles. Dog-ears are the second reason for banknote destruction in sorting centers behind soil. On the other hand, crumpling is more difficult to count as there is still no sensor to automatically detect this defect but is at the origin of banknote destruction and issue in supply chain. Two strategies were developed in this work. The first one consisted in introducing cellulose nanocrystals (CNCs) in the polyvinyl alcohol (PVOH) impregnation bath for the reduction of dog-ears, and the second one proposed the addition of a cellulose nanofibril (CNF) layer between the two fiber layers composing a classical banknote for the reduction of crumpling by increasing its internal rigidity.

This work has been performed in an industrial context. Therefore, **chapters II and III** proposed both fundamental understanding of the phenomena involved and applied research for the development of a new paper product (Figure 1). The most fundamental part has led to 4 scientific publications (3 are in submission) and participation to international conferences, while the most applied parts have led to 2 patents (1 in submission). New tools of characterization were also created (Quality index for CNF, dog-ears measurement) or adapted (Siebimm for micron-thick coatings, crumpling reproducibility and analysis).

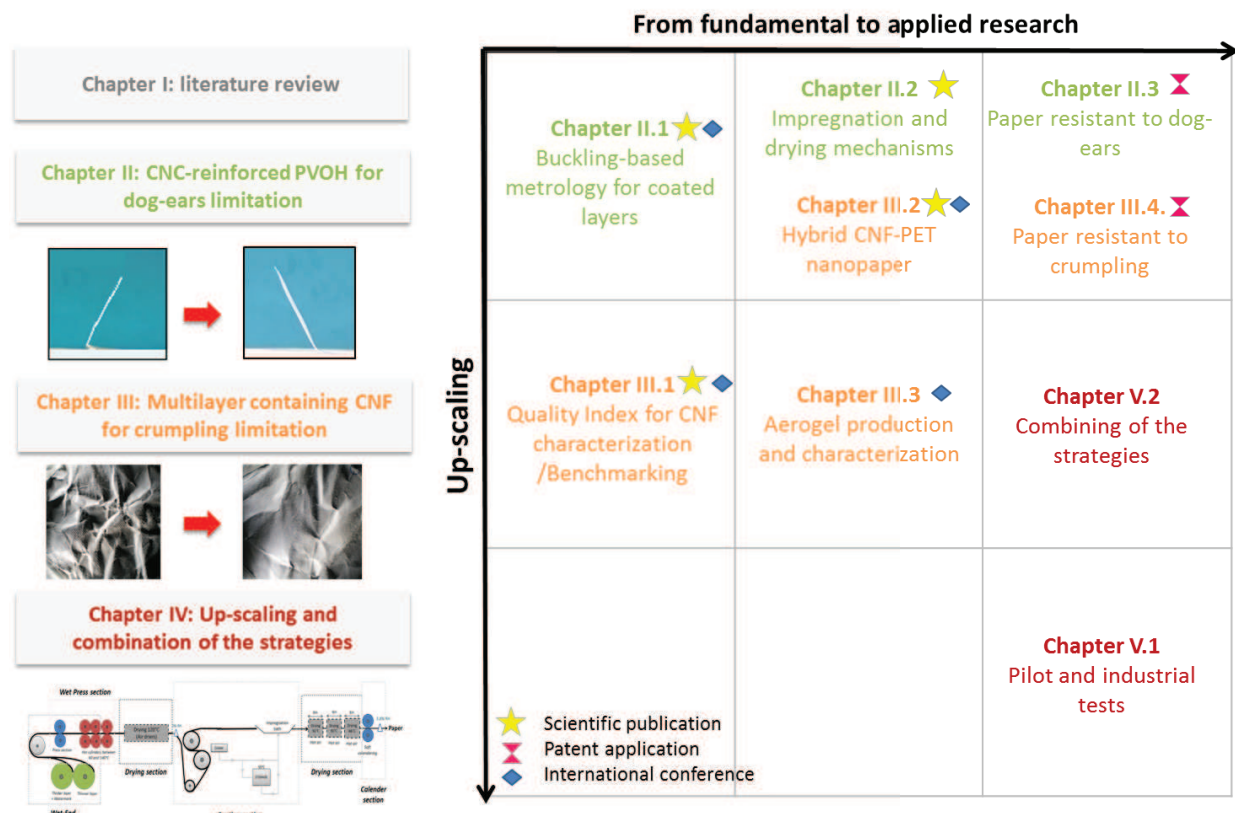


Figure 1: Schematic organization of the different chapters and valorization

Before starting this PhD project, very few studies investigated the improvement of paper crumpling or dog-ears (folding) resistance. The scientific literature focused on characterization and fundamental understanding of these mechanisms. Only a few patents reported some innovative solutions for decreasing these defects (Table 1) and all targeted security paper applications. Up to our knowledge, no solution was proposed with nanocellulose. Furthermore, the use of nanocellulose for security paper application was only patented once (Ratnakumar and Howland 2013) and it described the use of microfibrillated cellulose as a surface treatment to provide soil resistance. Since the beginning of this project in 2015, the situation has not really changed as only two more patents (except our patents) was reported: one for the production of crease-resistant security films and another one for the use of cellulose nanocrystals inside the banknote varnish in order to improve soil resistance as well as hydrophobic and oleophobic properties. This PhD manuscript, its publications and its patent provide then innovative solutions and a new understanding of these phenomena.

Table 1: Summary of patents dealing with the improvement of paper crumpling or folding resistance, or with nanocellulose for security paper application (except this PhD contribution)

	Paper resistant to crumpling	Paper resistant to fold or dog-ears	Use of nanocellulose in security paper
Patents Before 2015	1. Crease-resistant security film (Buck and McCord 1949), Arjowiggins Security	1. Fold-resistant cleaning sheet (Volpenhein and Ebrahimpour 2008), Procter and Gamble	1. A substrate for security documents (Ratnakumar and Howland 2013) De la Rue International
	2. Sheet for security documents having high printability and high handling resistance (Vallee and Halope 1997), Arjowiggins Security	2. Corner reinforcing watermarks on sheets (Howland and Pearson 2011), De la Rue International	-
	3. Security sheet comprising a transparent or translucent layer (Rosset 2004), Arjowiggins Security	3. Paper including watermarks and/or embossing (Pearson and Howland 2008), De la Rue International	-
	4. Sheet of Wrinkle-Resistant Paper (Sarrazin 2013), Arjowiggins Security	4. Security document (Roberty 2005), European Central Bank	-
Patent After 2015	5. Crease-resistant security film (Sarrazin 2016), Arjowiggins Security	-	2. Process for the surface treatment of a security document and associated security document (Le Berre et al. 2015) Oberthur Fiduciaire

Table 2 synthesizes the key results of the project. **Chapter II** was dedicated to the decrease of banknote dog-ears thanks to the paper impregnation with CNC reinforced PVOH. In this chapter, the buckling metrology has been adapted for the characterization of micron thick coatings (**Chapter II.1.**). This work allowed a better understanding of the impact of coating processes on the mechanical properties of the thin layer. It also permitted to conclude that the introduction of 10 wt% CNCs in the PVOH matrix strongly increased the layer Young’s modulus. This increase in layer Young’s modulus results from the intrinsic reinforcing effect of the nanocrystals but also from their ability to increase the PVOH crystallinity during isothermal drying (**Chapter II.2.**). The PVOH crystallinity is also

influenced by the drying system (convective or radiative) and temperature. By gathering the right amount of CNCs in the PVOH, the right nanomaterial source and surface chemistry, and the best drying conditions, the elastic angle recovery after folding was strongly increased by 20%. Furthermore, the creation of the fold and the risk of crack propagation after a fold were also reduced (**Chapter II.3.**). The feasibility of the method as well as the good impact of CNCs on paper dog-ears were confirmed at pilot scale, which favor a patent application. At industrial scale, unsatisfactory results were obtained as described in **chapter IV.1.**, but tracks for process optimization were proposed and new industrial tests are now in perspective.

Chapter III was dedicated to the use of a CNF layer in the bulk paper for decreasing the banknote crumpling deformation. Thanks to their high aspect ratio, surface area and hydrogen bonding capability, CNFs form a highly cohesive and entangled network. These properties explain the outstanding mechanical properties of CNFs but they are also responsible for decreasing the tear resistance of CNF-containing papers. As the increase in crumpling resistance can only be successful without damaging the collateral properties, a careful attention has been paid also to the tear resistance. Chapter III started with the creation of a new tool of characterization for CNFs, the quality index (**chapter III.1.**). Thanks to this tool, it was possible to make a quantitative ranking of existing CNF suspensions from commercial source and from lab productions, and select the appropriate suspensions for the crumpling resistance application. Then, a PET/CNF composite has been studied under the form of hybrid nanopapers, and it has been shown that the synthetic microfibers have a beneficial impact on tear and crumpling, in both the dry and wet state (**Chapter III.2.**). The optimum ratio to keep satisfying mechanical properties and ensure tear and crumpling resistance was found to be 10 wt% PET and 90 wt% CNF. In **chapter III.3.**, CNF was considered in a completely different structure called CNF foam. This material was expected to combine the outstanding properties of CNF with a highly porous structure hindering the tear propagation without the use of any additive. This part focused on a fundamental understanding of foam preparation and properties and proposed different strategies for the adaptation of this porous structure in a paper-making process. Finally, neat CNF, CNF with PET, or CNF in a porous form were included in the multilayer preparation (**Chapter III.3.**) for the creation of a crumpling resistant paper. This study confirmed the increase in crumpling resistance thanks to the CNF network and the increase in tear resistance thanks to the addition of PET or by using porous CNF. Such promising results were confirmed at pilot scale and a patent has been submitted. Today, the up-scale production of CNF foams and the adaptation in a paper-making process remain challenging, and this route should be considered as a preliminary study needing further developments. However, the addition of PET in the CNF suspension is fast and easily up-scalable. Consequently, this last strategy was considered as the most promising way for improving banknote crumpling and tear resistance. The next industrial trials forecasts to test this strategy if the implementation of a spray device between the two round shape formers is possible.

Table 2: Key results of the project and perspectives

Key results	Cellulose nanocrystals (CNCs) in impregnation bath	Cellulose nanofibrils (CNFs) as a 5 g.m ⁻² intermediate layer
Impact on banknote dog-ears (lab scale)	Principal strategy Successful increase of dog-ears resistance	(collateral impact) Beneficial impact
Impact on banknote crumpling (lab scale)	(collateral impact) Not significant	Principal strategy Successful increase of crumpling resistance and decrease of spring-effect
Impact on other mechanical properties (tensile properties, tear)	(collateral impact) Not significant	(collateral impact) Tear has been increased thanks to (i) addition of PET in the CNF suspension or (ii) use of CNF in a porous form
Best laboratory conditions	10 wt% CNCs – 90 wt% PVOH Dried 2 minutes with a 2500-W long wave IR	5 g.m ⁻² layer containing 90 wt% CNF and 10 wt% PET
Up scaling	CNC-reinforced PVOH in pilot machine (satisfying results) and in real paper machine (Unsatisfactory results)	Pilot test with a sprayed CNF layer (satisfying results)
Main issue	Impossibility do dry with IR at industrial scale, difficult to control impregnation and drying times, difficult to change drying temperature	Difficult to implement a spray device in the industrial paper machine
Perspective	New industrial test with optimized parameters	New industrial test with CNF spraying Test of CNF alone or CNF + PET

As a conclusion, this work provides interesting results for producing a banknote paper with improved resistance to dog-ears and crumpling deformations. No satisfactory solutions were proposed before this PhD and the use of nanocellulose in this project were also completely innovative. Positive results were achieved by respecting the two initial strategies, consisting in introducing CNCs in the PVOH impregnation bath for the limitation of dog-ears and introducing a CNF layer in the bulk paper for the limitation of crumpling. Among the different perspectives, optimizing the process conditions during industrial tests and testing the CNF spraying in paper machine were identified as priority objectives. New tests should be performed in summer 2018. Finally, we hope that this work will provide sustainable and profitable answers for the industrial partnership and extend the use of nanocellulose in paper security applications but also propose some understanding in nanocellulose field and its challenges.

References

- Buck GS, McCord FA (1949) Crease-Resistance and Cotton. Text Res J 19:216–247. doi: 10.1177/004051754901900405
- Howland P, Pearson NG (2011) Corner reinforcing watermarks on sheets. De la Rue International. EP1466755B1
- Le Berre M, Gillot J, Borde X (2015) Process for the surface treatment of a security document and associated security document. Oberthur Fiduciaire WO2015091873 A1
- Pearson NG, Howland P (2008) Paper including watermarks and/or embossings. De la Rue International. US7399513B2
- Ratnakumar R, Howland P (2013) A substrate for security documents. De La Rue International. WO 2013178986 A1
- Roberty G (2005) Security document. European Central Bank. EP 1800891 A1
- Rosset H (2004) Security sheet comprising a transparent or translucent layer. Arjowiggins Security. US20040023008A1
- Sarrazin P (2013) Sheet of Wrinkle-Resistant Paper. Arjowiggins Security. WO2013093872 (A1)
- Sarrazin P (2016) Crease-resistant security film. Arjowiggins Security. US9527332B2
- Vallee A, Halope C (1997) Sheet for security documents having high printability and high handling resistance. Arjowiggins Security. US5660919A
- Volpenhein ME, Ebrahimpour A (2008) Fold-resistant cleaning sheet. Procter and Gamble Co. US7423003B2

Résumé Français
-
Extended french abstract

Résumé Français – Extended French abstract

Contexte. En 1992 à l’occasion du traité de Maastricht, les pays membres de l’union européenne ont pris la décision officielle de créer l’Euro. Dix ans plus tard, les billets de banques ont commencé à circuler. Aujourd’hui, 20,2 milliards de billets Euros sont en circulation et 7 milliards sont fabriqués chaque année dans les papeteries et imprimeries européennes. La France est le premier producteur de billets de banque avec un volume annuel d’environ 2000 tonnes. Ces billets de banque, avant d’être symbole de richesse, sont des papiers à haute valeur ajoutée quotidiennement manipulés, échangés, pliés. Pour garantir la qualité visuelle et physique de ces papiers, les centres de tri détruisent les billets de banques endommagés ou remettent en circulation les billets de banque en bon état. Ainsi, la durée de vie d’un billet de banque se situe entre quelques mois et trois ans, en fonction de la dénomination du billet et du pays. La première raison de destruction des billets de banque en centre de tri est la salissure, suivie par les « dog-ears », ou plis qui apparaissent dans les coins des billets (Figure 1). Le froissement est aussi un défaut classique des billets de banque, mais il reste en dehors des statistiques car il n’y a pas de capteurs détectant ce défaut dans les centres de tri malgré les nombreuses destructions dont il est à l’origine.



Figure 1: Problèmes liés au dog-ears et au froissement des billets de banque

Défis associé aux dog-ears et au froissement. L’objectif de cette thèse est d’augmenter la résistance aux dog-ears et au froissement des billets de banque. En effet, ces deux défauts sont responsables d’une perte économique en réduisant la durée de vie des billets de banque et perturbent le fonctionnement des machines de tri pour différentes raisons. La première conséquence des dog-ears est l’augmentation de l’épaisseur dans la zone du coin plié, ce qui complique le transport automatique des billets de banque dans les machines de tri et peut provoquer des bourrages papier. Par ailleurs, cette augmentation de l’épaisseur limite le nombre de billets de banque dans les boîtes de conditionnement, ce qui cause une perte économique. Le coin plié peut également couvrir des signes de sécurité qui ne seront donc plus détectés par les machines automatiques et entraîneront la destruction du billet. De plus, les dog-ears peuvent également

affaiblir la couche barrière des billets de banque et engendrer la pénétration de la salissure. Enfin les coins cornés ont davantage de risque d'être déchiré.

La situation concernant les billets de banque froissés est plus complexe. Tout d'abord, les billets froissés peuvent être remis en circulation même s'ils ne répondent pas aux exigences de qualité visuelle, faute de détection du défaut dans les machines de tri. Par ailleurs, le froissement peut également augmenter l'épaisseur locale des billets et engendrer des problèmes de conditionnement. De plus, un « effet de ressort » peut apparaître résultant d'une perte de rigidité du papier, augmentant la tension nécessaire pour maintenir les billets dans leur boîte de conditionnement. Enfin, les billets de banque froissés en circulation sont affaiblis et les zones froissées peuvent être facilement déchirées. Dans le pire des cas, une perte de propriétés mécaniques entraîne la circulation de billets de banque flasques. Aujourd'hui, aucune solution satisfaisante n'existe pour la limitation de ces deux défauts.

Certains pays, comme l'Australie, le Canada ou la Nouvelle-Zélande, ont choisi les billets de banque en polymère pour augmenter la durée de vie, les propriétés mécaniques et la résistance à la salissure des billets. Cependant, ces billets de banque en plastique présentent certains désavantages tels que leur coût de production initial plus élevé et provoquent des problèmes de manipulation et d'adaptation aux machines automatiques de paiement ou de vente. Jusqu'à présent, l'Eurosystème a décidé de rester dans une stratégie utilisant des substrats papiers et examinant les vastes possibilités offertes par la nature pour gagner en performance.

Les nanocelluloses dans l'industrie papetière. Les nanocelluloses combinent les propriétés bien connues de la cellulose telles que la résistance mécanique, l'abondance et la biodégradabilité, avec les propriétés innovantes et exceptionnelles offertes par l'échelle nanométrique. Le terme "nano" désigne des matériaux ayant au moins une dimension inférieure à 100 nm. Deux types de nanocellulose peuvent être extraits de la fibre cellulosique brute: les nanofibrilles de cellulose («NFCs») et les nanocristaux de cellulose («NCCs»). Les NFCs sont obtenues après une désintégration mécanique de la fibre et se présentent sous forme de fibrilles longues et flexibles qui s'enchevêtrent, souvent imagées sous la forme de «spaghettis», dont le diamètre est celui d'un cheveu qui aurait été coupé par 1000 dans le sens de la largeur. Les NCCs sont obtenus après une hydrolyse acide des régions amorphes de la fibre, et ont la forme de cristaux petits et rigides qui peuvent être imagés comme des « grains de riz » dont le diamètre serait divisé par 10^6 (figure 2A). L'échelle nano de ces matériaux ainsi que leur haut facteur de forme confèrent une grande surface spécifique responsable de propriétés mécaniques impressionnantes. Par ailleurs, les NCCs et NFCs possèdent de nombreux groupes hydroxyles à leur surface qui leur permettent d'interagir entre eux ou dans une matrice, et qui permettent aussi aux NCCs et NFCs d'être fonctionnalisés avec divers agents chimiques (antimicrobiens, antioxydants,...). Grâce à leur performance dans diverses applications (papier, cosmétique, biomédicale,...), ces nanomatériaux suscitent un intérêt industriel qui augmente de façon exponentielle depuis une dizaine d'années comme on peut le voir avec l'évolution des brevets (figure 2B).

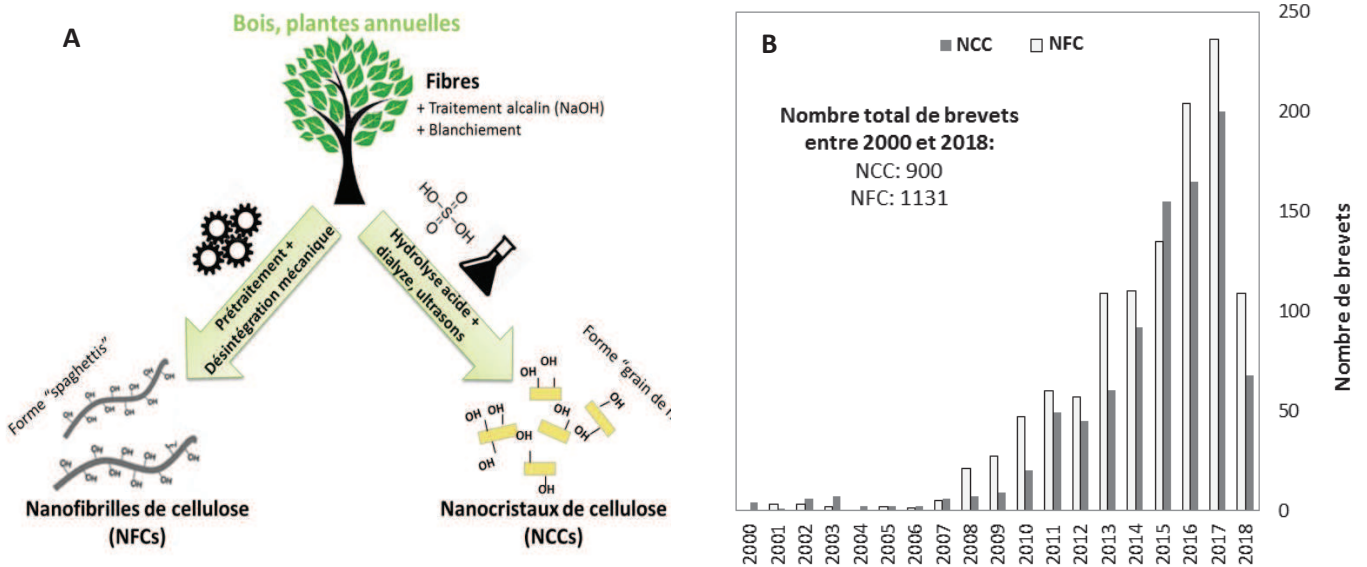


Figure 2: A) Description schématique des NFCs and NCCs et B) nombre de brevets publiés contenant des nanocelluloses. Basé sur une recherche SciFinder. Descripteurs pour les NFCs: Cellulose + CNF, Cellulose + MFC, Cellulose + NFC, Cellulose nanofibers, nanofibrillated cellulose, cellulose nanofibrils. Descripteurs pour les NCCs: Cellulose + CNC, Cellulose + NCC, Cellulose nanocrystals, Nanocrystalline cellulose, Cellulose nanowhiskers.

Le potentiel des nanocelluloses dans l'industrie papetière s'est révélé au cours de la dernière décennie. La transition s'est d'abord effectuée de la recherche à l'industrie à haute valeur ajoutée, mais s'est répandue aujourd'hui à l'industrie à fort volumes. En effet, les récentes avancées scientifiques ont permis de réduire les coûts de production des nanocelluloses ainsi que de proposer une meilleure connaissance et caractérisation de ces matériaux. Aujourd'hui, il existe de nombreuses sources commerciales à fort tonnages disponibles pour des applications industrielles. Il existe deux approches pour l'utilisation des nanocelluloses dans le papier: mettre les nanocelluloses dans la masse ou à la surface. Les nanofibrilles de cellulose sont principalement utilisées dans la masse pour améliorer les propriétés mécaniques humides et sèches, augmenter la teneur en charges, diminuer le raffinage des fibres ou diminuer le grammage du papier. A la fois les nanofibrilles et les nanocristaux de celluloses sont utilisés en surface, seuls ou en renfort de polymère, pour augmenter la résistance aux huiles, à l'air, aux graisses, à la vapeur d'eau, diminuer la rugosité, ou encore pour faciliter l'impression. Ces applications sont déjà utilisées dans les papiers traditionnels, dans les papiers qui ciblent des propriétés fonctionnelles supplémentaires, dans l'emballage alimentaire ou dans l'industrie du carton, mais aussi dans les papiers spéciaux et même dans les billets de banque. En effet, un brevet a été déposé il y a deux ans par Oberthur security qui propose l'utilisation de NCCs dans le vernis des billets de banque pour augmenter la résistance aux corps gras et à la salissure. Cependant, aucun brevet ni aucune publication n'ont jamais signalé l'utilisation de NCCs et NFCs pour diminuer le dog-ears ou le froissement.

Description des chapitres. Ce projet, nommé « RESIST », a pour but d'utiliser les NCCs et NFCs dans deux stratégies différentes pour limiter l'apparition de dog-ears ou du froissement des billets de banque. Le projet global est divisé en 4 phases et propose à la fois une recherche fondamentale et appliquée, jusqu'à la réalisation d'essais pilotes puis industriels sur machine de la Banque de France. Ces phases sont illustrées sur la Figure 3.

- **Phase 1 : Sélection des matières premières.** Cette étude préliminaire a été réalisée par les mêmes auteurs dans le cadre d'un mémoire de master, mais ne sera pas reportée dans ce manuscrit. Comme les billets de banque sont réalisés en fibre de coton, cette première phase a étudié la possibilité d'une production autonome de nanocellulose sans avoir recours à une source commerciale, à partir de la même fibre de départ (le coton) ou bien à partir d'eucalyptus. Ainsi, différents types de nanocellulose, greffées ou non avec des charges anioniques ou cationiques, ont été préparés et caractérisés. Ces suspensions ont été produites avec succès à l'échelle labo, avec des dimensions et des propriétés comparables à celles des sources commerciales. Une augmentation de la production de NFC a été proposée en adaptant l'équipement de super-broyeur Masuko du laboratoire avec un système de recirculation. En outre, la consommation d'énergie de ce traitement mécanique a également été réduite avec succès grâce à l'addition en faible quantité de charges abrasives, telles que le dioxyde de titane ou les fibres de verre. Cependant, une production supérieure à l'échelle labo des NCCs n'a pas été réalisée en raison des longues et minutieuses étapes de lavage (centrifugation et dialyses). La phase 1 a conclu que les NFCs pourraient être produites directement à partir des équipements de laboratoire tandis que les NCCs seraient fournis par des sources commerciales.
- **Phase 2: Addition de NCCs dans le bain d'imprégnation d'alcool polyvinylique (PVOH) pour diminuer le dog-ears.** Cette phase est décrite dans le **Chapitre II** de ce manuscrit. Un billet de banque est composé de deux couches de fibres de coton. A la fin de la machine à papier, le papier est imprégné dans un bain d'alcool polyvinylique (PVOH). La stratégie de ce chapitre consiste à introduire une petite quantité de NCCs pour renforcer la matrice PVOH. Ce nanocomposite a renforcé la surface des billets de banques via une augmentation de la rigidité et de la cristallinité du PVOH. Plusieurs paramètres ont été testés, notamment grâce à une nouvelle technique (SIEBIMM), et un optimum a été obtenu concernant la quantité de CNC (10% en CNC par rapport à la matrice) mais aussi le type de séchage (utilisation de l'infra-rouge). L'angle après pliage a ainsi considérablement été augmenté. L'addition de CNC favorise donc un retour élastique du coin ainsi plié pour retrouver une conformation plane. Ces résultats positifs ont été confirmés à l'échelle pilote ce qui a permis le dépôt d'un brevet.
- **Phase 3: Conception d'un multicouche contenant des NFCs pour la limitation du froissement.** Cette phase est décrite dans le **chapitre III** de ce manuscrit. Dans cette partie, une couche de NFCs de 5 g.m^{-2} est introduite entre les deux couches de fibres composant un billet de banque classique, l'une de grammage 25 g.m^{-2} et l'autre de grammage 60 g.m^{-2} .

Cette couche de NFCs a pour but d'augmenter la résistance au froissement. Comme les NFCs sont extrêmement sensibles à la déchirure, une attention particulière a été également portée sur la résistance à la déchirure du papier multicouche, et différentes stratégies comprenant le mélange de NFCs avec des fibres synthétiques de polyester ou des billes poreuses de NFCs ont été étudiées. Il a fallu mettre en place des outils de caractérisation de la qualité des NFCs et du froissement du papier. Les résultats avec l'ajout de NFC mais aussi avec celui de NFC + PET ont été très positifs pour éviter de froisser le papier et un deuxième brevet est en cours de submission.

- **Phase 4: Combinaison des deux stratégies et mise à l'échelle industrielle.** Cette phase est décrite dans le **chapitre IV** de ce manuscrit. Les études des deux chapitres précédents ont été menées indépendamment et à l'échelle du laboratoire. Ce dernier chapitre propose une transition de la recherche à l'industrie et décrit les essais qui ont été réalisés sur machine pilote et sur machine industrielle à la Banque De France. Ce chapitre rassemble également les deux stratégies dans un matériau final commun et étudie de manière symétrique l'influence des NCCs sur la résistance au froissement et l'influence des CNFs sur le dog-ears. Des confirmations et des questions peuvent être listées après cette partie appliquée. Ils mettent notamment en avant l'intérêt des NFCs pour la résistance au pli, la possibilité du passage à l'échelle industrielle et le rôle (positif) des étapes de post-fabrication du papier (lors de l'ajout d'éléments de sécurité).

En conclusion, ce projet a proposé deux nouvelles approches qui se sont toutes deux avérées positives pour améliorer les propriétés mécaniques des billets de banque. Le transfert à l'échelle industrielle est déjà en cours et de nouveaux essais sont prévus pour confirmer la validité des résultats. Il est également important de noter la volonté d'une meilleure compréhension et maîtrise des phénomènes avec des approches fondamentales en collaborations internationales et le développement de nouveaux outils de caractérisation. Nous espérons que ces travaux soient utiles à la communauté des nanocellulose et des papiers de sécurité.

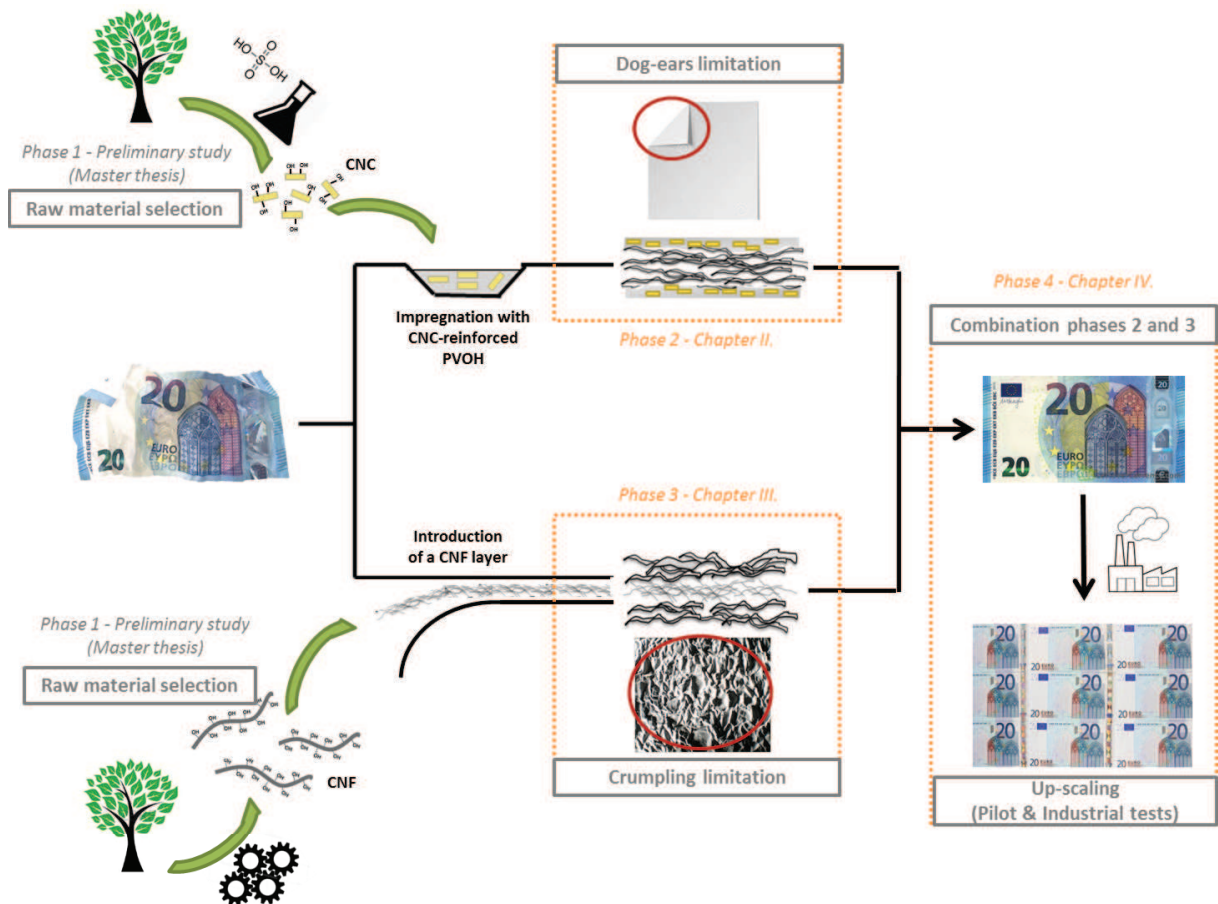


Figure 3: Description des deux stratégies pour limiter l'apparition du dog-ears et du froissement et organisation des chapitres

Résumé Anglais – English Abstract

The original feature of this work is the use of nanocellulose for limiting two security paper defects: corner folds, also called “dog-ears”, and crumpling. These defects, principally caused by daily handling of these high added value documents, are responsible for a decrease of paper visual and mechanical quality and constitute an economic loss. Nanocellulose can be divided into two different families: cellulose nanofibrils (CNFs) and cellulose nanocrystals (CNCs). CNFs are long and flexible materials with the ability to entangle and form a network strongly maintained by hydrogen bonds. CNCs are short and rigid materials whose outstanding mechanical properties make them good candidates for reinforcement in a polymer matrix. In this study, two strategies are proposed to incorporate these two kinds of nanocellulose in the security paper process. First, introduction of a CNF layer within the paper substrate is considered in order to increase the paper crumpling resistance. Then, impregnation of the paper with CNCs-reinforced polyvinyl alcohol (PVOH) is considered in order to increase the dog-ears resistance. Finally, these approaches are tested at pilot and industrial scales.

Keywords: Nanocellulose, Security paper, Crumpling, Corner folds, CNF, CNC

Résumé Français – French Abstract

Ce travail étudie la contribution des nanocelluloses pour limiter deux défauts courant dans les papiers sécurités: le froissement et les “cornes”, ou plis qui se manifestent dans les angles des papiers. Ces défauts sont principalement causés par une manipulation quotidienne de ces papiers à haute valeur ajoutée, et sont responsables d’une perte de qualité visuelle et mécanique ainsi que d’une perte économique. Les nanocelluloses peuvent être divisées en deux différentes familles de matériaux: les nanofibrilles de celluloses (NFCs) et les nanocristaux de cellulose (NCCs). Les NFCs sont longues et flexibles et peuvent facilement s’enchevêtrer pour former un réseau cohésif maintenu par de nombreuses liaisons hydrogène. Les NCCs sont des matériaux petits et rigides, et leurs impressionnantes propriétés mécaniques font d’eux des candidats intéressants pour être utilisés comme renfort de polymère. Dans cette étude, deux stratégies sont proposées pour incorporer ces deux types de nanocellulose dans la fabrication du papier sécurité. Premièrement, il est question d’introduire une couche de NFCs à l’intérieur du papier afin d’augmenter la résistance de ce papier au froissement. Ensuite, il est question d’imprégner ce papier avec de l’alcool polyvinylique renforcé par des NCCs afin d’augmenter la résistance aux cornes. Enfin, ces approches sont testées à l’échelle pilote et industrielle.

Keywords: Nanocellulose, Security paper, Crumpling, Corner folds, NFC, NCC